MODELING OF INDOOR AIR QUALITY AND EXPOSURE

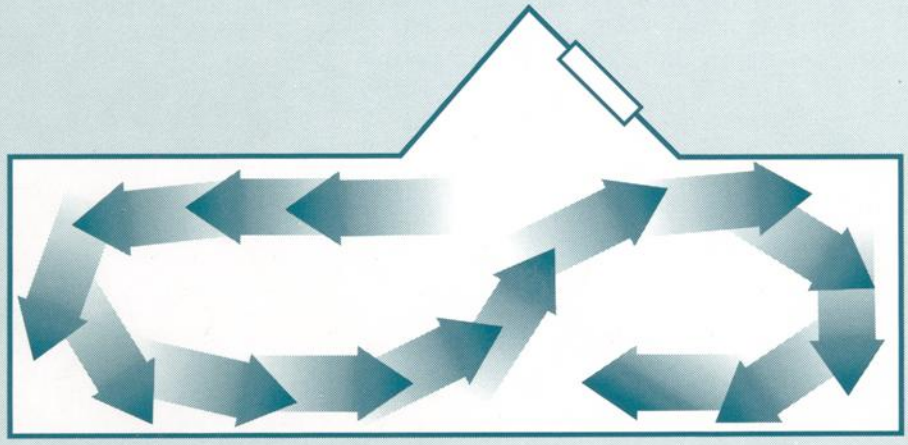

NIREN L. NAGDA EDITOR

ASTM STP 1205

STP 1205

Modeling of Indoor Air Quality and Exposure

Niren L. Nagda, editor

ASTM Publication Code Number (PCN)
04-012050-17

ASTM
1916 Race Street
Philadelphia, PA 19103

Library of Congress Cataloging-in-Publication Data

Modeling of indoor air quality and exposure / Niren L. Nagda, editor.
(STP; 1205)
"Contains papers presented at the symposium of the same name held in Pittsburgh, PA on 27–28 April 1992 . . . sponsored by ASTM Committee D–22 on Sampling and Analysis of Atmospheres and Subcommittee D22.05 on Indoor Air" — Foreword.
"ASTM publication code number (PCN): 04-12050-17."
Includes bibliographical references and indexes.
ISBN 0-8031-1875-9
1. Indoor air pollution—Mathematical models—Congresses.
2. Pollutants—Toxicology—Mathematical models—Congresses.
I. Nagda, Niren Laxmichand, 1946– . II. Series: ASTM special technical publication; 1205.
TD890.M64 1993
628.5'3'015118—dc20 93–31561
CIP

Photocopy Rights

Peer Review Policy

Each paper published in this volume was evaluated by three peer reviewers. The authors addressed all of the reviewers' comments to the satisfaction of both the technical editor and the ASTM Committee on Publications.

The quality of the papers in this publication reflects not only the obvious efforts of the authors and the technical editor, but also the work of these peer reviewers. The ASTM Committee on Publications acknowledges with appreciation their dedication and contribution to time and effort on behalf of ASTM.

Printed in Philadelphia, PA
September 1993

Foreword

This publication, *Modeling of Indoor Air Quality and Exposure*, contains papers presented at the symposium of the same name held in Pittsburgh, PA on 27–28 April 1992. The symposium was sponsored by ASTM Committee D-22 on Sampling and Analysis of Atmospheres and Subcommittee D22.05 on Indoor Air. Dr. Niren L. Nagda of ICF Incorporated in Fairfax, VA presided as symposium chairman and is the editor of the resulting publication.

Contents

Overview

Concern for the quality of air in buildings and exposures to toxic substances has been rising in recent years. Mathematical modeling of indoor air quality is commonly used to improve the understanding of chemical and physical processes that affect indoor pollutant concentrations and to predict indoor concentrations and human exposures under different situations.

Most indoor air quality models are based on the principle of conservation of mass: the accumulation of a contaminant is equal to the difference between the mass generated within or entering a particular air space and the mass leaving that air space. In this conceptual framework, pollutant concentrations are increased by emissions within a defined volume and by transport from other air spaces, including the outdoors. Similarly, concentrations are decreased by transport exiting the air space, by removal to chemical and physical sinks within the air space, or by conversion of the contaminant to other forms. Relationships are in the form of one or more differential equations representing the rate of accumulation and the contaminant gain and loss.

Models to quantify human inhalation exposure to contaminants need to consider air quality in various microenvironments such as residences, workplaces, and outdoors. Because many people spend a large fraction of their time indoors, inclusion of an indoor air quality model is an important component of total or 24-h exposure modeling. Another important component of exposure modeling is consideration of human activity patterns, that is, where and how people spend their time during the conduct of their daily activities.

In the past, simplifying assumptions have been made in modeling, such as a constant source rate over time, a negligible sink rate, steady-state conditions, or an isothermal air mass. In addition, activity patterns have not been considered or have been treated with simplistic assumptions. These may be appropriate assumptions under some limited circumstances but, to obtain greater generalizability and to better understand the behavior of indoor contaminants or the factors that affect exposures, it is important to examine situations in a more realistic manner.

This Special Technical Publication (STP) has been published as a result of the 1992 symposium entitled, "Modeling of Indoor Air Quality and Exposure" held in Pittsburgh, PA in an effort to present recent advances in various aspects of indoor air and exposure modeling. The papers presented at this symposium are grouped in three areas:

(1) Modeling and measuring sources and sinks,
(2) Model validation and application, and
(3) Modeling of exposures.

Research over the last several years has shown that emissions from indoor sources dominate indoor air concentrations and exposures much more so than factors such as ventilation. Understanding of complexities such as re-emitting sinks is just beginning. As sources and sinks are basic components of indoor air quality modeling, and considerations of sources and sinks are often linked, the papers on that subject form the first major section of the STP.

The second section of this STP contains papers that address a variety of indoor air quality modeling issues: validation of models, modeling of air flows, including consideration of computational fluid dynamics, and application of models to predict indoor air concentrations of contaminants. The third section extends considerations of indoor air quality modeling to exposure modeling. Activity patterns are treated as assumed scenarios, as measured profiles for specific individuals, and as general mobility patterns for subgroups defined by factors such as age and occupation.

Individuals who are involved in indoor air quality and exposure research can use this STP to assess the state-of-the-art, and as a foundation to further on-going research. The STP will assist environmental and public health officials with responsibilities in the areas of indoor air quality and public health in understanding the impact of various factors on indoor concentrations and exposure. With the diversity of topics covered in this STP, all focused towards modeling, it should be a valuable resource for undergraduate and graduate students and faculty.

The remainder of this overview provides some highlights of the papers included in the STP.

Modeling and Measuring Sources and Sinks

Clausen et al. determined time-varying profiles for emissions of cyclohexanone and phenol from a vinyl floor covering using two 234-L chambers and a much smaller, 0.035-L chamber. The emission rates of both compounds decreased rapidly during the first 24 h followed by a much slower decrease over the next several days. The experimental data for the initial period indicated evaporation-controlled emissions; the authors have suggested diffusion-controlled emissions for the period after the first 24 h. However, parameters for the diffusion-controlled model could not be reproduced with the data collected from this study.

Keating and McKone measured and modeled the water-to-air transfer efficiency for trichloroethylene (TCE) during showering using a specially constructed chamber and different nozzles. As expected, the nozzle producing smallest drop diameters had the highest transfer efficiency. Significant differences were observed between measured air concentrations and those predicted using transfer efficiencies and air exchange rates. The authors examined possible impacts of various factors such as measurement precision, aerosol concentrations, scavenging, deposition, and incomplete mixing. In a different study, Borrozzo et al. measured partition coefficients for TCE and ethanol to nylon, wool, polypropylene, jute, styrene-butadiene rubber (SBR), glass, cotton and polyester surfaces, as well as partition coefficients for chloroform, tetrachloroethylene, and p-dichlorobenzene to nylon, cotton, wool, and glass surfaces. For nonpolar species, sorption to polypropylene and SBR was greater than sorption to nylon or wool. For polar species, the opposite was true. The authors suggested that "*ad*sorption" can explain the majority of the experimental results but "*ab*sorption" may be a dominant mechanism in some cases. Since various components of a composite material may display different affinities for a single compound and different mechanisms of interaction, first-order kinetics may not adequately describe sorption of indoor volatile organic compounds.

Complexities of source and sink terms are further magnified when mixtures of compounds, such as environmental tobacco smoke, are considered. In such cases, it is not practical to measure or even model all constituents of the mixture as one considers their transport and removal in an indoor environment, thereby making the selection of suitable tracers an important issue in modeling. Eatough examined various components of environmental tobacco smoke (ETS) with respect to uniqueness to ETS, ease of determination at concentrations present in indoor air, and relationship to other components of ETS. The author contends that gas-phase 3-ethenylpyridine and isoprene, and particulate-phase solanesol could be better ETS tracers than nicotine and respirable particles, that have been used as tracers in the past.

The existence of re-emitting sinks for VOCs is well recognized, but the mechanisms by which VOC sinks operate are not well understood. Diffusion mechanisms have been considered to play a role in interactions of VOCs with indoor sinks. Dunn and Chen proposed and tested three unified, diffusion-limited mathematical models to account for such interactions. The phrase "unified" relates to the ability of the model to predict both in the sink accumulation and decay phases. A linear isotherm model adequately described data when a pillow functioning as a sink was exposed to ethylbenzene and a single-parameter diffusion model described pillow-sink/perchloroethylene data well, but neither could adequately describe data for carpet when exposed to ethylbenzene. A

hybrid, sorption/desorption model was required to describe carpet-sink/ethylbenzene data, consistent with the complex nature of that sink.

The concept of "deposition velocity," as used in describing the interaction between an airborne contaminant and indoor surfaces, is defined as the net flux of a species to a surface divided by the concentration of that species in air. Deposition velocities have been used in modeling the amount of a given substance removed by indoor surfaces. Nazaroff et al. discussed, measured, and modeled deposition velocities for four different species: fine particles, radon progeny, ozone, and nitrogen dioxide. The authors showed that the factors that may limit useful application of the concept include lack of uniform mixing in the indoor space, limited data on air motion near surfaces within buildings, spatial variability of deposition, and the inflexibility of the concept to deal with subsequent release or re-emission of contaminants into indoor air.

Sorption of contaminants on suitable filtration media is one means of improving the quality of air in buildings, yet models that fully accommodate filtration processes are not availble. Axley and Lorenzetti proposed models formulated as mass transport modules that can be combined with existing indoor air quality models. Four generic families of models proposed by the authors include: equilibrium adsorption, boundary layer diffusion, porous adsorbent diffusion transport, and convection-diffusion transport. The authors present applications of these models and propose criteria for selection of models that are based on the boundary layer/conduction heat transfer problem.

Model Validation and Application

Model validation is perhaps the weakest aspect of indoor air quality model development. Recognizing a critical need, ASTM has published a *Standard Guide for Statistical Evaluation of Indoor Air Quality Models* (ASTM D 5157) that provides quantitative tools for evaluation of indoor air quality models. These tools include statistical formulas for assessing the general agreement between predicted and measured values as well as for evaluating bias. The guide also proposes specific ranges of values for various statistical indicators that can be used in judging model performance.

As in the case of indoor air quality models in general, Guo observed that few source and sink models have been validated. The author outlined five major problems areas: (1) elusive model parameters, that result from attempts to model complex reality with a simple model, so that some adjustable parameters are necessary; (2) confusion in parameter estimation methods, specifically uncertainty in selecting appropriate regression models to accurately fit various portions of emissions decay; (3) uncertainty in scale-up and misleading scaling factors, for example, the commonly used ratio of air exchange rate to the chamber loading factor is incorrect unless the source is constant at steady state; (4) unspecified valid range, particularly the limited time over which a model is valid and the limited degree of air turbulence for which a model is valid; and (5) weakness in quantitative comparisons between models and observations, that is caused by an almost exclusive dependence upon graphic comparisons and a failure to use statistical methods.

Solutions suggested by Guo included the need to check the agreement between the model and multiple sets of observations as well as performing scale-up verification. This should be coupled with the use of statistical comparisons to complement graphic comparisons. Finally, he proposed that the key to developing relatively simple mass transfer models lies in selecting proper expressions for mass transfer coefficients, and he suggested criteria for choosing an expression. It was also noted that the degree of accuracy of model predictions necessary is an important consideration; in some cases, a simple model may do a reasonable job.

Girman expanded in some detail upon one of the concerns described by Guo: chamber air velocity and its effect on the scale-up of model results. Through simple modeling of air with chambers of different dimensions, Girman suggested that air velocities in small test chambers as currently operated may be essentially stagnant, possibly resulting in inaccurate emission factors. He proposed that boundary-layer effects be examined for a range of representative materials, es-

pecially wet sources, to determine the importance of controlling air velocities in small chambers. If chamber air velocities are currently too low to obtain representative emission factors, guidance for selecting appropriate operating conditions was suggested: operating chambers with high loading and high air exchange rates to produce representative chamber concentrations and representative air velocities. Other suggestions include varying the design of chamber air inlets and outlets.

Yamamoto et al. present a model that can be used as an analytical tool for engineers to evaluate potential ventilation performance and indoor-air-quality implications of a proposed indoor space design. The ventilation model is capable of determining distributions of time-averaged, steady-state flow fields, assuming isothermal conditions. Klobut demonstrated, through a modeling simulation, that unevenly distributed thermal load tends to increase the spread of contaminants in the building. His numerical simulations consider non-isothermal, two-way flow through large openings and illustrate differences among different scenarios, including an isothermal case with examples. Although his work represents an important step, the potential sources of uncertainties, especially those introduced by flow relations for each path, still need to be examined. The author urges a comprehensive verification of the simulation through measurements.

Jones and Waters dealt with the application of airflow and smoke modeling for building environmental design using three-dimensional computational fluid dynamics (CFD). CFD modeling can assist in design of a building in three main areas: (1) comfort, by predicting variation in thermal comfort due to air temperature and velocity and permitting optimization of space heating or cooling efficiencies; (2) health, by predicting ventilation effectiveness of the spatial distribution of fresh air; and (3) safety, by predicting the movement of smoke during a fire for a given smoke management strategy. The authors presented examples of applications of CFD modeling including design and assessment of natural ventilation strategies and prediction of smoke movement arising from accidental fires for the development of a smoke ventilation strategy.

As a number of buildings, especially in Europe, rely exclusively on natural means for ventilation, natural ventilation systems are important for indoor air quality. Panzhauser et al. pointed out that few generally accepted design rules and codes are available to assist in the design of natural ventilation systems. An effective design of natural ventilation systems could be achieved through properly designed and constructed window and shaft systems that consider regional climate, occupancy requirements, and geometric configuration of the building. Based on long-term studies of residual buildings in Austria, and mathematical modeling, the authors have developed a single-cell model to support the design and evaluation of natural ventilation systems. The model has undergone limited testing and enhancements are planned.

Applications of indoor air quality modeling to specific pollutants are presented in three papers: Panzhauser and Mahdavi predict formaldehyde concentrations and Wray et al. and Persily address radon. Panzhauser and Mahdavi extend the work on formaldehyde conducted almost 20 years ago to distinguish two types of formaldehyde sources, those that depend on indoor air conditions and those that do not. Their model calculates formaldehyde concentrations under steady-state and dynamic conditions for different sources, spaces and boundary conditions. Wray et al. used a model to make a comparative assessment of the effectiveness of subslab radon mitigation systems in residential structures. They found that, consistent with the measured data, a subslab depressurization system was more successful than a subslab pressurization system in reducing indoor radon concentrations. Persily presents results of a limited number of computer simulations of multizone airflow and radon transport for a simplified representation of a multi-family, high-rise building. His simulation considers the influence of two different radon source terms, indoor-outdoor temperature difference, and exterior wall leakage. Although the analysis is limited by the lack of measurement data, one conclusion of the study is that vertical shafts are critical pathways for air and radon transport in these tall buildings.

Modeling of Exposures

Sparks et al. have developed an indoor-air-quality based exposure model that enables analysis of individual exposures for a wide variety sources and sinks. Assuming certain activity scenarios, the model allows for calculating exposures in a multiroom residential environment. The authors provided examples to explain the impact of source emissions on exposures and modifications to those exposures due to behavior of sinks.

Rosenbaum and Anderson summarized a demonstration study of the use of dispersion modeling to estimate carcinogenic risk to residents of southern California from benzene emitted into the atmosphere. The model addresses exposures and risks due to inhalation of contaminants considering different geographic subregions, age-occupation groups, daily activities, and respiration rates. The impact of building ventilation rates on indoor air quality is considered, but indoor sources and sinks are not included in this model. With the exclusion of indoor sources and sinks in their model, the opportunity to test the correspondence between predicted and observed concentration is limited: the results of the model are in the same range as the measured outdoor benzene concentrations.

Koontz et al. described a model that is under development for estimating the distribution of Californians' indoor exposures to various pollutants. The model will address various contaminants such as VOCs, inorganic gases, and particulate matter. The model can either use existing indoor concentration and exposure information to generate exposure distributions across microenvironments or it can estimate indoor air concentration distributions for different microenvironments based on principles of indoor air quality modeling. The model utilizes recently collected data on individual activity profiles of California residents and will use Monte Carlo techniques to combine data on activity patterns, microenvironmental concentration distribution, and mass-balance parameters.

Behar et al. simulate exposures of a sample of residents in an urban area during the conduct of their daily lives and combine the exposure levels with pharmacokinetic models. The estimates of exposure are based on human activity patterns, indoor concentration distributions, and outdoor concentration distributions and are simulated using Monte Carlo techniques. The results indicate: (1) that contributions to exhaled air and arterial blood concentrations from indoor air exposures are large compared to those solely resulting from outdoor exposures, and (2) that changes in exposure rapidly translate into similar changes in blood and exhaled breath concentrations.

Niren L. Nagda

ICF Incorporated, vice president, 9300 Lee Highway, Fairfax, VA 22031; symposium chairman.

John Girman

U.S. Environmental Protection Agency, branch chief, Indoor Air Division; Washington, DC 20460; session chairman.

Leslie Sparks

U.S. Environmental Protection Agency, environmental engineer, Air & Energy Engineering Research Laboratory, Research Triangle Park, NC 27711; session chairman.

Barry Ryan

Harvard School of Public Health, associate professor, Cambridge, MA 02115; session chairman.

Charles Weschler

Bellcore, distinguished member of professional staff, Red Bank, NJ 07701; session chairman.

Modeling and Measuring Sources and Sinks

Per A. Clausen,[1] *Bjarne Laursen,*[1] *Peder Wolkoff,*[1] *Elke Rasmusen,*[1] *and Peter A. Nielsen*[2]

Emission of Volatile Organic Compounds from a Vinyl Floor Covering

REFERENCE: Clausen, P. A., Laursen, B., Wolkoff, P., Rasmusen, E., and Nielsen, P. A., **"Emission of Volatile Organic Compounds from a Vinyl Floor Covering,"** *Modeling of Indoor Air Quality and Exposure, ASTM STP 1205*, Niren L. Nagda, Ed., American Society for Testing and Materials, Philadelphia, 1993, pp. 3–13.

ABSTRACT: The emission of volatile organic compounds (VOCs) from a vinyl floor covering has been evaluated in two small climatic chambers and a microchamber using different air exchange rates and loading factors. The concentration versus time emission curves for cyclohexanone and phenol were decreasing. Evaluation of the emission data showed that a first order decay model was insufficient to describe the emission adequately. However, in spite of the different air exchange rates and chamber concentrations, the first order rate constant could be reproduced when the model was fitted to simultaneous measurements in the three chambers. This indicated that the emission was controlled by internal diffusion. A simplified model for emission controlled by internal diffusion in the source was developed, applying a diffusion coefficient which depends exponentially on the concentration in the source. This model described the emission curves satisfactorily. However, the model parameters were not reproducible, probably because the samples were inhomogeneous with respect to VOC content and effective thickness. All results indicated that the concentrations of cyclohexanone and phenol were almost homogeneous at test start (because of the wrapping of the samples during storage prior to testing) and that the emission after a short initial period became controlled by internal diffusion in the source.

KEY WORDS: vinyl floor covering, volatile organic compounds, emission, internal diffusion model

The purpose of the work presented here was to evaluate the emission of volatile organic compounds (VOCs) from a vinyl floor covering in chamber tests using different air exchange rates and loading factors. Initial examination of the emission data using a first order decay model showed that this model was insufficient to describe the emission adequately. However, it was indicated that the emission was controlled by internal diffusion. A model for emission controlled by internal diffusion in the source had to be developed. It was a requirement that the model should have few parameters to be estimated so it could be applied on a limited data set.

Theory

It is commonly assumed that the emission rates of VOCs from finite thin film sources decrease approximately by a first order decay, as shown in Eq 1,

$$R = R_0 \exp(-k_1 t) \tag{1}$$

[1]Research scientist, scientist, senior research scientist, and engineer, respectively, National Institute of Occupational Health, Lersø Parkalle 105, DK-2100 Copenhagen Ø, Denmark.
[2]Senior research engineer, Danish Building Research Institute, PO Box 119, DK-2970 Horshølm, Denmark.

where

R = emission rate, mg · m^{-2} · h^{-1},
R_0 = initial emission rate, mg · m^{-2} · h^{-1},
k_1 = first order rate constant, h^{-1}, and
t = time, h.

First order decay models incorporating sink and vapor pressure effects for concentration of an emission in a well-mixed chamber have been proposed by Dunn and Tichenor [*1*]. Solutions to the simplest model (that is, neglecting sink and vapor pressure effects) can be found by insertion of Eq 1 into the mass balance equation for the chamber,

$$V \cdot dC = A \cdot R \cdot dt - k_2 \cdot V \cdot C \cdot dt \tag{2}$$

where

C = chamber air concentration, mg · m^{-3},
A = area of source, m^2,
k_2 = air exchange rate, h^{-1}, and
V = chamber volume, m^3.

Given that $C = 0$ when $t = 0$, the solution to Eq 2 with Eq 1 inserted is

$$C = AR_0[\exp(-k_1 t) - \exp(-k_2 t)]/[V(k_2 - k_1)] \tag{3}$$

The first order decay model can be developed assuming that the emission is limited by evaporation from the surface (diffusion in the boundary layer) and that the concentration in the source is homogeneous [*2*]. However, internal diffusion in the source may become limiting. This implies that a concentration gradient will develop in the source. Dunn has proposed a model for an infinitely deep source [*3*]. However, this model is nonphysical for a finite source (for example, vinyl floor covering) in that a steady-state emission is reached. In addition, the diffusion coefficients of VOCs in a polymer matrix are probably not constant but depend strongly on the concentration of the VOC itself. Hansen [*4*] has shown that the exponential variation of the solvent-in-polymer diffusion coefficient is very important for lacquer film drying

$$D = D_0 \exp [kC(x)] \tag{4}$$

where

D = diffusion coefficient, m^2 · h^{-1},
D_0 = diffusion coefficient at zero concentration, m^2 · h^{-1},
k = proportionality constant, m^3 · mg^{-1}, and
$C(x)$ = concentration in the source at location x, mg · m^{-3}.

Model for Emission Controlled by Diffusion in the Source (Diffusion Model)

Consider the following cross-sectional schematic of the source and test chamber (Fig. 1). Let $C(x)$ denote the concentration of the VOC of interest at location x at any time, t, and let L denote the thickness (length) of the source. Assume that the diffusion coefficient $D = D_0 \exp [kC(x)]$ where D_0 and k are constants characteristic of the VOC of interest and the source matrix. This implies that, after a short initial period, there will be established a relatively stable concentration gradient profile which will be steep near the surface and almost flat in the remaining part of the

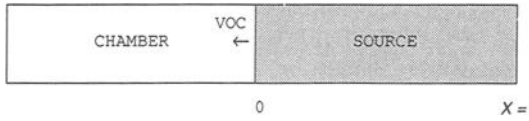

FIG. 1—*Cross-sectional schematic of the source and test chamber.*

source. After this initial period the flux will be F_s at the surface and decrease to zero at $x = L$. It is assumed that the flux at location x, $F(x)$, can be approximated by

$$F(x) = F_s\ (1 - x/L) \tag{5}$$

where

$F(x)$ = flux at location x in the source, mg · m^{-2} · h^{-1},
F_s = flux at the surface of the sources, mg · m^{-2} · h^{-1},
x = location in the source perpendicular to the surface, m, and
L = thickness (length) of the source, m.

The justification of this assumption is that the shape of the concentration gradient profile will be approximately constant during emission when the diffusion coefficient depends exponentially on concentration [*4*]. This implies that the removal rate (amount/time) of a VOC is approximately equal at all locations x (except just within the surface) and thereby $dF(x)/dx$ = constant.

Assuming that the movement within the source is controlled by Fick's Law $[dC(x)]/dx = F\ [(x)/D]$, the concentration gradient profile at any time can be found from the differential equation

$$dC(x)/dx = F_s(1 - x/L)/\{D_0 \exp\ [kC(x)]\} \tag{6}$$

Assuming that $C(x) = C_s$ when $x = 0$, the solution to Eq 6 is

$$C(x) = \{\ln\ [x/L_0 - x^2/(2 \cdot L \cdot L_0) + \exp\ (kC_s)]\}/k \tag{7}$$

where

$L_0 = D_0/kF_s$, m, and
C_s = surface concentration, mg · m^3.

The quantity L_0 depends on the flux at the surface and thereby the time. The mass of the VOC of interest in the source can be calculated as a function of the flux by integration of Eq 7. However, the second term in Eq 7 can be neglected for $x << L$ and for $x = L$ if $L >> L_0$. In the latter case the relative error for neglecting the second term is $\ln (2)/\ln(L/L_0)$. Approximation of the third term in Eq 7 [$\exp (kC_s)$] to 1 (C_s, very low) has only minor significance for the calculated mass of VOC in the source when $L >> L_0$. Thus, assuming that $L >> L_0$, Eq 7 can be approximated to

$$C(x) = \{\ln\ [(x/L_0) + 1]\}/k \tag{8}$$

The mass of VOC in the source as a function of the flux at the surface is then

$$M(F_s) = \int_0^L C(x)dx = \{(L + L_0) \ln\ [(L/L_0) + 1] - L\}/k \tag{9}$$

where

$M(F_s)$ = mass of VOC in the source, mg · m^{-2}.

The flux out of the source (the emission rate) can be found by differentiation of the mass emitted to the chamber

$$F_s = -dM/dt \tag{10}$$

It is assumed that $M(t)$ only depends on time through $F_s(t)$ so that

$$dM/dt = dM/dF_s \cdot dF_s/dt \tag{11}$$

Insertion of Eq 10 into Eq 11 and rearrangement gives

$$dF_s/dt = -F_s/(dM/dF_s) \tag{12}$$

Differentiation of Eq 9 with respect to F_s (dM/dF_s) and insertion into Eq 12 gives

$$dF_s/dt = kF_s^2/\{L_0 \ln [(L/L_0) + 1] - L\} \tag{13}$$

The functional form of $F_s(t)$ cannot be found from this differential equation. However, for $L \gg L_0$ (that is, F_s is large), Eq 13 simplifies to

$$dF_s/dt = -kF_s^2/L \tag{14}$$

Given that $F_s = F_0$ when $t = 0$, the solution to Eq 14 is

$$F_s(t) = 1/[(k/L)t + F_0^{-1})] \tag{15}$$

where

F_0 = initial flux at the surface, mg · m^{-2} · h^{-1}.

This model for emission controlled by internal diffusion in the source is valid when the diffusion coefficient depends exponentially on the concentration in the source. The model shows that the emission rate may be approximately proportional to $1/t$ when F_s is large and after a stable concentration gradient profile has been established. The model is not valid when F_s is small (that is, when $L \sim L_0$).

Experimental

Test Material

The vinyl floor covering was produced with an oak wood parquet look and had a smooth surface with "wood grain" grooves. It consisted of three layers: 0.3-mm wear layer, 0.7 to 1-mm foam layer, and approximately 1.5-mm synthetic felt backing. The VOC emission from the vinyl floor covering was evaluated prior to the chamber experiments by gas chromatography/mass spectrometry (GC/MS) [5]. The major VOCs in the emission from the floor covering were cyclohexanone, phenol, and 2,4,4-trimethyl-1,3-pentanediol diisobutyrate (TXIB).

TABLE 1—*Chamber data and test conditions for the FLEC and Chambers 1 and 2.*

Chamber	Air Exchange Rate, h^{-1}	Loading, $m^2 \cdot m^{-3}$	Volume, L	Temperature, °C	Relative Humidity, %RH
FLEC	169.5[a]	505	0.035	23	50
Chamber 1	0.12[b]	0.45	234	23	45
Chamber 2	0.25	0.45	234	23	45

[a]The air exchange rate decreased linearly over the test period following the equation $k_2 = 169.5 - 0.045 \cdot t$ (h^{-1}).

[b]Has been estimated from emission curves in a later experiment in the chamber [*11*] because the value controlling the air flow through the chamber had failed.

Chambers

The vinyl floor covering was tested in a flat, bell-shaped, efficiently ventilated microemission test cell made of stainless steel (FLEC) [*6*] and two small stainless steel chambers without fan stirring (Chambers 1 and 2) which complied with a Nordtest method [*7*]. Chamber data are shown in Table 1.

VOC Sampling and Analysis

VOCs in the chamber air were sampled in duplicate with separate pumps (Alpha-1®, Dupont®, Wilmington, DE) on Tenax® TA (Chrompach, Middleburg, The Netherlands) and analyzed by thermal desorption followed by capillary gas chromatography with flame ionization detection [*8*]. The pump flow was a nominal 40 mL/min. The sampling time was 0.5 h for all the FLEC samples and 1.0 h for all of the Chamber 1 and 2 samples. Breakthrough was checked for high content samples with sample backup tubes. Complete desorption of the cold trap was checked by a succeeding run of a blank tube, and complete desorption of sample tubes was checked by a cleaning procedure identical to the analysis procedure. All samples were analyzed within a week.

Sample Preparation

The vinyl floor covering was a representative sample taken out of a newly produced batch. It was wrapped in aluminum foil and stored in a nylon bag prior to the chamber testing. It was unwrapped immediately before insertion into the chambers.

Chamber Tests

The FLEC test was conducted as previously described [*6*], and the small chambers tests were conducted in compliance with a Nordtest method [*7*]. Prior to the tests the chambers were cleaned and background measurements were carried out. The samples were placed on the bottom part of Chambers 1 and 2 while the FLEC was placed onto the test material, which is the bottom part of the FLEC itself. The test start (time = 0) was established when the FLEC was placed onto the test material and when the doors to Chambers 1 and 2 were closed. The tests were started simultaneously in the three chambers. During 25 days, 8 and 5 duplicate samples were taken from Chambers 1 and 2, respectively, and 11 duplicate samples were taken from the FLEC during a period of 10 days.

Data Treatment and Calculations

All raw data were input to spreadsheets for calculation of chamber concentrations. The first order decay model parameters (k_1 and R_0) were obtained by fitting Eq 3 to the concentration versus time data with STATGRAPHICS routine for nonlinear regression using the standard regression parameters of the program [*9*]. The high air exchange rate in the FLEC (see Table 2) made it possible to approximate the diffusion model expression for the chamber concentration by the following equation

$$C = A \cdot F_s(t)/(V \cdot k_2), \text{ when } t >> 1/k_2 \tag{16}$$

The model parameters (k/L and F_0) were obtained by fitting Eq 16 to the concentration versus time data with STATGRAPHICS nonlinear regression. The diffusion model was fitted to the concentration versus time data from Chambers 1 and 2 using Eqs 2 and 15 in which $F_s(t)$ is substituted for R. The model parameters (k/L and F_0) were obtained by a simplex minimum search routine [*10*]. The entity to minimize was the squared deviation from the solution of Eqs 2 and 15 obtained by a fourth order Runge-Kutta method [*10*].

Results and Discussion

Description of the Emission Curves

The emission curves obtained in the FLEC and Chambers 1 and 2 are shown in Figs. 2 and 3 for cyclohexanone and phenol, respectively. The curves are based on the average of the duplicate measurements. The vinyl floor covering behaved as a decreasing source for cyclohexanone and phenol in all three chambers.

Analysis of the Emission Curves

The sink and vapor pressure effects under the test conditions are assumed to be insignificant for the shape of the emission curves of cyclohexanone and phenol because of their relatively high volatility as discussed previously [*2*]. Therefore, these effects are not incorporated in the models used in this work.

The high initial cyclohexanone concentration in the FLEC and the cyclohexanone concentration in Chamber 1 at 21 h (see Fig. 2) cannot be explained (predicted) by the diffusion model curves shown in Fig. 4. The wrapping on the vinyl floor covering sample prior to testing may have stopped the emission because the air concentrations of the emitting VOC at the surface may get very high. This may imply an almost homogeneous concentration in the floor covering at test start, resulting in a strong initial emission. The influence of a strong initial emission in the model fitting is circumvented by rejecting all data within the first 24 h.

The VOCs in the vinyl floor covering are distributed in all three layers. The amount of VOCs in the fluffy felt backing is probably much smaller than in the two other more dense layers. Therefore, it will only contribute a little to the emission from the wear layer. The diffusion in the foam layer is probably much faster than in the more compact wear layer. Thus, the diffusion through the wear layer becomes the limiting step and a concentration gradient will develop in this layer whereas the VOCs in the foam layer will be homogeneously distributed. If the amount of VOCs in the foam layer is much smaller than in the wear layer, the VOCs will be emitted as if only the wear layer existed. In the opposite case where the amount of VOCs in the foam layer is much larger than in the wear layer, the foam layer will function as a VOC reservoir for the wear layer, resulting in a slower decrease of the emission rate. This case cannot be described by the diffusion model but the effect corresponds approximately to an increased thickness of the source.

TABLE 2—*Results of the fitting of the diffusion model and the first order decay model to the emission data of cyclohexanone and phenol (see "Analysis of the Emission Curves").*

	Cyclohexanone				Phenol			
	Diffusion Model		Order Decay		Diffusion Model		Order Decay	
Chamber	$10^3 \cdot k/L$, $m^2 \cdot mg^{-1}$	F_0, $mg \cdot m^{-2} \cdot h^{-1}$	$10^4 \cdot k_1$, h^{-1}	R_0, $mg \cdot m^{-2} \cdot h^{-1}$	$10^3 \cdot k/L$, $m^2 \cdot mg^{-1}$	F_0, $mg \cdot m^{-2} \cdot h^{-1}$	$10^4 \cdot k_1$, h^{-1}	R_0, $mg \cdot m^{-2} \cdot h^{-1}$
FLEC	10[a]	1.77	61	1.28	64	0.15	46	0.13
	9[b]	1.36	43	0.97	59	0.14	36	0.11
Chamber 1	34	0.45	56	0.34	120	0.052	29	0.045
	34	0.45	53	0.31	137	0.057	39	0.048
Chamber 2	6	2.52	40	1.57	14[c]	0.11[c]	9[c]	0.10[c]
	6	2.77	54	1.82	31	0.14	28	0.13

[a]First row: estimates based on all data after 24 h.
[b]Second row: estimates based on simultaneous measurements in the three chambers at 72, 120, 168, and 240 h.
[c]These results are strongly influenced by the measurements at 600 h.

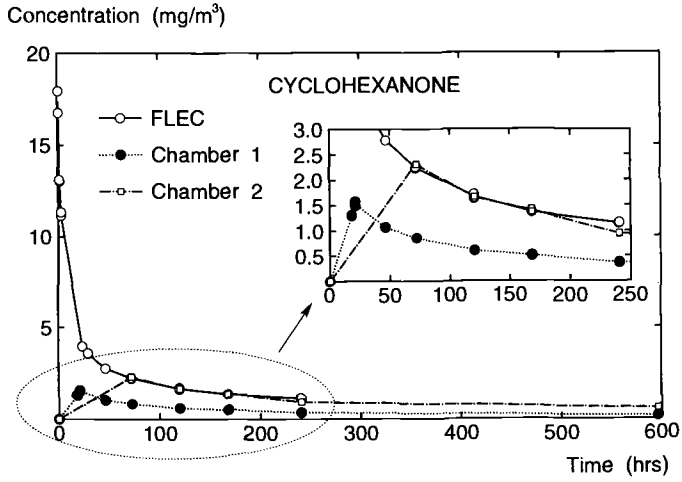

FIG. 2—*Cyclohexanone emission from the floor covering in the FLEC and the two small chambers.*

The result of these considerations is that the value of k cannot be isolated from the estimate of k/L because the distribution of VOCs in the different layers of the vinyl floor covering is unknown. The thickness L can be interpreted only in the case where most of the VOC content is in the wear layer.

The estimated value of the air exchange rate (k_2) and the loading factor has influence on the estimates of k/L, F_0, and R_0 but not k_1. For the FLEC and Chamber 2, k_2 has been estimated by measuring the flow through the chamber and dividing by the chamber volume (see Table 1). For Chamber 1, the air exchange rate has been estimated in a succeeding experiment by fitting the first order decay model to the emission data from a waterborne paint [*11*] (see Table 1). Hence, the air exchange rate of Chamber 1 is somewhat uncertain.

The models are fitted as described in the experimental section. The results are shown in Table 2. The first row shows estimates based on all data after 24 h. The second row shows estimates

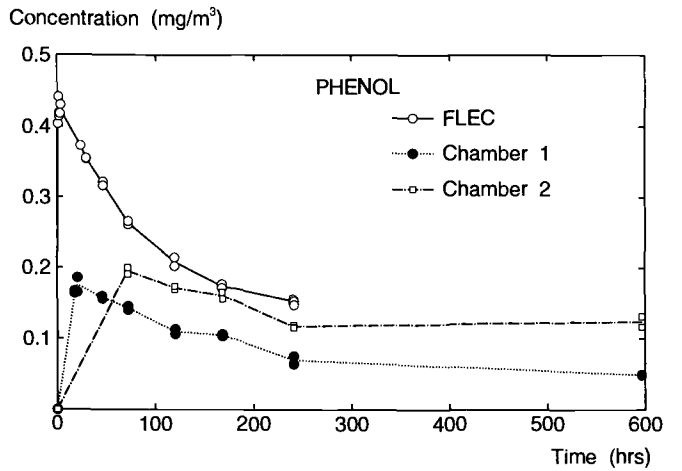

FIG. 3—*Phenol emission from the floor covering in the FLEC and the two small chambers.*

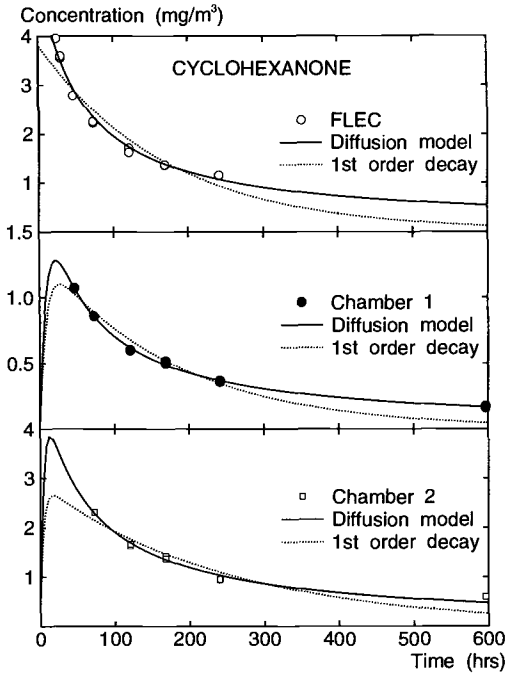

FIG. 4—*Model curves fitted to the measured concentrations of cyclohexanone in the FLEC and the two small chambers.*

based on four duplicate measurements performed simultaneously in the three chambers at 72, 120, 168, and 240 h [*6*].

First Order Decay Model—The decreasing part of the experimental curves is more curved than the first order decay model can accommodate for cyclohexanone and phenol, respectively, as shown in Figs. 4 and 5. In addition, the estimated first order rate constant (k_1) for each compound could not be reproduced in the chambers (see Table 2, first row for each chamber). This shows that the first order decay is a poor description of the emission from the vinyl floor covering. However, the k_1 values get much closer when the model is fitted to data sampled simultaneously in the three chambers (see Table 2, second row). Since k_1 is a measure of the emission rate decay, this shows that the curves had approximately the same decay rates at the same time. If the emission had been controlled by evaporation, much larger differences in the value of k_1 would have been expected as a result of the different air exchange rates and chamber concentration levels in the three chambers. Since this is not the case, this shows that the emission is independent of the air exchange rate and the chamber concentration. This indicates that the emission is controlled by internal diffusion.

The smaller k_1 for phenol (see Table 2, second row) may indicate a lower diffusion rate in the vinyl floor covering than for cyclohexanone.

The smaller values of R_0 for Chamber 1 reflect the lower chamber concentrations indicating sample inhomogeneity with regard to VOC content.

Diffusion Model—The decreasing part of the experimental curves are well described by the diffusion model as shown in Figs. 4 and 5 for cyclohexanone and phenol, respectively. However, the estimates of k/L and F_0 are not reproducible in the three chambers as shown in Table 2. The estimates of k/L appear to be dependent upon the experiment because the estimates of cyclohexanone and phenol correlate in the three chambers. This could be caused by different effective

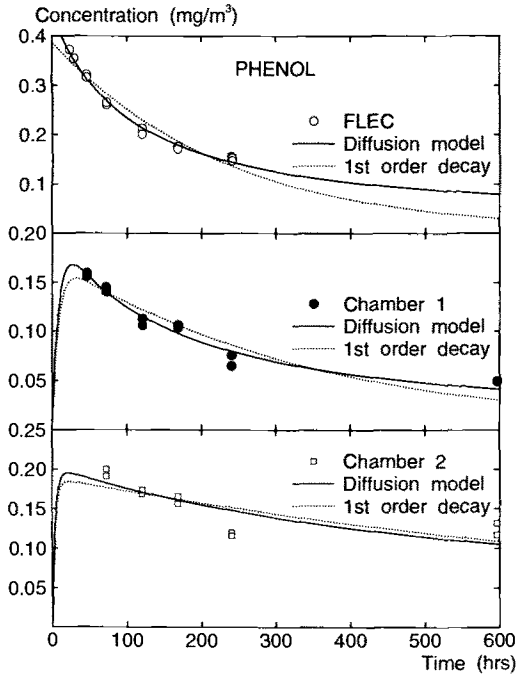

FIG. 5—*Model curves fitted to the measured concentrations of phenol in the FLEC and the two small chambers.*

thicknesses of the three samples. In addition, the estimates of both k/L and F_0 depend directly on the loading factor and air exchange rate (that is, a twofold increase of the air exchange rate approximately halves the estimate of k/L and doubles the estimate of F_0). The poor reproducibility may be caused by erroneous loading factors, air exchange rates, measurements of concentrations, and/or sample inhomogeneity with respect to VOC content, and effective thickness.

In spite of the nonreproducible estimates of k/L and F_0, the k/L values for phenol were several times larger than for cyclohexanone. This could reflect different interaction between phenol and the source matrix than for cyclohexanone.

The much lower values of F_0 in Chamber 1 may reflect the lower concentrations in this chamber and thereby may indicate sample inhomogeneity.

Comparison of the Two Models—F_0 and R_0 are essentially parameters of the same quantity, namely the initial emission rate. This is confirmed by the correlation of all the estimates based on the simultaneous measurements: $R_0 = 0.03 + 0.66 \cdot F_0$, $r^2 = 0.9992$.

Conclusion

The emission rate of cyclohexanone and phenol from a vinyl floor covering decreased with time. All results indicated that the concentrations of cyclohexanone and phenol in the vinyl floor covering were homogeneous at the start of the tests because of the wrapping of the samples prior to testing. After a short initial period, the emission became controlled by internal diffusion. Thus, changing the air exchange rate had little effect on the emission of cyclohexanone and phenol.

The experimental curves were more curved than the first order decay model could accommodate. However, in spite of different air exchange rates and chamber concentrations, the first order rate

constant seemed to be reproducible when the model was fitted to measurements made simultaneously in a micro chamber and two small chambers. This indicated that the emission was controlled by internal diffusion.

An internal diffusion model, applying a diffusion coefficient that depends exponentially on the concentration in the source, described the emission curves of cyclohexanone and phenol satisfactorily. However, the model parameters were not reproducible. This may have been caused by sample inhomogeneity with respect to VOC content and effective thickness. Other causes may also be erroneous loading factors, air exchange rates, and measurements of concentration. In spite of the nonreproducibility, the estimated model parameter (k/L) of phenol was always several times larger than for cyclohexanone in the same chamber.

Validation of the diffusion model requires a well-defined source, well-controlled and monitored test conditions, and testing over an extended period.

References

[1] Dunn, J. E. and Tichenor, B. A., "Compensating for Sink Effects in Emission Test Chambers by Mathematical Modeling," *Atmospheric Environment*, Vol. 22, 1988, pp. 885–894.

[2] Clausen, P. A., Wolkoff, P., Holst, E. and Nielsen, P. A., "Long Term Emission of Volatile Organic Compounds from Waterborne Paints–Methods of Comparison," *Indoor Air*, Vol. 1, 1991, pp. 562–576.

[3] Dunn, J. E., "Models and Statistical Methods for Gaseous Emission Testing of Finite Sources in Well-Mixed Chambers," *Atmospheric Environment*, Vol. 21, 1987, pp. 425–430.

[4] Hansen, C. M., "A Mathematical Description of Film Drying by Solvent Evaporation," *Journal of Oil Color Chemistry Association*, Vol. 51, 1968, pp. 27–43.

[5] Wolkoff, P., "Proposal of Methods for Developing Healthy Building Materials; Laboratory and Field Experiments," *Environmental Technology*, Vol. 11, 1990, pp. 327–338.

[6] Wolkoff, P., Clausen, P. A., Nielsen, P. A., Gustafsson, H., Jonsson, B., and Rasmusen, E., "Field and Laboratory Emission Cell: FLEC," *Healthy Buildings '91*, American Society of Heating, Refrigerating, and Air-Conditioning Engineers, Inc., Atlanta, 1991, pp. 160–165.

[7] Nordtest, "Building Materials: Emission of Volatile Compounds, Chamber Methods," Nordtest, *NT Build 358*, Espoo, Finland, 1990.

[8] Wolkoff, P., "Some Guides for Measurements of Volatile Organic Compounds Indoors," *Environmental Technology*, Vol. 11, 1990, pp. 339–344.

[9] STATGRAPHICS®, Statistical Graphics Corporation, Version 2.6, 1987.

[10] Press, W. H., Flannery, B. P., Teukolsky, S. A., and Vetterling, W. T., *Numerical Recipes in Pascal*, Cambridge University Press, New York, 1989.

[11] Clausen, P. A., "Emission of Volatile Organic Compounds from Waterborne Paint—The Effect of Film Thickness," (in preparation).

Garrett A. Keating[1] *and Thomas E. McKone*[2]

Measurements and Evaluation of the Water-to-Air Transfer and Air Concentration for Trichloroethylene in a Shower Chamber

REFERENCE: Keating, G. A. and McKone, T. E., **"Measurements and Evaluation of the Water-to-Air Transfer and Air Concentration for Trichloroethylene in a Shower Chamber,"** *Modeling of Indoor Air Quality and Exposure, ASTM STP 1205*, Niren L. Nagda, Ed., American Society for Testing and Materials, Philadelphia, 1993, pp. 14–24.

ABSTRACT: Indoor-air models for the transfer of contaminants from tap water to air typically rely on physical properties such as Henry's law constant, diffusion coefficients and so forth, and on room-air exchange rates to determine personal-air concentrations. These models do not address other potential sinks or sources for airborne contaminants that could affect exposure. A study was conducted to examine the buildup and decay of trichloroethylene (TCE) in the air of a 1 m^3 shower chamber into which water containing 210 μg/L TCE flowed through nozzles producing different flow rates (3 to 6 L/min) and droplet sizes (300 to 1500 μm). The concentrations of TCE in the air of the chamber and in the drain water were measured and the water-to-air transfer efficiency for the three nozzles was determined. The aerosol concentration and size distribution of aerosols generated by the nozzles were measured. Significant differences were observed between the measured air concentrations and the concentrations predicted by the transfer efficiencies and air exchange rate. These differences are observed to depend on the aerosol concentrations for the three nozzles. Consideration is given to processes such as deposition, incomplete mixing, scavenging, and measurement precision as explanations for these differences.

KEY WORDS: indoor air, shower, trichloroethylene, transfer efficiency, aerosols

Inhalation exposure from chemicals in drinking water has recently been recognized as a potentially significant route of exposure. Indoor air contamination from radon in potable water supplies has also been documented [*1,2*]. These observations imply that this phenomenon could apply to the volatile organic compounds (VOCs) found in trace amounts in groundwater. Experimental studies have shown that VOCs can enter the air phase from showers, causing significant exposure [*3–5*]. Based on these and other studies, models for indoor air contamination have calculated a range of exposure concentrations significantly higher than those currently permitted by regulatory agencies using ingestion as the principal route of exposure [*6,7*]. Given these findings, water quality standards based principally on ingestion as the route of exposure must be reevaluated to account for the multiple water uses that may contribute to exposure.

Before these standards can be addressed, validation of the models that quantify exposures from inhalation are needed. Indoor air models for water pollutants typically rely on physical properties of the contaminant, such as the Ostwald water/air partition coefficient to predict behavior. Alternatively, volatilization data for radon from a source may be used to predict the expected concentration in air of a contaminant from the same source. Both approaches are valid for predicting air

[1]Graduate field of Environmental Toxicology, Cornell University, 16 Fernow Hall, Ithaca, NY 14850.
[2]Senior scientist, University of California, Lawrence Livermore National Laboratory, Box 808, L-453, Livermore, CA 94550.

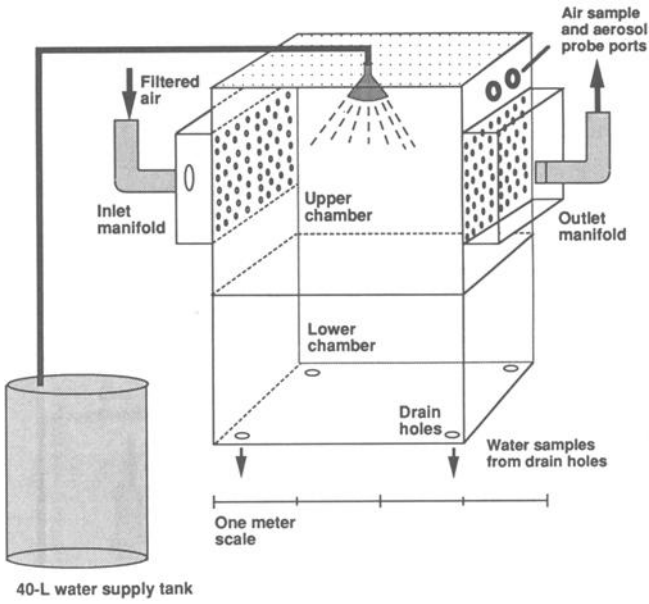

FIG. 1—*Illustration of the exposure chamber.*

concentrations; however, more complicated models are needed to accurately assess indoor exposure to water pollutants. Occupancy factors, deposition and resuspension rates of volatilized chemicals, and water use-factors are potential model parameters that could have a large impact on the ultimate exposure to volatile chemicals in drinking water.

The purpose of this study was to measure the volatilization of trichloroethylene (TCE) from a stream of water into an enclosed chamber and to monitor the subsequent change in the air concentration of TCE in the chamber for 1 h. Three shower nozzles, producing different droplet sizes and flow rates, were selected to generate a range of fine airborne aerosols (1 to 90 μm in diameter) in the chamber in order to examine the effect this would have on both stripping efficiency and the air concentrations of TCE.

Methods

Test Chemical

TCE (99.99%+ purity, Aldrich Chemical Co., Milwaukee, WI) was used as the test chemical for the shower simulations.

Simulation Chamber

Shower simulations were conducted in an exposure chamber (EC) [1.08 m × 0.75 m(w) × 1.3 m(h)] constructed in two parts: an 80-cm high PMMA and borosilicate plate glass upper section and a 50-cm deep welded high-density polypropylene base unit (Fig. 1). Prefiltered air was drawn through the EC by means of perforated side panels, creating a laminar or diffusive flow pattern through the EC. Water was supplied to the EC from a 40-L stainless steel tank under air pressure to the shower nozzle. The shower nozzle was centered in the EC approximately 120 cm from the

TABLE 1—*Droplet sizes, flow rates, and duration of flow for each nozzle.*

Nozzle	Droplet Size, μm	Flow Rate, L/min	Duration, min
1	1 500	4.2	8
2	300	2.8	10
3	1 000	6.0	5

floor of the EC. Water was drained from the bottom under mild suction through four drain holes (1 cm diameter) located in each corner of the EC.

Simulation Conditions

All shower simulations were conducted for 1 h at an EC air flow rate of 65 L/min. Prior to each simulation, the water tank was filled with deionized distilled water and TCE added directly to the tank by syringe. The water was then mixed and heated to a temperature ranging from 40 to 50°C. TCE concentrations of approximately 210 μg/L were used. A shower simulation consisted of running water into the chamber for periods up to 10 min during which time air and water samples were taken. After water flow to the EC stopped, the air was sampled for the remainder of the hour. Aerosol concentration was measured for the first 15 min of each simulation. Water and air temperatures were measured continuously during a simulation.

Water and Air Sampling and Analysis

Samples of EC drain water and air were taken in triplicate during a simulation. Water samples were taken from the tank just prior to the simulation and twice from the drain while water was flowing. Water samples were collected in 40-mL volatile organic analysis (VOA) glass vials, sealed with TFE-fluorocarbon-lined silicone septum screw-caps, and immediately refrigerated. Air samples (100 and 500 μL) were taken from within the EC at the height of the nozzle with Hamilton gas tight syringes (Fisher Scientific, Pittsburgh, PA) at 10 time-points over the 1-h simulation. Water and air samples were analyzed with a Photovac® 10A10 Gas Chromatograph equipped with a photoionization detector and an ambient temperature SE-30 packed column (Supelco, Bellefonte, PA). Air samples were analyzed immediately after being drawn from the EC by direct injection into the gas chromatograph. Water samples were analyzed using a headspace technique in which 20 mL of the sample were transferred to a 40-mL vial, shaken for 1 min and stored at room temperature for 1 h [*8*]. Air samples of the vial headspace were then taken by syringe and injected into the gas chromatograph. The results were quantified by comparison to a standard curve of known concentrations of TCE analyzed in the same manner.

Shower Nozzle Characteristics

Three shower nozzles were used to generate different droplet sizes. Nozzles 1 and 2 (Spraying Systems Co., Wheaton, IL.) were designed for commercial use in spraying devices. Nozzle 3 (Teledyne Water Pic®, Fort Collins, CO) was a water-saving nozzle designed for use in the shower. The droplet sizes (provided by the manufacturer), flow rates, and the duration of flow for each nozzle are shown in Table 1.

TABLE 2—*Supply tank and drain water concentrations measured at start of and during the simulations. Values are the average of three simulations per nozzle.*

	Water Concentration, μg/L (Standard Deviation)			Transfer Efficiency, % (Standard Deviation) From Water to Air	
		Drain Water			
Nozzle	Supply Tank at Start	Midway Through Shower	At End of Shower	Midway Through Shower	At End of Shower
1	206.22	28.77	30.82	86	84
	(55.26)	(5.93)	(7.97)	(0.01)	(0.03)
2	218.29	7.35	5.17	97	98
	(25.51)	(2.67)	(2.21)	(0.02)	(0.01)
3	210.12	25.79	17.16	86	88
	(29.00)	(4.10)	(10.94)	(0.04)	(0.1)

Aerosol Sampling

Aerosol size and concentration were measured during the first 15 min of a simulation by a hot-wire technique [*9*]. The Army Insecticide Measurement System (AIMS) Droplet Counter (KLD Labs, Huntington Station, NY) utilizes a hot-wire anemometer probe which is cooled when droplets come in contact with its thin platinum wire. Each droplet contacting the probe cools a wire length proportional to its diameter, thus reducing the probe's electrical resistance proportionally. The resultant electronic signal, which is droplet size dependent, is then conditioned by an electrical circuit in a manner that provides a droplet size distribution between 1.2 and 586 μm. The probe was positioned at the same height as the shower nozzle, and aerosol concentration was measured within the EC for the first 15 min of the 1-h simulation.

Results

The transfer efficiency of the three nozzles was found to be inversely related to the nozzle droplet size (Table 2). The transfer efficiency was calculated for each nozzle from the data in Table 2 with the following equation

$$\text{transfer efficiency} = \left\{1 - \frac{\text{mg TCE in water at time}_t}{\text{mg TCE in supply water tank}}\right\} \times 100\%$$

The efficiencies reported here are from 20 to 30% greater than those observed by others [*5,10*]; however, the shower nozzles used here produced droplets smaller than those produced by the standard shower nozzles used in the other studies. There were no significant differences in the transfer efficiency of the nozzles between the two times at which the drain water was sampled.

The relationship between droplet size and aerosol concentration was less evident. Table 3 reports the average concentration of the aerosols measured during the first 15 min of a simulation for each nozzle. Nozzles 2 and 3 resulted in aerosol concentrations of over 1000 aerosols/cm^3, while the aerosol concentration of Nozzle 1 was threefold less. This relationship shifts when the volume median diameter (VmD) for the three nozzles is considered. The VmD for Nozzles 1 and 2 are approximately equal whereas that of Nozzle 3 is half that of the other two nozzles. The percentage of aerosols in each size category did not differ significantly between nozzles (Fig. 2).

TABLE 3—*Aerosol conditions produced by the three shower nozzles.*

Nozzle	Aerosol Concentration, aerosols/cm^3	Volume Median Diameter,[a] μm	Shower Evaporation Rate, g/min
1	390	4.7	360
2	1125	16.3	3170
3	1022	7.1	975

[a] Diameter at which accumulated liquid volume of aerosols is one-half (VmD).

The buildup and decay of TCE air concentrations during the simulations followed a similar pattern for the three nozzles. The TCE air concentrations measured in the EC for Nozzles 1, 2, and 3 are shown in Figs. 3, 4, and 5, respectively. The air concentration of TCE rose steadily in the EC while the nozzles were operated. After the water was turned off, the concentration of TCE dropped rather rapidly until 20 min into the simulation, after which time the concentration slowly declined over the remainder of the simulation. The completion of the first air exchange of the EC occurs approximately at this time point. The peak air concentrations attained in these experiments are on the order of 0.004 mg/L.

To determine the shower evaporation rate, we first calculated the stationary droplet evaporation rate, (from Maxwell's Equation [*11*]) for each shower droplet size using the following equations

$$I = \frac{2\pi DMd}{RT}(p_\infty - p_0)$$

where

I = evaporation rate, grams H_2O/min,
d = drop diameter, μm,
D = diffusion coefficient of gas mixture (H_2O − air ≈ 0.219 cm^2/s),
M = molecular weight, grams per mole,
R = 62 360 cm^3-mm (Hg)/(°K mole), constant,
T = temperature in K,
p_∞ = vapor pressure of water at T = 40°C, mm Hg, and
p_0 = partial pressure of water vapor in chamber air, mm Hg.

To account for forced convection on the evaporation of the droplets, the stationary droplet evaporation rate was corrected by multiplying it by the Sherwood number, derived from the following equation [*12*]

$$Sh = 1.755 + 0.535Re^{1/2}Sc^{1/3}$$

where

Sh = Sherwood number,
Re = Reynolds number, and
Sc = Schmidt number.

We then summed the droplet evaporation rate for all droplets entering the EC per min (flow rate per min/droplet volume = number of droplets per min).

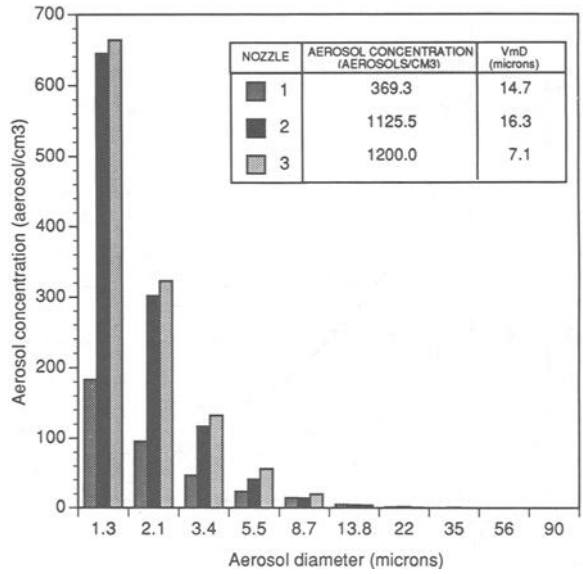

FIG. 2—*Size distribution of aerosols formed during simulations by the shower nozzles.*

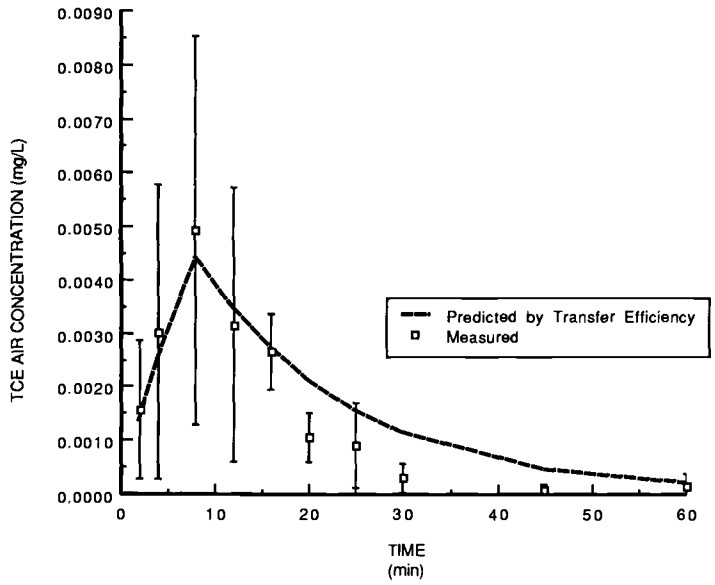

FIG. 3—*Predicted and measured TCE air concentrations for Nozzle 1.*

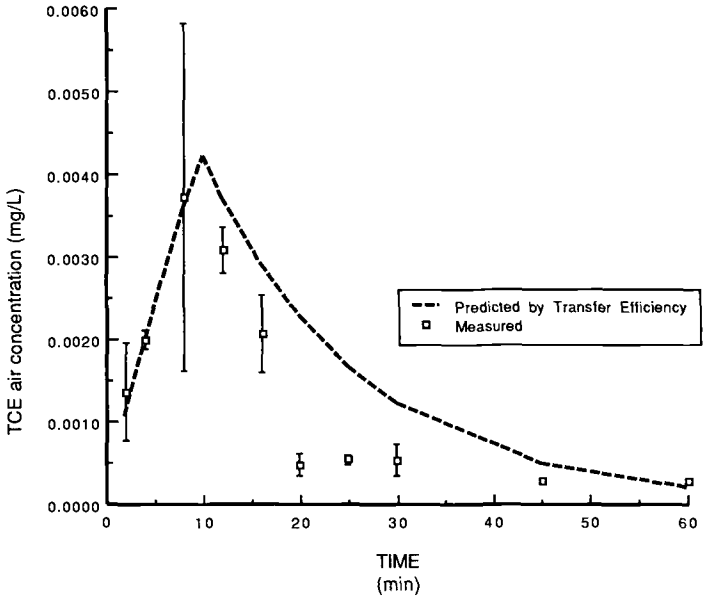

FIG. 4—*Predicted and measured TCE air concentrations for Nozzle 2.*

Discussion

The transfer of chemicals from water to air has been widely treated as a "two resistance" process with mass-transfer at the air-water interface reflecting resistance through both the liquid and gas phases at the droplet boundary [*13–15*]. For TCE, the water to air mass-transfer is expected to be dominated by the liquid phase resistance as TCEs apparent mass transfer coefficient in air is several orders of magnitude greater than its mass transfer coefficient in water [*7*]. For shower nozzles, this relationship implies that nozzles producing smaller droplets will facilitate the transfer of TCE from water to air through a decrease in the liquid resistance by generating a larger surface area per unit of water flow. The water-to-air transfer efficiencies of the shower nozzles in this study were in agreement with this relationship as shown in Table 2. Nozzle 2 produced the smallest drop diameter and had the highest transfer efficiency, whereas Nozzle 1, with the largest drop diameter, had the lowest transfer efficiency. This relationship between droplet size and transfer efficiency has been observed with standard-size shower nozzles as well [*16*].

The measured TCE air concentrations can be contrasted with the air concentrations projected for each nozzle based on its water-to-air transfer efficiency and on the chamber air-exchange rate. Assuming that all TCE not found in the drain water samples is transferred to the air of the EC, and assuming that this air volume is well mixed, an "expected" air concentration as a function of time during the simulation was calculated. To do so, the following equations describing the time-dependent inventory, $N(t)$, in milligrams of TCE in the EC were solved.

$$\frac{dN(t)}{dt} = -E_a \times \frac{N(t)}{V} C_w \times \epsilon \times F_w \quad \text{(when water is flowing)} \tag{1}$$

$$\frac{dN(t)}{dt} = -E_a \times \frac{N(t)}{V} \quad \text{(after the water is off)} \tag{2}$$

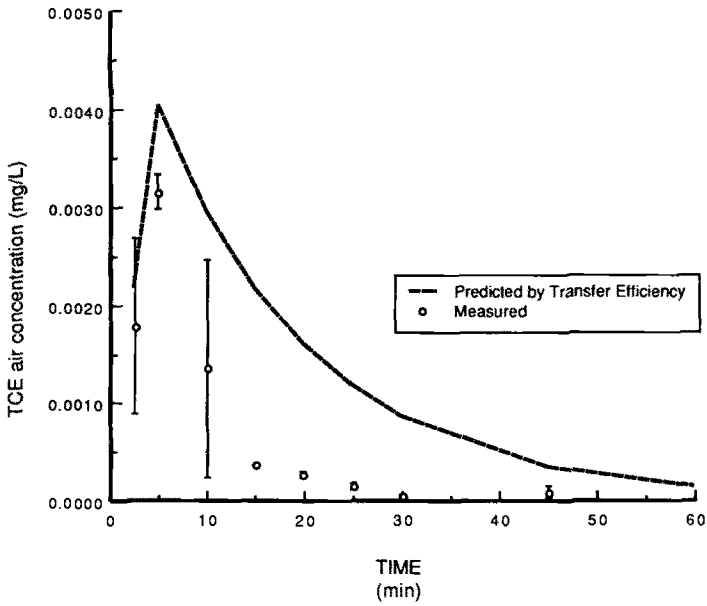

FIG. 5—*Predicted and measured TCE air concentrations for Nozzle 3.*

In these equations, E_a is the air exchange rate in the EC, 65 L/min; V is the volume of the EC, 1050 L; C_w is the TCE concentration in the inlet water, mg/L; ϵ is the transfer efficiency for TCE from water to air, no units; and F_w is the water flow rate through the nozzle when it is on, L/min. Assuming no inventory of TCE in the EC prior to the experiment, the solutions to these equations are

$$N(t) = \frac{C_w \times \epsilon \times F_w \times V}{E_a} [1 - \exp(-E_a t/V)] \quad \text{(when water is flowing)} \tag{3}$$

$$N(t) = \frac{C_w \times \epsilon \times F_w \times V}{E_a} \times \{\exp[-E_a(t - T)/V] - \exp(-E_a t/V)\} \quad \text{(after the water is off)} \tag{4}$$

where t is the elapsed time since the beginning of the experiment in min, and T is the length of time that the nozzle was on, in min. Using these calculations, we calculated the expected air concentrations of the three nozzles as the inventory, N, divided by the volume, V. These predicted air concentrations are plotted with the measured air concentrations in Figs. 3, 4, and 5.

As can be seen in Figs. 3, 4, and 5, there is a consistent difference both in the magnitude and the shape of the measured and predicted results for the three nozzles. We have identified a number of experimental factors and physical phenomena that could explain the discrepancy between the predicted and measured air concentrations. We first considered experimental variability and the precision of the air and water analyses as contributing to these differences. The precision of the air and water analyses was 6% and 8.5%, respectively. But this level of error is below the range of differences between the expected and measured air concentrations (10 to 50%). We then considered that a second and more likely source for the difference between the measured and expected air concentration could be experimental variability in the transfer efficiency for each nozzle. The

transfer efficiencies with standard deviations for each nozzle are reported in Table 2. However, the variability in the transfer efficiency cannot account for the difference between the measured and expected air concentrations. Taken together, measurement error and experimental variability could lead to differences of the magnitude seen here; however, such differences should occur randomly between nozzles rather than in the systematic manner observed in this study. In addition, neither measurement error nor experimental variability could account for the significant difference in shape between the measured and predicted time history of concentration. The slower than predicted rise in air concentration, rapid fall-off of concentration after the water flow stops, and the longer than predicted tail of the measured concentration suggests that there is evidence of a second compartment in this system. We considered that this second-compartment effect could be accounted for by incomplete mixing within the air volume, deposition of TCE onto surfaces, scavenging of TCE by water aerosols, or some combination of these processes. In the paragraphs below, we evaluate the plausibility of these processes as explanations for the discrepancy between measured and predicted results.

Operation of the EC could produce transient conditions during a simulation that could cause the air concentrations of TCE to differ from the levels estimated from the water-to-air transfer efficiency combined with air exchange rates. These conditions may be due to an experimental factor, such as the shower nozzle, or an intrinsic factor of the design and operating conditions of the EC, such as air flow patterns and the air exchange rate. In addition to droplet size, the shower nozzles differed in the extent to which they fogged the air and surfaces of the EC with water vapor. Droplet evaporation is presumably the source of water vapor that leads to the formation of aerosols and condensation of water on the walls within the EC. The aerosol concentrations for the different nozzles correspond with the evaporation rates calculated for each nozzle droplet (see Table 3). The correlation between aerosol concentration and the droplet evaporation rate suggests that aerosol formation within the EC results from condensation of water vapor rather than from droplet impact or droplet sheer at the nozzle. In generating both the smallest droplet and largest number of droplets per minute, Nozzle 2 released the largest mass of water vapor into the EC, whereas the effect is just the opposite in Nozzle 1. Condensation could also explain the relationship between the aerosol concentration and the VmD seen in Table 3. Assuming condensation as the mechanism of aerosol formation, the VmD (the diameter at which the accumulated volume of measured aerosol is one-half) can be interpreted as a measure of the growth of aerosols during a simulation. Of the three nozzles considered, Nozzle 2 saturated the EC with water vapor the fastest and maintained this condition the longest (approximately 10 min). Therefore, a greater proportion of the aerosols generated by Nozzle 2 grew to larger sizes, as reflected in the VmD. Nozzle 3 produced an aerosol concentration equivalent to that of Nozzle 2, but maintained these saturated conditions for only half of the time (approximately 5 min). The VmD for Nozzle 3 is half that of Nozzle 2.

The correlation between aerosol concentration and greater differences between the measured and expected air concentrations suggests that aerosols might play a role in lowering the peak TCE air concentration within the EC and in more rapidly removing the TCE following termination of water flow. This role may be to scavenge TCE from the air and release it back to the gas phase as the aerosols evaporate following termination of water flow. Alternatively, direct deposition of TCE onto the surfaces of the EC may explain a concentration history that differs from what is predicted from the simple model. The wetted surfaces of the EC could act as a bulk water phase and retain some mass of TCE while the nozzle is operating and then slowly release TCE as the air concentration diminishes over the remainder of a simulation. Nonetheless, though likely to have some effect, the concentration of aerosols and wetted wall surface do not supply sufficient volume to account for the difference between expected and measured TCE air concentrations. If treated as one bulk water phase, equilibrium considerations suggest that the volume of aerosols and surface water is insufficient to retain the amount of TCE that is needed to produce the "second-compart-

ment effect'' we observed. Based on the VmD and using Nozzle 2 as an example, we calculate the total volume of the aerosol in the EC as

$$4.5 \times 10^{-9} \text{ cm}^3 \text{ water/aerosol} \times 1125 \text{ aerosols/(cm}^3 \text{ air)} \times 1.053 \text{ m}^3 \times 1000 \text{ L /m}^3 = 0.0054 \text{ L}.$$

Similarly, we calculate the volume of water deposited on the walls of the EC, assuming a 1-mm layer of water on all six surfaces as

$$[2(1.03 \times 0.75) + 2(1.3 \times 1.08) + 2(1.08 \times 0.75)]\text{m}^2 \times 0.001 \text{ m} \times 1000 \text{ L/m}^3 = 6.0 \text{ L}.$$

The maximum measured air concentration for Nozzle 2 of 0.0037 mg/L and a Henry's law constant for TCE of 0.32 (at 20°C) would produce an expected TCE concentration in the aerosol and wall surface water of 0.012 mg/L. Thus, at equilibrium, the aerosol and surface water would be expected to hold 0.072 mg of TCE (6.0 L × 0.012 mg TCE/L). The total mass of TCE present in the air of the EC is 3.9 mg (0.0037 mg/L × 1053 L). Therefore, the aerosol and surface water could, at equilibrium, remove only an estimated 2% of the TCE that had transferred into the air of the EC. The differences between the measured and expected TCE air concentrations range from 10 to 50%, so it appears that TCE absorption by aerosols and deposition onto the EC walls cannot alone account for the difference.

Incomplete mixing of the air within the EC could also explain why the measured air concentrations did not achieve the levels predicted by the transfer efficiency. Calculations of the expected air concentrations assumed the EC was well mixed with a constant air exchange rate of 65 L/min. Air velocity measurements made with the AIMS probe recorded velocities of 85 cm/s while the nozzles were operated. Turbulent air currents generated while the nozzles were operated may have created areas of incomplete mixing with the EC. Once water flow to the chamber stopped, air exchange to the chamber returned to laminar flow, resulting in less variability in air measurements. There may also have been stratification of the TCE air concentrations along the descending path of the shower droplets. Air samples were taken at the same height as the shower nozzle and could represent incomplete volatilization of TCE from the droplet.

Though the experiments performed here do not support the conclusion that absorption of TCE onto aerosols and wall surfaces explains the less than expected air concentrations in the EC, the systematic observation of greater differences between the measured and expected air concentrations with experimental conditions resulting in higher aerosol concentrations suggests that this effect should be further studied. Enhanced aqueous phase partitioning of chemicals into rain and fog beyond levels predicted by equilibrium (that is, Henry's law ratio) has been observed for a wide range of chemicals [*17*]. Ligocki et al. [*18*] observed dissolved rain concentrations of TCE collected at air temperatures between 5 and 9°C that were 1.5 times greater than the equilibrium concentration calculated with the Henry's law constant at 25°C. Whereas these findings may be explained by the direct relationship between temperature and the Henry's constant, the results reported here are not likely to be due to enhanced aqueous phase partitioning since experimental conditions favored the vapor phase partitioning of TCE (water and air temperatures > 25°C). Another plausible hypothesis that needs to be addressed by further experimentation is the possible existence of a surface-area interaction between the vapor-phase TCE and the aerosols and surfaces of the EC. Under this hypothesis, the TCE would wet or condense on these surfaces by a process other then partitioning. A final hypothesis that also would require further experimentation is that the air volume of the EC is stratified into two mixing regimes that interact at different rates when the nozzles are on or off. Either of these two processes could be affected by the turbulent air flow in the EC while the nozzles are operated and then by removal of aerosols as the chamber returns to a laminar air flow pattern with the cessation of water flow.

Acknowledgments

This work was performed in part under the auspices of the U.S. Department of Energy (DOE) through Lawrence Livermore National Laboratory under Contract W-7405-Eng-48 with funding provided in part by the California Department of Toxic Substances Control (DTSC) through Memorandum of Understanding Agreement 91-T0038, in part by the Office of Research and Development of the U.S. Environmental Protection Agency (EPA) under Interagency Agreement Contract DW-8993-4285, and in part by a grant from the New Jersey Department of Environmental Protection (NJDEP), Office of Science and Research. The views expressed are those of the authors and not necessarily those of the DOE, EPA, CDHS, or NJDEP.

References

[1] Nazaroff, W. W., Doyle, S. M., Nero, A. V., and Sextro, R. G., "Potable Water use as a Source of Airborne Radon in U.S. Dwellings: A Review and Assessment," *Health Physics*, Vol. 52, 1987, p. 281.

[2] Prichard, H. M. and Gessel, T. F., "An Estimate of Population Exposures due to Radon in Public Water Supplies in the Area of Houston, Texas," *Health Physics*, Vol. 41, 1981, p. 599.

[3] Andelman, J. B., "Human Exposures to Volatile Halogenated Organic Chemicals in Indoor and Outdoor Air," *Environmental Health Perspectives*, Vol. 62, 1985, p. 313.

[4] Jo, W. K., Weisel, C. P., and Lioy, P. J., "Chloroform Exposure and Body Burden from Showering with Chlorinated Tap Water," *Risk Analysis*, Vol. 10, 1990, p. 575.

[5] McKone, T. E. and Knezovich, J. P., "The Transfer of Trichloroethylene (TCE) from a Shower to Indoor Air: Experimental Measurements and their Implications," *Journal of the Air and Waste Management Association*, Vol. 41, 1991, p. 832.

[6] Shehata, T. A., "A Multi-Route Exposure Assessment of Chemically Contaminated Drinking Water," *Toxicology and Industrial Health*, Vol. 1, 1985, p. 277.

[7] McKone, T. E., "Human Exposure to Volatile Organic Compounds in Household Tap Water: The Indoor Inhalation Pathway," *Environmental Science and Technology*, Vol. 21, 1987, p. 1194.

[8] Herzfeld, K. D. and Van der Gun, R. L., "Quantitative Determination of Volatile Organochlorine Compounds in Water by GC-Headspace Analysis with Dibromomethane as an Internal Standard," *Chemosphere*, Vol. 18, 1989, p. 1425.

[9] Mahler, D. S. and Magnus, D. E., "Hot-Wire Technique for Droplet Measurements," *Liquid Particle Size Measurement Techniques, ASTM STP 848*, J. M. Tishkoff, R. D. Ingelbo, and J. B. Kennedy, Eds., American Society for Testing and Materials, Philadelphia, 1984, pp. 153–162.

[10] Tancrede, M., Yanagisawa, Y., and Wilson, R., "Volatilization of Volatile Organic Compounds from Showers – 1. Analytical Method and Quantitative Assessment." *Atmospheric Environment*, Vol. 26A, 1992, p. 1103.

[11] Reist, P. C., *Introduction to Aerosol Science*, Macmillan Publishing Company, New York, 1984, pp. 204–207.

[12] Wedding, J. B., Kim, Y. J., and Dennison, R. S., "Mass Transfer from Water Droplets under Simulated Free-Fall Conditions," *Atmospheric Environment*, Vol. 20, 1986, p. 1039.

[13] Mackay, D. and Paterson, S., "Fugacity Models of Indoor Exposure to Volatile Chemicals," *Chemosphere*, Vol. 12, 1983, p. 143.

[14] Roberts, P. V. and Dandliker, P. G., "Mass Transfer of Volatile Aqueous Solution to the Atmosphere During Surface Aeration," *Environmental Science and Technology*, Vol. 17, 1983, p. 484.

[15] Andelman, J. B., "Inhalation Exposure in the Home to Volatile Organic Contaminants of Drinking Water," *Science and the Total Environment*, Vol. 47, 1985, p. 443.

[16] Giardino, N. J., Esman, N. A., and Andelman, J. B., "Modelling Volatilization of Trichloroethylene from a Domestic Shower Spray: The Role of Drop-Size Distribution," *Environmental Science and Technology*, Vol. 26, 1992, p. 1602.

[17] Glotfelty, D. E., Seiber, J. N., and Liljedahl, L. A., "Pesticides in Fog," *Nature*, Vol. 325, 1987, p. 602.

[18] Ligocki, M. P., Leuenberger, C., and Pankow, J. F., "Trace Organic Compounds in Rain – II. Gas Scavenging of Neutral Organic Compounds," *Atmospheric Environment*, Vol. 19, 1985, p. 1609.

John E. Borrazzo,[1]* *Cliff I. Davidson,*[1] *and Julian B. Andelman*[2]

Small Closed-Chamber Measurements for the Uptake of Trichloroethylene and Ethanol Vapor by Fibrous Surfaces

REFERENCE: Borrazzo, J. E., Davidson, C. I., and Andelman, J. B., **"Small Closed-Chamber Measurements for the Uptake of Trichloroethylene and Ethanol Vapor by Fibrous Surfaces,"** *Modeling of Indoor Air Quality and Exposure, ASTM STP 1205*, Niren L. Nagda, Ed., American Society for Testing and Materials, Philadelphia, 1993, pp. 25–41.

ABSTRACT: Recent efforts to quantify the effect of sorption on indoor concentrations of volatile organic compounds (VOCs) have indicated that indoor surfaces may behave as reservoirs for VOCs emitted from other sources. For the surface materials of greatest interest indoors, the interactions of airborne pollutants with such surfaces have not been very extensively studied. In this study, partition coefficients, defined as the ratio of the sorbed-phase to vapor-phase equilibrium concentrations, have been measured for sorption of trichloroethylene (TCE) and ethanol (EtOH) vapors by a variety of fibrous or polymeric surfaces. Several of these, nylon, wool, polypropylene, jute, and styrene-butadiene rubber (SBR), are important components of carpet. Glass, cotton, and polyester fibers have also been included. Results indicate that for TCE, sorption to the carpet backing materials polypropylene and SBR is more significant than sorption to the nylon or wool pile fiber; partition coefficients for the former are about 300 cm^3/g, while values for nylon are approximately 10 to 20 cm^3/g. The opposite was found to be true for EtOH, for which partition coefficients with respect to nylon fiber are on the order of 1000 cm^3/g, in contrast to those measured with respect to polypropylene or SBR, that are in the range of 20 to 40 cm^3/g. Because of the concentration and temperature dependence of the observed sorption effects, an explanation based on an adsorption mechanism was reasonable in most cases. Nevertheless, absorption may also play a role in partitioning, particularly for VOCs and polymers with similar solubility parameters, such as for TCE with respect to polypropylene or SBR. Because various components of a composite material such as carpet may exhibit very different affinities for a single compound as well as different mechanisms of interaction, models for sorption using first-order kinetics may not adequately describe sorption and desorption of VOCs indoors.

KEY WORDS: indoor air quality, heterogeneous reactions, gas, vapor, sorption, equilibrium, isotherms, specific surface area

Air quality in the indoor environment is determined by complex interactions of contaminant sources with transport and removal processes. Whether sorption represents a significant removal mechanism for vapor-phase organic compounds depends on both the equilibrium capacity of the surfaces present and the kinetics of uptake by the surfaces, as well as on the relative importance of other removal mechanisms such as ventilation. On the other hand, at least of equal importance is the extent to which surfaces might behave as reservoirs for organic compounds. In this case, such surfaces might act as secondary sources of indoor pollutants even after a primary source has

*Current address — Agency for International Development, Bureau for Research and Development, Office of Health, Washington, DC 20523-1817.

[1]Research assistant and professor, Carnegie Mellon University, Department of Civil Engineering, Pittsburgh, PA 15213.

[2]Professor, University of Pittsburgh, Graduate School of Public Health, Department of Environmental and Occupational Health, Pittsburgh, PA 15261.

been removed. Thus, desorption of a previously-sorbed organic vapor may result in elevated long-term concentrations.

Although the heterogeneous reaction of reactive pollutants such as nitrogen dioxide has been studied by numerous authors [*1–3*], the potential of indoor materials to act as sorbents for non-reactive organic compounds has not been examined as extensively. In this latter case, it is important to determine the magnitude of the sorbed-phase surface concentrations. Knowledge of the equilibrium extent of sorption allows the practical significance of sorption to be determined for limiting cases, and some realistic bounds may be established for kinetic effects. For example, Axley [*4*] has modeled the effect of sorption on the evolution of chamber air concentrations in which airborne and surface concentrations are in equilibrium; the analysis showed that such a model is a limiting case of models with greater physical bases.

This study is one component of a research program concerned with the emission, transport, and fate of volatile organic compounds (VOCs) during residential water use [*5,6*]. Trichloroethylene (TCE) has received the most extensive examination of its emissions, and for this reason, this nonpolar compound was selected for study here. Because different sorption effects may be found for polar and nonpolar species, particularly with respect to polar sorbents, ethanol (EtOH), which has a saturation vapor pressure comparable to that of TCE at typical indoor temperatures, was selected for comparison.

Of all indoor surfaces, fibrous materials have among the highest ratios of actual to projected surface area. Furthermore, as discussed by Nielsen [*7*], the presence of such surfaces may be related to occupant complaints of mucosal irritation. This surface type has been selected for study, with the additional requirement that each surface should be chemically and physically homogeneous. Many indoor materials, such as carpets, are actually composites, comprising several such homogeneous surfaces. The study of individual components allows the apportionment of sorption effects among the components. Such knowledge is important in understanding how potential modifications to indoor surface materials could affect sorption properties. This emphasis on studying homogeneous materials in conjunction with the deliberate selection of VOCs with different polarities represents the unique contribution of this study.

In focussing on the quantitative description of the partitioning obtained between the sorbed and vapor phases, this study has involved measurement of the partition coefficient, denoted by K. Here, K (cm^3/g) is defined as the ratio of the mass-based sorbed-phase concentration of a species C_s (ng/g) to its vapor-phase concentration C (mg/m^3) at equilibrium. Higher values of K thus correspond to stronger partitioning to the surface.

Literature Review

Few authors have quantified sorption effects for organic vapors with respect to indoor surfaces. Matthews et al. [*8*] found time scales on the order of days for the reversible uptake of formaldehyde on gypsum board. Berglund et al. [*9*] discovered that several organic compounds emitted from materials removed from a "sick" building were not original components; sorption of the compounds from the building air and subsequent reemission in the test chamber was assumed to be responsible. Korte and Gebefugi [*10*] demonstrated that sorbed concentrations of pentachlorophenol and lindane were higher on lambswool than on acrylic fiber, indicating that differences between fibrous surfaces may be significant. Seifert and Schmahl [*11*] studied sorption kinetics for twenty VOCs on plywood, nylon carpeting, and wool carpeting in a ventilated, well-mixed chamber. For a pulse input, they found that sorption and desorption processes could cause the typically straight-line plots for the decrease of log concentration versus time to become curved, indicating that reemission of sorbed-phase VOCs caused gas-phase concentrations to remain elevated above the detection limit longer than would be expected without sorption. A less volatile chemical, the pesticide lindane, was more strongly sorbed than the VOCs. In an earlier paper, we have more extensively reviewed the above studies [*12*].

Borrazzo et al. [*12,13*] investigated the sorption of TCE to nylon carpets in small glass/TFE-fluorocarbon chambers. A linear partition isotherm was found to be applicable, with a partition coefficient of about 60 cm^3/g. In related studies [*6*], inverse gas chromtography (IGC) was used in conjunction with nylon- and wool-packed columns to investigate the dependence of sorption on temperature and saturation vapor pressure (P_o). As would be expected, partition coefficients were smaller at 35°C than at 25°C. For the nine VOCs studied, ranging in P_o from ten to several hundred mm Hg, log K and log P_o were found to be inversely and linearly related. Partition coefficients for TCE were smaller than those found in the tests with carpet; a possible explanation was that the IGC tests involved only the nylon fiber as a sorbent surface, while the tests in small chambers were for intact carpet that contained other components with a greater affinity for the sorption of TCE.

Tichenor et al. [*14,15*] examined sorption to nylon carpet, a polyester-filled pillow, gypsum wallboard, ceiling tile, and window glass. Each surface was exposed in a ventilated stainless steel chamber to an atmosphere with a constant concentration of either tetrachloroethylene or ethylbenzene. Afterwards, a clean atmosphere was provided at the chamber inlet. Equilibrium sorbed-phase concentrations were estimated from the integrated VOC mass efflux from the chamber minus the mass in the chamber air at equilibrium. Partition coefficients were calculated using linear regressions of the sorbed phase equilibrium concentration versus that in the gas phase; R^2 values greater than 0.95 indicated that a linear fit to the data accounted for most of the observed variability. For the nylon carpet, assuming a typical carpet weight of 2000 g/m^2 of projected area, the partition coefficients reported by Tichenor et al. [*15*] can be converted to units consistent with those used here, yielding values of K on the order of 10^3 cm^3/g for both tetrachloroethylene and ethylbenzene.

Kjaer and Nielsen [*16*] measured the sorption and desorption of toluene and 2-butoxyethanol on nylon and wool fibers. Sorbed-phase concentrations were measured directly using an electronic microbalance. Following a twelve-hour exposure to constant gas-phase concentrations of these two compounds, it was found that the sorbed-phase wool fiber concentrations were higher than those for nylon fiber. In desorption studies, these authors found that complete desorption from the wool fibers was not attained during the course of the experiments, while desorption of toluene and butoxyethanol from the nylon fibers required 106 and 140 h, respectively.

Over the past two decades, analysis of gases in the headspace of multi-phase systems has become a standard technique for the determination of volatile components in a sorbed or dissolved phase. This method uses the chemical information contained in the gas phase to determine the composition of the condensed phase with which it is in contact. For a comprehensive review, see Ioffe and Vitenberg [*17*].

Several researchers have used such headspace analysis techniques in the examination of sorption and desorption processes. Pleil and Whiton [*18*] used a dynamic headspace method to qualitatively determine the emissions of volatile organic species from new carpeting. Peterson et al. [*19*] extended the dissolved-phase technique of Garbarini and Lion [*20*] to examine vapor-solid partitioning in the unsaturated zone. Partition coefficients for TCE were evaluated using alumina oxide coated with humic acid as the sorbent surface. Crittenden and coworkers [*21*] have used Tedlar bags to examine sorption equilibrium for TCE vapor/activated carbon systems. The flexible bag acts as a constant pressure container, allowing the extraction of a sample from the headspace with no change in the equilibrium concentrations.

Selection and Characteristics of Surface Materials

The authors are not aware of any survey data for the distribution of fiber types indoors. For this reason, 1986 end-use data for five applications compiled by the Textile Economics Bureau (101 Eisenhower Parkway, Roseland, NJ 07068) have been used to determine the most commonly occurring fiber types [*22*]. Two categories, consumer/industrial products and exported fiber, are not clearly of interest indoors. Another category, apparel, accounted for about 40% of all fiber

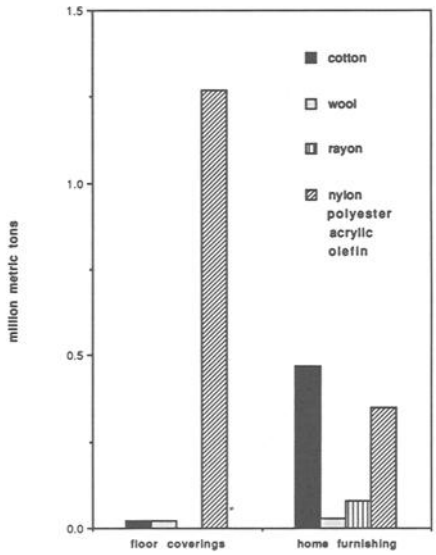

FIG. 1—*Breakdown by fiber type for two principal indoor fiber uses* [22].

production. However, the effect of sorption to apparel on indoor air concentrations is likely to be localized to those regions with high mass loadings, such as closets, that are otherwise relatively isolated from the remainder of an indoor space.

Two categories, floor coverings and home furnishings, can be considered to be almost exclusively of indoor application and account for nearly 40% of all fiber production. For these, the breakdown by fiber type is shown in Fig. 1. Nylon and wool are the predominant fibers used in carpet pile yarn, while polypropylene and jute are the predominant backing materials. The final important component of carpet is the styrene-butadiene rubber (SBR) latex used to hold the carpet together; this may account for nearly half of the carpet weight. Because of its potential importance, this surface was also studied here, even though it is not fibrous. Cotton and polyester, two fibers more important in home furnishings than in carpets, have also been included. A final addition is glass fiber, which was postulated to be useful as a noninteracting control surface.

Table 1 summarizes some of the properties of interest for these surface types. The presence of polar groups is a major factor in determining the hydrophilicity of fibrous materials, a direct measure of which is moisture regain. As indicated in Table 1, it is generally true that natural fibers cotton, jute, and wool show significantly greater sorption of water vapor than the synthetic substances polyester, polypropylene, and SBR. Nylon, another synthetic fiber, is moderately hydrophilic.

The glass transition temperature T_g is the temperature at which a polymeric substance or ordinary inorganic glass will soften; this is considerably below the melting point. T_g marks second-order transitions in physical and mechanical properties, such as density, specific heat, and diffusivity. This means that instead of exhibiting discontinuity in a plot of property versus temperature (as would molar volume at the liquid-vapor phase transition), it is the slope of such a plot that exhibits a more or less sharp discontinuity at T_g. The greater polymer segment mobility in fibers at temperatures above T_g means that, at such temperatures, absorption into the body of the fiber as well adsorption on its surface can play a role in uptake processes. The range in values for T_g in Table 1 reflect uncertainties due to the thermal history of the sample, structure and molecular weight of the polymer, the presence of impurities, the degree of crystallinity in the fiber or polymer, and a small effect of pressure at which the measurement is made [*23*].

TABLE 1—*Summary of surface properties [26,29,30].*

Surface	Transition Temperature, °C	Density, g/cm^3	Moisture Regain,[a] %	Solubility Parameter, (cal/cm^{-3})$^{1/2}$
Cotton	220–245	1.5	8, 17	12.5
Jute	220–245	1.5	12	12.5
Wool	...[b]	1.3	16–18	...
Nylon	40–50	1.14	4	11.2–11.7
Polyester[c]	60–85	1.38	0.4	10.5
Polypropylene	−35 to −13	0.91	0	8.4, 9.2–9.4
Styrene-butadiene rubber	−64 to −59	0.93	0	8.1–8.8

[a]At 65% relative humidity and 25°C.
[b]Not available.
[c]Polyethylene terephthalate.

The solubility parameter d is defined as the square root of the cohesive energy density, which is the energy change per unit volume for the isothermal vaporization of the saturated liquid to the ideal gas state at infinite volume. Solubility parameters increase with increasing polarity. For polymers, d is empirically determined using solvents with known solubility parameters; only polymers with values of d close to those of a given solvent will dissolve or swell in the presence of that solvent. From the values of d in Table 1, it appears that TCE (d = 9.3 [cal/cm^3]$^{1/2}$;) may swell polypropylene or SBR, while EtOH (d = 12.8 [cal/cm^3]$^{1/2}$) may swell the cellulose fibers of cotton or jute.

Nylon and wool fibers were obtained by cutting the pile off several new carpets. Sample Nylon I was a nylon 6 fiber (Allied Chemical). Nylon II and Nylon III were nylon 66 fibers (DuPont). Nylon I and Nylon II, intended for residential use, were very lightly dyed and appeared white; Nylon III was a commercial carpet dyed dark green. Detailed information about the origin and preparation of Wool Samples I and II was unavailable; both were light in color, indicating minimal or no dyeing.

Most modern carpet construction uses a two-layer backing. The primary backing, usually polypropylene, is used to hold the tufts of the pile yarn in place. SBR latex and a secondary backing add rigidity to the primary backing. The secondary backing (but not the latex) is sometimes omitted in commercial carpets. Samples of jute and polypropylene webbing materials used as secondary backing were obtained from a carpet manufacturer (J & J Industries, Dalton, GA). The specific masses of these samples were 300 and 120 g/m^2, respectively.

SBR was obtained in a 300 parts filler per hundred rubber (phr) formulation as a dried 0.051 cm film. $CaCO_3$ was used as the filler material. This film was cut into small pieces, typically 0.1 cm^2. The density of the dried latex was 1.5 g/cm^3 at 25°C, assuming a uniform film thickness. Based on the densities of the SBR and $CaCO_3$, a nonporous film of these materials would have a density of 2.3 g/cm^3. Thus, the porosity of the dried latex backing is about 35%.

Undyed polyethylene terephthalate (PET) polyester (Dacron® Hollofil 808) was obtained from the filling of a brand-new pillow. The cross-section of this fiber is essentially round, although it is slightly flattened on four sides. There are four distinct voids running axially through the fiber. This fiber has a weight of 5.5 denier (= grams per 9000 m) and a density of 1.38 g/cm^3 excluding the voids, or 1.27 g/cm^3 including the voids. Therefore, the voids occupy about 8.7% of the volume of the fiber.

Cotton fiber samples had been processed by the manufacturer 42–5001, (Absorbent Cotton Company, Inc., Valley Park, MI) using sodium hydroxide to remove some of the vegetable fats in the cotton. After removal from the sodium hydroxide bath, the cotton was bleached, rinsed, and dried.

The glass fiber used in this study was Pyrex® (Owens-Corning 3950) with a circular cross section, 8 μm in diameter, and a density of 2.5 g/cm^3.

Data Acquisition

Principles

Both static and dynamic headspace analysis techniques are available. Static methods apply to closed systems, while the dynamic method involves purging of the headspace. In the dynamic method, equilibrium partitioning may not be attained (although a steady-state condition may be). For this reason, static methods have been used here.

Principles for establishing equilibrium between a sorbed and dissolved phase have been described by Sontheimer et al. [*24*]; these are also applicable to gas-solid systems. The method involves the addition of known quantities of sorbent to vessels containing known quantities of solution (or in the gas phase, simply a known volume); initial concentrations are established in both the sorbed and dissolved (or gaseous) phases. Tests are conducted under isothermal conditions. Although sorbed-phase equilibrium concentrations are not measured directly, an indirect measurement is provided by the change in the gas-phase concentration from its initial value, based on the assumption that sorption processes are solely responsible for such changes. One of two possible approaches to the establishment of initial conditions was selected for this study, that which relies upon the establishment of a known initial gas-phase concentration and an initial sorbed-phase concentration of zero. Thus, based on the conservation of mass in the closed system, the partition coefficient K can be estimated as

$$K = (V/M_s)(C_o/C - 1) \tag{1}$$

where C and C_o are the equilibrium and initial gas-phase concentrations, respectively, V is the volume of the closed chamber, and M_s is the mass of the sorbent surface. The applicability of value of K estimated using Eq 1 to concentrations other than those at which K was determined depends on the linearity of the sorption isotherm. Note that Eq 1 can be re-expressed as:

$$C_s = (V/M_s)(C_o - C) \tag{2}$$

which is a form particularly useful in the determination of sorption isotherms when data at more than a single value of C are available.

The glass vials used as closed chambers in this study are fixed-volume containers. Thus, the VOC mass in the gas-phase is reduced as samples are withdrawn, with a resulting decrease in the gas-phase concentration as equilibrium is reestablished. However, this effect will be negligible if the withdrawn volume is much smaller than the headspace volume. In this study, the maximum total volume withdrawn was less than 1% of the headspace volume.

Assuming a linear isotherm and that the isosteric heat of sorption Q_{st} is independent of surface coverage, the use of a two-point approximation allows the estimation of Q_{st} from values of K at two temperatures

$$Q_{st} = -R \frac{\ln \dfrac{K_1 T_2}{K_2 T_1}}{\dfrac{1}{T_1} - \dfrac{1}{T_2}} \tag{3}$$

where R is the universal gas constant (8.314 J mol^{-1} K^{-1}), T is the absolute temperature in Kelvins, and the two subscripts refer to the two temperatures at which measurements were made.

Experimental Procedure

The method of surface area determination developed by Brunauer, Emmett, and Teller (BET) [25] was applied to the eleven surface samples. Despite uncertainties related to the variation of accessible surface area for sorbates other than nitrogen, this sorbate can be used reliably for the comparison of surface areas. The Quantasorb® Sorption System (Quantachrome Corporation, 6 Aerial Way, Syosset, NY 11791) was used for all tests. Each surface was outgassed at room temperature in a pure nitrogen carrier for a minimum of 2 h prior to testing. Data were gathered at relative partial pressures of 0.24 to 0.35 nitrogen. Good agreement was found between replicate measurements. Because of inaccuracy in measuring the small adsorbed volumes at relative partial pressures less than 0.24, specific surface areas were calculated on the basis of single-point measurements.

All samples were stored in a dessicator for several weeks prior to the start of the experiments. Two sets of eleven glass vials of 160 mL volume were filled with approximately 2 g of each of the eleven samples and sealed with a TFE-fluorocarbon valve. Two empty vials were used as controls; all surfaces within the empty control vials were glass except for the TFE-fluorocarbon closure. The temperature of the vials was controlled by immersion in a thermostatted water bath at either 25 or 35°C. The measurement of the partition coefficient at a single temperature for either TCE or EtOH for one set of eleven vials constituted a single experiment; replicate experiments involved simultaneous study of both sets of vials under identical conditions of loading and temperature. Aliquots of TCE/air or EtOH/air vapor mixtures were introduced to the headspace of the vials to establish an initial gas-phase concentration of about 100 mg/m^3. TCE and EtOH were examined separately to avoid any complicating synergistic effects.

Vapor samples of 50-μL were gathered directly from the headspace of the vials via syringe sampling through the TFE-fluorocarbon valve. Headspace concentrations were analyzed using GC/ECD for TCE and GC/FID for EtOH. Each vial was sampled twice; thus, each reported headspace concentration is the mean of two replicate chromatographic analyses. TCE calibration standards were prepared by dilution of liquid TCE in 10 mL of methanol and allowing complete evaporation of this liquid mixture in calibration vials identical in all aspects to those used in the sorption experiments. EtOH calibration standards were prepared by allowing small quantities of liquid EtOH to evaporate in Tedlar bags with an approximate volume of 10 L. Liquid TCE and EtOH were delivered by syringe; the amount delivered was determined gravimetrically. The volume of clean dilution air delivered to the Tedlar bags was determined using a wet test meter.

Preliminary experiments examining the change in concentration as function of time determined that sorption equilibrium was established within $2^1/_2$ h for TCE and within 1 day for EtOH.

For TCE at 25°C, further tests to obtain a partition isotherm over a broad range of concentrations were conducted. For each isotherm, seven initial concentrations ranging from 300 μg/m^3 to 300 mg/m^3 were established; the resulting partition isotherms spanned several orders of magnitude in gas-phase concentration.

Results

Estimates of specific surface area A_{sp} for the eleven samples are shown in Table 2. One method for assessing the accuracy of these results is to consider the result for the glass fiber. For a nonporous fiber of constant circular cross section,

$$A_{sp}(\mathrm{m^2/g}) = \frac{4}{p_f(\mathrm{g/cm^3})\,d_f(\mu\mathrm{m})} \tag{4}$$

where p_f and d_f are the fiber density and diameter, respectively. For the glass fiber, A_{sp} calculated

TABLE 2—*Specific surface area* A_{sp} *(in* m^2/g*) as measured here using nitrogen adsorption at 77 K. The uncertainty in* A_{sp} *reflects the imprecision in measurement of the adsorbed volume. For comparison, values from the literature* [31] *for several surfaces are also shown; the last column is for data reported based on the adsorption of water vapor.*

Surface[a]	A_{sp}	Surface[b]	A^c_{sp}	A^d_{sp}
Glass	0.22 ± 0.03	polyester	0.50	...[e]
Polyester	0.15 ± 0.06			
Cotton	0.87 ± 0.05	cotton	0.72	108
Polypropylene	0.35 ± 0.04			
Jute	0.18 ± 0.03			
SBR[f]	0.20 ± 0.06			
Nylon I	0.29 ± 0.04	nylon	0.31	45
Nylon II	0.16 ± 0.03			
Nylon III	0.26 ± 0.04			
Wool I	0.26 ± 0.05	wool	0.96	206
Wool II	0.29 ± 0.03			

[a]This study.
[b]Ref *31*.
[c]Nitrogen at 77 *K*.
[d]Water vapor at 298 *K*.
[e]Not reported.
[f]Styrene-butadiene rubber.

using Eq 4 is 0.2 m^2/g, in good agreement with the value obtained here using the BET method. Values of A_{sp} for surfaces other than cotton are on the order of 10^{-1} m^2/g. The specific surface area for cotton is somewhat greater, though at most by one order-of-magnitude.

The partition coefficients obtained for TCE and EtOH at 25 and 35°C, calculated using Eq 1, are summarized in Fig. 2. Since the concentrations in the glass-fiber-filled vials were not significantly different from those in the empty vials, concentrations measured in the empty control vials and the vials containing the glass fiber were used to estimate the initial concentration C_o in each experiment. Two general observations are apparent. First, partition coefficients for the polar compound EtOH are higher on the hydrophilic surfaces (cotton, jute, wool, and nylon) than on those that are more hydrophobic. In contrast, partition coefficients for TCE are higher on the hydrophobic surfaces than on those that are more hydrophilic. Polyester is an exception, with approximately the same partition coefficients for both TCE and EtOH. Second, when VOC/surface interaction is favored, partition coefficients are an order of magnitude larger for EtOH (10^3 cm^3/g) than for TCE (10^2 cm^3/g); this reflects the stronger nature of the polar-polar interactions relative to those due to nonspecific dispersion (Van der Waals) forces. The error bars in Fig. 4 represent the uncertainty in K estimated by Eq 1; this incorporates the measured uncertainty in C and C_o.

Based on these measurements, the values of Q_{st} calculated using Eq 3 are shown in Table 3. Negative values indicate an exothermic interaction. The minimum and maximum values in parentheses reflect the uncertainty in the estimate of K. Note that the values for EtOH sorption on polypropylene and SBR latex, as well as the value for TCE sorption on cotton, are highly uncertain. The remaining values for EtOH indicate that the heat of sorption is less than the heat of vaporization Q_v, that is approximately −9 kcal/mole. For TCE, Q_v is about −7 kcal/mole, and the results in Table 3 indicate that the heat of sorption is generally larger in magnitude than the heat of vaporization, supporting an explanation of the observed partitioning on the basis of adsorption. Q_{st} values for polypropylene and SBR latex are exceptions and are significantly lower than those for the other surfaces.

Figure 5 shows the results of the two experiments evaluating sorption of TCE at 25°C over a broad concentration range. Equation 2 has been used to estimate C_s. Figure 3 depicts the same

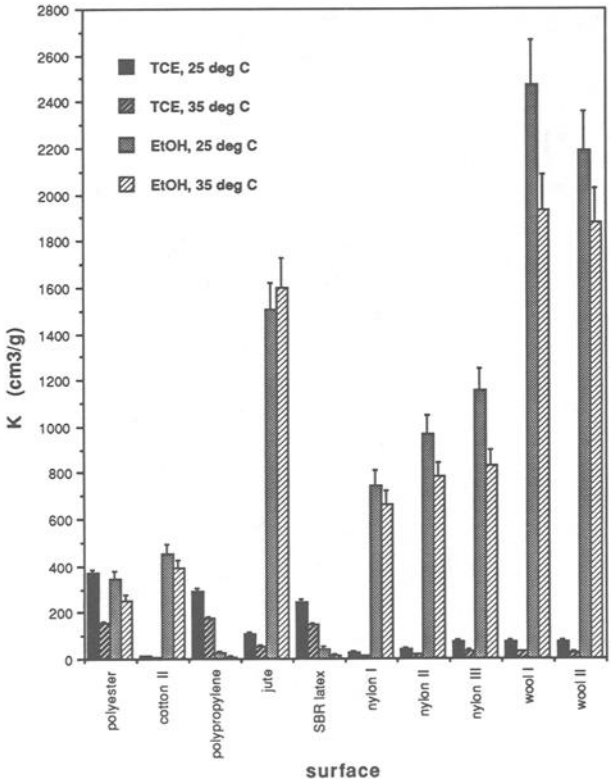

FIG. 2—*Partition coefficients for TCE and EtOH vapor measured at 25 and 35°C. Each data point is the average of two independent experiments. The coefficients of variation corresponding to the error bars indicated on the plot range from 8 to 90% with an average value of 16%; lower values of the partition coefficient are associated with larger coefficients of variation.*

data in the range of gas-phase concentrations from 0 to 35 mg/m^3. Because the range of equilibrium gas-phase concentrations spanned three orders of magnitude (from less than 0.25 mg/m^3 to over 250 mg/m^3), the data are also depicted on a log-log plot in Fig. 4.

The error bars in the plots account for two different sources of variability in C_s. One results from the uncertainty in the initial mass of TCE that was added to each of the vials, reflected in the variability in the measurements of C_o for each experiment. Although not independent of C, this uncertainty was not found to be directly proportional to C, so it became relatively smaller as C became larger, even though its magnitude increased.

The second source of uncertainty is that associated with replicate measurement of C from a single vial. This uncertainty is directly proportional to the concentration measured, and thus, for this case, the coefficients of variation of the C_s estimates are independent of C. The average value of the coefficient of variation for C_s due to this uncertainty was 0.78%, ranging from a minimum of 0.01% to a maximum of 4.96%.

Discussion

For comparison with the values of A_{sp} obtained here, typical literature values for A_{sp} are also shown in Table 2. Note that for the three hydrophilic surfaces, cotton, wool, and nylon, the sorption of water vapor increases the apparent specific surface area by several orders of magnitude. As

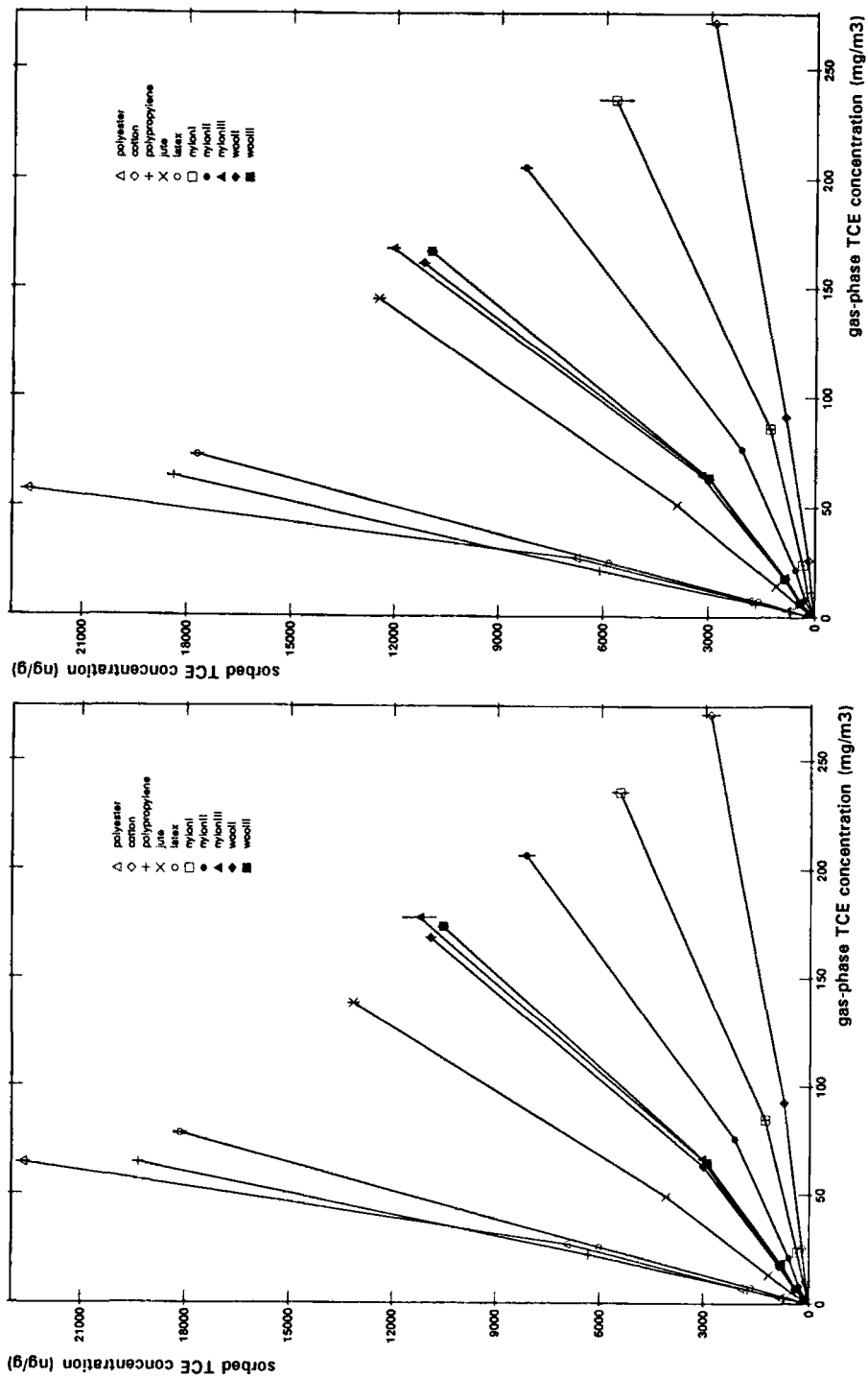

FIG. 3—*Sorption isotherms for TCE vapor with respect to ten surfaces at 25°C plotted in log-log coordinates.*

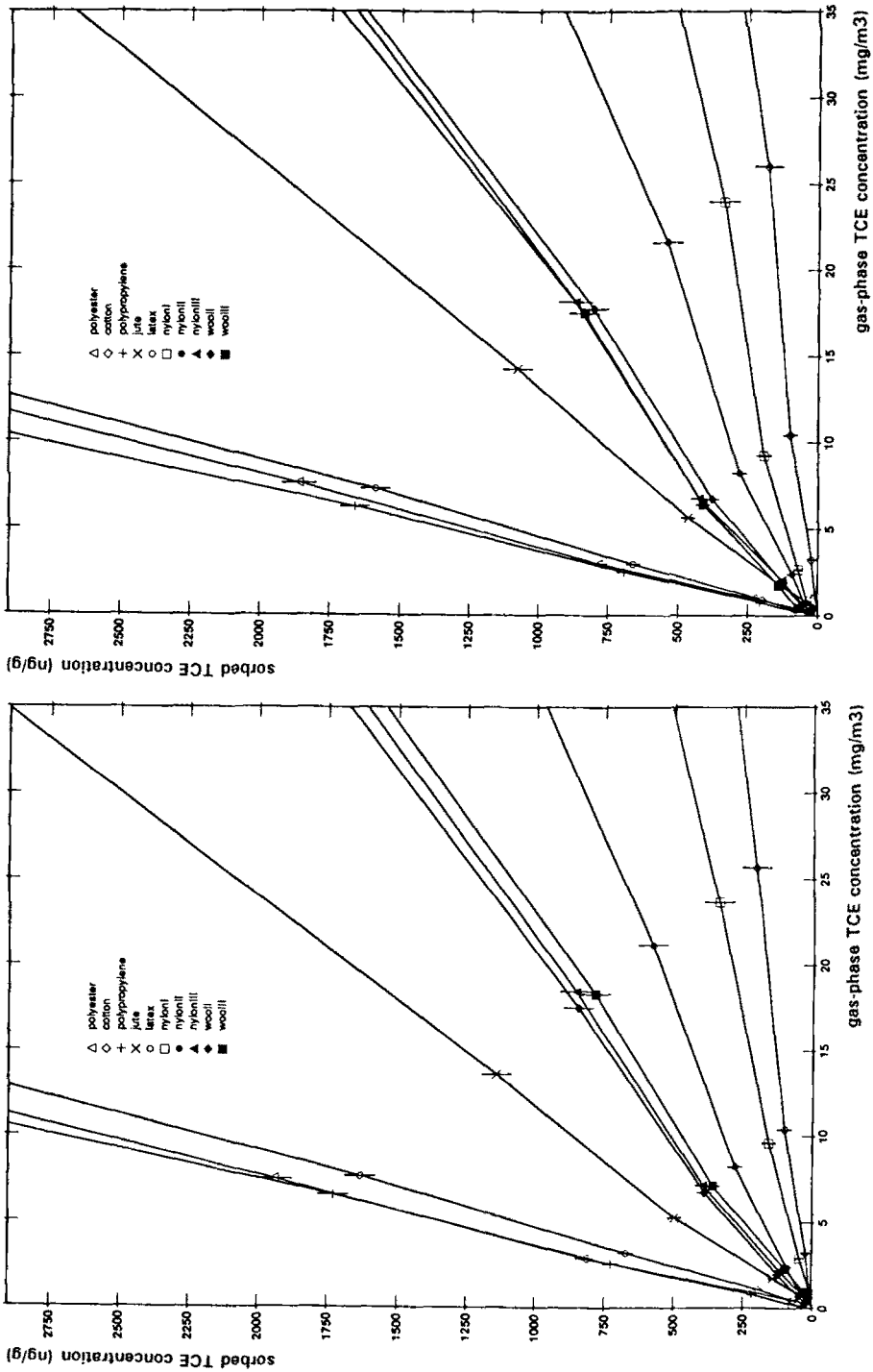

FIG. 4—*Sorption isotherms for TCE vapor with respect to ten surfaces at 25°C for the full range of concentrations studied.*

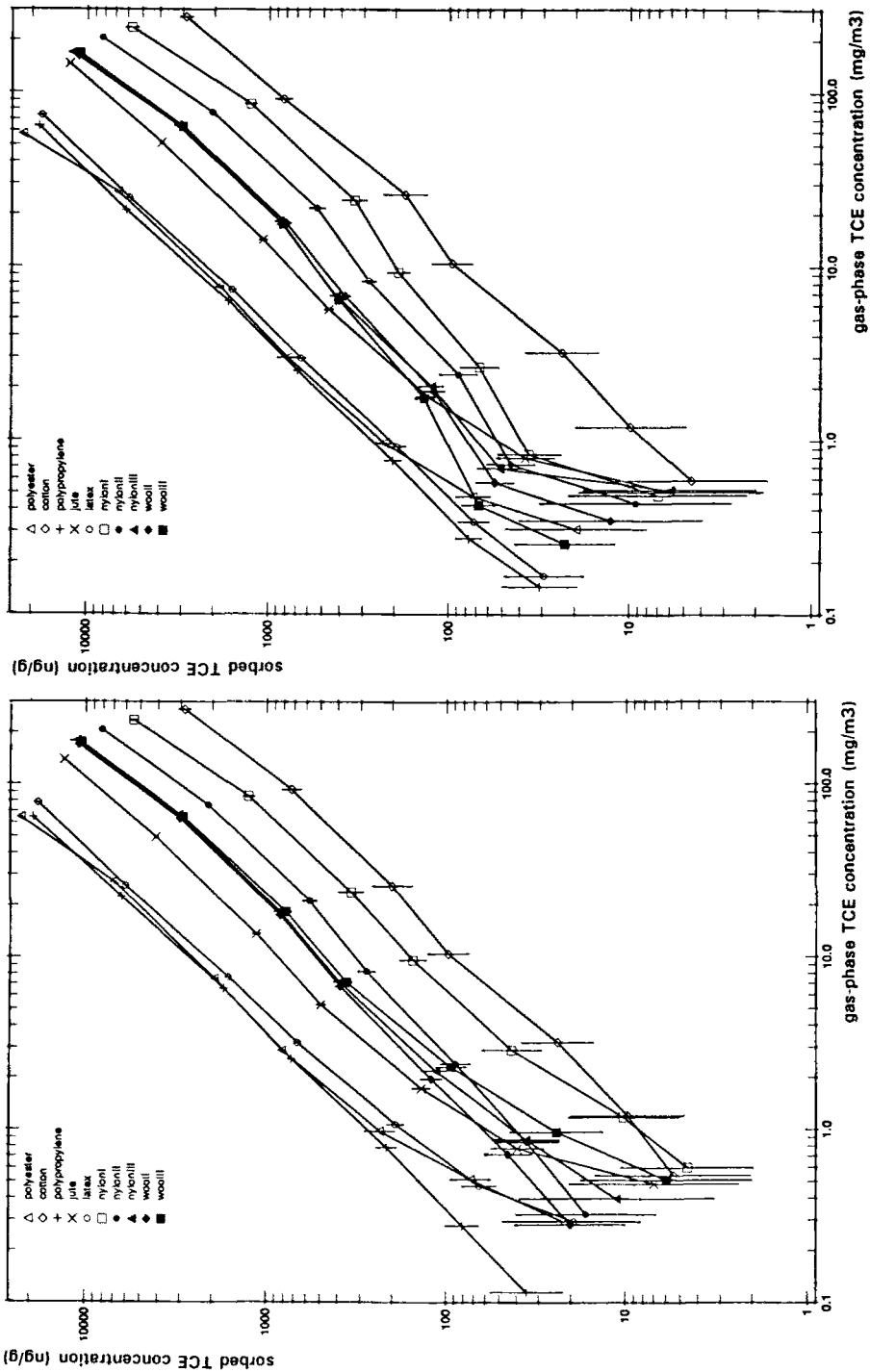

FIG. 5—*Sorption isotherms for TCE vapor with respect to ten surfaces at 25°C for equilibrium gas-phase concentrations up to 35 mg/m*^{3}.

TABLE 3—*Values of the heat of sorption* Q_{st} *(kcal/mole), computed from the temperature-dependency of the partition coefficient* K. *The values in parentheses reflect the uncertainty in* Q_{st} *due to uncertainty in the estimation of* K.

Surface	Q_{st} for TCE		Q_{st} for EtOH	
Polyester	−16.4	(−14.7, −18.0)	−6.6	(−2.9, −10.3)
Cotton	−22.8	(−8.7, −47.3)	−3.2	(0.1, −6.5)
Polypropylene	−9.6	(−8.0, −11.2)	−22.6	(−3.7, −70.4)
Jute	−12.3	(−9.9, −14.7)	0.5	(3.5, −2.4)
SBR	−9.5	(−7.8, −11.1)	−18.6	(−7.3, −33.3)
Nylon I	−15.3	(−8.9, −22.6)	−2.7	(0.4, −5.8)
Nylon II	−15.5	(−11.0, −20.4)	−4.5	(−1.4, −7.5)
Nylon III	−13.7	(−10.4, −17.1)	−6.6	(−3.6, −9.7)
Wool I	−16.3	(−13.0, −19.6)	−5.1	(−2.2, −8.0)
Wool II	−17.7	(−14.5, −21.2)	−3.4	(−0.5, −6.3)

mentioned above, all three of these fibers will sorb significant volumes of water, ranging from about 4% for nylon to over 18% for wool at standard conditions. Since water vapor swells these surfaces, and sorption is no longer localized, the applicability of the BET method in measuring surface areas using water vapor sorption is questionable. Reported values for surface area in the presence of water vapor or estimated using water vapor sorption have little meaning, except insofar as they indicate that swelling of the polymer by the water vapor has a significant impact on the physical structure of the fiber.

Water vapor sorption on hydrophilic fibers may have a significant impact on the simultaneous sorption of VOC vapors; it is not clear whether sorbed water vapor will enhance or inhibit the sorption of VOCs. This uncertainty limits the practical applicability of the results obtained in this study for hydrophilic surfaces, since indoor relative humidity is typically maintained at values between 40 and 60%.

As seen in Fig. 2, the sorption of relatively nonpolar TCE and the more polar compound EtOH are inversely related. These results suggest that the relative polarities of sorbate and surface material play an important, perhaps dominant role in determining the extent of sorption. Polyester is an exception, exhibiting approximately equal, moderately strong sorption effects with respect to both TCE and EtOH. The high T_g of polyester, relative to room temperature, as well as the small diffusion coefficient in the polymer, suggest that absorption will not play an important role in interactions with this fiber. The stronger temperature dependence (relative to the SBR and polypropylene surfaces) of the partition coefficients measured for TCE on the polyester fiber also suggests that partitioning is, in this case, governed by an adsorption phenomenon. Since BET polyester is formed from the condensation polymerization of polar and nonpolar molecules, the polymer retains some aspects of each with respect to its adsorption properties. This duality is also reflected in the bimodal nature of the distribution of solubility parameters of good solvents for polyester [*26*].

From the data in Figs. 3 and 5, it appears that the sorption isotherms are concave to the gas-phase concentration axis at lower concentrations and convex to this axis at higher concentrations. Such sigmoid-shaped isotherms are typical of physical adsorption. Note that the isotherms for SBR latex and polypropylene appear to be exceptions; these isotherms appear to be linear over the entire concentration range examined.

Regression analysis was used to determine whether the nonlinearity of the isotherms was statistically significant, given the larger relative uncertainties in the data at lower concentrations. A slope of unity for the regression line in log-space corresponds to a linear isotherm. The regression equation

$$\log C_s = a_1 \log c + a_2 \tag{5}$$

was used for this analysis. Since the variance about the regression line was not constant, it was necessary to weight the ordinate values inversely to the uncertainty in each value. As suggested by Ang and Tang [27], the inverse of the variance was used for the weighting scheme. In general, because of the uncertainty in the lower values of C, the deviation from linearity noted for several of the curves in this concentration range was not statistically significant and did not greatly influence the estimation of the regression parameters. Values of the estimated slope a_1 ranged from 1.03 to 1.16, based on the average of the values obtained by separate regressions for each of the two experiments. This implies that using a single estimate of K for the entire concentration range of interest will result in some error in the estimate of K. However, the values of a_1 are close enough to unity that such errors will be at most a factor of two and not an order-of-magnitude. Thus, the values of K estimated using the single-point method and shown in Fig. 2 are reasonable.

In considering the significance of the apparent nonlinearity in the isotherms of Figs. 3 and 5, it is important to remember that the mean value of a set of imprecise measurements may be accurate. Although lack of precision may prevent the statistical justification of nonlinearity, this effect may nevertheless be very real and may provide insight into the fundamental nature of the sorption process. The fact that two independent experiments exhibited the same type of sigmoid-shaped isotherms for eight of the ten surfaces suggests that more precise data would confirm the nonlinearity of the isotherms. Indeed, isotherms of this shape are typical of physical adsorption. On the other hand, such nonlinearities are of small practical significance when only order-of-magnitude estimates of the partition coefficients are of interest.

For systems in which the solubility parameters of the sorbate and sorbent are approximately equal, absorption of organic vapor molecules into the body of the fiber can be the dominant partitioning mechanism. Note that the only surfaces among those studied that are above their glass transition temperatures at room temperature are polypropylene and SBR latex (see Table 1), indicating that for these surfaces, solubilization of VOC molecules in the polymeric surface is possible. The solubility parameters for these surfaces also suggest that absorption of TCE, but not of EtOH, may occur. In addition, the apparent linearity of the isotherms for these two surfaces over a broad range of TCE concentrations also supports the notion that the partitioning mechanism is absorption, as does the observation that Q_{st} is approximately equal to Q_v.

With respect to TCE sorption, for surfaces other than polypropylene fiber and SBR, the strong temperature dependence of the partition coefficient results in larger values of $Q_{st} - Q_v$ (~8 kcal/mole) than those expected solely on the basis of weak interactions governed by dispersion forces (typically < 2 kcal/mole). However, the large uncertainty in the relatively small partition coefficients on which these estimates are based make definitive statements difficult.

Dipole-dipole interactions of EtOH with the polar surfaces likely explains the observed large partition coefficients; partition coefficients were an order-of-magnitude higher than for TCE. However, the weak temperature dependence of the data suggests that Q_{st} is less than Q_v, indicating that changes in the structure of the sorbent surface upon sorption of EtOH may complicate the thermodynamic analysis. The values of Q_{st} for polypropylene and the SBR latex are too uncertain to be meaningful.

It is important to remember that the physical preparation of the filled SBR film was different from that which would be used in carpet backings. Although we could locate no data for the sorption of organic vapors on dried SBR latex, Barrer [28] describes how the solubilities of several permanent gases (H_2, N_2, and O_2) in filled rubbers varied with the amount of filler. At least for several carbon black fillers, these solubilities increased over those of the unfilled rubbers. This suggests that for filler particles whose surfaces are not fully wetted by the rubber polymer, adsorption on the surfaces of the filler may enhance partitioning. For this reason, the geometry of the filled SBR latex used as carpet backing may be very important in determining its partitioning characteristics. The film used in the BET test was not foamed and so it is reasonable to expect that it would have low porosity, that was confirmed by both the low specific surface area and the

TABLE 4—*Fraction in the sorbed phase* f_s *of the total mass in a closed system at equilibrium. Values have been calculated at several values of the partition coefficient* K *(cm³/g) for a fiber mass-to-volume loading ratio typical of a carpeted room.*

K, cm³/g	f_s
10^0	0.001
10^1	0.01
10^2	0.09
10^3	0.5
10^4	0.9

density of the film. Filled SBR latex in carpet backing is foamed, and probably has a high porosity with more filler surface accessible for adsorption; one might expect that higher partition coefficients than those obtained in this study would result.

Implications and Conclusions

The effectiveness of a surface as a reservoir for a VOC is a function not only of the affinity of the surface for sorption of the VOC, but also its surface area or mass. Using assumptions about the mass loading of sorbent surfaces in the indoor environment, the partition coefficient K can be used to evaluate the significance of equilibrium sorption effects on indoor pollutant concentrations. The fraction f_s of the total mass in the sorbed phase for the limiting case of a closed chamber is given by

$$f_s = \frac{K(M_s/V)}{1 + K(M_s/V)} \tag{6}$$

where M_s is the sorbent mass and V is the chamber volume. As an example, for a room with a ceiling height of 2.5 m, the ratio of projected floor surface area to room volume would be approximately 0.4 m^{-1}. If the room contained a nylon pile carpet weighing 2000 g/m², then M_s/V is on the order of 1000 g/m³. Values of f_s corresponding to several values of K for this example scenario are shown in Table 4. Since partition coefficients for TCE with respect to the polypropylene and SBR latex were about 200 to 300 cm³/g and these surfaces account for about half the weight of the carpet, for this example about 10% of the total mass of TCE would be in the sorbed phase. Obviously, in the presence of additional sorbing surfaces or for VOC/surface systems exhibiting stronger sorption interactions, f_s would be greater. For EtOH, sorption to the nylon pile fiber yields a partition coefficient of approximately 800 cm³/g, resulting in an equilibrium sorbed phase fraction of about 30%.

Of course, most real systems are dynamic and do not behave as closed chambers. Thus, this calculation is intended only to demonstrate the limiting case.

Most indoor fibrous surfaces have fairly low specific surface areas when compared with sorbents such as activated carbon. For this reason, interactions governed by dispersion forces alone will not result in very extensive partitioning to the surfaces, at least for VOCs. Dipole-dipole interactions, that may play a role in the sorption of more polar substances, can yield much larger partition coefficients. The differences in partition coefficients exhibited by compounds of similar polarity are probably smaller than those due to specific interactions that will vary between compound families. For example, the two compounds of comparable volatility that were studied here, TCE

and EtOH, exhibited very different sorption effects with respect to the surfaces studied, both quantitatively and qualitatively.

Absorption may play a role as well as adsorption in determining the extent of partitioning. This could have been the case for the polypropylene and SBR surfaces with respect to the sorption of TCE, because partition coefficients for these surfaces were large while the temperature-dependency of the data indicated that energies of sorption were small. In addition, the sorption isotherms were linear over a broad range of concentrations, typical of solution isotherms.

The data suggest that nonlinearities in the sorption isotherms exist. However, on the basis of the experiments here, such behavior could not be rigorously confirmed. Such nonlinearities also do not appear to be of much practical significance, since they cause partition coefficients to vary, but only by at most a factor of two. Nevertheless, an understanding of the nature of such nonlinearities may prove useful in determining the fundamental mechanisms underlying the observed effects.

This study has shown that different components of a composite material such as carpet may exhibit very different affinities for a single compound, but entirely different behavior, both qualitatively and quantitatively, for another compound. This suggests that appropriate models for the kinetics of uptake on a particular surface may be dependent on compound properties such as polarity. Alternatively, any one model will need to account for several possible sorption steps or mechanisms, or both, not all of which would necessarily be significant in describing the interaction of a given surface and vapor. This is consistent with the observation of Tichenor et al. that first-order kinetics did not govern the behavior of uptake of tetrachloroethylene by nylon carpeting [*15*].

Finally, these partition coefficient data should be applied cautiously, particularly since they were gathered for pure sorbates, without any competing or synergistic effects of other compounds. In particular, water vapor, which normally is present at significant indoor concentrations, may greatly affect the sorption interactions considered here.

Acknowledgments

This research has been funded in part under U.S. Environmental Protection Agency (EPA) cooperative agreement CR-812761-02. This manuscript has not been subjected to EPA peer and administrative review policy, does not necessarily reflect its views, and no official endorsement should be inferred.

References

[*1*] Yamanaka, S., "Decay Rates of Nitrogen Oxides in a Typical Japanese Living Room," *Environmental Science & Technology*, Vol. 18, 1984, pp. 566–570.

[*2*] Spicer, C. W., Coutant, R. W., Ward, G. F., Gaynor, A. J., and Billick, I. H., "Removal of Nitrogen Dioxide from Indoor Air by Residential Materials," *Proceedings*, IAQ 1986, American Society of Heating, Refrigeration, and Air Conditioning Engineers (ASHRAE), Atlanta, GA, 1986, pp. 584–590.

[*3*] Brauer, M., Ryan, P. B., Suh, H. H., Koutrakis, P., Spengler, J. D., Leslie, N. P., and Billick, I. H., "Measurement and Modeling of Nitrous Acid in Indoor Air," *Proceedings*, Fifth International Conference on Indoor Air Quality and Climate, Toronto, Canada, 29 July–3 Aug. 1990, Vol. 2, pp. 293–298.

[*4*] Axley, J. W., "Adsorption Modelling for Building Contaminant Dispersal Analysis," *Indoor Air*, Vol. 1, No. 2, 1991, pp. 147–171.

[*5*] Andelman, J. B., "Inhalation Exposure in the Home to Volatile Organic Contaminants of Drinking Water," *Science of the Total Environment*, Vol. 47, 1985, pp. 443–460.

[*6*] Andelman, J. B., Giardino, N. J., Marshall, J., Esmen, N., Borrazzo, J. E., Davidson, C. I., Small, M., and Wilkes, C., "Exposure to Volatile Chemicals from Indoor Uses of Water," *Proceedings*, Air and Waste Management Association Symposium on Total Exposure Methodology, Las Vegas, NE, 27–30 Nov. 1989.

[7] Nielsen, P. A., "Potential Pollutants, their Importance to the Sick Building Syndrome, and their Release Mechanism," *Proceedings*, Fourth International Conference on Indoor Air Quality and Climate, Berlin, Germany, 17–21 Aug. 1987, Vol. 2, pp. 598–602.

[8] Matthews, T. G., Hawthorne, A. R., and Thompson, C. V., "Formaldehyde Sorption and Desorption Characteristics of Gypsum Wallboard," *Environmental Science & Technology*, Vol. 21, No. 7, 1987, pp. 629–634.

[9] Berglund, B., Johansson, I., and Lindvall, T., "Volatile Organic Compounds from Used Building Materials in a Simulated Chamber Study," *Environment International*, Vol. 15, 1989, pp. 383–387.

[10] Korte, F. and Gebefugi, I., "Avoidable and Unavoidable Exposition of Indoor Chemicals," *Proceedings*, Fourth International Conference on Indoor Air Quality and Climate, Berlin, Germany, 17–21 Aug. 1987, Vol. 1, pp. 239–242.

[11] Seifert, B. and Schmahl, H.-J., "Quantification of Sorption Effects for Selected Organic Substances Present in Indoor Air," *Proceedings*, Fourth International Conference on Indoor Air Quality and Climate, Berlin, Germany, 17–21 Aug. 1987, Vol. 1, pp. 252–256.

[12] Borrazzo, J. E., Davidson, C. I., and Andelman, J. B., "The Influence of Sorption to Fibrous Surfaces on Indoor Concentrations of Organic Vapors," *Proceedings*, Eighty-third Annual Meeting of the Air and Waste Management Association, Pittsburgh, PA, 24–29 June 1990.

[13] Borrazzo, J. E., Davidson, C. I., and Andelman, J. B., "Sorption of Organic Vapors to Indoor Surfaces of Synthetic and Natural Fibrous Materials," *Proceedings*, Fifth International Conference on Indoor Air Quality and Climate, Toronto, Canada, 29 July–3 Aug. 1990, Vol. 3, pp. 617–622.

[14] Tichenor, B. A., Guo, Z., Mason, M. A., and Dunn, J. E., "Evaluation of Indoor Air Pollutant Sinks for Vapor Phase Organic Compounds," *Proceedings*, Fifth International Conference on Indoor Air Quality and Climate, Toronto, Canada, 29 July–3 Aug. 1990, Vol. 3, pp. 623–628.

[15] Tichenor, B. A., Guo, Z., Dunn, J. E., Sparks, L. E., and Mason, M. A., "The Interaction of Vapor Phase Organic Compounds with Indoor Sinks," *Indoor Air*, Vol. 1, No. 1, 1991.

[16] Kjaer, U. and Nielsen, P. A., "Adsorption and Desorption of Organic Compounds on Fleecy Materials," *Proceedings*, Healthy Buildings IAQ 1991, American Society of Heating, Refrigerating, and Air-Conditioning Engineers (ASHRAE), Washington, DC, 4–8 Sept. 1991, pp. 285–288.

[17] Ioffe, B. V. and Vitenberg, A. G., *Head-Space Analysis and Related Methods in Gas Chromatography*, John Wiley & Sons, New York, 1984.

[18] Pleil, J. D. and Whiton, R. S., "Determination of Organic Emissions from New Carpeting," *Applied Occupational Environmental Hygiene*, Vol. 5, No. 10, October 1990, pp. 693–699.

[19] Peterson, M. S., Lion, L. W., and Shoemaker, C. A., "Influence of Vapor-Phase Sorption and Diffusion on the Fate of Trichloroethylene in an Unsaturated Aquifer System," *Environmental Science & Technology*, Vol. 22, 1988, pp. 571–578.

[20] Garbarini, D. R. and Lion, L. W., "Evaluation of Sorptive Partitioning of Nonionic Pollutants in Closed Systems by Headspace Analysis," *Environmental Science & Technology*, Vol. 19, 1985, pp. 1122–1128.

[21] Crittenden, J., personal communication, Michigan Technological University, 1990.

[22] Textile Economics Bureau, "Man-Made Fiber, Cotton and Wool End Use Survey," *Textile Organon*, Vol. 58, No. 9, 1987, pp. 205–226.

[23] Peyser, P., "Glass Transition Temperatures of Polymers," *Polymer Handbook*, J. Brandrup and E. H. Emmergut, Eds., John Wiley & Sons, New York, 1989.

[24] Sontheimer, H., Crittenden, J., and Summers, R. S., *Activated Carbon for Water Treatment*, Karlsruhe: DVGW-Forschungsstelle, 1988.

[25] Brunauer, S., Emmett, P. H., and Teller, E., "Adsorption of Gases in Multimolecular Layers," *Journal of the American Chemical Society*, Vol. 60, 1938, pp. 309–319.

[26] Weigmann, H.-D., "Interactions Between Fibers and Organic Solvents," *Handbook of Fiber Science and Technology: Volume I, Chemical Processing of Fibers and Fabrics, Fundamentals and Preparation: Part A*, M. Lewin and S. B. Sello, Eds., Marcel Dekker, Inc., New York, 1983.

[27] Ang, A. H.-S. and Tang, W. H., *Probability Concepts in Engineering Planning and Design*, John Wiley & Sons, New York, 1975.

[28] Barrer, R. M., "Discussion of: Absorption of Water by Polymers–Analysis in Terms of a Simple Model," (Hailwood, A. J. and Horrobin, S., Authors) *Transactions of the Faraday Society*, Vol. 42B, 1946, pp. 46–47.

[29] *Polymer Handbook*, J. Brandup and E. H. Immergut, Eds., John Wiley & Sons, New York, 1989.

[30] Cook, J. G., *Handbook of Textile Fibres*, Merrow Publishing Company Ltd., Watford, Great Britain, 1964.

[31] Morton, W. E. and Hearle, J. W. S., *Physical Properties of Textile Fibres*, Butterworths, London, 1962.

Delbert J. Eatough[1]

Assessing Exposure to Environmental Tobacco Smoke

REFERENCE: Eatough, D. J., **"Assessing Exposure to Environmental Tobacco Smoke,"** *Modeling of Indoor Air Quality and Exposure, ASTM STP 1205*, Niren L. Nagda, Ed., American Society for Testing and Materials, Philadelphia, 1993, pp. 42–63.

ABSTRACT: The assessment of environmental tobacco smoke exposure is complicated by the presence of significant amounts of organic material in both the gas and the particulate phase and by changes in the relative composition of the two phases with time. An understanding of both the chemical nature of fresh environmental tobacco smoke and the changes in its composition over time are needed in order to properly assess the impact of smoking on the nonsmoker in indoor environments. The dynamics of these changes in environmental tobacco smoke affect: (1) the chemical compounds to which the nonsmoker is exposed, (2) the chemical compounds that may be used to estimate the exposure of the nonsmoker to environmental tobacco smoke in the indoor environment, and (3) risk assessment of disease and irritant exacerbations associated with exposure of the nonsmoker to environmental tobacco smoke.

The chemical characteristics of environmental tobacco smoke that affect the assessment of exposure to environmental tobacco smoke are reviewed. The various components of environmental tobacco smoke that have been used to assess exposure are evaluated with respect to the following three criteria: (1) uniqueness to environmental tobacco smoke, (2) ease of determination at concentrations present in indoor air, and (3) relationship to other components of environmental tobacco smoke.

KEY WORDS: 3-ethenylpyridine, continine, deposition, environmental tobacco smoke, exposure, isoprene, mutagen, nicotine, respirable suspended particles (RSP), solanesol, UV-PM

The Chemical Composition of Fresh Environmental Tobacco Smoke

Environmental tobacco smoke consists of side-stream smoke generated by a burning cigarette, and mainstream smoke exhaled by the smoker. The major contribution to environmental tobacco smoke is from the side-stream smoke from a cigarette [*1*]. Side-stream and mainstream smoke produced during the smoking of a cigarette are similar chemically and qualitatively. However, significant quantitative differences exist between the two sources [*1–3*]. In addition, as the generated environmental tobacco smoke emissions are introduced into an indoor environment, substantial changes in the gas-particulate phase distribution of the chemical species present occurs [*1,2,4*].

Chemical Composition of Side-Stream Tobacco Smoke

The chemical composition of environmental tobacco smoke has been extensively discussed in reviews by the Surgeon General [*5*] and the National Research Council [*3*]. More recent data have been discussed in recent reviews [*1,2,6–10*] and in an International Agency for Research on Cancer (IARC) Monograph [*11,12*]. Included in the IARC Monograph and other publications is a review of the combustion conditions associated with the formation of both mainstream and side-stream tobacco smoke [*2,7,13,14*]. The major differences between mainstream and side-stream tobacco smoke arises from the lower combustion temperatures associated with the formation of side-stream tobacco smoke,

[1]Professor, Brigham Young University, Chemistry Department, Provo, UT 84602.

leading to an increase in the amounts of distillation products and a decrease in the amounts of combustion products present in the sidestream smoke. As a result, side-stream smoke is more alkaline than mainstream smoke [*7,15*]. This alkalinity results from the increased amounts of N-containing bases present as distillation products in the side-stream smoke aerosol. However, the combustion zone of mainstream smoke is more oxygen deficient than the combustion zone of side-stream smoke and, as a result, the CO_2/CO ratios are higher for side-stream smoke than for mainstream smoke.

The expected composition of potential tracers of environmental tobacco smoke in freshly generated side-stream tobacco smoke is given in Table 1. The amounts of most constituents in side-stream tobacco smoke are little affected by brand, tobacco moisture content, or mainstream combustion parameters for combustion of comparable amounts of tobacco [*1,2,7,16*]. Since side-stream tobacco smoke is responsible for most of the environmental tobacco smoke in indoor environments, environmental tobacco smoke composition in an indoor environment should be predictable from a knowledge of the number of cigarettes smoked as a function of time. This prediction will be altered by changes in the phase distribution and chemical composition of the environmental tobacco smoke as it ages in an indoor environment.

Gas-Particulate Phase Distribution of Some Compounds in Environmental Tobacco Smoke

Little is known about the distribution of organic compounds between the gas and particulate phases of environmental tobacco smoke [*1,3,7,17–22*]. Recent studies have shown that most of the volatile nitrogen containing compounds such as nicotine, myosmine, and pyridine are predominantly present in the gas phase of environmental tobacco smoke [*18–21,23–25*]. Acrolein, formaldehyde, and acetaldehyde are major toxic constituents of the gas phase of environmental tobacco smoke [*1,3,5*]. The distribution of many mutagenic and toxic compounds, or both, such as the N-nitrosamines, between the gas and particulate phases of environmental tobacco smoke is presently not known [*3,26,27*]. For most of the semivolatile organic compounds, the phase of the compound is not well known. The phase distribution of nicotine has been extensively studied. While nicotine is undoubtedly present primarily in the particulate phase in side-stream tobacco smoke generated in small combustion devices of only a few litres in volume [*7*], it is present as the gas phase species in side-stream tobacco smoke in a large chamber [*18,28*]. The equilibration from the particle to the gas phase is very rapid [*18,21,24,29,30*]. The more alkaline pH of side-stream tobacco smoke [*15*] may be, in part, responsible for the rapid displacement of the nonprotonated nicotine from the particles [*1,7*]. In addition to nicotine, nicotyrine, myosmine, pyridine and alkyl pyridine compounds are also present only, or predominantly, in the gas phase [*18,19,21,29*]. The identification of the gas-particle phase distribution of organic compounds of toxicological interest is an area of needed research.

There is an apparent difference in total mass in side-stream emissions from a cigarette in studies conducted using a small combustion and collection device, as compared to studies conducted using an environmental chamber [*2,13*]. The chamber studies give emission values which range from 6 to 11 mg particles per cigarette, while the other studies give values with 11 mg per cigarette as the lower end of the measurements. The differences can not be accounted for based on selective deposition loss of particles in the chamber experiments as the data are generally obtained in chambers immediately after combustion of the cigarette [*17,18,31,32*]. The difference appears to be real. Many of the organic constituents of side-stream tobacco smoke are volatile and losses of material from the particles as the smoke is diluted would be expected [*6,13,33,34*]. It is assumed in the data interpretation given in this review that this is the case. The amount of particulate matter in environmental tobacco smoke resulting from the combustion of a cigarette is assumed to be about 10 mg [*1,2,32*].

If the differences in particulate matter observed in the two types of chemical characterization experiments (chamber versus combustion apparatus) are due to volatilization of organic compounds

TABLE 1—*Gas and particulate phase compounds potentially useful as tracers of environmental tobacco. (Data are from Refs* 2, 17, 18, 19, 32, 47, 49, 85, 138, *and* 153*).*

Chemical Class	Class wt% of Particle	Examples of Identified Compounds	μmol Compound/mol CO		% Compound in Gas Phase
			Gas Phase	Particles	
Particles				4.22 ± 0.82 g/mol CO	
Mutagenicity				6.47 ± 1.15 revertants/μmol CO	
Alkanes/alkenes	3.6 ± 0.5	phytadiene	. . .[a]	138 ± 13	. . .[a]
		n-Hentriacontane	. . .[a]	93 ± 29	. . .[a]
		1,3-Butadiene	3100 ± 850	. . .[a]	100
		isoprene	19 200 ± 5600	. . .[a]	100
		solanesol	0	219 ± 43	0
Bases	10.9 ± 1.2	nicotine	12 500 ± 3600	393 ± 150	98.3 ± 1.4
		myosmine	375 ± 38	14.7 ± 1.7	96.1 ± 0.9
		nicotyrine	16 ± 6	10.6 ± 3.3	60 ± 20
		cotinine	18.2 ± 9.4	17.7 ± 7.0	54.6 ± 12.8
		pyridine	1180 ± 72	<5	100
		3-Ethenylpyridine	1370 ± 460	<5	100
		2-Ethenylpyridine	207 ± 36	<5	100
N-Nitrosoamines	<0.1	-nornicotine	1.0 ± 0.5	. . .[a]	. . .[a]
		-dimethylamine	4.4 ± 1.8	. . .[a]	. . .[a]
PAH	<0.1	pyrene	0.02 ± 0.01	. . .[a]	. . .[a]
		phenanthrene	0.11 ± 0.02	. . .[a]	. . .[a]
Inorganic	. . .[a]	NO	36 700 ± 3200	0	100
		NO_2	2520 ± 430	0	100
		HNO_3	96 ± 127	92 ± 55	44 ± 24
		HNO_2	4650 ± 1300	54 ± 40	98.7 ± 1.0
		SO_2 × sulfate	71 ± 52	71 ± 40	49 ± 23
		NH_3	51 900 ± 5400	155 ± 34	99.6 ± 0.2
		potassium	0	840 ± 150	0
		calcium	0	340 ± 100	0

[a]Not determined.

as the smoke is diluted into a room, then available data [*2,6*] suggest that about one-half of the generated side-stream particle mass is rapidly lost to the gas phase during dilution and aging in an indoor environment. Gas phase hydrocarbon measurements [*18,35*] and the results of radiotracer labeled experiments [*36,37*] are consistent with this hypothesis. The existence of large amounts of gas phase hydrocarbons that can be readily condensed back to particulate phase material has also been suggested by chamber experiments involving ultraviolet (UV) radiation or ozone oxidation of side-stream environmental tobacco smoke [*2,18,26,27,34*]. The concentration of particles present in the irradiated side-stream mixture doubles in less than one hour as a result of chemistry induced by the UV radiation. This includes the movement of most of the gas phase nicotine back to the particulate state [*17,18*]. Comparable chemistry apparently occurs [Environmental Protection Agency (EPA), unpublished results] in environments with unvented combustion heaters because of the presence of airborne particulate acids in these environments [*38*]. The gas phase compounds responsible for the UV/ozone oxidation chemistry are not currently known. The identification of gas phase compounds in environmental tobacco smoke may help determine which species are responsible for sensory irritation in sensitive individuals [*39–42*].

Changes During the Aging of Environmental Tobacco Smoke in an Indoor Environment

Environmental tobacco smoke is a complex mixture of gas and particulate phase compounds. During aging of environmental tobacco smoke in an indoor environment, changes in the chemical composition will occur. These changes will include coagulation of particles to alter the particle

size distribution [*17,43,44*], changes in the gas/particle distribution of semivolatile compounds [*18*], and possible chemical changes due to reactions [*18,29,30,34,45–47*]. In addition, the chemical composition of environmental tobacco smoke may be altered during aging in an indoor environment because of differences in the removal rate of various constituents as the environmental tobacco smoke is aged, is recirculated in the indoor environment, and is mixed with outside air [*26,27,34,46,48,49*].

Many gas phase components of environmental tobacco smoke have been shown to be rapidly removed in indoor environments. Several studies have shown that the removal rate of gas phase nicotine and other basic nitrogen compounds is much faster than the removal rates for particles, nonreactive gases such as CO [*13,18–21,25,29,30,32–34,48–52*], NO, gas phase hydrocarbons, or specific particulate phase compounds [*13,21,25,34,47–51,53,54*]. The relative removal rates may depend on local environmental factors such as wall coverings, furnishings, presence or absence of people, air flow, and so on. Thus, environmental tobacco smoke will be a constantly changing mixture due to loss of material as a result of adsorption or decomposition, and due to changes in gas/particulate phase equilibria for volatile species.

The effect of the differential loss of various constituents in environmental tobacco smoke in typical indoor environments on the relative composition of various species is best illustrated by comparing the concentrations of nicotine to fine particulate matter in both controlled and indoor atmospheres. The ratio of RSP to total nicotine has been reported by several investigators. Experiments conducted in chambers with inert walls or in experiments with minimal residence time of the generated side-stream smoke [*18,25,31,32,49,55*] give a ratio of about 2 to 4 g RSP/g nicotine in diluted side-stream tobacco smoke. Values determined in side-stream smoke emissions vary from 2 to 6 g RSP/g nicotine [*7,56–58*] with the higher values probably resulting from partial loss of some nicotine to the gas phase during sample collection on a filter [*28,55*]. The studies of environmental tobacco smoke conducted in non-TFE-fluorocarbon chambers give higher ratios of RSP to nicotine, probably because of the more rapid removal of gas phase nicotine by chamber components [*19,25,33,34,49–55*]. Results from decay studies in chamber or controlled environment experiments are shown in Fig. 1. The ratio of nicotine/RSP increases slightly with time in experiments conducted in a TFE-fluorocarbon chamber [*17,18*] because gas phase nicotine is stable in this environment, but the concentration of particles decreases by evaporation and by loss of particles to the chamber walls. In all the other study environments, the rate of decay of gas phase nicotine is significantly greater than the rate of loss of particles.

Steady-state experiments in other ventilated chambers with individuals present or in well controlled experimental indoor environments give values of around 10 to 15 g RSP/g nicotine [*16,32,34,48,59–61*]. This ratio is larger than would be seen if people (and the accompanying absorptive surfaces) were not present. For example, in studies in the chamber at the U.S. Environmental Protection Agency (EPA) [*32*], the ratio of RSP to nicotine when the chamber had people in it was 13 g RSP/g nicotine. In the empty chamber, the ratio was determined to be 3.0 g RSP/g nicotine, a ratio consistent with the value obtained for side-stream smoke [*7,56–58*] and in inert chambers [*17,18,49,55*]. It has been suggested that nicotine may be a good tracer of environmental tobacco smoke particles in indoor environments [*9,16,38*]. However, experiments conducted in indoor environments indicate that the observed ratio of particles to nicotine present in atmospheres dominated by smoking varies from 3 to 80 g RSP/g nicotine [*16,19,32,49–51,57,62–72*] (Fig. 2). The data from recent studies where nicotine was collected after a TFE-fluorocarbon-coated filter [*69,73*] are not included in Fig. 2 since the data appears to be outliers to the rest of the literature. In the study by Mumford et al. [*73*], PM_{10} and nicotine were not correlated in homes with smokers. It is possible that the data were affected by removal of nicotine in the inlet of the sampling system [*28*] or by the filter [*32*].

The ratio of RSP to nicotine for the data in Fig. 2 generally increases with increased residence time and decreased total nicotine concentrations, or both. This same trend is observed for the limited data that are available on concentrations of nicotine and concentrations of UV-PM [*50,75–*

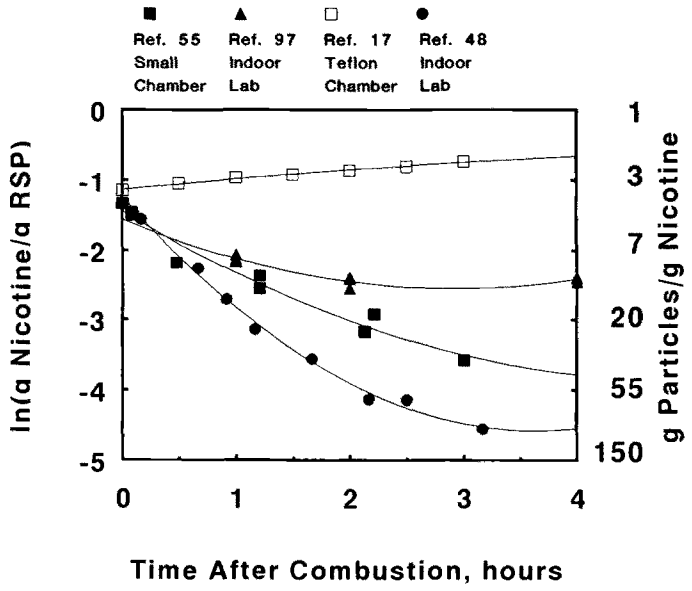

FIG. 1—*Change in the ratio of nicotine to RSP with time in chamber and controlled indoor experiments. Data are from the indicated references.*

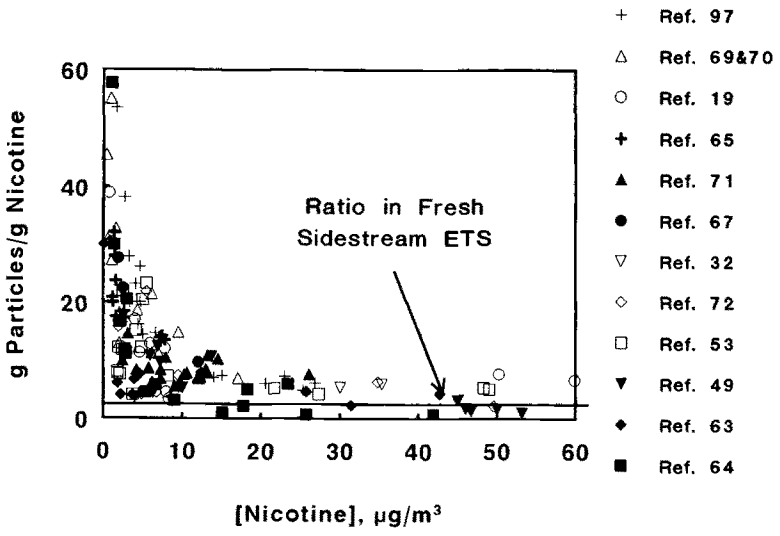

FIG. 2—*The ratio of RSP to nicotine as a function of nicotine concentration in indoor environments. Data are from the indicated references.*

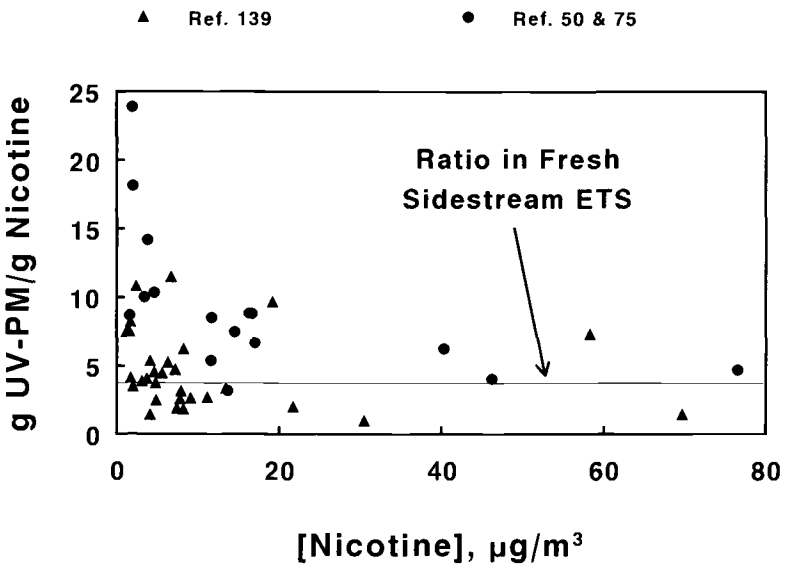

FIG. 3—*The ratio of UV-PM measured RSP to nicotine as a function of nicotine concentration in indoor environments. Data are from the indicated references.*

77] (Fig. 3). UV-PM is a measure of UV adsorption by a methanol extract of collected particulate matter. The resulting measure is referred to as UV-PM (UV-determined particulate matter). The UV-PM measurement is believed to be indicative of the RSP originating from environmental tobacco smoke [*78*]. Because of the rapid removal of nicotine from indoor environments, the use of nicotine as a tracer and of nicotine and its metabolites, cotinine and 3-hydroxycotinine, as biological markers for determining exposure to environmental tobacco smoke in studies of passive smoking has been questioned [*1,2,6,19,21,49*]. It has been argued that a direct plot of nicotine versus RSP, rather than the plot shown in Fig. 2, is a better measure of the use of nicotine as a surrogate for ETS particles. However, such a plot ignores the removal effects illustrated in Figs. 1 and 3, places greatest emphasis on environments with high exposure, and overestimates nonenvironmental tobacco smoke particles. The measurement of gas phase nicotine or even total nicotine will probably underestimate exposure to the particulate phase and possibly other components of environmental tobacco smoke. The predicted exposure to non-nicotine components in environmental tobacco smoke will be dependent on the comparability of the nicotine ratios to RSP in the indoor and other component data sets. The scatter in the data given in Figs. 2 and 3 indicate the magnitude of this underestimation could be a factor of 2 to 5 at nicotine concentrations of <10 μg nicotine/m^3 normally seen in indoor environments.

There are a few studies that report changes in the chemical composition of environmental tobacco smoke as it ages in an indoor environment. In the absence of external oxidizing agents or UV light, NO in environmental tobacco smoke is only very slowly converted to NO_2, HNO_2, and possible organic nitrogen-oxide compounds [*17,26,27,46*]. In the presence of a strong UV light source, this conversion is rapid [*17,26,27*]. In addition, under these extreme conditions, the photochemistry leads to the doubling of total particulate matter, the reduction of gas phase basic compounds, loss of solanesol, and photochemical alterations in the N-containing bases of environmental tobacco smoke [*17,18,26,27,34,47*]. Changes also occur in the composition of nitroso- and nitro-organic compounds upon exposure of environmental tobacco smoke to UV light or ozone, with some compounds disappearing and new compounds being formed [*26,27*]. The exact chemical

reactions taking place are not known. Under more realistic conditions where some oxidants are introduced into an indoor environment from the ambient air [*26,34*], the same reactions appear to occur but at a somewhat reduced rate.

These changes in environmental tobacco smoke composition over time complicate the assessment of health effects associated with exposure, and may preclude the accurate measurement of human exposure to specific compounds [*8*] without actual measurement of the compounds of interest.

Tracers of Exposure to Environmental Tobacco Smoke

The assessment of environmental tobacco smoke exposure is complicated by the presence of significant amounts of organic material in both the gas and the particulate phase, as well as by changes in the relative composition of the two phases with time. The development of accurate markers for estimating exposure to environmental tobacco smoke will be dependent on the determination of the chemical composition of both the gaseous and particulate components of environmental tobacco smoke, and the elucidation of changes in that composition with time in indoor environments. As summarized in the National Academy of Sciences review [*3*], a suitable tracer for quantifying environmental tobacco smoke exposure should be:

- unique or nearly unique to environmental tobacco smoke;
- easily detected in air, even at low smoking rates;
- similar in emission rate for a variety of tobaccos; and
- in constant proportion to compounds in ETS that affect human health.

One of the major shortcomings of many past studies is that only one measure of exposure to environmental tobacco smoke was determined. Therefore, there is no way to assess whether the concentration of the species studied is (or is not) related to the components in environmental tobacco smoke that may be hazardous to health.

Chemical tracers of environmental tobacco smoke frequently used to assess exposure in the past have included RSP, CO, NO_x, and nicotine. Recent reviews of environmental tobacco smoke studies by the National Academy of Sciences [*3*] and the U.S. Surgeon General [*5*] reach the same conclusion: the only tracers previously used in large studies that may be related to actual exposure to environmental tobacco smoke are concentrations of nicotine and RSP [*9*].

CO and NO_x as Tracers of Environmental Tobacco Smoke

Components of environmental tobacco smoke that are not specific to ETS, but which have been used to assess exposure to environmental tobacco smoke, include CO [*5,42,65,79–82*] and NO_x [*5,42,61*]. Both of these gases can be measured in indoor environments by a variety of techniques as illustrated in the referenced articles. Comparison of the chemical composition of environmental tobacco smoke in chamber experiments (Table 1) [*17,18,25,31,80,83*], and the relationship between CO concentrations and other constituents of environmental tobacco smoke in indoor environments suggests that the majority of the CO in indoor environments comes from sources other than environmental tobacco smoke.

Chamber experiments show the ratio of CO to RSP in environmental tobacco smoke is about 0.2 to 0.4 mol CO/g RSP (Table 1) [*18,31,80,83*]. The ratio of CO to RSP in restaurants impacted by modest levels of smoking has been reported to average about 4 [*65*] and 1.0 [*84*], and in a variety of homes and offices where smoking occurred at modest levels, the ratio of CO to RSP varies from 0.4 to 6 and averages 2 [*9*]. Even in environments such as taverns, discos, bus terminals, and restaurants, where the major source of particulate matter is from smoking, the CO to

RSP ratio varies from 0.4 to 1.5 and averages 0.7 mol CO/g RSP [*19,80,83*]. These ratios are all higher than seen in controlled chamber experiments. Measurements in restaurants of CO and UV-PM (a measure of particulate matter more specific to ETS, see next section) give a ratio of CO to UV-PM of 1.7 mol CO/g RSP [*84*], a ratio about five times that expected from environmental tobacco smoke. The recent study of environmental tobacco smoke in restaurants [*84*] included the determination of CO in the outdoor environment. The outdoor CO concentrations averaged about half of the indoor CO concentrations. Correcting the indoor restaurant data for the measured outdoor concentrations gives a minimum ratio of non-ambient CO to UV-PM of 0.9 mol CO/g UV-PM, about three times the expected ratio. All of these studies taken together show that the majority of the CO in indoor environments comes from sources other than environmental tobacco smoke. Similarly, the ratio of NO_x to RSP reported in indoor environments varies from values comparable to that found in environmental tobacco smoke to ratios that are higher by factors of up to 10 [*6,19*]. In addition, NO and NO_x have been shown to be only weakly correlated with CO from environmental tobacco smoke, even in a controlled indoor environment [*61*]. The results available to date show that the use of CO and NO_x concentrations as surrogates for ETS will significantly overestimate exposure to environmental tobacco smoke [*2,6*].

Nicotine and Nicotine Metabolites

The only tobacco specific compound that has been used extensively in the past to determine exposure to environmental tobacco smoke is nicotine [*9,16,19,21,32,49–52,59,60,62–69,71,73,77,81,82,84–94*]. It might be expected that determination of the concentration of nicotine in an indoor environment would give a good measure of exposure to environmental tobacco smoke. The use of nicotine as a tracer of environmental tobacco smoke is complicated because nicotine is found primarily in the gas phase [*18,25,28,59,60*] and because gaseous nicotine is removed at a faster rate than particulate phase nicotine or the particulate portion of ETS [*19,21,33,34,49,50*]. Thus, the concentration of gas phase nicotine underestimates exposure to the particulate phase of environmental tobacco smoke and possible to the concentration of many gas phase environmental tobacco smoke constituents [*33,34*], for example, see Figs. 2 and 3 and related discussion in text.

Estimation of exposure to environmental tobacco smoke based on the determination of nicotine has been done both by determining airborne concentrations of nicotine and also by determining the concentration of nicotine and its principal metabolite, cotinine, in body fluids [*4,63,66,88,89,95–129*]. Inhaled nicotine in environmental tobacco smoke is efficiently absorbed by the nonsmoker [*130*]. However, studies in which exposure has been determined by the use of questionnaires and dose measured by urine levels of nicotine and cotinine [*96,99,102–104,109–111,115–117,123*] have generally yielded poor correlations between exposure and dose.

In contrast, studies that have determined urine clearance of nicotine and cotinine, or both, and have also directly measured nicotine [*63,66,88,103,104,114,117,119,128*] or ETS [*88,121*] exposure have yielded much better correlations when the exposure occurred over a well-defined time period, and the urinary cotinine measurements were made over time intervals that are long compared to the rate of clearance of the compounds from the body [*88,97,101,114,119,128,132–136*], for example, see Fig. 4. The data in Fig. 4 have a linear regression slope of 0.12 ± 0.03 nmol cotinine/nmol nicotine with $r^2 = 0.92$. With a proper study design, nicotine exposure can be estimated reasonably well from cotinine data [*103*]. More frequently, the correlation between dose and exposure has been poor because the relationship between time of exposure and time of dose assessment was not known or controlled [*133,136*]. However, determination of exposure to ETS by measurement of gas phase (or total) nicotine probably underestimates exposure to many components of environmental tobacco smoke in most indoor environments. As discussed above, this

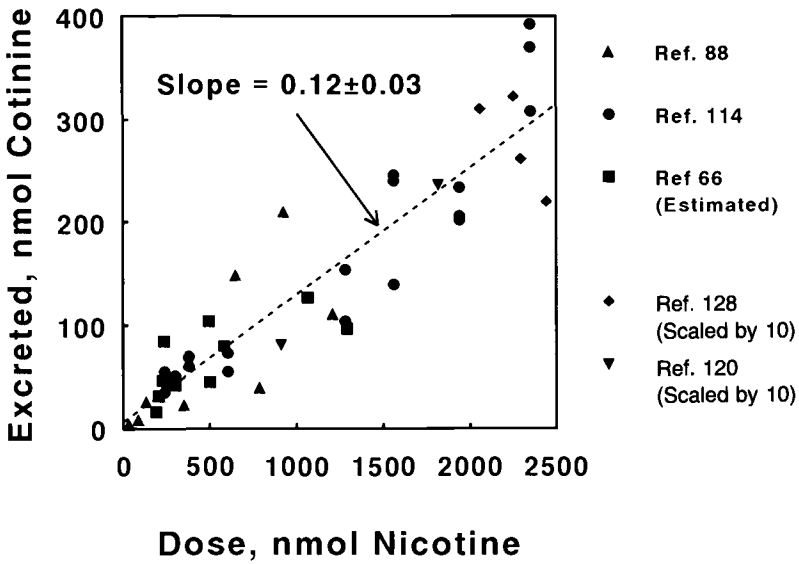

FIG. 4—*Cotinine versus measured exposure to atmospheric nicotine. Data are from the indicated references.*

is due to the rapid removal of gas phase nicotine as compared to many other constituents of environmental tobacco smoke. The usefulness of nicotine and cotinine as biomarkers of exposure to constituents of environmental tobacco smoke is limited by the viability of nicotine itself as a surrogate for environmental tobacco smoke.

Respirable Particulate Matter

Total RSP is the tracer for environmental tobacco smoke most extensively used in past studies [*3,5,9,16,137*] because of the ease with which it may be measured [*43,137*]. Even though RSP is elevated in environments where smoking is present, about one half of the RSP in these indoor environments comes from sources other than environmental tobacco smoke. Thus, RSP overestimates exposure to environmental tobacco smoke [*19,77,81,82,84,87,138*]. The measurement will be even more insensitive for the determination of ETS exposure as controls are implemented and the concentration of tobacco smoke decreases in controlled environments.

A technique that has the promise of being specific for particulate matter from environmental tobacco smoke is based on the measurement of the UV absorption of a methanol extract of the collected particulate matter [*50,77,78,82,84,139*]. The UV-PM measurement is better correlated with the estimated amount of environmental tobacco smoke than is the corresponding measurement of nicotine [*2,139*]. The measurement of UV-PM may provide a specific measure of particulate matter from only environmental tobacco smoke but additional work needs to be done to determine if other sources of RSP may contribute to the UV-PM concentrations.

Particulate Mutagens

Studies of particulate mutagens in indoor atmospheres suggest that environmental tobacco smoke may be the principal source of mutagenic compounds in particles present in indoor atmosphere [*32,66,73,83,140–144*]. While there are many potential sources of mutagens in the environment

[*145–148*], current data suggest that environmental tobacco smoke is the principal source of particulate mutagens in indoor environments, and that the emission rate of mutagenic material in the particulate phase of environmental tobacco smoke is constant [*32,83,73,144*]. The mutagenic activity of particulate matter in rooms where smoking is occurring is much higher than concentrations seen in the absence of smoking. The mutagenic activity is correlated with the number of cigarettes smoked [*73,83,143*] and is consistent with the results of chamber experiments [*32*]. However, the determination of particulate mutagens in indoor environments requires the use of specialized microsuspension techniques [*32,83,140,143,149*].

McCurdy, et al. [*68*] and Kado, et al. [*142*] have reported on the simultaneous determination of the mutagenicity of particulate matter, concentrations of RSP, and concentrations of nicotine in a bingo parlor and in a casino. Similar measurements have been made in residential environments with and without smoking present [*73,140*]. A comparison of the observed concentrations of RSP and mutagens [*6,32,66,68,73,83,140,150*] indicates that, in the environments studied, there is a background of nonmutagenic particulate matter of about 40 $\mu g/m^3$ (the data from Ref *73* have been corrected for an observed non-ETS mutagenic background) with increasing mutagenicity of the particulate matter as the concentration of environmental tobacco smoke RSP increases (Fig. 5). The mutagenicity of this ETS-RSP agrees with the mutagenicity of ETS determined in chamber studies [*32,83,144,149*]. The data also indicate that nicotine from environmental tobacco smoke is lost more rapidly than either RSP or mutagenicity in the indoor environment, and that the concentration of nicotine leads to an underestimation of environmental tobacco smoke particles and particulate mutagenicity [*6*]. The loss of nicotine may also explain the lack of correlation of RSP mutagenicity with biological measures of exposure, that is, urine concentrations of cotinine and nicotine in the population studied [*68*]. Further studies on the potential use of mutagenicity as a measure of exposure to environmental tobacco smoke are needed. It should be noted that urine mutagenicity cannot be used to asses exposure [*3,122,124,150,151*] because of the effect of other sources of mutagens, such as diet.

Other Potential Conservative Tracers of Environmental Tobacco Smoke

The fourth criteria from the National Academy of Sciences review of environmental tobacco smoke [*3*] listed in the introduction to this section on ETS tracers requires that a tracer for assessing exposure to environmental tobacco smoke be present in the indoor atmosphere in constant proportion to compounds in environmental tobacco smoke that affect human health. The tracer that has been emphasized in studies conducted to the present is gas phase nicotine. While gas phase nicotine meets the requirements of being unique to ETS, being easily measurable in the environment, and having a similar emission rate for many commercial brands of cigarettes, the concentration of nicotine relative to most other constituents of environmental tobacco smoke is not constant in an indoor environment. The initial data available on the two tracers, UV-PM [*50,78,139*] and particulate mutagens [*6,32,66,68,83,97,140*], indicate that these may be conserved relative to most components of environmental tobacco smoke in an indoor environment. It is not clear, however, that the measurement of these two tracers will be unique to environmental tobacco smoke, especially at low concentrations of emission and subsequent exposure to a population. In addition, neither of these two tracers can be used to develop techniques for the assessment of biomarkers for determining human dose. Additional tracers are needed.

The results from studies by Brigham Young University [*19,21,34,48,50*] and others [*21*] and a large study by R. J. Reynolds Tobacco Company [*33*] suggest that 3-ethenylpyridine may be a conservative tracer of environmental tobacco smoke in indoor environments. This compound is present at about the concentration expected relative to environmental tobacco smoke particulate matter in a variety of indoor environments [*19,21,34,50*].

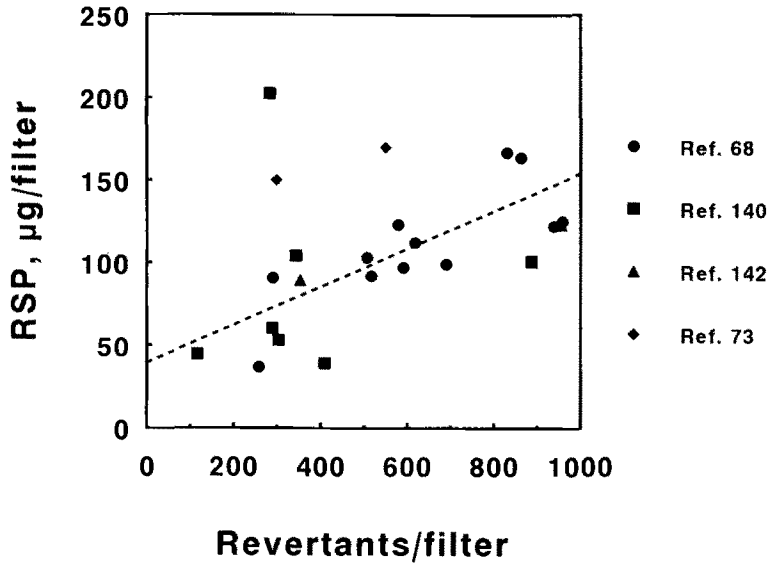

FIG. 5—*Plot of revertants/filter versus concentrations of RSP in environments with environmental tobacco smoke. Data are from the indicated references.*

It has been suggested that the amount of 3-ethenylpyridine observed to be present in experiments in a TFE-fluorocarbon chamber [*17,18*] was not related to the number of cigarettes burned [*8*]. However, this conclusion is based on a faulty interpretation of the chamber data. The ratio of 3-ethenylpyridine to the most stable constituent in the chamber experiments, CO, was independent of the number of cigarettes smoked. The ratio relative to RSP decreased with increasing the number of cigarettes smoked because the mass (relative to CO) increased with an increasing number of cigarettes as the equilibrium position for semivolatile organic compounds shifted towards the particulate phase with increasing concentrations of material in the chamber. The chamber data predict a ratio of 3-ethenylpyridine to environmental tobacco smoke RSP of 0.32 ± 0.08 nmol 3-ethenylpyridine/µg of ETS RSP.

The ratio seen in indoor environments with environmental tobacco smoke present is comparable to this expected value of 0.32 ± 0.08 nmol 3-ethenylpyridine/µg of ETS RSP. The ratio seen in experiments in the Pierce Laboratory experimental chamber [*47*] is 0.43 ± 0.06 nmol 3-ethenylpyridine/µg of ETS RSP. In environments with high concentrations of environmental tobacco smoke (discos [*19*]) the determined ratio was 0.20 ± 0.04 nmol 3-ethenylpyridine/µg of ETS RSP. In offices where smoking is present [*19*], the measured ratio was 0.35 ± 0.10 nmol 3-ethenylpyridine/µg of ETS RSP. These various ratios differ by a maximum of a factor of two. In contrast, the relative amount of nicotine present in indoor environments is lower by a factor of two to five than that expected, based on chamber experiments because of the selective loss of gas phase nicotine. The potential use of 3-ethenylpyridine as a tracer of RSP in environmental tobacco smoke should be studied further. 3-Ethenylpyridine is present only in the gas phase in the indoor environment and may be determined using passive sampling devices [*18*], diffusion denuders [*18,19,50*], or sorbent beds [*29,30,34*]. In fresh environmental tobacco smoke there is about nine times as much nicotine as 3-ethenylpyridine (Table 1). However, because of the selective loss of gas phase nicotine in indoor environments, the concentration of gas phase 3-ethenylpyridine in indoor environments is comparable to the concentration of gas phase nicotine [*19,21,34,50*]. 3-

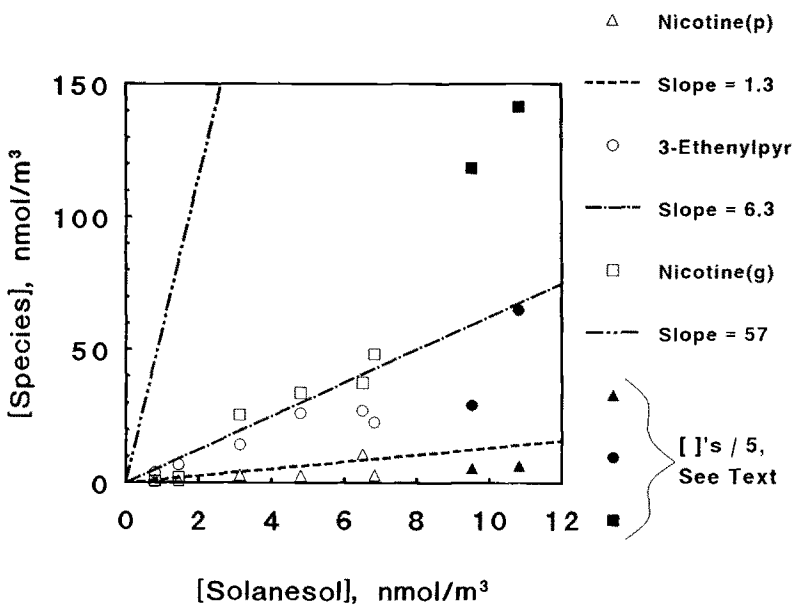

FIG. 6—*Concentrations of solanesol versus nicotine, 3-ethenylpyridine, and particulate nicotine in an office building with smokers present. The solid lines are the mole ratios to solanesol expected for each species based on the results given in Table 1. Data are from Refs* 19 *and* 47.

Ethenylpyridine may be determined with a detection limit comparable to that for nicotine using similar sampling systems.

A compound unique to the particulate phase of environmental tobacco smoke that should be studied as a potential tracer is solanesol [*21,47,152–154*]. Solanesol, (3,7,11,15,19,23,27,31,35-Nonamethyl-2,6,10,14,18,22,26,30,34-Hexatriacontanonaen-1-ol),

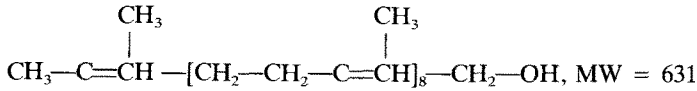

is a trisesquiterpenoid of trans-isoprene units that is present at about 3 wt% in the particles from environmental tobacco smoke (Table 1). The large molecular weight ensures that it will be present only in the particulate phase in environmental tobacco smoke. The compound can be collected by conventional indoor sampling systems and determined by gas chromatography [*47,61,153,154*], or supercritical fluid chromatography [*47*]. The limited data available to date [*21,61,47,91,152–154*], indicate that the concentration of solanesol in environmental tobacco smoke particles is conserved in the environment.

The concentrations of gas and particulate phase nicotine, and gas phase 3-ethenylpyridine are compared in Fig. 6 to concentrations of solanesol for experiments conducted in an office building [*19,47*]. The solid data points (concentrations on both the x and y axes divided by 5 in Fig. 6) were obtained in smoking offices and the open data points were obtained in other rooms in the office wing where no smoking occurred. The lines in Fig. 6 correspond to the mole ratio of nicotine(g) (57), 3-ethenylpyridine (6.3) and nicotine(p) (1.3) to solanesol expected in ETS based

on the data given in Table 1. The reasonable agreement between the ratio of 3-ethenylpyridine or particulate phase nicotine and ETS particulate phase solanesol with the ratio expected from the composition of fresh side-stream smoke is apparent. This agreement between observed and expected ratios is seen in both the rooms with smoking and in the rooms with recirculated air. In contrast, the effect of selective loss of gas phase nicotine from environmental tobacco smoke is apparent. Additional work on the use of 3-ethenylpyridine and solanesol as tracers of environmental tobacco smoke would appear to be warranted.

Two recent reports by Löfroth et al. [*32*] and Brunnemann et al. [*85*] of chamber studies of environmental tobacco smoke suggest that isoprene may be used as a gas phase tobacco smoke tracer in indoor environments. The amount of isoprene emitted in side-stream smoke is comparable to the amount of nicotine produced (Table 1). In addition, samples collected indoors and outdoors of a tavern indicate that background concentrations of isoprene may be negligibly small compared to the indoor concentration from environmental tobacco smoke [*32*]. Equally important, the ratio of isoprene to RSP, nicotine or particulate mutagenicity from environmental tobacco smoke in taverns [*32,85*] was comparable to that observed in the chamber studies. Additional work needs to be done in indoor environments with lower concentrations of environmental tobacco smoke to determine if isoprene is a conservative tracer and to establish if other sources, such as vegetation, may be significant.

Questionnaires as a Tool to Assess Exposure to Environmental Tobacco Smoke

Retrospective evaluation of exposure to environmental tobacco smoke by the use of questionnaires has been the principal research tool used in epidemiological studies [*3,5,12,86,96,155–157*]. The accuracy of relationships between responses to these questionnaires and the actual past exposure to environmental tobacco smoke is difficult to evaluate. However, errors in classifying smokers versus non- and never-smokers by this approach will generally result in the overestimation of health effects associated with environmental tobacco smoke due to misclassification and other effects [*3,9,109,158–161*]. Comparisons of estimated exposure from questionnaire data and from measured exposure to nicotine and respirable particles [*62,86,139,159*], or from measured concentrations of urinary [*62,96,109,162*] or salivary [*109,125*] cotinine give only modest correlation coefficients, indicating that better measures of long-term exposure are desirable. The actual exposure to environmental tobacco smoke in any given indoor environment will be a complex function of the rate of smoking, proximity to the smoker, room size and ventilation, and other factors generally not available in a data set [*86*]. When these factors are taken into account [*86*], the prediction of exposure from questionnaire data is significantly improved. Misclassification may occur in questionnaire results. For example, the relationship between questionnaire measured exposure to environmental tobacco smoke and measured urinary cotinine in primary school children [*96*] yielded a dose-response relationship (Fig. 7), but the high concentrations observed for the "no exposure" group indicates that misclassification is common in the data set [*125*], making quantification of the results difficult. While relationships between responses to questionnaires and the actual past exposure (either short- or long-term) is difficult to evaluate, questionnaires will continue to be the principal research tool for evaluating long-term exposure, as no other techniques are presently available.

Summary

Concentrations of nicotine and RSP in indoor environments have been extensively used to assess exposure to environmental tobacco smoke in past studies. Determination of these species provides an adequate measure of exposure in environments with heavy smoking. However, in environments

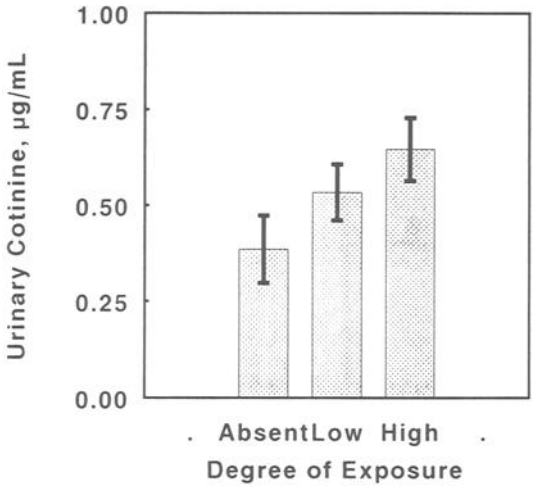

FIG. 7—*Questionnaire and urinary cotinine determined exposure of primary school children to environmental tobacco smoke. Data are from Ref* 96.

where the exposure is moderate to light, nicotine will tend to underestimate exposure to environmental tobacco smoke due to the selective loss of this species in indoor environments and RSP will overestimate exposure due to confounding sources. The potential magnitude of the exposure assessment error is probably about a factor of two to five underestimation for nicotine and a factor of about two overestimation for RSP. The use of cotinine as a biomarker for determining exposure to environmental tobacco smoke will be limited by the variability in nicotine as a marker of exposure. In spite of these shortcomings, these species are currently the best measures of exposure with well developed protocols for their use.

Gas phase 3-ethenylpyridine and isoprene, and particulate phase solanesol may be excellent tracers for assessing exposure to environmental tobacco smoke. However, the viability of these compounds as tracers for measuring exposure to environmental tobacco smoke has not yet been extensively tested. The relationships among these compounds, and between these compounds and other constituents of environmental tobacco smoke in indoor environments needs to be estabished. If 3-ethenylpyridine and isoprene, or both, are shown to be conservative tracers for both many gas phase constituents and for the particulate phase of environmental tobacco smoke, then these compounds could possibly serve as the basis for a tobacco specific passive monitor or for a biomarker for assessing exposure to environmental tobacco smoke.

References

[1] Guerin, M. R., Jenkins, R. A., Tomkins, B. A., *The Chemistry of Environmental Tobacco Smoke: Composition and Measurement*, M. Eisenberg, Ed., Indoor Air Research Series, Center for Indoor Air Research, Lewis Publishers, Boca Raton, 1992.

[2] Eatough, D. J., Hansen, L. D., and Lewis, E. A., "The Chemical Characterization of Environmental Tobacco Smoke," *Environmental Tobacco Smoke*, Proceedings of the International Symposium at McGill University, 1989, D. J. Ecobichon and J. M. Wu, Eds., Lexington Books, 1990, pp. 3–39.

[3] National Research Council, "Environmental Tobacco Smoke. Measuring Exposure and Assessing Health Effects," *National Research Council*, National Academy Press, Washington, DC, 1986, 337 pages.

[4] Proctor, C. J., Warren, N. D., Bevan, M. A. J., and Baker-Rogers, J., "A Comparison of Methods of Assessing Exposure to Environmental Tobacco Smoke in Non-Smoking British Women," *Environment International*, Vol. 17, pp. 287–297.

[5] U.S. Department of Health and Human Services, "The Health Consequences of Involuntary Smoking," *A Report of the Surgeon General*, U.S. Department of Health and Human Services, Washington, DC, 1986, 332 pages.

[6] Eatough, D. J., Hansen, L. D., and Lewis, E. A., "Methods for Assessing Exposure to Environmental Tobacco Smoke," *Combustion Processes and the Quality of the Indoor Environment*, Air and Waste Management Association, Jerome P. Harper, Ed., Niagara Falls, NY, 1989, pp. 183–200.

[7] Guerin, M. R., Higgins, C. E., and Jenkins, R. A., "Measuring Environmental Emissions from Tobacco Combustion: Sidestream Cigarette Smoke Literature Review," *Atmospheric Environment*, Vol. 21, No. 12, 1987, pp. 291–297.

[8] Hammond, S. K., "Evaluating Exposure to Environmental Tobacco Smoke," *Sampling and Analysis of Airborne Pollutants*, E. D. Winegar and L. H. Keith, Eds., Lewis, Ann Arbor, 1993, pp. 319—338.

[9] Leaderer, B. P., "Assessing Exposures to Environmental Tobacco Smoke," *Risk Analysis*, Vol. 10, 1990, pp. 19–26.

[10] Reasor, M. J., "The Composition and Dynamics of Environmental Tobacco Smoke," *Journal of Environmental Health*, Vol. 50, 1987, pp. 20–24.

[11] O'Neill, I. and Riboli, E., "IARC Approaches to Monitoring Exposure of Passive Smoking," *Toxicology Letters*, Vol. 35, 1987, pp. 29–33.

[12] *Environmental Carcinogens Methods of Analysis and Exposure Measurement*, IARC Scientific Publications 81, O'Neill, I. K., Brunneman, K. D., Doden, B., and Hoffmann, D., Eds., International Agency for Research on Cancer, Oxford University Press, Lyon, 1987.

[13] Baker, R. R. and Proctor, C. J., "The Origins and Properties of Environmental Tobacco Smoke," *Environment International*, Vol. 16, 1990, pp. 231–245.

[14] Baker, R. R., "Mechanisms of Smoke Formation and Delivery," *Recent Advances in the Tobacco Sciences*, Vol. 6, 1980, pp. 184–224.

[15] Brunnemann, K. D. and Hoffmann, D., "The pH of Tobacco Smoke," *Food Cosmetics Toxicology*, Vol. 12, 1974, pp. 115–124.

[16] Leaderer, B. P. and Hammond, S. K., "Evaluation of Vapor-Phase Nicotine and Respirable Suspended Particle Mass as Markers for Environmental Tobacco Smoke," *Environmental Science and Technology*, Vol. 25, 1991, pp. 770–777.

[17] Benner, C. L., Bayona, J. M., Lee, M. L., Lewis, E. A., Hansen, L. D., Eatough, N. L., and Eatough, D. J., "The Chemical Composition of Environmental Tobacco Smoke. II. Particulate-Phase Compounds," *Environmental Science and Technology*, Vol. 23, 1989, pp. 688–699.

[18] Eatough, D. J., Benner, C. L., Bayona, J. M., Caka, F. M., Richards, G., Lamb, J. D., Lewis, E. A., and Hansen, L. D., "Chemical Composition of Environmental Tobacco Smoke. I. Gas-Phase Acids and Bases," *Environmental Science and Technology*, Vol. 23, 1989, pp. 679–687.

[19] Eatough, D. J., Benner, C. L., Tang, H., Landon, V., Richards, G., Caka, F. M., Crawford, J., Lewis, E. A., Hansen, L. D., and Eatough, N. L., "The Chemical Composition of Environmental Tobacco Smoke. III. Identification of Conservative Tracers of Environmental Tobacco Smoke," *Environment International*, Vol. 15, 1989, pp. 19–28.

[20] Eatough, D. J., Benner, C. L., Bayona, J. M., Caka, F. M., Tang, H., Lewis, L., Lamb, J. D., Lee, M. L., Lewis, E. A., and Hansen, L. D., "Sampling for Gas Phase Nicotine in Environmental Tobacco Smoke with a Diffusion Denuder and a Passive Sampler," *Proceedings*, 1987 EPA/APCA Symposium on Measurement of Toxic and Related Air Pollutants, Research Triangle Park, NC, 1987, pp. 132–139.

[21] Neurath, G. B., Petersen, S., Duenger, M., Orth, D., Pein, F. G., "Gas-Particulate Phase Distribution and Decay Rates of Constituents in Ageing Environmental Tobacco Smoke," *Environment Technology*, Vol. 12, 1991, pp. 581–590.

[22] Sakuma, H., Kusama, M., Munakata, S., Obsumi, T., and Sugawara, S., "The Distribution of Cigarette Smoke Components between Mainstream and Sidestream Smoke. I. Acidic Components," *Beit. Tabakfors. International*, Vol. 12, 1983, pp. 63–71.

[23] Eatough, D. J., Benner, C., Mooney, R. L., Bartholomew, D., Steiner, D. S., Hansen, L. D., Lamb, J. D., and Lewis, E. A., "Gas and Particle Phase Nicotine in Environmental Tobacco Smoke," Paper 86-68.5, *Proceedings*, 79th Annual Meeting of the Air Pollution Control Association, 22–27 June, Minneapolis, MN, 1986.

[24] Eudy, L. W., Thome, F. A., Heavner, D. K., Green, C. R., and Ingebrethsen, B. J., "Studies on the Vapor-Particulate Phase Distribution of Environmental Nicotine by Selective Trapping and Detection Methods," Paper 86-38.7, *Proceedings*, 79th Annual Meeting of the Air Pollution Control Association, Minneapolis, MN, 1986.

[25] Thome, F. A., Heavner, D. L., Ingebrethsen, B. J., Eudy, L. W., and Green, C. R., "Environmental Tobacco Smoke Monitoring with an Atmospheric Pressure Chemical Ionization Mass Spectrometer/Mass Spectrometer Coupled to a Test Chamber," Paper 86-37.6, *Proceedings*, 79th Annual Meeting of the Air Pollution Control Association, 23–27 June, Minneapolis, MN, 1986.

[26] Eatough, D. J., "SFE/SFC Determination of Gas and Particulate Phase Compounds in Environmental Tobacco Smoke," Final report submitted to CIAR, March 1992.

[27] Eatough, D. J., Francis, E. S., Lewis, E. A., and Lee, M. L., "Determination of Nitrogen Containing Compounds in Environmental Samples by Supercritical Fluid Separation," *Measurement of Toxic and Related Air Pollutants*, Proceedings, 1991 EPA/AWMA International Symposium, Vol. 1, 1991, pp. 799–804.

[28] Caka, F. M., Eatough, D. J., Lewis, E. A., Tang, H., Hammond, S. K., Leaderer, B. P., Koutrakis, P., Spengler, J. D., Fasano, A., Ogden, M. W., and Lewtas, J., "An Intercomparison of Sampling Techniques for Nicotine in Indoor Environments," *Environmental Science and Technology*, Vol. 24, 1990, pp. 1196–1203.

[29] Tang, H., Richards, G., Gunther, K., Crawford, J., Lee, M. L., Lewis, E. D., and Eatough, D. J., "Determination of Gas Phase Nicotine and 3-Ethenylpyridine and Particulate Phase Nicotine in Environmental Tobacco Smoke with a Collection Bed-Capillary Gas Chromatography System," *High Resolution Chromatography and Chromatography Communication*, Vol. 11, 1988, pp. 775–782.

[30] Tang, H., Benner, C. L., Richard, G. H., Lee, M. L., Lewis, E. A., Hansen, L. D., and Eatough, D. J., "Monitoring of Environmental Tobacco Smoke Nicotine with a Sorbent Bed-Capillary Gas Chromatograph System," *International Journal of Environmental Analytical Chemistry*, Vol. 33, 1988, pp. 197–208.

[31] Heavner, D. L., Thome, F. A., Eudy, L. W., Ingebrethsen, B. J., and Green, C. R., "A Test Chamber and Instrumentation for the Analysis of Selected Environmental Tobacco Smoke (ETS) Components," Paper 86-37.9, *Proceedings*, 79th Annual Meeting of the Air Pollution Control Association, Minneapolis, MN, 1986.

[32] Löfroth, G., Burton, R. M., Forehand, L., Hammond, S. K., Sella, R. L., Zwerdinger, R. B., and Lewtas, J., "Characterization of Environmental Tobacco Smoke," *Environmental Science and Technology*, Vol. 23, 1989, pp. 610–614.

[33] Ogden, M. W. and Maiolo, K. C., "Comparative Evaluation of Diffusive and Active Sampling Systems for Determining Airborne Nicotine and 3-Ethenylpyridine," *Environmental Science and Technology*, Vol. 26, 1992, pp. 1737–1740.

[34] Tang, H., Eatough, D. J., Lewis, E. A., Hansen, L. D., Gunther, K., Belnap, D., and Crawford, J., "The Generation and Decay of Environmental Tobacco Smoke Constituents in an Indoor Environment," *Proceedings*, EPA/AWMA Symposium on the Determination of Toxic and Related Air Pollutants, Air and Waste Management Association, Raleigh, NC, May 1989, pp. 596–605.

[35] Ramsey, R. S., Moneyhun, J. H., and Jenkins, R. A., "Generation, Sampling and Chromatographic Analysis of Particulate Matter in Dilute Sidestream Tobacco Smoke," *Analytical Chim. Acta*, Vol. 236, 1990, pp. 213–220.

[36] Pritchard, J. N., Black, A., and McAughey, J. J., "The Physical Behavior of Sidestream Tobacco Smoke under Ambient Conditions," *Environmental Technology Letter*, Vol. 9, 1988, pp. 545–552.

[37] Pritchard, J. N., Black, A., and McAughey, J. J., "The Physical Behavior of Sidestream Tobacco Smoke under Ambient Conditions," *Indoor and Ambient Air Quality*, R. Perry and P. W. Kirk, Eds., Selper, London, 1988, pp. 49–56.

[38] Leaderer, B. P., Boone, P. M., and Hammond, S. K., "Total Particle, Sulfate and Acidic Aerosol Emissions from Kerosene Space Heaters," *Environmental Science and Technology*, Vol. 24, 1990, pp. 908–912.

[39] Cain, W. S., Tosun, T., See, L.-C., and Leaderer, B., "Environmental Tobacco Smoke: Sensory Reactions of Occupants," *Atmospheric Environment*, Vol. 21, 1987, pp. 347–353.

[40] Cain, W. W., Leaderer, B. P., Isseroff, R., Berglund, L. G., Huey, R. J., Lipsitt, E. D., and Perlman, D., "Ventilation Requirements in Buildings—I. Control of Occupancy Odor and Tobacco Smoke Odor," *Atmospheric Environment*, Vol. 6, 1983, pp. 1183–1197.

[41] Weber, A., "Acute Effects of Environmental Tobacco Smoke," *European Journal of Respiratory Disease*, (Supplement 133), Vol. 68, 1984, pp. 98–108.

[42] Weber, A. and Fischer, T., "Passive Smoking at Work," *International Archives of Occupational and Environmental Health*, Vol. 47, 1984, pp. 209–221.

[43] Ingebrethsen, D. J., Heavner, D. L., Angel, A. L., Conner, J. M., Steichen, T. J., and Green, C. R., "A Comparative Study of Environmental Tobacco Smoke Particulate Mass Measurements in an Environmental Chamber," *Journal of the Air Pollution Control Association*, Vol. 38, 1988, pp. 413–417, see also, Ingebrethsen, B. J., TCRC, Knoxville, TN, 13–16 Oct., 1986.

[44] Vu Duc, T. and Huynh, C. K., "Sidestream Tobacco Smoke Constituents in Indoor Air Modelled in an Experimental Chamber," *Toxicology Letters*, Vol. 35, 1987, pp. 59–65.

[45] Browne, C. L., Keith, C. H., and Alka, R. E., *Beitr. Tabak. Forsch.*, Vol. 10, 1980, pp. 81–90.

[46] Eatough, D. J., Lewis, L., Lamb, J. D., Crawford, J., Lewis, E. A., Hansen, L. D., and Eatough, N. L., "Nitric and Nitrous Acids in Environmental Tobacco Smoke," *Proceedings*, 1988 EPA/APCA Symposium on Measurement of Toxic and Related Air Pollutants, 1988, pp. 104–112.

[47] Tang, H., Richards, G., Lee, M. L., Lewis, E. A., Hansen, L. D., and Eatough, D. J., "Solanesol—A Tracer for Environmental Tobacco Smoke Particles." *Environmental Science and Technology*, Vol. 24, 1990, pp. 848–852.

[48] Lewis, E. A., Tang, H., Crawford, J. W., Hansen, L. D., and Eatough, D. J., "A Laboratory for the Study of Environmental Tobacco Smoke Components," Paper 88-76.7, *Proceedings*, 81st Annual Meeting of the Air Pollution Control Association, Dallas, TX, 19–24 June, 1988.

[49] Thompson, C. V., Jenkins, R. A., and Higgins, C. E., "A Thermal Desorption Method for the Determination of Nicotine in Indoor Environments," *Environmental Science and Technology*, Vol. 23, 1989, pp. 429–435.

[50] Eatough, D. J., Caka, F. M., Crawford, J., Braithwaite, S., Hansen, L. D., and Lewis, E. A., "Environmental Tobacco Smoke in Commercial Aircraft," *Indoor Air '90*, Proceedings of the 5th International Conference on Indoor Air Quality and Climate, Toronto, Canada, 29 July–3 Aug. 1990, Vol. 2, 1990, pp. 311–316.

[51] Malmfors, T., Thorburn, D., and Westlin, A., "Air Quality in Passenger Cabins of DC-9 and MD-80 Aircraft," *Environmental Technology Letters*, Vol. 10, 1989, pp. 613–628.

[52] Nagda, N., Fortmann, R., Koontz, M., and Konhein, A., "Investigation of Cabin Air Quality Aboard Commercial Airliners," *Proceedings*, 5th International Conference on Indoor Air Quality and Climate, Toronto, Canada, Vol. 2, 1990, pp. 245–250.

[53] Baker, R. R., Case, P. D., and Warren, N. D., "The Build-Up and Decay of Environmental Tobacco Smoke Constituents as a Function of Room Conditions," *Indoor and Ambient Air Quality*, R. Perry and P. W. Kirk, Eds., Selper Ltd., London, 1988, pp. 121–130.

[54] Brynnel, U. and Löfroth, G., "Environmental Tobacco Smoke in Public Places," *Environmental Hygiene*, III, Springer-Verlag, Heidelberg, in press, 1992.

[55] Badre, R., Guillerm, R., Abran, N., Bourdin, M., and Dumas, C., "Pollution Atmosphérique par le Fumée de Tabac," *Annal. Pharm. Franc.* Vol. 36, 1987, pp. 443–452.

[56] Sakuma, H., Kusama, M., Yamaguchi, K., Matsuki, T., and Sugawara, S., "The Distribution of Cigarette Smoke Components between Mainstream and Sidestream Smoke, II. Bases," *Beit. Tabakfors. Int.*, Vol. 12, 1984, pp. 199–209.

[57] Klus, H. and Kuhn, H., "Verteilung Verschiendener Tabakrauchbestandteile auf Haupt-and Nebenstromrauch," *Beit. Tabakforsch. Int.*, Vol. 11, 1982, pp. 229–265.

[58] Rickert, W. S., Robinson, J. C., and Collishaw, N., "Yields of Tar, Nicotine and Carbon Monoxide in the Sidestream Smoke from 15 Brands of Canadian Cigarettes," *American Journal of Public Health*, Vol. 74, 1984, pp. 228–231.

[59] Hammond, S. K. and Coghlin, J., "Field Study of Passive Smoking Exposure with Passive Sampler," *Indoor Air '87*, Proceedings of the Fourth International Conference on Indoor Air Quality and Climate, Vol. 2, B. Seifert, H. Esdorn, M. Fischer, H. Ruden, J. Wegner, Eds., Berlin (West), 17–21 Aug. 1987, Institute for Water, Soil and Air Hygiene, 1987, pp. 131–136.

[60] Hammond, S. K., Leaderer, B. P., Roche, A. C., and Schenker, M., "Collection and Analysis of Nicotine as a Marker for Environmental Tobacco Smoke," *Atmosphere Environment*, Vol. 21, 1987, pp. 457–462.

[61] Piade, J. J., Gerber, C., and Fink, W., "Assessment of ETS Impact on Office Air Quality, Part 2," *Indoor and Ambient Air Quality*, R. Perry and P. W. Kirk, Eds., Selper Ltd., London, 1988, pp. 594–601.

[62] Coultas, C. B., Samet, J. M., McCarthy, J. F., and Spengler, J. D., "A Personal Monitoring Study to Assess Workplace Exposure to Environmental Tobacco Smoke," *American Journal of Public Health*, Vol. 80, 1990, pp. 988–990.

[63] Coultas, D. B., Samet, J. M., McCarthy, J. F., and Spengler, J. D., "Variability of Measures of Exposure to Environmental Tobacco Smoke in the Home," *American Review of Respiratory Disease*, Vol. 142, 1990, pp. 602–606.

[64] Drake, J. W. and Johnson, D. E., "Measurements of Certain Environmental Tobacco Smoke Components on Long-Range Flights," *Aviation, Space and Environmental Medicine*, Vol. 61, 1990, pp. 531–542.

[65] Eudy, L., Heavner, D., Stancill, M., Simmons, J. S., and McConnell, B., "Measurement of Selected Constituents of Environmental Tobacco Smoke in a Winston-Salem, North Carolina Restaurant," *Indoor Air '87*, Proceedings, of the Fourth International Conference on Indoor Air Quality and Climate, Vol. 2, B. Seifert, H. Esdorn, M. Fischer, H. Ruden, J. Wegner, Eds., Berlin (West), 17–21 Aug. 1987, Institute for Water, Soil and Air Hygiene, 1987, pp. 126–130.

[66] Mattson, M. E., Boyd, G., Byar, D., Brown, C., Callahan, J. F., Corle, D., Cullen, J. W., Greenblatt, J., Haley, N. J., Hammond, S. K., Lewtas, J., and Reeves, W., "Passive Smoking on Commercial Airline Flights," *Journal of the American Medical Association*, Vol. 261, No. 6, 1989, pp. 867–872.

[67] McCarthy, J., Spengler, J., Chang, B-H., Coultas, D., and Samet, J., "A Personal Monitoring Study to Assess Exposure to Environmental Tobacco Smoke," *Indoor Air '87*, Proceedings of the Fourth International Conference on Indoor Air Quality and Climate, Vol. 2, B. Seifert, H. Esdorn, M. Fischer, H. Ruden, J. Wegner, Eds., Berlin (West), 17–21 Aug. 1987, Institute for Water, Soil and Air Hygiene, 1987, pp. 142–146.

[68] McCurdy, S. A., Kado, N. Y., Schenker, M. B., Hammond, S. K., and Benowitz, N. L., "Measurement of Personal Exposure to Mutagens in Environmental Tobacco Smoke," *Indoor Air '87*, Proceedings of the Fourth International Conference on Indoor Air Quality and Climate, Vol. 2, B. Seifert, H. Esdorn, M. Fischer, H. Ruden, J. Wegner, Eds., Berlin (West), Institute for Water, Soil and Air Hygiene, 1987, pp. 91–96.

[69] Miesner, E. A., Rudnick, S. N., Hu, F.-C., Spengler, J. D., Preller, L., Okaynak, H., and Nelson, W., "Particulate and Nicotine Sampling in Public Facilities and Offices," *JAPCA*, Vol. 39, 1989, pp. 1577–1582.

[70] Miesner, E. A., Rudnick, S. N., Hu, F.-C., Spengler, J. D., Preller, L., Okaynak, H., and Nelson, W., "Aerosol and ETS Sampling in Public Facilities and Offices," Paper 88-76, *Proceedings*, Annual Meeting of the Air Pollution Control Association, Dallas, TX, 1988.

[71] Muramatsu, M., Umemura, S., Okada, T., and Tomita, H., "Estimation of Personal Exposure to Tobacco Smoke with a Newly Developed Nicotine Personal Monitor," *Environmental Research*, Vol. 35, 1984, pp. 218–227.

[72] Turner, S. and Binnie, P. W. H., "An Indoor Air Quality Survey of Twenty-Six Swiss Office Buildings," *Proceedings*, 5th International Conference on Indoor Air Quality and Climate, Toronto, Canada, Vol. 4, pp. 27–32, 1990.

[73] Mumford, J. L., Lewtas, J., Burton, R. M., Henderson, F. W., Forehand, L., Allison, J. C., and Hammond, S. K., "Assessing Environmental Tobacco Smoke Exposure of Pre-School Children in Homes by Monitoring Particles, Mutagenicity, and Nicotine," *Measurement of Toxic and Related Air Pollutants*, Proceedings, 1989 EPA/AWMA International Symposium, 1989, pp. 606–610.

[74] Löfroth, G., "Removal of Gas Phase Nicotine by Teflon® Coated Filters," personal communication to D. J. Eatough, 1992.

[75] Eatough, D. J., Caka, F. M., Crawford, J., Braithwaite, S., Hansen, L. D., and Lewis, E. A., "Environmental Tobacco Smoke in Commercial Aircraft," *Atmosphere Environment*, Vol. 26A, 1992, pp. 2211–2218.

[76] Proctor, C. J., Warren, N. D., and Bevan, M. A. J., "An Investigation of the Contribution of Environmental Tobacco Smoke to the Air in Betting Shops," *Environmental Technology Letters*, Vol. 10, 1989, pp. 333–338.

[77] Oldaker, G. B., III, Perfetti, P. F., Conrad, F. W., Jr., Conner, J. M., and McBride, R. L., "Results from Surveys of Environmental Tobacco Smoke in Offices and Restaurants," *International Archives of Occupational and Environmental Health*, 1990, pp. 99–104.

[78] Conner, J. M., Oldaker, G. B., III, and Murphy, J. J., "Method for Assessing the Contribution of Environmental Tobacco Smoke to Respirable Suspended Particles in Indoor Environments," *Environmental Technology*, Vol. 11, 1990, pp. 189–196.

[79] Aviado, D. M., "Carbon Monoxide as an Index of Environmental Tobacco Smoke Exposure," *European Journal of Respiratory Disease*, Vol. 65, Supplement 113, 1983, pp. 47–60.

[80] First, M. W., "Environmental Tobacco Smoke Measurements: Retrospect and Prospect," *European Journal of Respiratory Disease*, Vol. 65, Supplement 113, 1983, pp. 9–16.

[81] Kirk, P. W. W., Hunter, M., Baek, S. O., Lester, J. N., and Perry, R., "Environmental Tobacco Smoke in Indoor Air," *Indoor and Ambient Air Quality*, R. Perry and P. W. Kirk, Eds., Selper Ltd., London, 1988, pp. 99–112.

[82] Proctor, C. J., Warren, N. D., Bevan, M. A. J., "Measurements of Environmental Tobacco Smoke in an Air-Conditioned Office Building," *Environmental Technology Letters*, Vol. 10, 1989, pp. 1003–1018.

[83] Löfroth, G., Ling, P. I., and Agurell, E., "Public Exposure to Environmental Tobacco Smoke," *Mut. Research*, Vol. 202, 1988, pp. 103–110.

[84] Oldaker, G. B., III, Ogden, M. W., Maiolo, K. C., Conner, J. M., Conrad, F. W., Jr., Stancill, M. W., and DeLuca, P. O., "Results from Surveys of Environmental Tobacco Smoke in Restaurants in Winston-Salem, North Carolina," *Proceedings*, 5th International Conference on Indoor Air Quality and Climate, Vol. 2, 1990, pp. 281–285.

[85] Brunnemann, K. D., Kagan, M. R., Cox, J. E., and Hoffmann, D., "Analysis of 1,3-Butadiene and Other Selected Gas-Phase Components in Cigarette Mainstream and Sidestream Smoke by Gas Chromatography-Mass Selective Detection," *Carcinogenesis*, Vol. 11, 1990, pp. 1863–1868.

[86] Coghlin, J., Hammond, S. K., and Gann, P. H., "Development of Epidemiologic Tools for Measuring Environmental Tobacco Smoke Exposure," *American Journal of Epidemiology*, Vol. 130, No. 4, 1989, pp. 696–704.

[87] Crouse, W. E. and Oldaker, G. B., III, "Comparison of Area and Personal Sampling Methods for Determining Nicotine in Environmental Tobacco Smoke," *EPA/AWMA Conference on Toxic and Related Air Pollutants*, 1990, pp. 562–566.

[88] Eatough, D. J., Caka, F. M., Crawford, J., Braithwaite, S., Hansen, L. D., and Lewis, E. A., "Cabin Air Quality: Cotinine as a Biomarker of Environmental Tobacco Smoke in Commercial Aircraft," *Measurement of Toxic and Related Air Pollutants*, Proceedings, 1990 EPA/AWMA International Symposium, 1990, pp. 542–549.

[89] Jarvis, M. J. and Russell, A. J., "Measurement and Estimation of Smoke Dosage to Non-Smokers from Environmental Tobacco Smoke," *European Journal of Respiratory Disease*, Vol. 65, Supplement 133, 1984, pp. 68–75.

[90] Muramatsu, M., Umemura, S., Fukui, J., Arai, T., and Kira, S., "Estimates of Personal Exposure to Ambient Nicotine in Daily Environment," *International Archives of Occupational and Environmental Health*, Vol. 59, 1987, pp. 545–550.

[91] Ogden, M. W., Nystrom, C. W., Oldaker, G. B., III, and Conrad, F. W., Jr., "Evaluation of a Personal Passive Sampling Device for Determining Nicotine Exposure in Environmental Tobacco Smoke," *EPA/AWMA Conference on Toxic and Related Air Pollutants*, 1989, pp. 552–558.

[92] Oldaker, G. B., III, Stancill, M. W., Conrad, F. W., Jr., Morgan, W. T., Collie, B. B., Fenner, R. A., Lephardt, J. O., Baker, P. G., Lyons-Hart, J., and Parrish, M. E., "Results from a Survey of Environmental Tobacco Smoke in Hong Kong Restaurants," *Environment International*, 1991, in press.

[93] Oldaker, G. B., III and Conrad, F. C., Jr., "Estimation of Effect of Environmental Tobacco Smoke on Air Quality Within Passenger Cabins of Commercial Aircraft," *Environmental Science and Technology*, Vol. 21, 1987, pp. 994–999.

[94] Vaughan, W. M. and Hammond, S. K., "Impact of 'Designated Smoking Area' Policy on Nicotine Vapor and Particle Concentrations in a Modern Office Building," *JAWMA*, Vol. 40, 1990, pp. 1012–1017.

[95] Biber, A., Scherer, G., Hoepfner, I., Adlkofer, F., Heller, W.-D., Haddow, J. E., and Knight, J., "Determination of Nicotine and Cotinine in Human Serum and Urine: An Interlaboratory Study," *Toxicology Letters*, Vol. 35, 1987, pp. 45–52.

[96] Casale, R., Colantonio, D., Dialente, M., Colorizio, V., Barnabei, R., and Pasqualetti, P., "Impaired Pulmonary Function in School Children Exposed to Passive Smoking," *Respiration*, Vol. 58, 1991, pp. 198–203.

[97] Curvall, M., Kazemi-Vala, E., Enzell, C. R., Olander, L., and Johansson, J., "Inhaled Amount of Tobacco Smoke During Passive Smoking," *Indoor Air '87*, Proceedings of the Fourth International Conference on Indoor Air Quality and Climate, B. Seifert, H. Esdorn, M. Fischer, H. Ruden, and J. Wegner, Eds., Berlin (West), 17–21 Aug. 1987, Institute for Water, Soil and Air Hygiene, Vol. 2, 1987, pp. 57–60.

[98] Etzel, R. A., "A Review of the Use of Saliva Cotinine as a Marker of Tobacco Smoke Exposure," *Preventive Medicine*, Vol. 19, 1990, pp. 190–197.

[99] Feyerabend, C., Higenbottam, T., and Russell, M. A. H., "Nicotine Concentrations in Urine and Saliva of Smokers and Non-Smokers," *British Medical Journal*, Vol. 284, 1982, pp. 1002–1004.

[100] Foliart, D., Benowitz, N. L., and Becker, C. E., "Passive Absorption of Nicotine in Airline Flight Attendants," *New England Journal of Medicine*, Vol. 308, 1983, p. 1105.

[101] Goldstein, G. M., Collier, A., Etzel, R., Lewtas, J., and Haley, N., "Elimination of Urinary Cotinine in Children Exposed to Known Levels of Sidestream Cigarette Smoke," *Indoor Air '87*, Proceedings of the Fourth International Conference on Indoor Air Quality and Climate, B. Seifert, H. Esdorn, M. Fischer, H. Ruden, and J. Wegner, Eds., Berlin (West), 17–21 Aug. 1987, Institute for Water, Soil and Air Hygiene, Vol. 2, 1987, pp. 61–67.

[102] Greenberg, R. A., Haley, N. J., Etzel, R. A., and Loda, F. A., "Measuring the Exposure of Infants to Tobacco Smoke. Nicotine and Cotinine in Urine and Saliva," *New England Journal of Medicine*, Vol. 310, 1984, pp. 1075–1078.

[103] Henderson, F. W., Reid, H. F., Morris, R., Wang, O.-L., Hu, P. C., Helms, R. W., Forehand, L., Mumford, J., Lewtas, J., Haley, N. J., and Hammond, S. K., "Home Air Nicotine Levels and Urinary Cotinine Excretion in Preschool Children," *American Review of Respiratory Disease*, Vol. 140, 1989, pp. 197–201.

[104] Henderson, F. W., Morris, R., Reid, H. F., Hu, P. C., Mumford, J. L., Forehand, L., Burton, R., Lewtas, J., Hammond, S. K., and Haley, N. J., "Serum and Urine Cotinine as Quantitative Measures of Passive Tobacco Smoke Exposure in Young Children," *Indoor Air '87*, Proceedings of the Fourth International Conference on Indoor Air Quality and Climate, B. Seifert, H. Esdorn, M. Fischer, H. Ruden, and J. Wegner, Eds., Berlin (West), 17–21 Aug. 1987, Institute for Water, Soil and Air Hygiene, Vol. 2, 1987, pp. 18–21.

[*105*] Husgafvel-Pursiainen, K., Sorsa, M., Engström, K., and Einistö, P., "Passive Smoking at Work: Biochemical and Biological Measures of Exposure to Environmental Tobacco Smoke," *International Archives of Occupational and Environmental Health*, Vol. 59, 1987, pp. 337–345.

[*106*] Jarvis, M. J., McNeill, A. D., Bryant, A., and Russell, M. A. H., "Factors Determining Exposure to Passive Smoking in Young Adults Living at Home: Quantitative Analysis Using Saliva Cotinine Concentrations," *International Journal of Epidemiology*, Vol. 20, 1991, pp. 126–131.

[*107*] Jarvis, M. J., "Application of Biochemical Intake Markers to Passive Smoking Measurement and Risk Estimation," *Mutation Research*, Vol. 222, 1989, pp. 101–110.

[*108*] Jarvis, M. J., Russell, M. A. H., Benowitz, N. L., and Feyerabend, C., "Elimination of Cotinine from Body Fluids: Implications for Noninvasive Measurement of Tobacco Smoke Exposure," *AJPH*, Vol. 78, 1988, pp. 696–699.

[*109*] Jarvis, M., Tunstall-Pedoe, H., Feyerabend, C., Vesey, C., and Salloojee, Y., "Biochemical Markers of Smoke Absorption and Self Reported Exposure to Passive Smoking," *Journal of Epidemiology and Community Health*, Vol. 38, 1984, pp. 335–339.

[*110*] Knight, G. J., Palomaki, G. E., Lea, D. H., and Haddow, J. E., "Exposure to Environmental Tobacco Smoke Measured by Cotinine I-Radioimmunoassay," *Clinical Chemistry*, Vol. 35, 1989, pp. 1036–1039.

[*111*] Langone, J. J., Cook, G., Bjercke, R. J., and Lifschitz, M. H., "Monoclonal Antibody ELISA for Cotinine in Saliva and Urine of Active and Passive Smokers," *Journal of Immunological Methods*, Vol. 114, 1988, pp. 73–78.

[*112*] Letzel, H., Fischer-Brandies, A., Johnson, L. C., Überla, K., and Biber, A., "Measuring Problems in Estimating the Exposure to Passive Smoking Using the Excretion of Cotinine," *Toxicology Letters*, Vol. 35, 1987, pp. 35–44.

[*113*] Lewis, L. J., Lamb, J. D., Eatough, D. J., Hansen, L. D., and Lewis, E. A., "The Determination of Nicotine and Cotinine by Ion Pair Reversed-Phase Chromatography," *Journal of Chromatographic Science*, Vol. 28, 1990, pp. 200–203.

[*114*] Lewis, E. A., Tang, H., Gunther, K., Belnap, D., Jensen, A., Hansen, L. D., Eatough, D. J., Balter, N. J., Schwartz, S. L., and Winiwarter, W., "Use of Urine Nicotine and Cotinine Measurements to Determine Exposure of Nonsmokers to Sidestream Tobacco Smoke," *Indoor Air '90*, Proceedings of the 5th International Conference on Indoor Air Quality and Climate, Toronto, 29 July–3 Aug. 1990, Vol. 2, 1990, pp. 151–156.

[*115*] Matsukura, S., Taminato, T., Kitano, N., Seino, Y., Hamada, H., Uchihashi, M., Nakajima, H., and Hirata, Y., "Effects of Environmental Tobacco Smoke on Urinary Cotinine Excretion in Nonsmokers," *New England Journal of Medicine*, Vol. 311, 1984, pp. 828–832.

[*116*] Pattishall, E. N., Strope, G. L., Etzel, R. A., Helms, R. W., Haley, N. J., and Denny, F. W., "Serum Cotinine as a Measure of Tobacco Smoke Exposure in Children," *AJDC*, Vol. 139, 1985, pp. 1101–1104.

[*117*] Roussel, G., Quang, L. E., Migueres, M. L., Roche, D., Mongin-Charpin, D., Chretien, J., and Ekindjian, O. G., "An Interpretation of Urinary Cotinine Values in Smokers and Non-Smokers," *Rev. Mal. Resp.*, Vol. 8, 1991, pp. 225–232.

[*118*] Russell, M. A. H., Jarvis, M. J., and West, R. J., "Use of Urinary Cotinine Concentrations to Estimate Exposure and Mortality from Passive Smoking in Non-Smokers," *British Journal of Addiction*, Vol. 81, 1986, pp. 275–281.

[*119*] Scherer, G., Conze, C., Meyerinck, L., Sorsa, M., and Adlkofer, F., "Importance of Exposure to Gaseous and Particulate Phase Components of Tobacco Smoke in Active and Passive Smokers," *International Archives of Occupational and Environmental Health*, Vol. 62, 1990, pp. 459–466.

[*120*] Scherer, G., Westphal, K., Adlkofer, F., and Sorsa, M., "Biomonitoring of Exposure to Potentially Genotoxic Substances from Environmental Tobacco Smoke," *Environment International*, Vol. 15, 1989, pp. 49–56.

[*121*] Scherer, G., Westphal, K., Sorsa, M., and Adlkofer, F., "Quantitative and Qualitative Differences in Tobacco Smoke Uptake Between Active and Passive Smoking," *Indoor and Ambient Air Quality*, R. Perry and P. W. Kirk, Eds., Selper Ltd., London, 1988, pp. 189–194.

[*122*] Scherer, G., Westphal, K., Hoepfner, I., and Adlkofer, F., "Biomonitoring of Exposure to Potentially Mutagenic Substances from Environmental Tobacco Smoke (ETS)," *Indoor Air '87*, Proceedings of the Fourth International Conference on Indoor Air Quality and Climate, B. Seifert, H. Esdorn, M. Fischer, H. Ruden, and J. Wegner, Eds., Berlin (West), Institute for Water, Soil and Air Hygiene, Vol. 2, 1987, pp. 109–114.

[*123*] Sepkovic, D. W., Haley, N. J., and Hoffmann, D., "Elimination from the Body of Tobacco Products by Smokers and Passive Smokers," *Journal of the American Medical Association*, Vol. 256, 1986, p. 863.

[*124*] Sorsa, M., Einistö, P., Husgafvel-Pursiainen, K., Järventaus, H., Kivistö, H., Peltonen, Y., Tuomi, T., and Valkonen, S., "Passive and Active Exposure to Cigarette Smoke in a Smoking Experiment," *Journal of Toxicology and Environmental Health*, Vol. 16, 1985, pp. 523–534.

[125] Strachan, D. P., Jarvis, M. J., and Feyerabend, C., "The Relationship of Salivary Cotinine to Respiratory Symptoms, Spirometry, and Exercise-Induced Bronchospasm in Seven-Year-Old Children," *American Review of Respiratory Disease*, Vol. 142, 1990, pp. 174–151.

[126] Wall, M. A., Johnson, J., Jacob, J., and Benowitz, N. L., "Cotinine in the Serum, Saliva, and Urine of Nonsmokers, Passive Smokers, and Active Smokers," *American Journal of Public Health*, Vol. 78, 1988, pp. 699–701.

[127] Willers, S., Svenonius, E., and Skarping, G., "Passive Smoking and Childhood Asthma. Urinary Cotinine Levels in Children with Asthma and in Referents," *Allergy*, Vol. 46, 1991, pp. 330–334.

[128] Winiwarter, W., Gunther, K., Belnap, D., Tang, H., Crawford, J., Hansen, L. D., Eatough, D. J., Lewis, E. A., Schwartz, S. L., and Balter, N. J., "Elimination of Nicotine and Cotinine by Nonsmokers Exposed to Sidestream Tobacco Smoke Under Controlled Conditions," *Proceedings*, EPA/A&WMA Specialty Conference, Total Exposure Assessment Methodology, November 1989, Las Vegas, NV, 1990, pp. 526–540.

[129] Yanagisawa, Y., Matsuki, H., and Spengler, J. D., "Evaluation of Tobacco Smoke Using Urinary Cotinine as an Indicator of Dose and Hydroxyproline as an Indicator of Effects," *Indoor Air '87*, Proceedings of the Fourth International Conference on Indoor Air Quality and Climate, B. Seifert, H. Esdorn, M. Fischer, H. Ruden, and J. Wegner, Eds., Berlin (West), 17–21 Aug. 1987, Institute for Water, Soil and Air Hygiene, Vol. 2, 1987, pp. 115–118.

[130] Iwase, A., Aiba, M., and Kira, S., "Respiratory Nicotine Absorption in Non-Smoking Females During Passive Smoking," *International Archives of Occupational and Environmental Health*, Vol. 63, 1991, pp. 139–143.

[131] Sepkovic, D. W., Axelrad, C. M., Colosimo, S. G., and Haley, N. J., Paper 87-80.2, presented at the Annual Meeting of the Air Pollution Control Association. New York, NY, 1987.

[132] Adlkofer, F., Scherer, G., Conze, C., Angerer, J., and Lehnert, G., "Significance of Exposure to Benzene and Other Toxic Compounds Through Environmental Tobacco Smoke," *Cancer Research Clinical Oncology*, Vol. 116, 1990, pp. 391–399.

[133] Balter, N. J., Eatough, D. J., and Schwartz, S. L., "Application of Physiological Pharmacokinetic Modeling to the Design of Human Exposure Studies with Environmental Tobacco Smoke," *Indoor and Ambient Air Quality*, R. Perry and P. W. W. Kirk, Eds., Printext Ltd., London, 1988, pp. 179–188.

[134] Curvall, M., Vala, E. K., Enzell, C. R., and Warren, J., "Simulation and Evaluation of Nicotine Intake During Passive Smoking: Cotinine Measurements in Body Fluids of Nonsmokers Given Intravenous Infusions of Nicotine," *Clinical Pharmacology Ther.*, Vol. 47, 1990, pp. 42–49.

[135] Kyerematen, G. A., Morgan, M. L., Chattopadhyay, B., deBethizy, J. D., and Vesell, E. S., "Disposition of Nicotine and Eight Metabolites in Smokers and Nonsmokers: Identification in Smokers of Two Metabolites that are Longer Lived than Cotinine," *Clinical Pharmacology Ther.*, Vol. 48, 1990, pp. 641–651.

[136] Schwartz, S. L., Ball, R. T., and Witorsch, P., "Mathematical Modelling of Nicotine and Cotinine as Biological Markers of Environmental Tobacco Smoke Exposure," *Toxicology Letters*, Vol. 35, 1987, pp. 53–58.

[137] Repace, J. L. and Lowery, A. H., "Indoor Air Pollution, Tobacco Smoke, and Public Health," *Science*, Vol. 208, 1980, pp. 305–309.

[138] Spengler, J. D., Treitman, R. D., Testeson, T. D., Mage, D. T., and Soczek, M. L., "Personal Exposures to Respirable Particulates and Implications for Air Pollution Epidemiology," *Environmental Science Technology*, Vol. 19, 1985, pp. 700–707.

[139] Carson, J. R. and Erikson, C. A., "Results from Survey of Environmental Tobacco Smoke in Offices in Ottawa, Ontario," *Environmental Technology Letters*, Vol. 9, 1988, pp. 501–508.

[140] Georghiou, P. E., Blagden, P., Snow, D. A., Winsor, L., and Williams, D. T., "Mutagenicity of Indoor Air Containing Environmental Tobacco Smoke: Evaluation of a Portable PM-10 Impactor Sampler," *Environmental Science Technology*, Vol. 25, 1991, pp. 1496–1500.

[141] Husgafvel-Pursiainen, K., Sorsa, M., Moller, M., and Benestad, C., "Genotoxicity and Polynuclear Aromatic Hydrocarbon Analysis of Environmental Tobacco Smoke Samples from Restaurants," *Mutagenesis*, Vol. 1, 1986, pp. 287–292.

[142] Kado, N. Y., McCurdy, S. A., Tesluk, S. J., Hammond, S. K., Hsieh, D. P. H., Jones, J., and Schenker, M. B., "Measuring Personal Exposure to Airborne Mutagens and Nicotine in Environmental Tobacco Smoke," *Mutation Research*, Vol. 261, 1991, pp. 75–82.

[143] Lewtas, J., Williams, K., Löfroth, G., Hammond, K., and Leaderer, B., "Environmental Tobacco Smoke: Mutagenic Emission Rates and Their Relationship to Other Emission Factors," *Indoor Air '87*, Proceedings of the Fourth International Conference on Indoor Air Quality and Climate, B. Seifert, H. Esdorn, M. Fischer, H. Ruden, and J. Wegner, Eds., Berlin (West), Institute for Water, Soil and Air Hygiene, Vol. 2, 1987, pp. 8–12.

[144] Lewtas, J., Goto, S., Williams, K., Chuang, J. C., Petersen, B. A., and Wilson, N. K., "The Mutagenicity of Indoor Air Particles in a Residential Pilot Field Study," *Atmosphere Environment*, Vol. 21, 1987, pp. 443–449.

[145] Albert, R. E., "Comparative Carcinogenic Potencies of Particulates from Diesel Engine Exhausts, Coke Oven Emissions, Roofing Tar Aerosols and Cigarette Smoke," *Environmental Health Perspectives*, Vol. 47, 1983, pp. 339–341.

[146] Alfheim, I. and Ramdahl, T., "Contribution of Wood Combustion to Indoor Air Pollution as Measured by Mutagenicity in Salmonella and Polycyclic Aromatic Hydrocarbon Concentration," *Environmental Mutagenesis*, Vol. 6, 1984, pp. 121–130.

[147] Austin, A. C., Claxton, L. D., and Lewtas, J., "Mutagenicity of the Fractionated Organic Emissions from Diesel, Cigarette Smoke Condensate, Coke Oven and Roofing Tar in the Ames Assay," *Environmental Mutagenesis*, Vol. 7, 1985, pp. 471–487.

[148] Lioy, P. J., Avdenko, M., Harkov, R., Atherhold, T., and Daisey, J. M., "A Pilot Indoor-Outdoor Study of Organic Particulate Matter and Particulate Mutagenicity," *JAPCA*, Vol. 35, 1985, pp. 653–657.

[149] Lewis, E. A., Eatough, D. J., Parrish, T. D., Francis, E. S., Booth, G. M., and Lee, M. L., "Combined Supercritical Fluid Chromatography/Microsuspension Mutagenicity Assay of Environmental Tobacco Smoke," *Proceedings*, 1992 EPA/AWMA Symposium on Measurement of Toxic and Related Air Pollutants, 1992, pp. 433–444.

[150] Kado, N. Y., Tsluk, S. J., Hammond, S. K., Woskie, S. R., Samuels, S. J., Schenker, M. B., "Use of a Salmonella Micro Pre-Incubation Procedure for Studying Personal Exposure to Mutagens in Environmental Tobacco Smoke," *Environmental Science Research*, Vol. 36, 1987, pp. 375–390.

[151] Sasson, I. M., Coleman, D. T., LaVoie, E. J., Hoffmann, D., and Wynder, E. L., "Mutagens in Human Urine: Effects of Cigarette Smoking and Diet," *Mutation Research*, Vol. 150, 1985, pp. 149–157.

[152] Ogden, M. W. and Maiolo, K. C., "Collection and Determination of Solanesol as a Tracer of Environmental Tobacco Smoke in Indoor Air," *Environmental Science Technology*, Vol. 23, 1989, pp. 1148–1154.

[153] Ogden, M. W. and Maiolo, K. C., "Gas Chromatographic Determination of Solanesol in Environmental Tobacco Smoke," *Journal of High Resolution Chromatography & Chrom. Commun.*, Vol. 11, 1988, pp. 341–343.

[154] Ogden, M. W. and Maiolo, K. C., "Collection and Analysis of Solanesol as a Tracer of Environmental Tobacco Smoke," *Indoor and Ambient Air Quality*, R. Perry and P. W. Kirk, Eds., Selper Ltd., London, 1988, pp. 77–88.

[155] Chinn, S. and Rona, R. J., "Quantifying Health Aspects of Passive Smoking in British Children Aged 5–11 Years," *Journal of Epidemiology and Community Health*, Vol. 45, 1991, pp. 188–194.

[156] Janerich, D. T., Thompson, W. D., Varela, L. R., Greenwald, P., Chorost, S., Tucci, C., Zaman, M. B., Melamed, M. R., Kiely, M., and McKneally, M. F., "Lung Cancer and Exposure to Environmental Tobacco Smoke in the Household," *New England Journal of Medicine*, Vol. 323, 1990, pp. 632–636.

[157] Sherrill, D. L., Krzyzanowski, Bloom, J. W., and Lebowitz, M. D., "Respiratory Effects of Non-Tobacco Cigarettes: A Longitudinal Study in General Population," *International Journal of Epidemiology*, Vol. 20, 1991, pp. 132–137.

[158] Balter, N., Schwartz, S. L., Kilpatrick, S. J., and Witorsch, P., "Causal Relationship Between Environmental Tobacco Smoke and Lung Cancer in Non-Smokers: Critical Review of the Literature," Paper 86-80.9, *Proceedings*, 79th Annual Meeting of the Air Pollution Control Association, 23–27 June, Minneapolis, MN, 1986.

[159] Coultas, D. B., Samet, J. M., Peake, G. T., McCarthy, J., and Spengler, J., "Reliability and Validity of Questionnaire Assessment of Involuntary Tobacco Smoke Exposure," *Indoor Air '87*, Proceedings of the Fourth International Conference on Indoor Air Quality and Climate, B. Seifert, H. Esdorn, M. Fischer, H. Ruden, and J. Wegner, Eds., Berlin (West), 17–21 Aug. 1987, Institute for Water, Soil and Air Hygiene, Vol. 2, 1987, pp. 121–125.

[160] Lebowitz, M. D., "Methodological Issues in the Epidemiological Investigations of Lung Cancer Related to Low-Level Risks," *International Journal of Epidemiology*, Vol. 19 (Supplement 1), 1990, pp. S43–S47.

[161] Moschandreas, D. J., Sterling, D. A., and Gibbons, R. D., "Perception of Daily Cigarette Consumption," *Indoor Air '87, Proceedings* of the Fourth International Conference on Indoor Air Quality and Climate, B. Seifert, H. Esdorn, M. Fischer, H. Ruden, and J. Wegner, Eds., Berlin (West), 17–21 Aug. 1987, Institute for Water, Soil and Air Hygiene, Vol. 2, 1987, pp. 147–151.

[162] Bauman, K. E., Greenberg, R. A., Strecher, V. J., and Haley, N. J., "A Comparison of Biochemical and Interview Measures of Exposure of Infants to Environmental Tobacco Smoke," *Evaluation of the Health Profession*, Vol. 12, 1989, pp. 179–191.

James E. Dunn[1] *and Tong Chen*[1]

Critical Evaluation of the Diffusion Hypothesis in the Theory of Porous Media Volatile Organic Compound (VOC) Sources and Sinks

REFERENCE: Dunn, J. E. and Chen, T., **"Critical Evaluation of the Diffusion Hypothesis in the Theory of Porous Media Volatile Organic Compound (VOC) Sources and Sinks,"** *Modeling of Indoor Air Quality and Exposure, ASTM STP 1205*, Niren L. Nagda, Ed., American Society for Testing and Materials, Philadelphia, 1993, pp. 64–80.

ABSTRACT: Recently, reports by both the U.S. Environmental Protection Agency (EPA) and a study committee of the Commission of the European Communities have alluded to diffusion mechanisms that may play a role in Volatile Organic Compound (VOC) interactions with indoor sinks. This paper proposes three alternative, diffusion-limited mathematical models to account for this interaction, using the linear isotherm model as a reference point. Their taxonomy is keyed to the nature of the vapor-sink interface. While the linear isotherm model gave an adequate description of data when a pillow-sink was challenged with ethylbenzene, a new single-parameter diffusion model gave a much improved description of data when the same pillow-sink was challenged with perchloroethylene. A hybrid, sorption/desorption, diffusion-limited model was the only plausible model when a carpet-sink was challenged with ethylbenzene. Some new computational aids, particularly interval-weighted least squares, are introduced in the context of model validation.

KEY WORDS: mathematical model, weighted least squares, linear isotherm, pillow, carpet, ethylbenzene, perchloroethylene, indoor air

The existence of indoor, re-emitting sinks for volatile organic compounds (VOC) is now well documented by Berglund et al. [*1*], Nielsen [*2*], Nielsen [*3*], and Tichenor et al. [*4*], among others, and an active, small-chamber testing program of this phenomenon is underway [*5*]. However, the mechanisms by which VOC sinks operate are not well understood.

Recently, both the U.S. Environmental Protection Agency (EPA) [*6*] and the Commission of the European Communities [*7*] published guidelines for use of small environmental test chambers to characterize organic emissions from indoor materials and products. Both reports list three fundamental processes that are thought to control the rate of emissions: (1) surface evaporative mass transfer, (2) surface desorption, and (3) diffusion within the material. Models based on the first two phenomena have been used with varying success to characterize volatile organic compound (VOC) sources [*8, 9*] and sinks [*5*]. While a diffusion limitation often has been alluded to in order to account for not infrequently observed VOC decay curves that are slower than negative exponential, mathematical formulations of this concept have been limited to linearized approximations of diffusion across the boundary layer [*10,11*]. Consistent with the need stated by Axley [*10*] for physical models based on diffusion processes in a porous media, we propose here several potential

[1]Professor and chairman, and research assistant, respectively, University of Arkansas, Statistics Division, Department of Mathematical Sciences, Fayetteville, AR 72701. Research by the senior author was supported under the United States Environmental Protection Agency (USEPA) Cooperative Agreement CR-818520-01-0.

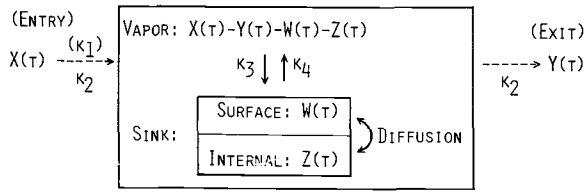

FIG. 1—*Mass balance schematic of alternative VOC sink models.*

models that account for diffusion-limited VOC sink effects and present statistical evidence that we have used to discriminate among their alternative forms.

All models presented here are unified models in the sense that they apply to the whole course of accumulation and decay. In actual applications of chamber studies to indoor air quality (IAQ), we will never be able to predict when we will be in an accumulation or decay phase, so that the same model must apply to both.

Admittedly, the functional forms of some of these models are formidable, often involving complex roots of a polynomial equation. However, since our aim was to attempt validation of these models exactly as postulated, we avoided simplifying approximations. The reader may wish to focus on the model assumptions that are given in the following section, rather than being immediately dismayed by the mathematical complexities of Table 1.

In what follows, we suppose that clean air is swept through a well-mixed test chamber of volume V containing a sink of surface area A at a constant rate of k_2 air exchanges per time unit. At time $t = 0$, VOC is introduced into the initially VOC-free test chamber at a constant rate of k_1 mass units per time unit. At time $t = t_0$, this source of VOC is removed and the VOC concentration is allowed to decay. The only available measurement is that of chamber, vapor-phase concentration, $C(t)$ at any time $t > 0$.

The following four, unified models for $C(t)$ were developed:

(1) linear adsorption isotherm model,
(2) diffusion-limited model with finite transfer coefficient,
(3) diffusion-limited model with an infinite transfer coefficient, and
(4) hybrid, diffusion-limited model with sorption phenomena at the vapor/sink interface.

The distinctions among these models are best visualized by an examination of a mass balance schematic given in Fig. 1

where

$X(t)$ = VOC mass introduced into the test chamber by time t,
$Y(t)$ = VOC mass swept from the test chamber by time t,
$W(t)$ = VOC mass subject to desorption at time t,
$Z(t)$ = VOC mass interior to the sink, subject to diffusion at time t;
k_3 = sorption rate constant for the sink,
k_4 = desorption rate constant for the sink,
$U(x, t)$ = VOC concentration at distance x interior to the sink at time t,
E = finite transfer coefficient between the vapor phase and the sink, and
k = diffusion coefficient of the VOC within the sink,

in terms of internally consistent units. $W(t)$ is associated with the surface of the sink, while $Z(t)$ occupies the porous structure. C_0, W_0, and Z_0 denote, respectively, initial values of $C(t)$, $W(t)$, and

$Z(t)$ at time $t = 0$. The function $G(t) = k_1 I_{(0,t_0)}(t)$ will be used throughout to describe an interrupted input in terms of an indicator function I.

Mathematical Models for Sinks

Linear Isotherm Model

Suppose that there is no penetration of VOC into the sink so that $Z(t) = 0$ for $t \geqq 0$. Mass balance is described by thin-film sorption properties of the sink as follows

$$\frac{dX}{dt} = G(t) \tag{1}$$

$$\frac{dY}{dt} = k_2(X - Y - W) = k_2 VC \tag{2}$$

$$\frac{dW}{dt} = \underset{\text{(sorption)}}{k_3(X - Y - W)} - \underset{\text{(desorption)}}{k_4 W} = k_3 VC - k_4 W \tag{3}$$

from which chamber vapor phase concentration is defined by

$$\frac{dC}{dt} = \frac{1}{V}\left[\frac{dX}{dt} - \frac{dY}{dt} - \frac{dW}{dt}\right] = \frac{G(t)}{V} - (k_2 + k_3)C + \frac{k_4 W}{V} \tag{4}$$

This model has appeared in Dunn and Tichenor [8], and in reparameterized form in Tichenor et al. [5], though in neither case as a unified model. Equating Eq 3 to zero yields the steady state, linear isotherm, $W = K_p C$, in terms of the partition coefficient [10] $K_p = k_3 V/k_4$. Solutions $C(t)$ and $W(t)$ are given in Table 1.

Diffusion-Limited Models

Suppose that the surface of the sink does not provide a physical barrier to VOC penetration, but that once a VOC molecule penetrates the surface of the sink, its movement is controlled by the 1-dimensional diffusion equation

$$U_t(x, t) = kU_{xx}(x, t), \; x \geqq 0, \tag{5}$$

where the orientation of the x axis is taken so that the vapor phase is to the left of the origin at $x = 0$ and the sink is to the right. Flux of VOC/unit surface area, immediately to the right of the interface, is $-kU_x(+0, t)$. If no sorption occurs on the surface of the sink, so that $W(t) = 0$ for $t \geqq 0$, then, in addition to Eq 1, mass balance equations are given by

$$\frac{dY}{dt} = k_2(X - Y - Z) = k_2 VC \tag{6}$$

$$\frac{dZ}{dt} = -kAU_x(+0, t) \tag{7}$$

and chamber vapor phase concentration is defined by

$$\frac{dC}{dt} = \frac{G(t)}{V} - k_2 C + \frac{kA}{V} U_x(+\ 0,\ t) \tag{8}$$

An initial model, which we termed the K & E diffusion model, resulted from imposing initial and boundary conditions

$$\#1 \quad U(x,\ 0) = 0 \text{ for } x \geqq 0 \quad \text{(the sink is empty initially)} \tag{9}$$

$$\#2 \quad \lim_{x \to \infty} U(x,\ t) = 0 \text{ for all } t \quad \text{(the sink is nonsaturable)} \tag{10}$$

$$\#3 \quad kU_x(+0,\ t) = E[U(+0,\ t) - C(t)] \quad \begin{pmatrix} \text{flux is driven by concentration} \\ \text{difference at the interface} \end{pmatrix} \tag{11}$$

However, in attempts to fit this model to actual data, E was estimated to be very large, for example, of order 1.0×10^{22} m/100 h. Therefore, we supposed that the transfer coefficient must dominate the flux rate and arrived at an alternative to boundary condition #3, namely.

$$\#3 \quad \lim_{E \to \infty} \frac{kU_x(\pm 0,\ t)}{E} = 0 \rightarrow U(+0,\ t) = C(t). \tag{12}$$

This seems reasonable as it corresponds to no discontinuity in VOC concentration at the interface. The result is termed a K-diffusion model. Solutions for $C(t)$, $Z(t)$, and $U(x,\ t)$ are given in Table 1 in terms of the complementary error function

$$\text{erfc}(x) = \frac{2}{\sqrt{\pi}} \int_x^\infty e^{-r^2}\, dr \tag{13}$$

Hybrid Diffusion Model

Suppose that the only pathway by which VOC may enter or leave a diffusion-limited sink is through sorbed material on the surface of the sink. Then, in addition to Eq 1, the following mass balance equations result

$$\frac{dY}{dt} = k_2(X - Y - W - Z) = k_2 VC \tag{14}$$

$$\frac{dW}{dt} = k_3(X - \underset{\text{(sorption)}}{Y} - W - Z) + \underset{\text{(diffusion)}}{AkU_x(+0,\ t)} - \underset{\text{(desorption)}}{k_4 W} = k_3 VC + AkU_x(+0,\ t) - k_4 W \tag{15}$$

where

$$Z(t) = A \int_0^\infty U(x,\ t)dx \tag{16}$$

TABLE 1—*Voc sink models arising from alternative mass balance assumptions.*

Linear Isotherm Model

$$C(t)=\frac{k_1}{k_2V}\left\{1+\frac{(k_2+\theta_2)e^{\theta_1 t}-(k_2+\theta_1)e^{\theta_2 t}}{\theta_1-\theta_2}\right\}-\frac{k_1}{k_2V}\left\{1+\frac{(k_2+\theta_2)e^{\theta_1(t-t_o)}-(k_2+\theta_1)e^{\theta_2(t-t_o)}}{\theta_1-\theta_2}\right\}I_{(t_o,\infty)}(t)+W_0\frac{k_4(e^{\theta_1 t}-e^{\theta_2 t})}{V(\theta_1-\theta_2)}+C_0\frac{(k_4+\theta_1)e^{\theta_1 t}-(k_4+\theta_2)e^{\theta_2 t}}{\theta_1-\theta_2}$$

$$W(t)=k_1k_3\left\{\frac{1}{k_2k_4}+\frac{e^{\theta_1 t}}{\theta_1(\theta_1-\theta_2)}-\frac{e^{\theta_2 t}}{\theta_2(\theta_1-\theta_2)}\right\}-k_1k_3\left\{\frac{1}{k_2k_4}+\frac{e^{\theta_1(t-t_o)}}{\theta_1(\theta_1-\theta_2)}-\frac{e^{\theta_2(t-t_o)}}{\theta_2(\theta_1-\theta_2)}\right\}I_{(t_o,\infty)}(t)$$
$$+C_0k_3V\frac{(e^{\theta_1 t}-e^{\theta_2 t})}{\theta_1-\theta_2}+W_0\frac{k_3k_4}{\theta_1-\theta_2}\left\{\frac{e^{\theta_1 t}}{k_4+\theta_1}-\frac{e^{\theta_2 t}}{k_4+\theta_2}\right\},$$

where $\theta_1,\ \theta_2=\{-(k_2+k_3+k_4)\pm[(k_2+k_3+k_4)^2-4k_2k_4]^{1/2}\}/2$[a].

K-diffusion Model ($E\to\infty$)

$$C(t)=\frac{k_1}{V}\left\{\frac{1}{k_2}+\frac{e^{\theta_1^2 t}\,\mathrm{erfc}(-\theta_1\sqrt{t})}{\theta_1(\theta_1-\theta_2)}-\frac{e^{\theta_2^2 t}\,\mathrm{erfc}(-\theta_2\sqrt{t})}{\theta_2(\theta_1-\theta_2)}\right\}-\frac{k_1}{V}\left\{\frac{1}{k_2}+\frac{e^{\theta_1^2(t-t_o)}\,\mathrm{erfc}(-\theta_1\sqrt{t-t_o})}{\theta_1(\theta_1-\theta_2)}-\frac{e^{\theta_2^2(t-t_o)}\,\mathrm{erfc}(-\theta_2\sqrt{t-t_o})}{\theta_2(\theta_1-\theta_2)}\right\}I_{(t_o,\infty)}(t)$$
$$+C_0\left\{\frac{\theta_1e^{\theta_1^2 t}\,\mathrm{erfc}(-\theta_1\sqrt{t})-\theta_2e^{\theta_2^2 t}\,\mathrm{erfc}(-\theta_2\sqrt{t})}{\theta_1-\theta_2}\right\},$$

$$Z(t)=\frac{Ak_1\sqrt{k}}{V}\left\{\frac{2\sqrt{t}}{k_2\sqrt{\pi}}-\frac{A\sqrt{k}}{k_2^2V}+\frac{e^{\theta_1^2 t}\,\mathrm{erfc}(-\theta_1\sqrt{t})}{\theta_1^2(\theta_1-\theta_2)}-\frac{e^{\theta_2^2 t}\,\mathrm{erfc}(-\theta_2\sqrt{t})}{\theta_2^2(\theta_1-\theta_2)}\right\}-\left\{\frac{2\sqrt{t-t_o}}{k_2\sqrt{\pi}}-\frac{A\sqrt{k}}{k_2^2V}+\frac{e^{\theta_1^2(t-t_o)}\,\mathrm{erfc}(-\theta_1\sqrt{t-t_o})}{\theta_1^2(\theta_1-\theta_2)}-\frac{e^{\theta_2^2(t-t_o)}\,\mathrm{erfc}(-\theta_2\sqrt{t-t_o})}{\theta_2^2(\theta_1-\theta_2)}\right\}$$
$$\cdot\frac{Ak_1\sqrt{k}}{V}I_{(t_o,\infty)}(t)+C_0\frac{A\sqrt{k}}{\theta_1-\theta_2}\left\{e^{\theta_1^2 t}\,\mathrm{erfc}(-\theta_1\sqrt{t})-e^{\theta_2^2 t}\,\mathrm{erfc}(-\theta_2\sqrt{t})\right\}+Z_0,$$

$$U(x,t)=\frac{k_1}{V}\left\{\frac{\mathrm{erfc}[x/(2\sqrt{kt})]}{k_2}+\sum_{i=1}^{2}\frac{(-1)^{1-1}e^{-x\theta_1/\sqrt{k}+\theta_1^2 t}}{\theta_1(\theta_1-\theta_2)}\,\mathrm{erfc}[x/(2\sqrt{kt})-\theta_1\sqrt{t}]\right\}-\frac{k_1}{V}\left\{\frac{\mathrm{erfc}[x/(2\sqrt{k(t-t_o)})]}{k_2}+\sum_{i=1}^{2}\frac{(-1)^{1-1}e^{-x\theta_1/\sqrt{k}+\theta_1^2(t-t_o)}}{\theta_1(\theta_1-\theta_2)}\,\mathrm{erfc}[x/(2\sqrt{k(t-t_o)})-\theta_1\sqrt{t-t_o}]\right\}I_{(t_o,\infty)}(t)$$
$$+C_0\sum_{i=1}^{2}\frac{(-1)^{1-1}\theta_1e^{-x\theta_1/\sqrt{k}+\theta_1^2 t}}{\theta_1-\theta_2}\,\mathrm{erfc}[x/(2\sqrt{kt})-\theta_1\sqrt{t}],$$

where $\theta_1,\ \theta_2=\{-A\sqrt{k}/v\pm[A^2k/V^2-4k_2]^{1/2}\}/2$[b].

TABLE 1—*Continued.*

Hybrid Diffusion Model

$$C(t) = \frac{k_1}{V}\left\{\frac{1}{k_2} + \sum_{i=1}^{4}(\theta_i + \sqrt{k} + k_4/\theta_i)e^{\theta_i^2 t}\,\mathrm{erfc}(-\theta_i\sqrt{t})\Big/\prod_{\substack{j=1\\ j\neq i}}^{4}(\theta_i - \theta_j)\right\} - \frac{k_1}{V}\left\{\frac{1}{k_2} + \sum_{i=1}^{4}(\theta_i + \sqrt{k} + k_4/\theta_i)e^{\theta_i^2(t-t_0)}\,\mathrm{erfc}(-\theta_i\sqrt{t-t_0})\Big/\prod_{\substack{j=1\\ j\neq i}}^{4}(\theta_i - \theta_j)\right\} I_{(t_0,\infty)}(t)$$

$$+ C_0\sum_{i=1}^{4}\theta_i(k_4 + \sqrt{k}\,\theta_i + \theta_i^2)e^{\theta_i^2 t}\,\mathrm{erfc}(-\theta_i\sqrt{t})\Big/\prod_{\substack{j=1\\ j\neq i}}^{4}(\theta_i - \theta_j) + W_0\frac{k_4}{V}\sum_{i=1}^{4}\theta_i e^{\theta_i^2 t}\,\mathrm{erfc}(-\theta_i\sqrt{t})\Big/\prod_{\substack{j=1\\ j\neq i}}^{4}(\theta_i - \theta_j),$$

$$W(t) = k_1k_3\left\{\frac{1}{k_2k_4} + \sum_{i=1}^{4}e^{\theta_i^2 t}\,\mathrm{erfc}(-\theta_i\sqrt{t})/[\theta_i\prod_{\substack{j=1\\ j\neq i}}^{4}(\theta_i - \theta_j)]\right\} - k_1k_3\left\{\frac{1}{k_2k_4} + \sum_{i=1}^{4}e^{\theta_i^2(t-t_0)}\,\mathrm{erfc}(-\theta_i\sqrt{t-t_0})/[\theta_i\prod_{\substack{j=1\\ j\neq i}}^{4}(\theta_i - \theta_j)]\right\} I_{(t_0,\infty)}(t)$$

$$+ C_0k_3V\sum_{i=1}^{4}\theta_i e^{\theta_i^2 t}\,\mathrm{erfc}(-\theta_i\sqrt{t})\Big/\prod_{\substack{j=1\\ j\neq i}}^{4}(\theta_i - \theta_j) + W_0\sum_{i=1}^{4}\theta_i(k_2 + k_3 + \theta_i^2)e^{\theta_i^2 t}\,\mathrm{erfc}(-\theta_i\sqrt{t})\Big/\prod_{\substack{j=1\\ j\neq i}}^{4}(\theta_i - \theta_j),$$

$$Z(t) = k_1k_3\sqrt{k}\left\{\frac{2\sqrt{t/\pi}}{k_2k_4} - \frac{(k_2+k_3)\sqrt{k}}{k_2^2k_4^2} + \sum_{i=1}^{4}\frac{e^{\theta_i^2 t}\,\mathrm{erfc}(-\theta_i\sqrt{t})}{\theta_i\prod_{\substack{j=1\\ j\neq i}}^{4}(\theta_i - \theta_j)}\right\} - k_1k_3\sqrt{k}\left\{\frac{2\sqrt{(t-t_0)/\pi}}{k_2k_4} - \frac{(k_2+k_3)\sqrt{k}}{k_2^2k_4^2} + \sum_{i=1}^{4}\frac{e^{\theta_i^2(t-t_0)}\,\mathrm{erfc}(-\theta_i\sqrt{t-t_0})}{\theta_i\prod_{\substack{j=1\\ j\neq i}}^{4}(\theta_i - \theta_j)}\right\} I_{(t_0,\infty)}(t)$$

$$+ C_0k_3V\sqrt{k}\sum_{i=1}^{4}e^{\theta_i^2 t}\,\mathrm{erfc}(-\theta_i\sqrt{t})\Big/\prod_{\substack{j=1\\ j\neq i}}^{4}(\theta_i - \theta_j) + W_0\sqrt{k}\sum_{i=1}^{4}(k_2 + k_3 + \theta_i^2)e^{\theta_i^2 t}\,\mathrm{erfc}(-\theta_i\sqrt{t})\Big/\prod_{\substack{j=1\\ j\neq i}}^{4}(\theta_i - \theta_j) + Z_0,$$

$$U(x,t) = \frac{k_1k_3}{A}\left\{\frac{\mathrm{erfc}[x/(2\sqrt{kt})]}{k_2k_4} + \sum_{i=1}^{4}\frac{e^{-x\theta_i/\sqrt{k}+\theta_i^2 t}\,\mathrm{erfc}[x/(2\sqrt{kt})-\theta_i\sqrt{t}]}{\theta_i\prod_{\substack{j=1\\ j\neq i}}^{4}(\theta_i - \theta_j)}\right\} - \frac{k_1k_3}{A}\left\{\frac{\mathrm{erfc}[x/(2\sqrt{k(t-t_0)})]}{k_2k_4} + \sum_{i=1}^{4}\frac{e^{-x\theta_i/\sqrt{k}+\theta_i^2(t-t_0)}\,\mathrm{erfc}[x/(2\sqrt{k(t-t_0)})-\theta_i\sqrt{t-t_0}]}{\theta_i\prod_{\substack{j=1\\ j\neq i}}^{4}(\theta_i - \theta_j)}\right\} I_{(t_0,\infty)}(t)$$

$$+ C_0\frac{k_3V}{A}\sum_{i=1}^{4}\theta_i e^{-x\theta_i/\sqrt{k}+\theta_i^2 t}\,\mathrm{erfc}[x/(2\sqrt{kt})-\theta_i\sqrt{t}]\Big/\prod_{\substack{j=1\\ j\neq i}}^{4}(\theta_i - \theta_j) + \frac{W_0}{A}\sum_{i=1}^{4}(k_2 + k_3 + \theta_i^2)\theta_i e^{-x\theta_i/\sqrt{k}+\theta_i^2 t}\,\mathrm{erfc}[x/(2\sqrt{kt})-\theta_i\sqrt{t}]\Big/\prod_{\substack{j=1\\ j\neq i}}^{4}(\theta_i - \theta_j),$$

where $\theta_1,\ldots,\theta_4$ solve $\theta^4 + \sqrt{k}\,\theta^3 + (k_2+k_3+k_4)\theta^2 + (k_2+k_3)\sqrt{k}\,\theta + k_2k_4 = 0$[c].

[a] Both real and negative.

[b] Both real and negative or complex conjugates.

[c] Real and negative or complex conjugates in pairs.

TABLE 2—*Summary of VOC sink data sets supplied by USEPA/AEERL.*

Data Set	VOC	A, m^2	V, m^3	k_1, μg/h	k_2, h^{-1}	n^a	Test Duration, h
Pillow-1	Ethylbenzene	0.266	0.0456	388.6	0.992	70	366.98
Pillow-2	Ethylbenzene	0.266	0.0456	330.6	0.955	70	366.97
Pillow-7	Perchloroethylene	0.266	0.0456	1196	0.923	115	167.75
Pillow-8	Perchloroethylene	0.266	0.0456	1208	0.925	105	165.75
Carpet-1	Ethylbenzene	0.14	0.053	432.6	0.949	80	408.08
Carpet-2	Ethylbenzene	0.14	0.0509	396.9	0.951	78	408.07

[a]Number of separate determinations in data set.

defines the mass in the interior of the sink at time t, and $U(x, t)$ is defined by the 1-dimensional diffusion (Eq 5). Equating Eq 15 to zero and solving for W defines the corresponding adsorption isotherm. From

$$\frac{dC}{dt} = \frac{1}{V}\frac{d(X - Y - W - Z)}{dt}$$

$$\frac{dC}{dt} = \frac{G(t)}{V} - (k_2 + k_3)C(t) - \frac{kA}{V}U_x(+0, t) + \frac{k_4}{V}W(t) - \frac{A}{V}\int_0^\infty U_t(x, t)dx \tag{17}$$

Initial condition #1 and boundary condition #2 were taken as in Eqs 9 and 10. With flux across the interface now proportional to the difference between inner and outer sink concentrations, boundary condition #3 became

$$kU_x(+0, t) = E[U(+0, t) - W/A] \tag{18}$$

so that $\lim_{E\to\infty} \frac{kU_x(+0, t)}{E} = 0$ suggested a second boundary condition, namely

$$\#3\ U(+0, t) = W/A \tag{19}$$

Table 1 gives solutions $C(t)$, $W(t)$, $Z(t)$, and $U(x, t)$ in terms of the complementary error function, usually with complex argument.

Methods of Model Validation

Six data sets, supplied by the Indoor Air Test Laboratory, Environmental Protection Agency/Air and Energy Engineering Research Laboratory (USEPA/AEERL) were used for model validation. Experimental details were described in Ref 5, and analyses based on the linear isotherm model were given there. The basic setup was 0.055 m^3 continuous flow test chambers with internal mixing fans. Critical details of individual tests are given in Table 2. The pillow material was described as "50% polyester-50% cotton fabric covering a polyester fiber fill," while the carpet material was described as "nylon fiber pile bound with styrenebutadiene latex to a jute backing." In all cases, input of VOC was terminated at $t_0 = 48$ h. Inspection of Table 2 will show that each successive pair of tests (Pillow-1 and Pillow-2, Pillow-7 and Pillow-8, Carpet-1 and Carpet-2) essentially were replications of each other.

All models were fitted to all data sets using least squares, as implemented by SAS procedure NLIN [*12*]. Necessarily, we were forced to write our own complex arithmetic routines in order to

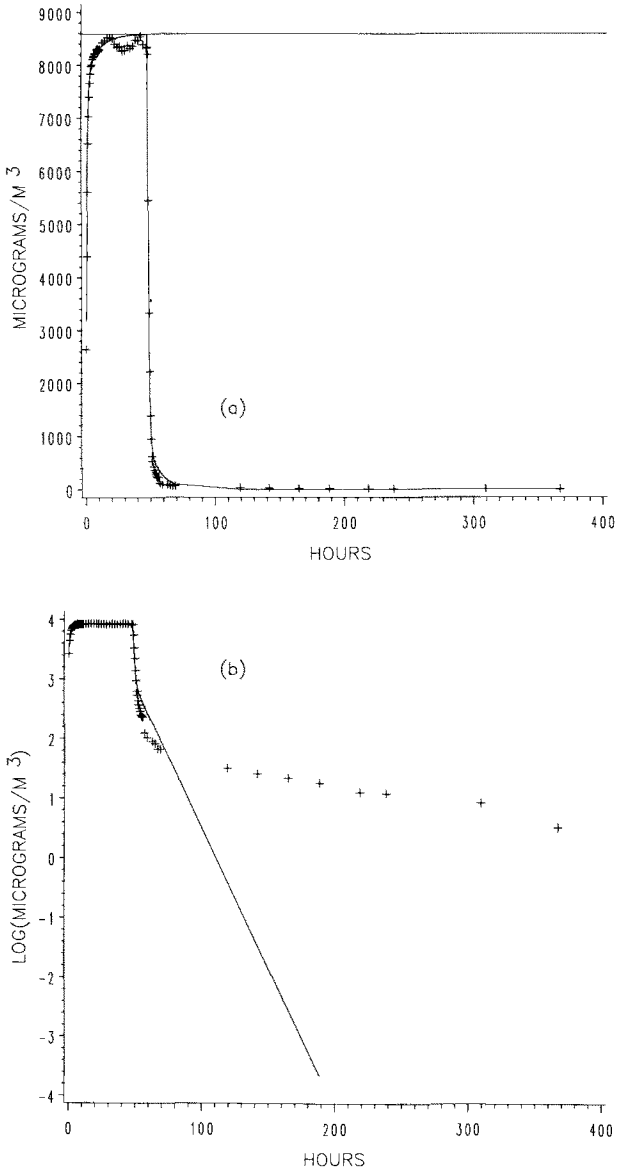

FIG. 2—*Fidelity of the Langmuir model to the Pillow-1 data. (a) Least squares fit of concentration in linear scale, and (b) least squares fit replotted in* $\log_{10}$ *scale of concentration.*

do so. The logical alternative, Fortran-based IMSL, was no more amenable in that the Fortran complementary error function does not accept a complex argument.

Figure 2(*a*) shows the fit of the linear isotherm model to the Pillow-1 data set. The solid curve represents the fitted model, while plus (+) represents an experimental determination. Concentration is expressed as $\mu g/m^3$. The horizontal line at 8591 $\mu g/m^3$ represents ultimate concentration given by $k_1/(k_2V)$, had the VOC source not been terminated. The fit looks quite good until replotted in Figure 1(*b*) in terms of log-concentration.

The problem is two-fold. First, Figure 2(*a*) represents a "point-weighted" (PW) fit in the sense that each data point has been given equal weight in determining the shape of the fitted curve. But since by choice, the technician sampled more frequently during the early stage of the experiment when chamber concentration was changing rapidly (consistent with good laboratory practice), this unequally weighted the influence of the passage of time on the fit. The solution, we felt, was to concentrate on the fact that each experiment produced one continuous response over time. That the technician took n determinations of chamber concentration at discrete times, $t_1, \ldots, t_n$, does not alter the conclusion. In order to compensate for the lack of continuous observation, we introduced an "interval weight" for each data point

$$w_i = (t_i - t_{i-1})/2 + (t_{i+1} - t_i)/2, \quad i = 1, \ldots, n-1$$

$$w_n = (t_n - t_{n-1})/2 \tag{20}$$

which reflects the amount of the experimental time axis represented by that data point, and performed all subsequent model fits using "interval-weighted" (IW) least squares.

The second problem stems from an increase in experimental error that is associated with increasing VOC concentration. This is evident in Figure 2(*a*), where more scatter of data appears about the trend line above 8000 $\mu g/m^3$ than at lower levels of the response. To compensate, we utilized the "transform both sides" (TBS) approach which has been explored extensively by Carroll and Ruppert [*13*]. Based on their method, let c_i and $C(t_i; \theta)$ represent, respectively, observed and theoretical VOC chamber concentrations at time t_i, and let $\lambda \geqq 0$ denote a parameter to be estimated in addition to (possibly vector-valued) θ. To do so, we applied IW least squares to the model

$$c_i^{\lambda} = C(t_i; \theta)^{\lambda} + e_i, \quad i = 1, \ldots n, \tag{21}$$

where e_i represents experimental error in the ith determination.

A practical implication of this model is that

$$\text{variance}[c_i] \propto C(t_i; \theta)^{2(1-\lambda)} \tag{22}$$

that is, the experimental error increases at a rate proportional to the $1 - \lambda$ power of the expected concentration. A value $\lambda = 0$ corresponds to a logarithmic transformation and implies a constant coefficient of variation.

Following Ref 13, we used IW least squares and TBS to fit all models in Table 1 to all data sets in Table 2 for equally spaced increments of λ over a range $0 \leqq \lambda \leqq 0.8$. By this approach, choice of λ reduced to maximizing the following, conditional log-likelihood function of λ, under the assumption that the experimental errors in Eq 21 are independent and normal with mean zero and variance σ^2

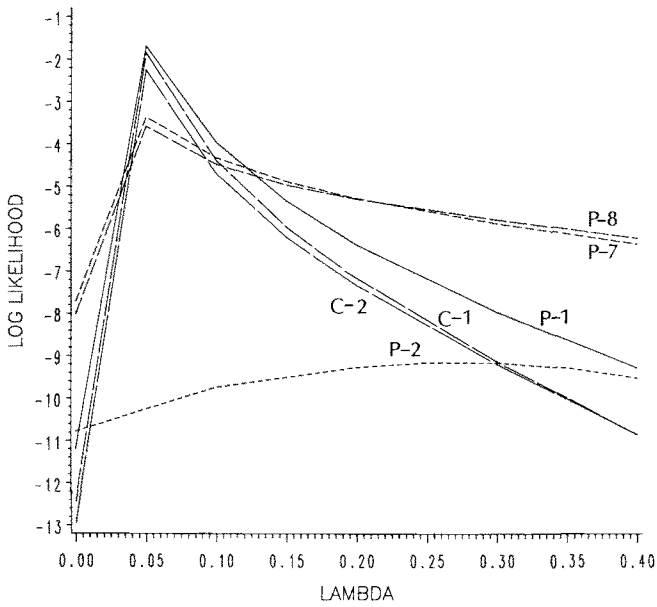

FIG. 3—*Log-likelihood plots to determine the optimal TBS power transformation when fitting the* K*-diffusion model to all data sets;* P = *pillow,* C = *carpet.*

$$L\{\lambda|\hat{\theta}\} = \sum_{i=1}^{n} w_i[(\lambda - 1)\ln(c_i) - 0.5\ln\{\mathrm{SSE}(\lambda)\}] \tag{23}$$

where $\mathrm{SSE}(\lambda) = \Sigma_{i=1}^{n} w_i[c_i^{\lambda} - C\{t_i; \hat{\theta}(\lambda)\}]^2$ and $\hat{\theta}(\lambda)$ denotes estimates of the model parameters conditional on λ. Figure 3 is representative of the results obtained. In this case, the *K*-diffusion model was fitted to each of the data sets in Table 2 using $\lambda = 0$, that is, TBS using a logarithmic transformation. Figure 3 shows a plot of $L\{\lambda|\hat{\theta}\ (\lambda = 0)\}$ for each of the six data sets. With the exception of the Pillow-2 data set (*P*-2), maximum *L* occurred in the region of $0 \leqq \lambda \leqq 0.05$. We considered this, and similar plots, which resulted by fitting the other models, to be sufficient evidence to base all comparisons of model validity in the following section on TBS using a logarithmic transformation ($\lambda = 0$). We did not feel justified in individual "tuning" of λ for each data set. If λ reflects the magnitude of experimental error, as suggested by Eq 22, then it should be relatively constant under conditions of constant test apparatus and quality of laboratory technique.

Results

Pillow Material Challenged with Ethylbenzene

Chamber conditions underlying the Pillow-1 and 2 data sets were the least well replicated, varying from 41 to 33% relative humidity, 22.7 to 23.1°C, and $k_1 = 389$ to 331 μg/h, respectively. Nevertheless, results presented in Table 3 were reproducible between replications for each of the models, with the exception of *k* in the hybrid model.

MSE is an estimator of σ^2 in the context of Eq 21, and is a measure of lack-of-fit. D.f. in Table 3 refers to the degrees of freedom associated with MSE. Based on this criterion, both the linear

TABLE 3—*Results Units: $k = m^2/100\ h$, k_3 and $k_4 = (100\ h)^{-1}$.*

Units: $k = m^2/100$ h, k_3 and $k_4 = (100\ h)^{-1}$.	
Pillow-1	Pillow-2
Linear Isotherm Model	
k_3 = 2.363, s.e. = 0.0859	2.408, s.e. = 0.0726
k_4 = 0.9284, s.e. = 0.0314	0.9084, s.e. = 0.0311
MSE = 9.23E-4 (68 d.f.)	6.45E-4 (65 d.f.)
K-diffusion Model	
k = 0.1930, s.e. = 0.0159	0.2114, s.e. = 0.0190
MSE = 1.99E-3 (69 d.f.)	2.16E-3 (66 d.f.)
Hybrid Diffusion Model	
k_3 = 3.442, s.e. = 0.213	3.811, s.e. = 0.196
k_4 = 1.748, s.e. = 0.277	1.990, s.e. = 0.352
k = 0.980, s.e. = 0.559	2.485, s.e. = 1.293
MSE = 7.41E-4 (67 d.f.)	3.09E-4 (64 d.f.)
Pillow-7	Pillow-8
Linear Isotherm Model	
k_3 = 3.596, s.e. = 0.141	4.155, s.e. = 0.203
k_4 = 2.180, s.e. = 0.0888	2.152, s.e. = 0.112
MSE = 3.13E-4 (103 d.f.)	4.87E-4 (103 d.f.)
K-diffusion Model	
k = 0.2190, s.e. = 0.00667	0.2989, s.e. = 0.0103
MSE = 1.04E-4 (104 d.f.)	1.24E-4 (104 d.f.)
Hybrid Diffusion Model	
k_3 = 15.17, s.e. = 4.25	59.17, s.e. = 22.2
k_4 = 45.36, s.e. = 19.7	304.0, s.e. = 161.7
k = 109.6, s.e. = 69.1	417.6, s.e. = 143.7
MSE = 4.35E-5 (101 d.f.)	1.24E-4 (102 d.f.)
Carpet-1	Carpet-2
Linear Isotherm Model	
k_3 = 3.331, s.e. = 0.289	3.770, s.e. = 0.942
k_4 = 1.405, s.e. = 0.0552	1.453, s.e. = 0.0547
MSE = 3.85E-3 (77 d.f.)	3.75E-3 (76 d.f.)
K-diffusion Model	
k = 0.6243, s.e. = 0.0647	0.6576, s.e. = 0.0782
MSE = 3.59E-3 (78 d.f.)	4.72E-3 (77 d.f.)
Hybrid Diffusion Model	
k_3 = 9.466, s.e. = 0.00054	13.09, s.e. = 0.311
k_4 = 4.831, s.e. = 0.152	5.766, s.e. = 0.0685
k = 0.3120, s.e. = 0.0385	0.3427, s.e. = 0.0326
MSE = 3.89E-4 (76 d.f.)	3.36E-4 (75 d.f.)

isotherm and the hybrid models gave superior fits compared to that of the *K*-diffusion model. Figures 4(*a*) to 4(*c*) demonstrate model adequacy in the logarithmic scale in which fitting occurred. Both linear isotherm and hybrid models cope very well with the sharp elbow that appeared late in the decay curve. By contrast, the *K*-diffusion model anticipated a longer period of VOC emissions and overestimated this part of the decay curve. Figures 4(*d*) to 4(*f*) show the same fitted models plotted in the original units of concentration. Clearly, fidelity to the decay phase on the part of both the linear isotherm and hybrid models left something to be desired during the accumulation phase. (Recall that both IW and fitting in the log scale tend to discount the early, large values.) Nevertheless, choice is between the linear isotherm and hybrid models. We prefer the former, since the large relative standard errors of k estimates for the hybrid model (57 and 52%, respectively) suggest that this may be a superficial parameter. Certainly, iterative convergence when fitting the hybrid model was slow to attain, and this often is indicative of an over-parameterized model.

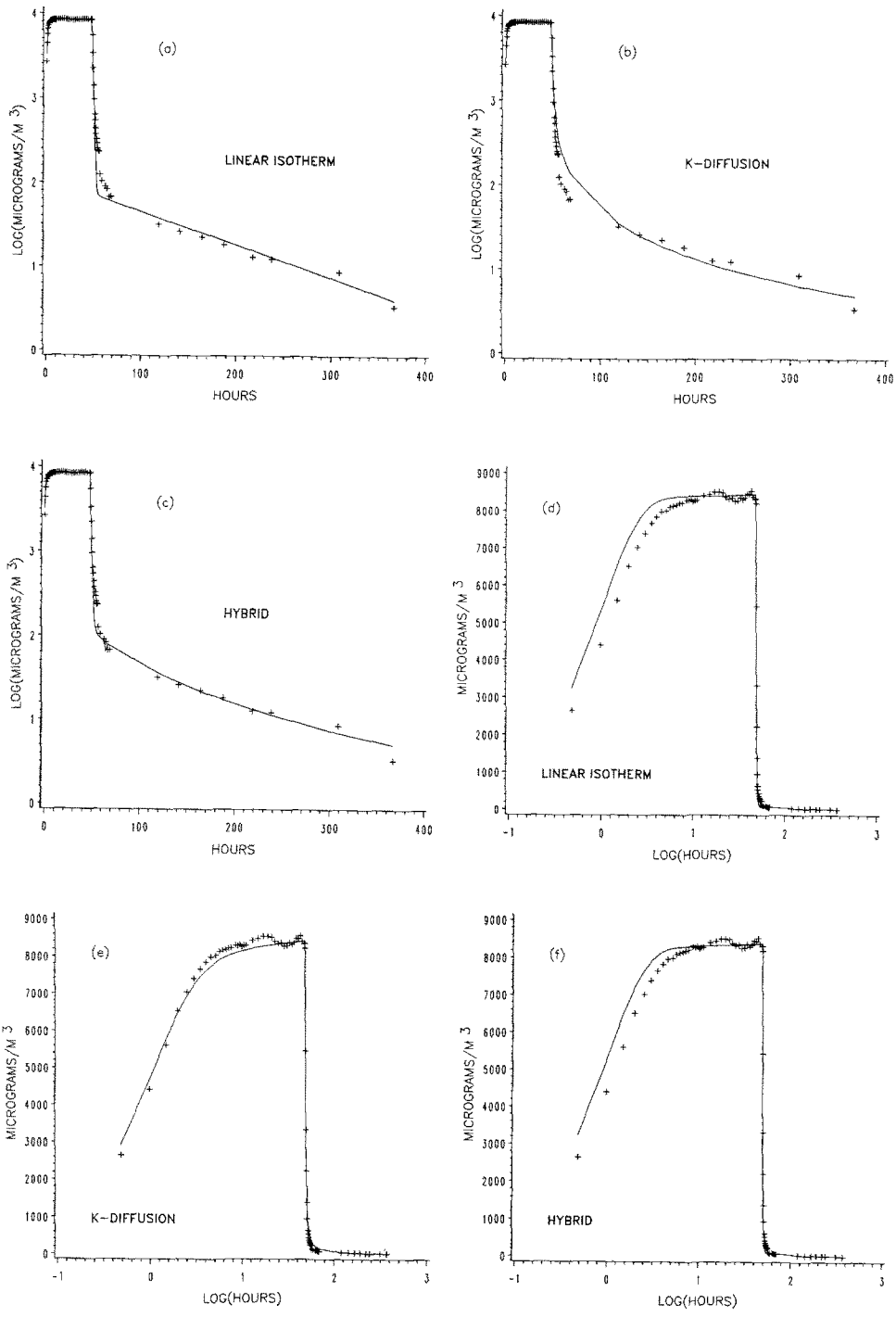

FIG. 4—*IW least squares model fits to pillow/ethylbenzene test chamber data (Pillow-1) in log_{10} scale of concentration, Figs. (a) through (c), and replotted in linear scale of concentration, Figs. (d) through (f).*

Therefore, we concluded that the sink effect of pillow material for ethylbenzene was dominated by thin-film, sorption phenomena, with insufficient evidence to identify a diffusion phenomenon as well.

Pillow Material Challenged with Perchloroethylene

Chamber conditions were well replicated in this case, being identically 45% relative humidity and 23.0°C, with k_1 = 1196 and 1208 μg/h, respectively. Figures 5(*a*) to 5(*f*) clearly demonstrate superior fits by the *K*-diffusion and hybrid models over that of the linear isotherm model. This is reinforced by a comparison of MSEs in Table 3. Here, the sharp elbow in the linear isotherm model decay curve works to its disadvantage. A choice of the *K*-diffusion model over the hybrid model is dictated by: (1) almost identical fits shown in the figures, (2) little reduction in MSE by adding sorption parameters, k_3 and k_4, in the presence of a diffusion term, (3) large relative standard errors for parameter estimates in the hybrid model, and (4) lack of reproducibility between replicates when fitting the hybrid model. Both (3) and (4) are indicative of an over-parameterized model. Since a sorption phenomenon seems to be ruled out by Fig. 5(*a*), we concluded that the sink effect of pillow material for perchloroethylene was dominated by a diffusion phenomenon with little evidence of a sorption/desorption effect.

Carpet Material Challenged with Ethylbenzene

Chamber conditions for the two replications were identically 43% relative humidity, 22.8 and 23.2°C, and k_1 = 433 and 397 μg/h, respectively. A comparison of Fig. 6(*c*) to Figs. 6(*a*) and 6(*b*) clearly demonstrates the superiority of the hybrid model over the linear isotherm and *K*-diffusion models during the decay phase. A comparison of MSEs in Table 3 also dictates a preference for the hybrid model. Relative standard errors of parameter estimates for the hybrid model were acceptably small, the estimates were reproducible between replicates, and iterative convergence was easily obtained for both data sets. In spite of poor fidelity to the data during the accumulation phase, as shown in Fig. 6(*f*), we concluded that the hybrid model had merit and that both diffusion and sorption/desorption phenomena were at play in the sink effect of carpet material in the presence of ethylbenzene. This is no surprise since the carpet material represents a complex mixture of natural and synthetic fibers and adhesive.

Discussion and Summary

The strongest case for the porous media, diffusion hypothesis was given by the excellent fit of the *K*-diffusion model to both pillow/perchloroethylene data sets. Even with only one adjustable parameter, *k*, the model fitted both the accumulation and decay phases very well even though data points during accumulation were heavily discounted by our fitting method. By contrast, the hybrid model fitted the decay phase of both carpet/ethylbenzene data sets very well, but its fidelity to the accumulation phase was less satisfactory. This places doubt on whether it truely is a unified model for this particular VOC/sink combination, since one would expect that a correct model fitted to one segment of the data should be able to predict any other segment of the data.

The apparent change in sink mechanism of pillow material that occurred when ethylbenzene was replaced by perchloroethylene is both interesting and puzzling. We believe the change over occurred, since it was reproducible, but its chemical basis escapes us.

Several worrisome details remain. The boundary condition of Eq 10 always has been suspect since it implies an infinitely deep sink. This is a standard heat equation assumption, but if it is to be replaced, with what? What does "depth" mean in terms of a pillow? Figure 7, based on parameters estimated from the excellent fit of the *K*-diffusion model to the Pillow-8 data set, is a

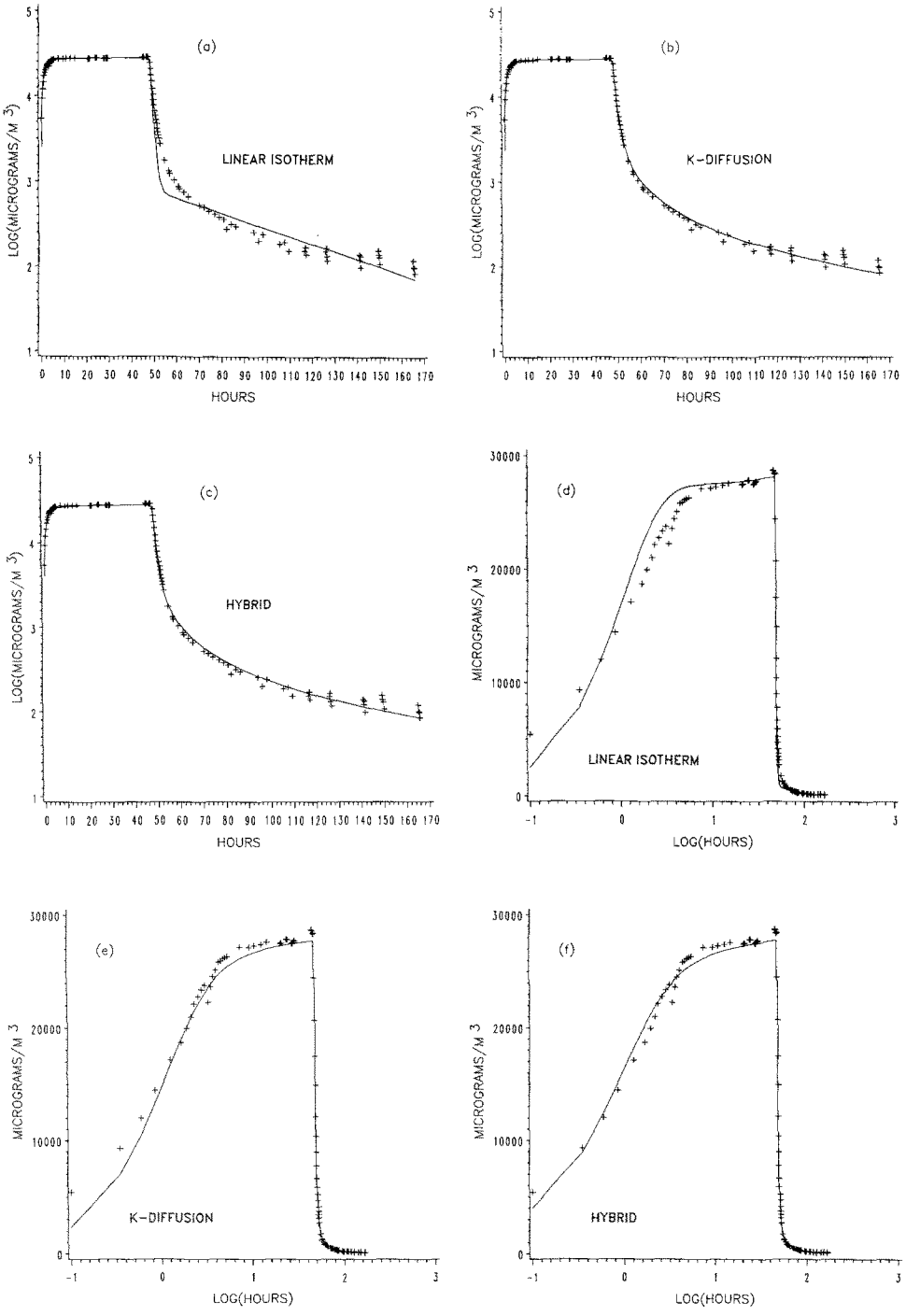

FIG. 5—*IW least squares model fits to pillow/perchloroethylene test chamber data (Pillow-8) in $\log_{10}$ scale of concentration, Figs. (a) through (c), and replotted in linear scale of concentration, Figs. (d) through (f).*

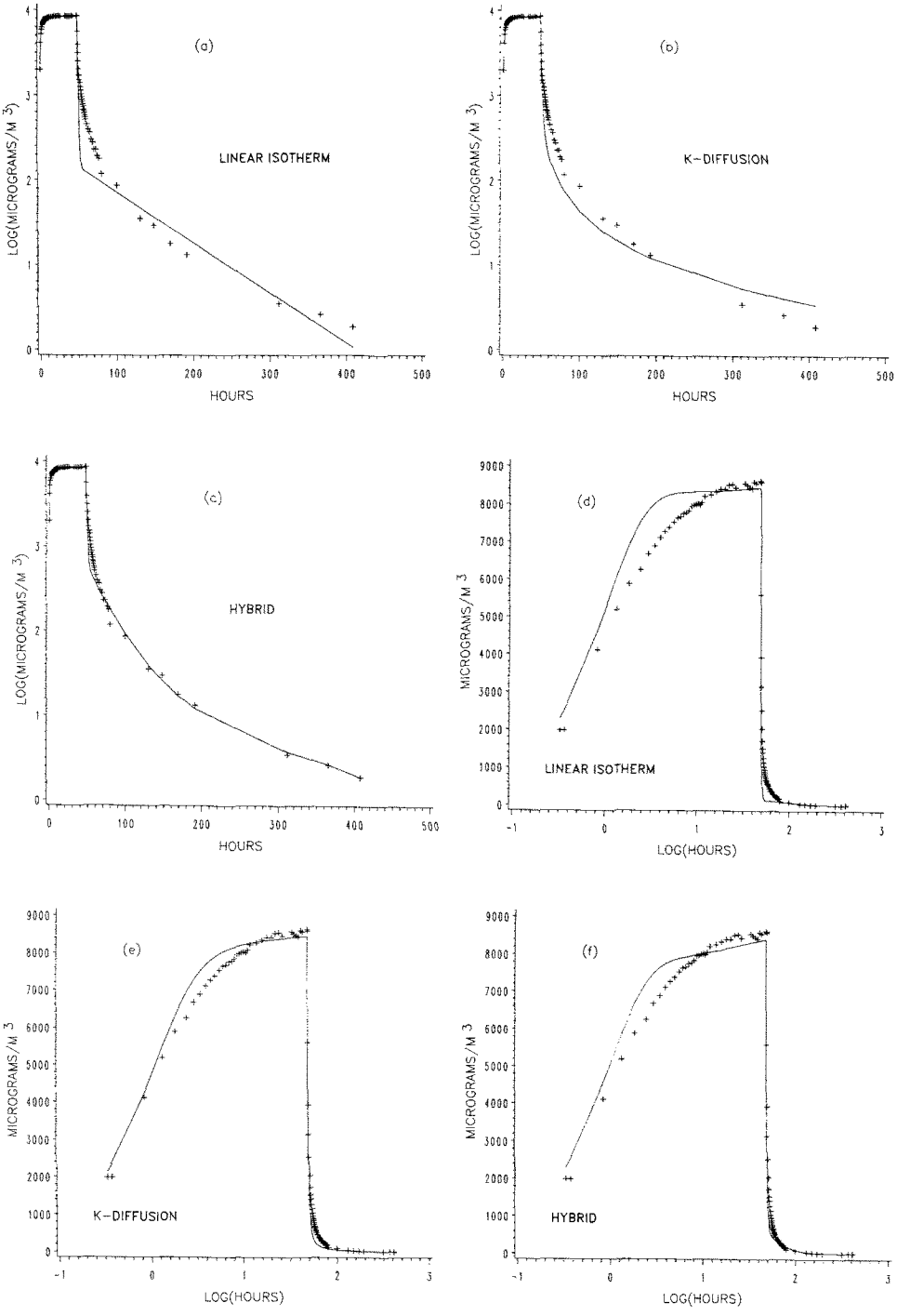

FIG. 6—*IW least squares model fits to carpet/ethylbenzene test chamber data (Carpet-1) in $\log_{10}$ scale of concentration, Figs. (a) through (c), and replotted in linear scale of concentration, Figs. (d) through (f).*

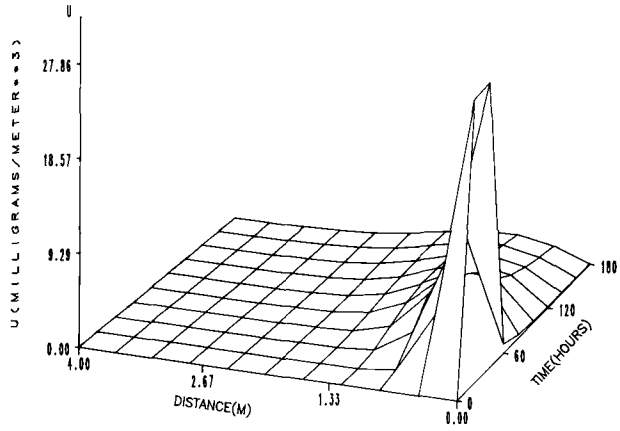

FIG. 7—*Estimated VOC concentration in the sink, based on the* K*-diffusion model fitted to the Pillow-8 data set.*

plot of VOC concentration as a function of distance of penetration into the sink and elapsed time. Can perchloroethylene molecules penetrate more than a meter into a pillow whose apparent thickness is only a few cm? This distance is suggestive of a diffusion pathway.

The diffusion-limited models presented here were developed because our interest was piqued by recalcitrant data sets resulting from pillow and carpet sorption studies and because of largely unsubstantiated speculation relating VOC emissions to porous diffusion. Because our confirmatory data was generated under dynamic test conditions, we largely focused on dynamic properties of the models. Steady-state properties, so familiar in adsorption science, were not useful in discriminating among the models. For example, $\lim_{t(<t0)\to\infty} C(t) = k_1/(k_2 V)$ and $\lim_{t(>t0)\to\infty} C(t) = 0$ for all three models characterized in Table 1. Admittedly, these models are not complete. So as to focus on dynamics, we defined models in terms of somewhat generic constants, then let data dictate the optimal choice of these constants, conditional on the dynamics of the model being correct. It is not implied that k_3, k_4, k, and E are global constants. They are assumed to be only locally constant within the course of an environmentally controlled experiment, and otherwise are dependent on temperature, chemical properties of the VOC, physical properties of the sink, and so forth. Clearly, the physical basis for these constants must be determined before the models have general application, say, in the building trades. Most recently, Guo and Tichenor [*11*] have illustrated an approach to VOC wet source modeling that combines both physical and chemical properties of the VOC with an experimental approach.

Acknowledgment

Research by the senior author was supported under the United States Environmental Protection Agency (US EPA) Cooperative Agreement CR-818520-01-0.

References

[*1*] Berglund, B., Johansson, I., and Lindvall, T., "Volatile Organic Compounds from Building Materials in a Simulated Chamber Study," *Environment International*, Vol. 15, 1989, pp. 383–388.

[2] Nielsen, P., "Potential Pollutants—Their Importance to the Sick Building Syndrome, and Their Release Mechanism," *Proceedings of Indoor Air '87*, Institute for Water, Soil, and Air Hygiene, Berlin, Vol. 2, 1987, pp. 598–602.

[3] Nielsen, P., "The Importance of Building Materials and Building Construction to the Sick Building Syndrome," *Proceedings of Healthy Buildings '88*, Swedish Council for Building Research, Stockholm, Vol. 3, 1988, pp. 391–399.

[4] Tichenor, B. A., Sparks, L. E., White, J., and Jackson, M., "Evaluating Sources of Indoor Air Pollution," Paper 88-110.2, presented at 81st Annual Meeting of the Air Pollution Control Association, Dallas.

[5] Tichenor, B. A., Guo, Z., Dunn, J. E., and Sparks, L. E., "The Interaction of Vapour Phase Organic Compounds with Indoor Sinks," *Indoor Air*, Vol. 1, 1991, pp. 23–35.

[6] Tichenor, B. A., "Indoor Air Sources: Using Small Environmental Test Chambers to Characterize Organic Emissions from Indoor Materials and Products," USEPA Report 600/8-89-074, U.S. Environmental Protection Agency, Washington, DC, 1989.

[7] DeBortoli, M. (co-coordinator), "Guideline for the Characterization of Volatile Organic Compounds Emitted from Indoor Materials and Products Using Small Test Chambers," Report 8, prepared by Working Group 8 of Community Cost Project 613, Commission of the European Communities.

[8] Dunn, J. E., "Models and Statistical Methods for Gaseous Emission Testing of Finite Sources in Well-mixed Chambers," *Atmospheric Environment*, Vol. 21, No. 2, 1987, pp. 425–430.

[9] Dunn, J. E. and Tichenor, B. A., "Compensating for Sink Effects in Emissions Test Chambers by Mathematical Modeling," *Atmospheric Environment*, Vol. 22, No. 5, 1988, pp. 885–894.

[10] Axley, J. W., "Adsorption Modeling for Building Contaminant Dispersal Analysis," *Indoor Air*, Vol. 2, 1991, pp. 147–171.

[11] Guo, Z. and Tichenor, B. A., "Fundamental Mass Transfer Models Applied to Evaluating the Emissions of Vapor-phase Organics from Interior Architectural Coatings," presented to the EPA/AWMA International Symposium on Measurement of Toxic and Related Air Pollutants, 3–8 May, Durham, NC, 1992.

[12] SAS Institute, Inc., *SAS User's Guide: Statistics*, Version 5, Cary, NC, 1985.

[13] Carroll, R. J. and Ruppert, D., "Power Transformations when Fitting Theoretical Models to Data," *Journal of the American Statistical Association*, Vol. 79, No. 386, 1984, pp. 321–328.

William W. Nazaroff,[1] *Ashok J. Gadgil*[2] *and Charles J. Weschler*[3]

Critique of the Use of Deposition Velocity in Modeling Indoor Air Quality

REFERENCE: Nazaroff, W. W., Gadgil, A. J., and Weschler, C. J., **"Critique of the Use of Deposition Velocity in Modeling Indoor Air Quality,"** *Modeling of Indoor Air Quality and Exposure, ASTM STP 1205*, Niren L. Nagda, Ed., American Society for Testing and Materials, Philadelphia, 1993, pp. 81–104.

ABSTRACT: Among the potential fates of indoor air pollutants are a variety of physical and chemical interactions with indoor surfaces. In deterministic mathematical models of indoor air quality, these interactions are usually represented as a first-order loss process, with the loss rate coefficient given as the product of the surface-to-volume ratio of the room times a deposition velocity. In this paper, the validity of this representation of surface-loss mechanisms is critically evaluated. From a theoretical perspective, the idea of a deposition velocity is consistent with the following representation of an indoor air environment. Pollutants are well-mixed throughout a core region which is separated from room surfaces by boundary layers. Pollutants migrate through the boundary layers by a combination of diffusion (random motion resulting from collisions with surrounding gas molecules), advection (transport by net motion of the fluid), and, in some cases, other transport mechanisms. The rate of pollutant loss to a surface is governed by a combination of the rate of transport through the boundary layer and the rate of reaction at the surface. The deposition velocity expresses the pollutant flux density (mass or moles deposited per area per time) to the surface divided by the pollutant concentration in the core region. This concept has substantial value to the extent that the flux density is proportional to core concentration. Empirically, the problem of human exposure to ozone in commercial buildings has been successfully modeled by using the deposition velocity to parameterize ozone removal onto indoor surfaces. The concept has also been applied in investigations of the indoor dynamics of other pollutant species. However, despite the successful application of this concept, caution is advised in using deposition velocity to characterize pollutant-surface interactions. Limitations that are explored in this paper include these: the presumption of uniform mixing throughout the core region may fail; deposition may vary strongly with position in an enclosure; certain classes of surface-pollutant reactions may not be represented adequately as a first-order loss process; transformation processes within the boundary layer may need to be considered in theoretical investigations; and transport rates through boundary layers may depend strongly on near-surface air flow conditions. Published results from experimental and modeling studies of fine particles, radon decay products, ozone, and nitrogen oxides are used as illustrations of both the strengths and weaknesses of deposition velocity as a parameter to indicate the rate of indoor air pollutant loss on surfaces.

KEY WORDS: indoor air quality, modeling, deposition, ozone, radon decay products, nitrogen oxides, particles

The interaction of air pollutants with interior surfaces strongly influences the indoor concentrations and fates of many species. Pollutant interactions with indoor surfaces may be viewed from two contrasting perspectives. In the context of human health concerns, such interactions are frequently beneficial. Pollutants that deposit or react on indoor surfaces are no longer available to be inhaled. On the other hand, material damage to objects kept in buildings is also a significant

[1]Civil Engineering Department, University of California, Berkeley, CA 94720.
[2]Indoor Environment Program, Energy and Environment Division, Lawrence Berkeley Laboratory, Berkeley, CA 94720.
[3]Bell Communications Research, 331 Newman Springs Road, Red Bank, NJ 07701.

concern. In this context, pollutant-surface interactions are generally detrimental, constituting an important factor in the degradation of items such as works of art and electronic equipment.

Accurate deterministic modeling of the concentrations and fates of indoor pollutants requires quantitative knowledge about the rates and outcomes of pollutant interactions at indoor surfaces. To date, most indoor air quality models have parameterized pollutant-surface interactions as a first-order loss mechanism. The loss rate is commonly evaluated as the product of two terms: the surface-to-volume ratio of the indoor space and the deposition velocity.

The central objective of this paper is to review and critique the utility of this approach. The core of the paper consists of three sections. In "Background" we provide a general overview of the deposition velocity concept: how it is defined, what factors govern its value, and how it is determined. We also discuss in this section the nature of near-surface air flows and pollutant-surface interactions. Under "Illustrations" we evaluate information on pollutant-surface interactions for four classes of pollutants: fine particles, radon decay products, ozone and nitrogen oxides. The third major section of the paper is entitled "Limitations." In this section, we explore transport and transformation issues that restrict the utility of the deposition velocity for representing pollutant-surface interactions.

In addition to its use in modeling indoor air, the deposition velocity concept is well established in the literature addressing outdoor air pollution problems. The interested reader is referred to the review article by Davidson and Wu [*1*] and the conference proceedings edited by Pruppacher et al. [*2*] for summaries of this topic.

Background

Definition of Deposition Velocity

The deposition velocity, v_d, is defined as the net flux density, F, of a species to a surface divided by the concentration, C, of that species in the air:

$$v_d = \frac{F}{C} \tag{1}$$

The normalizing airborne concentration is to be determined at a position that is sufficiently far from the surface so that the concentration does not vary (strongly) with position.

If the flux density is measured in units of pollutant mass per area per time, and the concentration is measured in units of pollutant mass per volume, then the ratio has units of length per time. The "deposition velocity" then represents an effective velocity. For a pollutant that has an average deposition velocity v_d, onto a surface of area S, the rate of pollutant mass loss by deposition would be $S \times F = S \times v_d \times C$. This loss rate is equivalent to the rate of mass removal by ventilation at an air flow rate of $S \times v_d$.

The attentive or experienced reader may recognize immediately two significant concerns about the concept of deposition velocity. The first pertains to the normalizing concentration. We have been somewhat (and necessarily) vague about where the concentration, C, should be determined. If the core of a room is not well mixed, then the deposition velocity may be strongly dependent on the position at which C is determined. A second concern relates to the surface area, S. For smooth surfaces such as linoleum flooring and window panes, the meaning of S is unambiguous. But problems may arise in specifying S for surfaces that are not smooth, such as carpets. These and other concerns about the deposition velocity will be discussed in subsequent sections of the paper.

Factors That Govern the Deposition Velocity

To set the context for subsequent discussion, it is helpful to think of pollutant interactions with surfaces on a molecular level. The series of events necessary for the interaction to occur may be divided into two groups: transport and transformation. Interaction of a species with a surface can only occur if a species constituent (a molecule for gases, an individual particle for aerosols) collides with the surface. Transport to the vicinity of the surface may occur by a variety of mechanisms including advection, diffusion, and, in the case of particles, gravitational settling, thermophoresis, electrostatic drift, etc. Once a species constituent strikes a surface, it may or may not interact and be lost from the air, depending on the nature and strength of the chemical and/or physical interactions that occur between the constituent and the surface.

In general, then, we may think of the deposition velocity as being governed by a combination of the rate of transport to a surface and the probability of transformation following collision with the surface. The processes operate in a sequential fashion, so that, if the processes proceed at different characteristic rates, the total loss rate is governed by the slower phenomenon. For some species, such as particles and highly reactive gases, transformation is a relatively probable consequence of collision, so that the deposition velocity is significantly influenced by the rate of transport to surfaces. For other species, the transformation probability may vary strongly with the nature of the surface material or surface conditions (for example, the amount of sorbed water), and this variability may control the local deposition velocity.

In sum, then, the deposition velocity is expected to be a function of the factors that govern transport and transformation. For a given species, transport will be governed by factors such as the indoor air flow conditions, particularly near surfaces, and details of the surfaces, including shape and orientation. The transformation probability for a given species will depend on surface composition, possibly modified by previously deposited species.

Conceptual Value of Deposition Velocity

If the deposition velocity for a particular species in a given indoor environment is known, then the rate of species loss from indoor air by surface interaction may be calculated. In many cases, surface loss is a significant removal mechanism. An accurate quantitative estimate of this rate of loss is essential for understanding the relationship between indoor concentrations and other governing variables.

Consider the case of first-order irreversible removal of a species by surface interaction. The relationship between the deposition velocity and the rate of change of indoor concentration due to surface loss may be represented by

$$\left(\frac{dC}{dt}\right)_{\text{surface-loss}} = -\frac{C}{V}\int_S v_d(s)\, ds = -C\,\frac{S}{V}\,\overline{v_d} \tag{2}$$

where V is the volume of the room, $v_d(s)$ is the deposition velocity of the species onto the surface at position s, and ds is the area of a differential surface element. The integration is to be carried out over all room surfaces, the total area of which is S. The second "equal" sign in Eq 2 may be considered to define the area-weighted mean deposition velocity, $\overline{v_d}$.

If a species is irreversibly deposited or sorbed onto a surface, then the local rate of surface accumulation may also be computed from the deposition velocity:

$$\frac{dM(s)}{dt} = C\, v_d(s) \tag{3}$$

where $M(s)$ represents the mass of the species accumulated on a surface at position s per unit area.

Illustrative Applications

Human Exposure to Ozone—Indoor ozone concentrations can be a significant fraction of outdoor concentrations [*3*, and references therein]. Because of the large amount of time spent indoors, indoor ozone exposures (concentration × time) can be substantial and are sometimes greater than outdoor exposures, even though indoor concentrations are normally less than those outdoors. The contribution of indoor to total exposures is especially important when one considers possible chronic health effects resulting from long-term ozone exposure [*4*].

The ozone encountered in most indoor environments has infiltrated from outdoors [*5*]. In some cases, it is generated indoors by sources such as electrostatic air cleaners and photocopy machines [*6*]. In the absence of indoor emission sources, its concentration can be estimated from the outdoor ozone concentration, the air-exchange rate, and the rate of removal on indoor surfaces. The last factor depends directly on the deposition velocity. Knowledge of the deposition velocity allows one to estimate indoor ozone levels from outdoor values and readily available building parameters.

Accumulation of Particles on Cultural Artifacts and Electronic Equipment—Airborne particles can deposit on cultural artifacts causing soiling and material damage [*7,8*]. Airborne particles, especially fine-mode particles, can also deposit on sophisticated electronic equipment, resulting in equipment failures [*9*]. If the deposition velocities of particles in different size ranges are known, one can calculate the rate at which particles accumulate on surfaces. Such information has been used to develop predictions of the benefits and costs derived from improving air quality in telephone switching offices [*10*]. In a similar vein, the information can be used in choosing filtration systems, in estimating "time to failure," and in evaluating potential risks to cultural artifacts and electronic equipment under different heating, ventilating, and air-conditioning (HVAC) scenarios.

Nature of Near-Surface Air Flow and Its Role in Pollutant Deposition

Near-surface air flow in rooms is controlled by a combination of natural convection, induced by heat transfer at surfaces, and forced convection, induced, for example, by the operation of mechanical ventilation systems. In cases when the indoor air is not being circulated with furnace-fans (for residences) or HVAC systems (for commercial buildings), natural convection may be the dominant mechanism inducing air motion. Many other factors may also influence indoor air flow: infiltration of wind through cracks, mechanical air exhaust (for example, clothes dryers, bathroom fans), the stack effect, thermal plumes from hot surfaces (for example, office equipment, residential ovens), and mixing fans. The general characteristics of natural convection motion of fluid in enclosures has been mathematically analyzed by Gill [*11*] and Quon [*12*] and confirmed by several experimental and numerical investigations [*13*].

In the steady state, air flow can be visualized in terms of the flow paths (called stream lines) of parcels of air as they move through space. In laminar flow, the air parcels follow these paths exactly. In turbulent flow, the stream lines represent the paths taken by air parcels after averaging over the turbulent fluctuations. Owing to the definition of stream lines, air parcels cannot cross them. For two-dimensional flows, adjacent stream lines represent boundaries within which a given mass of fluid flows, without crossing the stream lines on either side. As a result, when two adjacent stream lines separate from each other, the fluid flow in between them must slow down (to keep the fluid mass flux constant). As the stream lines get closer together, the fluid flow between them must accelerate to keep the mass flux constant.

The flow of a viscous fluid, such as air in a room, can be analyzed with the following approximation: The air is assumed to behave as a viscous fluid only within thin layers (typical thickness of about 1 to 2 cm for room air motion) which line the solid surfaces in the room. The air away from these thin layers behaves as if it were an ideal (that is, nonviscous) fluid. This approximation is known as the boundary layer approximation, and has been applied with great success to a large

variety of viscous fluid flow problems. The thin layer of fluid lining the solid surfaces is called the boundary layer. The thickness of this *momentum* boundary layer corresponds to the distance from a surface at which the air velocity approaches its free stream value. The thickness depends on the momentum diffusivity of the fluid, as given by its kinematic viscosity—0.15 $cm^2\ s^{-1}$ for air.

The boundary layer concept can also be used to describe the near-surface variation of temperature and contaminant-species concentrations. The *thermal* boundary layer thickness depends on the thermal diffusivity of the fluid—0.2 $cm^2\ s^{-1}$ for air. Since the thermal diffusivity for air has the same magnitude as the momentum diffusivity, the momentum and thermal boundary layers have about the same thickness.

For contaminants in air, different species diffusivities give rise to concentration boundary layers of different thicknesses. Gaseous species with molecular weights close to that of air have diffusivities comparable to the thermal diffusivity of air, and for these species the *concentration* boundary layers will have a thickness similar to those of the momentum and temperature boundary layers. In this case, mass transfer across the concentration boundary layer can be approximately analyzed from studies of heat transfer in corresponding circumstances [*14,15*].[4]

In contrast to low molecular weight gases, particles have small diffusion coefficients. Consequently, the particle concentration boundary layers are much thinner than the momentum boundary layers.[5] One result of this point is that surface roughness may be large enough to strongly influence particle transport across the boundary layer while having little effect on momentum or heat transfer. Another complication towards understanding particle transport to indoor surfaces is that processes other than diffusion and advection—such as thermophoresis, gravitational settling, inertial drift, and electrostatic migration—are frequently important.

Within the boundary layers, there is little air motion in the direction perpendicular to the solid surface. Consequently, almost all transport across a boundary layer must occur by mechanisms other than advection (for example, diffusion, electrostatic drift, thermophoresis, gravitational settling). The effective rate of diffusive transport to a surface is approximately given by the diffusion coefficient divided by the boundary layer thickness. In a thicker boundary layer, the transport rate relative to the concentration outside the boundary layer is reduced.

The thicknesses of the boundary layers are influenced by the intensity and nature of near surface air flow. The boundary layers are thinner when the fluid outside them is fast moving, and thicker when the fluid moves slowly. In the idealized case of natural convection flow along an isolated isothermal vertical surface, the momentum boundary layer thickness varies in proportion to $(x/|\Delta T|)^{1/4}$ where x is the distance along the surface in the direction of flow and $|\Delta T|$ is the absolute value of the temperature difference between the surface and the air. For forced laminar flow parallel to a flat plate, the momentum boundary layer thickness scales as $(x/U_\infty)^{1/2}$ where U_∞ is the free stream air velocity.

When the transport of species across the boundary layer is diffusion controlled, it can be visualized by studying the isopleths of species concentrations, especially near the surfaces. Diffusion is driven by concentration gradients; a large gradient of concentration implies relatively rapid diffusive transport down the gradient. A high density of concentration isopleths near a surface then implies a large change in species concentration over a small distance, and hence large concentration gradient and deposition flux. Conversely, a large spacing of concentration isopleths near a surface implies small concentration gradients and small deposition rates.

[4]Note, however, that natural convection heat transfer results must be applied with caution: In typical indoor environments, temperature gradients are large enough to induce flow whereas concentration gradients are not.

[5]Note an important distinction: for a given species a thinner boundary layer implies a larger rate of transport to a surface; however, for a comparison between species under given flow conditions, the species having the slower rate of diffusive transport will tend to have a thinner boundary layer.

Nature of Surface Reactions

Under conditions encountered in most indoor environments, when submicron particles or unattached radon decay products come in contact with a surface, they adhere. To a first approximation, adhesion is complete and irreversible. Particles are bound primarily by van der Waals forces, although gravity and electrostatic interactions may also contribute. The smaller a particle, the more important are the van der Waals interactions.

When gas-phase molecules encounter a surface, a fraction of the collisions may be ineffective (that is, some molecules may make contact with a surface and reenter the boundary layer unchanged). There are other ensuing possibilities: reversible sorption, irreversible sorption, and sorption followed by chemical transformation. Chemical transformations include decomposition reactions, acid-base reactions, and oxidation-reduction (redox) reactions. The progress of a heterogeneous gas reaction depends on the nature of both the adsorbate and the adsorbent, and such reactions are frequently catalyzed by the adsorbing surface (heterogeneous or contact catalysis) [*16*]. In catalyzed processes, the chemisorbed gas sometimes assumes the role of a reaction intermediate, with the result of enhancing the overall rate of the reaction. If the catalyzed reaction is bimolecular, it may be faster simply because the concentrations of the reactive species are higher on the surface than in the gas phase [*17*].

When a gas decomposes on a surface, the reaction rate is normally proportional to θ, the fraction of the surface covered by the adsorbate. In such a heterogeneous reaction, three simple cases can arise [*16*]: if only a small amount of the surface is covered, $\theta = bP$ (where b is the adsorption coefficient and P is the partial pressure of the adsorbate gas), and the gas's rate of heterogeneous decomposition will be first order; at moderate surface coverages, $\theta = bP^{1/n}$, where $0 < n < 1$, and the decomposition rate will be a fractional order; if the surface coverage is almost complete, $\theta \sim 1$ and the gas's decomposition proceeds at a zero-order (that is, concentration independent) rate. Most gas phase pollutants encountered indoors are present at low concentrations (10^{-10} to 10^{-7} atm). At such low partial pressures, the resultant surface coverage would be small and decomposition reactions are therefore expected to proceed at a first-order rate.

Redox reactions tend to have large activation energies and consequently proceed at relatively slow rates. Contact catalysis can certainly increase the rate at which such reactions occur, but acid/base reactions tend to be faster still (and hence their rates are normally transport controlled). A dramatic example of the potential importance of acid/base surface processes comes from an early study by Wilson [*18*]. In a test room (volume: 47 m^3; surface area: 124 m^2), the deposition velocity of SO_2 was measured to be 1×10^{-2} cm s^{-1} under normal conditions. When the walls and floor were then painted with a "strong solution of sodium carbonate," the deposition velocity increased by about a factor of seven. The carbonate ion is an effective base, substantially increasing the capacity of the surface to absorb the acidic SO_2.

Indoor surfaces are commonly basic (gypsum, concrete, nylon, etc.) Consequently, acid/base reactions tend to be significant for acidic gases (for example, SO_2, HNO_3, HCl, HONO). For basic gases, such as NH_3, important acidic surfaces encountered indoors are typically those associated with wood and paper products.

The presence of moisture can influence interactions with surfaces; the influence can range from reaction at the surface of a moisture film to reaction within an aqueous layer. As the relative humidity of a room increases, moisture films develop on various surfaces within the room—the thickness of these films depends on the nature of the surface. For example, at 50% RH most common metal surfaces have between one and three molecular layers of adsorbed water [*19*]. Gases can dissolve in a moisture film. Given the small partial pressures of indoor pollutants, the resulting solutions would be fairly dilute. Under these conditions, the solubility of the gas is proportional to its partial pressure (Henry's Law). However, tabulated values of Henry's Law constants are based on experiments with bulk water. Water films on surfaces tend to have more structure than

TABLE 1—*Methods for determining deposition velocity.*

Method	Application	Illustrative References
Analysis of transient data[a]	ozone	Mueller [20]; Sabersky et al. [21]
	combustion appliance emissions	Traynor et al. [22]
Analysis of steady-state data[a]	ozone	Weschler [3]
	radon decay products	Knutson [23]
Measurement of deposited flux and airbone concentrations[a]	fine particles	Ligocki et al. [24]
	radon decay products	Toohey et al. [25]
Theoretical mass transport analysis	particles and reactive gases	Nazaroff and Cass [26]
	radon decay products	Nazaroff et al. [27]

[a]These methods may be employed in full-scale rooms or in experimental chambers. Examples of the latter include ozone decomposition experiments of Sabersky et al. [21] and radon decay product deposition experiments of Vanmarcke et al. [28].

bulk water and this will alter the value of the constant appropriate for a given dissolution process [19]. In evaluating this effect, the polarity and structure of the surface is important, as well as the nature of the dissolving species. In addition to dissolution processes, water can influence surface chemistry. For example, acid/base reactions may be facilitated as the proportion of Bronsted acid (proton donor) sites increases with increasing surface water [17]. Similar enhancements can occur for hydrolysis and water assisted decomposition reactions.

Methods of Determining Deposition Velocity

Methods that have been employed for evaluating the deposition velocity of species in indoor air are presented in Table 1. A brief discussion of each method is presented below.

The first two methods listed in Table 1 are based on a representation of a room or building as a continuous-flow stirred-tank reactor (CFSTR). A commonly derived expression for the rate of change of indoor pollutant concentration, based on a material balance, is as follows:

$$\frac{dC}{dt} = \lambda_v C_{out} - \lambda_v C - \overline{v}_d \frac{S}{V} C \tag{4}$$

where C_{out} is the outdoor species concentration and λ_v is the air-exchange rate, that is, the total rate of outdoor air flow into the building divided by the building volume. Other terms are as defined previously (see Eq 2). In this representation, the following assumptions are made: no filtration of pollutants from outside air on entry, no direct indoor emissions of pollutants, first-order depositional loss onto surfaces, and no homogeneous production or decay of the species. Note specifically that this equation is not properly formulated to described radon decay product dynamics [23]. If the variables other than C are constant for a given situation, then the solution to Eq 4 is

$$C(t) = C_{out} \frac{\lambda_v}{\lambda_v + \overline{v}_d \frac{S}{V}} \left(1 - \exp\left[-\left(\lambda_v + \overline{v}_d \frac{S}{V}\right)t\right]\right) + C(0) \exp\left[-\left(\lambda_v + \overline{v}_d \frac{S}{V}\right)t\right] \tag{5}$$

where $C(0)$ is the concentration at time $t = 0$. The first term on the right-hand side of Eq 5 reflects the growth toward the steady-state result

$$\frac{C(\infty)}{C_{out}} = \frac{\lambda_v}{\lambda_v + \overline{v_d}\frac{S}{V}} \tag{6}$$

The second term on the right-hand side of Eq 5 reflects the decay of an initial concentration, $C(0)$, of contaminant in the room owing to removal by ventilation and deposition.

To determine deposition velocity from analysis of transient data, an initially elevated indoor concentration of the pollutant is established, for example, by indoor emission of a species such as NO_2 from a gas-fired range [*22*]. Subsequently, the concentration decay is monitored as a function of time. If the initial pollutant concentration is much larger than the steady-state concentration (that is, $C(0) >> C(\infty)$) then it is appropriate to neglect the first term on the right-hand side of Eq 5 in interpreting the results. A linear least-squares regression is fitted to $\ln [C(t)/C(0)]$ versus time; the slope of this regression is $b_1 = -(\lambda_v + \overline{v_d}\, S/V)$. The ventilation rate, λ_v, may be determined from a similar experiment in which a nonreactive (that is, $\overline{v_d} = 0$) tracer gas, such as SF_6, is injected into the room and monitored over time. The deposition velocity is then evaluated as $\overline{v_d} = -(b_1 + \lambda_v) \times (S/V)^{-1}$. If the rate of pollutant entry from outdoor air or from other sources cannot be neglected, the method must be adjusted to fit the more complex functional form of Eq 5, for example, by nonlinear least squares, to extract the deposition velocity.

The deposition velocity also may be inferred from the analysis of steady-state data using Eq 6, rewritten as follows:

$$\overline{v_d} = \frac{\lambda_v\,(C_{out} - C(\infty))}{\frac{S}{V}\,C(\infty)} \tag{7}$$

For this equation to be valid, the outdoor concentration must be approximately constant over a period of at least several times the quantity $(\lambda_v + \overline{v_d}\, S/V)^{-1}$. This method works well when entry from outdoor air is the dominant indoor source of a species.

The most direct means of determining deposition velocity is based on measurement of deposition flux density and the airborne concentration. In this case, the defining relationship, Eq 1, may be used directly to determine the deposition velocity. For the most part, this approach is only feasible for condensed matter. This is the only experimental method that can provide information on spatial dependence of deposition. The key limitation is the difficulty in measuring surface accumulation of contaminants. Even where measurement techniques exist, long sampling periods are usually required to accumulate sufficient mass to exceed minimum detection limits.

Each of the three techniques described above may be employed in experimental chambers as well as in rooms in buildings. A central advantage of conducting experiments in chambers is that governing variables such as the type of surface and the near-surface air flow conditions may be more effectively controlled than in a room. Also, elevated species concentrations may be used, simplifying the measurement requirements. However, air flow conditions in buildings are generally not well understood and air flow conditions in chamber studies of deposition have usually not been well characterized. Consequently, it is difficult to reliably extrapolate results from chambers to buildings.

Much of the interest in deposition arises for species that interact strongly with surfaces. For particles and highly reactive gases, the deposition velocity is expected to be limited by the rate of mass transport of pollutants to surfaces. Provided that the near-surface air flow conditions are sufficiently well understood, theoretical mass-transport analysis may be used as a basis for deter-

TABLE 2—*Measurement and model prediction results for indoor deposition velocities of fine particles to vertical surfaces.*

Species	v_d (cm s^{-1})	Comments; References
Fine-mode sulfate	0.003–0.005	2 telephone buildings (Wichita, KS and Lubbock, TX); ion chromatographic analysis; 120 surface samples from 6 equipment frames; 3 months air sampling; Sinclair et al., 1985 [*29*].
Fine-mode sulfate	0.004, 0.005	2 telephone buildings (Neenah, WI and Newark, NJ); ion chromatographic analysis; 500 surface samples from 25 equipment frames; 1 year air sampling; Sinclair et al., 1990a [*30*] and Sinclair et al., 1988 [*31*].
Fine-mode sulfur	0.003	1 apartment (Helsinki); PIXE analysis; apiezon/Nuclepore membrane filter deposition coupons; 4 week exposure; intermittent air sampling; Raunemaa et al., 1989 [*32*]
Fine-mode sulfate	0.0002–0.001	5 museums (Southern CA); ion chromatographic analysis; TFE-fluorocarbon membrane filter deposition plates; 2 months summer and 2 months winter exposure; air sampling every 6th day; Ligocki et al., 1990 [*24*]
0.5-μm diameter particles	0.0001–0.002	5 museums (Southern CA); single particle analysis; mica deposition plates; 2 months summer and 2 months winter exposure; air sampling every 6th day; Ligocki et al., 1990 [*24*]
0.5-μm diameter particles	0.00002–0.0004	5 museums (Southern CA); model results based on surface-air temperature differences, near-wall air velocities, and assumed air-flow regimes; Nazaroff et al., 1990, Table 5 [*8*]

mining deposition velocities. Nazaroff and Cass [*26*] have reported results of such analyses for three model air flow conditions: homoegeneous turbulence, forced laminar flow parallel to an isolated flat plate, and natural convection flow induced by heat-transfer at surfaces. Such analyses could also be extended to predict deposition velocities in cases in which surface transformations limit loss rates, provided that the surface reaction rates could be adequately characterized.

Illustrations

In this section, experimental and theoretical information on deposition velocity is summarized for several species or classes of species—fine particles, radon decay products, ozone, and nitrogen oxides. For each of these contaminants, indoor deposition is at least potentially significant. Furthermore, several studies have been published on the rates of indoor-surface interactions for each use. The central aims of this section are, first, to provide quantitative information on the observed deposition velocities of a range of compounds of interest and, second, to synthesize the information in a manner that emphasizes the limits of our present understanding.

Fine Particles

The deposition of fine particles to indoor surfaces is normally a smaller sink than ventilation (both exfiltration and exhaust). Consider fine-mode sulfate particles with a mean deposition velocity ($\overline{v_d}$) of 0.003 cm s^{-1} (see Table 2), a room with a surface-to-volume (S/V) ratio of 2.9 m^{-1} and a ventilation rate (λ_v) of 1/h. For this case, the first-order rate constant for removal by deposition onto surfaces is 0.87×10^{-4} s^{-1} ($\overline{v_d} \times S/V$), while the first-order rate constant for removal by ventilation is 2.8×10^{-4} s^{-1} (λ_v). Obviously, higher ventilation rates and smaller deposition velocities would decrease further the relative importance of deposition as a sink. However, although

ventilation may dominate surface removal, particle deposition remains a concern due to the cumulative damage to surfaces that it can cause.

Table 2 lists measured indoor deposition velocities (to vertical surfaces) for fine-mode sulfate, fine-mode sulfur and 0.5 μm particles. The deposition velocities of these species should be comparable: most of the fine-mode sulfur is present as sulfate salts [*33*]; the mass median diameter of fine-mode sulfate is approximately 0.5 μm [*34*]; and sulfate particles typically constitute the majority of the particles in this size range [*33,35*]. The entries provide interesting comparisons among studies by three separate research groups using distinct sampling and analytical procedures. Table 2 also includes results from a modeling effort [*8*] applied to one of the measurement studies [*24*].

As reported in Table 2, the deposition velocities measured by Ligocki et al. [*24*] and modeled by Nazaroff et al. [*8*] are much smaller than those measured by Sinclair et al. [*29–31*] and Raunemaa [*32*]. This may reflect real differences or measurement artifacts. In each study, the reported deposition velocities have been calculated as the ratio of measured surface accumulation rates (that is, flux densities) to measured airborne concentrations. The low accumulation rates mandate extended sampling intervals followed by state-of-the-art analytical procedures—challenging conditions for obtaining accurate results. In both the "telephone" and "museum" studies, the periods during which airborne concentrations were measured do not match those during which accumulation rates were determined. However, it appears unlikely that the actual average airborne concentrations could vary sufficiently from the sampled airborne concentrations to explain the differences in deposition velocities among studies.

Sinclair et al. [*36*] examined location-to-location differences in airborne concentrations and surface accumulation rates at the Newark and Neenah sites. At Newark, air samplers were deployed at ten indoor locations; at Neenah, eleven; and airborne sampling was conducted over four intervals of four to five weeks each. At both Newark and Neenah, the airborne concentrations were remarkably constant (the standard deviation was only 2% of the mean), while accumulation rates varied by a factor of five. The investigators concluded that the measured differences in accumulation rates from location to location were due to differences in deposition velocities. (The values reported in Table 2 are averages.)

Similarly, the differences among the measured deposition velocities listed in Table 2 may simply reflect different surfaces and near-surface airflows at the switching offices and museums. The sampled surfaces at the switching offices were metallic and an integral part of the equipment; the sampled surfaces at the museums were either TFE-fluorocarbon or mica surrogates and were sometimes thermally isolated from the walls. The switching offices have mechanical HVAC systems and these systems operate almost continuously. Not all of the museums have mechanical HVAC systems, and among those that do, some operate only intermittently. Furthermore, the surfaces sampled at the switching offices were either protruding or recessed relative to the plane of the equipment frames. In contrast, the surrogate surfaces employed at the museums were positioned, in some cases, so as to minimize disturbance of air flows along walls. Hence, one would expect turbulence and near-surface airflows to be greater in the switching office studies than in the museum studies.

The focus of this section has been ~0.5 μm diameter particles. However, the variation of deposition velocities with particle size is also of importance. There is a tendency for modeled deposition velocities [*8*] to show more of a decrease with increasing particle size than is observed in experiments [*24*]. This phenomenon may be due to a measurement bias [*8*]. However, refinements may also be necessary in the model (for example, incorporating the effect on deposition of disruption of the boundary layer caused by air passing over thin deposition plates).

Radon Decay Products

The indoor concentrations of radon and its decay products are determined by two factors: the rate with which they enter or are generated in the building, and the rate with which various processes remove or transform them. Apart from radioactive decay, the following processes lead

TABLE 3—*Deposition velocity of unattached radon progeny: experimental and numerical simulation results.*

Enclosure (Species)	v_d (cm s^{-1})	Comments; References
50-L cylindrical drum (^{218}Po)	0.033–0.047	Small dimensions probably led to slower air motion than in real rooms leading to low estimate of v_d; McLaughlin and O'Byrne, 1984 [*40*]
1000-L aluminum chamber (^{212}Pb)	0.11	Chamber contained a large stirring paddle. This and the longer life of ^{212}Pb both contribute to the large estimate of v_d; Cox and Penkett, 1972 [*42*]
Large basement (^{218}Po)	0.10–0.50	Deposition velocity derived from model and measured values of deposited activity and attached fraction. Deposition velocity found to vary with location and qualitatively correlated with air flow; Scott, 1983 [*43*]
Utility room (^{218}Po)	0.44	Analysis of deposited activity based on a model. They assumed 10% unattached progeny. Knutson [*23*] states that reanalysis of their data assuming a more realistic value for unattached fraction (30–40%) yields a deposition velocity of 0.14 cm s^{-1}; Toohey et al., 1984 [*25*]
26 m^3 room (^{212}Pb and ^{218}Po)	0.055–0.52	Analysis of deposited activity based on a model. Both ^{212}Pb and ^{218}Po activities measured separately. Unattached fraction estimated. Room had fan. Higher values of deposition velocity correspond to fan on, lower values to fan off; Bigu, 1985 [*41*]
3 m × 3 m enclosure (^{212}Pb and ^{218}Po)	0.01–0.17	Numerical modeling of deposition from solving governing equations for natural convection and progeny transport from first principles. The tabulated range reflects averages over enclosure surfaces under a variety of conditions. The deposition velocity was found to vary strongly as a function of position, with peak local values near corners as high as 0.29 cm s^{-1}. Deposition velocity was also predicted to increase significantly with rate of attachment to particles; Nazaroff et al., 1992 [*27*]; Gadgil et al., 1992 [*44*]

to removal or transformation of radon progeny: attachment to airborne particles (which greatly reduces their diffusivity, and thus affects rates of diffusion-controlled processes), deposition onto indoor surfaces, and removal from the indoor environment by ventilation. The full dynamics of the fate of decay products can be specified with equations that determine the concentrations of the various species based on given rate constants. Such a model was first formulated by Jacobi [*37*] and refined by Porstendörfer et al. [*38*]. A good presentation is given by Knutson [*23*].

Because of their smaller mass and correspondingly larger diffusivity, the unattached progeny provide a much larger radioactive dose to the bronchi of the lung per atom inhaled than is attributable to the attached radon progeny [*39*]. Deposition onto walls and other solid indoor surfaces is a significant removal mechanism for unattached progeny, again because of their relatively large diffusivity. Deposition of unattached ^{218}Po thus plays an important role in influencing the radiological dose to the lung from exposure to indoor radon.

Key work towards obtaining experimental values of the deposition velocity for the unattached radon progeny has been reviewed by Knutson [*23*]. Particularly since 1980, there have been several experiments conducted with the aim of determining the deposition velocity. Experiments have been conducted in laboratory-scale chambers [*40*] and also in full-scale rooms [*25,41*]. Deposition velocities of unattached radon decay products have also been predicted by solving the fundamental equations governing (1) air motion in the enclosure and (2) radon progeny transport and dynamics. Table 3 summarizes the results obtained in several studies.

The numerical simulations predict that deposition velocities of unattached decay products increase with increasing rate of attachment to particles. The simulations also predict variation in

deposition velocity with position of more than one order of magnitude, owing to variations in local air motion and boundary layer thickness [*27,44*]. In general, however, the predicted deposition velocities are significantly smaller than those determined by experiment. Unfortunately, the reports of experimental measurements are not adequately specific with respect to the location where the deposition velocities were measured, and have included inadequate characterization of the air flow in the enclosures. Thus, the discrepancy between the numerical predictions and the experimental results may be owing to differences in the near-surface air motion characteristics, or to some as-yet-ignored aspect of the deposition process. More completely characterized experiments are needed to resolve this issue.

Ozone

The removal of ozone by indoor surfaces is a first order process [*20,21*]. Table 4(*a*) lists rate constants for this process derived from experiments where ozone was introduced into a room, the space was sealed, and the decay of ozone monitored (that is, analysis of transient data). Table 4(*b*) lists rate constants obtained from reported indoor/outdoor (I/O) ratios and air-exchange rates (λ_v) (that is, analysis of steady-state data). Tables 1(*a*) and 1(*b*) also list ozone deposition velocities, calculated using estimated values for the surface-to-volume ratio in the various indoor settings. These deposition velocities range from 0.015 cm s^{-1} in a stainless steel room to 0.075 cm s^{-1} in a clean room. However, for most of the sites the numbers are remarkably similar, clustering about 0.04 cm s^{-1}.

The deposition velocities appear to be sensitive to indoor air flow conditions. Consider the fifth and sixth entries in Table 4(*a*). These measurements were made within the same room; in one case, the central ventilation system fan was "off" (v_d = 0.025 cm s^{-1}); in the other, the fan was "on" (v_d = 0.046 cm s^{-1}). Higher air exchange rates may also increase transport to surfaces, and, hence, deposition velocities. In Table 4(*b*), the deposition velocity measured in the clean room (λ_v = 30 h^{-1}, v_d = 0.075 cm s^{-1}) is larger than those measured at the other indoor sites.

There are a number of basic issues regarding deposition velocities reported for ozone in various indoor settings:

Site-to-site variability—In chamber studies, Sabersky et al. [*21*] demonstrated that different surfaces scavenge ozone at markedly different rates. For a freshly exposed plate glass or aluminum surface, v_d was 0.001 cm s^{-1}; for cotton muslin or lamb's wool, v_d was 0.11 cm s^{-1}. Materials such as linen, nylon and plywood had values between these extremes. *Why, then, are the values in Table 4 so similar from site-to-site and study-to-study?* A possible explanation is that, since many different materials are encountered within a building, and since these materials tend to be similar from structure to structure, then, the "average" deposition velocity will be similar from structure to structure. An alternative explanation invokes moisture films or indoor surfaces. The thickness of such films is a function of the relative humidity and the nature of the surface. However, if a thin film of water can promote the surface decomposition of ozone, moisture films may promote similar rates of ozone decay on quite different surfaces. This concept will be expanded in what follows.

Aging of surfaces—In the same chamber studies cited above, Sabersky et al. [*21*] demonstrated that ozone's deposition velocity to an "aged" surface (exposed to ozone for several days) is significantly smaller than to a fresh surface. For aged plate glass or aluminum, v_d was 0.0005 cm s^{-1}; for aged cotton muslin, 0.015 cm s^{-1} and for aged lamb's wool, 0.0004 cm s^{-1}. All the materials studied demonstrated an aging effect; some also demonstrated "reverse aging" (for example, after several days with no ozone exposure, the deposition velocity to a plywood specimen was comparable to that measured for freshly exposed plywood). Similarly, Mueller et al. [*20*] found that the decomposition rate of ozone in an aluminum chamber was strongly dependent on the extent of prior ozone exposure and decreased by a factor of five with progressive aging of the aluminum surfaces. They also reported "reverse aging;" ozone decomposed at a rate closer to a "fresh" value after the chamber had been ozone-free over a weekend. *Does "aging" affect dep-*

TABLE 4—*Measured rate constants for ozone decay on indoor surfaces,* $v_d \times \frac{S}{V}$, *and inferred average deposition velocity* v_d.

a. Values based on observed first-order decay in isolated rooms.

Interior Space	$v_d \times \frac{S}{V}$ (s^{-1})	v_d (cm s^{-1})	Comments; References
Aluminum room, 11.9 m^3	0.9×10^{-3}	0.027	S/V = 3.3 m^{-1}; Mueller et al., 1973 [20]
Stainless steel room, 14.9 m^3	0.4×10^{-3}	0.015	S/V = 2.7 m^{-1}; Mueller et al., 1973 [20]
Bedroom, 40.8 m^3	2.0×10^{-3}	0.062	S/V = 3.3 m^{-1}; Mueller et al., 1973 [20]
Office, 55.2 m^{-3}	1.1×10^{-3}	0.039	S/V = 2.8 m^{-1}; Mueller et al., 1973 [20]
Home; no forced air movement	0.8×10^{-3}	0.025	estimated S/V = 3.3 m^{-1}; Sabersky et al., 1973 [21]
Home; furnace fan on	1.5×10^{-3}	0.046	estimated S/V = 3.3 m^{-1}; Sabersky et al., 1973 [21]
Department store	1.2×10^{-3}	0.043	estimated S/V = 2.8 m^{-1}; Thompson et al., 1973 [45]
Office, 24.1 m^{-3}	1.1×10^{-3}	0.039	estimated S/V = 2.8 m^{-1}; Allen et al., 1978 [6]
Office, 20.7 m^3	1.2×10^{-3}	0.043	estimated S/V = 2.8 m^{-1}; Allen et al., 1978 [6]

b. Values based on reported indoor-outdoor concentration ratio (I/O) and air-exchange rate (λ_v)

Interior Space	λ_v (h^{-1})	I/O	$v_d \times \frac{S}{V}$ (s^{-1})	v_d (cm s^{-1})	Comments; References
Office/Lab	5.5	0.57	1.2×10^{-3}	0.043	est. S/V = 2.8 m^{-1}; Shair and Heitner, 1974 [46]
Office/Lab	5.5	0.63	0.9×10^{-3}	0.032	est. S/V = 2.8 m^{-1}; Shair and Heitner, 1974 [46]
Office/Lab	3.6	0.50	1.0×10^{-3}	0.035	est. S/V = 2.8 m^{-1}; Shair and Heitner, 1974 [46]
Museum	2.0	0.41	1.2×10^{-3}	0.043	est. S/V = 2.8 m^{-1}; Nazaroff & Cass, 1986 [47]
Museum	0.3	0.07	1.2×10^{-3}	0.043	est. S/V = 2.8 m^{-1}; Nazaroff & Cass, 1986 [47]
Office/Lab	4	0.5	1.1×10^{-3}	0.039	est. S/V = 2.8 m^{-1}; Weschler et al., 1992 [48]
Office/Lab	8	0.7	0.9×10^{-3}	0.032	est. S/V = 2.8 m^{-1}; Weschler et al., 1992 [48]
Office	0.6	0.2	0.7×10^{-3}	0.025	est. S/V = 2.8 m^{-1}; Weschler et al., 1992 [48]
Lab	10	0.8	0.7×10^{-3}	0.025	est. S/V = 2.8 m^{-1}; Weschler et al., 1992 [48]
Cleanroom	30	0.8	2.1×10^{-3}	0.075	est. S/V = 2.8 m^{-1}; Weschler et al., 1992 [48]

osition velocities measured within selected buildings? Perhaps. In studies by Weschler et al. [*48*] the authors report smaller I/O values during winter, when the outdoor ozone levels are low, than during spring, summer, and fall. In these comparisons, the sampling sites and the air exchange rates are basically unchanged from season to season. It may be that during winter, ozone's deposition to the lightly exposed surfaces increases (reverse aging). In spring, summer and fall, when outdoor ozone values are higher, the surfaces remain "aged." However, there are alternative explanations for this seasonal effect [*48*]. More work is necessary to understand the detailed mechanism of aging, why some materials revert to "fresh" behavior in as little as a day, and how these processes relate to deposition within actual buildings.

Effect of moisture—Mueller et al. [*20*] observed that the rate constant for ozone decomposition in an aluminum chamber was highly dependent on relative humidity. At 28% RH, the first-order constant was 2.5×10^{-5} s^{-1}; at 55% RH, 5.7×10^{-5} s^{-1}; and at 87% RH, 9.6×10^{-4} s^{-1}. Note that the latter value is similar to those listed in Table 4. Cox and Penkett have also reported a significant increase in ozone deposition velocity with increasing relative humidity in an aluminum and glass chamber [*42*]. Ryan et al. [*49*] have reported a humidity dependence for the decomposition of ozone on a latex-painted glass surface. They found that the decomposition rate increased sevenfold from 9% RH to 91% RH. *What is the mechanism underlying these observations, and what effect does relative humidity have on ozone deposition velocities in buildings?* The former question will be addressed in the next paragraph. Regarding the latter point, on a clean aluminum surface, one would expect the amount of adsorbed water to vary from about half a monolayer at 10% RH to more than six layers at 80% RH [*19*]. Surfaces encountered indoors are not "clean;" they have normally accumulated fine and coarse particles (see above). Inorganic salts comprise 25 to 50% of the fine particle mass [*50,51*]. These salts will have a resulting deliquescence point lower than that of any single component in the mixture [*52*]. Even at moderate RH values, due to accumulated salts, indoor surfaces may possess sufficient water for ozone decomposition to proceed at the limiting rate reported by Mueller et al. [*20*].

Chemical nature of ozone-surface reactions—Ozone is the most powerful oxidant commonly encountered indoors and can oxidize many of the compounds it encounters. In the case of a "dangling" carbon bond, the oxidation might be written: O_3 + surface-C $\Rightarrow$ surface-CO + O_2. Additional reactions can result in the release of CO or CO_2 from the surface. However, if the surface does not contain "activated" carbon or unsaturated bonds, these reactions tend to be slow. A second pathway to ozone loss is surface-induced dissociation. The primary step can be shown as: $O_3 \Rightarrow O + O_2$. The presence of water, especially under basic conditions, can facilitate such a process [*53*]. Water-assisted dissociation may be responsible for the observed effect of relative humidity on ozone decomposition [*20,42*]. It may also help explain the deposition velocities listed in Table 4, which otherwise appear to be too fast for "aged" surfaces. To elaborate, even the most reactive aged surfaces (lamb's wool, cotton muslin and neoprene) in the studies of Sabersky et al. [*21*] have deposition velocities (0.004 cm s^{-1} to 0.015 cm s^{-1}) a factor of two to three smaller than those measured in most indoor studies (Table 4). The indoor surfaces in the tabulated building studies are certainly "aged." However, unlike the surfaces in the chamber study, they are not clean. This may be an important difference, especially if the contaminants are hygroscopic.

An interesting hypothesis (which remains to be tested) emerges from the above discussion. Perhaps the commonality among indoor surfaces is that they are not clean. Enough water may be associated with accumulated particles (as a consequence of ionic constituents) that the dominant decomposition pathway on soiled indoor surfaces is water-assisted dissociation.

Nitrogen Oxides

The presence of nitrogen oxides in indoor air has attracted considerable attention, in part because NO_2 is a criterion pollutant. Furthermore, indoor concentrations are sometimes much higher than those outside due to the emissions from unvented combustion appliances, including gas ranges, gas ovens and kerosene-fired space heaters.

TABLE 5—*Measured rate constants for nitrogen dioxide decay on indoor surfaces,* $v_d \times \frac{S}{V}$.

Reference	$v_d \times \frac{S}{V}$ (s^{-1})	Comments
Wade et al., 1975 [*54*]	2.3×10^{-4}	1 experiment in home, NO_2 generated by gas range and oven
Özkaynak et al., 1982 [*55*]	$(0.8 \pm 0.5) \times 10^{-4}$	7 experimental runs in house, NO_2 generated by gas range
Traynor et al., 1982 [*56*]	$(3.6 \pm 1.9) \times 10^{-4}$	11 experimental runs in research house, NO_2 generated by range gas
Yamanaka, 1984 [*57*]	1.2×10^{-4} (RH = 50%) 2.3×10^{-4} (RH = 60%) 3.3×10^{-4} (RH = 70%)	27 runs in one house (Japan); NO_2 generated by gas and kerosene fired space heaters; additional loss attributed to homogeneous decay in the range $(2.3–4.8) \times 10^{-4}$ s^{-1}
Traynor et al., 1985 [*58*]	$(0.6 \pm 0.4) \times 10^{-4}$	6 experimental runs in one house; NO_2 generated by unvented gas-fired space heater
Spicer et al., 1989 [*59*]	$(2.2 \pm 1.7) \times 10^{-4}$	11 runs in up to 5 residences; outliers excluded; NO_2 generated by gas range

Experimental measurements have revealed significant rates of loss of NO_2 by reaction on indoor surfaces. First-order loss rates from several studies, excluding the effects of ventilation, are in the range (0.6 to 3.6) $\times$ 10^{-4} s^{-1} (see Table 5). Assuming that these rates reflect heterogeneous processes, and taking a typical value of S/V as 2.8 m^{-1}, the corresponding average deposition velocity is in the range 0.0002 to 0.012 cm s^{-1}, about an order of magnitude lower than the indoor deposition velocities inferred for ozone. Several of these studies also reported NO loss rates, and these are significantly lower than the values for NO_2, from essentially zero to about 3 $\times$ 10^{-6} s^{-1}.

Yamanaka's studies [*57*] reveal a significant effect of relative humidity on surface loss rates, with higher RH leading to increased v_d. In chamber studies of the uptake of NO_2 by a variety of indoor materials, Miyazaki [*60*] found modest to moderate increases in v_d with increasing humidity. Spicer et al. [*59*] reported no effect of increased humidity on NO_2 loss to wallboard, decreasing loss rates to cement block and increasing loss rates to wool carpet and furnace filters.

Yamanaka's investigation of indoor NO_2 decomposition presents a puzzling result [*57*]. To exclude surface reactions in some experimental runs, he covered all of the interior surfaces with polyethylene sheeting (shown to be essentially nonreactive with NO_2 both by his studies and by Spicer et al. [*59*]). In these runs, for relative humidities above 55%, he still observed a net loss of NO_2, correcting for that due to ventilation, of (2.2 to 4.8) $\times$ 10^{-4} s^{-1}. The mechanism for this loss rate is not clear. Indoor lighting levels are not high enough to cause such a large rate of consumption of NO_2 (typically indoor photolysis rates would be three or four orders of magnitude lower than outdoor levels, not one to two orders of magnitude as implied here). A candidate homogeneous reaction is with ozone: $O_3 + NO_2 \rightarrow NO_3 + O_2$; however, the O_3 concentration would have to be improbably high—250 to 500 ppb—to yield the observed decay rates, given the reaction rate constant (at 298 K) of 0.05 ppm^{-1} min^{-1}.

Miyazaki [*60*] and Spicer et al. [*59*] have used chamber studies to investigate NO_2 loss to a variety of specific interior materials. Reported deposition velocities vary markedly in each study, from effectively zero to more than 0.1 cm s^{-1}. The highest loss rates are associated with wallboard, cement block, and wool carpet. Glass and plastic are relatively ineffective at removing NO_2.

The study of Spicer et al. [*59*] also included an investigation of the fate of NO_2 upon reaction with surface materials. They observed significant conversion to NO, which was subsequently released to the gas phase, and formation of nitrite (NO_{2-}) and nitrate (NO_{3-}) ions which remain bound to the surface. The appointment of reacted NO_2 among these fates depended significantly upon the surface material. The investigators were unable to account for the fate of a substantial fraction of the reacted NO_2.

Studies of heterogeneous NO_2 loss rates in houses cited in Table 5 were all based on cases in which NO_x levels were elevated due to operation of a combustion appliance. There is some evidence to suggest that these loss coefficients *may* overestimate the heterogeneous removal of NO_2 from indoor air in the absence of indoor emissions. For example, consider the report by Nazaroff and Cass [*47*] of modeling and measurement results for nitrogen oxides in a Southern California museum. In this case, in the absence of indoor sources, the average measured indoor NO + NO_2 concentration was 85 ppb, compared with 92 ppb as the average measured outdoor concentration. Modeling predictions based on an NO_2 deposition velocity of 0.006 cm s^{-1} (in the middle of the range cited above) and no deposition of NO yielded an average indoor NO + NO_2 concentration of only 73 ppb. With the deposition velocity of NO_2 set to zero, the predicted average indoor concentration of NO + NO_2 was 89 ppb, much closer to the measured result. (The predicted decline from 92 ppb outdoors to 89 ppb indoors is a result of homogeneous chemical reactions.)

Additional studies have suggested that the heterogeneous reaction of NO_2 on indoor surfaces may lead to the production of gaseous nitrous acid [*47,61,62*]. This possibility is a particular concern because of the role played by nitrous acid in forming carcinogenic nitrosamines.

Finally, Salmon et al. [*63*] measured the apparent deposition velocity of nitric acid to vertical surfaces in five museums in Southern California. The determinations were based on measurement

of nitrate ion collected on nylon surfaces (minus the particulate nitrate contribution determined by deposition onto TFE-fluorocarbon surfaces), divided by the mean indoor concentration. The apparent deposition velocities resulting from these experiments were very high, up to 2.4 cm/s, which was as much as an order of magnitude larger than an estimate based on mass-transport considerations. Among the explanations suggested by the authors was the conversion of NO_2 to nitrous acid on the nylon surfaces, followed by ozone-induced oxidation of nitrite ion (NO_2^-) to nitrate (NO_2^-).

Limitations

Transport-Related Issues

Failure of Uniform Mixing—Deposition velocity is defined as the flux density to a surface divided by the core concentration. For the concept to be meaningful, there must be an identifiable core region. The minimum expectation of the core is that it is well mixed (that is, has uniform species concentration).

Furthermore, if one considers the boundary layers on the solid surfaces to be the main diffusive barriers to species transport to the solid surfaces, then, the well-mixed core region should extend to the outer limits of the boundary layers lining the solid surfaces.

Such a core region will not necessarily exist in all situations, as noted in the following two examples:

(1) Consider a room with a poorly insulated flat roof. On a sunny summer day, the ceiling of the room may become hotter than any other room surface. If the ventilation rate is low, and the windows are closed, the air in the room will become stratified, with the hottest layer of air stagnant and trapped near the ceiling. In this case, the core of the room air may not be well mixed. Deposition velocities may be limited by mass transport in the vertical direction through the core region, rather than by transport through thin boundary layers adjacent to surfaces.

(2) Let radon-220 be suddenly and uniformly distributed in a room-size air-tight enclosure with adiabatic top and bottom surfaces, and with two of its opposite surfaces maintained isothermally at different temperatures. Assume that the enclosure has a large extent in the third dimension, so that the problem becomes essentially two dimensional. Within a few minutes, all the radon will decay through its first progeny, ^{216}Po, to the relatively long-lived ^{212}Pb (half-life 10.6 h). The air flow in the enclosure is characterized by fast moving boundary layers lining the vertical walls, and crossing the adiabatic ceiling and floor, with a relatively stagnant central core that is poorly coupled advectively to the air in the boundary layers. Lead-212 is removed throughout the room at a steady rate by radioactive decay, and in addition, ^{212}Pb in the boundary layers is also removed by deposition on the walls. Owing to the poor advective coupling of the boundary layers to the core region, transport of ^{212}Pb from the core to the boundary layer region occurs primarily by diffusion, leading to a strong gradient of ^{212}Pb concentration within the poorly mixed core, (particularly in the vertical direction). The concentration of the species throughout the room drops steadily owing to radioactive decay; however, because deposition velocity is defined as the species flux divided by the core concentration, the ratio reaches a steady state. A difficulty in evaluating the deposition velocity for this system lies in defining the location of this "core." Because the core concentration is so strongly stratified, selection of a different sized region as the "core" leads to a different denominator, and a different value for the deposition velocity [*27*].

In the United States, residential buildings are not commonly equipped with mechanical ventilation systems. The circumstances sketched above may apply at times in such buildings, and the

assumption of a well-mixed core may fail. On the other hand, a recent summary of data from mechanically ventilated commercial buildings suggests that for a given room in the building, the air is well mixed, although there are differences in the age of air in different rooms [*64*]. The results of this study indicate that poorly mixed core regions are not likely to be a limitation in applying the concept of deposition velocity to mechanically ventilated buildings.

Spatial Variability of Deposition—Another limitation to the concept of a deposition velocity arises from the spatial variation in the deposition flux. This restricts the applicability of a deposition velocity derived or measured at one location or under one set of conditions for predicting the deposition flux at another location or under another set of conditions.

As one illustration, consider the case of a species whose reactivity with surfaces varies according to the nature of the surface. Ozone's low reactivity with glass, relative to other materials, is a good example. The deposition velocity for the species measured as its net flux to a local surface would be different, even under identical flow conditions, if another more reactive material were substituted in place of glass. The average deposition velocity of ozone on indoor surfaces may be experimentally measured by observing the loss rate of ozone in the room. In two rooms with glass making up different proportions of their interior surfaces, the results will be different simply because of different surface-weighted reactivities for ozone.

As another example, consider the deposition of radon progeny discussed earlier, except in this case consider ^{222}Rn (half life 3.8 days), and the deposition of unattached ^{218}Po (half life 3.04 min). The fundamental equations governing fluid flow and those governing the transport, generation and decay of radon progeny have been solved numerically for selected boundary conditions, and for a range of governing parameters [*27,44*]. The model yields predictions of local deposition velocity that vary by more than an order of magnitude within the enclosure. The variation in deposition velocity is attributable to two factors: differences with position in the thickness of the boundary layer that must be diffusively crossed by the species, and the air flow patterns (such as corner eddies) that influence the replenishment rates of the species to the outer edge of the local boundary layer. In this case, the enclosure surfaces are considered to be perfect sinks. However, use of a single average value of deposition velocity, derived from experiments that deduce it from the loss rate of ^{218}Po from the room air, would lead to inaccurate predictions of local deposition of the species. These results, although calculated for radon progeny, are also likely to be valid for the deposition of nonradioactive species.

Differences with position in the deposition velocity of unattached radon decay products have been observed experimentally [*43*]. In a field study, Scott measured radon progeny deposition onto different surfaces of a well-ventilated basement room of a commercial building during winter. By measuring the activity deposited on the surface of an alpha detector, and also on different room surfaces, he obtained estimates of the deposition velocity for unattached ^{218}Po of 0.45 cm s^{-1} for inside surfaces of exterior walls, 0.35 cm s^{-1} for interior walls, and 0.2 cm s^{-1} for horizontal surfaces. Scott reports that the walls of the room were distinctly cooler than the average room air, and that, using a smoke generator, he could visualize the boundary layers descending down the cold walls. The trends in his findings are consistent with the numerical modeling results for ^{218}Po deposition discussed above. The highest deposition rates would be found on thermally active surfaces (namely the cold exterior walls), and the smallest on the relatively inactive ceiling and floor surfaces. Scott's results support the surface variability of deposition flux predicted by the simulations. His deposition velocity values are significantly larger than those numerically predicted for enclosure surfaces; however, the air flow and surface geometry conditions of his experiments are not sufficiently described to permit a rigorous comparison.

The important implications of this spatial variability are twofold. First, in using deposition velocity data derived from species loss rates measures in room air, one must exercise caution in predicting the local deposition flux at a specific position on the room surface. The local deposition velocity may well be many times larger or smaller than the average obtained from the species loss

rate in the room. Secondly, experimental measurements of deposition velocity that are based on measurement of local deposition flux (e.g., using a filter paper attached to a wall) should not be assumed to apply directly to the entire interior surface.

Influence of Near-Surface Air Flow—Available experimental evidence demonstrates that for species with significant deposition velocities, deposition can be enhanced by promoting mass transport to surfaces. For example, Wilson [*18*] reported that stirring the air in a room significantly increased the rate of SO_2 loss onto indoor surfaces. In chamber studies, Miyazaki [*60*] showed that the use of a mixing fan increased the rate of NO_2 removal onto interior surfaces; for one carpet sample, the deposition velocity was increased by a factor of three relative to unstirred conditions. Sabersky et al. [*21*] found that the use of an internal recirculation fan increased the ozone decomposition rate in a house from 8×10^{-4} to 15×10^{-4} s^{-1}.

Modeling calculations also show that the mass-transport limited deposition velocity can be greatly influenced by near-surface air flow conditions. For example, long-term average deposition velocities predicted for 0.5 μm particles onto walls in five museums varied from 2×10^{-5} at the Norton Simon Museum to 44×10^{-5} cm s^{-1} at the Getty Museum [*8*]. The factor of 20 difference among these sites was largely ascribed to an apparent difference in air flow regimes. The ventilation design at the Norton Simon Museum promoted low velocity laminar flow parallel to the walls, whereas the system at the Getty Museum generated turbulent flow with relatively high near-surface velocities.

Two important implications arise from the dependence of deposition velocity on air flow conditions. First, a control opportunity is presented. Additional mixing could be used to promote pollutant deposition onto indoor surfaces when the primary objective is to reduce human exposure. In settings where material preservation is a primary concern, such as museums, air flow conditions could be managed to reduce the rate of pollutant mass transport to surfaces.

The second important implication of the relationship between air flow conditions and deposition velocity is the need for awareness in extrapolating results from one setting to another. Deposition velocities determined for one indoor environment can only be applied to another to the extent that the air flow conditions are similar. This issue presents particular problems in attempts to make use of chamber studies of pollutant-surface interactions for predicting behavior in buildings. In most chamber studies, air flow conditions have been too poorly specified to be of direct use towards this end.

Other Deposition Mechanisms—The transport of all pollutants to surfaces is influenced by advection and diffusion. Particle deposition, however, presents special problems because of the potential importance of other transport mechanisms, including gravitational settling, thermophoresis, electrostatic drift, and inertial drift. This feature, among others, makes the theoretical analysis of particle deposition challenging. Furthermore, in extrapolating particle deposition rates from one setting to another, not only must the near-surface air flow conditions be similar, as discussed above, but the strength of any other dominant transport process must also be comparable. For example, the deposition of particles from natural convection flow to smooth vertical surfaces is predicted to be very strongly influenced by whether the surface is cooler or warmer than the adjacent air [*65*]. The average deposition velocity of 0.3 μm diameter particles to a 1-m high plate that is 1 K cooler than the adjacent air is 1.1×10^{-4} cm s^{-1}. If the same plate is 1 K warmer than the adjacent air, the deposition velocity would be reduced to 0.04×10^{-4} cm s^{-1}.

Transformation-Related Issues

Nature of Reactions at Surfaces—The use of a constant value for the deposition velocity is only appropriate for surface processes, such as sorption or chemical reaction, that do not change with time or with magnitude of exposure. (Actually, the standard concept of "deposition velocity" can

still be used if the change with time is slow relative to the deposition process; an example is the aging of surfaces upon exposure to ozone [*20,21*].) Certain surface processes may not satisfy these constraints.

- If the rate of removal is governed by the rate of chemisorption, it may change as the sorption capacity of the surface is approached. Such a phenomenon is likely to occur for surfaces with limited sorption sites or for situations where the gas-phase concentration of the sorbent is very large.
- Just as the sorption capacity of a surface can be reached, so also can the catalytic capacity (when the catalytically active sites are all occupied). As this condition is approached, the process can evolve from a first-order to a zero-order reaction.
- Conditions may change in such a way that previously adsorbed species are now desorbed (for example, a sudden increase in the temperature of a surface).
- Chemical transformations at the surface, followed by partial release of the product, may complicate the assignment of a "deposition velocity" to the product. Consider a situation where HONO is present in the gas phase and is also created by chemical transformation of NO_x at surfaces (with subsequent release). The net flux of HONO to a surface may well be a nonlinear function of the core concentration of HONO, and may change with time, even to negative values, as the relative airborne concentrations of NO_x and HONO vary.
- Different species may compete for the same surface sites. Ozone can displace water from active sites on charcoal [*66*]. In a similar fashion, one compound could displace another sorbed compound as the chemicals present within an indoor environment varied.
- Some surface reactions are simply not first order. Such is the case in bimolecular surface reactions where neither reactant is in pseudo-first order excess.

For these and other reasons, surface removal may not be a first order process. If the removal process is not first order, then the rate coefficient for this process is no longer simply the product of the surface-to-volume ratio of the room times a deposition velocity. Indeed, the standard concept of a "deposition velocity" no longer applies—the flux density to the surface is not linearly proportional to the core concentration.

The significance of these processes is largely unknown. However, investigators should be cautious in applying a deposition velocity to species that have very large indoor concentrations, to surfaces that undergo relatively sudden temperature changes, to indoor environments whose chemical constituents change rapidly and dramatically, and to species that may be generated by surface chemistry.

Influence of Homogeneous Reactions—For species that are produced or decay homogeneously, the deposition velocity can be influenced by the production/decay rate. An example comes from a recent study by Nazaroff et al. [*27*] that reports numerical predictions of local deposition velocities of unattached ^{218}Po and ^{212}Pb to the surfaces of square two-dimensional enclosures under laminar natural convection flow. Polonium-218 has a relatively short half-life (3.04 min), while that of ^{212}Pb is significantly longer (10.6 h). Owing to these differences in their rates of decay (and generation), ^{218}Po and ^{212}Pb are not expected to have identical deposition velocities, even if their diffusivity were the same. The study results indicate that the production and decay of ^{218}Po alter its spatial distribution relative to that of ^{212}Pb even under identical airflow conditions. Hence, the deposition velocities for ^{218}Po are larger than those for ^{212}Pb. The latter species, because of its 10.6 h half-life, behaves as a stable species with respect to the time scale of convective motion.

The above illustration involves radioactive generation and decay. However, the concept applies to any situation in which species are produced or decay homogeneously on a time scale comparable to or faster than that of transport across a boundary layer. For example, gas-phase reactions between ozone and nitric oxide could modify the spatial distribution of the less abundant reactant. The

occurrence of such reactions within a boundary layer could alter the concentration gradient and thereby result in a change in the flux density to the surface relative to the core concentration.

Investigators are cautioned to take into consideration the effects of homogeneous transformations when using results from one species to predict deposition velocities for other species.

Concluding Remarks

As a scientific topic, the issue of air pollutant interaction with indoor surfaces is at a juvenile stage of development. The achievements to date might be summarized as follows:

- Introduction of the concept of deposition velocity as a means of parameterizing the loss process. This representation has proven useful for pedagogical purposes and as a tool for achieving a first-order quantitative description of the process.
- Generation of experimental information on the deposition velocity for several important classes of indoor pollutants and in a number of specific indoor settings.
- An emerging understanding of the factors that govern the deposition velocity.
- Predictions of the deposition velocity under mass-transport limited conditions for several canonical indoor air flow scenarios.
- Application of the concept of deposition velocity in indoor air quality models to deterministically predict indoor pollutant concentrations. The concept has also been used to interpret experimental studies of the factors governing indoor concentrations.

On the other hand, it is possible to identify many important aspects of the topic about which present knowledge is unsatisfactory, or at least unsatisfying. These include the following:

- Knowledge of surface transformation processes is weak. Only very recently have efforts towards understanding the chemical reactions that occur between air pollutants and indoor surfaces been reported. Phenomena such as "aging" of surfaces and the relative humidity dependence of the deposition velocity for certain species cannot yet be explained.
- The concept of deposition velocity is inflexible with respect to processes that lead to subsequent release of contaminants into indoor air. We know that such phenomena occur. The persistent odor of cigarette smoke is direct evidence of a reversible deposition process. The surface conversion of NO_2 to gaseous nitrous acid is another example. However, we cannot yet describe the rates of these processes quantitatively.
- Detailed understanding is lacking of the air motion near surfaces within buildings. A primary source of evidence of this limitation is the persistent difficulty in reconciling the deposition velocity predictions based on mass-transport analysis with experimental results.

Given the importance of exposure—both of humans and of sensitive materials—to air pollutants in buildings, it behooves investigators to develop a better understanding of pollutant-surface interactions. To do so will require the combined efforts of experts on transport processes and surface chemistry in concert with scientists and engineers knowledgeable about the important issues in indoor air quality. Progress on this frontier holds the promise of increasing society's ability to beneficially manage the indoor environments in which we live and work.

Acknowledgment

We gratefully acknowledge that financial support for this research was provided by the following sources: (1) National Science Foundation under Grant No. BCS-9057298; (2) the Office of Exploratory Research, U.S. Environmental Protection Agency; and (3) Director, Office of Energy

Research, Office of Health and Environmental Research, of the U.S. Department of Energy under Contract No. DE-AC03-76SF00098. C.J.W gratefully acknowledges a sabbatical from Bell Communications Research and a position as a visiting scientist at Lawrence Berkeley Laboratory during which this paper was formulated.

References

[1] Davidson, C. I. and Wu, Y.-L., "Dry Deposition of Particles and Vapors," *Acidic Precipitation, Volume 3: Sources, Deposition, and Canopy Interactions*, S. E. Lindberg, A. L. Page, and S. A. Norton, Eds., Springer-Verlag, New York, 1990, pp. 103–216.

[2] Pruppacher, H. R., Semonin, R. G., and Slinn, W. G. N., Eds., *Precipitation Scavenging, Dry Deposition, and Resuspension*, Vol. 2, Elsevier, New York, 1983.

[3] Weschler, C. J., Shields, H. C., Naik, D. V., "Indoor Ozone Exposures," *Journal of the Air Pollution Control Association*, Vol. 39, 1989, pp. 1562–1568.

[4] Absil, M., Narducci, P., Whitfield, R., Richmond, H. M., "Chronic Lung Injury Risk Estimates for Urban Areas Having Ozone Patterns Similar to Those in the Northeast," *Tropospheric Ozone and the Environment II: Effects, Modeling and Control*, Air and Waste Management Association, Pittsburgh, PA, 1992, in press.

[5] Yocum, J. E., "Indoor-Outdoor Air Quality Relationships: A Critical Review," *Journal of the Air Pollution Control Association*, Vol. 32, 1982, pp. 500–520.

[6] Allen, R. J., Wadden, R. A., Ross, E. D., "Characterization of Potential Indoor Sources of Ozone," *American Industrial Hygiene Association Journal*, Vol. 39, 1978, pp. 466–471.

[7] Baer, N. S. and Banks, P. N., "Indoor Air Pollution: Effects on Cultural and Historical Materials," *International Journal of Museum Management Curatorship*, Vol. 4, 1985, pp. 9–20.

[8] Nazaroff, W. W., Ligocki, M. P., Ma, T., Cass, G. R., "Particle Deposition in Museums: Comparison of Modeling and Measurement Results," *Aerosol Science and Technology*, Vol. 13, 1990, pp. 332–348.

[9] Weschler, C. J. and Shields, H. C., "The Impact of Ventilation and Indoor Air Quality on Electronic Equipment," *ASHRAE Transactions*, Vol. 97, 1991, pp. 455–463.

[10] Weschler, C. J., "Predictions of Benefits and Costs Derived from Improving Indoor Air Quality in Telephone Switching Offices," *Indoor Air*, Vol. 1, 1991, pp. 65–78.

[11] Gill, A. E., "The Boundary-Layer Regime for Convection in a Rectangular Cavity," *ASME Journal of Fluid Mechanics*, Vol. 26, 1966, pp. 515–536.

[12] Quon, C., "Free Convection in an Enclosure Revisited," *ASME Journal of Heat Transfer*, Vol. 99, No. 2, 1977, pp. 340–342.

[13] Bauman, F., Gadgil, A. J., Kammerud, R., Altmayer, E., and Nansteel, M., "Convective Heat Transfer in Buildings: Recent Research Results," *ASHRAE Transactions*, Vol. 89, 1A, 1982, pp. 215–233.

[14] Kays, W. M. and Crawford, M. E., *Convective Heat and Mass Transfer*, Second Edition, McGraw Hill, New York, 1980.

[15] Bejan, A., *Convection Heat Transfer*, Wiley Interscience, New York, 1984.

[16] Moore, W. J., *Physical Chemistry*, 3rd edition, Prentice Hall, Englewood Cliffs, 1963, pp. 302–305.

[17] Adamson, A. W., *Physical Chemistry of Surfaces*, 4th edition, Wiley, New York, 1982, pp. 626–629.

[18] Wilson, M. J. G., "Indoor Air Pollution," *Proceedings of the Royal Society, Series A*, Vol. 307, 1968, pp. 215–221.

[19] Phipps, P. B. P. and Rice, D. W., "The Role of Water in Atmospheric Corrosion," *Corrosion Chemistry*, ACS Symposium Series Vol. 89, American Chemical Society, Washington, 1979, pp. 235–261.

[20] Mueller, F. X., Loeb, L., Mapes, W. H., "Decomposition Rates of Ozone in Living Areas," *Environmental Science and Technology*, Vol. 7, 1973, pp. 342–346.

[21] Sabersky, R. H., Sinema, D. A., Shair, F. H., "Concentrations, Decay Rates, and Removal of Ozone and Their Relation to Establishing Clean Indoor Air," *Environmental Science and Technology*, Vol. 7, 1973, pp. 347–353.

[22] Traynor, G. W., Anthon, D. W., and Hollowell, C. D., "Technique for Determining Pollutant Emissions from a Gas-Fired Range," *Atmospheric Environment*, Vol. 16, 1982, pp. 2979–2987.

[23] Knutson, E. O., "Modeling Indoor Concentrations of Radon's Decay Products," *Radon and Its Decay Products in Indoor Air*, W. W. Nazaroff and A. V. Nero, Eds., Wiley, New York, 1988, pp. 161–202.

[24] Ligocki, M. P., Liu, H. I. H., Cass, G. R., John, W., "Measurements of Particle Deposition Rates Inside Southern California Museums," *Aerosol Science and Technology*, Vol. 13, 1990, pp. 85–101.

[25] Toohey, R. E., Essling, M. A., Rundo, J., and Wang, H., "Measurements of the Deposition Rates of Radon Daughters on Indoor Surfaces," *Radiation Protection Dosimetry*, Vol. 7, 1984, pp. 143–146.

[26] Nazaroff, W. W. and Cass, G. R., "Mass-Transport Aspects of Pollutant Removal at Indoor Surfaces," *Environmental International*, Vol. 8, 1988, pp. 567–584.

[27] Nazaroff, W. W., Kong, D., and Gadgil, A. J., "Numerical Investigations of the Deposition of Unattached ^{218}Po and ^{212}Pb from Natural Convection Enclosure Flow," *Journal of Aerosol Science*, Vol. 23, 1992, pp. 339–352.

[28] Vanmarcke, H., Landsheere, C., Van Dingenen, R., and Poffijn, A., "Influence of Turbulence on the Deposition Rate Constant of the Unattached Radon Decay Products," *Aerosol Science and Technology*, Vol. 14, 1991, pp. 257–265.

[29] Sinclair, J. D., Psota-Kelty, L. A., Weschler, C. J., "Indoor/Outdoor Concentrations and Indoor Surface Accumulations of Ionic Substances," *Atmospheric Environment*, Vol. 19, 1985, pp. 315–323.

[30] Sinclair, J. D., Psota-Kelty, L. A., Weschler, C. J., Shields, H. C., "Measurement and Modeling of Airborne Concentrations and Indoor Surface Accumulation Rates of Ionic Substances at Neenah, Wisconsin," *Atmospheric Environment*, Vol. 24A, 1990, pp. 627–638.

[31] Sinclair, J. D., Psota-Kelty, L. A., Weschler, C. J., "Indoor/Outdoor Ratios and Indoor Surface Accumulations of Ionic Substances at Newark, NJ," *Atmospheric Environment*, Vol. 22, 1988, pp. 461–469.

[32] Raunemaa, T., Kulmala, M., Saari, H., Olin, M., Kulmala, M. H., "Indoor Air Aerosol Model: Transport Indoors and Deposition of Fine and Coarse Particles," *Aerosol Science and Technology*, Vol. 11, 1989, pp. 11–25.

[33] Seinfeld, J. H., *Atmospheric Chemistry and Physics of Air Pollution*, John Wiley & Sons, New York, 1986, p. 738.

[34] Milford, J. B. and Davidson, C. I., "The Sizes of Particulate Sulfate and Nitrate in the Atmosphere—A Review," *Journal of the Air Pollution Control Association*, Vol. 37, 1987, pp. 125–134.

[35] Finlayson–Pitts, B. J. and Pitts, J. N., *Atmospheric Chemistry*, John Wiley & Sons, New York, 1986, p. 1098.

[36] Sinclair, J. D., Psota-Kelty, L. A., Weschler, C. J., Shields, H. C., "Deposition of Airborne Sulfate, Nitrate and Chloride Salts as it Relates to Corrosion of Electronics," *Journal of the Electrochemical Society*, Vol. 137, 1990, pp. 1200–1206.

[37] Jacobi, W., "Activity and Potential α-Energy of ^{222}Radon and ^{220}Radon-Daughters in Different Air Atmospheres," *Health Physics*, Vol. 22, 1972, pp. 441–450.

[38] Porstendörfer, J., Wicke, A., and Schraub, A., "The Influence of Exhalation, Ventilation and Deposition Processes Upon the Concentration of Radon (^{222}Rn), Thoron (^{220}Rn) and Their Decay Products in Room Air," *Health Physics*, Vol. 34, 1978, pp. 465–473.

[39] James, A. C., "Lung Dosimetry," *Radon and Its Decay Products in Indoor Air*, W. W. Nazaroff and A. V. Nero, Eds., Wiley, New York, 1988, pp. 259–309.

[40] McLaughlin, J. P. and O'Byrne, F. D., "The Role of Daughter Product Plateout in Passive Radon Detection," *Radiation Protection Dosimetry*, Vol. 7, 1984, pp. 115–119.

[41] Bigu, J., "Radon Daughter and Thoron Daughter Deposition Velocity and Unattached Fraction Under Laboratory-Controlled Conditions and in Underground Uranium Mines, *Journal of Aerosol Science*, Vol. 16, 1985, pp. 157–165.

[42] Cox, R. A. and Penkett, S. A., "Effect of Relative Humidity on the Disappearance of Ozone and Sulphur Dioxide in Contained Systems," *Atmospheric Environment*, Vol. 6, 1972, pp. 365–368.

[43] Scott, A. G., "Radon Daughter Deposition Velocities Estimated from Field Measurements," *Health Physics*, Vol. 45, 1983, pp. 481–485.

[44] Gadgil, A. J., Kong, D., and Nazaroff, W. W., "Deposition of Unattached ^{218}Po and ^{212}Pb under Natural Convection Flow in Enclosures: A Numerical Investigation," submitted to *Radiation Protection Dosimetry*, 1992.

[45] Thompson, C. R., Hensel, E. G., Kats, G., "Outdoor-Indoor Levels of Six Air Pollutants," *Journal of the Air Pollution Control Association*, Vol. 23, 1973, pp. 881–886.

[46] Shair, F. H. and Heitner, K. L., "Theoretical Model for Relating Indoor Pollutant Concentrations to Those Outside," *Environmental Science and Technology*, Vol. 8, 1974, pp. 444–451.

[47] Nazaroff, W. W. and Cass, G. R., "Mathematical Modeling of Chemically Reactive Pollutants in Indoor Air," *Environmental Science and Technology*, Vol. 20, 1986, pp. 924–934.

[48] Weschler, C. J., Shields, H. C., Naik, D. V., "Indoor Ozone: Recent Findings," *Tropospheric Ozone and the Environment II: Effects, Modeling and Control*, Air and Waste Management Association, Pittsburgh, PA, 1992, in press.

[49] Ryan, P. B., Koutrakis, P., Bamford, S. Reiss, R., "Ozone Reactive Chemistry in Indoor Microenvironments: Effects on Exposure," in *Tropospheric Ozone and the Environment II: Effects, Modeling and Control*, Air and Waste Management Association, Pittsburgh, PA, 1992, in press.

[50] Walker, M. V. and Weschler, C. J., "Water-Soluble Components of Size-Fractionated Aerosols Collected After Hours in a Modern Office Building," *Environmental Science and Technology*, Vol. 14, 1980, pp. 594–597.

[51] Gray, H. A., Cass, G. R., Huntzicker, J. J., Heyerdahl, E. K., Rau, J. A., "Characteristics of Atmospheric Organic and Elemental Carbon Particle Concentrations in Los Angeles," *Environmental Science and Technology*, Vol. 20, 1986, pp. 580–589.

[52] Wexler, A. S. and Seinfeld, J. H., "Second-Generation Inorganic Aerosol Model," *Atmospheric Environment*, Vol. 25A, 1991, pp. 2731–2748.

[53] Sehested, K., Corfitzen, H., Holcman, J., Fischer, C. H., Hart, E. J., "The Primary Reaction in the Decomposition of Ozone in Acidic Aqueous Solutions," *Environmental Science and Technology*, Vol. 25, 1991, pp. 1589–1596.

[54] Wade, W. A., III, Cote, W. A., and Yocum, J. E., "A Study of Indoor Air Quality," *Journal of the Air Pollution Control Association*, Vol. 25, 1975, pp. 933–939.

[55] Özkaynak, H., Ryan, P. B., Allen, G. A., and Turner, W. A., "Indoor Air Quality Modeling: Compartmental Approach with Reactive Chemistry," *Environmental International*, Vol. 8, 1982, pp. 461–471.

[56] Traynor, G. W., Apte, M. G., Dillworth, J. F., Hollowell, C. D., and Sterling, E. M., "The Effects of Ventilation on Residential Air Pollution Due to Emissions from a Gas-Fired Range," *Environment International*, Vol. 8, 1982, pp. 447–452.

[57] Yamanaka, S., "Decay Rates of Nitrogen Oxides in a Typical Japanese Living Room," *Environmental Science and Technology*, Vol. 18, 1984, pp. 566–570.

[58] Traynor, G. W., Girman, J. R., Apte, M G., Dillworth, J. F., and White, P. D., "Indoor Air Pollution Due to Emissions from Unvented Gas-Fired Space Heaters," *Journal of the Air Pollution Control Association*, Vol. 35, 1985, pp. 231–237.

[59] Spicer, C. W., Coutant, R. W., Ward, G. F., Joseph, D. W., Gaynor, A. J., and Billick, I. H., "Rates and Mechanisms of NO_2 Removal from Indoor Air by Residential Materials," *Environmental International*, Vol. 15, 1989, pp. 643–654.

[60] Miyazaki, T., "Adsorption Characteristics of NOx by Several Kinds of Interior Materials," *INDOOR AIR: Chemical Characterization and Personal Exposure*, Vol. 4, B. Berglund, T. Lindvall and J. Sundell, Eds., Swedish Council for Building Research, Stockholm, 1984, pp. 103–110.

[61] Pitts, J. N., Jr., Wallington, T. J., Biermann, H. W., and Winer, A. M., "Identification and Measurement of Nitrous Acid in an Indoor Environment," *Atmospheric Environment*, Vol. 19, 1985, pp. 763–767.

[62] Febo, A. and Perrino, C., "Prediction and Experimental Evidence for High Air Concentration of Nitrous Acid in Indoor Environments," *Atmospheric Environment*, Vol. 25A, 1991, pp. 1055–1061.

[63] Salmon, L. G., Nazaroff, W. W., Ligocki, M. P., Jones, M. C., and Cass, G. R., "Nitric Acid Concentrations in Southern California," *Environmental Science and Technology*, Vol. 24, 1991, pp. 1004–1013.

[64] Fisk, W. J., Faulkner, D., and Prill, R. J., "Air Exchange Effectiveness of Conventional and Task Ventilation for Offices," report LBL-31652, Lawrence Berkeley Laboratory, Berkeley, CA, December 1991.

[65] Nazaroff, W. W. and Cass, G. R., "Particle Deposition from a Natural Convection Flow onto a Vertical Isothermal Flat Plate," *Journal of Aerosol Science*, Vol. 18, 1987, pp. 445–455.

[66] Abel, W. A., "Destruction of Ozone," report ASHRAE RP169, American Society of Heating, Refrigeration and Air-Conditioning Engineers, Atlanta, 1976, pp. 38.

James W. Axley[1] *and David Lorenzetti*[1]

Sorption Transport Models for Indoor Air Quality Analysis

REFERENCE: Axley, J. W. and Lorenzetti, D., **"Sorption Transport Models for Indoor Air Quality Analysis,"** *Modeling of Indoor Air Quality and Exposure, ASTM STP 1205*, Niren L. Nagda, Ed., American Society for Testing and Materials, Philadelphia, 1993, pp. 105–127.

ABSTRACT: Sorption filtration is presently being investigated as one means to control the quality of air in buildings, yet methods to integrate models of sorption filtration devices with multi-zone indoor air quality analysis procedures, to enable rational design of these devices, have not appeared.

This paper reviews the theoretical bases of sorption models recently developed for multizone contaminant dispersal analysis and presents new work to extend these models to the problem of sorption filtration modeling. Four generic families of models are presented that account for (1) the equilibrium limits of reversible sorption processes with or without (2) boundary layer diffusion transport at the adsorbent surface and (3) diffusion transport within the adsorbent proper, and, for filtration devices, (4) convection-diffusion transport within the filtration medium. All models are formulated as mass transport elements that may be directly assembled with existing elements to model contaminant dispersal in multizone building/HVAC systems of arbitrary complexity. A comparison of the model families is made, criteria are presented to aid in the selection of the model family to use, and results of first applications of these models are presented that provide some validation of the theory.

KEY WORDS: indoor air quality, adsorption, desorption, sorption filtration, multi-zone model, exposure

Nomenclature

A_s	Projected (that is, exposed) surface area of the adsorbent (m^2)
${}^{\alpha}C$	Air-phase concentration of species α (g · α/g · air)
${}^{\alpha}C^*$	Air-phase concentration of species α near the surface of the adsorbent (g · α/g · air)
${}^{\alpha}C_e$	Air-phase equilibrium concentration of species α (g · α/g · air)
${}^{\alpha}\hat{C}_e$	So-called reduced concentration of (g · α/g · air)
${}^{\alpha}C_{sat}$	Saturation air-phase concentration (g · α/g · air)
${}^{\alpha}C_{se}$	Sorbed-phase equilibrium concentration of species α (g · α/g · sorbent)
${}^{\alpha}C_{so}$	Sorbed-phase concentration corresponding to complete coverage by a single layer of adsorbate (g · α/g · sorbent)
${}^{\alpha}C'_{so}$	Sorbed-phase concentration corresponding to the practically complete filling of micropores within the sorbent when the air-phase is saturated (g · α/g · sorbent)
D	Dubinin-Radushkevich parameter (dimensionless)
${}^{\alpha\text{-air}}D$	Molecular diffusivity of species α in air (m^2/s)
${}^{\alpha\text{-air}}\mathcal{D}({}^{\alpha}C)$	Effective diffusion coefficient of the adsorbate-adsorbent system (m^2/s)
${}^{\alpha}E$	System excitation, (g · α/s)
${}^{\alpha}f$	Equilibrium sorption function for species α on a specific adsorbent (g · α/g · air)
${}^{\alpha}g$	Species α generation rate within the adsorbent per unit length (g · α/m · s)

[1]Associate professor and doctoral student, respectively, Building Technology Program, Massachusetts Institute of Technology, Cambridge, MA 02139.

$^{\alpha}G$ Species α generation rate within the room or chamber (g · α/s)
$^{\alpha}G_s$ Species α generation rate within the adsorbent (g · α/s)
$^{\bar{h}}m$ Average *film* mass transfer coefficient (m/s)
$^{\alpha}K_P$ *Partition* coefficient (g · air/g · sorbent)
$^{\alpha}K_L$ Langmuir isotherm coefficient (g · air/g · α)
$^{\alpha}K_{BET}$ BET isotherm coefficient (g · air/g · α)
M Mass of air in the volume of the room (g · air)
M_{eff} Effective participating mass of the room-sorbent system (g · air)
M_{seff} Effective participating mass of the sorbent (g · air)
M^{e}_{seff} Effective participating mass of the sorbent for each finite element e (g · air)
M_s Mass of sorbent, (g · sorbent)
Sc Schmidt number, the ratio of the kinematic viscosity of air ν to the molecular diffusivity of the species in air ($^{\nu/\alpha\text{-air}}D$)
Sh A dimensionless form of the film coefficient equal to the quotient ($^{\bar{h}}m^{L}/^{\alpha\text{-air}}D$), where L is a characteristic length
T Temperature (°C, K)
P Pressure (Pa)
w Mass flow rate of air into a room or chamber (g · air/s)
$^{\alpha}w'$ Mass transport rate of species α relative to the bulk flow through the porous adsorbent (g · α/s)
$^{\alpha}w_s$ Mass transport rate of species α into the adsorbent (g · α/s)
$^{\alpha}w_{diff}$ Mass transport rate of species α through the adsorbent by diffusion (g · α/s)
$^{\alpha}w_{con\text{-}dif}$ Mass transport rate of species α through the filtration medium by convection and diffusion combined (g · α/s)
$^{\alpha}w_{\delta}$ Net mass transport rate of species α through the boundary layer δ, (g · α/s)
$^{\alpha}w_{\delta\text{-}ads}$ Boundary layer adsorption mass transport rate (g · α/s)
$^{\alpha}w_{\delta\text{-}des}$ Boundary layer desorption mass transport rate (g · α/s)
x Distance perpendicular to the plane of the adsorbent sheet (m)
δx^{e} Element thickness (m)
ϵ Porosity of the adsorbent
ρ Air density, (g · air/m^3)
ρs Bulk density of the adsorbent, (g · sorbent/m^3)

Air pollutants are known to be adsorbed and desorbed from building materials, furnishings, and other contents—the persistence of odor provides the obvious evidence of this—but can sorption transport significantly alter the dispersal dynamics of air pollutants in buildings? Some experimental studies indicate that, indeed, the impact of sorption transport may be significant in some cases and attempts have been made to model the adsorption dynamics involved [*1–6*]. However, these empirical and semi-empirical models fall short of that which would be needed to evaluate the impact of sorption transport in a practical context.

This paper will review the theory underlying more general sorption transport models developed in earlier studies for the purposes of practical multizone indoor air quality analysis [*7–9*]. These models were formulated using element assembly techniques and, following approaches taken for moisture transport modeling [*10–16*], are based on fundamental principles of adsorption science limited here, however, to isothermal sorption dynamics. They provide the means to identify the conditions under which sorption transport can significantly alter contaminant dispersal in building airflow systems and can be used to extend the existing multi-zone theory to predict the quality of air in buildings.

The past decade of research has placed a central emphasis on source-control, ventilation, and particle-filtration strategies to mitigate indoor air problems. Multizone contaminant dispersal and

airflow analysis tools have been developed to evaluate the efficacy of these strategies and, thereby, aid designers attempting to implement them. In recent years, attention has turned to the possibility of using sorption filtration devices to extend the arsenal of mitigation strategies [*17–19*].

Specifically, researchers at the National Institute of Standards and Technology (NIST) have developed a test method and apparatus to measure the single-pass effectiveness of building sorption filtration media, and available gas sorption theory has been adapted, with success, to predict the time varying sorption characteristics of a single-pass sorption device challenged by an air stream containing a single contaminant component of steady concentration delivered to the filtration device at a steady airflow rate [*20*]. However, building sorption filtration devices are challenged by air streams containing contaminants of varying concentrations delivered at varying airflow rates due in part to the dynamic interaction of the filtration device and the building airflow systems and, in part, to time varying source emission rates. Furthermore, in many instances two or more contaminant components may be expected to compete for sorption sites within the filtration medium, complicating both the mechanics and modeling of the sorption process.

The practical design of sorption filtration devices intended to be used to control the quality of air in buildings will therefore demand the development of sorption filtration component models that can account for: (1) the dynamic interaction of the filtration device and the building airflow systems, (2) the possibility of time varying or discontinuous supply airflow rate to the filtration device, and (3) the possibility of multi-component sorption competition within the sorption medium. This paper will present sorption filtration models that will answer the first two needs, and future studies will be directed toward extending these models to account for the multi-component case.

To proceed, some fundamental principles of adsorption science will be reviewed. The application of these principles to modeling adsorption dynamics in single rooms will then be considered and from these single room (single-zone) models element equations for equilibrium adsorption, boundary layer diffusion, and porous adsorbent diffusion transport will be extracted that may be used for general multizone analysis. A sorption filtration model based on a finite element approximation of the governing convection diffusion equation for a porous filtration medium will be presented. It will be shown that simpler sorption filtration models can be assembled from the basic sorption element equations developed earlier that may provide adequate accuracy for the current state of the art and the results of practical applications of these models will be described.

Fundamental Principles

Adsorption, the separation of a substance from one phase (indoor air in the present context) and the accumulation of that substance on the surface of another phase (here, building materials and filtration media) is just one step of several that together determine the nature of the adsorption dynamics. In the building context, adsorbate species are transported via convection and molecular and turbulent diffusion transport processes from the bulk air-phase to locations near the adsorbent. At this point, diffusion transport processes alone take over to move the adsorbate first through the boundary layer surrounding the adsorbent and then through the porous interstices of the adsorbent to near-surface locations of the solid portions of the adsorbent. Finally, the actual adsorption processes come into play to bind the adsorbate to activated adsorbent surface locations. Simultaneously, desorption processes release adsorbate within the porous structure of the adsorbent that are then transported to the bulk air-phase by these same processes. The rate of species transport to and from the surface-bound locations is thus determined by dispersal processes within in the building/HVAC system, by boundary layer diffusion processes near the adsorbent, by porous diffusion processes within the adsorbent, and by the adsorption process itself at the solid surface locations within the adsorbent. It is somewhat ironic that the rate of the adsorption process is invariably practically instantaneous, and thus we shall simply ignore the kinetics of this step. The

limitations placed on this step by equilibrium considerations are all-important, however, and will be central to all subsequent discussion.

Sorption Equilibria

Under normal conditions of temperature and pressure, physical and some chemical adsorption processes may be considered to be a more or less reversible transformation between two alternative phases of the adsorbate—the free phase and the adsorbed phase—where the adsorbent may be thought to activate the transformation process not unlike a catalyst in a chemical tranformation

$$\text{Free Phase} \xrightarrow{\text{Adsorbent}} \text{Adsorbed Phase} + \Delta H$$

where ΔH is the heat of adsorption released.

For closed systems under steady conditions the rate at which adsorbate molecules (or ions) α bind to adsorbate surfaces will eventually equal the rate at which they are released and the concentration of the free and adsorbed phases will remain constant at their respective equilibrium values, ${}^{\alpha}C_e$ and ${}^{\alpha}C_{se}$. (Here concentration for both phases will be expressed in terms of mass fraction, following one of the common conventions used in the adsorption and chemical engineering literature.)

In functional notation, we may say that the free-phase equilibrium concentration of species α, ${}^{\alpha}C_e$, is related to the adsorbed-phase concentration, ${}^{\alpha}C_{se}$, and the thermodynamic state of the system determined by temperature, T, and the free-phase pressure, P, as

$$ {}^{\alpha}C_{se} = {}^{\alpha}f({}^{\alpha}C_e, T, P) \tag{1}$$

where ${}^{\alpha}f$ is a function that is unique for each adsorbate-adsorbent system.

When reported for isothermal conditions at atmospheric pressure these equilibrium relations are identified as adsorption isotherms. Experimentally determined adsorption isotherms are often approximated by one of several models. Four representative models are the Linear, Langmuir, BET, and Polanyi DR models [*21*]

Linear Model

$$ {}^{\alpha}C_{se} = {}^{\alpha}K_P^{\alpha}C_e \tag{2}$$

Langmuir Model

$$ {}^{\alpha}C_{se} = \frac{{}^{\alpha}C_{so}{}^{\alpha}K_L{}^{\alpha}C_e}{1 + {}^{\alpha}K_L{}^{\alpha}C_e} \tag{3}$$

BET Model

$$ {}^{\alpha}C_{se} = \frac{{}^{\alpha}C_{so}{}^{\alpha}K_{\text{BET}}{}^{\alpha}\hat{C}_e}{(1 + {}^{\alpha}\hat{C}_e)(1 - {}^{\alpha}\hat{C}_e + {}^{\alpha}K_{\text{BET}}{}^{\alpha}\hat{C}_e)}; \quad {}^{\alpha}\hat{C}_e \equiv \frac{{}^{\alpha}C_e}{{}^{\alpha}C_{\text{sat}}} \tag{4}$$

Polanyi DR

$$ {}^{\alpha}C_{se} = {}^{\alpha}C'_{so} \exp\left[-D\left\{\ln\left(\frac{{}^{\alpha}C_{\text{sat}}}{{}^{\alpha}C_e}\right)\right\}^2\right] \tag{5}$$

The Linear and Langmuir models are likely to be appropriate for the adsorption of ambient levels of volatile organic compounds (VOCs) on building materials, the BET model would be appropriate for adsorption of water on building materials, and the Polanyi DR model is the model of choice for sorption of VOCs on granulated activated carbon (GAC) where capillary condensation in microporous interstices (pore filling) is important. In these models, the Partition, Langmuir and

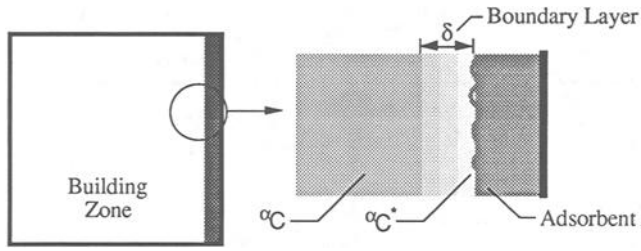

FIG. 1—*Boundary layer diffusion.*

BET "constants," ${}^{\alpha}K_P$, ${}^{\alpha}K_L$ and ${}^{\alpha}K_{BET}$, have an Arrhenius type dependency on temperature [*22–24*] while the Dubinin-Radushkevich parameter D is proportional to the square of the absolute temperature of the system; ${}^{\alpha}C_{so}$, is the sorbed concentration corresponding to complete coverage of a single layer of adsorbate (constant for a given system and independent of temperature for the Langmuir assumption of a fixed number of sites available for adsorption) while ${}^{\alpha}C'_{so}$ is the sorbed concentration corresponding to the practically complete filling of micropores within the sorbent when the air-phase is saturated; and ${}^{\alpha}\hat{C}_e$ is the so-called reduced concentration, a ratio of the equilibrium to the saturation air-phase concentration, ${}^{\alpha}C_{sat}$.

Boundary Layer Diffusion

Adsorbent surfaces may be thought to be separated from the bulk air by a film or boundary layer over which the species concentration varies from a near-surface, air-phase concentration, ${}^{\alpha}C^{*}$, to the bulk air-phase concentration in the room or zone, ${}^{\alpha}C$, as illustrated in Fig. 1. If mass transport is due only to molecular and turbulent diffusion processes (that is, there is no bulk flow of adsorbate through the boundary layer and adsorbent due to pressure gradients), then the net mass transport rate from the bulk phase to the surface, ${}^{\alpha}w_{\delta}$, may be approximated using steady-state mass transfer relations from boundary layer theory of the general form

$$ {}^{\alpha}w_{\delta} = {}^{\bar{h}}m\rho A_s({}^{\alpha}C - {}^{\alpha}C^{*}) \tag{6} $$

where ${}^{\bar{h}}m$ is the average film mass transfer coefficient, ρ is the film density, the average of the bulk and surface densities, and A_s is the projected (that is, exposed) surface area of the adsorbent.

The average mass transfer coefficient may be measured directly (for example, see Ref *5*), measured indirectly using the naphthalene sublimation technique [*25*], estimated from published heat transfer correlations (for example, see Refs *26* and *27*) using the so-called heat and mass transfer analogy, or estimated from published mass transfer correlations. Mass transfer correlations, typically, relate a dimensionless form of the film coefficient, the Sherwood number, *Sh*, with the surface flow Reynolds number, *Re*, and the air-phase Schmidt number, *Sc*. White provides useful correlations for flow parallel to a flat plate, a flow condition that may be considered to be representative of airflow past interior building surfaces [*25*]; Glicksman and Kirwan provide correlations for flow through fixed beds that may prove useful for modeling sorption filtration media [*28,29*]. (See, also, the closely related correlations for particle deposition velocity discussed by Nazaroff [*30,31*].)

Porous Diffusion in Flat Adsorbent Sheets

Transport within effective adsorbents invariably involves a complex variety of processes including:

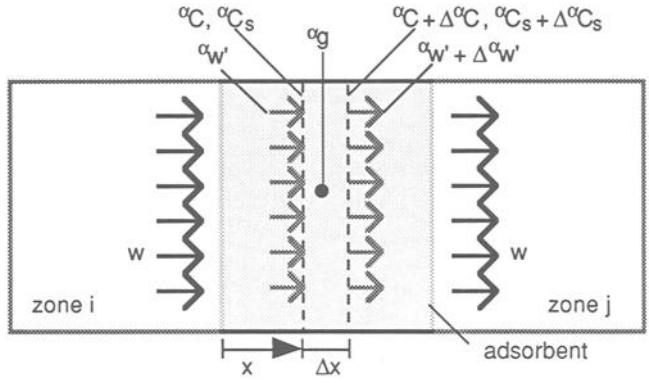

FIG. 2—*Convection-diffusion with adsorption in a flat adsorbent.*

- molecular, Knudsen, and surface diffusion within macroporous interstices (that is, interstices that are large relative to the molecular dimensions of the adsorbate),
- diffusion processes influenced by the potential field of the adsorbent surfaces within microporous interstices that are specific to the surface characteristics of the adsorbent and the nature of the adsorbate, and
- bulk transport due to Poiseuille flow driven by pressure gradients [*23,32,33*].

Macroporous diffusion and microporous diffusion, at low air-phase adsorbate concentrations, in flat adsorbent sheets or panels may be modeled *analogously* to Fick's Law as

$$ {}^{\alpha}w' = -\rho A_s {}^{\alpha\text{-air}}\mathcal{D}({}^{\alpha}C)\frac{\partial {}^{\alpha}C}{\partial x} \tag{7} $$

where ${}^{\alpha}w'$ is the mass transport rate of species α relative to the bulk flow through the porous adsorbent, ${}^{\alpha\text{-air}}\mathcal{D}({}^{\alpha}C)$ is the effective diffusion coefficient of the adsorbate-adsorbent system that, in general, depends upon the species air-phase concentration, its physical properties, and the physical characteristics of the adsorbent [*23,32,33*], and x is the coordinate direction perpendicular to the plane of the adsorbent sheet.

Consider now a flat adsorbent panel separating two building zones, as diagrammed in Fig. 2, with diffusion transport ${}^{\alpha}w'$, superimposed upon a bulk flow, w from Zone i to Zone j. At position x in the adsorbent, the air-phase and adsorbed-phase concentrations are ${}^{\alpha}C$ and ${}^{\alpha}C_s$, respectively. Accounting for a change of these values over a small distance Δx and the possibility of species generation (or removal) in the adsorbent ${}^{\alpha}g$ we may directly write a species mass balance for the Δx slice

$$ w[{}^{\alpha}C - ({}^{\alpha}C + \Delta {}^{\alpha}C)] + [{}^{\alpha}w' - ({}^{\alpha}w' + \Delta {}^{\alpha}w')] + {}^{\alpha}g\Delta x = \rho A_s \epsilon \Delta x \frac{\partial {}^{\alpha}C}{\partial t} + \rho_s A_s \Delta x \frac{\partial {}^{\alpha}C_s}{\partial t} \tag{8} $$

where ρ is (now) the density of the air-phase, ρ_s is the bulk density of the adsorbent, and ϵ is the porosity of the adsorbent.

In the limit, $\Delta x \rightarrow 0$, Eq 8 becomes

$$ -w\frac{\partial {}^{\alpha}C}{\partial x} - \frac{\partial {}^{\alpha}w'}{\partial x} + {}^{\alpha}g = \rho A_s \epsilon \frac{\partial {}^{\alpha}C}{\partial t} + \rho_s A_s \frac{\partial {}^{\alpha}C_s}{\partial t} \tag{9} $$

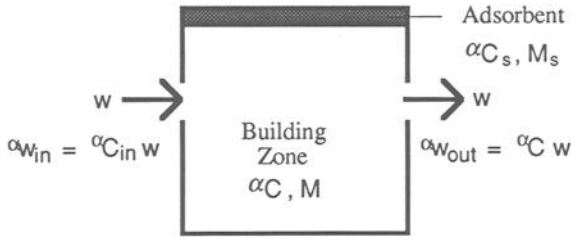

FIG. 3—*Single-zone equilibrium adsorption (EA) model.*

Equation 9 is a differential species mass balance relation that is quite general, but not yet in a form that is useful. We shall modify this expression by first assuming that adsorption is practically instantaneous so that $^{\alpha}C$ and $^{\alpha}C_s$ are related by the equilibrium relation $^{\alpha}C_s = {}^{\alpha}f(^{\alpha}C)$ and then introduce the porous diffusion relation defined by Eq 7 to obtain

$$\rho A_s {}^{\alpha\text{-air}}\mathcal{D}\,\frac{\partial^2 {}^{\alpha}C}{\partial x^2} + {}^{\alpha}g = \left(\rho A_s \epsilon + \rho_s A_s \frac{\partial {}^{\alpha}f}{\partial {}^{\alpha}C}\right)\frac{\partial {}^{\alpha}C}{\partial t} + w\,\frac{\partial {}^{\alpha}C}{\partial x} \tag{10}$$

This equation that has the form of the one-dimensional convection-diffusion equation—although here with possibly nonlinear coefficients due to the terms $^{\alpha\text{-air}}\mathcal{D}$ and $\partial {}^{\alpha}f/\partial {}^{\alpha}C$—shall be identified as the one-dimensional convection-diffusion-adsorption equation. This equation is similar to those used to model the dynamics of adsorption in packed columns or chromatographic columns [*33,34*].

Building Sorption Dynamics

The forgoing principles may be directly applied to the problem of modeling adsorption dynamics in buildings. We will focus consideration on the single-zone case, moving from simple models to more complete models, and from these results extract element equations that can be used for general multi-zone contaminant dispersal analysis.

EA: Equilibrium Adsorption Model

Consider a single well-mixed zone containing a volume of air of mass M and a quantity of adsorbent of mass M_s with air flowing into and, by continuity, out of the zone at a mass flow rate w, as illustrated in Fig. 3. Given the species concentration in the zone $^{\alpha}C$ and that of the air flowing into the zone $^{\alpha}C_{in}$, the species mass flow rates into and out of the zone are as shown on the figure and thus the species mass balance may be written as

$$w\,{}^{\alpha}C + M\frac{d\,{}^{\alpha}C}{dt} + M_s\frac{d\,{}^{\alpha}C_s}{dt} = {}^{\alpha}G + {}^{\alpha}G_s + w\,{}^{\alpha}C_{in} \tag{11}$$

where we have admitted the possibility of species generation in the zone air, $^{\alpha}G$, and in the adsorbent, $^{\alpha}G_s$.

If now we make the simplifying assumption that the adsorbate concentration within the adsorbent is uniform, and the zone air at all times remains in equilibrium with the adsorbent (that is, $^{\alpha}C_s = {}^{\alpha}f(^{\alpha}C)$) then the mass balance assumes a form that is similar to that defining the dilution dynamics alone

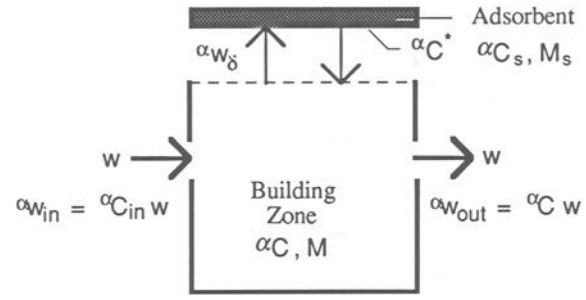

FIG. 4—*Single-zone boundary layer diffusion controlled (BLDC) model.*

$$w^{\alpha}C + M_{\text{eff}} \frac{d^{\alpha}C}{dt} = {}^{\alpha}E \; ; \; M_{\text{eff}} = \left(M + M_s \frac{d^{\alpha}f}{d^{\alpha}C}\right) \tag{12}$$

where the terms on the right-hand side of Eq 11 have been collected into a single term, the system excitation ${}^{\alpha}E$, and an effective participating mass of the system, M_{eff}, appears as the sum of the zone air mass plus the adsorbent mass scaled by the slope of the adsorption isotherm. For the Linear adsorption isotherm the effective mass is simply $M_{\text{eff}} = (M + M_s {}^{\alpha}K_P)$. From an element assembly point of view [*35*] the adsorbent simply contributes an additional storage element with capacitance equal to $M_s(d^{\alpha}f/d^{\alpha}C)$ or, equivalently, sorption mass transport may be modeled using the equilibrium adsorption element equation

$$\text{EA Element} \quad {}^{\alpha}w_s = M_s\left(\frac{d^{\alpha}f}{d^{\alpha}C}\right)\frac{d^{\alpha}C}{dt} \tag{13}$$

Equation 12, the single-zone equilibrium adsorption or EA model, may be solved to determine the time variation of zone-air concentration ${}^{\alpha}C$, and from this solution the adsorbent concentration response may be recovered using the assumed equilibrium relation ${}^{\alpha}C_s = {}^{\alpha}f({}^{\alpha}C)$. The assumption of equilibrium adsorption is reasonable when boundary layer diffusion, porous diffusion, and adsorption transport rates are rapid relative to flow transport dynamics. This is likely to be the case when the adsorbent is well distributed in the zone and when zone air concentrations are changing slowly.

BLDC: Boundary Layer Diffusion Controlled Model

Consider the same zone where, now, we isolate the adsorbent and the zone in separate control volumes linked by boundary layer mass transport ${}^{\alpha}w_\delta$, as shown in Fig. 4. Two mass balance relations may be written for this system idealization, one for the zone air and one for the adsorbent

$$w^{\alpha}C + \bar{h}_m \rho A_s({}^{\alpha}C - {}^{\alpha}C^*) + M\frac{d^{\alpha}C}{dt} = {}^{\alpha}G + w^{\alpha}C_{\text{in}} \tag{14a}$$

$$-\bar{h}_m \rho A_s({}^{\alpha}C - {}^{\alpha}C^*) + M_s\frac{d^{\alpha}C_s}{dt} = {}^{\alpha}G_s \tag{14b}$$

If we now make the simplifying assumption that the species concentration within the adsorbent is uniform and the air at the surface of the adsorbent at all times remains in equilibrium with the

adsorbent (that is, ${}^{\alpha}C_s = {}^{\alpha}f({}^{\alpha}C^*)$) then we obtain two equations in two unknown variables, ${}^{\alpha}C$ and ${}^{\alpha}C^*$, the zone and near-surface air-phase concentrations

$$\begin{bmatrix} w + \bar{h}_m \rho A_s & -\bar{h}_m \rho A_s \\ -\bar{h}_m \rho A_s & \bar{h}_m \rho A_s \end{bmatrix} \begin{Bmatrix} {}^{\alpha}C \\ {}^{\alpha}C^* \end{Bmatrix} + \begin{bmatrix} M & 0 \\ 0 & M_{\text{seff}} \end{bmatrix} \begin{Bmatrix} \dfrac{d^{\alpha}C}{dt} \\ \dfrac{d^{\alpha}C^*}{dt} \end{Bmatrix} = \{{}^{\alpha}\mathbf{E}\} \tag{15a}$$

$$M_{\text{seff}} = M_s \frac{d^{\alpha}f}{d^{\alpha}C^*} \tag{15b}$$

where the terms on the right hand side of Eqs 14*a* and 14*b* have been collected in a single system excitation vector $\{{}^{\alpha}\mathbf{E}\}$. For this model, then, an effective participating mass of the absorbent appears that is simply equal to the second term of the total effective mass obtained for the EA model. Note, also, that the first array, the transport array of Eq. 15*a*, can be written as the sum of a symmetric and an asymmetric array

$$\begin{bmatrix} w + \bar{h}_m \rho A_s & -\bar{h}_m \rho A_s \\ -\bar{h}_m \rho A_s & \bar{h}_m \rho A_s \end{bmatrix} = \begin{bmatrix} w & 0 \\ 0 & 0 \end{bmatrix} + \bar{h}_m \rho A_s \begin{bmatrix} 1 & -1 \\ -1 & 1 \end{bmatrix} \tag{16}$$

The first array on the right-hand side is due to flow transport, and the second array is due to boundary layer transport and is, in fact, the transport matrix of a boundary layer transport element equation

BL Element

$$\begin{Bmatrix} {}^{\alpha}w_{\delta\text{-ads}} \\ {}^{\alpha}w_{\delta\text{-des}} \end{Bmatrix} = \bar{h}_m \rho A_s \begin{bmatrix} 1 & -1 \\ -1 & 1 \end{bmatrix} \begin{Bmatrix} {}^{\alpha}C \\ {}^{\alpha}C^* \end{Bmatrix} \tag{17}$$

where ${}^{\alpha}w_{\delta\text{-ads}}$ and ${}^{\alpha}w_{\delta\text{-des}}$ are the boundary layer adsorption and desorption mass transport rates, respectively.

This system of two ordinary differential equations may be solved to determine the time variations of the zone and the near-surface air-phase concentrations, α_C and ${}^{\alpha}C^*$ and from this solution the adsorbent concentrations response may be recovered using the assumed equilibrium relation. An analysis of this system of equations may be found in an earlier publication [*7*] where it is shown that, for a linear adsorption isotherm, this model simplifies to the EA model when the rate of diffusion transport is large relative to the airflow rate (that is, when $\bar{h}_m \rho A_s >> w$).

The assumptions underlying this model are justified when boundary layer diffusion is slow relative to porous diffusion—a criterion similar to the Biot criterion used in heat transfer (see Ref *14*.) For this reason we will identify this model as the Boundary Layer Diffusion Controlled or BLDC model.

BLPD: Boundary Layer and Porous Diffusion Model

Reconsider the same zone again where now we isolate the zone in one control volume and spatially discretize the adsorbent into n slices linking it, by boundary layer mass transport ${}^{\alpha}w_{\delta}$, to the zone control volume as illustrated in Fig. 5. In this idealization, the primary dependent variables are again air-phase concentrations but now we will attempt to determine the spatial variation of air-phase concentration within the adsorbent pore structure with the discrete variables ${}^{\alpha}C_1$, ${}^{\alpha}C_2$, . . . ${}^{\alpha}C_n$. Following the strategies employed above, we will assume that the pore air-phase concen-

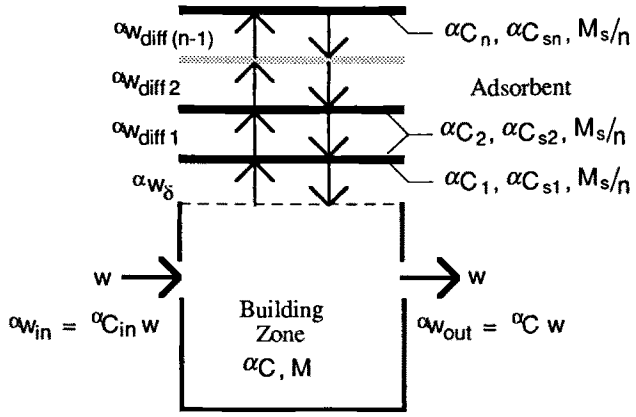

FIG. 5—*Single-zone boundary layer porous diffusion (BLPD) model.*

trations remain in equilibrium with the adsorbed-phase concentrations or ${}^{\alpha}C_{si} = {}^{\alpha}f({}^{\alpha}C_i)$; $i = 1, 2, \ldots r$.

The mass balance relation for the zone air may be formed directly (it will be similar to Eq 14*a*) but the formation of the mass balance for the adsorbent slices is a bit more challenging. Two approaches are available. In the first approach we may simply treat each slice as a control volume and formulate mass balances using average concentrations for the slice (for example, see Refs *11* and *13*). The second approach, which will be taken here, is the Finite Element Approach wherein (1) the form of the spatial variation of the concentration (shape function) is assumed for each slice and is related to the discrete concentration variables, (2) a governing differential equation is identified (in our case it is the one-dimensional convection-diffusion-adsorption equation presented in Eq 10) and the assumed shape functions are substituted, (3) a minimization principle (for example, the Galerkin Method) is applied to formulate element equations, and (4) the element equations are assembled to form the system equations.

The application of the Finite Element Method to the one-dimensional convection-diffusion equation and element assembly techniques are discussed elsewhere [*35*,*36*]. Here we shall assume no Poiseuille-type flow in the adsorbent and, therefore, need only consider the slightly simpler problem of one-dimensional diffusion with equilibrium adsorption. For linear shape functions, lumped mass, and no generation within the adsorbent, the resulting porous diffusion-adsorption element equations, or, equivalently, mass balance equations for transport from node i to j are

$$\text{PDA Element} \begin{Bmatrix} {}^{\alpha}w_{\text{diff-}i} \\ \alpha w_{\text{diff-}j} \end{Bmatrix} = \frac{\rho A_s {}^{\alpha\text{-air}}\mathcal{D}}{\delta x^e} \begin{bmatrix} 1 & -1 \\ -1 & 1 \end{bmatrix} \begin{Bmatrix} {}^{\alpha}C_i \\ {}^{\alpha}C_j \end{Bmatrix} + M^e_{\text{seff}} \begin{bmatrix} 1 & 0 \\ 0 & 1 \end{bmatrix} \begin{matrix} \dfrac{d^{\alpha}C_i}{dt} \\ \dfrac{d^{\alpha}C_j}{dt} \end{matrix} \tag{18a}$$

$$M^e_{\text{seff}} = \frac{A_s \delta x^e}{2} \left(\rho\epsilon + \rho_s \frac{\partial {}^{\alpha}f}{\partial {}^{\alpha}C} \right) \tag{18b}$$

where δx^e is the element thickness (i.e., the thickness of each slice). For this lumped mass formulation an element effective mass, M^e_{seff}, appears, completely analogous to the EA and BLDC effective mass contributions, that is equal to the mass of adsorbent within one half of the slice scaled by the slope of the adsorption isotherm plus the mass of the air within the pores of this half-slice.

The complete system of equations for this third single-zone Boundary Layer Porous Diffusion (BLPD) model will not be presented due to space limitations. Suffice it to say it is simply a slight modification and extension of Eq 15*a* with $n - 1$ additional equations. This system of equations may be solved to determine the $n + 1$ air-phase concentrations and then the adsorbent concentrations may be recovered using the equilibrium relation. The assumptions underlying this model are not very restrictive; therefore, we should expect this model to provide the best estimate of system response, although at the cost of extra complexity and computation.

Discussion

Model Variants—The models developed above are each based on the general functional expression for sorption isotherms, Eq 1. The substitution of a specific isotherm relation yields a specific member of each family of models. With the four isotherm relations defined above, Eqs 2 through 5, we obtain the Linear, Langmuir, BET, and Polanyi DR members of the EA, BLDC, and BLPD families. Other adsorption isotherms can also be used directly.

In all cases, the slope of the isotherm (i.e., $\partial^{\alpha} f/\partial^{\alpha} C$) for the current state of free-phase/adsorbed-phase concentration is required. In many situations it is likely that the free-phase/adsorbed-phase concentration response will fall within a range over which this slope may be relatively constant, and thus a linearized approximation to the isotherm (for example, using a truncated Taylor's expansion) may be used to avoid this source of nonlinearity.

Model Selection—The BLPD model family provides the most complete idealization of the zone-adsorbent system but requires an estimation of the effective diffusion coefficient and, possibly, the porosity, mean pore radius, and other physical characteristics of the absorbent—data that may be hard to come by. It is also rather complex and therefore somewhat more difficult to implement. The question arises, then: When can the simpler EA or BLDC models be expected to be accurate? Following the basic strategy of the Biot criteria used in the related boundary layer/conduction heat transfer problem we may establish model selection criterion based on a three-part ratio

$$w : \bar{h}_m \rho A_s : \rho A_s{}^{\alpha\text{-}air} \mathcal{D} / \delta x \tag{19}$$

where δx is the total thickness of the flat adsorbent sheet or panel. When the last two terms are large relative to the first, then the EA model may be expected to be accurate; when the first two terms are of the same magnitude yet smaller than the third term, then the BLDC model may be expected to be accurate; and when the last term is small or of a similar magnitude to the other terms, then the complete BLPD model should be used.

Multizone Analysis—The models developed above presumed that adsorption was local to the single zone being considered. For multi-zone modeling of adsorption that is local to a given zone it is theoretically and physically consistent to expect that the same elements—Eqs 13, 17, or 18, or a combination thereof—used to assemble these single-zone models may be used directly to model either EA, BLDC, or BLPD dynamics local to each zone in question. Indeed, one may directly consider a mixed model wherein some zones include EA assemblages (for example, due to curtain fabric adsorption), others include BLDC adsorption (for example, due to carpet adsorption), while yet others include BLPD adsorption dynamics (for example, moisture adsorption in wood construction).

Application

Silberstein at NIST studied the formaldehyde (HCHO) adsorption and desorption dynamics of a 1.2 m by 2.4 m specimen of 0.013-m-thick gypsum board that was attached to one wall of a 1.22 m by 2.44 m by 0.61 m test chamber [*4*]. The test chamber was placed in a closed environment

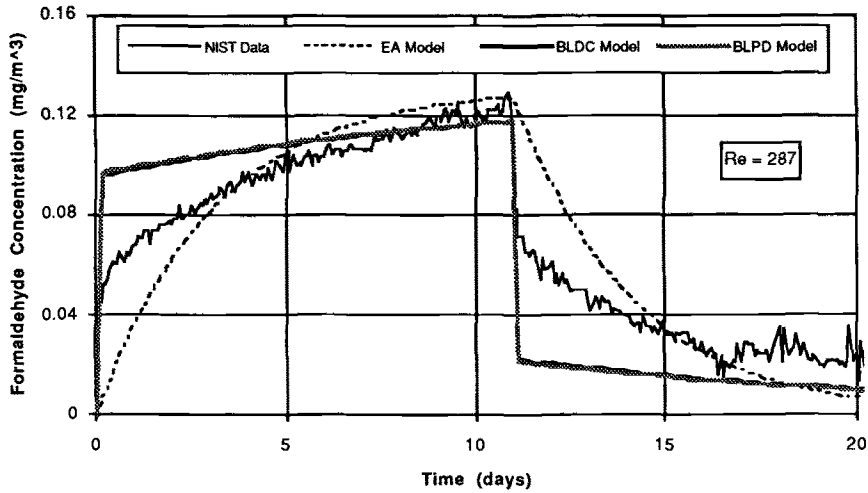

FIG. 6—*HCHO sorption on gypboard:* Re_L = *287.*

maintained at 23°C and 50% RH, a constant fresh airflow rate through the chamber of approximately one air change per hour was maintained, and HCHO gas was introduced into the chamber at a constant rate for eleven days. This test was modeled with the EA, BLDC, and BLPD models using the linear adsorption isotherm with a partition coefficient of 5.5 g · air/g · gypboard (other details have been reported earlier [*9*]. The average mass transfer coefficient was estimated to be 6.6×10^{-5} m/s using a correlation with the boundary layer Reynolds number given by White [25]. The Reynolds number was estimated to be RE_L = 287 by assuming a velocity profile within the chamber similar to that which would occur in a duct with the same volumetric flow rate. The comparison of measured response to predicted response is shown in Fig. 6 for Re_L = 287 and in Fig. 7 for a Reynolds number ten times this value (i.e., an average mass transfer coefficient $\sqrt{10}$ 6.6×10^{-5} m/s).

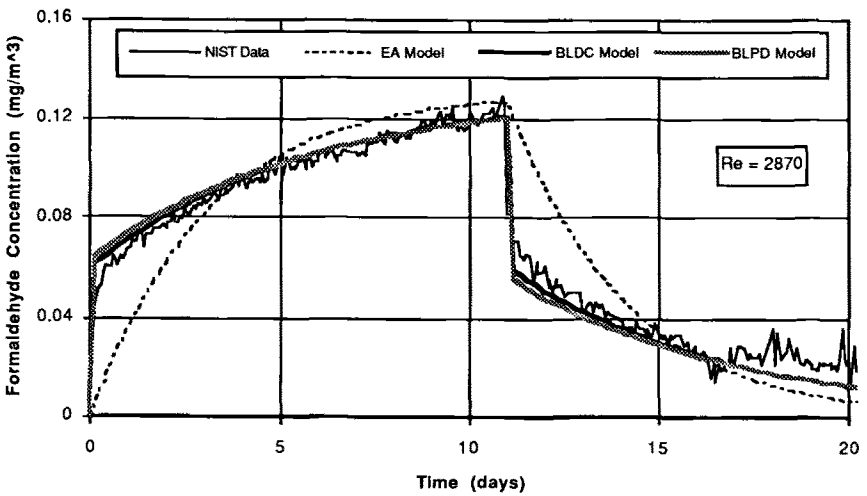

FIG. 7—*HCHO sorption on gypboard:* Re_L = *2870.*

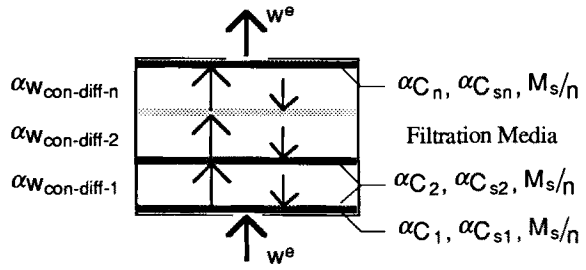

FIG. 8—*Discretization of sorption filter medium.*

The measured and predicted responses are seen to be of exponential nature with time constants on the order of days while the nominal time constant of the test chamber, based on the airflow rate of one air change per hour, was just one hour. Thus, in this case adsorption transport has indeed a significant impact. The EA model, being a single-degree-of-freedom model, approximates the response with a single exponential and provides a reasonable estimate of the overall response but does not capture the early rapid rise of the adsorption and rapid fall of the desorption phases. The BLDC model is a two-degree-of-freedom model and, as such, the response is represented by the sum of two exponentials. Here, these two exponentials have very different time constants and, as a result, the BLDC captures the early rapid rise of the adsorption and fall of the desorption phases.

For this case the mass transport ratios are, for $Re_L = 287$

$$w : \bar{h}_m \rho A_s : \rho A_s{}^{\alpha\text{-air}} \mathcal{D} / \delta x = 2200 : 817 : 5320$$

and for $Re_L = 2870$

$$w : \bar{h}_m \rho A_s : \rho A_s{}^{\alpha\text{-air}} \mathcal{D} / \delta x = 2200 : 2580 : 5320$$

so we should expect the BLDC and BLPD models to yield similar results; the results bear this out. It is seen that the results are sensitive, however, to the boundary layer mass transfer. With a tenfold increase in Reynolds number (that is, a $\sqrt{10}$ increase in mass transfer) we move from a poor to a very good prediction of response.

Sorption Filtration Dynamics

If we assume airflow within a building sorption filtration device is axial and radial mass transport is small relative to longitudinal transport, then sorption filtration mass transport in this device may reasonably be modeled using the one-dimensional convection-diffusion-adsorption equation, Eq 10. To do so, the finite element method may again be applied.

Finite Element Model of Sorption Filtration

To approximate a solution to the one-dimensional convection-diffusion-adsorption equation we follow the same steps previously discussed for the development of the porous-diffusion element equations, but now include the possibility of a Poiseuille-type bulk airflow in the porous adsorbent. We begin by spatially discretizing the filter medium into n slices as illustrated in Fig. 8, distributing the total mass of the medium M_s to each slice, and obtain the following convection-diffusion-adsorption element equations

$$\text{CDA Element} \begin{Bmatrix} {}^{\alpha}w_{\text{con-diff-}i} \\ {}^{\alpha}w_{\text{con-diff-}j} \end{Bmatrix} = [[{}^{\alpha}\mathbf{f}^{e}_{\text{diff}}] + [{}^{\alpha}\mathbf{f}^{e}_{\text{conv}}]] \begin{Bmatrix} {}^{\alpha}C_i \\ {}^{\alpha}C_j \end{Bmatrix} + M^{e}_{\text{seff}} \begin{bmatrix} 1 & 0 \\ 0 & 1 \end{bmatrix} \begin{matrix} \dfrac{d^{\alpha}C_i}{dt} \\ \dfrac{d^{\alpha}C_j}{dt} \end{matrix} \tag{18a}$$

where now the transport matrix is the sum of two component matrices, the first accounting for diffusion transport as before

$$[{}^{\alpha}\mathbf{f}^{e}] = \frac{\rho A_s{}^{\alpha\text{-air}}\mathcal{D}}{\delta x^{e}} \begin{bmatrix} 1 & -1 \\ -1 & 1 \end{bmatrix} \tag{18b}$$

and the second accounting for convective transport

$$[{}^{\alpha}\mathbf{f}^{e}_{\text{conv}}] = \frac{\mathrm{w}^{e}}{2} \begin{bmatrix} 1 & 1 \\ -1 & -1 \end{bmatrix} + \frac{\phi w^{e}}{2} \begin{bmatrix} 1 & -1 \\ -1 & 1 \end{bmatrix} \tag{18c}$$

The so-called upwind parameter, $0 \leq \phi \leq 1$, is introduced to control numerical stability (at the cost of artificial diffusion) during the solution phase, and w^{e} is the air mass flow rate through the filter medium. The effective mass M^{e}_{seff} is as before, Eq 18*b*.

It may be shown that an assemblage of these element equations (that is, corresponding to a given sorption filter) is equivalent to a tanks-in-series idealization, a series of equivalent well-mixed compartments linked by flow elements, for those cases when full upwinding, $\phi = 1$, is used [*37*]. This suggests another strategy that will be explored below.

Tanks-in-Series Models

The convection-diffusion-adsorption element equations would be appropriate for a sorption filtration medium with a homogeneous distribution of micro and small macro pores. Regrettably, gaseous sorption filtration media do not fit this description. Sorption filters for building air cleaning applications are likely to be either fixed beds of activated carbon pellets 0.5 to 5 mm in diameter supported in a rectangular frame or a particle filter loaded with these same activated carbon pellets (for example, nonwoven polyester or open-cell foam filled with activated carbon pellets and binder). Therefore, building sorption filtration chambers are made up of sheets of carbon-containing filters separated by air spaces, and the filter medium itself contains voids ranging in size from the pore structure of the support medium down to the interstitial voids between clumps of activated carbon pellets. The microporous structure is limited to individual pores alone.

Actual building sorption filtration devices are likely to be better modeled using a tanks-in-series approach. The three families of single-zone building sorption dynamics models presented above are attractive candidates for this purpose (that is, using a more appropriate model for porous diffusion in pellets for the BLPD case). To apply this strategy we would simply assemble a series of the single-zone EA, BLDC, or modified BLPD models to simulate the behavior of the filtration device as a whole. Figure 9 illustrates this strategy for the EA tanks-in-series model, the BLDC and the modified BLPD tanks-in-series models follow directly from this example. This is equivalent to the spatial discretization used in the finite element approach where now each single-zone is configured to represent a slice of the total filtration system and the total mass of the sorption medium M_s is distributed to each zone. Now, however, we account for the air in the relatively large air spaces within the filtration chamber and distribute it evenly (here) to each zone.

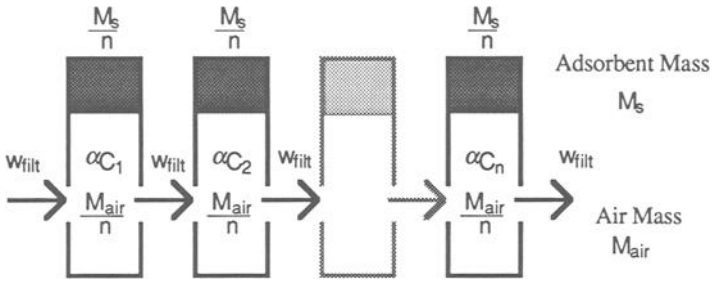

FIG. 9—*EA tanks-in-series model of filtration system.*

Application

Activated carbon filtration systems are commonly installed in buildings to control odor, yet few researchers have investigated the response of activated carbon challenged by the trace levels of contaminants commonly found in indoor air. An early investigation of the sorption capacity of activated carbon for acetaldehyde (CH_3CHO), benzene (C_6H_6), and 1,1,1-trichloroethane (CH_3CCl_3) was not promising [*17,18,38*]. Subsequent independent investigations by Liu [*39*] of the sorption capacity for heptane (C_7H_{16}) and decane ($C_{10}H_{22}$) and Graham [*40*] of the sorption capacity for benzene indicated dramatically higher sorption capacities and questioned the experimental procedure used in the earlier study. Both Liu and Graham used a coconut-based GAC.

Sorption Isotherms—The equilibrium sorption data reported by Liu and Graham were used to establish sorption isotherms for subsequent analysis. For the purposes of this study, the Polanyi DR isotherm model, Eq 5, was fitted to the equilibrium sorption data reported by Liu for heptane and by Graham for benzene. The air-phase saturated concentration ${}^{\alpha}C_{sat}$ for each species was determined for saturation vapor pressures reported in the *Handbook of Chemistry and Physics* [*41*] leaving two model parameters, ${}^{\alpha}C'_{so}$ and D, to be determined by a nonlinear least squares procedure. The results of this exercise are shown in Fig. 10.

Filtration Device Simulation—Liu investigated the response of a small, packed-bed filter to a constant inlet airflow at each of four constant challenge (inlet) concentrations of heptane: 118, 15, 2.7, and 0.5 ppm. The filter bed contained 6 g of granulated activated carbon within a cylindrical glass chamber 2.54 cm in diameter and 2.54 cm long. Heptane was injected into air maintained at 50% RH and ambient temperature. This air was passed through the filter maintaining a superficial velocity of 25.4 cm/s and exit concentrations were measured over time until complete breakthrough was realized. Results were reported in terms of the ratio of exit concentration to inlet concentration or breakthrough.

This filtration device was modeled using both the EA tanks-in-series model and the BLDC tanks-in series model, designated as EA and BLDC models, respectively. The Polanyi DR isotherm reported above was used in both cases. For the BLDC tanks-in-series model, the boundary layer mass transfer coefficient was estimated using correlations reported by Glicksman [*28*] with the particle Reynolds number estimated to be 65, and consequently the Sherwood number equal to 20 ± 5. The molecular diffusivity of heptane was assumed to be 0.1 cm^2/s. Carbon particles were assumed to be approximately spherical with a mean diameter of 4 mm. All values were based on atmospheric pressure and ambient temperature.

Figure 11 compares the results of the simulations using the EA model, employing five separate cells (tanks), and the BLDC model, employing ten, to measured data. These curves are commonly called breakthrough curves—as the activated carbon approaches equilibrium the contaminant in the entering gas no longer is adsorbed and simply "breaks through" the filter to the exit. In all cases the EA tanks-in-series models provided a reasonable estimate of the ultimate breakthrough

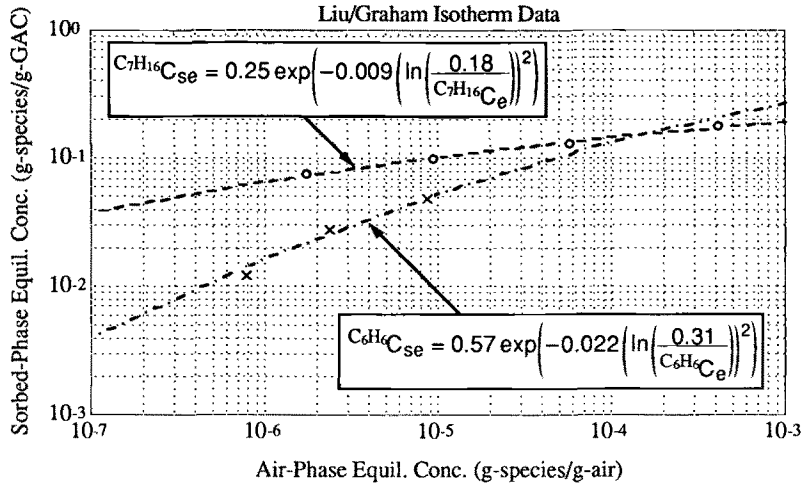

FIG. 10—*Sorption equilibrium data and Polanyi DR isotherms for heptane and benzene on coconut-based granulated activated carbon (GAC). (Liu's heptane data are indicated by* o *markers; Graham's benzene data by* x *markers.)*

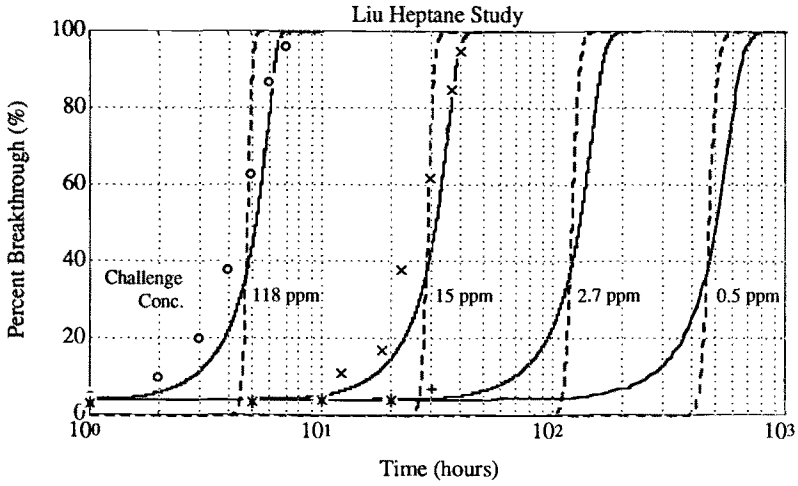

FIG. 11—*Heptane* breakthrough *curves for Liu's test filtration device. Solid lines are based on a 10-cell BLDC tanks-in-series simulation, dashed lines on a 5-cell EA tanks-in-series simulation, and markers present measured data:* o *for 118 ppm,* x *for 15 ppm,* + *for 2.7 ppm, and* * *for 0.5 ppm challenge concentrations, respectively.*

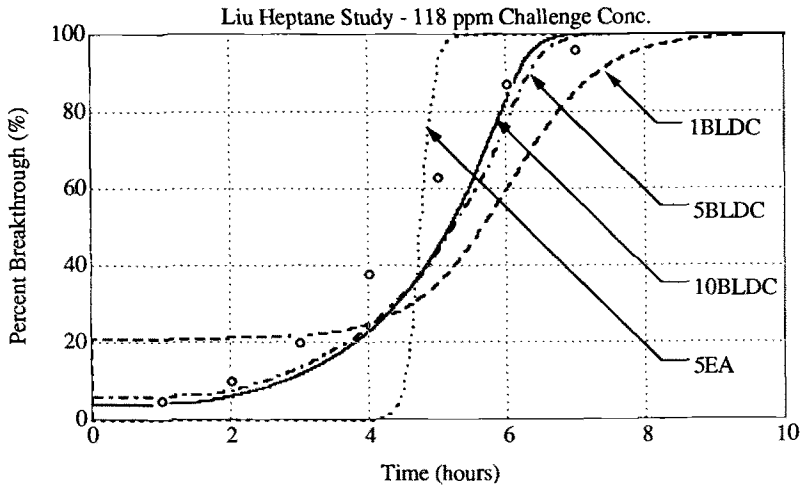

FIG. 12—*Comparison of simulated* breakthrough *curves for a 5-cell EA and 1, 5, and 10-cell BLDC tanks-in-series models at 118 ppm challenge concentration. Markers present measured data.*

time of the filter but significantly underestimated the breakthrough percentage up until that time. The BLDC model provided an accurate estimation of the percentage of breakthrough at all times, although during the period of rapid change it somewhat underestimated the response. Furthermore, the BLDC model of this system proved to be numerically stiff (that is, characterized by widely varying system time constants) and, as a result, demanded state-of-the-art numerical methods for its solution. The close correspondence between measured results and the BLDC model results suggest that, in this case, sorption is boundary layer diffusion controlled.

In chemical process simulation, increasing the number of cells used in a tanks-in-series simulation approaches the limiting case of plug flow [*42*]. The EA tanks-in-series model exhibits this behavior, but the BLDC model is a bit more complex. Figure 12 compares computed responses for 1-cell, 5-cell, and 10-cell BLDC models. Although the computed breakthrough becomes more abrupt with a greater number of cells, the results converge to a response that falls short of the extreme plug flow breakthrough. In this case, a 10-cell idealization was practically convergent; 20-cell and 100-cell models produced results practically identical to the 10-cell results shown.

Boundary layer diffusion controlled absorption is, by its physical nature, sensitive to the mass transfer rate at the boundary layer and, thus, the mass transfer coefficient used to model it. The estimation of an appropriate (effective) boundary layer mass transfer coefficient is fraught with uncertainty. As noted above, the mass transfer coefficient used in this study corresponded to a Sherwood number of 20 ± 5. Figure 13 shows modeled responses using the convergent 10-cell BLDC model for mass transfer coefficients corresponding to Sherwood numbers of 10, 20, and 30, respectively. As expected, computed results are particularly sensitive to this parameter.

Building/Filtration System Simulation—The sorption filtration models presented above were formulated so that they may be directly assembled with other contaminant dispersal elements [*35*] to form idealizations of building/HVAC systems of arbitrary complexity. To provide an example of the utility of such an integration, a simple investigation was made of a representative problem—the performance of an activated carbon filtration system in a laboratory setting.

A hypothetical laboratory, 3 m by 6 m by 6 m, ventilated with outdoor air at a constant rate of 1 air change rate per hour (ACH) ACH was modeled as a single well-mixed zone. A 10-cell BLDC tanks-in-series filter model, using the Polanyi isotherm for benzene presented in Fig. 10, was linked

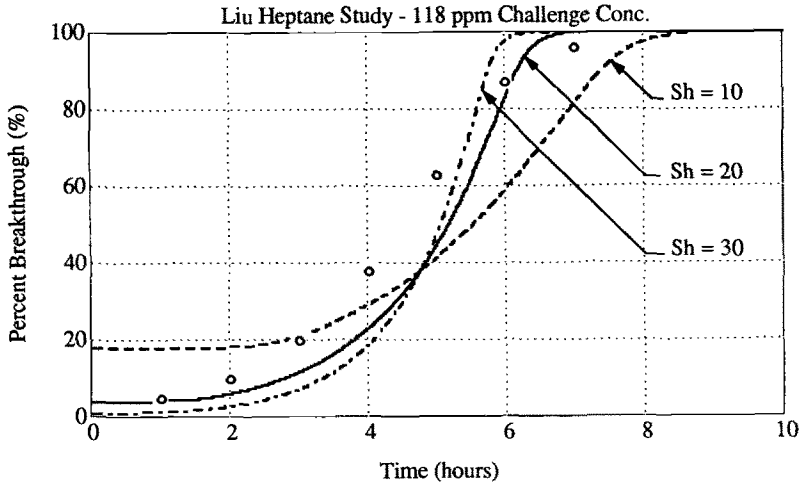

FIG. 13—*Comparison of simulated* breakthrough *curves for a 10-cell BLDC tanks-in-series model using boundary layer mass transfer coefficients corresponding to Sherwood numbers of 10, 20, and 30, respectively, at 118 ppm challenge concentration. Markers present measured data.*

to the laboratory idealization to account for an activated carbon recirculation filtration system. A diagram of this idealization is shown in Fig. 14. It was assumed that (1) the filtration system included a 0.61 m by 0.61 m by 0.61 m filtration chamber and was operated daily from 7:00 am to 5:00 pm, recirculating lab air at 10 ACH, (2) outdoor benzene concentration remained constant at 20 ppb, and (3) at 8:00 am daily a spill of 0.2 cm^3 of liquid benzene occurred (e.g., resulting from a daily transfer of benzene from a storage container to a smaller container) that completely volatilized within 0.10 h. The complete, well-mixed, instantaneous volatilization of the spilled benzene would result in a peak indoor benzene concentration of 500 ppb above ambient indoor levels: this value and the outdoor concentration used are representative of actual conditions that exist in building environments [*43*].

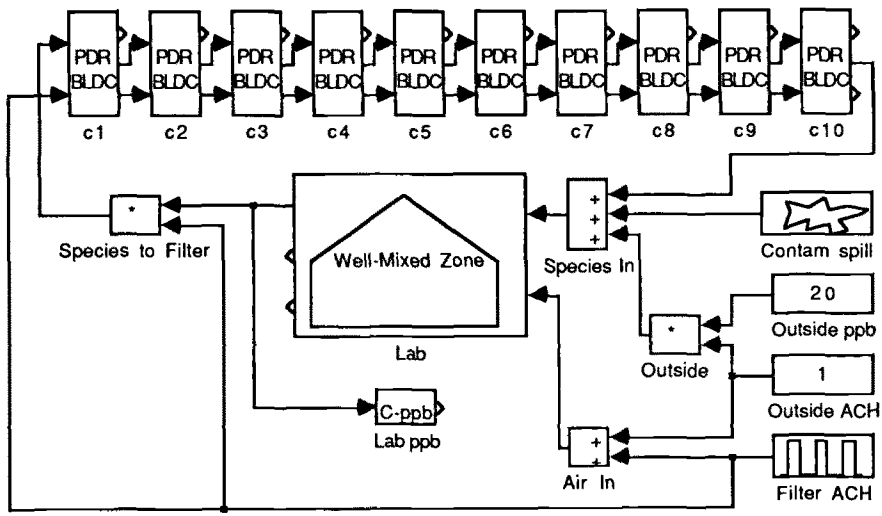

FIG. 14—*Diagram of the lab-filtration system idealization.*

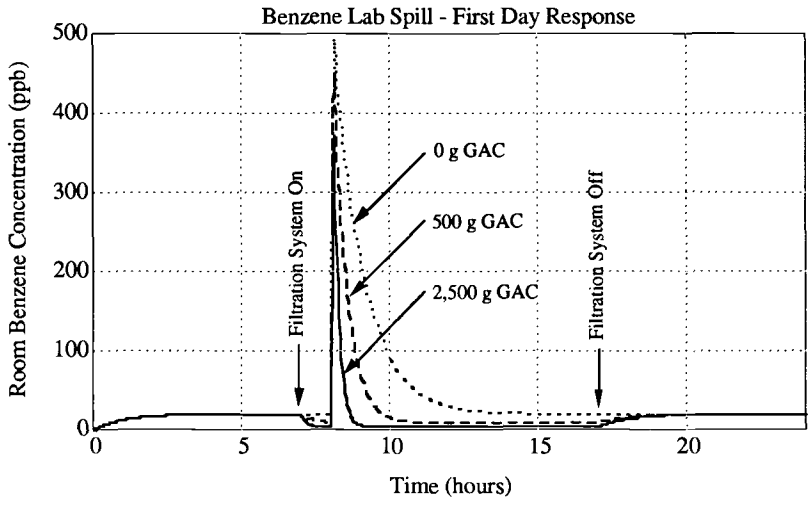

FIG. 15—*Simulation results for the first day response for a 0.2 cm³ C_6H_6 spill in a 108 m³ lab with a filtration systems containing 500 and 2 500 g of GAC operated at 10 ACH from 7:00 am to 5:00 pm.*

The response of the system was computed for the first day of operation using 500 and 2 500 g of activated carbon, both relatively small amounts, and compared to the response one would obtain without filtration. The results of this analysis are shown in Fig. 15. During the first day's response the filtration system not only effectively mitigates the impact of the spill but maintains indoor C_6H_6 levels below outdoor levels. While the larger amount of activated carbon reduces both peak concentrations and integrated exposure, as expected, even the very small amount of 500 g of activated carbon proves to have a significant impact on the quality of air within the lab.

To gain some insight into the long-term behavior of this hypothetical sorption filtration system the response was computed for the first 30 days using only 500 g of activated carbon. Figure 16 presents the complete response results, and Fig. 17 presents a detail of these results. Again this impractically small amount of activated carbon has sufficient capacity to effectively mitigate the

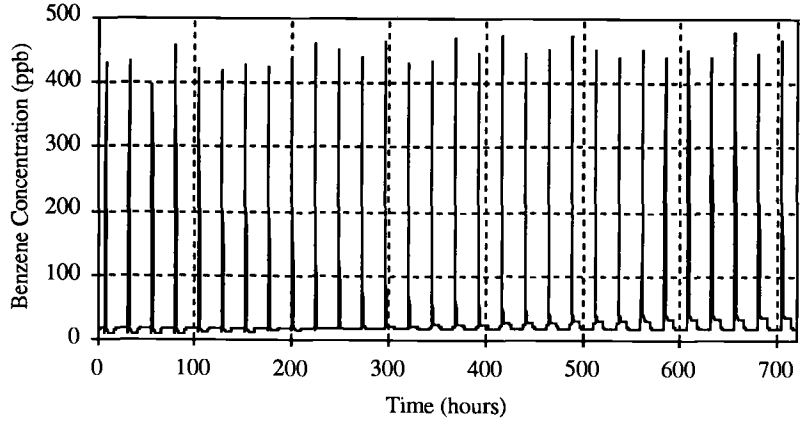

FIG. 16—*Simulation results for the first 30 days' response for a daily 0.2 cm³ C_6H_6 spill in a 108 m³ lab with a filtration systems containing 500 g of GAC.*

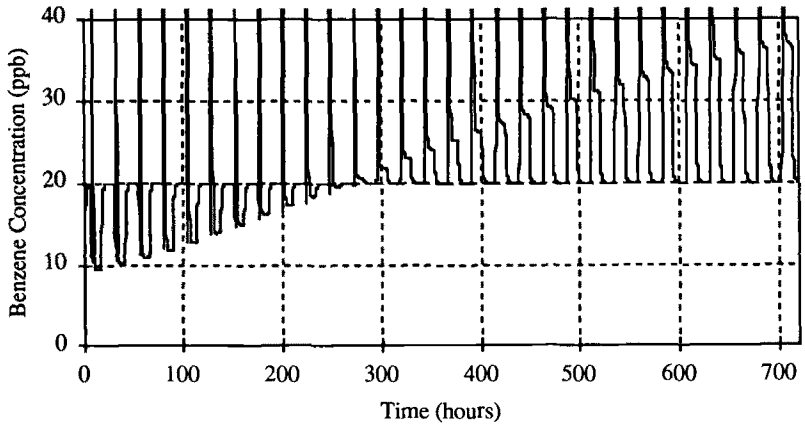

FIG. 17—*Detail of simulation results for the first 30 days' response for a daily 0.2 cm^3 C_6H_6 spill in a 108 m^3 lab with a filtration systems containing 500 g of GAC. The vertical scale has been clipped to reveal the gradual buildup of C_6H_6 levels from 10 to 40 ppb during operating hours.*

impact of the daily benzene spill. However, a close examination reveals that the filtration system loses the capacity to maintain indoor C_6H_6 levels below outdoor levels after eleven days of operation, and thereafter indoor levels increase daily as C_6H_6 is desorbed from the activated carbon during filtration system operation. This secondary problem could be mitigated by purging the filtration system with outdoor air after-hours—an operational scheme that may be readily investigated using the sorption models presented here—but this example has served its purpose and we will not continue.

Conclusion

Three families of adsorption dynamics models, based upon fundamental principles of adsorption science, have been presented and their use for sorption filtration analysis has been outlined. These models account for: (a) the equilibrium limits of reversible sorption processes, (b) boundary layer diffusion transport at the adsorbent surface, or (c) diffusion transport within the adsorbent proper, or a combination thereof. Individual members of the model families are distinguished by the sorption equilibrium model used in the model formulation. Importantly, the parameters of these models (the equilibrium adsorption characteristics of the adsorbate-adsorbent system being considered, the mass transfer coefficient associated with boundary layer transport, and the effective diffusivity of the adsorbate within the adsorbent) may be measured directly using standard test procedures or may be estimated using available theory; that is to say, the models presented are fundamentally based and not empirically determined.

Criteria are presented, analogous to the Biot criteria used in heat transfer, that provide a basis for model selection. First comparisons with experimental results have been promising, showing that accurate predictions of response may be realized if the appropriate model is employed as indicated by the criteria. In the cases studied, it was apparent that dynamic predictions were sensitive to: (a) the value of the boundary layer mass transfer coefficient for boundary layer limited diffusion and (b) the mesh refinement for porous diffusion limited dynamics. This sensitivity reflects the physical sensitivity of the systems and is not a numerical artifact.

The models presented apply to adsorption processes that are *local* to a zone; therefore, it is argued, these models may be directly integrated with existing multi-zone contaminant dispersal analysis methods to model local sorption dynamics. Element equations to do this are presented.

The use of special assemblages of these elements, tanks-in-series assemblages, to model sorption filtration devices is discussed and related to a finite element formulation of the one-dimensional convection-diffusion-adsorption equation. Results obtained from the application of these sorption filtration models appear to be reasonable and promising but cannot presently be validated for want of measured data.

Consideration has been limited to isothermal, reversible sorption of single components. However, the element assembly approach taken is compatible with the element assembly formulation of building thermal models developed earlier [*44*], thus it is expected that the generalization to non-isothermal conditions will be straightforward. Modeling sorption of complex mixtures represents the significant challenge for the future as single component conditions simply do not exist in buildings. There is an indication, however, that this problem may find a relatively simple resolution for sorption transport under the trace concentration levels present in buildings [*45,46*].

Acknowledgment

The first phase of the research reported here was supported by the Indoor Air Quality and Ventilation Group of the U.S. National Institute of Standards and Technology through funding provided by the U.S. Department of Energy.

References

[*1*] Dunn, J. E. and Tichenor, B. A., "Compensating for Wall Effects in IAQ Chamber Tests by Mathematical Modeling," *Proceedings*, 80th Annual Meeting of Air Pollution Control Association, New York, 1987.

[*2*] Dunn, J. E., "Models and Statistical Methods for Gaseous Emission Testing of Finite Sources in Well-Mixed Chambers," *Atmospheric Environment*, Vol. 21, No. 2, 1987, pp. 425–430.

[*3*] Seifert, B. and Schmahl, H. J., "Quantification of Sorption Effects for Selected Organic Substances Present in Indoor Air," *Indoor Air '87*, Institute for Water, Soil, and Air Hygiene, Berlin, 1987.

[*4*] Silberstein, S., "A Gypsum Wallboard Formaldehyde Sorption Model," National Institute of Standards and Technology, Gaithersburg, MD, 1989.

[*5*] Matthews, T. G., Hawthorne, A. R., and Thompson, C. V., "Formaldehyde Sorption and Desorption Characteristics of Gypsum Wallboard," *Environmental Science and Technology*, Vol. 21, No. 7, 1987, pp. 629–634.

[*6*] Borrazzo, J. E. and Davidson, C. I., "The Influence of Sorption to Fibrous Surfaces on Indoor Concentrations of Organic Vapors," *Proceedings*, Eighty-Third Annual Meeting of the Air and Waste Management Association, Pittsburgh, PA, 1990.

[*7*] Axley, J. W., "Adsorption Modeling for Macroscopic Contaminant Dispersal Analysis," National Institute of Standards and Technology, 1990.

[*8*] Axley, J. W., "Adsorption Modeling For Building Contaminant Dispersal Analysis. Indoor Air," *International Journal of Indoor Air Quality and Climate*, Vol. 1, No. 2, 1991, pp. 147–171.

[*9*] Axley, J. W., "Reversible Sorption Modeling for Multi-Zone Contaminant Dispersal Analysis," *Building Simulation '91*, 20–22 Aug. 1991, Nice-Sophia Antipolis, France, International Building Performance Simulation Association.

[*10*] Cleary, P. and Sherman, M., "Seasonal Storage of Moisture in Roof Sheathing," Lawrence Berkeley Laboratory, Applied Science Division, 1984.

[*11*] Cunningham, M. J., "Modeling of Moisture Transfer in Structures—I. A Description of a Finite-Difference Nodal Model," *Building and Environment*, Vol. 25, No. 1, 1990, pp. 55–61.

[*12*] Keresteciogiu, A., "Combined Heat and Moisture Transfer in Building Systems and Their Effect on Contaminant Distribution," *Building Systems: Room Air and Air Contaminant Distribution*, Allerton House, University of Illinois, Urbana-Champaign, American Society of Heating, Refrigeration, and Air-Conditioning Engineers, Atlanta, 1988.

[*13*] Shukuya, M. and Saito, M., "Simulation of Indoor Air Humidity Using Control Volume Heat and Moisture Balance Method," *Energy and Buildings*, Vol. 14, 1990, pp. 373–384.

[*14*] Thomas, W. C. and Burch, D. M., "Experimental Validation of a Mathematical Model for Predicting Water Vapor Sorption at Interior Building Surfaces," *ASHRAE Transactions*, Vol. 96, Part 1, 1990.

[15] Pedersen, C. R., "A Transient Model for Analyzing the Hygrothermal Behavior of Building Constructions. in Building Simulation '91," Sophia-Antipolis, Nice, France, International Building Performance Simulation Association, 1991.

[16] Delsante, A. E., "A Response-Factor Method for Calculating Coupled Heat and Moisture Transfer in Buildings," in *Building Simulation '91*, Sophia-Antipolis, Nice, France, International Building Performance Simulation Association, 1991.

[17] Ramanathan, K., Owen, M. K., Debler, V. L., Kosusko, M. A., and Sparks, L. E., "Air Cleaners for Volatile Organic Compounds in Indoor Air," *Proceedings*, ASHRAE/SOEH Conference: The Human Equation: Health and Comfort: IAQ '89, San Diego, CA, American Society of Heating, Refrigeration, and Air-Conditioning Engineers, Atlanta, 1989.

[18] Viner, A. S., Ramanathan, K., Hanley, J. T., Smith, D. D., Ensor, D. S., and Sparks, L. E., "Air Cleaners for Indoor Air Pollution Control," in *Indoor Air Pollution*, J. G. Kay, G. E. Keller, and J. F. Miller, Eds., Lewis Publishers, Chelsea, MI, 1991, pp. 115–131.

[19] Porco, R. D., "Chemical Gaseous Filtration," *ASHRAE Transactions*, Vol. 95, Part 2, 1989.

[20] Mahajan, B. M., "A Method for Measuring Effectiveness of Gaseous Contaminant Removal Filters," National Institute of Standards and Technology, 1989.

[21] Yang, R. T., *Gas Separation by Adsorption Processes*, Butterworth's Series in Chemical Engineering, H. Brenner, Ed. Butterworths, Boston, 1987.

[22] Andelman, J. B., Giardino, N. J., Marshal, J., Esmen, N. A., Borrozzo, J. E., Davidson, C. I., Small, M., and Wilkes, C., "Exposure to Volatile Chemicals from Indoor Uses of Water," *Symposium: Total Exposure Methodology: A New Horizon*, Las Vegas, Air & Waste Management Association, 1989.

[23] Ruthven, D. M., *Principles of Adsorption and Adsorption Processes*, John Wiley & Sons, New York, 1984.

[24] *Adsorption Technology: A Step-by-Step Approach to Process Evaluation and Application*, F. L. Slejko, Ed., Marcel Dekker, Inc., New York, 1985.

[25] White, F. M., *Heat and Mass Transfer*, Addison-Wesley Publishing Co., New York, 1988.

[26] Khalifa, A. J. N. and Marshall, R. H., "Validation of Heat Transfer Coefficients on Interior Building Surfaces Using a Real-Sized Indoor Test Cell," *International Journal of Heat Mass Transfer*, Vol. 33, No. 10, 1990, pp. 2219–2236.

[27] Spitler, J. D., Pedersen, C. O., and Fisher, D. E., "Interior Convective Heat Transfer in Buildings With Large Ventilative Flow Rates," *ASHRAE Transactions*, Vol. 97, Part 1, 1991.

[28] Glicksman, L. R. and Joose, F. M., "Heat and Mass Transfer in Fixed Beds at Low Reynolds Numbers," *Proceedings*, ASME/AIChE 18th National Heat Transfer Conference, San Diego, CA, American Society of Mechanical Engineers, New York, 1979.

[29] Kirwan, D. J., "Mass Transfer Principles," *Handbook of Separation Process Technology*, R. W. Rousseau, Ed., John Wiley, New York, 1984, pp. 60–128.

[30] Nazaroff, W. M. and Cass, G. R., "Mass Transfer Aspects of Pollutant Removal at Indoor Surfaces," *Indoor Air '87*, Institute for Water, Soil, and Air Hygiene, Berlin, 1987.

[31] Nazaroff, W. M. and Cass, G. R., "Mathematical Modeling of Indoor Aerosol Dynamics," *Environmental Science Technology*, Vol. 23, No. 2, 1989, pp. 157–166.

[32] Satterfield, C. N., *Heterogeneous Catalysis in Practice*, McGraw-Hill, New York, 1980.

[33] Suzuki, M., *Adsorption Engineering*. Kodansha–Elsevier, Tokyo–Amsterdam, 1990.

[34] Greenkorn, R. A., *Flow Phenomena in Porous Media. Energy, Power, and Environment*, P. N. Powers and W. Meier, Eds., Marcel Dekker, Inc., New York, 1983.

[35] Axley, J. W., "Multi-Zone Dispersal Analysis by Element Assembly," *Building and Environmment*, Vol. 24, No. 2, 1989, pp. 113–130.

[36] Huebner, K. H. and Thornton, E. A., *The Finite Element Method for Engineers, Second Edition*, John Wiley & Sons, New York, 1982.

[37] Axley, J. W., "Progress Toward a General Analytical Method for Predicting Indoor Air Pollution in Buildings: Indoor Air Quality Modeling Phase III Report," U.S. DOC, National Institute of Standards Technology, Gaithersburg, MD, 1988.

[38] Ramanathan, K., Debler, V. L., Kosusko, M., and Sparks, L. E., "Evaluation of Control Strategies for Volatile Organic Compounds in Indoor Air," *Environmental Progress*, Vol. 7, No. 4, 1988, pp. 230–235.

[39] Liu, R.-T., "Removal of Volatile Organic Compounds in IAW Concentrations with Short Bed Lengths," *Proceedings*, Indoor Air '90: The 5th International Conference on Indoor Air Quality and Climate, Toronto, Canada, Canada Mortgage and Housing Corporation, 1990.

[40] Graham, J. R. and Bayati, M. A., "The Use of Activated Carbon for the Removal of Trace Organics in the Control of Indoor Air Quality," in Indoor Air '90: The 5th International Conference on Indoor Air Quality and Climate, Toronto, Canada, Canada Mortgage and Housing Corporation, 1990.

[41] *Handbook of Chemistry and Physics*, The Chemical Rubber Co., Cleveland, OH, 1969.

[42] Nauman, E. B. and Buffham, B. A., *Mixing in Continuous Flow Systems*, John Wiley & Sons, New York, 1983.

[43] "Indoor Air Quality: Organic Pollutants," World Health Organization, Berlin, 1989.

[44] Axley, J. W., "DTAM1: A Discrete Thermal Analysis Method for Building Energy Simulation: Part I Linear Thermal Systems with DTAM1 Users Manual," U.S. DOC, National Institute of Standards Technology, Gaithersburg, MD, 1988.

[45] Jonas, L. A., Sansone, E. B., and Farris, T. A., "Prediction of Activated Carbon Performance for Binary Vapor Mixtures," *American Industrial Hygiene Association Journal*, Vol. 44, No. 10, 1983, pp. 76–719.

[46] Liu, R.-T., "Modeling Activated Carbon Adsorbers for the Control of Volatile Organic Compounds in Indoor Air," *Proceedings*, Far East Conference on Environmental Quality, November 1991, Hong Kong, American Society of Heating, Refrigeration, and Air-Conditioning Engineers, Atlanta, 1991.

Model Validation and Application

Zhishi Guo[1]

On Validation of Source and Sink Models: Problems and Possible Solutions

REFERENCE: Guo, Z., **"On Validation of Source and Sink Models: Problems and Possible Solutions,"** *Modeling of Indoor Air Quality and Exposure, ASTM STP 1205*, Niren L. Nagda, Ed., American Society for Testing and Materials, Philadelphia, 1993, pp. 131–144.

ABSTRACT: While model validation remains the weakest part of the entire process of indoor air quality (IAQ) model development, special problems have made the validation of indoor source and sink models even more difficult. Many source and sink models have been developed, but few have been properly validated. Major problems with current procedures include: elusive model parameters, confusion in parameter estimation methods, uncertainty in scale-up and misleading scaling factors, unspecified validity ranges, and weakness in quantitative comparisons between models and experimental observation.

To improve validation procedures, we have identified a number of potential areas including: proper definition of validation scope, proper use of statistical comparison methods, development of mass transfer indices to bridge the gap between test chambers and real buildings, and development of a cooperative effort to build a source and sink database to facilitate validation.

KEY WORDS: model validation, source, sink, indoor air quality

Model validation is the process of evaluating the usefulness, accuracy, and limitation of a model under various application conditions. While validation remains the weakest part in the entire process of indoor air quality (IAQ) model development, validating of source and sink models has its own special difficulties. In fact, although many source and sink models have been developed, few have been properly validated.

General discussions on model validation can be found in the literature [*1–4*], but the special problems associated with source and sink models remain untouched. This paper identifies the major problems with current practice in validating source and sink models and discusses some possible solutions. Most of the problems raised came from examining the author's own practice in model validation, and some came from reviewing other researchers' work. Although this paper is focused on validation, the author has found it difficult to completely separate model validation from model building. Some discussions here may be applicable to both steps.

Purposes of Validating Source and Sink Models

Why must we validate source and sink models? Before answering this question, we need to briefly discuss how they are developed and how they are used. It is generally agreed that, before any satisfactory verification scheme is adopted, it is necessary to determine the primary purpose or purposes to be served by the verification [*4*].

The development of source and sink models relies heavily on experimental observations and understanding of the mechanisms. From chamber data, one can often calculate the emission rate based on mass balance equations. For example, if we assume that the adsorption of pollutants on

[1]Staff scientist, Acurex Environmental Corporation, PO Box 13109, Research Triangle Park, NC 27709.

chamber walls is negligible, the mass balance for an area source in a chamber in an infinitesimal time period dt is

Mass increased in chamber = Mass emitted − Mass exfiltrated

or

$$V\frac{dC}{dt} = S\,R(t) - Q\,C \tag{1}$$

where

V = chamber volume,
C = chamber concentration,
S = area of the source,
$R(t)$ = emission rate at time t, and
Q = inlet/outlet air flow rate.

Let $L = S/V$ be the loading factor and $N = Q/V$ be the air exchange rate, we then have

$$R(t) = \frac{dC/dt + N\,C}{L} \tag{2}$$

When the concentration data have reasonable time resolution, the term dC/dt can be well represented by $\Delta C/\Delta t$. The data represented by empty squares in Fig. 1 is an example of using Eq 2 to calculate the emission rates from the chamber concentration data. The source tested was an indoor coating product. A total of 1.82 g of the product was applied to a 0.021 m^2 oak board, and tested for total organic emissions in a 53-L stainless steel chamber. The chamber was kept at 23°C and 45% relative humidity and the air exchange rate was 0.514 h^{-1}.

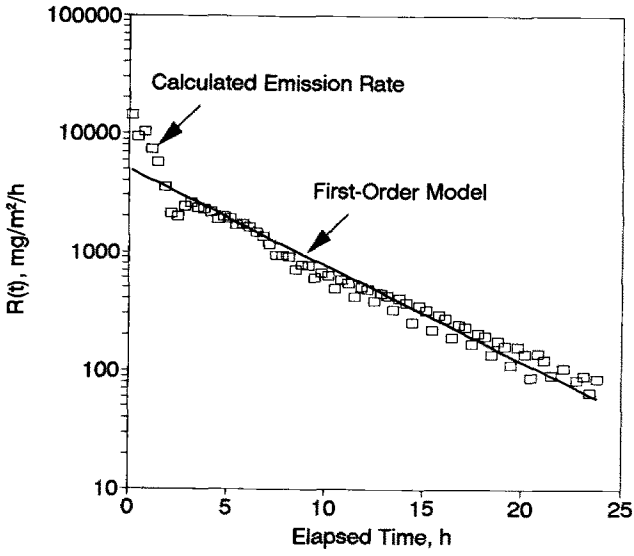

FIG. 1—*Calculated VOC emission rate for an indoor coating product based on chamber concentrations and first-order model prediction.*

Direct calculation of the adsorption and desorption rate is impossible because the two processes occur simultaneously, but it is possible to calculate the net mass transfer rate for the pollutant to or from the sink surface.

Base on experimental observations, a model can be developed in different ways. For the convenience of discussion, we can roughly divide all source and sink models into two categories, statistical models and fundamentally based models.

To find a statistical model suitable to the data in Fig. 1, basic knowledge of analytic geometry will convince us that the emission pattern in Fig. 1 can be approximated by a first order decay model [5]

$$R(t) = R_0 \, e^{-kt} \tag{3}$$

where

R_0 = initial emission rate and
k = first order decay constant.

The next step is to estimate the model parameters, the constants (or coefficients) in a model's expression. In this case, we need to determine the values for R_0 and k that could give the best agreement between the model prediction and observation. The solid line in Fig. 1 was obtained by log-linear regression imposed on the emission rate data.

In most cases, however, model parameters are estimated by fitting the model to concentration data. This is especially true for sink models. No matter what data are used, such model development depends heavily on statistical estimations.

To develop fundamentally based models, or mass transfer models, one needs to understand the physical-chemical phenomena involved, such as evaporation, adsorption, molecular diffusion in the air-surface interface, and molecular diffusion within the source. The parameters of a mass transfer model often have well-defined physical meanings such as vapor pressure, molecular weight, mole fraction, adsorption energy, diffusivity, and boundary layer thickness. Most parameters are obtained either directly from the literature or from well-established models. Therefore, parameter estimation for mass transfer models does not rely heavily on curve-fitting. In some cases, however, one or two of the parameters may have to be estimated empirically. It should be pointed out that, among existing source and sink models, many are neither pure statistical models nor pure mass transfer models.

Like any other model, a source or sink model is at best a simplification and approximation of a real source or sink. Therefore, no one should expect the model to represent reality perfectly. There is a definite need, however, to know how good the agreement would be under certain conditions between the model and reality. In other words, we need some estimation of the model's predictive error.

A model may give satisfactory prediction in one case but fail in another. Then we must know the conditions under which the model gives acceptable prediction, and those under which the model fails. We also need to know the sensitivity of the model to its parameters.

Source and sink models are seldom used alone. In most cases, they are part of an IAQ model. Since both source and sink models serve the IAQ model, any predictive errors they generate can be propagated during an IAQ simulation. We need to know how the inaccuracy of a source or sink model could affect the IAQ simulation output.

In summary, the purposes of validating source and sink models may include the following:

- estimating the model's predictive error by comparing the predicted values to observed ones;
- defining validity range and validity conditions,
- defining conditions of failure;

- defining the applicability of the model (good for a single product, type of product, or several types of products);
- estimating the model's sensitivity to its parameters, and, if possible;
- estimating the model's propagated error in IAQ simulation.

For those who want to use source and sink models, proper validation will provide them with a clear view of the conditions for reliable model application and the uncertainty they may expect under certain conditions. Such information may prevent the user from misusing the models. For those who develop source and sink models, proper validation may enable them to learn how to improve their models and how to develop more advanced models.

Major Problems with Current Validation Procedures

Variable Model Parameters

Most statistical models have at least one variable parameter, the parameter that is determined through statistical estimation and whose value changes as the environmental conditions change. Parameters R_0 and k in Eq 3 are such variable parameters. Unlike physical parameters (such as boiling point, vapor pressure, diffusivity, and air velocity), these parameters are sensitive to any change of the environment. The modelers often find it difficult to choose proper values under certain given conditions. The following example illustrates how those parameters may vary with test conditions.

A wood stain product was tested for its organic emissions in small environmental chambers [*5*]. The concentration data were fit by the first-order source model. Test conditions and estimated emission factors are summarized in Table 1. As one can see, both R_0 and k vary over a wide range. Unless correlations are found between these parameters and the environmental conditions (such as air exchange rate, loading factor, application rate, and degree of air turbulence), there is no way to tell what values to choose for R_0 and k under certain given conditions.

TABLE 1—*Total organic emissions from wood stain.*

Chamber type	166 L with a slow stirrer
Air exchange rate range	0.35 to 4.6, h^{-1}
Application rate range	23 to 26, g m^{-2}
Chamber loading range	0.1 to 1.3, m^{-1}
Range of estimated R_0	2.2 to 27, g m^{-2} h^{-1}
RSD (mean)	7%
RSD (range)	3 to 12%
Range of Estimated k	0.24 to 2.41, h^{-1}
RSD (mean)	11%
RSD (range)	4 to 16%

(N/L)—A Misleading Scaling Factor

The ratio of air exchange rate (N) over chamber loading factor (L) has been one of the most commonly used scaling factors in chamber experimental design and model validation. The concept behind this factor is that, if we double the chamber loading and the air exchange rate simultaneously, the two effects will be canceled out, and the resulting chamber concentration should be the same [*6*]. This assumption is correct if, and only if, we are dealing with a constant source at steady

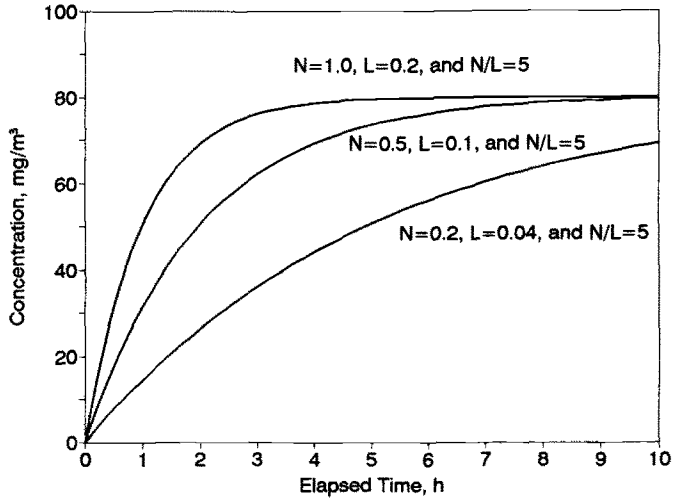

FIG. 2—*Improper use of (N/L)-constant source at nonsteady state.*

state. The problem is that it has been used far beyond the above limitations. It is theoretically incorrect to apply such a scaling factor to either nonsteady state situations or nonconstant sources, or both. To illustrate this problem, let us look at two theoretical concentration models. Equation 4 is the expression for a constant source and Eq 5 for the first order decay source [5]

$$C(t) = \frac{L\,R}{N}(1 - e^{-Nt}) \tag{4}$$

$$C(t) = \frac{L\,R_0}{N - k}(e^{-kt} - e^{-Nt}) \tag{5}$$

where

$C(t)$ = the chamber concentration,
R = emission rate for constant source,
L = chamber loading,
N = air exchange rate, and
t = time.

Figures 2 and 3 were plotted based on Eqs 4 and 5, respectively, assuming that chamber volume = 1 m^3 and $R = R_0 = 400$ $mg/m^2/h$. Figure 2 shows that, for the same constant source, the same *N/L* may not yield the same concentration curve if steady state is not approached, and Fig. 4 shows that, for a given finite source, very different concentration curves are obtained with the same *N/L*.

Confusion in Parameter Estimation

Estimating the parameters for a given model from a given set of data can also be confusing because there are many ways to fit a model to data. For example, to fit the first order model to the indoor coating data described above, we have many ways of estimating R_0 and k. For illustration purposes, four different regression methods are discussed here: (1) using nonlinear regression to

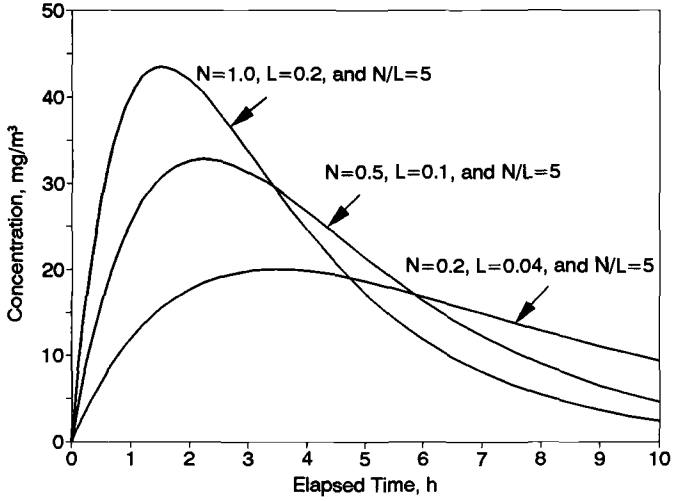

FIG. 3—*Improper use of (N/L)-finite source.*

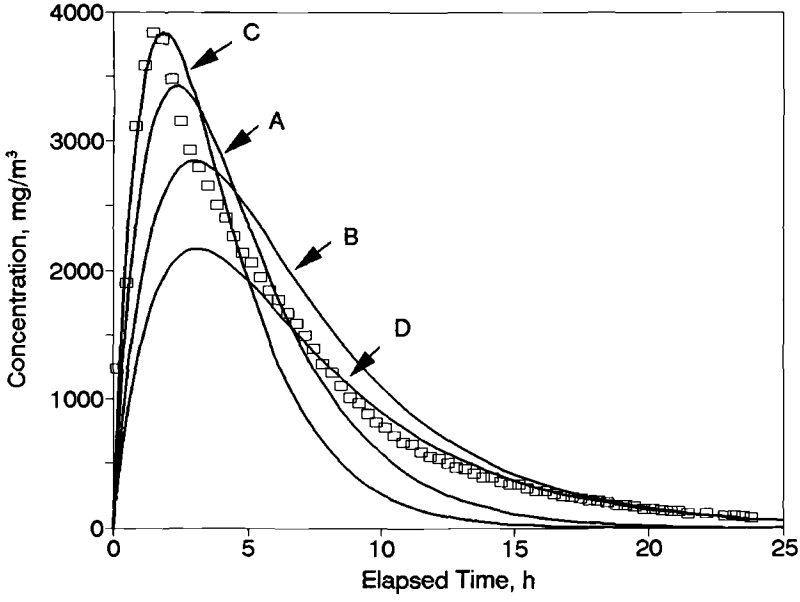

FIG. 4—*The effects of parameter estimation methods on model performance-normal scale.*

TABLE 2—*Estimated emission factors with four regression methods.*

	Method 1	Method 2	Method 3	Method 4
Model	Eq 5	Eq 5	Eq 3	Eq 3
Data type	concentration data	concentration data	rate[a]	rate[a]
Data scale	normal	log	normal	log
Regression	nonlinear	nonlinear	nonlinear	linear
R_0, g m^{-2} h^{-1}	10.1	6.68	14.0	4.96
Relative Standard Deviation (RSD)	4.2%	5.8%	4.3%	2.3%
k, h^{-1}	0.356	0.208	0.599	0.186
RSD	5.1%	2.5%	6.1%	2.0%

[a]Rate = emission rate data.

fit Eq 5 to the concentration data without any data transformation, (2) using nonlinear regression to fit Eq 5 to the concentration data with logarithmic transformation, (3) using nonlinear regression to fit Eq 3 to directly calculated emission rate data (as shown in Fig. 1), and (4) using linear regression to fit Eq 3 to directly calculated emission rate with logarithmic transformation. The different results are given in Table 2. Parameters obtained from Method 3 appeared to be the best in catching the peak (Fig. 4) and also the worst in tracing the tail as illustrated in the semi-log plot (Fig. 5). Just the opposite, Curve D looked the worst in the high concentration region but gave the best prediction in the tail. The other two curves fell between the two extremes. The questions then become which estimation method should we choose, and which set of parameters should we report?

The Effect of Data Range

Many indoor sources last for a long period of time, and the effect of indoor sinks lasts even longer. Tracking such long term effects can be very costly and time-consuming. People usually have to develop and validate their models by using chamber data within a limited time period. It is clear that, unless the validity range is defined, the statement of "validated" can be very confusing.

The following is an example of this problem. We tested the emission of ethylbenzene from a piece of 0.113 m^2 duct liner in a 53-L chamber (0.54 air change per hour, 23°C, and 45% relative humidity). The sample was taken from the air handling system in a test house and was previously exposed to ethylbenzene polluted indoor air. Using the first 10 h of chamber data, we found that the simple first-order model (Eq 3) fit the data adequately (Fig. 6). The model prediction failed after 10 h and the double exponential model $R(t) = R_1 \exp(-k_1 t) + R_2 \exp(-k_2 t)$ seemed more suitable to the wider data range (Fig. 7). After 120 h, however, it failed too. A second-order model, $R(t) = R_0/(1 + ktR_0)$, fit the data almost perfectly within 400 h (Fig. 8). It is difficult to tell if or when the second order model fails beyond 400 h.

Obviously, selection of data range plays an important role in both model building and validation. Without specifying the validity range of a model, the whole validation becomes meaningless. Information on conditions of model failure is especially important to IAQ modelers, for IAQ simulation programs do not turn off a source or a sink automatically.

The Effect of Air Velocity and Turbulence

The degree of air turbulence above the source or sink surface can alter the rate of mass transfer in both directions. This means that a model validated in one chamber may not work at all in another if the air turbulence conditions are significantly different.

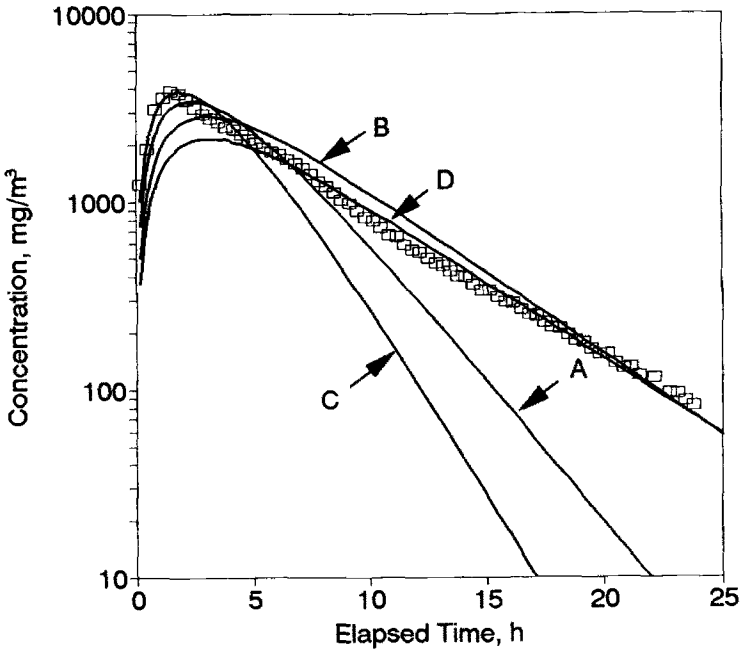

FIG. 5—*The effects of parameter estimation methods on model performance-log scale.*

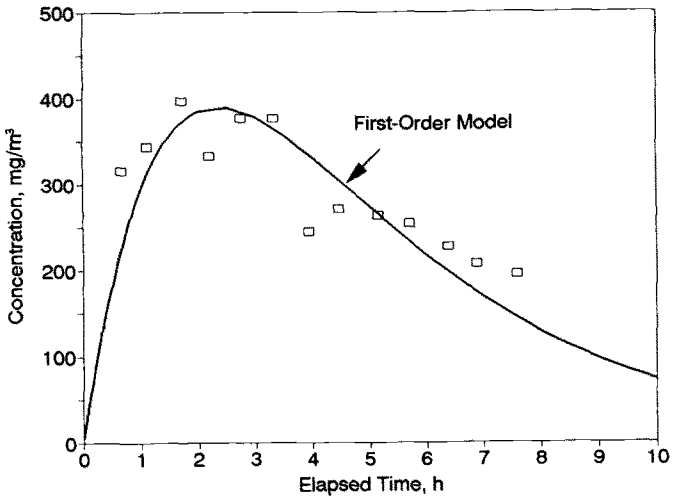

FIG. 6—*Modeling the reemission of ethylbenzene from polluted duct liner—10 h data.*

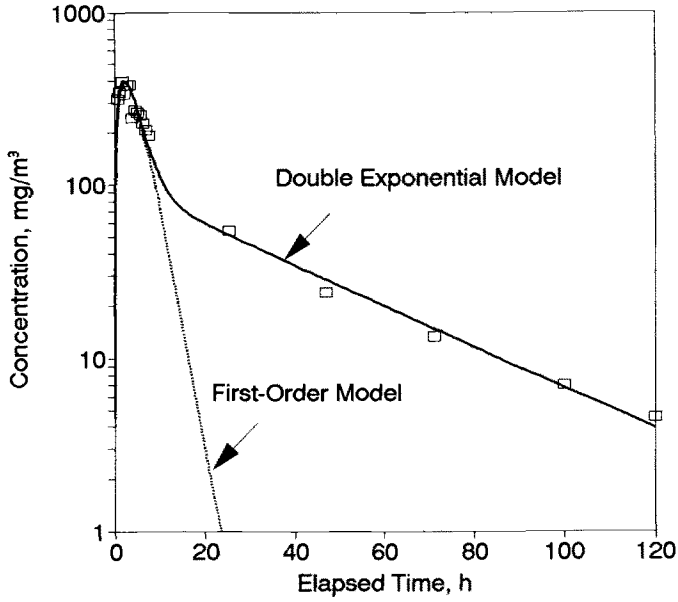

FIG. 7—*Modeling the reemission of ethylbenzene from polluted duct liner—120 h data.*

To show how the degree of air turbulence affects the model parameters, we did a set of preliminary sink tests in a two-chamber experimental system [*7*]. A piece of wallboard was placed in the test chamber and insulted by a first-order decay ethylbenzene source. To alter the air circulation conditions, a small biscuit fan was placed inside the test chamber (fan speed could be adjusted by varying the voltage). Tests were conducted with the fan at 50, 70, and 110 V, respectively, and all other conditions were kept the same. Figure 9 shows one of the test results and the fitting of the dynamic Langmuir sink model [*7,8*] to the data. The estimated model parameters, adsorption rate constant k_a and desorption rate constant k_d, are given in Table 3. It seems that both adsorption and desorption were accelerated by the increased air circulation. During these tests, we did not

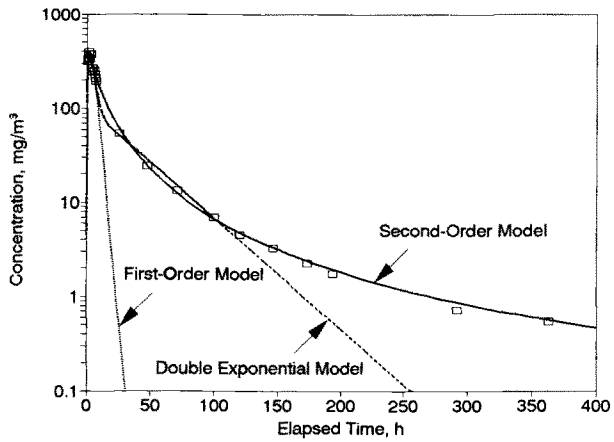

FIG. 8—*Modeling the reemission of ethylbenzene from polluted duct liner—400 h data.*

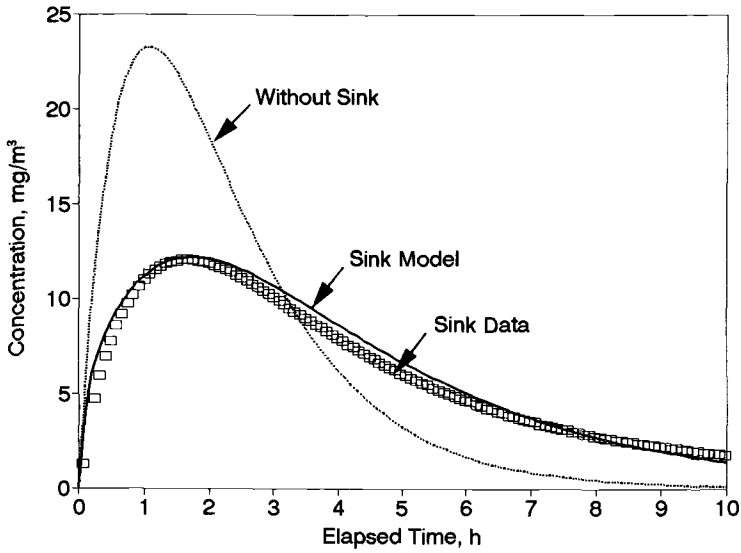

FIG. 9—*Dynamic sink test and model prediction.*

measure the fan speed and air velocity in the chamber; therefore, the results presented below should be considered as a qualitative illustration. Since air movement and turbulence conditions in a building can be significantly different from that in a chamber, the applicability of chamber results to real buildings has been challenged. This so-called "scale-up" problem has been the most troublesome in validating source and sink models.

TABLE 3—*The estimated adsorption rate constant* (k_a) *and desorption rate constant* (k_d) *at three fan speeds.*[a]

Fan Voltage (*V*)	50	70	110
$k_a \pm RSD$, m h^{-1}	0.64 ± 5.9%	0.91 ± 6.0%	1.23 ± 12%
$k_d \pm RSD$, h^{-1}	1.48 ± 6.4%	1.44 ± 7.0%	2.54 ± 6.7%

[a]Sink material, 0.14 m^2 wallboard; pollutant, ethylbenzene; air exchange rate = 1.2 h^{-1}; temperature = 23°C; and relative humidity = 45%.

Oversimplified Illustration of the Goodness of Fit

Checking the agreement between model prediction and observation can also be misleading. So far, most modelers, including the author [*9*], have tried to show the validity of their models by presenting the model prediction and observation together in a diagram. The authors would then claim that the presented model had been "validated" (or sometimes more cautiously, "preliminarily validated"). While there is nothing wrong with graphical comparison, something is missing here. What does "validated" or "preliminarily validated" mean? There have to be some criteria so that the model developer and, more importantly, the user can make an objective and quantitative judgment. Statistical methods for verification comparisons are available; unfortunately, many of us often neglect those useful tools.

Special Problems with Fundamentally-Based Models

Mass transfer models are preferred to statistical models because the former emphasize the physical understanding of the real mechanisms and because their parameters are usually well defined. But these types of models have their own problems.

To model very complex reality with relatively simple models, the modelers have to exclude whatever they consider "unnecessary" details and focus on one or two mechanisms. Due to the omission of the remaining mechanisms, the resulting models are often unusable unless some fuzzing factors are introduced. These variables often make the mass transfer models less attractive because they have made the mass transfer models undistinguishable from empirical models.

Mass transfer models are often much more complicated than their corresponding statistical models. It is commonly true that a mass transfer model has better "validity" than a statistical model, but is more difficult to use than the latter due to its complexity.

Recommendations

Three Levels of Validation

As just discussed, the primary purpose of validating source or sink models is to make sure they represent reality close enough under certain conditions so that they can be used in IAQ simulation without bringing in excessive propagation errors. Keeping this in mind, we can divide the validation process into three steps: (1) checking the agreement between the model and a single set of observations, (2) checking the agreement between the model and multiple sets of observations, and (3) verification of scale-up.

After a model is formulated, it is usually compared to a single set of observations to determine if the model represents the real pattern in that particular case reasonably well. If there are variable parameters in the model, they can be estimated by this step. If the model concept is poor, the model may not "survive" this step at all.

Since many, if not all, source and sink models contain variable parameters, one set of parameters that give satisfactory prediction in one event may not work in others. By comparing the model with a few sets of data, one can either fine-tune the parameters or find correlations between the values of parameters and test conditions. The author believes that not all existing source and sink models can survive this validation step.

The last step, scale-up verification, requires data from either real buildings or large test chambers. Without this step, the usefulness of a model cannot be justified.

Some Aspects in Validation Procedures

When comparing a model with observation, the modeler should clearly specify the conditions under which the observation was obtained. This will allow the modeler and the potential users to distinguish the conceptual errors of the model from those of the data. The list of conditions should include, but not be limited to, the following information:

- chamber specification (type, material, volume, shape, temperature, humidity, pressure, and so fourth);
- sample specification (material, size, sample preparation, and position in the chamber);
- air exchange rate;
- description of air movement in the chamber (qualitative description such as inlet/outlet pipeline design, with or without forced mixing and quantitative description such as surface velocity, Reynold's number, or other fluid dynamic parameters);
- sampling and analytical methods;

- data quality, and
- data range.

If some or all the model parameters are estimated using statistical means, a detailed description of the approach used should be given as follows:

- the equation used in the regression (it may or may not be the source or sink model itself);
- independent and dependent variables;
- statistical method (linear regression, nonlinear regression, or other methods); and
- data transformation (no transformation, logarithmic transformation or, in more general terms, Box-Cox power transformation).

When comparing a model to multiple sets of observations, the chamber data should include:

- observations under at least two air exchange rates and
- observations under at least two loading factors.

If a model is statistically based, the sensitivity of a model to its parameters, and the dependence of model parameters on environmental conditions (such as air exchange rate, loading factor, and degree of air turbulence) should be described.

When performing scale-up verification, data from large test chambers are preferred to those from buildings because the conditions in a building are difficult to control. The most important uncontrolled factors include varying air exchange rate, multiple air zones, and strong adsorption on many different surface materials. If the model parameters established from previous validation steps need further adjustment in scale-up, such adjustment should be justified.

Finally, validity range and validity conditions should be specified.

Making Comparisons More Objectively

Graphic comparison of model performance is absolutely necessary, but using it alone is not enough. Statistical tools should be used to complement graphical comparison.

Quite a few statistical methods are available in making comparisons [*10,11*]. At least one statistical verification method should be used along with graphical comparisons. The modeler should make careful selection among those methods because different validation purposes require different statistical techniques. The danger of using any goodness-of-fit index in model verification is illustrated by Benarie [*4*]. Besides, some methods may not be suitable to our particular situation. We should emphasize the importance of physically understanding the model during validation. Some statistical comparison techniques do not help very much in this aspect.

Dealing with Scale-Up Problems

Source and sink models based on basic mass transfer theories have received ever-increasing attention by the indoor air community in recent years [*12–14*]. Many of us, who have been frustrated by elusive statistical models, believe that fundamentally based models are the final solution to our problems, especially to the scale-up problem. Mass transfer models for emission and adsorption are not new, they can be found in many mass transfer monographs. The problem is that people can rarely find a proper model from the existing engineering literature that can be used by IAQ modelers on an "as is" basis because the processes being modeled are too complicated for those models.

To develop relatively simple mass transfer models, we need to select proper expressions for mass transfer coefficients (or mass transfer resistance). Criteria for selecting good expressions may include:

- they should separate the properties of the environment from those of the source or sink,
- they should be simple enough to be used in source or sink models,
- they can be measured independent of source and sink models, and
- they can be correlated to more complicated boundary layer models.

Making a Cooperative Effort by Building a Source and Sink Database

Generating quality data to validate a model can be very costly and time-consuming. A modeler may have the talent to develop scientifically sound models but may not have the ability or resources to generate good quality data. This has left little choice to the modelers: they often have to accept whatever data they can get, regardless of the suitability of the data to serve their validation purposes.

All modelers would benefit if some organization (a professional society or university, for example) would assume the responsibility for collecting source and sink data from volunteer research organizations and build an indoor source and sink database. Such a cooperative effort could make a great difference in easing the shortage of quality data.

Conclusions

As stated earlier, the major purpose of this paper has been to raise issues regarding the validation of source and sink models. We have identified a number of potential problem areas in IAQ modeling. Due to the great difficulty in validating indoor source and skin models, we cannot expect all the problems to be solved overnight. Improvement can only be made gradually. Besides, as long as a new model is built on a sound scientific basis, the model can be published without complete validation. The model developer should be allowed to leave part of the validation work to other researchers. Validating a model is as important as creating one, and can be an original contribution to science.

Acknowledgment

Research was supported by the U.S. Environmental Protection Agency (EPA), Contract 68-DO-0141. This work has been subject to the Agency's peer and administrative review and has been approved for publication. However, it does not necessarily reflect the views of the Agency and no official endorsement should be inferred.

References

[1] Ingles, D. M., *What Every Engineer Should Know About, Volume 15: Computer Modeling and Simulation*, Marcel Dekker, Inc., New York, 1985.

[2] Knox, J. B., "Model Validation: Purpose and Expectations," Lawrence Livermore National Laboratory Report UCRL-91664, Oct. 1984.

[3] Morrison, F., *The Art of Modeling Dynamic Systems*, John Wiley & Sons, Inc., New York, 1991.

[4] Benarie, M. M., *Urban Air Pollution Modeling*, MIT Press, Cambridge, MA, 1990.

[5] Tichenor, B. A. and Guo, Z., "The Effect of Ventilation on Emission Rates of Wood Finishing Materials," *Environment International*, Vol. 17, 1991, pp. 317–323.

[6] Matthews, T. G., Wilson, D. L., and Thompson, A. J., "Interlaboratory Comparison of Formaldehyde Emissions from Particleboard Underlayment in Small-Scale Environmental Chambers, *Journal of the Air Pollution Control Association*, Vol. 37, 1987, pp. 1320–1326.

[7] Krebs, K. A. and Guo, Z., "A Two-Chamber Design for Testing the Sink Effect with Dynamic Concentration Profiles," *Proceedings,* 1992 U.S. EPA/AW & MA International Symposium: Measurement of Toxic and Related Air Pollutants, Air and Waste Management Association, Pittsburgh, 1992.

[8] Tichenor, B. A., Guo, Z., Dunn, J. E., Sparks, L. E., and Mason, M. A., "The Interaction of Vapour Phase Organic Compounds with Indoor Sinks," *Indoor Air*, Vol. 1, 1991, pp. 23–35.

[9] Guo, Z., Dunn, J. E., Tichenor, B. A., Mason, M. A., and Krebs, K. A., "On Representing Reversible Sinks in Indoor Air Quality Models," *Proceedings,* 5th International Conference on Indoor Air Quality and Climate, Vol. 4, 1990, pp. 177–182.

[10] Panofsky, H. A. and Brier, G. W., *Some Applications of Statistics to Meteorology*, Pennsylvania Publication, University Park, 1968.

[11] Hanna, A. R., "Air Quality Model Evaluation and Uncertainty," *Journal of Air Pollution Control Association*, Vol. 38, 1988, pp. 406–412.

[12] Nazaroff, W. W. and Cass, R. G., "Mass Transfer Aspects of Pollutant Removal at Indoor Surfaces," *Proceedings,* 4th International Conference on Indoor Air Quality and Climate, Institute for Water, Soil, and Air Hygiene, Berlin, Germany, 1987, pp. 244–248.

[13] Gunnarsen, L., "Air Velocities and Indoor Emission," presented at CIB-W77 Symposium, New Haven, 1991.

[14] Axley, J. W., "Adsorption Modeling for Building Contaminant Dispersal Analysis," *Indoor Air*, No. 2, 1991, pp. 147–171.

John R. Girman[1]

Simple Modeling to Determine Appropriate Operating Conditions for Emission Testing in Small Chambers*

REFERENCE: Girman, J. R., **"Simple Modeling to Determine Appropriate Operating Conditions for Emission Testing in Small Chambers,"** *Modeling of Indoor Air Quality and Exposure, ASTM STP 1205*, Niren L. Nagda, Ed., American Society for Testing and Materials, Philadelphia, 1993, pp. 145–148.

ABSTRACT: Much of the mass-balance modeling of concentrations produced by indoor sources has been based upon emission rates obtained from small chamber testing. The suitability of emission rates used as inputs to such models is important and can depend upon the operating conditions of small test chambers. However, these operating conditions to date have largely been established on the basis of intuitive choices, that is, what appears reasonable in simulating actual full-scale indoor environments, rather than a critical examination of factors that can affect emissions. In this paper, the consequences of these choices are examined, and this examination suggests that air in chambers, as currently operated, may be stagnant. This indicates the need to measure air velocities under current operating conditions. Suggestions for improving chamber operating conditions are presented that may produce more accurate emission rates.

KEY WORDS: model inputs, air velocity, loading factor, emission rate, small test chamber, emission testing, ventilation rate

Many activities rely upon accurate mass-balance modeling, for example, exposure assessment from particular indoor sources and product emission comparisons. Much of the mass-balance modeling of concentrations produced by indoor sources has been based upon emission rates obtained from small chamber testing. The suitability of the emission rates used as model inputs is important and can depend upon the operating conditions of the test chamber. However, operating conditions for small chamber emission testing to date have largely been established on the basis of intuitive choices, that is, what appears reasonable in simulating actual full-scale indoor environments.

To this end, it is thought that concentrations produced in the chamber by a material sample should be similar to those concentrations found in full-scale indoor environments where the material is used. This is important because of analytic considerations and because of concerns for the effect of equilibrium on emission rates. Ventilation rates employed are generally similar to those found in indoor environments, in part, because of the desire to produce appropriate concentrations and perhaps, in part, because of the notion that this will produce air velocities in the chamber similar to those found in full-scale indoor environments. If chamber concentrations and ventilation rates are to be similar to those in full-scale indoor environments, then it follows that the chamber loading factor (the amount of the sample, expressed in surface area exposed or mass of sample, or both, per unit volume of the chamber) must approximate that of full-scale indoor environments.

[1]Analysis branch chief, Indoor Air Division, U.S. Environmental Protection Agency (USEPA), Washington, DC 20460.

*This paper represents the views of the author and not necessarily the views of the U.S. Environmental Protection Agency.

However, when the volume of a space is reduced (as occurs when going from a full-sized room to a small test chamber) and the loading factor and the ventilation rate are held constant, some other parameter must change. As this paper will attempt to demonstrate, in the absence of some other means of controlling the air flow (such as using fans within the chamber), the parameter that changes from that of full-scale indoor environments is the air velocity.

Current Practice in Small Test Chamber Operation

Using emission testing for floor coverings as an example, typical operating conditions and parameters can be examined. These are as follows: chamber volume, 0.050 m^3; temperature, 23°C; relative humidity, 50%; loading factor for a floor covering, 0.41 m^2/m^3; and ventilation rate, 1 h^{-1} (one air change per h). The air velocity is unspecified.

If we assume that the chamber is a cube, each side of the chamber is 36.8 cm. If the carpet sample is square, each side of the carpet is 14.3 cm. One air change per hour in the chamber corresponds to an air flow into the chamber of 0.50 m^3/h or 13.9 cm^3/s. (the temperature and relative humidity are parameters that can be readily controlled in the test chamber over a range of conditions and do not interact with the other parameters in the manner addressed in this paper.)

The air velocity in the chamber can be estimated as follows. Assume all the air flows uniformly through a vertical plane perpendicular to the surface of the carpet, that is, maximum flow across the surface of the carpet. Then the velocity through this plane of 1354 cm^2 (36.8 × 36.8 cm) is 0.0103 cm/s (13.9 cm^3/s divided by 1354 cm^2). Of course it is improbable that the air in a chamber flows across the chamber with complete uniformity in this manner. However, it is not unlikely that its velocity in the chamber averages to about this order of magnitude, 0.01 cm/s. This is a very low velocity relative to air velocities that have been measured in indoor environments and to which materials in indoor environments are exposed.

Measured Air Velocities in Indoor Environments

Mathews et al. determined a median air velocity of 5.3 cm/s in six occupied houses [*1*]. Gammage and Hawthorne reported air drift velocities ranging from 1 to 20 cm/s inside residences [*2*]. In office settings similar velocities have been reported: 2 to 20 cm/s with an average of 10 cm/s by Lorch and Straub [*3*]; 2 to 25 cm/s with typical values between 10 to 15 cm/s by Hart and Int-Hout [*4*]; and a mean air velocity of 8 cm/s by Schiller and Arens [*5*]. Christianson et al. have recommended 10 cm/s for use as a "standard room condition" when comparing products used in residences [*6*]. The air velocities measured in indoor environments support this choice.

The example above suggests that air in small test chambers as they are currently operated is essentially stagnant and that air velocities are two or possibly even three orders of magnitude lower than they should be for realistic testing. The isothermal conditions under which chamber testing occurs serves to exacerbate stagnant conditions, since even convective flow is low. These low velocities have possible consequences for the emission rates measured in small chambers.

Emission rates for a particular chemical are affected by the concentration of that chemical in the boundary layer above the material. This is especially true for materials with high emission rates (for example, "wet" materials), that have the potential to produce concentrations in the boundary layer approaching the equilibrium concentrations for particular chemicals. Thus, concentrations in the boundary layer must also be realistic in order to measure realistic emission rates. However, the boundary layer is determined, in part, by the air velocity across the material surface and air velocities two orders of magnitude too low would be expected to produce emission rates lower than would be found in actual indoor environments.

A Possible Chamber Redesign and Its Effect

Small test chambers could be redesigned with a different shape to increase air velocities in them to 10 cm/s. While retaining a 0.050 m^3 chamber size, the chamber width could be reduced to 14.3 cm, consistent with a square sample and a loading factor of 0.41 m^2/m^3. If, again, all the air passes through a plane perpendicular to the carpet sample and the ventilation rate is 1 h^{-1}, corresponding to a volumetric flow into the chamber of 0.50 m^3/h or 13.9 cm^3/s, then 13.9 cm^3/s divided by the desired air velocity, 10 cm/s, yields the area of the plane, 1.39 cm^2. Since the width of the chamber is 14.3 cm, the chamber height would be only 0.097 cm, which is clearly impractical. Moreover, to maintain a volume of 0.050 m^3 would require a chamber length of 360 m.

Still, the above exercise suggests how chambers should be designed and operated. Such a "redesigned" chamber may provide more accurate emissions than those of current practice. The "redesigned" chamber allows for appropriate concentrations and air velocities, but its low height and extreme length are completely impractical. Moreover, less than 0.1% of the chamber volume is used, the part with the sample. The rest of the volume serves only to provide space so that the loading factor and chamber ventilation rate approximate those of actual indoor environments. However, these are not the critical operating parameters. Instead, the chamber concentration and the air velocity are the important operating parameters. It appears that small test chambers should be operated with sufficiently high ventilation rates to obtain chamber air velocities near 10 cm/s and with sufficiently high loading factors so that the chamber concentrations will be near those measured in typical indoor environments. Alternatively, chambers could be operated with recirculated air or with small, internal mixing fans (provided they were shown not to unduly perturb the temperature, or introduce or remove contaminants). Air velocities in the chambers near the surface of the sample being tested should be confirmed by measurement for a given chamber configuration and operating conditions.

Conclusion

Because of the importance of obtaining accurate input (that is, emission rates) for mass-balance modeling, chamber operating conditions must be carefully considered and selected. In the first phase of learning to use small test chambers to determine emission rates, chamber operating conditions have been selected largely by intuition in an attempt to mimic the conditions found in indoor environments. However, we have now gained sufficient experience in using such chambers that we should begin to examine critically the operating parameters selected for these chambers.

These operating parameters need not exactly mimic all "real world" conditions. Indeed, because of the smaller volume of test chambers, they can not. Instead, the important parameters (chamber concentration and air velocity) must be correctly selected for accurate representation so that results transfer accurately to full-scale indoor environments.

Modeling boundary layer effects on emissions for a range of representative materials (in particular, wet sources) is needed to determine the extent to which air velocities must be controlled when measuring emission rates. Chamber air velocities in chambers currently in use should be measured to determine whether they are appropriate. If they are not, the following considerations may provide guidance in selecting operating conditions for small emission test chambers:

(1) The chamber concentration is an important factor because of equilibrium and analytical considerations, especially for high emitting materials.
(2) The air velocity over the surface of the materials is also important because of equilibrium considerations.
(3) The ventilation rate of the chamber is not important except to the extent it affects the chamber concentration and air velocity.

(4) The chamber volume is not important except to the extent that (a) it affects the chamber concentration and air velocity, (b) wall effects become important, or (c) the chamber size becomes too large or too small for practical use.

References

[1] Matthews, T. G., Thompson, C. V., Wilson, D. L., and Hawthorne, A. R., "Air Velocities Inside Domestic Environments: an Important Parameter for Passive Monitoring," *Environment International*, Vol. 15, pp. 545–550, 1989.

[2] Gammage, R. B. and Hawthorne, A. R., "Current Status of Measurement Techniques and Concentrations of Formaldehyde in Residences, *Advances in Chemistry, Series 210*, American Chemical Society, Washington, DC, 1985, pp. 117–130.

[3] Lorch, F. A. and Straub, H. E., "Performance of Overhead Slot Diffusers with Simulated Heating and Cooling Conditions," *ASHRAE Transactions*, Vol. 89, Part 1B, 1983, pp. 200–211.

[4] Hart, G. H. and Int-Hout, D., "The Performance of a Continuous Linear Air Diffuser in the Perimeter Zone of an Office Environment," *ASHRAE Transactions*, Vol. 86, Part 2, 1980, pp. 107–124.

[5] Schiller, G. E. and Arens, E. A., "Thermal Comfort in Office Buildings," *ASHRAE Journal*, Oct., Vol. 39, 1988, pp. 26–32.

[6] Christianson, L. L., Riskowski, G. L., and Zhang, J. S., "Simulating Residential Room Conditions," *Building Systems: Room Air and Air Contaminant Distribution*, American Society of Heating, Refrigerating, and Air-Conditioning Engineers (ASHRAE), Atlanta, GA, 1989, pp. 218–220.

Toshiaki Yamamoto,[1] *David S. Ensor,*[1] *and Leslie E. Sparks*[2]

Modeling of Indoor Air Quality for a Personal Computer

REFERENCE: Yamamoto, T., Ensor, D. S., and Sparks, L. E., **"Modeling of Indoor Air Quality for a Personal Computer,"** *Modeling of Indoor Air Quality and Exposure, ASTM STP 1205*, Niren L. Nagda, Ed., American Society for Testing and Materials, Philadelphia, 1993, pp. 149–157.

ABSTRACT: A menu-driven ventilation model for a personal computer was developed that is capable of determining the distributions of time-averaged, two-dimensional, steady-state flow fields and particulate or gaseous contaminants under isothermal conditions for a given particulate/gaseous diffusion coefficient. The model was written for a personal computer so that engineers can use it as a tool to evaluate a potential ventilation performance in indoor space yet to be designed.

The model's computational speed is extremely fast (a few minutes) with reasonable accuracy. This paper discusses the computational algorithm and user interactiveness for the use of this model. Case studies were performed for a simple indoor environment. Ventilation effectiveness in relation to the locations of the supply air duct and the contaminant source was investigated.

KEY WORDS: air flow, model, numerical simulation, indoor air, turbulence, ventilation, contamination, concentration

Most of the software developed to compute airflow distribution and concentration profiles within rooms require either a mainframe or super computer [*1–5*]. Some of these software models have been developed to predict airflow in cleanrooms constructed for the electronics industry [*6–9*]. However, these models have limited use because most engineers lack access to mainframe computers. Even the most complex model contains assumptions affecting the accuracy of the prediction and may not adequately account for the details of room configuration, supply/return air duct location, source location, and inflow velocity.

The aim of this project was to provide software tools for estimation of airflow distribution and particulate or gaseous contaminant transport that can be used by engineers responsible for indoor air quality. The software was developed for personal computers that are now available to almost everyone. By making some compromises with respect to the detail of the computations, it was possible to provide computational times compatible with the capabilities of personal computers.

During the course of software development, fast-direct solution schemes requiring no iteration have been incorporated into the model. Also, the algorithm developed caused no computational errors associated with the selection of grid size [*7*]. For a wide range of practical situations, a personal computer provides adequate capability to predict the general behavior of contaminant dispersion in a room and to design a ventilation system. The software is also designed to take advantage of the personal computer's interactive ability. These advantages included reduction of errors by inputting data through the use of menus and reduction of misinterpretation of the results through graphical displays of output.

[1]Research mechanical engineer and center director, respectively, Research Triangle Institute, PO Box 12194, Research Triangle Park, NC 27709.

[2]Senior chemical engineer, U.S. Environmental Protection Agency, Air and Energy Engineering Research Laboratory, Research Triangle Park, NC 27711.

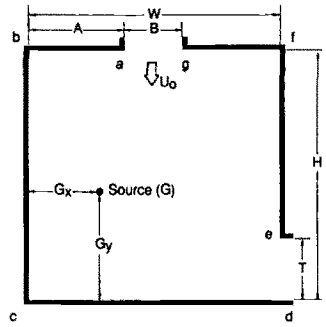

FIG. 1—*Room outline and variables.*

Figure 1 shows the configuration of a room and the variables for which the supply (B) and exhaust (T) dimensions and inlet locations (A), room width (W), room height (H), inflow velocity (U_o), source strength (G), and source location (G_x, G_y) can be specified. The model can predict the distribution of steady-state flow field and the effective turbulent diffusion coefficient. These predictions are then incorporated into the particle diffusion model to solve the particle or gaseous contaminant distributions within a significantly shorter computational time (a few minutes).

Because the room is assumed to be in an isothermal condition, the model does not take into account buoyancy forces. However, the qualitative effects of the placement of the supply air duct, the location of the source on the contaminant distribution, and basic design data for ventilation effectiveness can be determined.

User-Friendly Software

This model is highly interactive, permitting the user to control the flow of the program. Menus display the choices of the room configurations and operating parameters along with several lines of text on the screen and a flashing cursor. The user chooses a desired action by positioning the cursor and pressing <Enter>. Examples of operating menus are shown in Figs. 2 and 3. When the computation is completed, all necessary data files are created for contour plotting of streamlines,

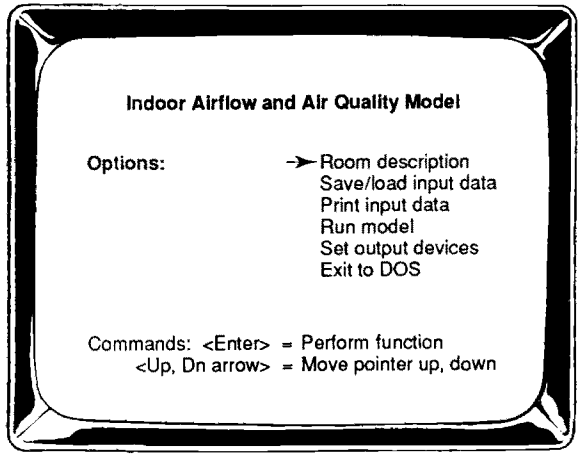

FIG. 2—*Example of an operating menu for indoor airflow and air quality model.*

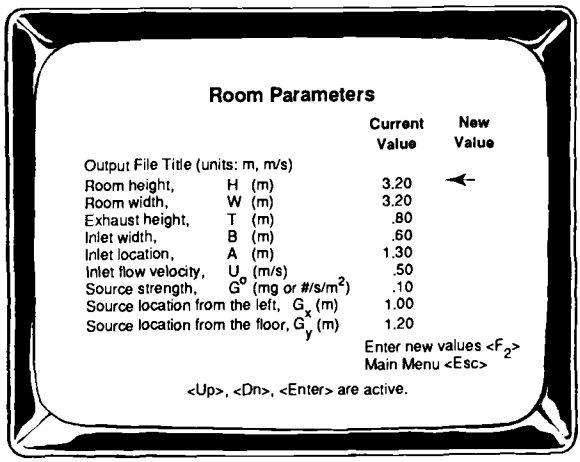

FIG. 3—*Example of data entry menu.*

turbulent kinetic energy distribution, kinetic energy dissipation rate, contaminant concentration profile, and velocity diagrams. Figure 3 shows the default values of the room parameters.

Computational Scheme

The model incorporates a new computational scheme to solve a standard two-dimensional k-ϵ turbulence model. The Navier Stokes equations and Reynolds stress equations can be expressed in the form of a vorticity-stream function. Instead of the five normally used, the governing equations are reduced to four: stream function equation, vorticity equation, turbulent kinetic energy equation, and energy dissipation rate equation. These four equations are expressed in finite difference form and solved simultaneously with appropriate boundary conditions. When the room con-

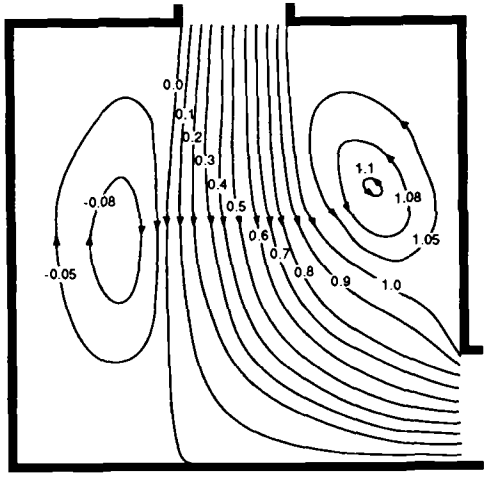

FIG. 4(*a*)—*Airflow streamlines in the room (inflow velocity of 0.5 m/s).*

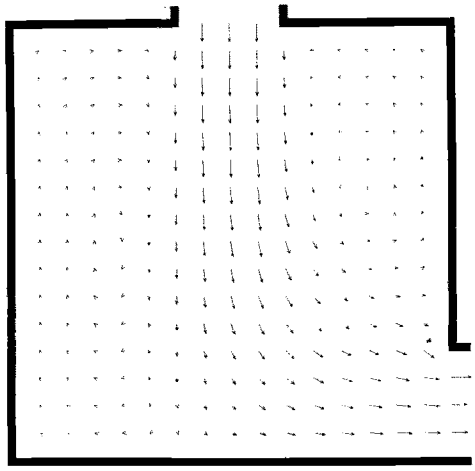

FIG. 4(*b*)—*Time-averaged velocity distributions in the room (inflow velocity of 0.5 m/s).*

figuration and the flow field are determined, the particle diffusion equation can be solved. A particle diameter of 1 μm was assumed for this simulation.

When solving the stream function equation (Poisson type equation), the model uses a new solution method called the fast-direct-solution (FDS) method [*10*] instead of a conventional iteration method such as the successive-over-relaxation method. Because this FDS method requires no iterations, no computational propagation errors associated with the selection of the grid size occur. By employing the vorticity-stream function and the FDS method, we are able to reduce considerably the computational time. This permits a personal computer to be used at the starting level of computation. In this model, a grid point mesh of 17 × 17 was used which produces a computational result almost identical to that of a grid point mesh of 25 × 25. The detailed formulation, computational procedures, and the discussions relating to the grid point mesh have been described previously [*7*].

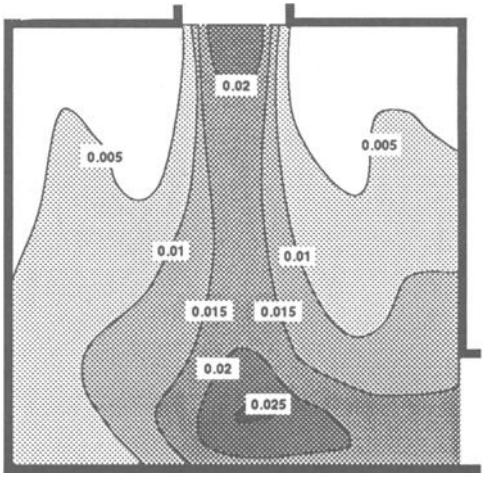

FIG. 5—*Distribution of the effective turbulent diffusion coefficient.*

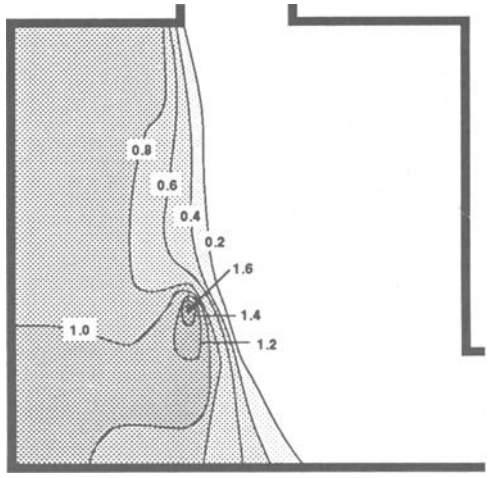

FIG. 6—*Steady-state contaminant concentration distribution when the source is placed at the left-hand side.*

The boundary conditions used for this simulation were: nonslip conditions along *a–b–c–d* and *e–f–g* (Fig. 1), uniform flow velocity along the supply duct (*a–g*), and parallel flow along the exhaust duct (*d–e*). All the detailed boundary conditions used for this simulation were discussed in Ref *7* although the room configuration was not the same.

Numerical Results and Discussion

Figure 4(*a*) shows the airflow streamlines in a room where a supply duct is placed at the center of the ceiling and an exhaust duct is located at the bottom of the side wall. The diagram shows two large recirculation (or eddy) zones, one on each side of the main airflow path. The strength of flow recirculation was slightly greater for the right-hand side. The strength of recirculation is

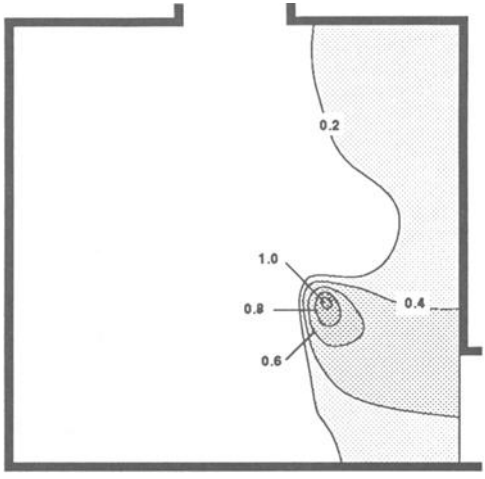

FIG. 7—*Steady-state contaminant concentration distribution when the source is placed at the right-hand side.*

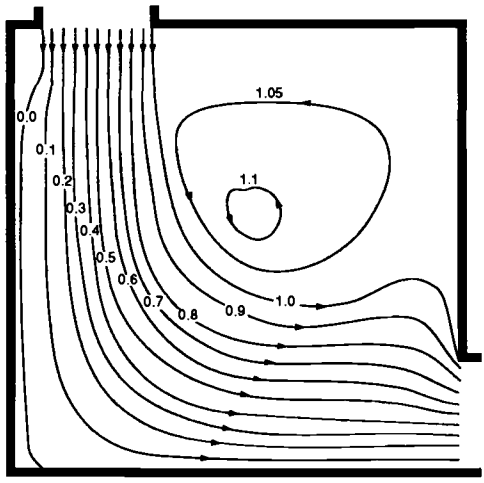

FIG. 8(*a*)—*Airflow streamlines when the supply air duct is at the left side.*

an index of how strongly contaminants can be entrained and trapped in the recirculation zone. Once trapped in such a recirculating zone, contaminants rarely escape unless a strong external force, such as electrostatic force, is present. Flow recirculation is clearly not a favorable condition. In Fig. 4(*b*), which shows the time-averaged velocity distributions, note that the fluid velocity is nondimensionalized by the inflow velocity of 0.5 m/s.

Because it is used as the measure of airflow mixing, the distribution of the effective contaminant diffusion coefficients is important. The contaminant diffusion coefficient consists of the diffusion due to Brownian motion for particles, or molecular diffusion for gaseous contaminants, and diffusion due to the turbulent kinetic energy. The diffusion due to Brownian motion depends on particle size. The value of 2.76×10^{-11} m^2/s, which corresponds to a 1-μm particle size, was used. On the other hand, the diffusion due to turbulence was determined by solving the kinetic energy and the dissipation rate equations. The summation of these two diffusion coefficients is shown as the normalized effective turbulent diffusion coefficient distribution (Fig. 5). Because the turbulent

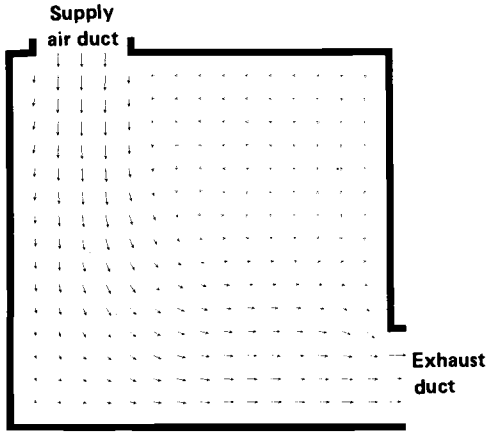

FIG. 8(*b*)—*Velocity vectors when the supply air duct is on the left-hand side.*

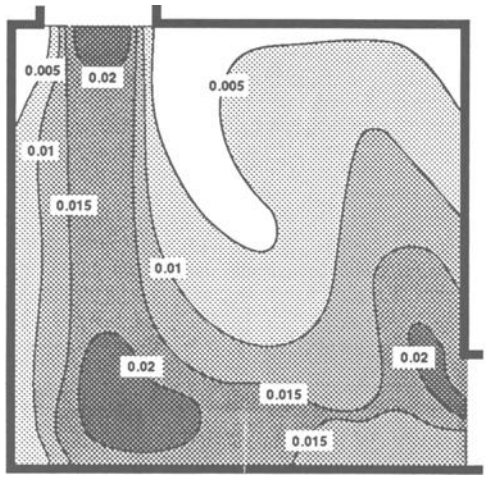

FIG. 9—*Distribution of the effective turbulent diffusion coefficient when the supply air duct is at the left-hand side.*

diffusion coefficients were nondimensionalized by BU_o (see Fig. 1), the actual turbulent diffusion coefficients (m^2/s) are 0.2 times the values shown in Fig. 5. As shown, the highest rate of diffusion occurs at near the bottom of the main flow path. Because the effective turbulent diffusion coefficient reflects the degree of air mixing, a greater degree of contaminant mixing takes place in the region of higher diffusion rate. The next highest rate of diffusion appears in the vicinities of inflow and outflow and the main flow stream region. In general, as distance from the main airflow path increases, the rate of contaminant diffusion decreases.

Figure 6 shows the steady-state contaminant concentration distribution that occurs when the source is placed at the left side of the main airflow stream. Note that the contaminant level shown in Fig. 6 is a relative value. On the left-hand side of the main airflow stream, the contaminant concentration is significantly higher than on the right-hand side; very few contaminants are present

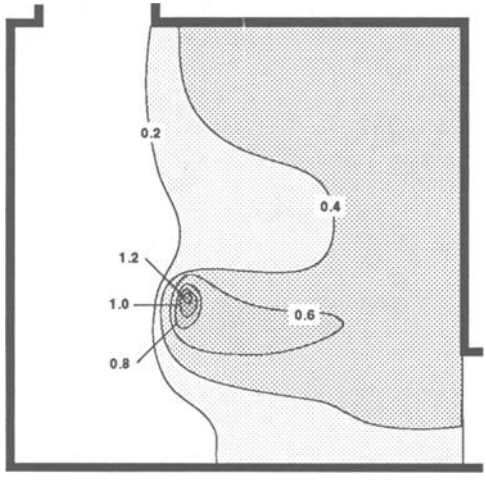

FIG. 10—*Contaminant concentration profile when the source is at the left-hand side.*

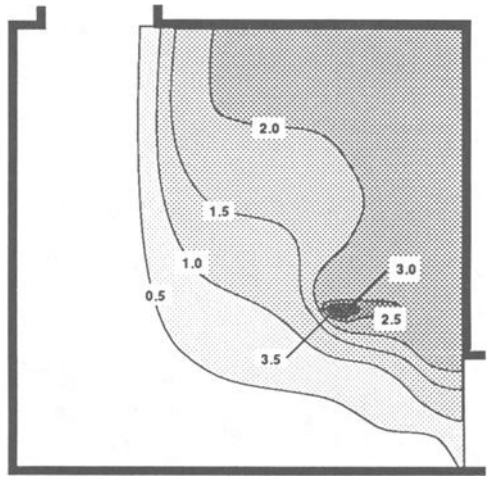

FIG. 11—*Contaminant concentration distribution when the source is at the right-hand side.*

on the right-hand side of the main airflow stream. This suggests that, in spite of contaminant diffusion, the main airflow stream behaves like an air curtain separating the two sides of the room.

Placing the source at the right-hand side of the room creates the contaminant concentration distribution shown in Fig. 7. Because the source is located in the main airflow stream, the average concentration is significantly lower (less than one-third) than shown in Fig. 6. Although most of the contaminants are swept away by the main airflow, some are diffused to the upper-right section of the room.

In Figs. 8(*a*) and 8(*b*), the airflow distribution is completely modified, and only one large recirculation (or eddy) zone is observed at the upper-right corner of the room. These effects are caused by shifting the supply air duct to the left.

Figure 9 shows the distribution of the effective turbulent diffusion coefficient for the case represented in Figs. 8(*a*) and 8(*b*). The relative value remains about the same (see Fig. 5) although its distribution is significantly changed. In other words, the effective turbulent diffusion coefficient is higher along the main airflow path and becomes lower in the stagnation region.

Figure 10 shows the contaminant concentration profile for a source at the left-hand side. Because the source is located in the main flow streamline, the average concentration is significantly smaller than with the supply duct located at the center (Fig. 6).

Figure 11 shows the contaminant concentration distribution when the source is moved to the right-hand side. In this instance, most of the contaminants remain in the upper-right-hand corner, indicating poor ventilation. The average concentration is more than three times higher than shown in Fig. 10. All these examples demonstrate that the ventilation effectiveness is greatly affected by the source location and the airflow distribution in a room. The model is able to provide quantitative information on the ventilation performance and thus can be used as a design tool for indoor air quality (IAQ) engineers.

The computational times for this model using various personal computers were compared with the time required to run the commercially available FLUENT code on a main frame computer. The computational time for this model using a grid of 17 × 17 was 5 min with a 286 machine at 8 MHz, 1.0 min with a 386 at 33 MHz, and 0.5 min on a 486 at 33 MHz. When the grid mesh was increased to 25 × 25, the computational time was increased to 15 min with a 286 at 8 MHz and 2.5 min with 386 at 33 MHz. When the FLUENT code (QUICK scheme) was used with the

same conversion criteria, the computational time was 16 min for a 17 × 17 grid and 39 min with a 25 × 25 grid. The shorter computational time for this model is attributed to fewer governing equations and the new computational scheme. The computational results for both cases appear to agree reasonably well even with a grid point mesh of 17 × 17. However, the investigation should be extended to cover a greater variety of cases. Also, experimental investigations should be performed for the model verification.

Conclusions

A user-friendly, two-dimensional ventilation model was developed to provide an analytical tool for engineers who need to solve indoor air quality engineering problems. The model operates on a personal computer with appropriate accuracy and resolution, and provides rapid analysis of airflow and particulate or gaseous contaminant concentration distribution so that indoor air quality problems and ventilation systems can be evaluated.

References

[1] Kurabuchi, T., Sakamoto, Y., and Kaizuka, M., "Numerical Prediction of Indoor Airflows by Means of the k-ϵ Turbulence Model," *Proceedings of Building Systems: Room Air and Air Contaminant Distribution*, American Society of Heating, Refrigeration, and Air-Conditioning Engineers, Atlanta, 1989, pp. 57–67.

[2] Murakami, S. and Kato, S., "Current Status of Numerical and Experimental Methods for Analyzing Flow Field and Diffusion Field in a Room," *Proceedings of Building Systems: Room Air and Air Contaminant Distribution*, American Society of Heating, Refrigeration, and Air-Conditioning Engineers, Atlanta, 1989, pp. 39–56.

[3] Baker, A. J. and Kelso, R. M., "On Validation of Computational Fluid Dynamics Procedures for Room Air Motion Prediction," *ASHRAE Transactions*, Vol. 96, 1990, pp. 760–774.

[4] Kelso, R. M., Wilkening, L. E., Schaub, E. G., and Baker, A. J., "Computational Simulation of Kitchen Airflows with Commercial Hoods," *Proceedings*, 1992 ASHRAE Winter Meeting, American Society of Heating, Refrigeration, and Air-Conditioning Engineers, Atlanta, 1992, 3565.

[5] Chen, Q., and Jiang, Z., "Significant Questions in Predicting Room Air Motion," *Proceedings*, 1992 ASHRAE Winter Meeting, American Society of Heating, Refrigeration, and Air-Conditioning Engineers, Atlanta, 1992, AN-92-9-1.

[6] Shanmugavelu, I., Kuehn, T. H., and Liu, B. Y. H., "Numerical Simulation of Flow Fields in Clean Rooms," *Proceedings of the Institute of Environmental Sciences*, Institute of Environmental Sciences, Mt. Prospect, IL, 1987, pp. 298–303.

[7] Yamamoto, T., Donovan, R. P., and Ensor, D. S., "New Computational Scheme for Two-Dimensional k-ϵ Model," *Proceedings of the IES Annual Meeting*, Institute of Environmental Sciences, Mt. Prospect, IL, 1991, pp. 108–112.

[8] Busnaina, A. A. and Abuzeid, S., "Accuracy of Numerical Modeling of Fluid Flow in Clean Rooms," *Proceedings of the Institute of the Environmental Sciences*, Institute of Environmental Sciences, Mt. Prospect, IL, 1989, pp. 245–250.

[9] Kuehn, T. H., Pui, D. Y. H., and Gratzek J. P., "Experimental and Numerical Results for Airflow and Particle Transport in a Microelectronics Clean Room," *Proceedings*, 1992 ASHRAE Winter Meeting, American Society of Heating, Refrigeration, and Air-Conditioning Engineers, Atlanta, 1992, AN-92-9-2.

[10] Nakamura, S., *Computational Methods in Engineering and Science with Applications to Fluid Dynamics and Nuclear Systems*, A Wiley-Interscience Publication, John Wiley and Sons, New York, 1977, pp. 418–430.

Krzysztof Klobut[1]

Theoretical Evaluation of Impact of Return Air and Thermal Load on Air Quality in a Multizone Building

REFERENCE: Klobut, K., **"Theoretical Evaluation of Impact of Return Air and Thermal Load on Air Quality in a Multizone Building,"** *Modeling of Indoor Air Quality and Exposure, ASTM STP 1205*, Niren L. Nagda, Ed., American Society for Testing and Materials, Philadelphia, 1993, pp. 158–172.

ABSTRACT: The computer programs published so far enabled the computation of airflows assuming constant temperatures or the calculation of air temperatures assuming constant airflows. Recently, a new microcomputer program was developed in which thermal conditions were considered when predicting the spread of contaminants in buildings. The program enabled simultaneous dynamic simulations of contaminant distribution, airflows, and temperatures in a multizone building. Using the new program, the dynamic distributions of contaminant concentration and air quality in an example building were determined with and without the recirculation of ventilation air, with different thermal loads and with several door positions. For comparison, some simulations were repeated in isothermal conditions. The results showed that a high thermal load increased the spread of contaminant. Recirculation of the ventilation air had a deteriorative impact on the air quality in the simulated building. There was a clear difference in the air qualities predicted by the respective simulations carried out with and without thermal analysis. It is believed that the inclusion of thermal analysis considerably improved the calculation method for the evalution of contaminant distribution in a building.

KEY WORDS: multizone model, calculation techniques, modeling, air recirculation, thermal load, airflow, temperature, contaminant, air quality

Nomenclature

$A_{i,j}$	Section area of flow path from node i to node j, m^2
A_{iw}	Surface area of wall at node i, m^2
A_{ww}	Surface area of window, m^2
a	Dummy variable in model of large operning, m/s^2
C_d	Coefficient of discharge
C_i	Concentration of contaminant at node i, pol (or volume ppm or kg/m^3 or g/kg dry air)
C_i^a	Thermal capacity of air at node i, J/K
C_{iw}^w	Thermal capacity of wall at node i, J/K
c_p	Specific thermal capacity of air, J/(kg K)
G_i	Strength of contaminant source at node i, olf (or L/h or kg/s)
g	Acceleration due to gravity, m/s^2
H	Height of large opening, m
$K_{i,j}$	General coefficient of pressure loss

[1]Scientist, Helsinki University of Technology, Laboratory of Heating, Ventilating, and Air Conditioning, Otakaari 4, SF-02150 Espoo, Finland.

$L_{i,j}$ Length of flow path from node i to node j, m
$m_{i,j}$ Mass flow of air from node i to node j, kg/s,
N Number of nodes in building network
PPD Predicted percentage dissatisfied, %
p_i Absolute pressure at node i, Pa
Δp Pressure difference, Pa
Δp_x Pressure difference producing net flow of air through large opening, Pa
Δp_u Pressure difference simulating effect of turbulence in model of large opening, $\Delta p_u = 0.003$ Pa
Q_c Thermal load by convection, W
Q_r Thermal load by radiation, W
$q_{i,j}$ Volume flow of air from node i to node j, m^3/s
q_1 Inflow of air to room through large opening, m^3/s
q_2 Outflow of air from room through large opening, m^3/s
q_{net} Net flow of air through large opening, m^3/s
$S_{i,j}$ Stack effect in flow path from node i to node j, Pa; head generated by fan, Pa
t_0 Outdoor air temperature, °C
t_i Temperature of air at node i, °C
t_{iw} Surface temperature of wall at node i, °C
t_{iwr} Temperature of surface of hemisphere, °C
t_{iwx} Temperature of air on opposite side of wall at node i (for example, outdoor air temperature for external wall), °C
Δt Temperature difference, K
U_{iw} Overall heat transfer coefficient of wall at node i, $W/(m^2 K)$
U_{ww} Overall heat transfer coefficient of window, $W/(m^2 K)$
V_i Volume of zone associated with node i, m^3
v_x Mean velocity of air in large opening, m/s
W Width of large opening, m
α_c Convection heat transfer coefficient, $W/(m^2 K)$
α_r Radiation heat transfer coefficient, $W/(m^2 K)$
η Filter effect, $-$, $0.0 \leq \eta \leq 1.0$
ρ_i Density of air at node i, kg/m^3
ρ_m Mean density of air in large opening, kg/m^3
τ Time, s

In the past few years a considerable amount of scientific effort has gone into the development and improvement of models for predicting indoor airflows and contaminant concentrations in buildings. A number of new computer programs have been developed. For example, MULTIC, CONTAM, and COMIS [*1–3*] are designed for the simulation of contaminant concentrations; AIRNET [*4*] performs the calculation of airflows by infiltration, between indoor zones and in ventilation ducting. Work is in progress on DTFAM [*5*], for coupled airflow and thermal analysis, but the program has not yet been published.

Contaminants are not simulated in DTFAM. In the other programs, the temperatures are assumed to be constant. However, the changes in the outdoor and indoor air temperatures do occur in reality, and, combined with the thermal behavior of the building structure, they have an impact on the interzonal airflows distributing airborne pollutants in the system.

Therefore, a new program, TFCD [*6–8*], for microcomputers, was recently developed in which thermal conditions were considered. TFCD enables the simultaneous dynamic simulation of temperatures, air flows, contaminant concentrations, and air quality in terms of predicted percentage of dissatisfication due to contaminant concentration.

Prior to this publication the program was further improved by including the filter effect and calculation of the concentration dose. The following is a brief report of the fundamentals of the models used in TFCD. This is followed by the simulation results obtained with TFCD.

Fundamentals of TFCD

The program is intended for a microcomputer to enable simulations covering a short period of time, for example, one day. The source code of the program is written in Fortran 77.

The building is simulated using a network model. The nodes of the network are placed outdoors at the envelope of the building, in the ventilation ducting and in indoor zones. The branches of the network represent airflow paths. The program is capable of simulating a system consisting of at most 40 nodes.

Model Equations

Calculation of Temperatures—The thermal model of the room presented in Ref *9*, was adapted to calculate the temperatures at the indoor nodes of the building network. Each zone of the building was represented by one node by assuming that the air inside the zone was instantly and perfectly mixed. A set of differential equations was written for each indoor zone

$$\frac{dt_i}{d\tau} C_i^a = \sum_{j \neq i}^{N} m_{j,i} c_p (t_j - t_i) + \sum_{iw=1}^{10} \alpha_c A_{iw} (t_{iw} - t_i) + Q_c + U_{ww} A_{ww} (t_0 - t_i) \tag{1}$$

$$\frac{dt_{iw}}{d\tau} C_{iw}^W = \frac{A_{iw}(t_{iwx} - t_{iw})}{\dfrac{1}{U_{iw}} - \dfrac{1}{\alpha_c + \alpha_r}} + \alpha_c A_{iw}(t_i - t_{iw}) + \alpha_r A_{iw}(t_{iwr} - t_{iw}) + Q_r \tag{2}$$

The set for a node has one equation for air temperature (Eq 1) and as many equations for wall temperature (Eq 2) as there are walls in the space (maximum ten) associated with the node. This set of equations is solved at each time step for all of the indoor nodes of the network.

Calculation of Airflows—The airflows and pressures in the building network are calculated from the set of differential equations written for each network node [*10*]

$$V_i \frac{d\rho_i}{d\tau} + \sum_{j \neq i}^{N} m_{i,j} = 0 \tag{3}$$

$$\frac{L_{i,j}}{A_{i,j}} \frac{dm_{i,j}}{d\tau} - p_i + p_j + \frac{K_{i,j} |m_{i,j}| m_{i,j}}{2} = S_{i,j} \tag{4}$$

Equations 3 and 4 must both be fulfilled for all the nodes simultaneously. The general coefficient of pressure loss, $K_{i,j}$ in the model Eq 4, is calculated from the formula

$$\Delta p_{i,j} = \frac{K_{i,j} m_{i,j}^2}{2} \tag{5}$$

Depending on the pressure-flow characteristics of the flow path, Eq 5 has a different form. At present, the program is able to handle nine types of flow paths [*6–8*]. They are: duct, damper, fan, crack leakage as power law, crack leakage as quadratic equation, logarithmic element, polynomial

approximation, large opening between vertically adjacent spaces (simplified to one-way flow approximated by orifice equation), and large opening between horizontally adjacent spaces.

Equations 3 and 4 are used to predict the airflows as one-way flows. In large openings two-way flows occur. These are calculated using an additional model. It consists of a large number of equations which have different forms, depending on the temperature difference and the position of the neutral levels. The complete set of model equations and associated theory may be found from Ref *1*. Some of these equations are [*1*]

Isothermal case and $\Delta p_x < \Delta p_u$

$$q_1 = \frac{1}{2} C_d W H \left[\frac{2(\Delta p_u - \Delta p_x)}{\rho_m}\right]^{0.5} \tag{6}$$

$$q_2 = \frac{1}{2} C_d W H \left[\frac{2(\Delta p_u + \Delta p_x)}{\rho_m}\right]^{0.5} \tag{7}$$

Isothermal case and $\Delta p_x \geq \Delta p_u$

$$q_1 = 0 \tag{8}$$

$$q_2 = \frac{1}{2} C_d W H \left\{\left[\frac{2(\Delta p_x + \Delta p_u)}{\rho_m}\right]^{0.5} + \left[\frac{2(\Delta p_x - \Delta p_u)}{\rho_m}\right]^{0.5}\right\} \tag{9}$$

Nonisothermal case and neutral levels intersect the opening

$$q_1 = \frac{1}{6} C_d W H \left(\frac{aH}{2}\right)^{0.5} \left\{\left[1 - \frac{4(\Delta p_x + \Delta p_u)}{\rho_m a H}\right]^{1.5} + \left[1 - \frac{4(\Delta p_x - \Delta p_u)}{\rho_m a H}\right]^{1.5}\right\} \tag{10}$$

$$q_2 = \frac{1}{6} C_d W H \left(\frac{aH}{2}\right)^{0.5} \left\{\left[1 + \frac{4(\Delta p_x + \Delta p_u)}{\rho_m a H}\right]^{1.5} + \left[1 + \frac{4(\Delta p_x - \Delta p_u)}{\rho_m a H}\right]^{1.5}\right\} \tag{11}$$

The dummy variable, a, in Eqs 10 and 11 is defined as

$$a = \frac{2g\Delta\rho}{\rho_m} \tag{12}$$

where Δp is the difference of air densities. Pressure difference Δp_x is the driving force for the net flow rate, q_{net}, that, in turn, is a difference between the outflow, q_2, and the inflow, q_1. The pressure difference Δp_u is assumed to be a constant 0.003 Pa describing the effect of turbulence and operating in opposite directions over both half areas of the opening. The discharge coefficient, C_d, was derived from tracer gas experiments and is calculated from the formula [*1*]

$$C_d = 3.7v_x + 6.4v_x e^{-\Delta t} - 0.90e^{-\Delta t} + 0.96 \tag{13}$$

where Δt is the difference between the air temperatures on both sides of large opening, and v_x is the mean velocity corresponding to the net flow rate through the opening

$$v_x = \frac{q_{net}}{HW} = \frac{q_2 - q_1}{HW} \tag{14}$$

The model equations for large opening are valid for [*1*]

$$0 \leq v_x \leq 0.05 \text{ m/s} \quad \text{and} \quad 0 \leq \Delta t \leq 3.0$$

Calculation of Contaminant Concentrations—It was assumed that the contaminant is instantly and perfectly mixed with the air in the zone and is passive. The mass balance equation for the contaminant is written for each node of the network.

$$\frac{dC_i}{d\tau} V_i = G_i + \sum_{j \neq i}^{N} q_{j,i} C_j (1 - \eta) - \sum_{j \neq i}^{N} q_{i,j} C_i \tag{15}$$

Once the airflows have been determined, the contaminant concentrations in the system are solved from Eq 15.

Evaluation of Air Quality—The perceived air quality may be quantified in terms of predicted percentage dissatisfied (PPD) [*11*] as

$$\text{PPD}_i = \begin{cases} 395 \exp(-3.25\, C_i^{-0.25}) & \text{for } C_i \leq 31.3 \text{ decipol} \\ 100\% & \text{for } C_i > 31.3 \text{ decipol} \end{cases} \tag{16}$$

where C_i is the perceived air pollution [*11*], that is, the concentration, expressed in decipols. The air quality at each node of the network is evaluated in the program by means of Eq 16.

Concentration Dose—Based on contaminant concentration, the integrated dose is calculated in the program at each network node according to Harber's Law [*12*] from the formula.

$$\text{Dose}_i = \int_0^{\text{exposure time}} C_i(\tau) d\tau \tag{17}$$

Solution Methodology and Strategy

Model Eqs 1 and 2 for air and wall temperatures are explicitly discretized and solved according to the Euler method. This solution method requires minimal computational effort but the time step must be short enough to avoid stability problems. The program has a subroutine for analyzing the stability and calculating the upper limit for the time step [*6,7*].

Fully implicit discretization is applied to model Eqs 3 and 4 for airflows and pressures. Thus, potential stability problems are avoided. The discretization and linearization are done according to Ref. *10*. The linear matrix equation is created and solved by means of standard LU-decomposition and the back substitution method [*13*]. The iterative solution is considered to be found when the residuals of the discretized equations are less than 0.0001 kg/s (Eq 3) and 0.001 Pa (Eq 4).

The contaminant mass balance Eq 6 is implicitly discretized and rearranged to obtain a linear matrix equation that is solved for the vector of concentration by means of the same solver as was previously used to determine the airflows.

The important benefit of using the explicit Euler method to calculate the temperatures is that the iterations between the temperatures and airflows can be avoided. Thus, the sequence of computations is clear (Fig. 1) and the computation time is shortened.

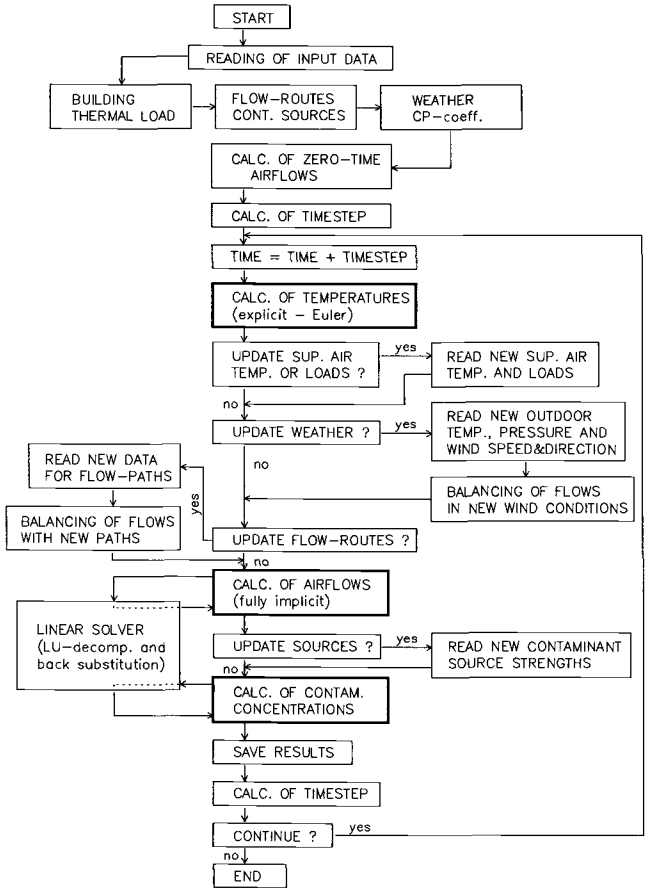

FIG. 1—*Simplified block diagram of the TFCD program.*

Reliability and Application Constraints

The performance of the numerical models and solution methods used in the program was tested in a number of validation cases [*6,7*].

In the isothermal cases, the simulations performed with TFCD were compared with more sophisticated programs using the constant temperature approach. An example of such a comparison is calculation of contaminant concentrations in building shown on top in Fig. 2. The mass flow rates given in Fig. 2 correspond to 0.5, 1.0, and 2.0 air changes per hour in the configuration [*3*]. The assumed outdoor concentration is a constant $100 \cdot 10^{-6}$g/kg dry air, and the initial concentrations in both rooms are $1000 \cdot 10^{-6}$ g/kg dry air. The plot at the bottom in Fig. 2 shows the evolutions of concentrations in the system as predicted by the program COMIS [*3*] and TFCD. Both rooms follow the same evolution and practically no difference is observed between the predictions of both programs, (Fig. 2). The nonisothermal simulations with TFCD in other applications were compared to measurements. Very good agreement of the results was obtained in all the cases [*6,7*].

In TFCD, the outdoor air temperature is assumed to be equal at all outdoor nodes. The thermal model does not explicitly solve the heat conduction problem in the wall (Eq 2). Instead, the lumped-

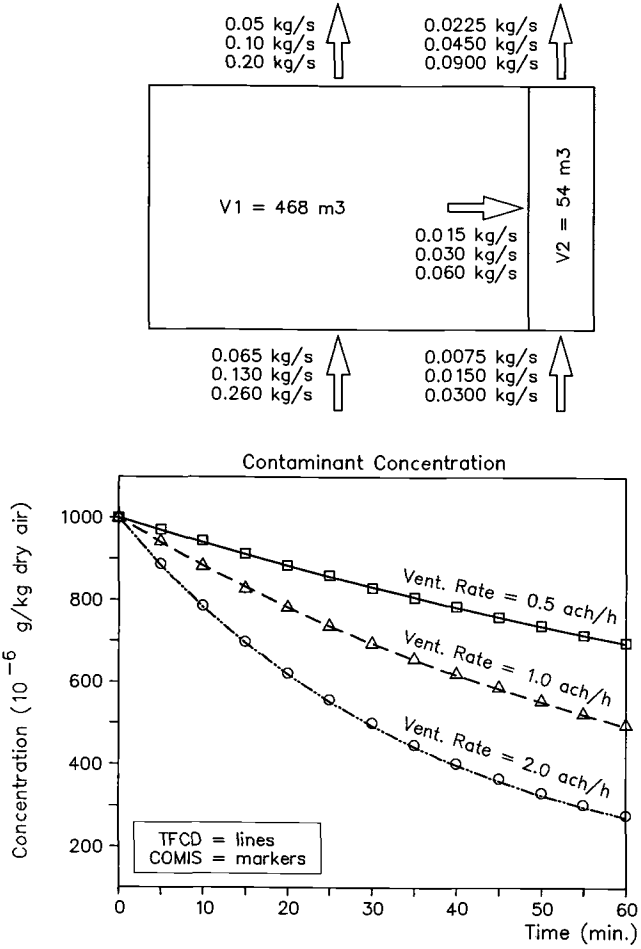

FIG. 2—*Compared evolution of contaminant concentrations computed with COMIS [3] and TFCD [6,7].*

analysis [*14*] is used to account for the thermal capacity of the wall. This simplification is allowed for the wall construction that is not particularly massive. It may also be applied when the penetration depth of the heat wave into the wall is small [*9,14*], that is often the case of simulation covering a relatively short period of time. The Biot number, less than 0.1, is the validity criteria of the lumped-approach [*14*].

The large-opening model showed strong sensitivity to the temperature difference and the size of the opening, but not to the magnitude of the net flow in theoretical calculations using four openings with widely changing temperature differences (0.0 through 2.0 K) and net flows (0.5 through 100 L/s), [*6,7*]. Incorporated in MULTIC [*1*], the model was used in the comparison of the simulation results to data measured in the field and it worked satisfactorily [*15*]. The parameters for the large-opening model were derived from the measurements made under conditions usually existing in dwellings [*1*]. Therefore, the TFCD is expected to be the most reliable in similar applications.

The basic simplification used in TFCD is the assumption of perfect mixing of air and contaminant within the zone. Therefore, the choice of zones has a decisive effect on the calculated results.

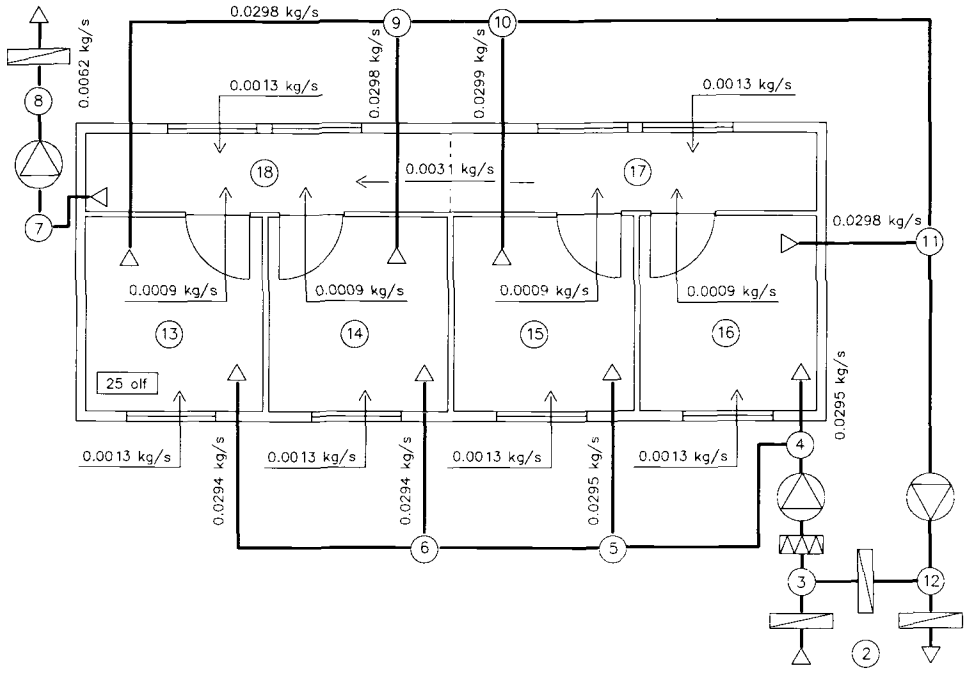

FIG. 3—*Plan of the example building used in the simulations.*

Reliability of the solution strategy used in TFCD was checked for the application presented in the following chapter of the paper. The solutions were computed for three diminishing time steps: (a) automatically calculated by the program (it varied from 30 to 120 s during the simulation), (b) 30 s, and (c) 10 s. All the obtained results were identical, which means that a convergent solution has been found. The time required to perform the simulations was (a) 5 min, (b) 7 min, and (c) 22 min, respectively.

The present version of TFCD works well and may readily be used for research purposes. However, a comprehensive verification by means of measurements must still be carried out in order to gain general confidence in the program as a whole.

Example Application

Part of a fictive office building (Fig. 3) was used in a number of simulations. Rooms 13 through 16 all had equal dimensions and were mechanically ventilated at an equal air exchange rate of approximately 1.85 $(m^3/h)/m^3$. The pressure in corridor Zones 17 and 18 was approximately 0.5 Pa lower than in the rooms. The doors of the rooms were assumed to be of poor tightness in order to avoid remarkable changes in the balance of airflows in the system in case of opening the door. Further details of the system are given in Refs *6 through 8*.

A contaminant source of 25 olf was placed at Node 13. The outdoor temperature was a constant 20°C and the wind velocity was 0 m/s in all of the cases. The air supply temperature was 20°C in the isothermal simulations and 17°C in the nonisothermal simulations. All of the airflows given in Fig. 3 are the results of computation at time = zero. All of the simulations covered a period of 8 h.

The point of interest was the effect of the thermal load and recirculation of the ventilation air on the spread of contaminant from the point of generation to the rest of the system with different

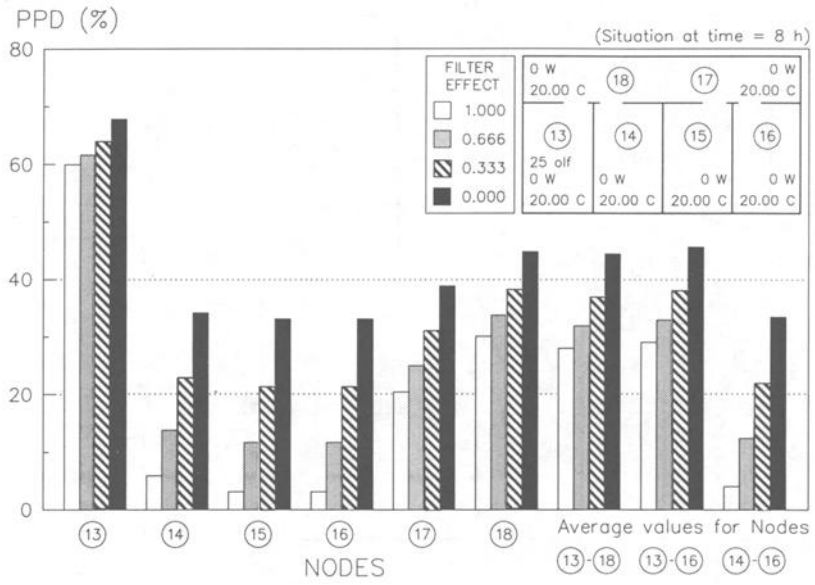

FIG. 4—*Final air quality in the simulated building in the isothermal case.*

door positions. The thermal loads by convection imposed on the rooms varied from 0 to 40 W/m^2. The flow of contaminant with recirculated air was controlled by means of a filter placed before the supply fan in Flow Path 3 to 4 (see Fig. 3). The filter effect varied from 0 to 1. These limit values would correspond to variation in the amount of recirculated return air in the supply air from approximately 57.2% (damper 12 to 3 fully open) to 0% (damper 12 to 3 closed), respectively, if the filter was not used.

The results of the simulations are presented in Figs. 4 through 11. In Figs. 4 through 10, the concentrations are expressed in terms of PPD (Eq 16) in order to evaluate the air quality. Figures 4 through 8 and Fig. 11 show the situations at the end of the simulation, that is, at time = 8 h.

Discussion of Simulation Results

In the first simulation (Fig. 4), the isothermal case was considered. All the doors were open and the filter effect varied from 0 to 1. The recirculation of the air had little effect on the air quality at node 13. In the rest of the system the poorer the filter performance was, the more the air quality deteriorated (Fig. 4).

The same simulation was repeated in a nonisothermal situation with equal thermal loads (Fig. 5) and with different thermal loads (Fig. 6). At Node 13, the air quality is better than in the isothermal case, but it is worse in the rest of the system. The application of different thermal loads results in the more efficient spreading of contaminant to nodes 15 and 16, that are far from the source, *cf* Figs. 5 and 6. This may be explained by the temperature difference between the zones 17 and 18 (see final temperatures given in upper-right corner of Figs. 5 and 6), because the two-way airflows in large openings are very sensitive to temperature difference.

When the doors of Rooms 14 through 16 were closed (Fig. 7) the air moved through the cracks as one-way flows towards the corridor. Closing the doors protected these rooms from contaminant penetration only with perfect filter performance (filter effect equal to one). In all other cases, penetration occurred and the air qualities were equal (Fig. 7), due to equal ventilation rates.

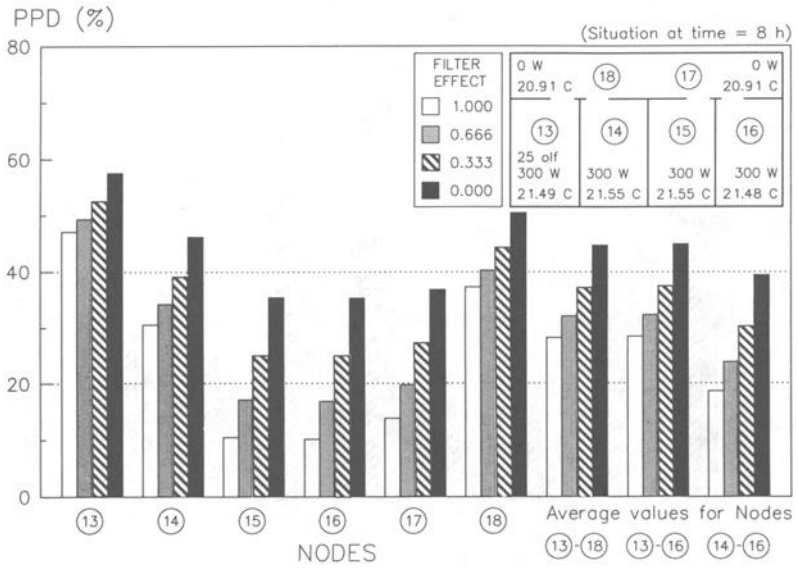

FIG. 5—*Final air quality in the simulated building in the nonisothermal case with equal thermal loads.*

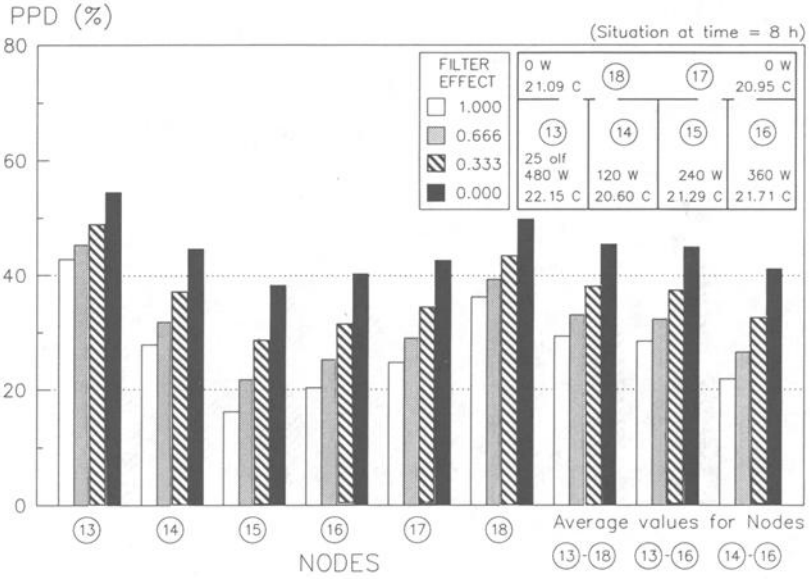

FIG. 6—*Final air quality in the simulated building in the nonisothermal case with different thermal loads.*

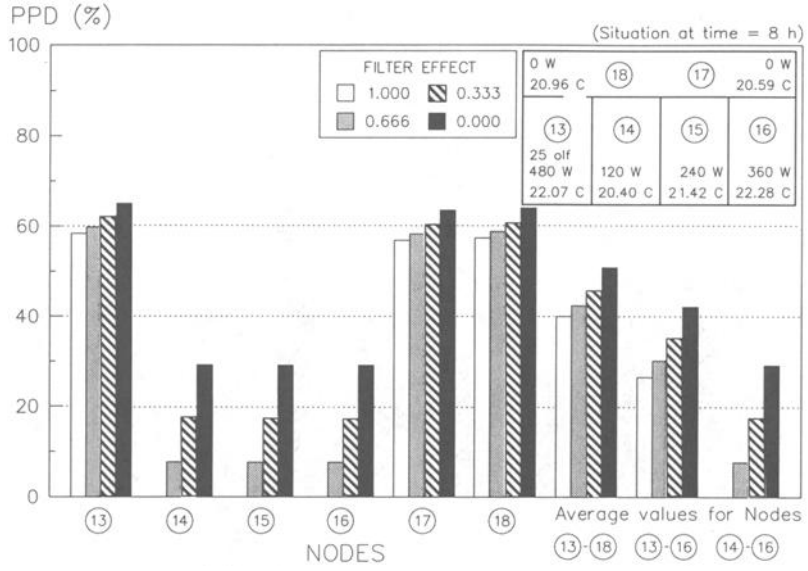

FIG. 7—*Final air quality in the simulated building in the nonisothermal case with different thermal loads when 3 doors are closed.*

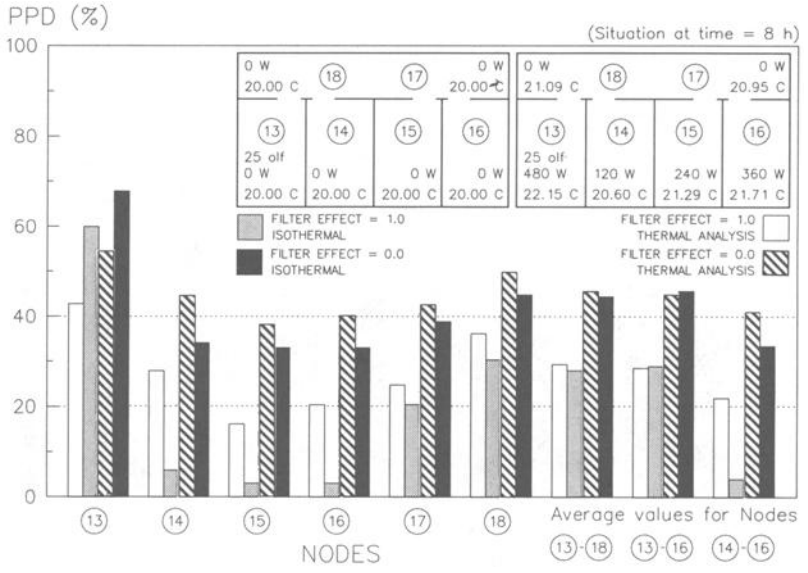

FIG. 8—*Compared final air quality in the simulated building in the isothermal and nonisothermal cases.*

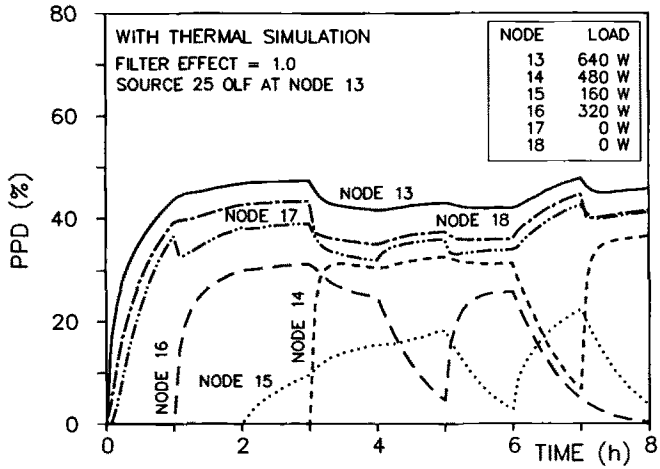

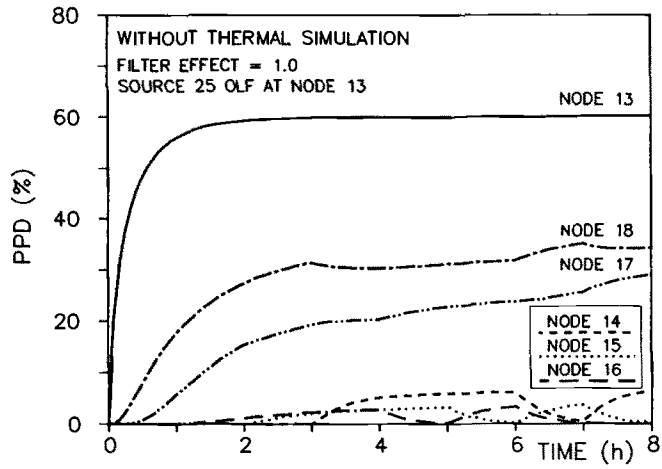

SCHEDULE									
	DOOR 13	OPEN	OPEN	OPEN	OPEN	OPEN	OPEN	OPEN	OPEN
	DOOR 14	CLOSED	CLOSED	CLOSED	DPEN	OPEN	OPEN	CLOSED	OPEN
	DOOR 15	CLOSED	CLOSED	OPEN	OPEN	OPEN	CLOSED	OPEN	CLOSED
	DOOR 16	CLOSED	OPEN	OPEN	OPEN	CLOSED	OPEN	CLOSED	CLOSED

FIG. 9—*Compared histories of air quality in the simulated building in the isothermal and nonisothermal cases (filter effect = 1) when the door positions are changed during simulation.*

In Fig. 8 the comparison is made between the isothermal and nonisothermal simulations in the case with all the doors open. The isothermal simulation predicts poorer air quality (higher PPD value) in Room 13 containing contaminant source and better air quality (lower PPD value) in all other spaces of the system than the nonisothermal simulation. Poor filter performance (or correspondingly the recirculation of air without filtration) leads to deterioration of the air quality as predicted by both the isothermal and the nonisothermal simulations. In the isothermal simulation this effect is less pronounced in Room 13 and more pronounced in the rest of the system than it is in the nonisothermal simulation (Fig. 8).

In the last case studied (Figs. 9 through 11) the door of Room 13 stayed open and the positions of the other doors were changed during the simulation. The simulation was performed in an iso-

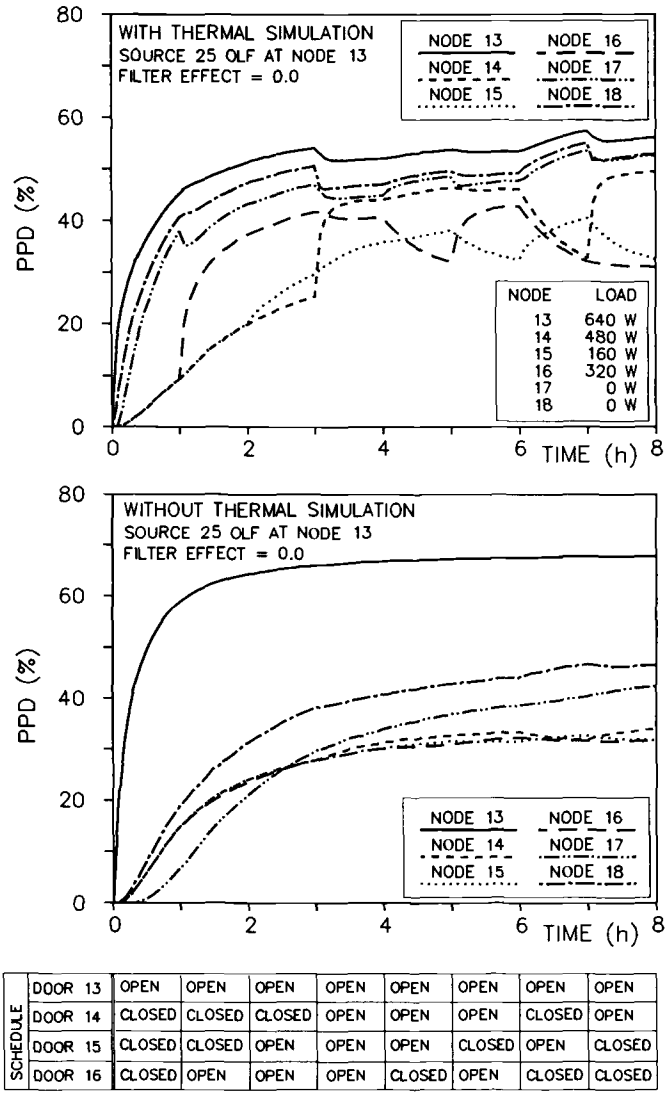

FIG. 10—*Compared histories of air quality in the simulated building in the isothermal and nonisothermal cases (filter effect = 0) when the door positions are changed during simulation.*

thermal and in a nonisothermal situation where the loads in rooms varied from 10 to 40 W/m^2. The histories of the air quality in the system in both situations are given in Figs. 9 and 10 (the schedule for the positions of the doors is shown at the bottom of the figures). The isothermal curves give the impression that the position of the doors does not have much impact on the air quality in rooms while the nonisothermal curves display a very strong effect (Figs. 9 and 10). Clear difference between the isothermal and nonisothermal predictions is obtained again when they are compared in terms of the concentration doses (Fig. 11). These differences prove the importance of thermal analysis in the proper prediction of temperature-sensitive airflows in large openings, which play an important role in distributing contaminant in the system.

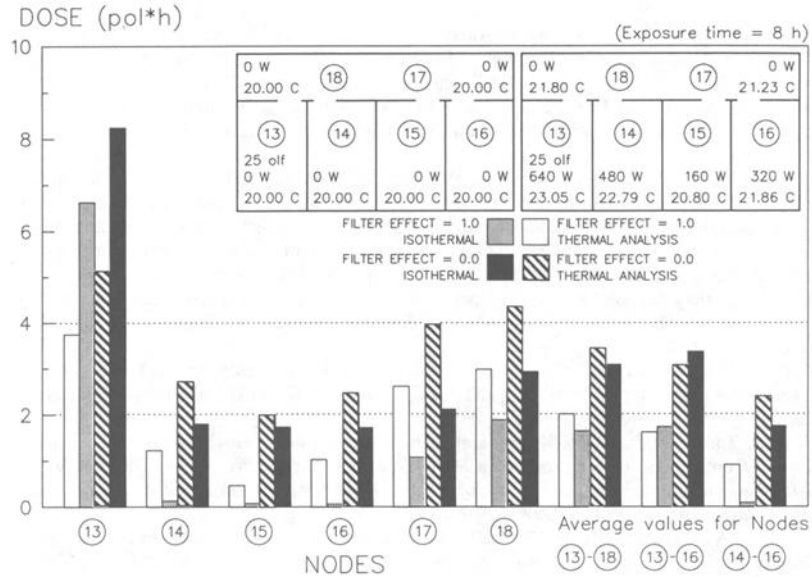

FIG. 11—*Compared concentration doses in the simulated building in the isothermal and nonisothermal cases when the door positions are changed during simulation.*

Conclusions

By means of numerical simulations, it has been shown that a high and unevenly distributed thermal load has an increasing effect on the spread of contaminant in the building, if the interior air temperatures are not controlled. The two-way airflows in large openings have a major influence on the contaminant transport within the building. The recirculation of return air without filtration or with imperfect filter performance leads to deterioration of the indoor air quality.

The isothermal simulations ignore the time variation of the temperature-dependent airflows in large openings, that results in underestimation of the spread of contaminant in the building. The nonisothermal approach is an appropriate means to account for the dynamic changes (for example, position of the doors, the magnitude of the thermal load, and so forth) that have an effect on the air temperatures and, consequently, on the airflows. It is therefore believed that the inclusion of thermal analysis considerably improved the method for evaluating the contaminant spread in the building.

Acknowledgments

The computer program was developed within the frames of a project financed by the Finnish Ministry of Trade and Industry. The preparation of this report was financed by the Technology Development Centre of Finland. The financial support from both institutions is gratefully acknowledged.

References

[*1*] Sirén, K., "A Computer Program to Calculate the Concentration Histories and Some Air Quality Related Quantities in a Multi-Chamber System," *Report 18*, Institute of Energy Engineering, Helsinki University of Technology, Espoo, Finland, 1986.

[2] Axley, J., "Progress Toward a General Analytical Method for Predicting Indoor Air Pollution in Buildings," *Indoor Air Quality Modeling Phase III*, Report NBSIR 88-3814, National Bureau of Standards (now National Institute of Standards and Technology), Gaithersburg, MD, July 1988.

[3] Feustel, H. E. and Raynor-Hoosen, A., Eds., "Fundamentals of the Multizone Airflow Model-COMIS," *Technical Note AIVC 29* (Related Project), Air Infiltration and Ventilation Centre, Coventry, Great Britain, May 1990.

[4] Walton, G. N., "AIRNET – A Computer Program for Building Airflow Network Modeling," Report NISTIR 89-4072, National Institute of Standards and Technology, Gaithersburg, MD, April 1989.

[5] Axley, J. and Grot, R., "The Coupled Airflow and Thermal Analysis Problem in Building Airflow System Simulation," *ASHRAE Transactions 1989*, American Society of Heating, Refrigerating, and Air Conditioning Engineers, Inc., Atlanta, GA, Vol. 95, Part 2, pp. 621–628, June 1989.

[6] Klobut, K., "Calculation of Airflows, Temperatures and Contaminant Concentrations in Multi-Zone Buildings," Licentiate's Thesis, Faculty of Mechanical Engineering, Helsinki University of Technology, Espoo, Finland, April 1991.

[7] Klobut, K., "Distribution of Contaminants in Buildings by Air Recirculation and Other Airflows," *Report B31*, Laboratory of Heating, Ventilating and Air Conditioning, Helsinki University of Technology, Espoo, Finland, May 1991.

[8] Klobut, K., Tuomaala, P., Sirén, K. and Seppänen, O., "Simultaneous Calculation of Airflows, Temperatures and Contaminant Concentrations in Multi-Zone Buildings," *Proceedings*, 12th AIVC Conference on Air Movement and Ventilation Control Within Buildings, Air Infiltration and Ventilation Centre, Coventry, Great Britain, Vol. 3, Sept. 1991, pp. 103–122.

[9] Borresen, B. A., "Thermal Room Models for Control Analysis," *ASHRAE Transactions 1981*, American Society of Heating, Refrigerating, and Air Conditioning Engineers, Inc., Atlanta, GA, Vol. 87, Part 2, 1981, pp. 251–261.

[10] Juslin, K. and Siikonen, T., "Solution Methods for Pipe Network Analysis," *Proceedings*, IAEA/NPPCI (International Atomic Energy Agency; Working Group on Nuclear Power Plant Control Instrumentation) Specialists' Meeting held in Espoo, Finland, Sept. 1983, Symposium Report 41 Nuclear Power Plant Training Simulators, National Research Centre of Finland, Espoo, Finland, 1984, pp. 285–299.

[11] Fanger, P. O., "Introduction of the olf and decipol Units to Quantify Air Pollution Perceived by Humans Indoors and Outdoors," *Energy and Buildings*, Vol. 12, No. 1, pp. 1–6, April 1988.

[12] Wilson, D. J. and Zelt, B. W., "The Influence of Non-Linear Human Response to Toxic Gases on the Protection Afforded by Sheltering-in-Place," Paper presented at the OECD/UNEP (Organization for Economic Cooperation and Development and the United Nations Environment Programme) Workshop on Emergency Preparedness and Response, Boston, MA, May 1990.

[13] Press, W. H., Flannery, B. P., Teukolsky, S. A., and Vetterling, W. T., *Numerical Recipes, The Art of Scientific Computing*, Cambridge University Press & Numerical Recipes Software, 1988.

[14] Myers, G. E., *Analytical Methods In Conduction Heat Transfer*, McGraw-Hill Book Company, 1971.

[15] Sirén, K., Helenius, T., "The Estimation of Concentration Histories in Dwellings in Unsteady Conditions," *Proceedings*, 2nd International Conference ROOMVENT-90 on Engineering Aero- and Thermodynamics of Ventilated Room, Session D1-9, Oslo, Norway, 13–15 June, 1990.

Phil Jones[1] *and Richard Waters*[2]

The Practical Application of Indoor Airflow Modeling

REFERENCE: Jones, P. and Waters, R., **"The Practical Application of Indoor Airflow Modeling,"** *Modeling of Indoor Air Quality and Exposure, ASTM STP 1205*, Niren L. Nagda, Ed., American Society for Testing and Materials, Philadelphia, 1993, pp. 173–181.

ABSTRACT: This paper discusses the application of three-dimensional computational airflow and smoke modeling to building environmental design. It is particularly concerned with the integration of modeling into the design process. The principles of airflow and smoke modeling techniques are discussed in terms of:

- definition of building geometry and boundary conditions,
- skills and resources required to carry out modeling, and
- visualization of results.

The integration of modeling into the design process can be applied at two levels:

- to assist in the development of design solutions at the early concept design stage and
- to assess the design at detailed design stage.

During both stages, close liaison with the design team is essential. It is also necessary to be able to carry out the modeling work in "design time." Results should be of a good visual quality in order to be easily understood by the design team and the client. This paper relates to a range of design projects. In each project, the use of modeling has had a significant impact on the design solution. This paper concludes that computational airflow modeling, if carried out by skilled personnel, can reduce the risk of building failure due to unsatisfactory environmental performance.

KEY WORDS: building simulation, environmental design, airflow, smoke management, computational fluid dynamics (CFD), indoor air

The provision of comfortable, healthy, and safe environments is fundamental to the success of a building. These requirements are becoming of greater importance as concern increases over the indoor environment and as buildings become spatially more complex.

Traditional design techniques do not adequately consider the spatial variation of the environmental parameters, either in naturally ventilated or air-conditioned spaces. In many cases over-engineering, with its capital and running-cost penalties, has been adopted in an attempt to reduce the risk of failure.

In recent years, advanced computational numerical techniques have been used in building design to improve environmental design prediction. No single technique can accomplish all the requirements of design that includes daylighting and acoustics, in addition to the thermal criteria considered in this paper). However, techniques based on Computational Fluid Dynamics (CFD) procedures are increasingly being used to tackle airflow and thermal design problems.

[1] University of Wales College of Cardiff, Welsh School of Architecture, Bute Building, King Edward VII Avenue, Cardiff, United Kingdom, CF1 3AP.

[2] Design Flow Solutions, CBTC, Senghenydd Road, Cardiff, United Kingdom, CF2 4AY.

There are three main areas where CFD modeling can assist the environmental designer:

- **Comfort**—To predict the variation in thermal comfort due to air temperature and air speed. In addition, by simulating the heat distribution, space heating (or cooling) efficiencies can be optimized.
- **Health**—To predict the ventilation effectiveness in relation to the spatial distribution of fresh air. Inadequate air distribution is often associated with "sick building syndrome" (SBS) complaints [*1*].
- **Safety**—To predict the movement of smoke during the development of a fire, for a given smoke-management strategy, and to relate the smoke movement to evacuation routes and times. Also, to predict the spread of contaminants within a space, for example, from chemical process (this area is not discussed in this paper, but the techniques used are similar).

This paper discusses two major applications of three-dimensional computational modeling, namely, airflow and smoke movement prediction to building environmental design. It is particularly concerned with the integration of modeling into the design process.

The paper first summarizes the principles of CFD modeling, then discusses its application to building design, and follows on to describe some of the main design application areas.

Principles of CFD Modeling

Numerical airflow modeling is based on solving a set of partial differential equations that describe the variation of velocity, temperature, pressure and turbulence parameters, and sometimes contaminant concentration, within a prescribed space. These parameters are calculated at discrete points throughout the space. Most models are generally based on the same computational procedures [*2,3*].

The model used in this paper was a three-dimensional cartesian model based on the finite volume approach. It used a fixed viscosity turbulence model that assumes a constant viscosity throughout the space. This approach has been used by a number of workers in the building simulation field for predominantly naturally ventilated spaces [*3*].

The success in the application of airflow models is largely dependent on the suitability of the model and the skills of the operator in dealing with the following building-related aspects:

(1) **Geometry**—This involves the definition in sufficient detail of the geometry of the space and its contents, and prescribing a sufficient number of calculation points for describing the pattern of airflow. There are practical limits on detail because the more calculation points that are used, the greater will be the computer storage required and the longer the time to achieve a solution.

(2) **Boundary conditions**—This involves the definition of sources of heat and mass transfer within the solution domain, including heat transfer at surfaces, air inlet and outlet at vents or windows, and the heat and air delivered and distributed from mechanical systems. In order to describe these boundary conditions, a set of submodels must be included in the airflow model that may be relatively simple or complex, depending on what is appropriate to the application. These include:

- radiation models to account for surface-to-surface heat transfer or for solar gains,
- surface heat transfer models to account for heat loss from, or gain to, the fabric due to external conditions and thermal capacity effects;
- ventilation models to predict airflow through windows and vents, that will require pressure/volume flow-rate relationships depending on the size and nature of the opening; and

- models for describing the dynamic performance of mechanical systems for heating/cooling ventilation and smoke control.

Once a solution has been obtained, it is essential to have suitable post-processing graphics in order to provide visualization of the results in a form suitable for communicating to other members of the design team.

Design Application

The aim of CFD modeling is to predict the movement of air and smoke and the distribution of heat in building spaces. This must be carried out by suitable skilled personnel, in "design time" (that is, to provide results within the time-scale required by a design-team) and within reasonable cost limits.

When considering the application of CFD modeling as part of a design, the following organizational issues must be considered:

(1) **Personnel skills**—In defining both the geometry and boundary conditions for a specific simulation and interpreting the results, a considerable amount of knowledge, experience, and judgement is required, relating to both building design and the operation of the numerical airflow models (and an understanding of the assumptions and approximations that they use). Most principal users of CFD computer models within the building design profession are currently at Ph.D. level.

(2) **Design time "turn-around"**—For modeling to be of use as a design tool, it must be able to be carried out in design time. In many cases, this may be the main limitation on the level of detail applied to a particular project. The environmental designer should assess the appropriate level of detail for a project in order to be able to operate within design time requirements.

There are two stages in the design process where the application of modeling is required, namely:

(1) **Concept design**—To explore the implications of design options—this is carried out during the early stages of a design and in close collaboration with the design team. The architect should liaise with the environmental designer at concept design stage in order to explore basic strategies. Figures 1, 2, and 3, that are discussed in the following sections, are examples of the type of simulations that might be quickly carried out during the early part of a design; in the example series of simulations presented in Figures 1, 2, and 3, design options for naturally ventilated spaces are considered.

(2) **Detailed design**—To test a proposed design—this would usually be carried out during the detailed design stage and ideally following from the concept design. The purpose of this simulation would be to consider the building in greater detail in order to fine-tune the design. It could also apply to investigating an existing building that may exhibit environmental problems. Figures 4 and 5, that are discussed in the following sections, are examples of detailed design simulations for air and smoke movement in atria.

A cost analysis of the use of CFD modeling as part of the design process is outside the scope of this paper. However, costs should be relatively small in comparison with physical scale modeling. In many cases, the costs can be recovered by the more accurate prediction of engineering requirements, for example, reducing equipment sizing and identifying problems at an early stage in the design, that could be costly to correct at a later date.

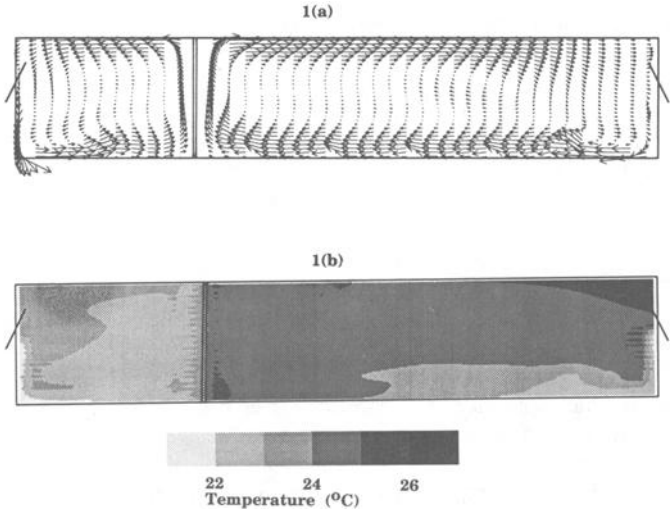

FIG. 1—*Vertical section through two offices, the left is 4.5 m deep and the right is 11.5 m deep. The conditions are for a warm summer day, external air temperature of 21°C, with windows open on external walls. Fig. 1(a) shows the pattern of air movement. Fig. 1(b) shows the air temperature contours. Office depths deeper than about 6 m are difficult to cool by natural ventilation.*

Application Areas

The range of application areas for CFD applied to the thermal and air movement aspects of environmental design is extensive. Some of the current mainstream design application areas are discussed as follows.

Natural Ventilation

Many modern buildings employ a natural ventilation strategy in order to promote energy efficiency, health, and to reduce capital costs. This is an ideal application area for CFD as the internal environmental conditions are very much related to the spatial arrangement and its interaction with external conditions. CFD airflow modeling can explicitly simulate this type of situation.

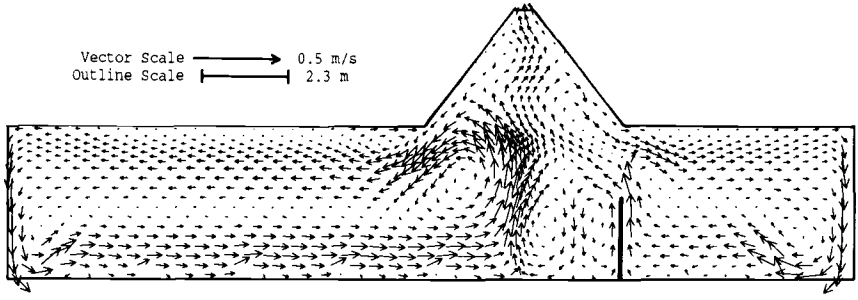

FIG. 2—*Vertical section through an open-plan area, with work zones on either side of a central atrium, showing patterns of air movement. The space is naturally ventilated with openings in the two external side walls and in the atrium roof. The stack effect developed in the atrium is used to ventilate the relatively deep plan space to the left and the narrower plan space to the right.*

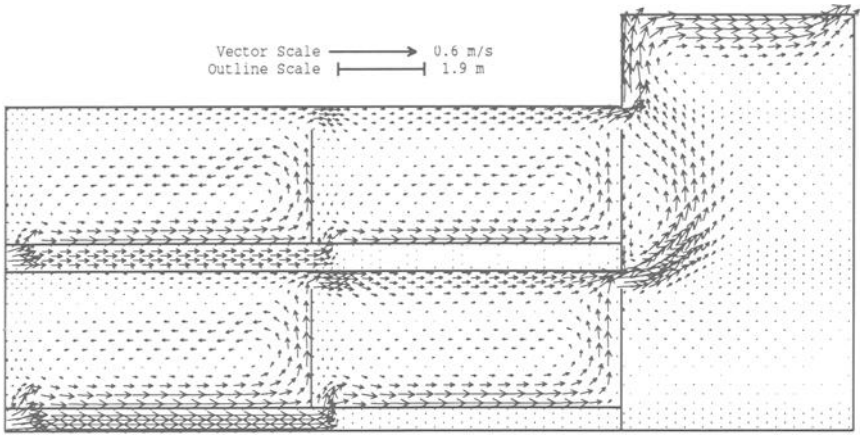

FIG. 3—*Vertical half-section through a two-story office with a central atrium, with symmetry assumed about the center of the atrium. The building is naturally ventilated, and the air-flow pattern shows air being drawn in from outside through vents to the floor voids, thus reducing noise break-in from outside. The stack effect in the atrium draws air from the offices, and exhausts it at high level in the atrium. The under floor delivery allows the partitioning of the space.*

Natural ventilation is traditionally associated with narrow-plan offices, where no worker is further than about 6 m from a window. As the plan gets deeper, the internal space becomes difficult to ventilate and it can suffer from a buildup of internal heat gains. Figure 1 presents a vertical section of adjacent 4.5 and 11.5 m width offices for summer conditions. The wider plan office suffers from high temperatures in the inner zone.

If the work spaces can open onto a central atrium, then the stack effect developed in the atrium can be used to draw air through the deeper plan spaces, thus allowing natural ventilation of deeper plan buildings. Figure 2 presents an example of a naturally-ventilated building with work spaces on either side of an atrium. Conditions are for summertime ventilation. It is important to size the windows and to provide variable opening control to allow for both winter and summer ventilation requirements.

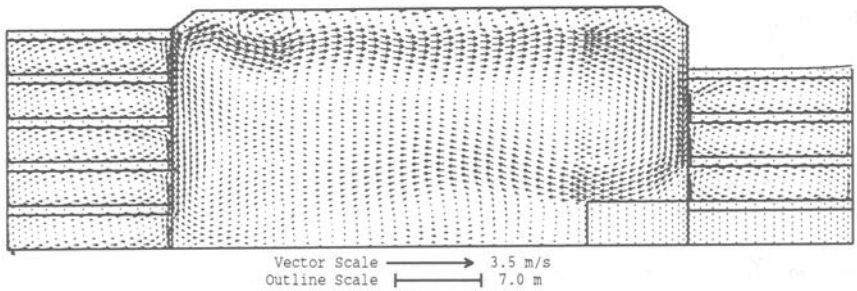

FIG. 4—*Vertical section through a five-floor office building with a large central atrium. The air flow pattern is shown for a winters day, with an external air temperature of 5°C. There is some infiltration through gaps around windows in the external walls and around vents in the atrium roof. There are openable louver windows between the offices and the atrium. Air flows from outside into the offices through to the atrium and out through the atrium roof. The overall ventilation rate was predicted to be 0.15 ac/h for the whole building with 0.5 ac/h in the offices.*

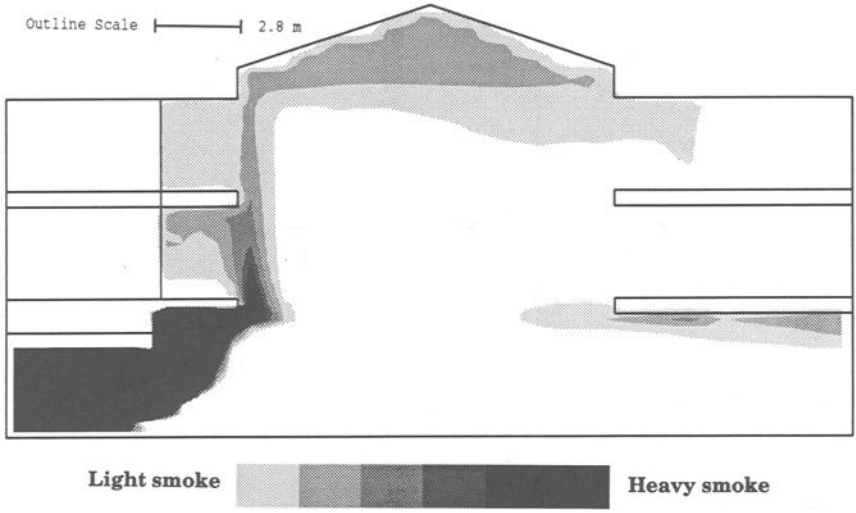

FIG. 5—*Vertical section through the center of a three-story office block with a medium-sized central atrium. A fire has developed over a period of 4 min in the office on the ground floor. Smoke rises up through the atrium where it is mechanically exhausted through a duct around the edge of the atrium roof. Smoke entrains into the upper balconies and travels under the lower balcony to the opposite side of the atrium (there are no smoke channels or curtains under the balconies).*

Two problems associated with the design of natural ventilation, as in the previous example, are external noise break-in through open windows and the need for open plan spaces to allow airflow through the building. Solutions to these problems can be explored with CFD modeling. Figure 3 presents a section through a two-level atrium office (with a symmetry axis about the center of atrium) for summer conditions. Air is drawn in through the floor void by the natural stack effect generated in the atrium. This method of air delivery can reduce the effects of external noise and allow for some degree of internal partitioning.

Figure 4 presents a detailed design study of an office building with a large central atrium [*4*]. Again, the stack effect in the atrium is used to draw air through the 14-m deep offices. Occasions of overheating occur at offices on higher levels where the stack effect, and consequently the ventilation rate, is reduced.

Air Conditioning

CFD modeling can be readily applied to the prediction of air movement, heat distribution, and ventilation effectiveness in air-conditioned offices [*5*], auditoriums, airport terminals, industrial buildings, and so on. Room air distribution is rarely considered in detail in the design process, especially in relation to room furnishing, room scenery, and complex spatial geometries. Airflow modeling can be used to design for adequate amounts of fresh air to reach the occupied region of a space without causing discomfort from drafts of too high or too low an air temperature.

CFD can also be used to consider hybrid situations, that employ a mix of air-conditioning and natural ventilation. For example, a deep plan office might use window opening at the perimeter and mechanical ventilation in the inner zone.

Smoke Movement

In complex buildings, for example, buildings with atriums, the smoke ventilation strategy in the event of a fire can have a major influence over the building design. Smoke movement can be simulated in fire situations, for natural or mechanical smoke-extract systems. The fire can be developed with time, smoke ventilators opened or mechanical smoke-extract fans switched on at the appropriate time, and smoke curtains or shutters activated. The simulation can examine the smoke situation at any time during the fire development and the results can be related to evacuation strategies. Figure 5 presents a section through a three-dimensional time dependent simulation of smoke movement in an office building with a central atrium. The smoke contours relate to a time 4 min after the start of the fire. The smoke spreads from the office into the atrium office building with an atrium. Smoke-extract fans extract smoke from the atrium roof. The smoke can be seen to entrain into the upper balcony areas and also "wrap" around the ground floor level of the atrium under the first floor balcony. This illustrates the importance of being able to explicitly model the geometry of the space for this type of modeling.

External Wind

So far, the discussion has been concerned with the application of CFD to internal air and smoke movement. CFD can also be used to predict the effect of wind around buildings. There are two areas where the simulation of wind effects around buildings are of importance. The first is the simulation of wind in relation to external comfort in the vicinity of pedestrian routes, external spaces around buildings, and external parts of the building such as balconies and roof gardens. The second application area is in the prediction of wind induced pressures around the envelope of the building, especially related to ventilation openings and smoke vents. Wind effects can counteract design strategies based on "natural" buoyancy-induced air or smoke extract systems and can cause cross-contamination from flues, cooling towers or exhaust louvers to ventilation openings or fresh air supply louvers.

Validation

In order to promote the use of CFD modeling as part of the design process, the modeling techniques must be continually validated. There are three levels of validation that have been applied to the modeling work discussed in this report.

(1) **Design validation**—This involves the validation of models when used in a design, against simple design tools and empirical relationships; for example, equations for predicting mean room air velocity in a room [2]. This should be carried out on every project and is the main reason why models should be used by experienced building environmental designers. This procedure also acts as a check to ensure that the model has been correctly set up. CFD procedures should agree with design tools. Their main role is to provide additional and more detailed information rather than a different kind of information.

(2) **Qualitative validation**—Comparisons have been carried out with smoke movement tests on full-scale buildings and scale models. For example, the simulation in Fig. 5 has been favorably compared to measurements of air movement in the atrium space as measured using neutral-buoyancy balloons [*4*]. The simulation in Fig. 5 has been compared favorably to physical scale modeling of smoke movement (unpublished design work).

(3) **Quantitative validation**—The results from CFD simulations have been compared to measured values of air speed and air temperatures in real buildings. Again, the atrium of Fig. 5

has been the subject of measurement and modeling comparisons with regards to air temperatures, air speeds, and ventilation rates [*4*]. Other validation work has been carried out on industrial buildings, using pressurization measurements to establish air leakage characteristics of the building that can then be used to predict ventilation rates and internal conditions, and to compare with simpler zonal airflow models [*6*].

Conclusions

Numerical airflow/smoke models can be used to develop and test design solutions at acceptable costs and within "design time," provided that the work is carried out by personnel experienced in the use of CFD techniques and environmental design.

Airflow and smoke movement models have the advantage that:

- they can take account of the specific geometry of the space and its contents, that can have a major influence on air or smoke movement;
- allow designers to visualize complex situations and indicate problem areas so that problems can be corrected at an early stage in the design and at minimum cost. They can improve design, allow for innovation, reduce over-engineering, and reduce costs in general. They can be used to help explain to regulatory authorities the implications of certain design innovations;
- simulations can be carried out in design time, providing quick feedback of a range of options to the design team; and
- costs are relatively low.

However, CFD simulations of buildings need to be carried out by specialists if the results are to be of any use. These specialists need to understand:

- the design process, timescales, and areas of responsibility;
- building physics, fabric, services, and environmental criteria; and
- CFD techniques—It is also essential to have source code to work with as most complex buildings require a unique set of boundary conditions, that general-purpose CFD codes can not always satisfy.

The accuracy of the results is largely determined by the skills of the environmental designer in setting up the problem, the capabilities of the particular code, and the approximations and assumptions made with regards to the boundary conditions and the spatial definition. The simulations presented in this paper have shown that where comparisons with measurements have been made, the results have been favorable.

Acknowledgment

The simulations reported in this paper were carried out using the Computational Fluid Dynamics computer models DFS-AIR and DFS-SMOKE, that are the property of Design Flow Solutions, UK.

References

[1] Jones, P. J., "Office Environments and Sick Building Syndrome," *Memorandum to the Environmental Committee on Indoor Pollution, HMSO*, Vol. 2, 1991, pp. 360–365.

[2] Jones, P. J., Whittle, G. E., *Airflow Modelling Review Project*, Two Volumes, Dept. of Energy, Crown Copyright, 1990.

[3] Jones, P. J., Whittle, G. E., "Computational Fluid Dynamics for Building Air Flow Predictions—Current Status and Capabilities," *Building and Environment*, Vol. 27, No. 3, 1992, pp. 321–338.

[4] Jones, P. J., Whittle, G. E., *Gateway II Atrium Building—Airflow Modelling, Dept of Energy (ETSU S 1323)*, Crown Copyright, 1992, p. 10.

[5] Jones, P. J., "Room Air Distribution and Ventilation Effectiveness in Air Conditioned Offices," *Proceedings*, 5th International Conference on Indoor Air Quality and Climate, Vol. 4, Toronto, Canada, 1990, pp. 133–138.

[6] Jones, P. J., Alexander, D. K., and Powell, G., "The Simulation of Infiltration Rates and Air Movement in a Naturally Ventilated Industrial Building," *Proceedings*, 12th AIVC Conference, Ottawa, Canada, Sept. 1991.

Erich Panzhauser,[1] *Ardeshir Mahdavi,*[1] *and Alfred Fail*[2]

Simulation and Evaluation of Natural Ventilation in Residential Buildings

REFERENCE: Panzhauser, E., Mahdavi, A., and Fail, A., **"Simulation and Evaluation of Natural Ventilation in Residential Buildings,"** *Modeling of Indoor Air Quality and Exposure, ASTM STP 1205*, Niren L. Nagda, Ed., American Society for Testing and Materials, Philadelphia, 1993, pp. 182–196.

ABSTRACT: Natural ventilation comprises various systems such as infiltration and exfiltration (for example, through cracks, leakages), window ventilation, as well as shaft ventilation. A considerable number of buildings rely exclusively on natural means for ventilation. This underscores the importance of natural ventilation systems for indoor air quality. Nevertheless, few generally accepted design rules and codes are available to assist the designer in the task of dimensioning and control of natural ventilation systems. The successful performance of most natural ventilation systems rely on occupants' behavior. However, the computer-aided simulation of the performance of these systems could support the designer in creating the necessary framework for appropriate behavioral patterns. This could be achieved through properly dimensioned, constructed, and located window and shaft systems while responding to specific geometrical configurations and climatic situation of the building as well as to the health- and comfort-related occupancy requirements. Based on mathematical modeling and long-term empirical studies of residential buildings in Austria, a simulation model was developed to predict the air flow rates and, thus, the air exchange rates between indoor rooms and exterior environment. The comparison of the field measurements with the corresponding simulation results showed an encouraging correlation.

KEY WORDS: natural ventilation systems, infiltration, window and shaft ventilation, air change, modeling ventilation

A considerable number of buildings (especially residential buildings) rely exclusively on natural means (infiltration and exfiltration as well as window and shaft ventilation) for ventilation and air exchange. Nevertheless, few generally accepted design tools and related codes are available to support the design of natural ventilation systems. The successful performance of most natural ventilation systems rely on occupants' behavior. However, the computer-aided simulation of the performance of these systems could support the designer effectively to create the necessary framework for appropriate behavioral patterns. This could be achieved through properly dimensioned, constructed, and located window and shaft systems, while responding to specific geometrical configurations and climatic situation of the building, as well as to the health and comfort related occupancy requirements. This paper presents the empirical and theoretical background of a design supporting simulation model (LUFT) for predicting the air flow rates in naturally ventilated buildings.

[1]Professor and university assistant, respectively, Institut für Hochbau, Technische Universitat Wien, Karlsplatz 13, A-1040 Vienna, Austria.

[2]Associate professor, Carnegie Mellon University, Center for Building Performance and Diagnostics, Department of Architecture, Pittsburgh, PA 15213-3890.

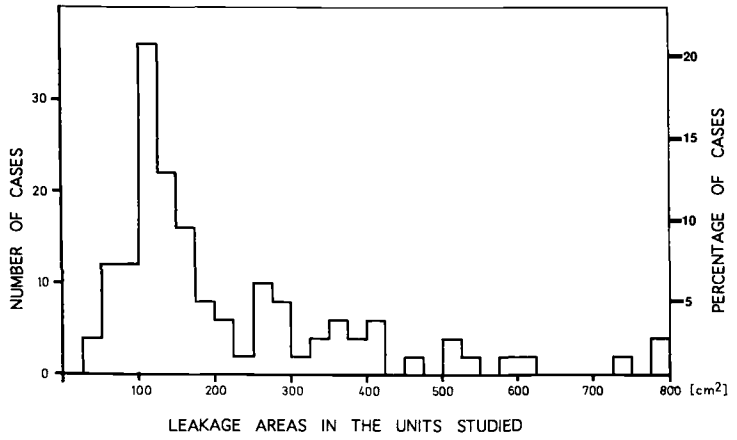

FIG. 1—*Statistical distribution of the empirically determined leakage areas ("A_4") in about 100 residential units in Austria.*

Empirical Background

To gain an original understanding of the indoor air quality of naturally ventilated residential buildings in Austria, extensive empirical studies were conducted [*1–4*]. The main motivation behind these studies was the problem of design methods for providing an adequate fresh air rate to indoor rooms, for pollutant dilution, and humidity control.

For the majority of the long-term measurements, the "constant gas emission method" was applied. Short-term measurements were carried on based on the "decreasing gas concentration method." In a large number of cases, the "pressure method" was used as well [*5*]. As an example of the results of these extended field measurements, Fig. 1 shows the statistical distribution of the empirically determined leakage areas in residential units. The air leakage areas "A_4" (the effective leakage area derived for a indoor/outdoor pressure differential of 4 Pa, [*6*]) were found to vary considerably between 50 cm^2 and 900 cm^2 in residential units (average area = 85 m^2 with a standard deviation of ± 25 m^2).

A strong correlation was found between measured leakage areas and air exchange rates (Fig. 2). However, in specific cases, significant deviations from this correlation can be observed. These deviations are mainly a consequence of special building geometries (for example, layouts with or without potential for cross ventilation) and topographic conditions, or both (for example, shielding effects of buildings).

From the measurements of the air exchange rates (due to air infiltration) in habitable rooms (Fig. 3) the following conclusions can be derived:

(1) In general statistical terms, air infiltration is not a function of the age of the building, but depends on building construction type, maintenance of the windows, and the effectiveness of shaft ventilation.

(2) Air infiltration, in massive constructions (with well-maintained wood windows) in winter ($\Delta t = 20 \pm 2$ K), allows air exchange rates of about 0.31 ± 0.07 h^{-1}. Given a complementary window ventilation (in accordance with typical occupant's window ventilation patterns observed in Austria) and a moderate moisture production, this value would provide sufficient humidity control [*1*].

(3) Air infiltration, in massive constructions with effective shaft ventilation, as well as in wood constructions in winter, allows air exchange rates of about 0.62 ± 0.07 h^{-1}. In buldings

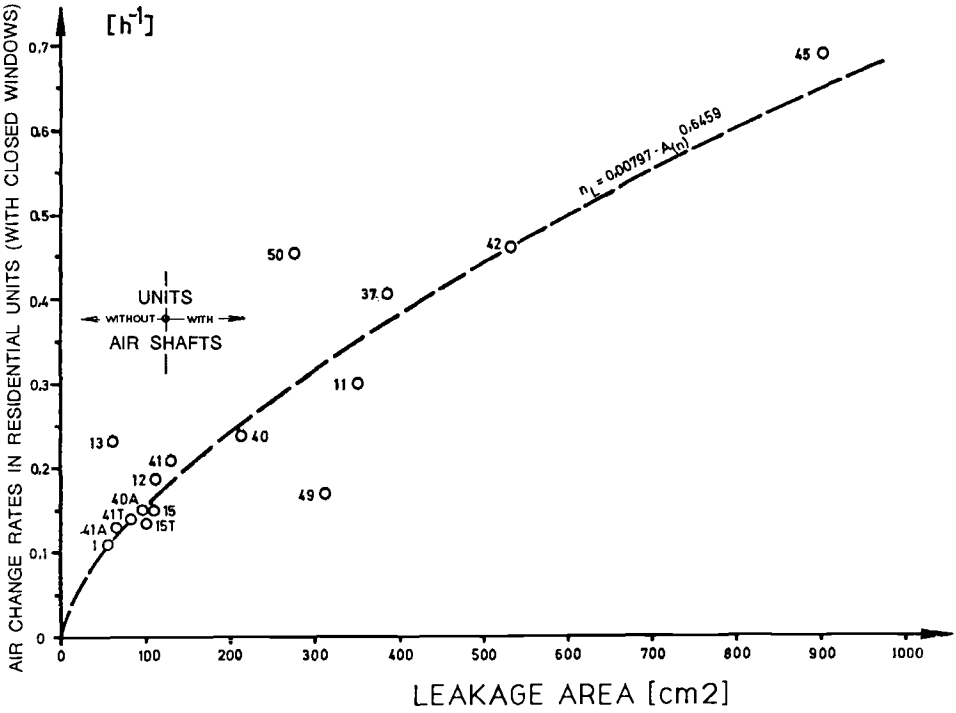

FIG. 2—*Correlation between measured leakage areas and measured air exchange rates (measurements under winter conditions; temperature difference = 20 K, wind velocity = 2 m · s^{-1}).*

with this level of air exchange, moisture is rarely a problem. However, in case of buildings in exposed locations and strong winds, both draft and room temperature drops may occur.

(4) Air infiltration, in massive constructions with very tight windows in winter, allows air exchange rates of only about 0.15 ± 0.07 h^{-1}. In these buildings, insufficient humidity control and insufficient dilution of air pollutants must be expected, even in the units with a window ventilation frequency typical for most occupants.

Empirical investigations of the effectiveness of the shaft ventilation systems (with no dedicated air intake ducts), and their contribution to the total air exchange, showed that, in units with shafts (for example, in centrally located bathrooms), the fresh air rates do not reach the expected calculation-based values (Fig. 4). Apparently, the traditional approach of dimensioning of shafts, based on building codes or classical technical literature (for example Ref *7*), does not necessarily guarantee the expected ventilation rates. Although a number of parameters can cause poor shaft performance, in-depth analysis of the measurement results [*1*] showed that the air flow resistance through the building enclosure has the most important effect on the effectiveness of shaft ventilation.

Empirical studies of the window ventilation showed the importance of window ventilation regulating devices (for example, fixing devices for operable window sash). As an interesting example, Fig. 5 shows the measured air volume flow through a window (length = 1.1 m, height = 1.45 m) equipped with a fixing device that allows for 12 different opening positions. Position 0 means window is closed. Position 12 corresponds to a maximum slot width of 14 cm. Opening Positions 1 to 12 correspond to geometric leakage area from 0.03 m^2 to 0.36 m^2. Measurements were carried

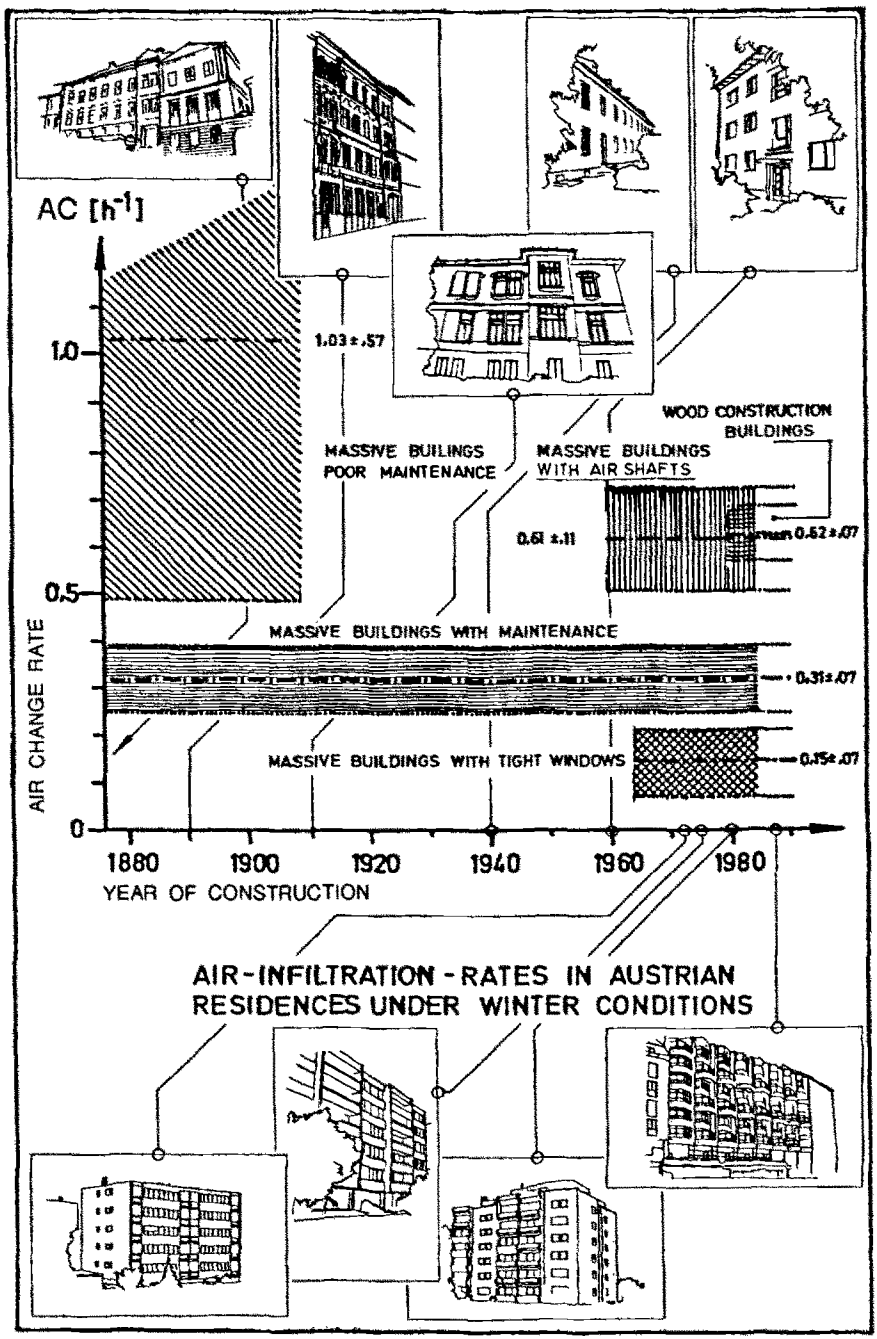

FIG. 3—*Air infiltration rates in Austrian residential buildings (winter conditions).*

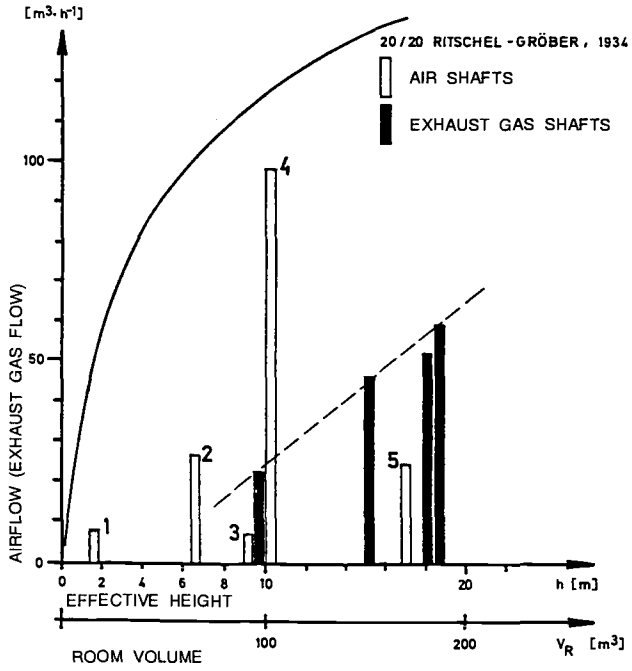

FIG. 4—*Comparison between the measured and calculated volume flows for rooms with shaft ventilation (since the heating system was shut down during the measurements, the mentioned exhaust gas shafts functioned similar to the ordinary air shafts).*

out in a room with one window under winter conditions with no wind influence. This figure demonstrates that the fresh air flow into the room can be controlled more effectively by changing a tilt and turn window into an adaptable window, using a simple fixing device.

The above-mentioned empirical studies of infiltration, as well as window and shaft ventilation, show the complex pattern and some interdependencies of the involved parameters of the natural ventilation systems. This offers a suitable basis for the critical study of some classical calculation procedures, as well as the further development and validation of more advanced algorithms.

Model Description

Based on technical literature [*6,8–10*], mathematical modeling, and empirical studies, a simulation model was developed to predict the air flow rates and, thus, the air exchange rates between indoor rooms and exterior environment. It was designed to assist the designer in the task of dimensioning and control of natural ventilation systems.

Mathematical Formulation

The calculation of air exchange due to infiltration is based on an approach formulated in [*6*]

$$V_t = A_4 3^{-1}(gh\Delta T/T)^{0.5}(1 + R/2)\{1 - X^2/(2 - R)^2\}^{-1.5} \quad (1)$$

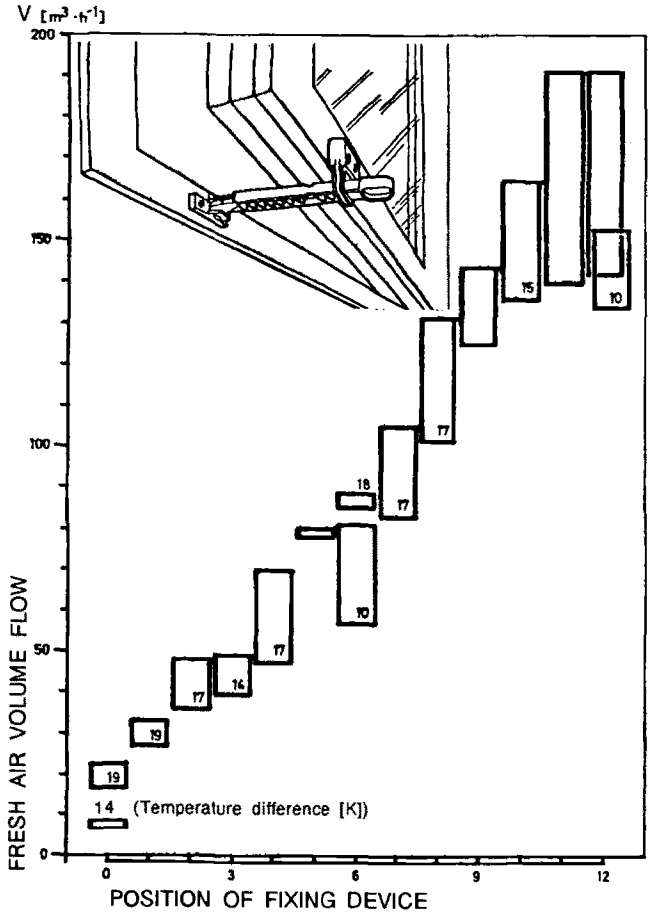

FIG. 5—*Measured air volume flow through a window (length = 1.1 m, height = 1.45 m) depending on the position of a fixing device. This device has 12 opening positions. Position 0 means window is closed. Position 12 corresponds to a maximum slot width of 14 cm (measurements in a room with one window under winter conditions with no wind influence).*

where

V_t = volume flow due to the stack effect, $m^3 \cdot s^{-1}$,
A_4 = effective leakage area, m^2,
g = acceleration of gravity, $m \cdot s^{-2}$,
h = effective height, m,
ΔT = inside-outside temperature difference, K, and
T = inside temperature, K.

R (the fraction of leakage in the floor and ceiling) is given by

$$R = (A_c + A_f)/A_4 \tag{2}$$

where

A_c, A_f = effective leakage areas of ceiling and floor, m^2.

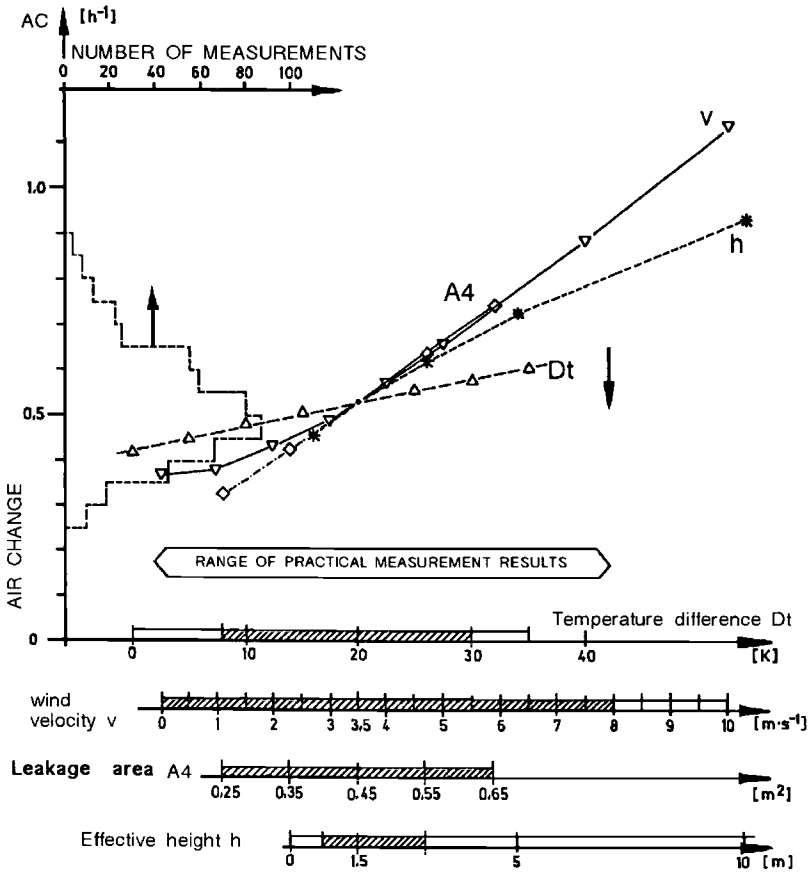

FIG. 6—*Comparison of calculated infiltration-based air change values and statistical distribution of about 600 measured air change values in a residential building (under winter conditions).*

The effective leakage distribution parameter X is given by

$$X = (A_c - A_f)/A_4 \tag{3}$$

The volume flow V_w (in $m^3 \cdot s^{-1}$) due to the wind effect is given by

$$V_W = A_4 v C_A (1 - R)^{1/3} [\alpha \cdot (H_c/10)^{\nu}/\alpha_m (H_m/10)^{\nu m}] \tag{4}$$

where

C_A = generalized shielding coefficient,
α, ν = terrain class constants for the buildings site,
α_m, ν_m = terrain class constants for the measurement site,
H_c = height of the ceiling above terrain, m, and
H_m = height of wind measurement point above terrain, m.

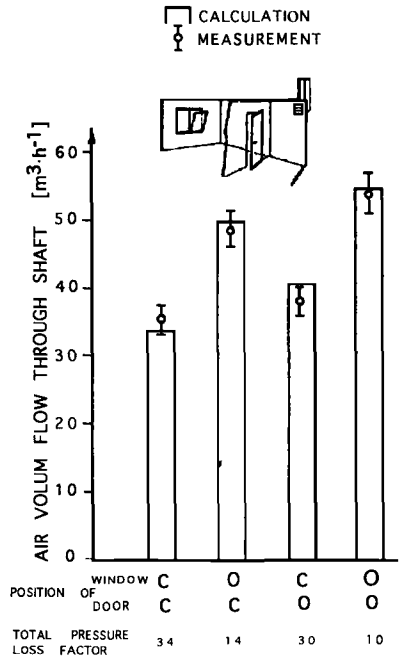

FIG. 7—*Measured versus calculated values for air volume flow in the shaft of a residential unit (O, window/door is open; C, window/door is closed).*

The calculation of the volume flow V_s (in $m^3 \cdot s^{-1}$) due to the shaft ventilation is principally based on Ref *8*. However, modifications to this basic model were necessary to account for the pressure loss effects due to the infiltration through the window and door slots

$$V_s = A_s[(\rho_a \cdot 2 \cdot g \cdot H_s \Delta T/T + \rho_a(v_c^2 c_{pi} - v_s^2 C_{pa})]/\rho_i(\Sigma\zeta_j + \lambda \cdot l/d_H)^{0.5} \quad (5)$$

where

A_s = shaft cross section, m^2,
ρ_a = density of outside air, $kg \cdot m^{-3}$;
ρ_i = density of inside air, $kg \cdot m^{-3}$;
H_s = effective height of the shaft, m,
v_c = wind velocity at the ceiling level, $m \cdot s^{-1}$;
v_s = wind velocity at the head of the shaft, $m \cdot s^{-1}$;
c_{pi} = pressure coefficient for interior space,
c_{pa} = pressure coefficient at the head of the shaft,
ζ = pressure loss factor (defined in fluid dynamics as the dimensionless quotient of pressure loss or pressure difference Δp due to a resistance and the "undisturbed" fluid pressure q),
λ = friction factor (derived from mean shaft roughness, k_m, mean air velocity, and hydraulic diameter d_H);
l = flow distance in shaft, m; and
d_H = hydraulic diameter, m.

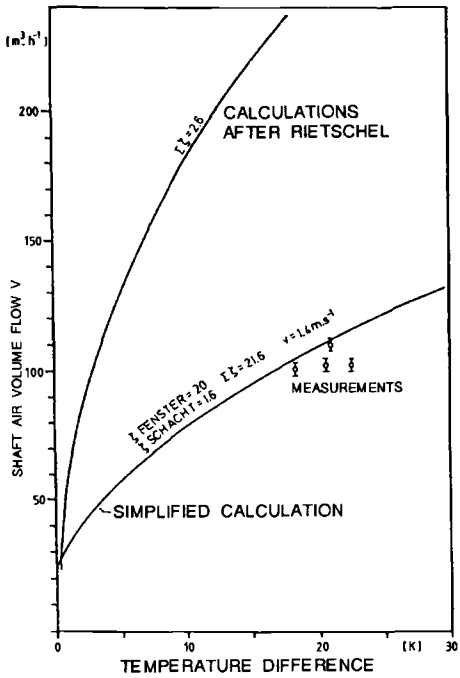

FIG. 8—*The relation between temperature difference and shaft related fresh air volume. Measurements versus calculations, effective shaft height = 10 m, shaft cross section = 0.2 × 0.2 m.*

The calculation of the voume flow $V_{a,t}$ (in $m^3 \cdot s^{-1}$) due to the temperature driven window ventilation is based on an analytical expression in Ref *11*

$$V_{a,t} = A_g 0.142(2gH_w\Delta T/T)^{0.5} \tag{6}$$

where

A_g = area of the window opening(s), m^2, and
H_w = height of the window, m.

The calculation of the volume flow $V_{a,w}$ due to the wind driven window ventilation, is based on the BERNOULLI equation applied for building related air flow processes [*9,12,13*]. It can be derived from the assumption of the balance of the air flows into ($V_{a,w,e}$ in $m^3 \cdot s^{-1}$) and out of ($V_{a,w,o}$ in $m^3 \cdot s^{-1}$) the room

$$V_{a,w,e} = (c_{pae} - c_{pi})^{0.5} v_a A_{ge} \epsilon \tag{7}$$

$$V_{a,w,o} = (c_{pi} - c_{pao})^{0.5} v_a A_{go} \epsilon \tag{8}$$

where

c_{pae}, c_{pao} = pressure coefficient for the facade with incoming/outgoing air flow,
v_a = wind velocity at the mid-height level of the window, $m \cdot s^{-1}$;
A_{ge} = area of the window opening in the facade with incoming air flow, m^2;

A_{go} = area of the window opening in the facade with outgoing air flow, m^2; and
ϵ = contraction coefficient.

Assuming a root-mean-square additive rule, for infiltration and shaft ventilation, the total fresh air volume flow V_{tot} (in $m^3 \cdot s^{-1}$) can be calculated according to the following formula

$$V_{tot} = (V_t^2 + V_w^2 + V_s^2)^{0.5} \tag{9}$$

Similarly, for window ventilation the total fresh air volume flow V_{tot} (in $m^3 \cdot s^{-1}$) can be calculated according to the following formula

$$V_{a,tot} = (V_{a,t}^2 + V_{a,w}^2)^{0.5} \tag{10}$$

Program Description

The simulation program LUFT is structured in terms of two main sections: Program section FUGE calculates the total fresh air volume flow (using the infiltration/exfiltration method) for configurations with or without shafts. Stack effect, wind effect, and shaft effect are considered separately. Program section FENSTER calculates the total fresh air volume flow due to window ventilation (large outlets/inlets). Input data consists surrounding parameters (C_A, α, ν, α_m, ν_m, H_m, ΔT, T), building parameters (A_s, H_w, H_s, A_4, T, A_c, A_f, k_m) and fluid dynamics parameters (c_{pa}, c_{pae}, c_{pao}, ζ). Output data include V_s, V_w, V_t, V_{tot}, AC (for infiltration/exfiltration, shaft ventilation) and $V_{a,t}$, $V_{a,w}$, $V_{a,tot}$, and c_{pi} (for window ventilation).

Comparison of Measurement and Calculation Results

As a general overivew, Fig. 6 shows the comparison of the calculated infiltration-based air change values (for variations of the parameters wind velocity, temperature difference, leakage area, and effective height) and the statistical distribution of about 600 measured values. These measurements were carried out during a two-year period (under winter conditions) in a 85 m^2 residential unit. Given a set of default values (temperature difference = 20 K, wind velocity = 2.5 $m \cdot s^{-1}$, leakage area = 0.04 m^2, and effective height = 1.5 m), calculations were performed for parametric variations of temperature difference (8 to 30 K), wind velocity (0 to 8 $m \cdot s^{-1}$), leakage area (0.025 to 0.065 m^2) and effective height (0.75 to 2.7 m). Figure 6 demonstrates, in general statistical terms, the level of agreement between the calculation results (air change rates) and the statistical distribution of the measurements.

Figure 7 shows both measured and calculated values for air volume flow in the shaft of a residential unit (with wooden frame windows without special sealing) for different configurations of window and door openings. This figure shows a positive correlation between measurements and calculations (the pressure loss factors were determined based on studies in Refs *2*, *14*, and *15*).

Figure 8 shows the relation between temperature difference and shaft related fresh volume. It includes results of both simplified calculations based on program LUFT (with equal indoor and outdoor air densities) and calculations after [7] (applied without air intake flow resistance and air suction effect) as well as a few measured values. As can be seen from this figure, the resistances against the incoming air flow must be taken into consideration for more realistic results.

Figure 9 shows the total fresh air volume flow for a residential unit (90 m^2, wooden frame windows) as a function of various configurations of the openings of one window (effective leakage area for closed window = 0.028 m^2, for tilted window = 0.064 m^2) and two shafts (effective height = 13 m, cross section = 0.12 × 0.12 m). It includes both measured and calculated values. The mean deviation of the measurements from the calculations was 5.6 ± 3.2%.

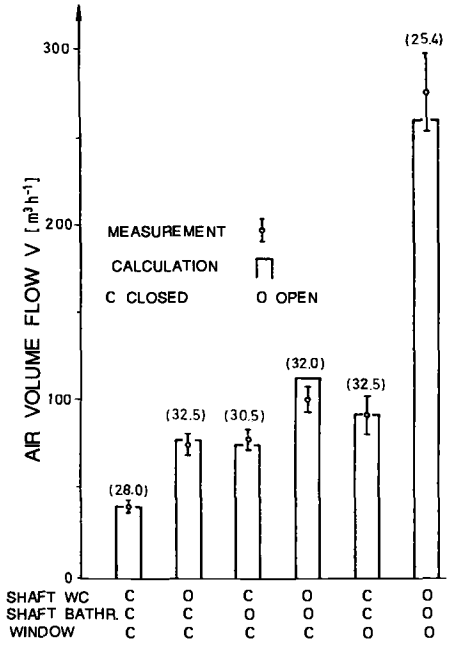

FIG. 9—*Measured and calculated values for total fresh air volume flow for a residential unit as a function of various configurations of the openings of one window and two shafts (wind velocity < 0.2 m · s^{-1}).*

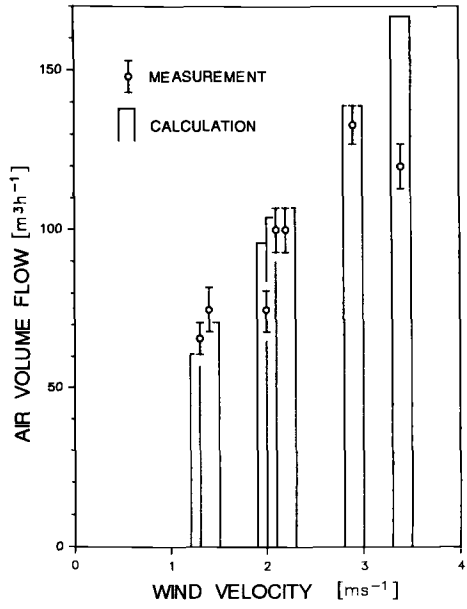

FIG. 10—*Air flow rates in a residential unit due to the cross ventilation as a function of wind velocity (measurements versus calculations).*

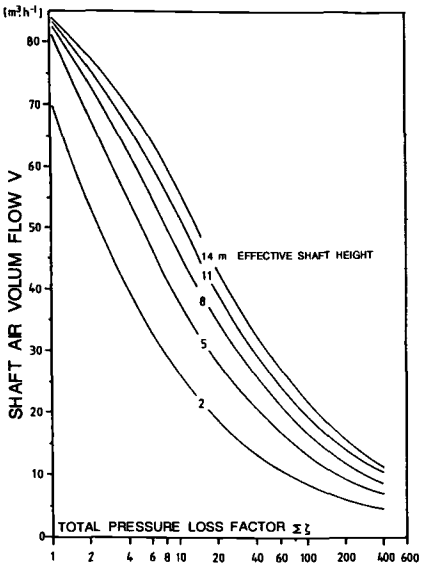

FIG. 11—*Fresh air volume flow as a function of total pressure loss factor and the effective shaft height (based on simulation results using program LUFT).*

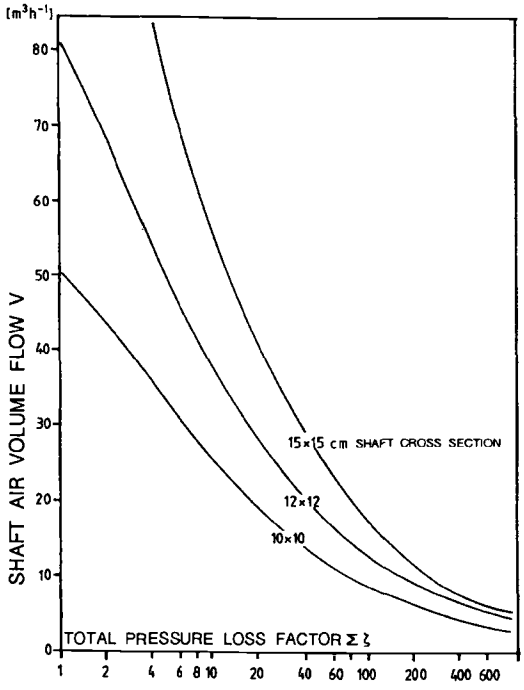

FIG. 12—*Fresh air volume flow as a function of total pressure loss factors and the shaft cross section (based on simulation results using program LUFT).*

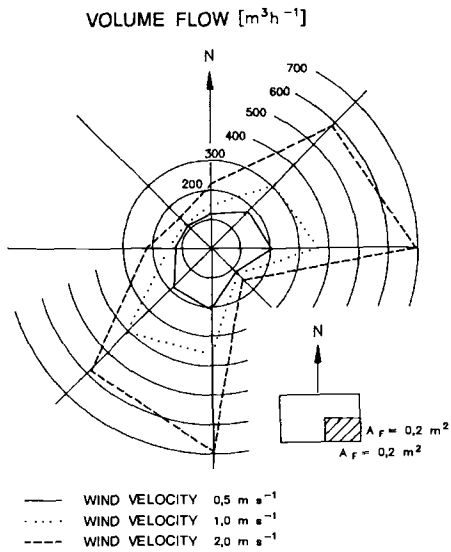

FIG. 13—*Air volume flow in a room due to a (diagonal) cross ventilation as a function of wind direction and velocity (based on simulation results using program LUFT).*

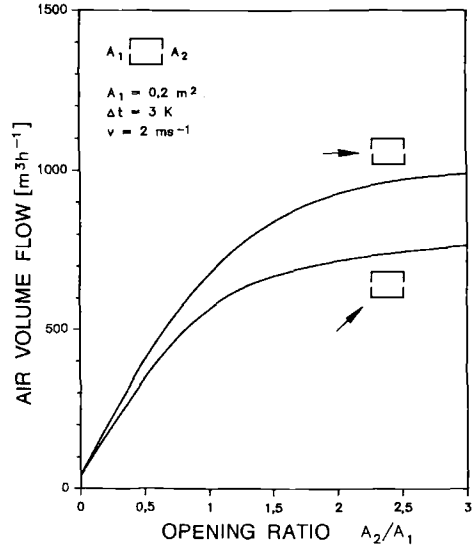

FIG. 14—*Air volume flows in a room as a function of outlet (A2) to inlet (A1) opening ratio for two different wind directions.*

Figure 10 shows the air flow rates in a residential unit due to the cross ventilation as a function of wind velocity. It includes both calculation results and measured values. The southwest facade had an outlet of 0.075 m^2 and the northeast facade had an inlet of 0.022 m^2. The correlation was found to be satisfactory (mean deviation of measurements from the calculations <10%) although default values for pressure coefficients were used.

Parametric Studies

To demonstrate the practical applicability of the simulation program for design purposes, a number of parametric studies were performed. The impact of some of the major parameters of shaft and window ventilation on the effectiveness of the natural ventilation systems was studied.

Figure 11 shows the fresh air volume flow as a function of total pressure loss factor and the effective shaft height (parameters: shaft cross section = 0.12 × 0.12 m, temperature difference = 20 K, wind velocity = 3 $m \cdot s^{-1}$, terrain class = III, wind pressure factor = −0.5, average roughness of shaft internal surfaces = 0.003 m). It demonstrates clearly that in low-rise buildings with very tight envelopes, minimum necessary volume flow rates can not be achieved through natural shaft ventilation. However, Fig. 11 is based on calculation for a 0.12 × 0.12 m shaft cross section. Significantly larger cross sections would allow for higher volume flow rates. Figure 12 demonstrates the importance of larger shaft cross sections and low total pressure loss factors for the effectiveness of natural shaft ventilation.

As an example of parametric studies of window ventilation, Fig. 13 shows the volume air flow in a room caused by (diagonal) cross ventilation as a function of wind direction and velocity. It demonstrates the very large dynamic range of wind-triggered window ventilation and the importance of wind direction for the effectiveness of the system.

The following example (Fig. 14) deals with the effect of different inlet and outlet areas on the air volume flows. It can be seen from this example that by increasing the outlet/inlet opening ratio beyond a certain level, the corresponding volume flows do not increase significantly.

Conclusion

Based on long-term empirical studies on residential buildings in Austria, as well as on mathematical modeling, a simulation program (single-cell model) was developed to support the design and evaluation of natural ventilation systems. The comparison of simulation results and field measurements showed an encouraging correlation. It is intended that the model will be enhanced, both in terms of its general applicability (for example, high-rise buildings and multicell configurations) and its user interface.

References

[1] Panzhauser, E., Fail, A., Haiduk, E., Ertl, H., Schwarz, K., Etrl, T., and Kaderle, A., "Luftwechselzahlen in österreichischen Woghungen," Wien, BMfBuT, 1985.

[2] Ertl, H., Fail, A., Panzhauser, E., Boisits, R., Heiduk, E., and Mahdavi, A., "Natürliche Schachtlüftung, Messung - Beurteilung - Planung," Wohnhabitat Bd. 3, Wien, *Archivum Oecologiae Hominis*, 1987.

[3] Haider, M., Heindel, W., Knötig, H., Mahdavi, A., and Panzhauser, E., "Bedeutung von Pufferräumen," Wohnhabitat Bd. 6, Wien, *Archivum Oecologiae Hominis*, 1991.

[4] Panzhauser, E., Fail, A., Haider, M., Heindel, W., Knötig, H., and Mahdavi, A., "Die Planung der (konventionellen) Fensterlüftung," Wohnhabitat Bd. 5, Wien, *Archivum Oecologiae Hominis*, 1991.

[5] Kronvall, J., "Airtightness - Measurements and Measurement Methods," Swedish Council for Building Research, D 8, Stockholm, 1980a.

[6] Sherman, M. H., "Air Infiltration in Buildings," Lawrence Berkeley Laboratory, LBL-10712, 1980.

[7] Rietschel, H. and Gröber, H., "Leitfaden der Heiz- und Lüftungstechnik," 11, Aufl. Berlin, Springer, 1938.

[8] Hausladen, G., "Wohnungslüftung. Untersuchung der verschiedenen Lüftungsarten bzw. Lüftungspraktiken unter Hygienischen, Bauphysikalischen und Energetischen Gesichtspuntken," *Fortschr. Ber. VDI Zschr.*, Reiche 6, Nr. 73. Düsseldorf VDI-Vlg., 1980.

[9] Sockel, H., "Aerodynamik der Bauwerke," Braunschweig (Viehweg), 1984.

[10] Sherman, M. H. and Grimsrud, D. I., "Infiltration-Pressurization Correlation: Simplified Physical Modeling," LBL-10163, Lawrence Berkeley Laboratory, 1980.

[11] Brown, W. B. and Solvason, K. R., "Natural Convection through Rectangular Openings in Partitions," Part 1: Vertical Partitions, *Int. V. Heat and Mass Transfer 5*, pp. 859–868, 1962.

[12] Wiren, B. G., "Effects of Surrounding Buildings on Wind Pressure Distribution and Ventilation Losses for Single-Family Houses, *Bulletin M85:19*, Part 2: 2-Storey Terrace Houses," The National Swedish Institute for Building Research, 1987.

[13] Wiren, B. G., "Effects of Surrounding Buildings on Wind Pressure Distribution and Ventilation Losses for Single-Family Houses, Part 1: 1 1/2-Storey Detached Houses," Research Report TN:2, The National Swedish Institute for Building Research, 1985.

[14] Esdorn, N. and Rheinländer, N., "Zur rechnerischen Ermittlung von Fugendurchlaßkoeffizienten und Druckexponenten für Bauteilfugen," *Heizung, Lüftung, Klimatechnik, Haustechnik*, Vol. 29, Nr. 3, 1978.

[15] Kronvall, J., "Air Flows in Building Components," Report TVBH-1002, Lund Institute of Technology, Division of Building Technology, 1980b.

Erich Panzhauser[1] *and Ardeshir Mahdavi*[2]

A Computational Model for the Prediction and Evaluation of Formaldehyde Concentration in Residential Buildings

REFERENCE: Panzhauser, E. and Mahdavi, A., **"A Computational Model for the Prediction and Evaluation of Formaldehyde Concentration in Residential Buildings,"** *Modeling of Indoor Air Quality and Exposure, ASTM STP 1205*, Niren L. Nagda, Ed., American Society for Testing and Materials, Philadelphia, 1993, pp. 197–210.

ABSTRACT: Over the last few years, increasing attention has been paid to the problem of indoor air pollution and especially critical indoor formaldehyde concentrations. Some recent developments in the building's interior systems and components (new materials, new furniture elements, and so forth) combined with some features of modern construction technology (for example, air-tight windows and envelopes), has aggravated the risk of potentially hazardous pollutant concentrations. As a practical contribution to the solution of the problem of formaldehyde concentration in Austrian residential buildings, a computer-aided model was developed to simulate the processes of formaldehyde emission and concentration in indoor air. Using this interactive model, the effective concentrations of formaldehyde can be simulated and represented for a variety of input data (emission sources, temperature, relative humidity, air exchange rates, and so forth). This model can be used by building owners, managers, designers, and occupants. To gather the necessary empirical data, a diagnostic unit was constructed to test a number of commonly applied products in the Austrian building market (mainly furniture elements and particle boards).

KEY WORDS: formaldehyde concentration, residential buildings, particle boards, HCHO-emission and absorption test-box, fixed sources and emitters, formaldehyde mass balance

Certain levels of formaldehyde (HCHO) have probably always existed in indoor rooms in residential buildings. However, until 30 to 40 years ago, the main sources of formaldehyde have been combustion processes and the use of detergents and disinfectants, or both. These rather "temporary" formaldehyde emissions occurred in rooms that were normally well-ventilated. As a result, for a relatively long time, no major concern was expressed with regard to possible negative effects of high HCHO concentrations in indoor rooms.

As a consequence of the recent development of new materials and their application in buildings (interior finishes, furniture systems, and so forth), introduction of "continuous" formaldehyde emission sources into the interior spaces has increased. This development, coupled with trends towards more air-tight building enclosures and uncoordinated saving efforts (through the reduction of ventilation heat losses) has aggravated the problem of critical HCHO-concentrations in indoor air.

To address this problem within the context of residential buildings in Austria, studies were conducted with regard to existing HCHO-concentration levels in residential buildings as well as the theoretical foundations for simulation of formaldehyde emission and concentration in indoor

[1]Professor, Institut für Hochbau, Technische Universität Wien, Karlsplatz 13, A-1040 Vienna, Austria.
[2]Associate professor, Carnegie Mellon University, Center for Building Performance and Diagnostics, Department of Architecture, Pittsburgh, PA 15213-3890.

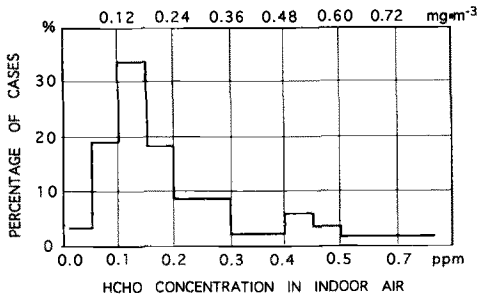

FIG. 1—*Distribution of the measured HCHO-concentration levels in 100 Austrian residential units.*

air. As a result of these studies, a computer-based model was developed. Using this interactive model, the effective concentrations of formaldehyde can be simulated and represented (numerically and graphically, or both) for a variety of input data (emission sources, temperature, relative humidity, air exchange rates, and so forth).

Experimental Studies

To obtain reliable information concerning the existing HCHO-concentrations in residential buildings, measurements were carried out in about 100 residential units [*1,2*]. According to this investigation, higher levels of HCHO-concentration occur mainly in households with smokers, in households with natural gas stoves, in insufficiently ventilated rooms, and in rooms that have been totally or partially refurnished in the five-year period prior to the measurements.

Figure 1 shows the distribution of the measured HCHO-concentration levels. The concentrations in the units that have been the subject of HCHO-related complaints were more than 0.06 mg · m^{-3} in 97% of the cases, and more than 0.12 mg · m^{-3} in 79% of the cases.

A statistical analysis was carried out to investigate possible correlations between the measured HCHO-concentration levels and factors such as outdoor and indoor air conditions (air temperature, relative humidity), natural gas as energy source for cooking purposes, area and volume of formaldehyde emission sources (carpet, furniture components, and so forth), smoking or nonsmoking households, and number of occupants.

In all these cases either no correlation was found or the correlation was of very low significance. The correlation between the measured HCHO-concentrations in the indoor air and the formaldehyde sources, as well as window material (wood, plastic, metal), was found to be of low significance. Through more advanced modeling of HCHO emissions from various sources, it was possible to further investigate the complex relationships between HCHO emission and the environmental factors (temperature of air, building elements and emission sources, and relative humidity) as well as occupant's behavior (window ventilation frequency, occupancy duration, and so forth). Based on the results of this investigation, requirements were formulated with regard to data assessment (products specification, relevant building related configurations, occupant's behavior, and so forth), and simulation procedures were developed for providing the necessary information to occupants, building developers, facility managers, and designers.

Formaldehyde Prediction Model

Through field diagnostics, the existing HCHO-concentration levels can be determined. However, this information is insufficient for the evaluation of pollution levels in indoor rooms under different conditions. For example, from field diagnostics no sufficient basis can be derived for the clarifi-

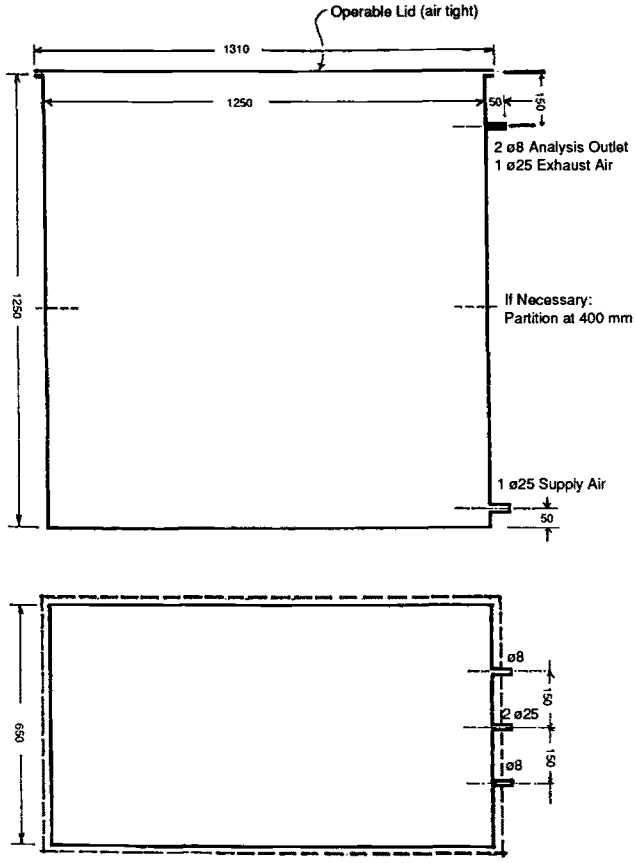

FIG. 2—*Test-box for the determination of the HCHO-emission.*

cation of important questions with regard to the source intensities and for the estimation of the impact of factors such as emission source areas, air exchange rates, and temperature and humidity changes.

To support the professional building related consulting activities concerning the formaldehyde concentration in Austrian residential buildings, a computer model was developed. This model can be used to advise occupants and building developers as well as designers.

Product's Specification

To collect the necessary empirical data for the model (mainly emission characteristics of interior elements and systems), a diagnostic unit was constructed to test a number of commonly applied products in the Austrian building market (mainly furniture elements and particle boards). This unit consists of two measurement boxes with ventilation and heating units, a measurement unit (for the assessment of climatic data and concentration values), and a data processing unit. Figure 2 shows the schematic plan of the HCHO-emission test-box. Figure 3(*a*) shows the arrangement for the measurement of source emission. Figure 3(*b*) shows a two-box arrangement for the measurement of both emission and absorption. Further details of the testing procedure are described in Ref *1*.

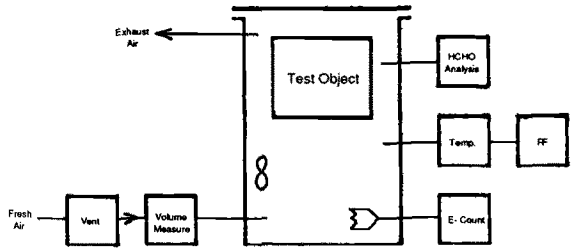

A) 1-BOX PROCEDURE

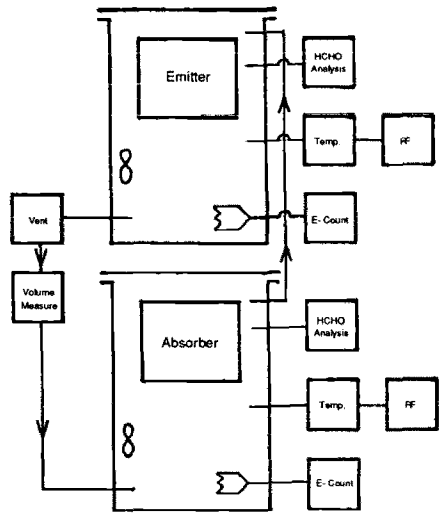

B) 2-BOX PROCEDURE

FIG. 3—*Measurement configurations for HCHO-emission and -absorption processes; (a) arrangement for emission measurement and (b) arrangement for emission and absorption measurement.*

Theoretical Foundation

The theoretical basis for the mathematical models used in the model (formaldehyde emission of sources, relevant data for the case of temperature and water content imbalance, and formaldehyde mass balance) utilizes a number of methods and approaches [*1,3–5*].

A distinction is made between "fixed sources" and "emitters." The HCHO emission from the fixed sources is not a function of the indoor air conditions, but depends only on time. The HCHO emission of the emitters is, however, assumed to be influenced by the indoor room conditions, particularly by its HCHO concentration.

The HCHO mass flow from an emitter into the surrounding room air is a function of indoor air conditions (relative humidity ϕ, temperature T), emitter (moisture content ρ_w, temperature T_K), and its surface (area F, properties specified by χ^*, and the characteristic velocity K). The description of HCHO mass flow from an emitter is based on the following assumptions. (1) The driving force for q is the difference between the HCHO partial pressure p in room air and a "virtual" HCHO equilibrium partial pressure p' in room air under the condition of temperature and moisture equilibrium between emitter and room air. (2) Emitter is considered to be an infinite HCHO source,

thus p is only a function of ρ_w and T_K. (3) q is proportional to F. (4) HCHO is treated as an ideal gas. Thus, p is simply defined as a function of HCHO partial density in the room air ρ, the gas constant for HCHO (R_F) and the room air temperature T

$$p = \rho R_F T \tag{1}$$

Based on these assumptions, the HCHO mass flow due to an emitter can be derived according to the following equation

$$q = F \chi^*(\rho_w, T_K)[p'(\rho_w, T_K) - p] \tag{2}$$

or

$$q = \chi^* \cdot R_F F(p'/R_F - \rho T) \tag{3}$$

χ^* is a factor given by "HCHO-conductance value" χ divided by the gas constant for HCHO (R_F). Thus, given "conductance value"

$$\chi = \chi^*(\rho_w, T_K)R_F, \tag{4}$$

and "equilibrium value"

$$R' = p'(\rho_w, T_K)/R_F, \tag{5}$$

the following mass flow equation can be derived

$$q = \chi F(R' - \rho T) \tag{6}$$

Data for the Case of Temperature and Moisture Imbalance

In the case of temperature and moisture imbalance, experimental data suitable for use in Eq 6 are difficult to obtain. In order to apply the data gained under the conditions of temperature and moisture equilibrium to more general cases, the following approach was selected. First, the concept formulated in Eqs 2 and 6 was compared to an approach for the description of the HCHO mass flow [*3,4*] that is based on the following assumptions. (1) Emitter and room air are in temperature and moisture equilibrium. (2) The driving force for q is the difference between the HCHO partial density ρ in room air and an "asymptotic HCHO partial density" ρ' in room air under the condition of temperature and moisture equilibrium between emitter and room air. (3) q is proportional to surface area, F. (4) The impact of the surface properties of the emitters on q can be described through the factor "characteristic velocity" K.

Based on these assumptions, the HCHO mass flow due to an emitter can be derived [*5,6*]

$$q = K(\phi, T_K)F[\rho'(\phi, T_K) - \rho] \tag{7}$$

According to Ref *5*, the dependency of the asymptotic partial density ρ' on the relative humidity ϕ and the emitter temperature T_K (= T according to Assumption 1) is given by

$$\rho' = \rho'_o \cdot [1 + D(\phi - \phi_o)]e^{-c[1/T - 1/To]} \tag{8}$$

where ρ_o' is the asymptotic HCHO partial density in the room air for the emitter's temperature $(T_K)_o$ and the relative humidity ϕ_o. C ("temperature parameter") and D ("humidity parameter") must be determined experimentally for different emitters. The mass flow formulation in Eq 7 is based on Assumption 1 and assumes that the emitter and the room air are not only in temperature equilibrium but also in moisture equilibrium. Thus, in this equation the term water content ρ_w is not considered. The connection to the more general case of temperature and moisture imbalance is carried out through the sorption term

$$\phi' = \phi'(\rho_w, T_K) \tag{9}$$

The sorption term describes the relationship between ρ_w and ϕ' for a given T_K. Thus, using Eq 9, it is possible to determine for a certain ρ_w and a certain emitter temperature T_K the relative humidity of the room air that is in temperature and moisture equilibrium with the emitter.

For the case of temperature equilibrium between emitter and room air, a limited version of Eq 6 can be formulated as follows

$$q = \chi(\rho_w, T_K)F[R'(\rho_w, T_K) - \rho T_K] \tag{10}$$

Comparing this limited version of the HCHO mass flow formation of Eq 6 with Eq 7, the following relationships can be derived

$$\chi(\rho_w, T_K) = K(\phi', T_K)/T_K \tag{11}$$

$$R'(\rho_w, T_K) = \rho'(\phi', T_K)T_K \tag{12}$$

Based on these relations, it is possible to derive the necessary data for the case of moisture and temperature imbalance from measurements carried out under temperature and moisture equilibrium between the emitter and the room air for the asymptotic partial density ρ' and the characteristic velocity K.

It is important to emphasize that in the right-hand side of Eqs 11 and 12, ϕ' is the relative humidity given by sorption isotherm of the emitter for the emitter's temperature T_K and the emitter's moisture content. ρ_w. Therefore, it does not refer to the actual relative humidity, but to a "virtual relative humidity" of that air, that would be in temperature and moisture equilibrium with the emitter. Taking this into consideration, the following relation can be derived for the equilibrium value based on Eqs 8 and 12

$$R'(\rho_w, T_K) = \rho_o'[1 + D(\phi' - \phi_o)]T_K \cdot e^{-c\{1/T_K - 1/To\}} \tag{13}$$

Formaldehyde Mass Balance

The HCHO partial density in the air is determined through the fixed sources, emitters and the air change. The time-dependent change of the HCHO mass in the room air ($V_F \cdot d\rho/dt$) can be calculated based on the contributions of the fixed sources (with source intensity Q_j), emitters (HCHO mass flow q_i) and the HCHO exhaust due to air change (product of air flow rate, m_L and HCHO partial density in the room air, ρ)

$$V_F \frac{d\rho}{dt} = \sum_{j=1}^{m} Q_j + \sum_{i=1}^{n} q_i - m_L\rho \tag{14}$$

The combination of Eqs 6 and 14 gives

$$V_F \frac{d\rho}{dt} = \sum_{j=1}^{m} Q_j + \sum_{i=1}^{n} \chi_i F_i [R_i' - \rho T] - m_L \rho \tag{15}$$

Equation 15 can be interpreted as a first order linear differential equation for the partial HCHO density ρ in room air

$$V_F \frac{d\rho}{dt} + \left[m_L + T \sum_{i=1}^{n} \chi_i F_i \right] \rho = \sum_{i=1}^{n} \chi_i F_i R_i' + \sum_{j=1}^{m} Q_j \tag{16}$$

Assuming the time constant τ

$$\tau = \frac{V_F}{m_L + T \sum_{i=1}^{n} \chi_i F_i} \tag{17}$$

and the asymptotic partial density ρ_∞

$$\rho_\infty = \frac{\sum_{i=1}^{n} \chi_i F_i R_i' + \sum_{j=1}^{m} Q_j}{m_L + T \sum_{i=1}^{n} \chi_i F_i} \tag{18}$$

Equation 16 can be modified in the following manner

$$\tau \frac{d\rho}{dt} = \rho = \rho_\infty \tag{19}$$

and for constant coefficients

$$\rho = (\rho_o - \rho_\infty) e^{-t/\tau} + \rho_\infty \tag{20}$$

Parametric Studies

Impact of Air Change and "Room Load"

In Austria the particle board class "E1" is considered to be appropriate for the application in furniture and interior finishes. A particle board of this class was examined with the measurement box test. C_{eq} (asymptotic concentration for an air change $AC = 0$) and K (characteristic velocity) were found to be 0.32 mg · m^{-3} and 0.378 m · h^{-1}, respectively. The equilibrium concentration C_s was found to be 0.0756 mg · m^{-3} (that is, <0.12 mg · m^{-3}). The question is whether the application of particle boards of this class would ensure that actual HCHO concentrations in rooms will not exceed certain critical limits (for example, 0.12 mg · m^{-3}).

In order to answer this question, the simulation program was used to predict the C_s values for the following conditions that are typical of many residential units (Table 1).

The simulation results are shown in Fig. 4. Based on these results, the following conclusions can be made. In the case of low fresh air rates (V_F = 12.5 to 25 m^3 · h^{-1}) that occur in rooms with

TABLE 1—*Boundary conditions for the parametric study illustrated in Fig. 4.*

Free Air Volume of the Living Room, V_F	50 m^3
Room temperature, ϑ_R	22.5°C
Relative air humidity, φ_R	45%
Fresh air volume flow, V_L	12.5–100 $m^3 \cdot h^{-1}$
Air change, n_L (= V_L/V_F)	0.25–2 h^{-1}
Total emitter area, F	12.5–100 m^2
Room load, B_R (= F/V_F)	0.25–2.0 m^{-1}

very tight windows, even smaller emitter areas ($F < 50$ m^2, $B_R < 1$ m^{-1}) result in HCHO concentrations considerably higher than the $C_{s,max} = 0.12$ mg $\cdot$ m^{-3}. In the case of higher fresh air rates ($V_F = 25$ to 50 $m^3 \cdot h^{-1}$) that occur in rooms with windows of "normal" tightness, only larger emitter areas ($F > 50$ m^2, $B_R = 1$ m^{-1}) result in HCHO concentrations higher than the $C_{s,max} = 0.12$ mg $\cdot$ m^{-3}. However the resulting concentrations regularly exceed 0.06 mg $\cdot$ m^{-3}.

Based on these observations it can be concluded that the HCHO emitting building components should carry appropriate specifications (C_{eq}, K) necessary for predictive calculations of HCHO concentrations in realistic settings.

Impact of the Moisture Content of the Emitter

As elements of furniture systems or as building components, particle boards are usually in moisture equilibrium with the indoor room air. If this is not the case (for example, due to local water vapor condensation), the simulation program can consider the higher HCHO emission rates

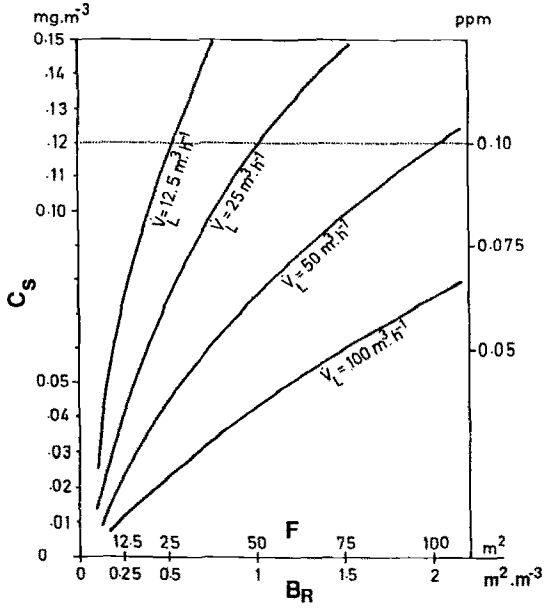

FIG. 4—*Simulated HCHO concentrations in a living room with particle board-based furniture.*

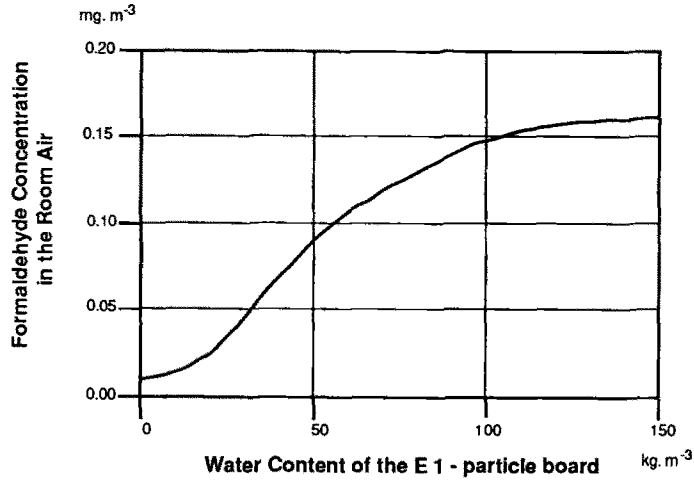

FIG. 5—*HCHO concentration in the room air as a function of the moisture content of an "E1" particle board.*

due to the effect of hydrolyzation. As an example, Fig. 5 demonstrates the HCHO concentration in the room air as the function of the moisture content of an "E1" particle board. This particle board causes, under "standardized" conditions, an HCHO concentration C_s of 0.0877 mg · m^{-3}. This corresponds per definition to the emitter-room temperature and moisture equilibrium for a relative humidity of 45%. In the case of deviation from this humidity value, significant changes occur in the HCHO concentration in room air. For dry particle boards the concentration decreases considerably. Hydrolized boards emit considerably more formaldehyde. If the moisture content of the board exceeds 60 kg · m^{-3}, the HCHO concentration will exceed the $C_{s,max}$ threshold value of 0.12 mg · m^{-3}.

Case Studies

The model can be effectively applied to evaluate the risk of high HCHO concentrations in indoor room air as the result of the interaction of HCHO emitters/sources and given spatial configurations/ boundary conditions. In the following, some examples of the application of the simulation model for the calculation of HCHO concentrations in rooms of residential units are presented. The simulation results and the possibilities of concentration reduction (avoidance of strong HCHO emitters, local exhaust at HCHO source, reduction of the emitter areas, increasing the fresh air rates, and artificial thermal aging of the emitter) are discussed.

Living Room with Book Case

The HCHO concentration was simulated for a living room (floor area = 23.58 m^2 and free volume = 48.0 m^3) with a strong HCHO emitting particle board base book case (area = 20 m^2). The results of simulation show the HCHO concentrations as a function of room air temperature (Fig. 6), relative humidity (Fig. 7), and fresh air rate (Fig. 8).

For an air change rate of 1 h^{-1}, a HCHO concentration C_s of 0.46 mg · m^{-3} must be expected. In the case of very tight windows without additional ventilation (AC < 0.3 h^{-1}) the resulting concentration would be C_s > 1.1 mg · m^{-3}. In order to avoid HCHO concentrations higher than 0.12 mg · m^{-3}, a continuous fresh air rate of 225 m^3 · h^{-1} would be necessary. This means that

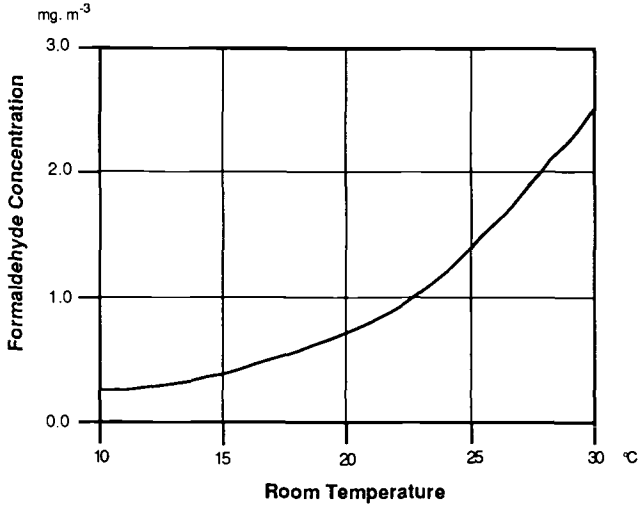

FIG. 6—*HCHO concentrations in a living room as a function of room air temperature (relative humidity = 55%, fresh air rate = 15 $m^3 \cdot h^{-1}$).*

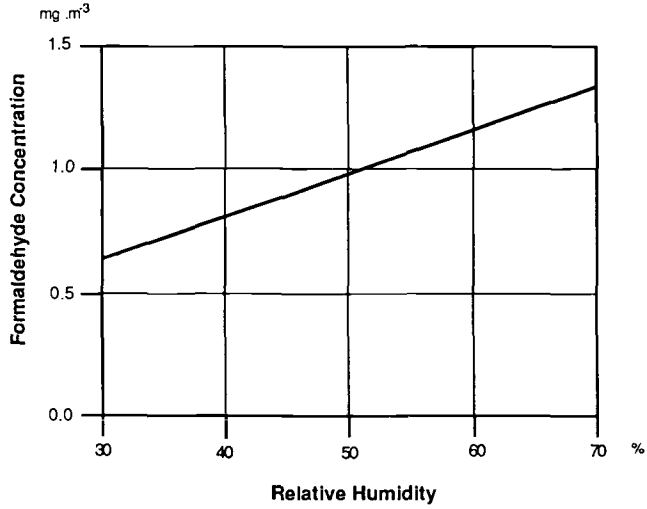

FIG. 7—*HCHO concentrations in a living room as a function of relative humidity (temperature = 22.5°C, fresh air rate = 15 $m^3 \cdot h^{-1}$).*

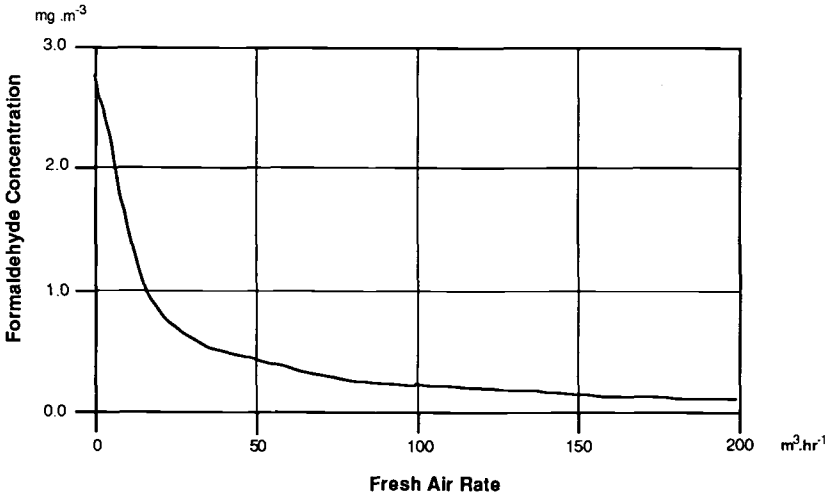

FIG. 8—*HCHO concentrations in a living room as a function of fresh air rate (temperature = 22.5°C, relative humidity = 55%).*

the problem of intensive HCHO emission due to the book case can not be solved appropriately through increased ventilation rates; the necessary high air change rates would cause draft effects in winter as well as low room temperatures and increased heating costs. Under summer conditions higher indoor room temperatures would cause even higher HCHO emission rates, so that without supporting mechanical ventilation, acceptable concentration levels could not be maintained. Thus, an adequate solution in this case would be either the removal of the book case or its treatment with a diffusion hampering coating that would reduce the HCHO emission down to a sufficiently low level.

Kitchen

The HCHO concentration was simulated for a kitchen (floor area = 6.30 m^2 and free volume = 13.9 m^3) with two alternative particle board types ("E2" and "E1") for kitchen furniture and two alternative stoves (gas and electric). Table 2 shows the results of simulation for the four resulting configurations under the assumption of similar boundary conditions (air temperature = 22.5 °C, relative humidity = 55%, and fresh air rate = 13.90 $m^3 \cdot h^{-1}$).

From this table it can clearly be seen that the dominant contributor to HCHO concentration in this case is the "E2"-particle board used in the kitchen furniture. Thus, changing from gas to electric stove while keeping this particle board leads only to an insignificant reduction in HCHO

TABLE 2—*HCHO concentration in a kitchen for four configurations of fixed emission sources and emitters.*

Stove	Emission Class of the Particle Board	C_s (HCHO Asymptotic Concentration in the Room Air)
Gas	E2	0.75 mg · m^{-3}
Gas	E1	0.13 mg · m^{-3}
Electric	E2	0.663 mg · m^{-3}
Electric	E1	0.032 mg · m^{-3}

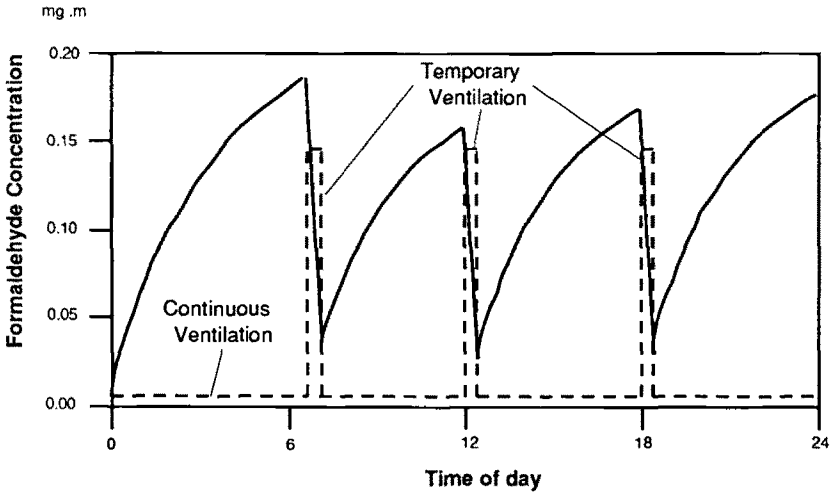

FIG. 9—*HCHO concentration in indoor air as a function of ventilation (continuous ventilation = 25 m^3 h^{-1}, temporary ventilation = 1200 $m^3 \cdot h^{-1}$, 3 × 20 min).*

concentration. Using kitchen furniture with particle boards of lower emission intensity combined with a slight increase of ventilation rates would allow for acceptable concentration values.

Transient Simulation of HCHO Concentrations

The previously described model has been extended to account for dynamic changes in boundary conditions (for example, fresh air rates). Although the integration of this module in the model, particularly in terms of an extended graphical output, is yet to be completed, simulations for time dependent boundary conditions can already be carried out and numerical results can be obtained.

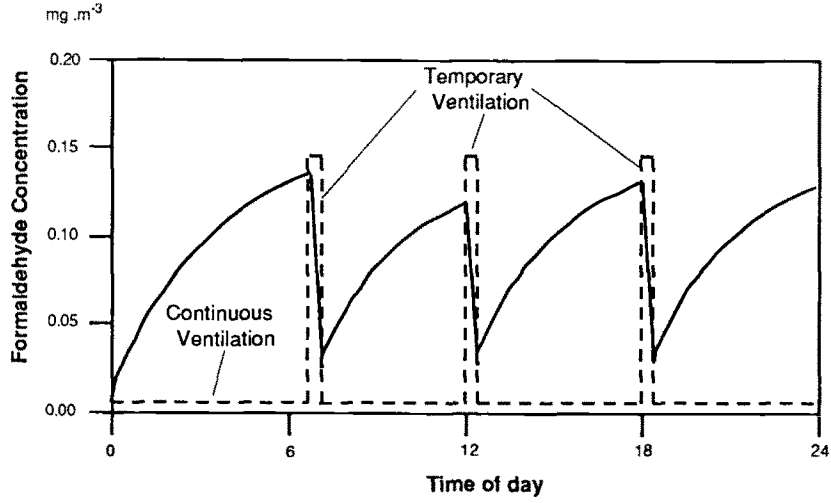

FIG. 10—*HCHO concentration in indoor air as a function of ventilation (continuous ventilation = 50 $m^3 \cdot h^{-1}$, temporary ventilation = 1200 $m^3 \cdot h^{-1}$, 3 × 20 min).*

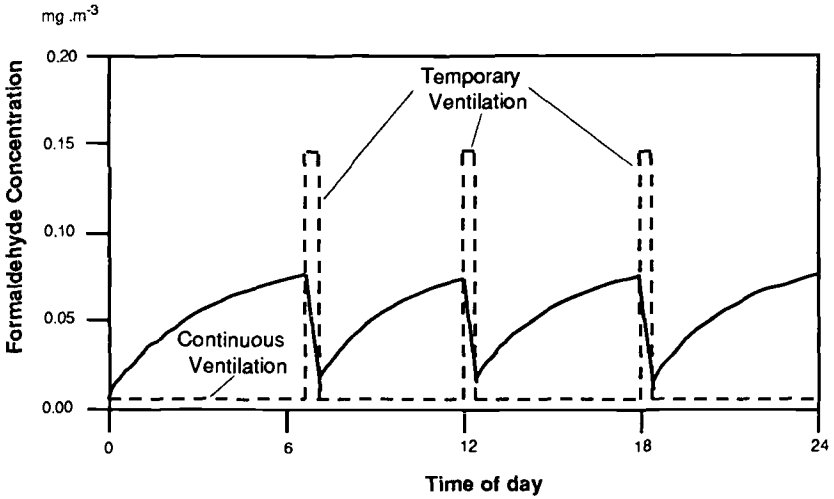

FIG. 11—*HCHO concentration in indoor air as a function of ventilation (continuous ventilation = 100 $m^3 \cdot h^{-1}$, temporary ventilation = 1200 $m^3 \cdot h^{-1}$, 12 × 20 min).*

The following example demonstrates this capability through the simulation of the time-dependent HCHO concentration in a residential unit (room volume = 200 m^3) with a strong HCHO emitter (a book case made of 10 m^2 "E2" particle board). The simulation results are illustrated in Figs. 9 to 12.

Figure 9 shows that in the case of low continuous ventilation (that is, tight windows), temporary ventilation has only a short-term effect in terms of the reduction of HCHO concentration. The peaks of HCHO concentration are higher than 0.15 mg $\cdot$ m^{-3}. A slight increase in continuous ventilation allows the concentrations to sink down to 0.12 mg $\cdot$ m^{-3} (Fig. 10). The effect of short-term ventilation is again limited. Figure 11 demonstrates the effectiveness of higher continuous

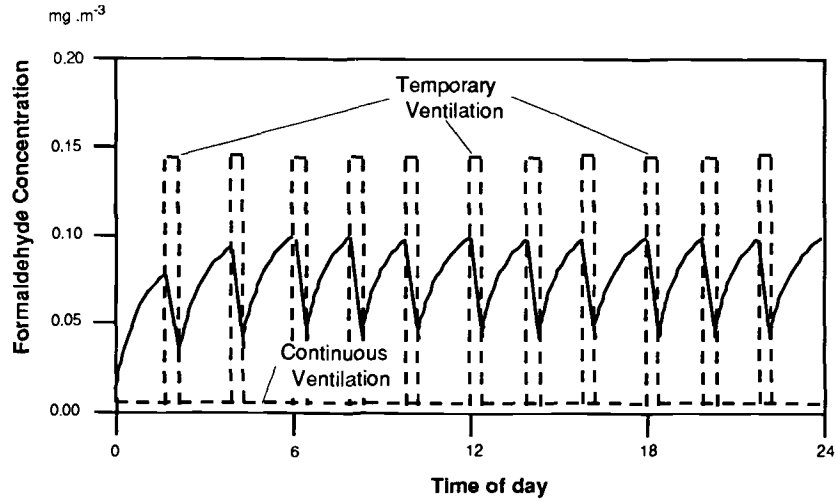

FIG. 12—*HCHO concentration in indoor air as a function of ventilation (continuous ventilation = 25 $m^3 \cdot h^{-1}$, temporary ventilation = 1200 $m^3 \cdot h^{-1}$, 3 × 20 min).*

ventilation rates. In order to achieve comparable effects with temporary ventilation, it would have to be repeated every 10 min (Fig. 12).

Conclusion

Adequate product specification procedures (that is, the declaration of the asymptotic HCHO concentration and the characteristic velocity) and the application of appropriate simulation programs allow the understanding and prediction of the interaction between HCHO sources/emitters and different spatial configurations. A computer-based model is presented for the steady-state and transient calculation of the concentrations of formaldehyde for different sources, spaces, and boundary conditions. Future development includes the extension of the materials database, incorporation of more advanced rule-based interactive evaluation tools, and the enhancement of the graphical interface for the transient simulation mode.

References

[1] Panzhauser, E., Fail, A., Ertl, H., Bednar, H., Hanappi, G., Heindl, W., Knötig, G., Scheidl, K., Terschak, S., and Wogrolly, E., *Formaldehydbelastung in Österreichischen Wohnungen*, Archivum Oecologiae Hominis, Wien (Vienna), 1987.

[2] Panzhauser, E. and Mahdavi, A., "Formaldehyd-Berater-Programm," *Environmental Technology 88*, Linz, Austria, 1987, pp. 243–247.

[3] Andersen, I., Lundquist, G. R., and Mölhave, L., "Liberation of Formaldehyde from Particleboard. A Mathematical Model," *Ugeskr. Laeg.* Vol. 136, 1974, pp. 2145–2150.

[4] Andersen, B., Lundquist, G. R., and Mölhave, O., "Indoor Air Pollution Due to Chipboard Used as a Constuction Material," *Atmospheric Environment*, Vol. 9, 1975, pp. 1124–1127.

[5] Berge, A., Mellegaard, B., Hanetho, P., and Ormstad, E. B., "Formaldehyde Release from Particleboard-Evaluation of a Mathematical Model," *Holz als Roh- und Werkstoff*, Vol. 38, 1980, pp. 251–255.

[6] Hoetjer, J. J., "Introduction to a Theoretical Model for the Splitting of Formaldehyde from Composition Board," *Report Methanol Chemie Nederland*, Delfzijil, 1978.

Craig P. Wray[1] *and Gren K. Yuill*[2]

Simulation and Description of the Performance of Radon Mitigation Systems

REFERENCE: Wray, C. P. and Yuill, G. K., **"Simulation and Description of the Performance of Radon Mitigation Systems,"** *Modeling of Indoor Air Quality and Exposure, ASTM STP 1205*, Niren L. Nagda, Ed., American Society for Testing and Materials, Philadelphia, 1993, pp. 211–225.

ABSTRACT: Several mitigation techniques such as subslab depressurization and subslab pressurization have been used recently to reduce indoor radon concentrations to acceptable levels. Unfortunately, there is a lack of understanding of the mechanisms that influence the effectiveness of these systems and of their impact on the building and surrounding soil. As a result, no systematic approach has been established to determine which remedial procedure to implement in a given situation.

The objective of the work described here was to use a microcomputer program to make a comparative assessment of the effectiveness of subslab radon mitigation systems in an unoccupied house and to identify potential problems associated with their operation. For each of the mitigation systems, the following steady-state parameters were predicted: airflows into and out of the house (above-grade and below-grade), pressures in the house, soil airflow and pressure fields, interzone airflows, differential pressures, and radon levels throughout the soil and in the house. Comparisons of the program predictions with results obtained using hand-calculations, with predictions of other programs, and with experimental data were used to validate the program.

Program predictions for the unoccupied house showed that the lowest indoor radon levels occurred when the subslab depressurization system was used. Most of the air removed by this system came from inside the basement. Simulation results also indicated that the house was adequately ventilated when the subslab depressurization system operated. However, they showed the subslab pressurization system did not adequately ventilate the house, because most of the air exhausted from the house and supplied to the soil by this system returned to the house through the basement. These predictions were confirmed by field monitoring of the house and of ten other houses with subslab depressurization systems.

The results obtained indicate it is unlikely that cold air drawn through the soil by subslab depressurization systems could cause the soil to freeze near the footings. However, the flow of air from the basement could depressurize the basement enough to create two problems: (1) excessive inflow of cold outside air, which would waste heating energy and (2) furnace backdrafting.

KEY WORDS: modeling, simulation, computer program, indoor air quality, buildings, multizone, ventilation, pollutant, radon, mitigation

In the past, methods have been applied independently to analyze airflows and radon transport in mechanical ventilation systems, to predict soil gas flow and radon concentration fields, and to estimate infiltration, natural ventilation, interzone airflows, and radon levels for buildings [*1–15*]. Crude superposition models [*16–19*] intended to account for nonlinear interactions were then used to combine the predictions of these separate models. This approach cannot be used to simulate subslab ventilation systems, because these systems couple the building and the soil surrounding it.

[1]MacInnis Engineering, 1151 Horseshoe Way, Richmond, BC, Canada, V7A 4S5.

[2]Professor, Pennsylvania State University, Department of Architectural Engineering, Engineering "A," Room 213, University Park, PA 16802.

A new approach that integrates airflow and contaminant dispersal analysis models was developed that allows buildings, soil, and their ventilation systems to be simulated simultaneously. The microcomputer program that implements this hybrid approach is a practical research tool that can be used to gain a better understanding of radon transport, which will lead to the improvement of existing mitigation techniques and the formulation of mitigation strategies. This paper describes that program, the input data required to use it, its validation, and its application in a comparative assessment of the performance of subslab ventilation systems.

Simulation Program Description

A microcomputer program called CONAIR [*16,17,20,21*] was used in this project. The program was developed for multizone airflow and contaminant dispersal analyses. It is capable of solving for soil pressure and flow fields, room pressures, interzone airflows, HVAC system airflows, and flows across a building envelope, taking into account the effects of buoyancy, wind, building features, and soil characteristics. CONAIR includes a wind flow model that can estimate the distribution of wind pressure coefficients on all four sides of a building, and that can account for the effects of terrain on the wind velocity profile. It also contains a model that accounts for two-way buoyancy-driven airflows in large openings such as doorways. The program calculates steady-state airflow rates on an hour-by-hour basis using hourly weather data such as wind velocity, wind direction, and outdoor temperature.

CONAIR can predict time-varying or steady-state radon concentrations under the influence of these airflow rates. It determines the concentrations at discrete points within the building and in the soil surrounding it. The program can model: steady-state and time-varying radon mass transport, or both, due to air movement (infiltration, exfiltration, interzone airflows, and HVAC system airflows), removal of radon from the air by radio-chemical processes, and steady-state or time-varying generation of radon in the soil. Provisions for simulating one-dimensional convection-diffusion processes in the soil are included in the program.

Program Input Data

For each radon mitigation technique, a single-network finite-element steady-state representation of a house, the heterogeneous soil surrounding its foundation, and the mitigation system was developed. Indoor nodes were connected to each other and to the outdoor node with convective flow elements, while the soil nodes were connected to each other by convective-diffusive flow elements. Nodes just below the soil surface were connected to the outdoor node at the soil surface by convective-diffusive flow elements. The house was coupled to the soil using convective-diffusive flow elements to represent a crack at the basement floor-wall perimeter. Constant-flow convective elements were used to represent the subslab mitigation systems, which supplies air to or exhaust air from a node in the subslab region immediately beneath the center of the floor slab. The total network size was 606 nodes and 1642 elements.

House Description

An unoccupied house located in a suburban area of Winnipeg, Manitoba was used as the basis for the simulations. Figure 1 shows a plan view of the main floor of the house. This house is a one-story bungalow having a floor area of approximately 100 m^2 (not including the basement), an Equivalent Leakage Area (ELA) of 15.4×10^{-3} m^2 with all intentional openings sealed, and a total volume of 446.48 m^3. The walls of the house are of typical wood-frame construction, using 38-mm wide and 140-mm deep studs. The basement in this house is unfinished. The top of its poured concrete floor slab is 1.26 m below grade level. The slab is 75-mm thick and has dimensions

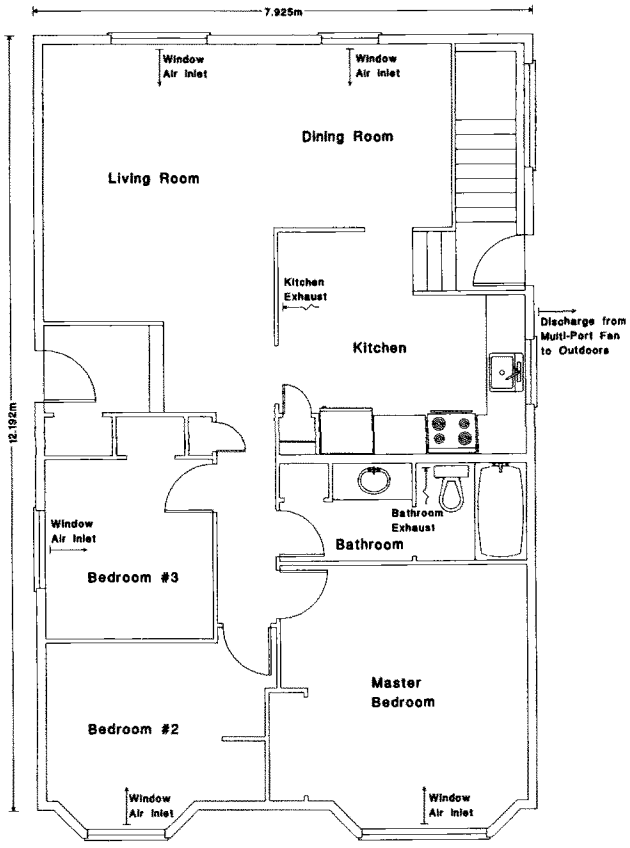

FIG. 1—*Plan view of main floor of house.*

of 7.5 by 11.8 m. It has a lapped and caulked polyethylene moisture barrier underneath it. A layer of small-diameter gravel with a total thickness of 125 mm is located immediately beneath the moisture barrier. Subslab perforated piping connects the sump pit and drain tile system. The basement walls are poured concrete with a thickness of 200 mm. Heating for the house is provided by electric baseboard heaters, which maintains the temperature of each room of the house at a constant 20°C.

For the simulations, the house was divided into the following seven zones: (1) basement, (2) kitchen/dining room/living room, (3) hallway joining living room, bathroom, and bedrooms; (4) bathroom, (5) master bedroom, (6) bedroom 2, and (7) bedroom 3. The kitchen, living room, and dining room of the simulated house were lumped together as one zone, because there are no significant flow resistances between these regions. The only leaks considered between indoor zones were interior doorways, which were simulated as if the doors were wide open.

The house is ventilated by a multiport central exhaust fan that runs continuously. The fan is located in the basement. Except for the bathroom and hallway, there is a damper-controlled outdoor-air inlet in each room to provide replacement outdoor air for the air that is exhausted. The fan is capable of exhausting air from as many as six locations with a total design flow rate of 62×10^{-3} m^3 s^{-1}. In the house, air is continually exhausted at a design flow rate of 17.5×10^{-3} m^3 s^{-1} directly from the kitchen and the same amount from the bathroom. To emulate a basement

suction system, a duct from the exhaust fan was placed to exhaust air directly from the basement at a continuous design flow rate of 27×10^{-3} m^3 s^{-1}. This system was implemented only to provide a controllable baseline for comparing the performance of the subslab mitigation systems. The use of this system is not recommended, because it will tend to depressurize the basement and increase radon entry rates. To emulate a subslab depressurization system, a duct was run from a floor slab penetration to connect the above-mentioned piping and drain tile system to the exhaust fan. The design flow rate in that duct was 27×10^{-3} m^3 s^{-1}. No air was exhausted directly from the basement in this case. Subslab pressurization was achieved by directing all of the exhaust air from the exhaust fan to the subslab region through a duct connected to the floor slab penetration. The design flow rate in that duct was 62×10^{-3} m^3 s^{-1}. In this case, additional air was exhausted directly from the kitchen at a design flow rate of 27×10^{-3} m^3 s^{-1}.

All exterior windows and doors were simulated in their closed position, so the only source of natural ventilation in the house was infiltration and exfiltration driven by wind and stack effects through unintentional leaks in the house envelope and through the damper-controlled outdoor-air inlets. Using the total ELA of the house, which was obtained from blower door tests that used an approach adapted to the project objectives [*22*], using assumptions of leakage area distributions based on surface area, and using the American Society of Heating, Refrigerating, and Air-Conditioning Engineers (ASHRAE) [*23*] estimates of door and window component leakages, inputs were developed for the airflow analysis section of CONAIR to characterize the magnitude and location of the unintentional leaks in the building envelope.

The damper-controlled outdoor-air inlets were modeled using empirical airflow data [*22*]. The ELA of each air inlet in the fully-open position was 2.4×10^{-3} m^2 and the flow exponent was 0.57. In the so-called "fully-closed" position, these tests indicated the ELA of the air inlet was reduced to 68% of that in the fully-open position. The air inlets were positioned so those in the living room were fully open, while those in the bedrooms were fully closed. These positions are typical of those that would be used during normal daytime occupancy.

Foundation and Soil Characteristics

Figure 2 shows the geometrical configuration of the basement and surrounding heterogeneous soil for the house. The configuration is based on that used by Loureiro [*8,9*]. Only one quarter of the soil block is modeled, because symmetry around the basement is assumed. Except for the surface of the soil at grade and the surface immediately below the basement perimeter crack, it was assumed there is no flow across the outer boundaries of the quarter soil block.

The dimensions used to model the basement and the soil surrounding it were: L_x = 14.450 m, L_y = 16.600 m, L_z = 11.460 m, l_{x-aggr} = 0.500 m, l_{y-aggr} = 0.500 m, l_{z-aggr} = 0.125 m, l_x = 3.745 m, l_y = 5.895 m, l_z = 1.260 m, t_x = 0.200 m, t_y = 0.200 m, t_z = 0.075 m, C_x = 0.005 m, and C_y = 0.005 m. The width of the gap between the backfill and foundation walls was assumed to be zero.

The soil block was defined with silt in the primary soil region and with small-diameter gravel beneath the floor slab. A looser-packed silt was specified in the backfill region, because the house is still relatively new. Over time, it is expected that the packing of the soil in this region will become similar to that in the primary region. These soil types are based only on observations at the building site, because field investigations to determine the soil types or their physical properties were beyond the scope of the project. The soil in each region was assumed to be a porous medium with no open channels or fractures. It was also assumed that: soil properties are constant and isotropic within each distinct region of the soil surrounding the basement, the soil gas in the pore spaces can be treated as a single-phase gaseous mixture of air and radon, and that soil gas density was constant, so the soil gas could be considered incompressible.

To use CONAIR to represent the soil, several parameters had to be specified for each node and flow element, or both, in each of the different soil regions. These included: (1) the depth of each

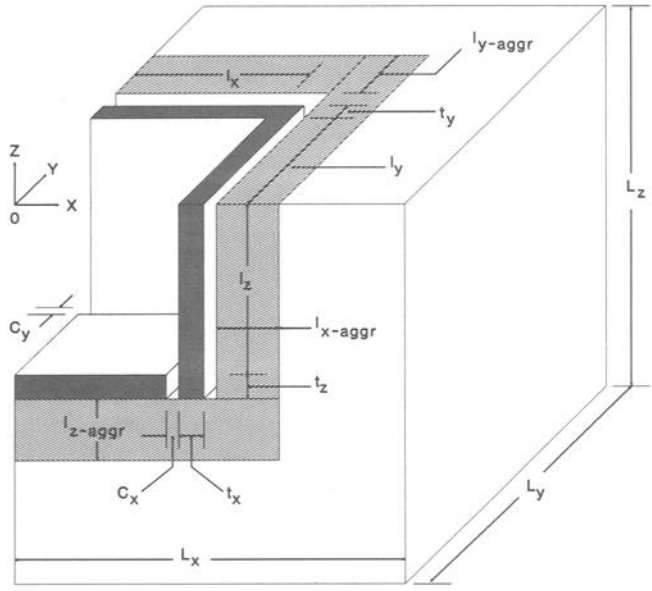

FIG. 2—*Basement and soil block geometrical configuration.*

node below grade, (2) the mass of air in the control volume surrounding each node, (3) the radon generation rate for each node, which depends on the radium-226 (^{226}Ra) concentration; (4) the soil particle density, the porosity, and the radon emanation fraction at that node, (5) the gas flow resistance in each element, which depends on the permeability, length, and cross-sectional area of that element; (6) the bulk radon diffusion coefficient in each element, and (7) the mass of air per unit length in each element. The manual calculation and specification of these parameters are prone to error and were too time consuming to carry out within the scope of the project. Thus, a computer program [*24*] was developed and used to subdivide the soil into hundreds of nodes using a non-uniform three-dimensional grid [*8,9*]. The soil was subdivided into eight layers in the *x*-direction, eight layers in the *y*-direction, and ten layers in the *z*-direction. The program then determined the parameters described above and generated CONAIR input files.

The ^{226}Ra concentrations were assumed to be 11 Bq kg^{-1} for the gravel and 110 Bq kg^{-1} for the silts. These concentrations tend to increase with decreasing grain size [*25*]. Since the gravel has large grain sizes, a value near the minimum found in the literature was used for the gravel [*26–28*]. A higher concentration was used for the silts for two reasons. First, the silts have much smaller grain sizes than the gravel. Second, calibrated-modeling exercises for the basement suction case indicated that high ^{226}Ra concentrations in the backfill and primary soil regions were necessary to explain the high soil radon concentrations measured in the soil surrounding the house [*29*].

The soil particle density of all the soils was assumed to be 2650 kg m^{-3}. Nazaroff and Nero [*28*] state that this soil particle density is typical of most soils and that only rarely is the density outside the range from 2600 to 2800 kg m^{-3}.

The porosities of the soils were assumed to be 0.4 for the gravel and 0.5 for the silts. These values are based on values found in the literature [*5,25,28*].

The radon emanation fractions were assumed to be 0.20 for the gravel and 0.35 for the silts. These fractions are based on the range of values listed in the literature [*27,28,30*]. The emanation fraction for the silts is typical of most moist soils [*5*]. A lower fraction was used for the gravel,

because it has a larger grain size. Emanation fractions tend to decrease with increasing grain size [*25*].

The permeabilities of the soils were assumed to be: 5.0×10^{-8} for the gravel, 2.5×10^{-12} m^2 for the silt in the primary region, and 2.5×10^{-11} m^2 for the silt in the backfill region. These values are based on values found in the literature [*5,27,28*]. A higher permeability was used for the silt in the backfill to account for the looser packing in that region.

The bulk radon diffusion coefficients for the soils were assumed to be 3.65×10^{-7} m^2 s^{-1} for the gravel and 3.50×10^{-8} m^2 s^{-1} for the silts. These values are based on those found in the literature [*28,31*]. A lower coefficient was used for the silts than for the gravel, because the silts are assumed to be moister than the gravel. As the moisture content of a soil increases, the diffusion coefficient decreases as a function of the fourth power of the moisture content [*28*]. Diffusion of radon through the concrete foundation was assumed to be negligible.

Basement wall footings were not modeled, because it was assumed the subslab region and bottom of the backfill region are coupled and have flow resistances several orders of magnitude lower than the rest of the soil. Ignoring these footings is not expected to significantly affect the program predictions in the cases considered here. However, further research should be carried out to quantify the effect footings have on program predictions.

Meteorological Data and Outdoor Concentrations

All of the simulations were carried out using an outdoor dry-bulb temperature of −23.5°C, based on monitored data [*29*]. However, wind speed and direction data were not monitored. Thus, a wind speed of 3.2 m s^{-1} and a wind direction from the north was used, based on data collected at the local airport during the monitoring period. A constant outdoor air pressure of 101.325 kPa was used for all of the simulations.

Data describing the variation of soil temperatures in the soil block were not available. Furthermore, measuring or simulating this temperature field was beyond the scope of the project. Thus, the soil was assumed to be isothermal. Its temperature was 7°C, which is based on the average soil temperature measured just outside the basement walls at footing level [*29*]. Further research should be carried out to quantify the interdependency of soil temperatures and soil gas flows.

Radon concentrations in outdoor air are usually in the range of 3.7 Bq m^{-3} to 14.8 Bq m^{-3} [*28,32*]. Thus, a typical value of 7.4 Bq m^{-3} was assumed for the cases simulated in this project.

Program Validation

CONAIR has been validated by comparing its predictions with those of other available programs or solution techniques to determine whether the predictions of CONAIR are reliable.

AIRNET is one of the programs on which CONAIR is based. Walton [*33*] has compared the predictions of AIRNET with those of ESPAIR [*34*], which is a separate airflow analysis program included in the ESP building thermal analysis program. AIRNET and ESPAIR were used to solve a large airflow network that represents a four-story building with six rooms, a hallway, an elevator shaft, and a stairwell on each floor. Both programs solved the same airflow and pressure fields, but AIRNET was significantly faster than ESPAIR (a factor of approximately 1000). Walton also described 14 analytical validation tests he carried out to demonstrate the performance of AIRNET. In all cases, AIRNET predictions matched the analytical results. These cases were also analyzed using CONAIR. Its predictions were exactly the same as those of AIRNET.

CONAIR has also been validated through comparisons with four other airflow analysis programs that use different solution techniques. Three of these programs (SCAFA, LINEAR, and SIMLOOP) have been developed by Yuill and Associates [*35*]. The fourth program was ASCOS [*36*]. In the comparisons of the predictions of these five programs, the same case was run in each program. The case involved a five-story building with an atrium, a zoned smoke control system, stairwell

pressurization, and atrium exhaust. This building had 66 zones and 170 airflow paths. All programs predicted the same zone pressures, element pressure drops, and flows.

CONTAM 87, another program on which CONAIR is based, has been validated internally by the National Institute of Standards and Technology (NIST) [*37*], through one interprogram comparison and two comparisons of program predictions with measured data. In addition, the program has been externally validated by another interprogram comparison [*38*]. For the cases for which input data were available, CONAIR predictions were identical to those of CONTAM 87. Another external interprogram comparison was used to validate SMOKESIM [*35*], which is a smoke transport simulation program based on CONAIR. This latter comparison involved measured data [*39*].

CONTAM 88 [*19*] is similar to CONAIR in that it combines AIRMOV [*40*] and CONTAM 87 into a single program. AIRMOV was a precursor of AIRNET. CONTAM 88 has also been applied to the simulation of radon and radon daughter movement within a 12-story apartment building [*19*]. However, that work did not simultaneously model airflows, pressures, radon generation, and radon transport in the soil and in the building.

The input file generator program used for CONAIR is based on algorithms used in the computer programs PRESSU and MASTRA [*8,9*]. MASTRA uses the same air-phase radon transport equation as used by Rogers and Nielson in RAECOM [*14,15*] and by the Lawrence Berkeley Laboratory team in STAR [*12,13,41*]. Like these other programs, MASTRA does not account for the normally negligible effects of liquid-phase radon transport and surface diffusion of radon.

An important difference between the present work and the subsoil radon transport models described above is that they deal only with subsoil flow, using an assumed basement pressure. CONAIR uses a simultaneous solution of the air and radon transport through the soil and through the house. It considers the house as a multizone space and includes the effects of buoyancy, wind, ventilation fans, and leakage areas across internal partitions and the building envelope.

Loureiro [*8,9*] carried out tests to determine whether the predictions of his programs behaved as expected. Several of these tests involved comparisons of program predictions for simple test cases with hand-calculated results obtained using fundamental principle models. He also carried out sensitivity studies to determine the effects of house size, disturbance pressure, crack width, soil permeability, soil porosity, and bulk diffusivity of radon in soil on the predictions of PRESSU and MASTRA. These sensitivity analyses indicated that the variations in program predictions exhibited the expected behavior. However, these results do not verify the accuracy of the programs.

Loureiro also employed analytical techniques to test the subroutine used by PRESSU and MASTRA that implements the widely accepted Thomas algorithm [*42*] for solving transport equations. In these tests, this subroutine was used to solve for heat flow in a one-dimensional bar and in a two-dimensional surface. The heat flow predictions generated using this subroutine agreed well with the results obtained analytically.

Validations of PRESSU and MASTRA have also been carried out by Fisk et al. [*41*] and by Revzan et al. [*12*], using both analytical and experimental comparisons. Good agreement was obtained. A later report by Gadgil et al. [*13*] describes the development of a non-Darcy transport model, "non-Darcy STAR," to better simulate the high flow velocities that can occur in subslab aggregate. A non-Darcy model was not considered in the present case because the maximum velocities simulated were less than 5% of that described in the latter reference (1.1 m/s). The only exceptions occurred within 4 mm of the basement perimeter crack and of the penetration through the slab for the subslab ventilation system, where soil gas velocities were predicted to be as high as 2.1 m/s. Exact analytical models [*10*] have been used to check the predictions of Loureiro's programs for homogeneous soils, in the absence of diffusion. Excellent agreement was reported. Diffusion was neglected in that comparison because analytical models that include this phenomenon are not presently available.

CONAIR and its input file generator program were also validated through a program-program comparison with PRESSU and MASTRA. A 600-node representation of a basement and heterogeneous soil block without any mechanical ventilation systems was specified in PRESSU. On the

TABLE 1—*Summary of predicted airflows across house and soil control surfaces.*

Flow Balance On	From	To	Flow ($\times 10^{-3}$ m^3 s^{-1})	Comment
		BASEMENT SUCTION		
	Outdoors	house	61.6	infiltration
House	Soil	house	0.4	infiltration
	House	outdoors	62.0	exhaust
Soil	Outdoors	soil	0.4	infiltration
	Soil	house	0.4	exfiltration
		SUBSLAB DEPRESSURIZATION		
	Outdoors	house	61.6	infiltration
House	House	soil	26.6	exfiltration
	House	outdoors	35.0	exhaust
	Outdoors	soil	0.4	infiltration
Soil	House	soil	26.6	infiltration
	Soil	outdoors	27.0	exhaust
		SUBSLAB PRESSURIZATION		
	Outdoors	house	9.0	infiltration
House	Soil	house	62.1	infiltration
	House	outdoors	9.1	exfiltration
	House	soil	62.0	exhaust
	Outdoors	soil	0.1	infiltration
Soil	House	soil	62.0	supply
	Soil	house	62.1	exfiltration

basis of the three-dimensional finite-difference grid generated by PRESSU, a CONAIR airflow network representation of the same soil block and basement was also developed using the input file generator program. The pressure and airflow rate predictions of CONAIR and PRESSU were identical. The radon concentration predictions of CONAIR and MASTRA were identical.

Simulation Results

To summarize the predicted airflow data, consider the entire house as a control volume, the soil block as a control volume, and each room indoors as a control volume. Each control volume is enclosed by a control surface. Table 1 summarizes the predicted infiltration, supply, exfiltration, and exhaust airflows across the house and soil control surfaces for each of the three different systems: basement suction, subslab depressurization, and subslab pressurization. Tables 2 through 4 summarize the predicted infiltration, supply, interzone, exfiltration, and exhaust airflows across the control surfaces for each zone for these cases. These latter three tables also list the predicted radon concentrations for each zonal control volume. The predicted disturbance pressure fields and radon concentration fields in the soil surrounding the basement are not presented in this paper because of their size.

Basement Suction

For the basement suction case, Table 2 shows the predicted radon concentration in the basement was 259 Bq m^{-3}. In the living room, the concentration was 115 Bq m^{-3}. These levels are similar to those measured in the house: 300 and 111 Bq m^{-3}, respectively [*29*]. Therefore, the model of the house and of its surrounding soil appears to be a reasonable approximation.

TABLE 2—*Summary of predicted zonal airflows–basement suction.*

Flow Balance On	From	To	Flow ($\times 10^{-3}$ m^3 s^{-1})	Comment[a]
Soil	Outdoors	soil	0.4	infiltration (7.4 Bq m^{-3})
	Soil	basement	0.4	exfiltration (21 $\times$ 10^3 Bq m^{-3} average)
	Outdoors	basement	8.9	infiltration (7.4 Bq m^{-3})
	Soil	basement	0.4	infiltration (21 $\times$ 10^3 Bq m^{-3} average)
Basement	Living room	basement	43.7	interzone (115 Bq m^{-3})
	Basement	living room	26.0	interzone (259 Bq m^{-3})
	Basement	outdoors	27.0	exhaust (259 Bq m^{-3})
	Outdoors	living room	31.9	infiltration (7.4 Bq m^{-3})
	Basement	living room	26.0	interzone (259 Bq m^{-3})
	Hallway	living room	3.3	interzone (7.4 Bq m^{-3})
Living room	Living room	basement	43.7	interzone (115 Bq m^{-3})
	Living room	outdoors	17.5	exhaust (115 Bq m^{-3})
Bedroom 3	Outdoors	bedroom 3	5.4	infiltration (7.4 Bq m^{-3})
	Bedroom 3	hallway	5.4	interzone (7.4 Bq m^{-3})
Master bedroom	Outdoors	master bedroom	10.0	infiltration (7.4 Bq m^{-3})
	Master bedroom	hallway	10.0	interzone (7.4 Bq m^{-3})
Bedroom 2	Outdoors	bedroom 2	5.5	infiltration (7.4 Bq m^{-3})
	Bedroom 2	hallway	5.5	interzone (7.4 Bq m^{-3})
Bathroom	Hallway	bathroom	17.5	interzone (7.4 Bq m^{-3})
	Bathroom	outdoors	17.5	exhaust (7.4 Bq m^{-3})

[a]For each flow, the radon concentration listed is the average level predicted for the control volume from which the flow originated.

Subslab Depressurization

The subslab depressurization system significantly reduced basement and main floor radon levels, in comparison to the basement suction system, as shown in Tables 2 and 3. Throughout the house, the predicted levels were all slightly less than that outdoors (7.4 Bq m^{-3}) when the subslab depressurization system operated. These low indoor levels occurred because no radon entered the basement from the soil, and because the radon in the outdoor air decayed as it entered the house. Monitored data confirmed this behavior [*29*].

Tables 2 and 3 show that for most rooms in the house, the predicted airflows in this case were similar to those for the basement suction case. This was expected, because the house operated under similar depressurizations in both cases. However, the predicted flows between the basement and soil were significantly different. Instead of air flowing from the soil into the basement as predicted in the basement suction case, Table 1 shows that air flowed from the basement into the soil in this case (26.6 $\times$ 10^{-3} m^3 s^{-1}). Thus, almost all (98%) of the air exhausted from the soil was from the basement. The rest of the air exhausted from the soil (0.4 $\times$ 10^{-3} m^3 s^{-1}) was due to leakage through the soil from outdoors. Most of the air leaking through the soil passed through the backfill region into the subslab region. This behavior is expected, because the backfill was significantly more permeable (factor of ten) than the primary soil region.

The predicted radon concentrations in the subslab region when the subslab depressurization system was operating were significantly lower than those when the basement suction system was operating. For the basement suction case, the predicted radon concentrations at the basement floor perimeter crack ranged from 17 $\times$ 10^3 Bq m^{-3} to 24 $\times$ 10^3 Bq m^{-3}. For the subslab depressurization case, these concentrations were similar to those indoors (7.4 Bq m^{-3}). At the point at which soil gas was exhausted from the subslab region, the predicted radon concentrations increased to 433

TABLE 3—*Summary of predicted zonal airflows–subslab depressurization.*

Flow Balance On	From	To	Flow ($\times 10^{-3}$ m^3 s^{-1})	Comment[a]
	Outdoors	soil	0.4	infiltration (7.4 Bq m^{-3})
Soil	Basement	soil	26.6	infiltration (7.4 Bq m^{-3})
	Soil	outdoors	27.0	exhaust (433 Bq m^{-3})
	Outdoors	basement	8.9	infiltration (7.4 Bq m^{-3})
Basement	Living room	basement	43.7	interzone (7.4 Bq m^{-3})
	Basement	living room	26.0	interzone (7.4 Bq m^{-3})
	Basement	soil	26.6	exfiltration (7.4 Bq m^{-3})
	Outdoors	living room	31.9	infiltration (7.4 Bq m^{-3})
	Basement	living room	26.0	interzone (7.4 Bq m^{-3})
Living room	Hallway	living room	3.3	interzone (7.4 Bq m^{-3})
	Living room	basement	43.7	interzone (7.4 Bq m^{-3})
	Living room	outdoors	17.5	exhaust (7.4 Bq m^{-3})
Bedroom 3	Outdoors	bedroom 3	5.4	infiltration (7.4 Bq m^{-3})
	Bedroom 3	hallway	5.4	interzone (7.4 Bq m^{-3})
Master bedroom	Outdoors	master bedroom	10.0	infiltration (7.4 Bq m^{-3})
	Master bedroom	hallway	10.0	interzone (7.4 Bq m^{-3})
Bedroom 2	Outdoors	bedroom 2	5.5	infiltration (7.4 Bq m^{-3})
	Bedroom 2	hallway	5.5	interzone (7.4 Bq m^{-3})
Bathroom	Hallway	bathroom	17.5	interzone (7.4 Bq m^{-3})
	Bathroom	outdoors	17.5	exhaust (7.4 Bq m^{-3})

[a]For each flow, the radon concentration listed is the average level predicted for the control volume from which the flow originated.

Bq m^{-3} with the subslab depressurization system, and to 79 $\times$ 10^3 Bq m^{-3} with the basement suction system. The reductions in subslab radon concentrations with the subslab depressurization system were due to the dilution airflows from the basement into the soil and due to the slight increase in dilution flow through the soil from outdoors.

Subslab Pressurization

A comparison of Tables 3 and 4 shows the indoor radon levels increased when the subslab pressurization system operated compared to those when the subslab depressurization system operated. This trend was also found in monitored data [*29*]. Predicted radon levels were similar almost everywhere in the house when it operated with subslab pressurization. This behavior can be explained by the predicted airflow patterns in the soil and in the house.

The subslab pressurization system supplied air at a rate of 62 $\times$ 10^{-3} m^3 s^{-1} from inside the house (livingroom and bathroom) to the soil. As Table 1 shows, almost all of this air then passed through the subslab region and back into the basement through the crack at the floor perimeter. It is not clear if all of the air supplied to the soil from the house reentered through this crack, because a very small amount of soil gas (5 $\times$ 10^{-6} m^3 s^{-1}) was predicted to flow from the soil to outdoors. There was no exfiltration or exhaust from the basement, so all of the soil gas entering the basement flowed from the basement through the doorway to the living room.

In the living room in this case, there was some exfiltration due to wind and stack effects, unlike in the other two cases. However, the exfiltration was predicted to be only 5% of the total airflow leaving the living room. A large fraction (57%) of the air leaving the living room was supplied directly to the soil. Another large fraction (28%) flowed into the hallway, from which most (79%) of the air was drawn into the bathroom and supplied directly to the soil. This meant that the

TABLE 4—*Summary of predicted zonal airflows–subslab pressurization.*

Flow Balance On	From	To	Flow ($\times 10^{-3}$ m^3 s^{-1})	Comment[a]
	Outdoors	soil	0.1	infiltration (7.4 Bq m^{-3})
Soil	Living room	soil	44.5	supply (525 Bq m^{-3})
	Bathroom	soil	17.5	supply (492 Bq m^{-3})
	Soil	basement	62.1	exfiltration (2.5×10^3 Bq m^{-3} average)
	Outdoors	basement	3.8	infiltration (7.4 Bq m^{-3})
Basement	Soil	basement	62.1	infiltration (2.5×10^3 Bq m^{-3} average)
	Living room	basement	7.1	interzone (525 Bq m^{-3})
	Basement	living room	73.0	interzone (537 Bq m^{-3})
	Outdoors	living room	4.7	infiltration (7.4 Bq m^{-3})
	Basement	living room	73.0	interzone (537 Bq m^{-3})
Living room	Living room	basement	7.1	interzone (525 Bq m^{-3})
	Living room	hallway	22.2	interzone (525 Bq m^{-3})
	Living room	outdoors	3.9	exfiltration (525 Bq m^{-3})
	Living room	soil	44.5	exhaust (525 Bq m^{-3})
	Outdoors	bedroom 3	0.5	infiltration (7.4 Bq m^{-3})
Bedroom 3	Bedroom 3	hallway	0.4	interzone (7.4 Bq m^{-3})
	Bedroom 3	outdoors	0.1	exfiltration (7.4 Bq m^{-3})
Master bedroom	Hallway	master bedroom	3.2	interzone (496 Bq m^{-3})
	Master bedroom	outdoors	3.2	exfiltration (481 Bq m^{-3})
Bedroom 2	Hallway	bedroom 2	1.7	interzone (496 Bq m^{-3})
	Bedroom 2	outdoors	1.7	exfiltration (481 Bq m^{-3})
Bathroom	Hallway	bathroom	17.5	interzone (496 Bq m^{-3})
	Bathroom	soil	17.5	exhaust (492 Bq m^{-3})

For each flow, the radon concentration listed is the average level predicted for the control volume from which the flow originated.

subslab region, basement, living room, hallway, and bathroom acted like a duct system for soil gas flow. Some dilution of the soil gas occurred in the basement and in these rooms through infiltration of outside air. However, Table 1 shows that only 13% of the airflows entering the house were from above grade. It is important to note that Canadian Standards Association (CSA) Standard F326.1-M1989 [*43*] does not permit ventilation systems to recirculate air that is exhausted from the bathroom and kitchen.

Table 4 shows that the indoor radon levels predicted for the subslab pressurization case were significantly higher than those measured: 144 Bq m^{-3} in the basement and 81 Bq m^{-3} in the living room [*29*]. The reason for these higher levels appears to be primarily due to the use of a different location for pressurization (further from the floor crack). This meant that pressurization airflows could not reach all of the subslab region near the crack to dilute radon levels, particularly at the corner of the basement. The predicted radon levels at the crack ranged from 533 Bq m^{-3} at the centerline of the slab to 9.8×10^3 Bq m^{-3} at the corner. These levels are significantly higher than those predicted for the subslab depressurization case. Further research should be carried out to examine the sensitivity of these systems to different soils and to a wider range of configurations.

To reduce the indoor radon levels when the subslab pressurization system operates, the balance of subslab pressurization flows from the subslab vent into the crack must be altered so that more pressurization air flows to the outdoors than into the basement. One method of changing the balance of airflows in the subslab region is to seal the basement floor perimeter crack. However, if the sealants degrade over time, the soil gas flows through the crack will increase, which will result in increased indoor radon levels. An additional step should be to reduce the resistance to soil gas flow outside the basement between the subslab region and outdoors.

An alternative method for reducing indoor radon levels is to reduce subslab radon levels by increasing subslab pressurization airflows through the region. Increased subslab pressurization airflows would increase ventilative energy losses to the soil, but these would be partially offset through reduced conduction heat losses through the basement floor slab and, to a limited extent, through the basement walls. Another significant drawback to increase these flows is that a larger, more expensive fan would be required. This could cause unacceptable noise levels and could lead to excessive air velocities caused by increased airflows from the basement to the main floor.

Finally, Table 4 shows that the predicted outdoor airflows into the house did not meet the requirements of CSA Standard F326.1-M1989 [*43*] in the case of subslab pressurization. The basement received only 38% of the required airflow (10×10^{-3} m^3 s^{-1}), while the kitchen/living room/dining room combination received only 31% of the required airflow (15×10^{-3} m^3 s^{-1}). The bedrooms were virtually unventilated relative to the standard's requirements (5×10^{-3} m^3 s^{-1}) per room. Of the three bedrooms, only Bedroom 3 received ventilation, and that was only 9% of that required. The addition of another ventilation system incorporating a heat recovery device is necessary if this system is to meet the airflow requirements of CSA Standard F326.1-M1989 [*43*] and is to avoid significant increases in ventilation energy losses. For comparison, it should be noted that in general, the airflow requirements of that standard were met when either the basement suction system or the subslab depressurization system was operated.

It must be noted that if the central exhaust fan used in the subslab venting systems failed or was turned off, these systems could cause higher indoor radon levels than would otherwise occur if the systems were not present. The duct leading from the subslab region was connected to the indoor space through the fan. With no forced flow into or out of the subslab region through this duct, the duct would act to increase the area of leaks in the basement floor slab. Flow of radon-laden soil gas through the duct into the fan plenum could occur. This gas could then be delivered to the main floor without any dilution from outdoor air infiltrating into the basement. Although a backdraft damper in the duct could in theory obviate such a condition, it might be difficult in practice to design a low cost, low pressure drop damper that would be airtight when closed. Without a backdraft damper, this failure scenario would always occur in the absence of fan-driven flow in a subslab pressurization system, unless outdoor air was used to pressurize the subslab region. However, the considerable potential for soil freezing and foundation damage in that mode precludes that approach. For subslab depressurization systems using ducts leading directly outdoors through a fan, and not connected to the indoor space, the lack of fan-driven flow would not be as significant a concern. In that case, the duct from the subslab vent could act as a passive stack, although the buoyancy-driven flows through this duct would be significantly lower than the flows driven by the fan.

Conclusions

The subslab depressurization system was more successful than the subslab pressurization system at reducing indoor radon concentrations, as predicted by the computer simulations, and as confirmed by monitored data.

Most of the air removed from the house by the subslab depressurization system was drawn through the basement floor, not through the soil. This means that there is little danger of subslab depressurization systems causing soil to freeze under the footings of this house, but the basement may be depressurized (leading to furnace backdrafting) and may be over-ventilated (leading to unnecessary heat loss).

Recommendations

Further computer simulations and tests should be carried out using different soils and for a wider range of configurations to confirm the conclusion that freezing of the soil under footings is not likely to be a problem. The project would also determine the interdependency of soil temperatures

and soil gas flows around foundations and would quantify the effect footings have on program predictions. In particular, this work should be based on a real house surrounded by soil that is highly permeable to air, to create a worst case condition. The house should have thermocouples buried under the footings and around the house. It should have a permanently installed subslab depressurization system. An identical house without subslab depressurization should be tested and simulated for comparison.

Acknowledgments

The work described in this paper was carried out with the assistance of a grant from the Canada Mortgage and Housing Corporation (CMHC) under the terms of the External Research Program. The views expressed are those of the authors and do not represent the official views of CMHC.

References

[1] Jacobi, W., "Activity and Potential α-Energy of ^{222}Radon- and ^{220}Radon-Daughters in Different Air Atmospheres," *Health Physics*, Vol. 22, May 1972, pp. 441–450.

[2] Porstendörfer, J., Wicke, A., and Schraub, A., "The Influence of Exhalation, Ventilation and Deposition Processes upon the Concentration of Radon (^{222}Radon), Thoron (^{220}Radon) and their Decay Products in Room Air," *Health Physics*, Vol. 34, May 1978, pp. 465–473.

[3] Kusuda, T., Silberstein, S., and McNall, P. E., Jr., "Modelling of Radon and its Daughter Concentrations in Ventilated Spaces," *Journal of the Air Pollution Control Association*, Vol. 30, No. 11, 1980, pp. 1201–1207.

[4] Hernandez, T. L. and Ring, J. W., "Indoor Radon Source Fluxes: Experimental Tests of a Two-Chamber Model," *Environment International*, Vol. 8, 1982, pp. 45–57.

[5] DSMA Atcon Ltd., "Review of Existing Instrumentation and Evaluation of Possibilities for Research and Development of Instrumentation to Determine Future Levels of Radon at a Proposed Building Site," Report of DSMA Atcon Ltd. to Atomic Energy of Canada Ltd., Toronto, 18 Jan., 1983.

[6] Scott, A. G. and Eaton, R. S., "Understanding Radon Transport into Houses," *Radiation Protection Dosimetry*, Vol. 7, Nos. 1–4, 1984, pp. 251–253.

[7] DSMA Atcon Ltd., "A Computer Study of Soil Gas Movement into Buldings," *Report of DSMA Atcon Ltd. to Health and Welfare Canada*, 5 March, 1985.

[8] Loureiro, C. O. Abriola, L. M., Martin, J. E., and Sextro, R. G., "Three-Dimensional Simulation of Radon Transport into Houses with Basements under Constant Negative Pressure," *Environmental Science and Technology*, Vol. 24, 1990, pp. 1338–1348.

[9] Loureiro, C. O., "Simulation of the Steady-State Transport of Radon from Soil into Basements under Constant Negative Pressure," Ph.D. Dissertation, University of Michigan, Ann Arbor, 1987.

[10] Mowris, R. J. and Fisk, W. J., "Modelling the Effects of Exhaust Ventilation on ^{222}Rn Entry Rates and Indoor ^{222}Rn Concentrations," *Health Physics*, Vol. 54, No. 5, 1988, pp. 491–501.

[11] Nazaroff, W. W., "Predicting the Rate of ^{222}Rn Entry from Soil into the Basement of a Dwelling Due to Pressure-Driven Airflow," *Radiation Protection Dosimetry*, Vol. 24, Nos. 1–4, 1988, pp. 199–202.

[12] Revzan, K. L., Fisk, W. J., and Gadgil, A. J. "Modeling Radon Entry into Houses with Basements: Model Description and Verification," *Indoor Air 2*, 1991, pp. 173–189.

[13] Gadgil, A. J., Bonnefous, Y. C., Fisk, W. J., Prill, R. J., and Nematollahi, A., "Influence of Subslab Aggregate Permeability on SSV Performance," Lawrence Berkeley Laboratory Report LBL-31160, 1991.

[14] Rogers, V. C. and Nielson, K. K., "Correlations for Predicting Air Permeabilities and ^{222}Rn Diffusion Coefficients of Soils," *Health Physics*, Vol. 61, No. 2, 1991, pp. 225–230.

[15] Rogers, V. C. and Nielson, K. K., "Multiphase Radon Generation and Transport in Porous Materials," *Health Physics*, Vol. 60, No. 6, 1991, pp. 807–815.

[16] Wray, C. P. "Development and Application of a Multizone Airflow and Contaminant Dispersal Analysis Microcomputer Program for Simulating Radon and Radon Progeny Transport and Accumulation in Soils and Houses with Basements," M.Sc. thesis, Department of Mechanical Engineering, University of Manitoba, 1990.

[17] Wray, C. P. and Yuill, G. K., "Development of Models to Characterize Soil Gas Flow and Radon Entry into Basements," *Proceedings*, Fifth International Conference on Indoor Air Quality and Climate, Toronto, Ontario, 1990.

[18] Kiel, D. E. and Wilson, D. J., "Influence of Natural Ventilation on Total Building Ventilation Dominated by Strong Fan Exhaust," *ASHRAE Transactions*, American Society of Heating, Refrigerating, and Air-Conditioning Engineers, Vol. 93, Part 2, 1987.

[19] Grot, R. A. and Axley, J. W., "Structure of Models for the Prediction of Air Flow and Contaminant Dispersal in Buildings," *Proceedings*, 11th Air Infiltration and Ventilation Center (AIVC) Conference, Ventilation System Performance, Belgirate, Lake Maggiore, Italy, September 1990.

[20] Wray, C. P. and Yuill, G. K., "Dynamic Multi-Compartment Modelling: The Transport of Radon and its Decay Products Indoors," *Proceedings*, International Symposium on Radon and Radon Reduction Technology, Atlanta, GA, 1990.

[21] Yuill, G. K. and Wray, C. P., "A Microcomputer Program for Evaluating the Performance of Buildings Equipped with Ventilator Window/Baseboard Heating Systems," *Proceedings*, 1989 Annual Solar Energy Society of Canada, Inc. (SESCI) Conference. Penticton, BC, 1989.

[22] Yuill, G. K. and Comeau, G. M., "Demonstration and Performance Testing of the Laminar Airflow Super Window-Humidity Controlled Air Inlet-Baseboard Heating (LAFSW/HCAI/BH) System in a Winnipeg House," *Proceedings*, 1989 Annual SESCI Conference. Penticton, BC, 1989.

[23] *ASHRAE Handbook of Fundamentals*, American Society of Heating, Refrigerating and Air-Conditioning Engineers, Inc., Atlanta, 1989.

[24] Yuill and Associates, "Computer Simulation of the Transport of Soil Gas, Indoor Air, and Atmospheric Air into a Subslab Venting System," Report of G. K. Yuill and Associates Ltd. to Canada Mortgage and Housing Corporation, 19 Aug., 1991.

[25] Nazaroff, W. W., Moed, B. A., Sextro, R. G., Revzan, K. L., and Nero, A. V., "Factors Influencing Soil as a Source of Indoor Radon: Framework for Assessing Radon Source Potential," Lawrence Berkeley Laboratory Report LBL-20645, Berkeley, 1989.

[26] Nero, A. V. and Nazaroff, W. W., "Characterising the Source of Radon Indoors," *Radiation Protection Dosimetry*, Vol. 7, Nos. 1–4, 1984, pp. 23–39.

[27] Sextro, R. G., Moed, B. A., Nazaroff, W. W., Revzan, K. L., and Nero, A. V., "Investigations of Soil as a Source of Indoor Radon," *American Chemical Society (ACS) Symposium Series 331-Radon and Its Decay Products: Occurrence, Properties, and Health Effects*, American Chemical Society, Washington, DC, 1987, pp. 10–29.

[28] Nazaroff, W. W. and Nero, A. V., Jr., *Radon and Its Decay Products Indoors*, John Wiley and Sons, New York, 1988.

[29] Yuill and Associates, "Preliminary Investigation Concerning the Impact of Subslab Ventilation on Radon Entry Rate, Soil Temperature, and Energy Consumption," Report of G. K. Yuill and Associates Ltd. to Canada Mortgage and Housing Corporation, 25 Feb., 1991.

[30] Bruno, R. C., "Sources of Indoor Radon in Houses: A Review." *Journal of the Air Pollution Control Association*, Vol. 33, No. 2, 1983, pp. 105–109.

[31] Nazaroff, W. W., "Entry by Pressure-Driven Flow or Molecular Diffusion? A Reassessment of ^{222}Rn Concentrations Measured in an Energy Efficient House," *Health Physics*, Vol. 55, No. 6, 1988, pp. 1005–1014.

[32] Bodansky, D., Robkin, M. A., and Stadler, D. R., *Indoor Radon and Its Hazards*, University of Washington Press, Seattle, 1989.

[33] Walton, G. N., "AIRNET—A Computer Program for Building Airflow Network Modelling," Report of U.S. National Institute of Standards and Technology (NIST, formerly NBS), April 1989.

[34] ABACUS, *ESP—A Building and Plant Energy Simulation System, Version 5, Release 3*, University of Strathclyde, Scotland, 1986.

[35] Yuill and Associates, "Evaluation of Algorithms for Analysis of Smoke Control Systems, ASHRAE Research Project 618-RP," Final Report of G. K. Yuill and Associates Ltd. to American Society of Heating, Refrigerating and Air-Conditioning Engineers, Inc., (ASHRAE), 30 Dec., 1991.

[36] Klote, J. H. and Milke, J. A., *Design of Smoke Management Systems*, American Society of Heating, Refrigerating and Air-Conditioning Engineers, Inc. (ASHRAE), Atlanta, 1992.

[37] Axley, J., "Progress Toward a General Analytical Method for Predicting Indoor Air Pollution in Buildings—Indoor Air Quality Modelling: Phase III Report," Report of U.S. National Bureau of Standards to U.S. Environmental Protection Agency (EPA) NBSIR 88-3814, July, 1988.

[38] Sparks, L. E., "Indoor Air Quality Model Version 1.0," Report of U.S. Environmental Protection Agency, Air and Energy Engineering Research Laboratory, EPA-600/8-88-097a, Research Triangle Park, NC, Sept. 1988.

[39] Said, M. N. A. and MacDonald, R. A., "An Evaluation of a Network Smoke Control Model," *ASHRAE Transactions* Vol. 97, Part 1, 1991.

[40] Walton, G. N. "A Computer Algorithm for Predicting Infiltration and Interroom Airflows," *ASHRAE Transactions*, Vol. 90, Part 1, 1984.

[41] Fisk, W. J., Flexser, S., Gadgil, A. J., Holman, H.-Y, Modera, M. P., Narasimhan, T. N., Nuzum, T., Revzan, K.L., Sextro, R. G., Smith, A. R., Tsang, Y. W., and Wollenberg, H. A., "Monitoring and Modelling for Radon Entry into Basements: A Status Report for the Small Structures Project," Lawrence Berkeley Laboratory Report LBL-27692, Berkeley, CA, Sept. 1989.

[42] Patankar, S. V., *Numerical Heat Transfer and Fluid Flow*, McGraw-Hill Book Company, New York, 1980.

[43] Canadian Standards Association (CSA), CSA Preliminary Standard F326.1-M1989: Residential Mechanical Ventilation Requirements, Canadian Standards Association, Rexdale, Ontario, Canada, 1989.

Andrew K. Persily[1]

Modeling Radon Transport in Multistory Residential Buildings

REFERENCE: Persily, A. K., "**Modeling Radon Transport in Multistory Residential Buildings,**" *Modeling of Indoor Air Quality and Exposure, ASTM STP 1205*, Niren L. Nagda, Ed., American Society for Testing and Materials, Philadelphia, 1993, pp. 226–242.

ABSTRACT: Radon concentrations have been studied extensively in single-family residential buildings, but relatively little work has been done in large buildings, including multistory residential buildings. The phenomena of radon transport in multistory residential buildings is made more complicated by the multizone nature of the airflow system and the numerous interzone airflow paths that must be characterized in such a system. This paper presents the results of a computer simulation of airflow and radon transport in a twelve-story residential building. Interzone airflow rates and radon concentrations were predicted using the multizone airflow and contaminant dispersal program CONTAM88. Limited simulations were conducted to study the influence of two different radon source terms, indoor-outdoor temperature difference and exterior wall leakage values on radon transport and radon concentration distributions.

KEY WORDS: airflow, contaminant dispersal, indoor air quality, multizone, radon, residential buildings

There has been a great deal of research and other activity in the area of radon buildings in recent years. This research has focused primarily on problem identification, mitigation, and source modeling in single-family residential buildings. Recently, attention has turned towards large buildings such as schools, commercial buildings, and multifamily residential buildings. While the fundamental issues regarding the relationship between radon, ventilation, and building features in small buildings is by no means resolved, radon in large buildings is a more complex problem due to the multizone nature of airflow and contaminant dispersal in large buildings. Multizone airflow systems have been studied by the infiltration and ventilation research community for many years, and many significant technical issues remain to be resolved.

In this paper the issue of radon transport in a multifamily residential building is studied with the multizone airflow and contaminant dispersal model CONTAM88 [*1*]. Such a modeling exercise is necessarily constrained by current limitations in existing knowledge regarding both multizone airflow prediction and characterization of radon source strengths. While a sound physical understanding exists regarding multizone airflow systems, the ability to predict the actual airflow rates is limited by the difficulty in representing a building as a multizone airflow system and a lack of data for the many inputs required to calculate the airflow rates in such a system.

In order to predict interzone airflow rates, one must identify an appropriate representation of the building in question as a collection of zones that exchange air with each other and with the outdoors. Identifying an appropriate multizone representation of a building that captures the important airflows, without including an unnecessarily large number of zones, is quite challenging and requires insight and experience with buildings and airflow in buildings. Once the zones of the

[1]Group leader, National Institute of Standards and Technology (NIST), Building and Fire Research Laboratory, Building 226, Room A313, Gaithersburg, MD 20899.

building have been selected, one must determine the leakage characteristics of the airflow paths between these zones. These leakage characteristics can be described as leakage areas at a particular reference pressure or as empirical leakage coefficients based on a power law relation between the airflow rate and the pressure difference between the two zones. Air leakage through openings and the means for characterizing this leakage are described in Chapter 23 of the *ASHRAE Handbook of Fundamentals* [2]. Only limited measurements exist of the leakage characteristics of the various airflow paths in buildings, and the measured values for any particular component, such as doors or windows, cover a wide range of leakage levels. Some leakage data are available in the *ASHRAE Handbook* [2] and other references [3], but when modeling a given building, the appropriate values for the numerous leakage paths in the building are not known unless they have been measured by component pressurization testing. In general, there are far too many leakage paths in a building, even a small building, to determine all of the leakage characteristics. It is not entirely clear whether one needs to know all of this detailed information to understand airflow and contaminant dispersal in a building, but in order to predict airflow in a multizone building, values for the leakage coefficients of the interzone airflow paths must be selected.

Characterization of the radon source strength and its dependence on other variables is another area where the limitations of current knowledge restrict the ability to model radon in multizone airflow systems. The rate at which radon enters a building depends on the rate of production of radon in the ground beneath the building, the permeability of the soil and other materials beneath the building, the nature and extent of openings in the building-ground boundary, and the pressure difference across this boundary [4]. Only limited work has been done on how best to describe the dependence of the rate at which radon enters a building on these factors. In the modeling effort described in this paper, the functional form of the radon source term is very simple and the numerical coefficients for inclusion in the source term are only approximations. Recent work on radon entry models has included finite difference modeling of air and radon transport through the soil beneath the house [5,6] and experimental investigations of the dependence of the radon entry rate on pressure [7,8] and radon source potential of soil [9]. A great deal of additional work is needed to understand radon entry and the most appropriate manner in which to model the radon entry rate in a given building.

CONTAM88

The analysis in this paper was conducted using CONTAM88, a multizone airflow and contaminant dispersal model developed at the National Institute for Standards and Technology (NIST) [1]. This model predicts air movement and contaminant concentrations in a multizone building system given a description of that system as a number of well-mixed zones, along with information on the leakage characteristics of the paths connecting those zones, any mechanical ventilation occurring in the building, contaminant sources and sinks, wind pressure coefficients for the building exterior surfaces, and interior and exterior environmental conditions. Based on this information, CONTAM88 calculates the airflow rates between all of the zones, with one of the zones being the outdoors, and the contaminant concentrations in the zones. A companion program NBSAVIS, also developed at NIST, is employed to develop the building description files used by CONTAM88. NBSAVIS is a menu-driven program used to create files describing the zones of the building, the leakage paths between these zones, any mechanical ventilation within the building, and the contaminant sources.

Detailed discussions of both NBSAVIS and CONTAM88 are contained in Ref 1. CONTAM88 itself is essentially a combination of two programs developed previously at NIST: AIRNET [10], which calculates interzone airflows, and CONTAM87 [11], which predicts contaminant dispersal in multizone systems.

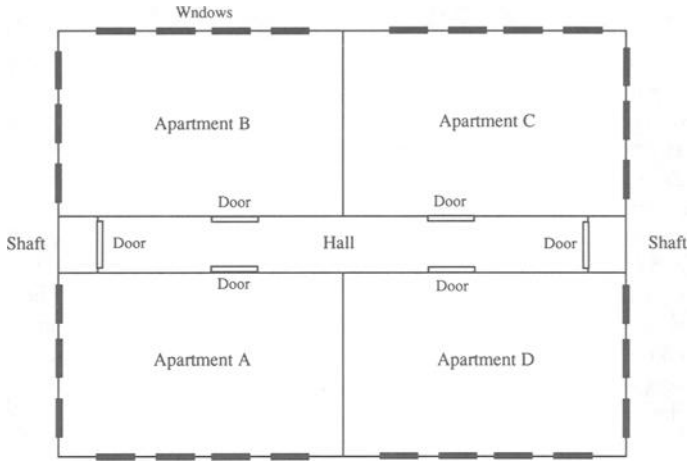

FIG. 1—*Typical floor plan.*

The Building Model

The analyses in this paper were carried out on a twelve-story apartment building with four apartments on each floor and a basement. Several different configurations of the building were modeled in order to study the impact of particular building features on air and radon transport within the building. Most of the modeling runs were conducted on a very simplified building representation, referred to as the base case. A typical floor plan of the base case building is shown in Fig. 1, and an elevation is shown in Fig. 2. The horizontal dimensions of the building are 30 by 22.5 m. The ceiling height of each floor is 2.5 m, and the basement is 2 m below grade, and therefore the roof is 30.5 m above grade. As seen in the figures, the building contains two vertical

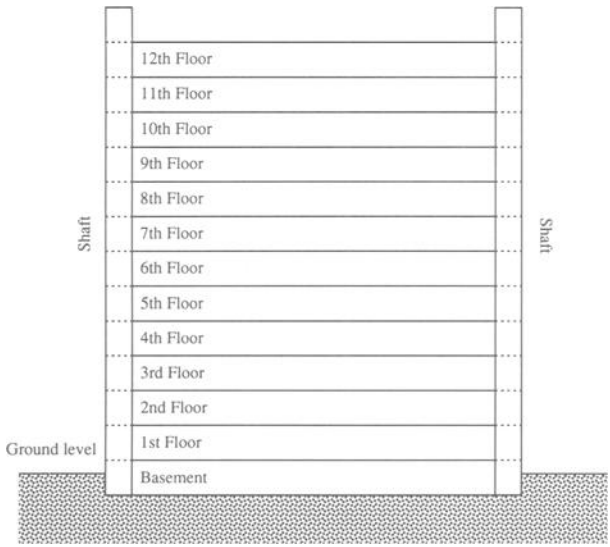

FIG. 2—*Building elevation.*

TABLE 1—*Values assumed for the leakage areas.*

Exterior Walls	3.0 cm^2/m^2
Exterior Doors	
elevator	29 cm^2
stair	29 cm^2
Windows	
basement	1.35 cm^2
upper floors	7.5 cm^2
Interior Walls	
apartment	2 cm^2/m^2
elevator shaft	5 cm^2/m^2
stair shaft	5 cm^2/m^2
Interior Doors	
apartment	75 cm^2
elevator	150 cm^2
stair	150 cm^2
Interior Floors	0.5 cm^2/m^2

shafts at either end of a central hall, an elevator shaft and a stairway. These shafts have horizontal dimensions of 2.5 by 2 m, and the hall is 26 by 2.5 m. These shafts extend from the basement, which is not subdivided into rooms, all the way up to the roof of the building. These shafts are open from the basement to the roof, but in the building model they are divided horizontally at each floor level in order to allow the calculation of vertical gradients in radon concentration within the shafts. All zones, including the shaft zones, are assumed to be perfectly mixed. Doors connect the hallway to each apartment, the hallway to the elevator and stair shafts, and these shafts to the basement. In addition, there are doors to the outside located at the roof level of the two shafts. There are four windows on the long wall of each apartment and three on the short wall.

Using NBSAVIS, this multizone system is described in terms of the zones, their volumes, and the leakage paths between the zones. The leakage of the interior and exterior walls, the windows, and the interior and exterior doors are based on information contained in Chapter 23 of the *ASHRAE Handbook of Fundamentals* [*2*] and the *Design of Smoke Management Systems* [*3*]. The *ASHRAE Handbook* contains a range of leakage values for these various elements and a value in the middle range of each element was selected for the base case. The values assumed for the leakage areas of interest are listed in Table 1.

In addition, a leakage area of 2.5 cm^2/m was assumed to exist at the wall-floor joints and wall-ceiling joints in each apartment. The leakage areas between the vertical sections of the elevator and stair shafts are assumed to be equal to the cross-sectional area of the shafts. All leakage areas are based on a reference pressure of 4 Pa and a discharge coefficient of 1.0. All leakage paths are characterized by a flow exponent of 0.6. As can be seen above, no distinction was made between the leakage characteristics of the elevator and stair shafts in the base case, although field measurements have shown differences to exist [*12*]. As described in the following section on the radon source model, the leakage area of the basement floor was assumed to be 0.0085 cm^2/m^2, with a flow exponent of 1.0.

Radon Source Model

Two models of radon entry rate were used in these simulations, one with the radon entry rate dependent on pressure and the other assuming a pressure independent radon source. These very simple models were based on consideration of the research that has been done on radon entry

measurement and modeling [*4–9*].[2] The first model assumes that the radon entry rate depends on the pressure difference between the basement floor and outside, specifically that the radon entry rate is equal to a radon entry coefficient times the pressure difference raised to the power x. In order to employ this model, one needs values for the radon entry coefficient in units of Bq/s-m^2-Pa^x and the power x that describes the dependence of radon entry on pressure difference. In order to determine the radon concentration of the air entering the basement from the ground, and to complete the inputs for calculating the interzone airflow rates, one needs values for the air leakage coefficient for the basement floor in units of m^3/s-m^2-Pa^n (or in units of leakage area) and the pressure exponent n. For both radon entry and air leakage through the basement floor, the pressure exponents x and n were assumed to equal 1.0. Little data exists for this basement floor leakage coefficient, and a value for the leakage area of 0.0085 cm^2 per m^2 of basement floor area was used in this model. Similarly, there have been few determinations of the radon entry coefficient.

In order to obtain a reasonable value for the radon entry coefficient, CONTAM88 was used to simulate infiltration and radon entry in a two-story house with an exterior envelope leakage area of 940 cm^2. Given an indoor-outdoor air temperature difference of 20 K, the radon entry coefficient was varied until a radon concentration of about 100 Bq/m^3 was obtained in the house. Under these conditions, the radon entry coefficient was equal to 0.02 Bq/s-m^2-Pa, and this value was used in the simulations of the twelve-story residential building.

The second radon entry model was based on the assumption that the radon entry rate is independent of the pressure difference between the basement and the outdoors. This model is based on the concept that there is a limited amount of radon generated under the building in question and that all of this radon is available to enter the building. Therefore, if the pressure in the basement is below that in the soil, then all of the radon enters the basement.[2] If the pressure in the basement is positive relative to the ground, then no radon enters the basement. This first order model has been suggested by some field measurements in which the radon entry increased with pressure difference up to a point and then remained constant as the pressure difference increased further [*7,8*]. In this second model of radon entry, the air leakage coefficient of the basement floor was the same as in the pressure dependent model. The radon entry coefficient was again determined from a CONTAM88 simulation of a two-story house. In order to obtain about 100 Bq/m^3 in the house, the pressure independent source term was equal to 0.05 Bq/s-m^2.

These models of radon entry are obviously oversimplified representations of a very complex phenomena. They ignore the important issues of soil properties such as radium content and permeability, as well as spatial variations in these properties. Temporal variations, such as those induced by moisture effects, are also ignored.

Simulations Run

In order to gain some insight into radon transport in multifamily, high-rise residential buildings, several cases were run in this modeling study. These cases are listed in Table 2. The base case described above was run at a series of indoor-outdoor air temperature differences ranging from 1 to 40 K for the two different radon source models presented earlier. Although CONTAM88 is capable of modeling wind effects, all cases were run at zero wind speed in this study. The base case employing the pressure-dependent radon source term is referred to as FT04, while the base case with the pressure independent source is referred to as FT05. Several modifications were made to the base case, and these were all run at an indoor-outdoor temperature difference of 20 K using both radon source models. In all of the runs, the ambient radon concentration was assumed to equal 10 Bq/m^3.

[2]Personal communication with Terry Brennan, president, Camroden Associates, Oriskany, NY.

TABLE 2—*Summary of simulation results.*

FT04	Base case, pressure dependent radon source
FT05	Base case, pressure independent radon source
FT06	Asymmetric elevator and stair leakage, pressure dependent radon source
FT07	Asymmetric elevator and stair leakage, pressure independent radon source
FT08	Exterior wall leakage 50% of base case, pressure dependent radon source
FT09	Exterior wall leakage 50% of base case, pressure independent radon source
FT10	Exterior wall leakage 200% of base case, pressure dependent radon source
FT11	Exterior wall leakage 200% of base case, pressure independent radon source
FT12	50 L/s exhaust fan in every apartment, pressure dependent radon source
FT13	50 L/s exhaust fan in every apartment, pressure independent radon source

In the first alternate case, the symmetry between the elevator and stair shaft leakage was removed. More reasonable values for the leakage of the shaft walls and the interior doors to these shafts were used in these simulations [*12*]. The modifications to the base are shown in Table 3. These "asymmetric" cases are designed as FT06 and FT07 for the pressure-dependent and the pressure-independent radon source terms, respectively.

Alternate cases were also run in which the leakage of the exterior walls was reduced to one-half the value in the base case. These are referred to as FT08 and FT09 for the pressure-dependent and pressure-independent radon sources. The leakage of the exterior walls, as compared to the base case, was doubled in cases FT10 and FT11. In cases FT12 and FT13, a 50 L/s exhaust fan was added to each apartment. Cases FT08 through FT13 are all based on the symmetric values of the elevator and stair shaft leakage.

The simulations of the twelve-story building run on CONTAM88 involved 92 building zones and about 1250 openings. Solution of the steady-state airflow equations required about 40 s on a 386 personal computer with a math coprocessor and a 20-mHz clock speed. The cases with the exhaust fans in the apartment increased the solution time by about 10 s. CONTAM88 obtained the airflow rate solution after about nine iterations in all cases. The solution of the steady-state radon concentrations required an additional 5 s.

Results

Each simulation determined the airflow rate through and the pressure difference across each of the 1254 openings in the building model and the radon concentration in each of the 92 zones. A schematic summary of the results for the base case with the pressure dependent radon source (FT04) is shown in Fig. 3. The figure shows the calculated airflow rate in kilograms per second between each type of zone (shaft, hall, and apartment), and between each zone type and the outdoors. Any apparent deviations from a perfect mass balance of an individual zone are due to rounding off of the results for inclusion in the figure. The calculated radon concentration in becquerels per cubic meter is also shown in each zone. As can be seen in the figure, vertical flow up the elevator and stair shafts is a major mechanism for air and radon transport within the building.

TABLE 3—*Modifications to the base case.*

Interior Walls	
elevator shaft	8 cm^2/m^2
stair shaft	2 cm^2/m^2
Interior Doors	
elevator	250 cm^2
stair	100 cm^2

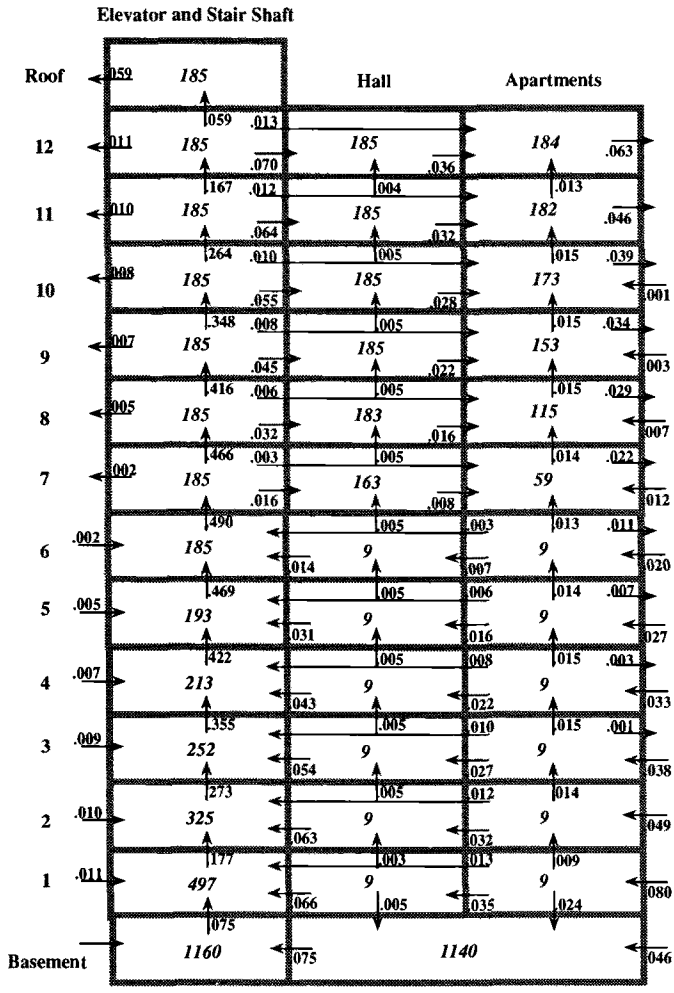

FIG. 3—*Schematic representation of the base case FT04.*

Air flows into the shafts from the outdoors, the basement, and the hallways and apartments on floors one through six. On floors seven and higher, air flows out of the shafts and into the apartments, hallways, and outdoors. Therefore, the radon concentrations in the halls and apartments on floors one through six are close to the outdoor concentration. The difference between the outdoor concentration of 10 Bq/m^3 and the indoor concentration on these lower floors 9 Bq/m^3 is due to density differences between the indoor and outdoor air. The radon concentrations in the hall and apartments increase from floors seven and higher as the airflow rate from the shafts to these zones increase. The stack effect in these shafts is so strong that air from the first floor hall and apartments is actually pulled down into the basement of the building. Regarding the ventilation of the apart-

ments themselves, outdoor air infiltrates into these apartments on floors one through ten and exfiltrates on floors three through twelve. Air infiltrates into and exfiltrates out of the same apartment because of the pressure relationship based on the relative values of the exterior wall leakage and the resistance to vertical airflow within the building. The phenomena of the stack effect in tall, multizone buildings is addressed by Tamura and Wilson [13]. The airflow rate results obtained for the base case with the pressure independent radon source, FT05, are identical. The radon concentrations are lower by a factor of four in all zones due to the magnitude of the source terms used in the two models. The relative radon concentrations throughout the buildings are identical in the pressure independent case. The predicted radon levels in these buildings scale linearly with the radon entry coefficients discussed earlier for both radon source models. These coefficients are generally quite building specific, and therefore the radon concentrations predicted in these simulations should be considered in relation to each other and should not be considered as relevant to actual concentrations in a particular building or group of buildings.

The base case model was run for several different indoor-outdoor air temperature differences. These results are summarized in Tables 4 and 5 for cases FT04 (pressure dependent source) and FT05 (pressure independent source). The first four columns of each table contain the indoor-outdoor temperature difference, the whole building air change rate in air changes per hour, the pressure difference between the basement floor and the outdoors, and the rate at which radon enters the basement. The last four columns contain the radon concentration that enters the basement from the ground and the concentration in the basement, the twelfth story apartments and the average of all the apartments, all in units of becquerels per cubic meter. Note that the predicted radon concentrations for FT05 are much lower than those for FT04. This is simply a reflection of the value of the radon entry coefficient for the two models. Of more interest is the dependence of these concentrations on temperature difference and building configuration.

The whole building air change rates for cases FT04 and FT05 are identical and the calculated air change rates are plotted against temperature difference in Fig. 4. As discussed in the *ASHRAE Handbook of Fundamentals* [2], the pressure difference due to temperature difference is linear with temperature difference. In these simulations, the airflow rate through the openings is a function of the pressure difference raised to the power 0.6. A simplistic consideration of the relationship between pressure difference and airflow rate would lead to the expectation that the whole building air change rate would depend on the temperature difference raised to the power 0.6. In fact, due to the nonlinear nature of the problem, the calculated air change rates for the building depend on the temperature difference raised to power 0.74.

The pressure difference across the basement floor, which induces airflow into the basement from the ground, depends linearly on the indoor-outdoor air temperature difference. Since the airflow rate into the basement from the ground is assumed to be linear with pressure difference, this airflow rate also varies linearly with temperature difference. Therefore, in case FT04, the rate of radon entry into the basement varies linearly with temperature difference. Of course, the rate of radon entry into the basement in case FT05 is independent of temperature difference. The radon concentration in the basement depends on both the radon entry rate and the air change rate of the basement, the latter quantity being a complex and nonlinear function of temperature and pressure.

Figure 5 is a plot of the basement radon concentration versus temperature difference for cases FT04 and FT05. In the case of the pressure dependent radon source, FT04, the basement radon concentration depends on the temperature difference to the power 0.32. The first order model discussed by Cavallo [7,8], would predict a power of 0.4. In case FT05, the radon entry rate is constant, and therefore as the temperature difference and the basement air change rate increase, the basement concentration decreases. The basement radon concentration in case FT05 depends on the temperature difference raised to the power -0.68. The simple first order model suggested by Cavallo [7,8] would predict a power of -0.6.

TABLE 4—*Summary of results for base case FT04.*

T_{in}-T_{out}, K	Building Air Change Rate, h^{-1}	Basement Floor Pressure Difference, Pa	Basement Radon Entry Rate, Bq/s	Radon Concentration, Bq/m^3			
				Entering from Ground	Basement	12th Floor Apartment	Average of Apartments
1	0.02	0.5	7	39 100	477	87	41
5	0.06	2.4	32	38 800	692	117	52
10	0.10	4.8	64	38 500	882	145	63
15	0.13	7.3	97	38 100	1020	166	70
20	0.15	9.9	131	37 800	1140	184	77
23	0.17	11.4	152	37 600	1200	194	80
25	0.18	12.5	166	37 500	1240	200	82
30	0.21	15.2	202	37 100	1330	214	88
35	0.23	18.0	239	36 800	1410	227	92
40	0.25	20.8	277	36 400	1480	239	97

TABLE 5—*Summary of results for base case FT05.*

T_{in}-T_{out}, K	Building Air Change Rate, h^{-1}	Basement Floor Pressure Difference, Pa	Basement Radon Entry Rate, Bq/s	Radon Concentration, Bq/m^3			
				Entering from Ground	Basement	12th Floor Apartment	Average of Apartments
1	0.02	0.6	33	162 000	2320	389	162
5	0.06	2.9	33	33 500	715	120	53
10	0.10	5.9	33	16 600	460	79	37
15	0.13	8.9	33	10 900	355	63	30
20	0.15	12.0	33	8000	295	53	26
23	0.17	13.9	33	6900	269	49	23
25	0.18	15.1	33	6300	255	47	23
30	0.21	18.4	33	5200	225	43	22
35	0.23	21.8	33	4400	203	39	20
40	0.25	25.3	33	3700	185	36	19

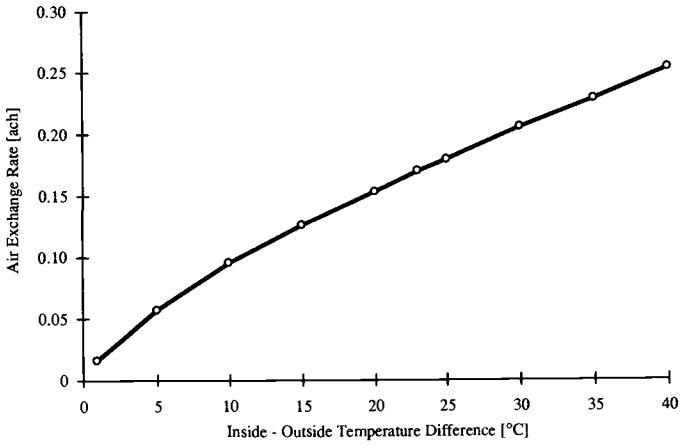

FIG. 4—*Whole building air change rate for the base case FT04.*

The radon concentrations in the twelfth-floor apartments and the average concentration for all of the apartments have essentially the same dependence on temperature difference as the basement concentration, that is, an exponent of about 0.3 in case FT04 and an exponent of −0.7 in case FT05.

The remaining simulations, described in Table 2, were all run at an indoor-outdoor temperature difference of 20 K. The results of these simulations are presented in Table 6. The first three columns of the table contain the case designation, the whole building air change rate in air changes per hour, the pressure difference across the basement floor, and the radon entry rate. The last four columns contain the radon concentration entering through the basement floor, in the basement and in the twelfth-floor apartments, and the average concentration in all of the apartments.

In cases FT06 and FT07, the symmetry between the elevator and stair shafts was eliminated by changing the leakage areas of the interior shaft walls and the interior doors leading from these shafts. These modifications in turn eliminate the symmetry of the calculated airflow rates and radon concentrations, making a graphical presentation of the results similar to that shown in Fig. 3 impossible. The overall results, that is, the whole building air change rate, the radon entry rate,

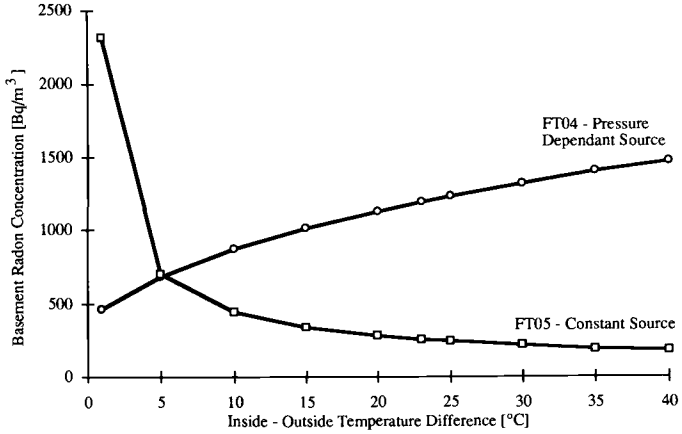

FIG. 5—*Predicted pressure difference across the basement floor.*

TABLE 6—*Summary of simulation results.*[a]

Case	Building Air Change Rate, h^{-1}	Basement Floor Pressure Difference, Pa	Basement Radon Entry Rate, Bq/s	Radon Concentration, Bq/m^3			
				Entering from Ground	Basement	12th Floor Apartment	Average of Apartments
FT04	0.15	9.9	131	37 800	1140	184	77
FT05	0.15	9.9	33	8050	295	53	26
FT06	0.16	10.3	137	37 800	1150	185	78
FT07	0.16	10.3	33	7740	283	51	26
FT08	0.12	11.2	148	37 800	1550	243	106
FT09	0.12	11.2	33	7270	354	61	31
FT10	0.25	8.5	113	37 800	833	125	47
FT11	0.25	8.5	33	9090	251	43	20
FT12	0.39	11.8	157	37 800	1420	176	62
FT13	0.39	11.8	33	6910	307	44	20

[a]Interior-exterior temperature difference equals 20 K in all cases.

the basement radon concentration, and the average radon concentration in the apartments, are very close to the base cases FT04 and FT05, as seen in Table 6. However, the changes in the shafts wall and interior door leakage areas change the airflow patterns within the building and the resultant radon concentration distribution. The airflow rates up the elevator shaft and between the elevator shaft and the apartments and hall, are much larger than in the base case. Correspondingly, the airflow rates up the stair shaft are lower and between the stair shaft and the floors are also lower. There is a larger flow rate of high radon concentration basement air into the elevator shaft than into the stair shaft, and therefore there are higher radon concentrations in the elevator shaft than in the stair shaft. Apartments A and B, which are closest to the elevator shaft, have higher radon concentrations than Apartments C and D. This difference is more pronounced on floors seven through ten than on the top two floors of the building. Also, air flows from Apartments C and D to Apartments A and B on the lower six floors of the building, and in the opposite direction on the upper six floors. This case shows the significant changes in internal airflow patterns and radon transport that can result from a limited modification in the leakage characteristics of interior partitions.

In cases FT08 and FT10, the exterior wall leakage was one-half and twice that of the base case respectively. Figure 6 is a schematic representative of the results of FT08, identical in format to Fig. 3. The tighter exterior walls result in a larger radon entry rate into the basement and less dilution of the radon that does enter by outdoor air change. The radon concentrations in the building are therefore significantly larger than in case FT04. Figure 7 shows the results for case FT10 with the leakier exterior walls. In this case, the radon entry rate is lower than in the base case and there is more dilution of the radon that does enter the building. These factors result in significantly lower radon concentrations in case FT10 than in the base case. The ratio of the average radon concentration in the apartments for the tight-wall case (FT08) to the loose-wall case (FT10) with the pressure dependent source is 2.55. The ratio of the base case average (FT04) to the loose-wall case (FT10) is 1.79. These ratios for the pressure independent source cases are 2.00 (FT09/FT11) and 1.55 (FT05/FT11), respectively. The radon concentrations in the pressure independent cases are less influenced by wall tightness because the source does not change, and the radon concentration is only affected by the difference in the dilution and air change rate.

In case FT12, a 50 L/s exhaust fan was included in every apartment. The results for this case are shown in Fig. 8. The operation of the exhaust fans increases the pressure difference across the basement floor, and therefore increases the radon entry rate into the building. However, the exhaust fans also increase the infitration into the apartments. The increased dilution of the radon in the building more than compensates for the increased radon entry, and the radon levels are lower than in the base case.

Summary and Discussion

This paper presents the results of a limited number of computer simulations of multizone airflow and radon transport for a simplified representation of a multifamily, high-rise building. A limited number of the building features in this representation were modified to study the impact of the leakage of exterior walls, the airtightness of interior partitions, and the operation of ventilation systems on the calculated airflow patterns and on the radon distribution within the building. Based on these simulations, limited as they were, some insights were gained into radon transport in this building type.

First, vertical shafts are critical pathways for air and radon transport in these tall buildings. Significant quantities of air flows through these shafts, transporting radon and perhaps other contaminants between the floors of the building. Under heating conditions, these shafts pull air from the lower floors, including the basement, and deposit this air and its contents on the upper floors. The number of floors that feed into the shafts and the number that are fed by the shafts depend

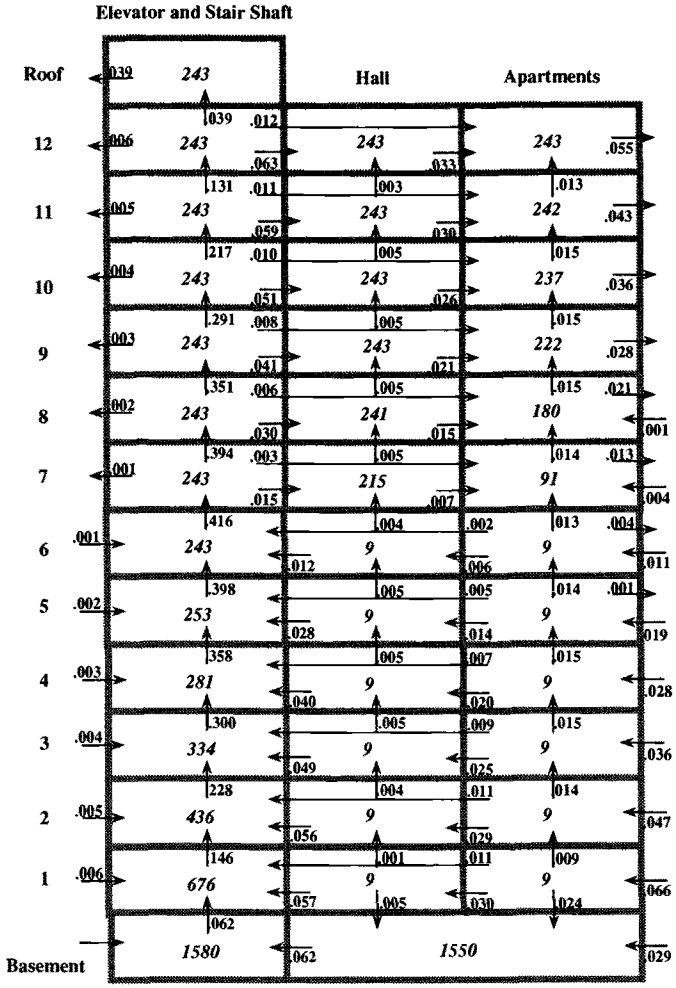

FIG. 6—*Schematic representation of case FT08—tight exterior wall.*

on the leakage characteristics of the interior partitions. In these simulations, the elevator and stair shafts served as these critical vertical pathways. In real buildings, other less obvious shafts may exist, including plumbing and other service chases, and interior and exterior wall cavities.

These simulations also demonstrate that airflow within multizone buildings and the resultant radon concentrations are complex and nonlinear functions of numerous factors: (1) the layout of the building especially the existence of vertical shafts, (2) the leakage characteristics of the exterior walls and the interior partitions, (3) the nature of the radon source, and (4) the existence and nature of mechanical ventilation in the building. The manner in which these factors interact to determine internal airflow patterns and radon distribution within large, multizone buildings is quite complex

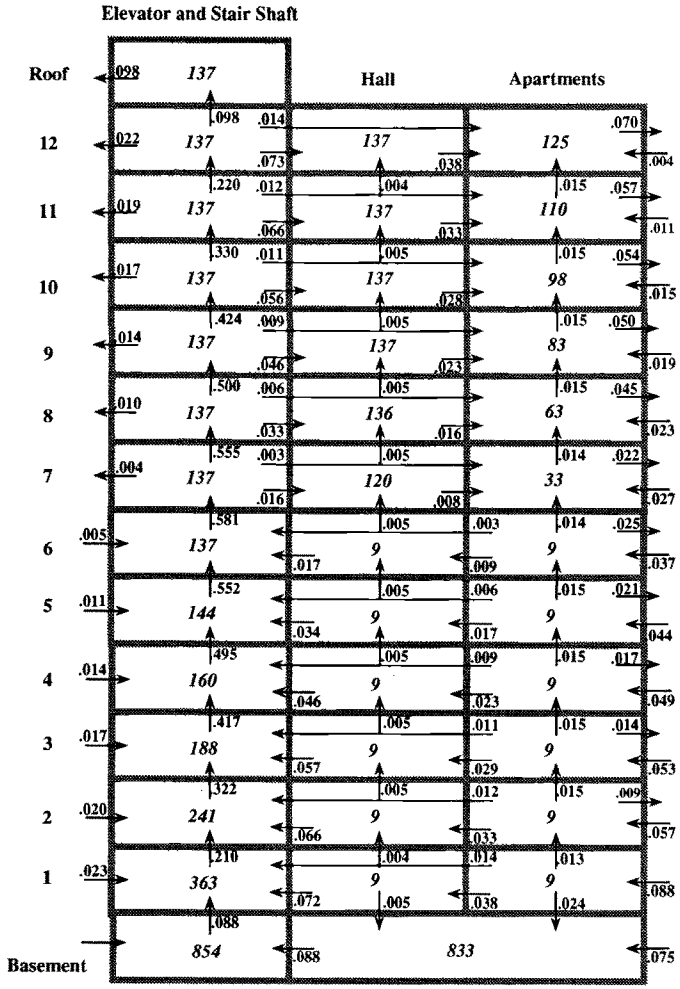

FIG. 7—*Schematic representation of case FT10—leaky exterior walls.*

and generally does not lend itself to an intuitive approach. For example, operating exhaust fans in a building with a pressure dependent radon source might be expected to increase radon concentrations. However, in the simulations presented in this paper, the nature of the interzone and exterior wall leakage characteristics led to decreased radon concentrations in the apartments. Under other circumstances of building layout and leakage and radon source characteristics, exhaust fan operation could instead increase radon concentrations.

These simulations employed both a pressure dependent and a pressure independent radon source term. While research activities are being conducted to understand the complex problem of radon entry into buildings, these simple models have proven useful in these simulations. The pressure

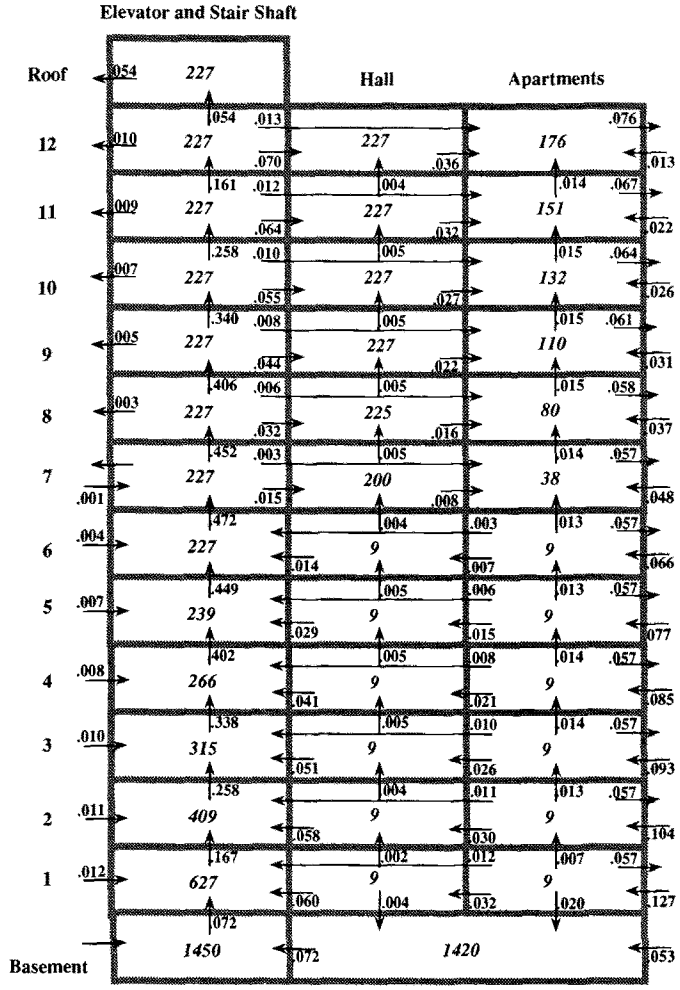

FIG. 8—*Schematic representation of case FT12—exhaust fans.*

dependent radon source yields a radon entry rate that is affected by the indoor-outdoor temperature difference, exhaust fan operation, and the tightness of the exterior walls and interior partitions. However, the resultant radon levels in the occupied space may not necessarily increase with an increasing radon entry rate, as the radon distribution within the building is also affected by the airflow pattern in the building. The pressure independent radon source yields a situation in which the overall radon levels within the building decrease under any circumstance that increases the building air change rate. The change in radon levels within the occupied spaces of the building however, is a more complex function of interior airflow patterns. The appropriateness of these models for real buildings will be determined by ongoing research into radon entry into buildings.

Further study of radon transport and other multizone airflow and contaminant dispersal problems lends itself to the analysis performed in this paper using the program CONTAM88. Performing such simulations is relatively straightforward, although data requirements exist for the leakage characteristics of the numerous interzone airflow paths. Additional computer modeling of the numerous factors affecting radon transport in multifamily, high-rise buildings are needed to develop a deeper understanding of this complex problem. These computer simulations need to be supplemented with field investigations to obtain the input data needed for the models and to verify the predictions.

Acknowledgments

The author extends his appreciations to Terry Brennan for many stimulating discussions on radon source models and to W. Stuart Dols for his assistance in preparing this report.

References

[1] Grot, R. A., "User Manual NBSAVIS CONTAM88," NISTIR 4585, National Institute of Standards and Technology (NIST), Gaithersburg, MD, 1991.

[2] *ASHRAE, Handbook of Fundamentals*, American Society of Heating, Refrigerating, and Air-Conditioning Engineers, Inc., Atlanta, GA, 1993.

[3] Klote, J. H. and Milke, J. A., *Design of Smoke Management Systems*, ASHRAE Publication, American Society of Heating, Refrigerating, and Air-Conditioning Engineers, Inc., Atlanta, GA, 1992.

[4] Nazaroff, W. W., Moed, B. A., and Sextro, R. G., "Soil as a Source of Indoor Radon: Generation, Migration, and Entry," *Radon and Its Decay Products in Indoor Air*, W. W. Nazaroff and A. V. Nero, Jr., Eds., John Wiley & Sons, New York, 1988.

[5] Revzan, K. L. and Fisk, W. J., "Modeling Radon Entry into Houses with Basements: The Influence of Structural Factors," LBL-28109, Lawrence Berkeley Laboratory, Berkeley, CA, 1990.

[6] Revzan, K. L., Fisk, W. J., and Gadgil, A. J., "Modeling Radon Entry into Houses with Basements: Model Description and Verification," *Indoor Air*, Vol. 2, 1991, pp. 173–189.

[7] Cavallo, A., Gadsby, K. J., Reddy, T. A., and Socolow, R., "The Effect of Natural Ventilation on Radon and Radon Progeny Levels in Houses," *Proceedings*, Fifth International Symposium on Natural Radiation in the Environment, Salzburg, Austria, 1991.

[8] Cavallo, A., Gadsby, K. J., and Reddy, T. A., "The Effect of Natural and Forced Basement Ventilation on Radon Levels in Single Family Dwellings," Center for Energy and Environmental Studies, Princeton University, Princeton, NJ, 1991.

[9] Nazaroff, W. W. and Sextro, R. G., "Technique for Measuring the Indoor ^{222}Rn Source Potential of Soil," *Environmental Science and Technology*, Vol. 23, No. 4, 1989, pp. 451–458.

[10] Walton, G. N., "AIRNET-A Computer Program for Building Airflow Network Modeling," NISTIR 89-4072, National Institute of Standards and Technology (NIST), Gaithersburg, MD, 1989.

[11] Axley, J., "Progress Toward a General Analytical Method for Predicting Indoor Air Pollution in Buildings-Indoor Air Quality Modeling Phase III Report," NBSIR 88-3814, National Bureau of Standards [Presently National Institute of Standards and Technology (NIST)], Gaithersburg, MD, 1988.

[12] Tamura, G. T. and Shaw, C. Y., "Air Leakage Data for the Design of Elevator and Stair Shaft Pressurization Systems," *ASHRAE Transactions*, Vol. 82, Part 2, 1976, pp. 179–190.

[13] Tamura, G. T. and Wilson, A. G.,"Building Pressures Caused by Chimney Action and Mechanical Ventilation," *ASHRAE Transactions*, Vol. 73, Part 2, 1967, pp. II.2.1–II.2.12.

Modeling of Exposures

Leslie E. Sparks,[1] *B. A. Tichenor,*[1] *and J. B. White*[1]

Modeling Individual Exposure from Indoor Sources

REFERENCE: Sparks, L. E., Tichenor, B. A., and White, J. B., **"Modeling Individual Exposure from Indoor Sources,"** *Modeling of Indoor Air Quality and Exposure, ASTM STP 1205*, Niren L. Nagda, Ed., American Society for Testing and Materials, Philadelphia, 1993, pp. 245–256.

ABSTRACT: Individual exposure to air pollutants is determined by the behavior of indoor sources and sinks and activity patterns. This paper discusses a model that allows analysis of individual exposure for a wide range of sources and sinks. Emphasis of the discussion is on exposures to volatile organic compounds (VOCs) from commonly used sources. The effects of source and sink behavior on exposure are complex. Important factors include source strength, source decay rate, rates to the sink, re-emissions from the sink, and building operation parameters such as ventilation rate. Sources provide the primary exposure and dominate exposure while the source strength is strong. Sinks modify exposure by reducing peak concentrations and, because of re-emissions from sinks, by increasing the time of relatively high concentrations. Exposures from several different sources are analyzed both with and without sinks and under a range of different building operation scenarios. The need for standard scenarios in evaluating the effects of sources on individual exposure is discussed. Model concentration predictions are compared with data from an indoor air quality (IAQ) test house.

KEY WORDS: indoor air quality (IAQ) model, exposure, sources, sinks, activity patterns

Indoor air quality (IAQ) is determined by the interactions of sources, sinks, and air movement between rooms and between the building and the outdoors. Sources may be located in rooms, in the heating, ventilation, and air-conditioning (HVAC) system, or outdoors. There may be sinks (i.e., materials that adsorb indoor pollutants) in the same locations. Sinks may also act as sources by re-emitting the pollutants collected in them. Individual exposure to pollutants from indoor sources is determined by the combination of indoor pollutant concentrations and individual activity patterns.

A personal computer model, EXPOSURE, to predict in-room pollutant concentrations and individual exposure to the pollutants is being developed as part of the EPA's IAQ program. The model is intended as a tool to allow analysis of IAQ situations. The analyses provided by the model can assist in providing guidance in finding ways to reduce exposure to indoor air pollutants.

General Mathematical Framework of the Model

EXPOSURE is a multi-room model based on an earlier model called INDOOR [*1*]. EXPOSURE allows calculation of pollutant concentrations based on source emission rates, room-to-room air movement, air exchange with the outdoors, and indoor sink behavior.

[1]Air and Energy Engineering Research Laboratory, U.S. Environmental Protection Agency, Research Triangle Park, NC 27711.

Each room is considered to be well mixed. The validity of the well-mixed assumption was verified in several experiments in the EPA IAQ test house [*1*] and by data reported by Maldonado [*2*].

A mass balance for room i of N rooms gives

$$V_i \frac{dC_i}{dt} = C_{i\text{IN}}Q_{i\text{IN}} - C_{i\text{OUT}}Q_{i\text{OUT}} + S_i - R_i \tag{1}$$

where V_i is the volume of the room, C_i is the pollutant concentration in the room, $C_{i\text{IN}}$ is the concentration entering the room, $Q_{i\text{IN}}$ is the air flow into the room, $C_{i\text{OUT}}$ is the concentration leaving the room, $Q_{i\text{OUT}}$ is the air flow leaving the room, S_i is the source term, R_i is the removal term, and the subscript i refers to room i for a room in a set of multiple rooms, $i = 1, 2, \ldots, N$, where N is the number of rooms. The removal term, R_i, includes pollutant removal by air cleaners and sinks. Typical units for the terms in Eq 1 are: V, m^3; C, mg/m^3; t, h; Q, m^3/h; S, mg/h; and R, mg/h.

The well-mixed assumption requires that $C_{i\text{OUT}}$ equals C_i. Equation 1 can be rewritten as

$$V_i \frac{dC_i}{dt} = C_{i\text{IN}}Q_{i\text{IN}} - C_iQ_{i\text{OUT}} + S_iR_i \tag{2}$$

Equation 2 is one of a set of similar equations that must be solved simultaneously in a multiple room model.

EXPOSURE uses a fast discrete time step algorithm developed by Yamamato et al. [*3*] to solve the series of equations. The algorithm is based on the assumption that for sufficiently small time steps, dt, the source and sink terms and all neighboring concentrations are constant. Under this assumption, there is an exact solution to the set of equations. The algorithm uses this exact solution to calculate the concentration under varying conditions at the end of each time step. The method is stable for all time steps and is accurate for sufficiently small time steps. (The size of the time step depends on how rapidly concentrations are changing. In general a time step of one minute is small enough for situations when concentrations are changing rapidly, and time steps of several minutes are adequate when concentrations are near steady-state. The time step must be sufficiently small to capture the changes in source behavior.)

Source Terms

The ability of any model to predict indoor air pollutant concentrations depends on the accuracy of the source models incorporated into the model. EXPOSURE uses source models developed as a part of the EPA's source characterization research program and source models provided in the literature. The model incorporates a wide range of emission characteristics to allow simulation of the range of sources encountered in indoor spaces. Several sources are allowed in each room.

The model includes a database of source emission rates for these various sources based on research conducted by the Indoor Air Branch, Air and Energy Engineering Research Laboratory, of the EPA. The user can add to the database and can override the database emission rates.

Generally sources can be divided into three categories:

(1) Long-term steady-state sources such as moth cakes,
(2) On/off sources such as heaters, and
(3) Decaying sources such as painted surfaces.

TABLE 1—*Emission rates for selected indoor pollutant sources.*

Source	S_0, mg/m²-h	k, 1/h	S_A, mg/m²-h
Wood stain	17 000	0.4	1000
Polyurethane	20 000	0.25	1000
Wood floor wax	20 000	6.0	10 000
Moth crystals	12 000	0	0
Dry-cleaned clothing	1.6	0.03	0
Liquid nails	10 000	1	0

Some sources also have short-term emissions associated with using the source. For example, a painted surface has a long-term decaying emission and a short-term emission associated with the act of painting. The short-term emission is defined as the application emission.

The most common source model used in EXPOSURE is given by

$$S = S_0 e^{-kt} + S_A \qquad \text{for } t \leq t_A$$

and

$$S = S_0 e^{-kt} \qquad \text{for } t > t_A \tag{3}$$

where S is the emission rate (mass/unit source/time), S_0 is the initial emission rate, k is a decay constant (1/time), t is the elapsed time, S_A is the application emission rate (mass per unit source size), and t_A is the application time. This type of source term allows simulation of a wide range of source types. For a steady-state source, k is zero. For sources without an application phase, S_A and t_A are zero.

S_0 and k can be determined from chamber studies (see ASTM D 5116, Guide for Small-Scale Environmental Chamber Determinations of Organic Emissions from Indoor Materials/Products; see also Ref *4*). In many cases all of the emissions are accounted for by S_0 and k as determined by chamber studies. However, there are sources, such as wood stain, paint, and floor wax, where significant emissions may not be accounted for by the chamber studies. These emissions occur while the source is being used (for example, while a floor is being waxed) and during the time it takes to place the source in the chamber. The emissions during the time the source is being used are termed application emissions. The values of S_A can be estimated or at least bounded from large chamber studies, test house studies, mass balance analysis of small chamber studies, or other experiments.

A series of experiments to estimate the emissions during application has been completed. The data for these experiments have not been fully analyzed. Preliminary data analysis indicates that the application emissions for wood stain and varnish are less than 5% of the total emissions.

Estimates of source terms for several sources are given in Table 1. These data are based on experiments conducted in the EPA's small chambers and in the EPA's IAQ test house.

Sink Terms

Research in the EPA test house [*1*,*5*,*6*] and in the small chamber laboratory [*6*] has shown that sinks (i.e., surfaces that remove pollutants from indoor air) play a major role in determining indoor pollutant concentrations. These sinks may be reversible or irreversible. A reversible sink re-emits the material collected in it, and an irreversible sink does not. Sink behavior depends on the pol-

lutant, on the nature of the sink, and on environmental factors such as temperature, air velocity, and humidity. A sink may appear to be irreversible when the pollutant concentration is high and then become reversible when the pollutant concentration is low. Considerable research is necessary to define the behavior of sinks. Sink models have been published by Tichenor et al. [6] and Axley [7].

The sink model used in EXPOSURE is based on research of Tichenor et al. [6]

$$R_s = k_a C A_{\text{sink}} - k_d M_S^n A_{\text{sink}} \tag{4}$$

where R_s is the rate to the sink (mass per unit time), k_a is the sink rate constant (length per time), C is the in-room pollutant concentration (mass per length cubed), A_{sink} is the area of the sink (length squared), k_d is the re-emission or desorption rate constant (1/time if $n = 1$), M_s is the mass collected in the sink per unit area (mass per length squared), and n is some exponent (generally $n = 1$).

Experimental data in the EPA test house and small chambers show that, for typical gaseous organic pollutants of interest in indoor air, k_a ranges from about 0.1 to 0.5 m/h, the sink re-emission rate, k_d, is about 0.008/h, and n is 1. Experiments are underway to provide better estimates of k_a and k_d for a wide range of pollutants and sink materials.

The impact of sinks on individual exposure depends on the activity patterns. Sinks slightly reduce the peak exposure of individuals spending 24 h/day in a building and have no impact on their cumulative exposure. Sinks, because they change the emission/time characteristics of pollutant concentrations, can have major impacts on the exposure of individuals with other activity patterns. These impacts are discussed in detail in the example calculations later in the paper.

Exposure

Exposure is concerned with the concentration a person is in contact with and the length of time the contact lasts. There are two types of exposure of interest: the instantaneous exposure and the cumulative exposure. The instantaneous exposure is the exposure at any time, t, and lasts for a short time, dt. The cumulative exposure is the total or integrated exposure over the time of interest. The nature of the pollutant and the effects of the pollutant determine which type of exposure is more important.

Because the most common route for exposure to indoor air pollutants is via inhalation, it is convenient to define inhalation exposure, E_i, as

$$E_i = C(t)bvdt \tag{5}$$

where $C(t)$ is the pollutant concentration at time t, b is the breathing rate, and v is the volume per breath. The exposure defined by Eq 5 is instantaneous; i.e., the exposure at any instant in time, t. As a simplifying assumption the instantaneous inhalation exposure can be looked at as the amount of material inhaled in a single breath. The peak exposure is the maximum of the instantaneous exposure versus time curve.

The cumulative inhalation exposure, E_{ic}, is given by

$$E_{ic} = \int_{t_1}^{t_2} C(t)bvdt \tag{6}$$

The cumulative inhalation exposure is the total amount inhaled during the time interval t_1 to t_2.

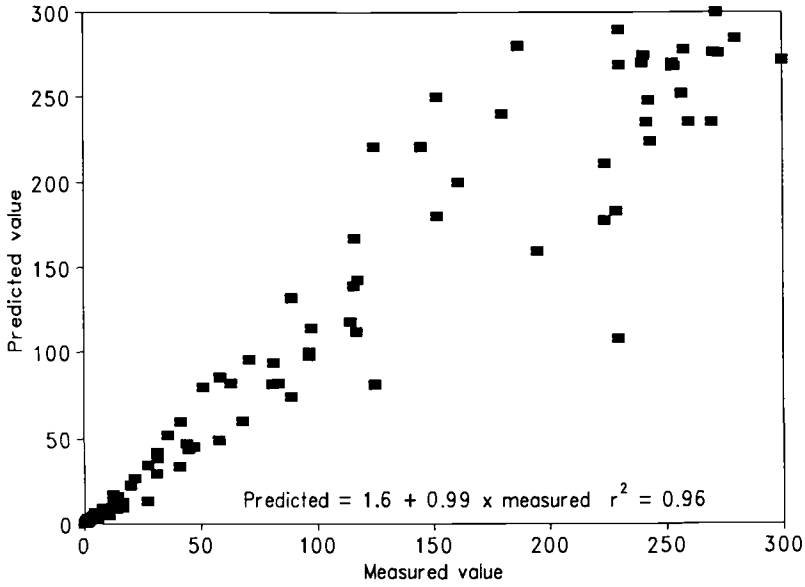

FIG. 1—*Predicted versus measured concentrations for test house experiments.*

The advantage of defining inhalation exposure is that the exposures calculated by the computer can be used in inhalation risk analyses without requiring the user to manually calculate the amount breathed. Note that no assumptions are made about the amount of material actually retained by the lungs.

For exposure by mechanisms other than inhalation, the instantaneous exposure, E, to a pollutant at time t is the concentration, $C(t)$, the person is in contact with at time t

$$E = C(t)dt \tag{7}$$

The cumulative exposure from t_1 to t_2 is given by

$$E_c = \int_{t_1}^{t_2} C(t)dt \tag{8}$$

Calculation of exposure requires the pollutant concentration, the time exposed to the concentration, and (for inhalation exposure) the breathing rate and volume per breath. The time exposed to the concentration depends on the individual activity pattern.

An activity pattern, in the context of the model, is defined by providing the time a person enters and leaves the various rooms of the building, or leaves the building for the outdoors. The model allows up to ten room changes per day. The model is based on a 24-h day. The activity patterns (and most source usage patterns) in the model repeat from day to day.

The model provides instantaneous exposure time plots and cumulative exposure time plots for individual activity patterns. The instantaneous exposure allows identification of high exposure situations and of the peak exposure.

While the model was designed to allow assessment of impact of indoor air pollution sources and sinks and IAQ control options on individual exposure from specific activities, it can also be

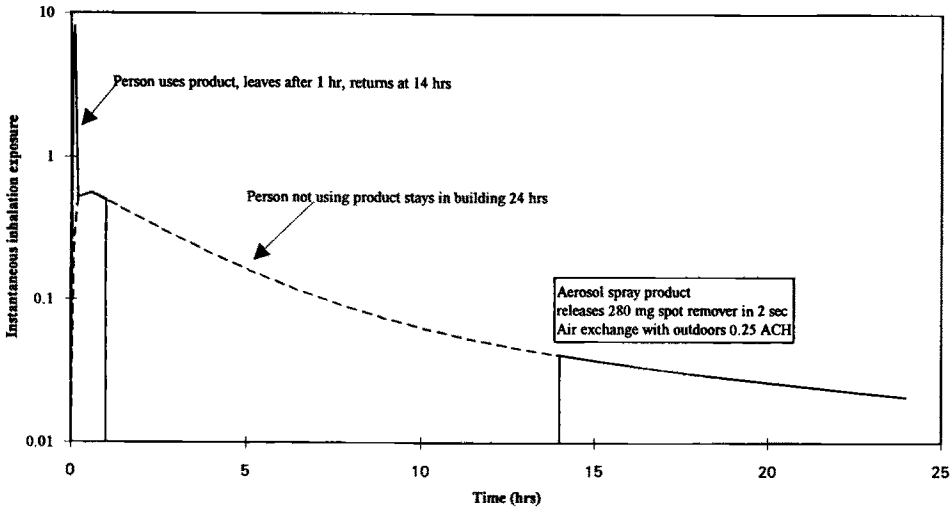

FIG. 2—*Instantaneous inhalation exposure to VOC from use of aerosol spray product.*

used to help estimate population exposures if data on population activity patterns are available. The model can be run for each activity pattern and then the results can be weighted according to the population statistics.

Model Verification

The model predictions of concentration versus time have been compared to experimental data from the EPA IAQ test house. In all cases the agreement between predictions and experiment has been good. Predicted versus measured concentrations for many of these experiments are plotted in

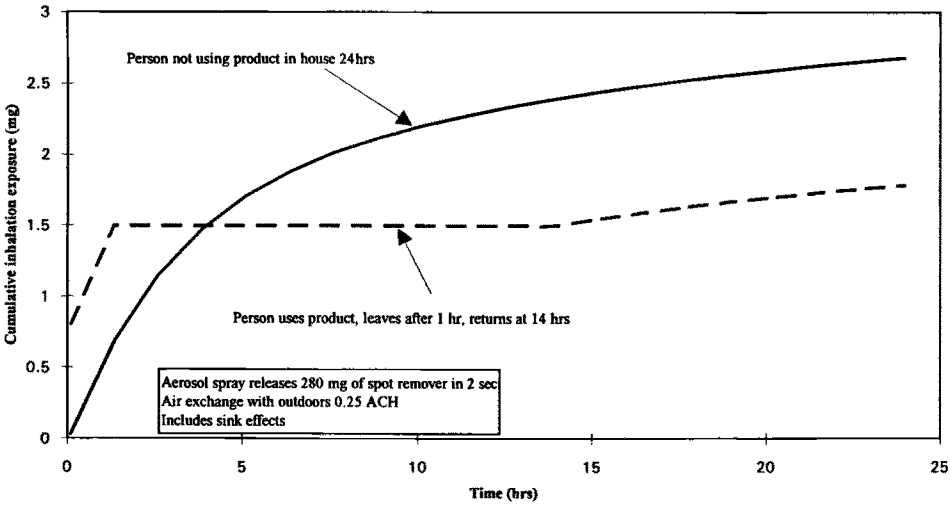

FIG. 3—*Cumulative inhalation exposure to VOC from use of aerosol spray product.*

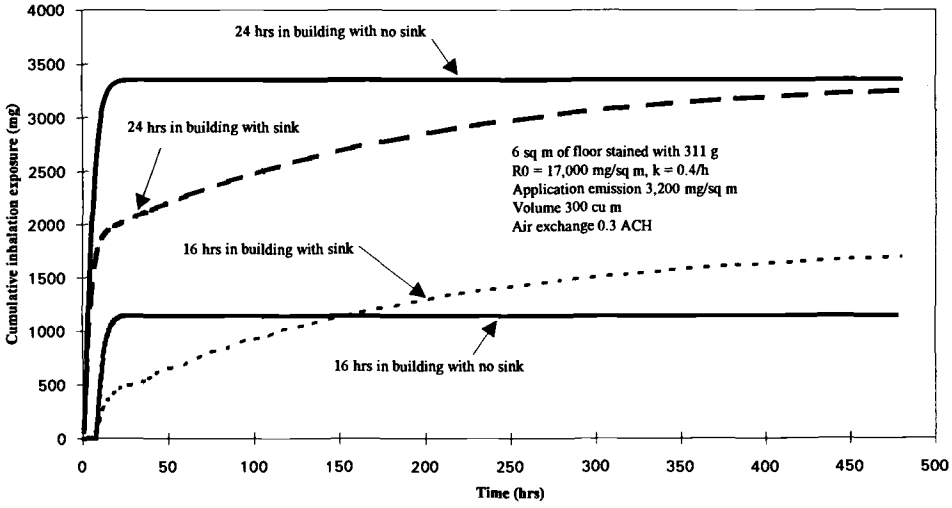

FIG. 4—*Cumulative exposure to VOC from wood stain.*

Fig. 1. Details of the comparisons between model predictions and indoor pollutant concentration are given by Sparks et al. [*8,9*].

Exposure Predictions

The examples in this section demonstrate some of the model's capabilities. The first example is calculation of the exposure to an aerosol spray product. The activity patterns are for a person who uses the product in a bathroom for ten minutes, moves to the living room and then leaves the building after one hour; and for a person who does not enter the bathroom where the source was used, but stays in the building for 24 hours. This example is based on an aerosol spray experiment conducted in the EPA IAQ test house. The test house is divided into seven zones. Values of sink terms are k_a = 0.1 m/h, k_d = 0.008/h for carpet and 0.1/h for all other surfaces. The instantaneous and cumulative inhalation exposures for the two individuals are given in Figs. 2 and 3, respectively. Note that, while the initial instantaneous exposure for the person using the product is much higher than for the other person, the cumulative exposure for the person using the product is less. However, the exposure for the person using the product may be somewhat underestimated in this example. The local concentration near the person is somewhat higher for several minutes than the average room concentration. EXPOSURE can deal with this situation if a pseudo room with a volume of about 5 m^3 and an airflow rate between 30 m^3/h with the rest of the room is defined. (This recommendation is based on preliminary experiments and detailed fluid flow modeling.) For

TABLE 2—*Emission rate factors for three sources.*

Source	S_0, mg/m^2-h	k, 1/h	Total Emission, mg/m^2-h
A	25	0.05	500
B	100	0.1	1000
C	8000	4.0	2000

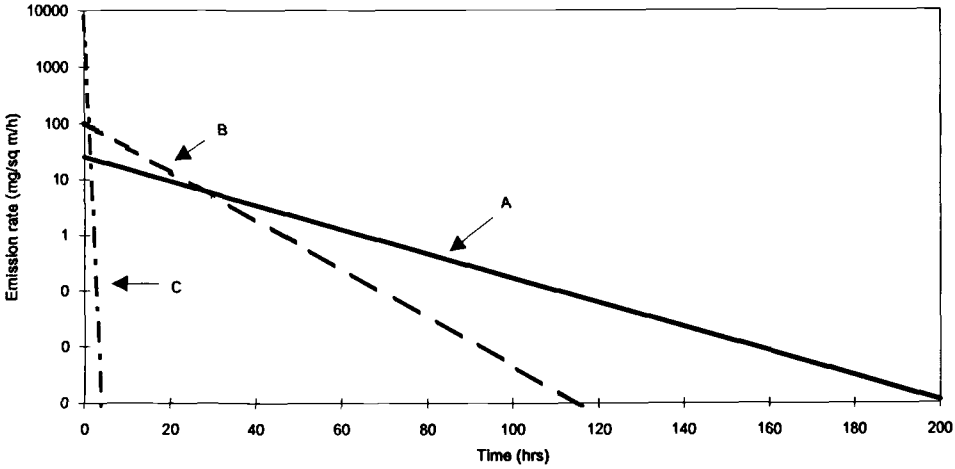

FIG. 5—*Emission rates for three products.*

the case shown in Fig. 2, the difference in exposures is not great because the volume of the bathroom is relatively small (20 m^3).

The second example shows the exposure due to wood stain, a "typical wet source." Because of adsorption and re-emission from sinks, the exposure lasts for a considerable time. The cumulative exposures for a person spending 24 h in the building and for a person spending 16 h in the building (starting 8 h after the stain is applied) are shown in Fig. 4 both with and without a sink. Note the major effect of the sink on the exposure of the person spending partial time in the building. The source term is given by Table 1. Sink terms are the same as those used in the aerosol spray example.

The two examples model experiments conducted in the EPA test house. All model input is based on the conditions in the test house at the time of the experiments. The model predictions of concentration versus time for both cases are in excellent agreement with the test house data.

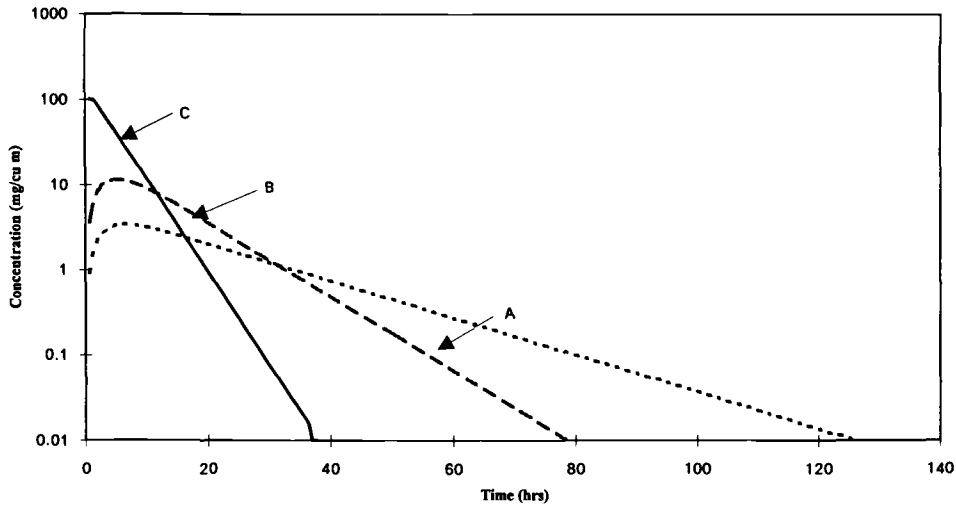

FIG. 6—*In-building concentrations of three products with no sinks.*

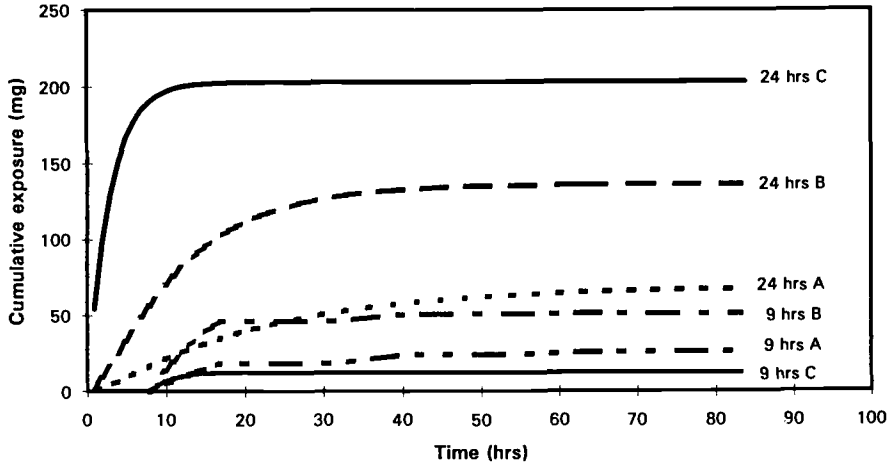

FIG. 7—*Cumulative exposure to three products with no sinks.*

Importance of Scenario

The importance of the scenario used to evaluate the impact of a given source on exposure can be demonstrated by looking at the impact of three sources on exposure. The source characteristics of the three sources are given in Table 2. The emission rate as a function of time for the three sources are shown in Fig. 5. Two activity patterns are analyzed: a person who spends 24 h/day in the building and a person who spends 9 h/day (from 8:00 am to 5:00 pm) in the building. Sink terms used in the model calculations are: k_a = 0.1 m/h and sink k_d = 0.008 m/h.

The first scenario is for a ventilation rate of one air change per hour (ACH) and no sinks. The concentration time profiles for the three sources are given in Fig. 6, and the cumulative exposures as a function of time are given in Fig. 7. The calculations show that for this scenario, Source C has the greatest impact on peak concentration and thus on peak exposure and on cumulative

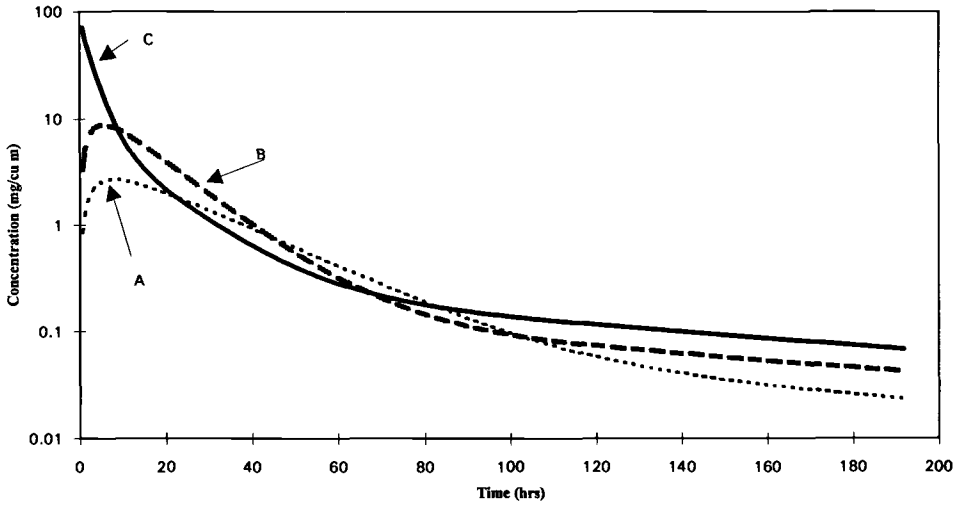

FIG. 8—*In-building concentrations of three products with sinks.*

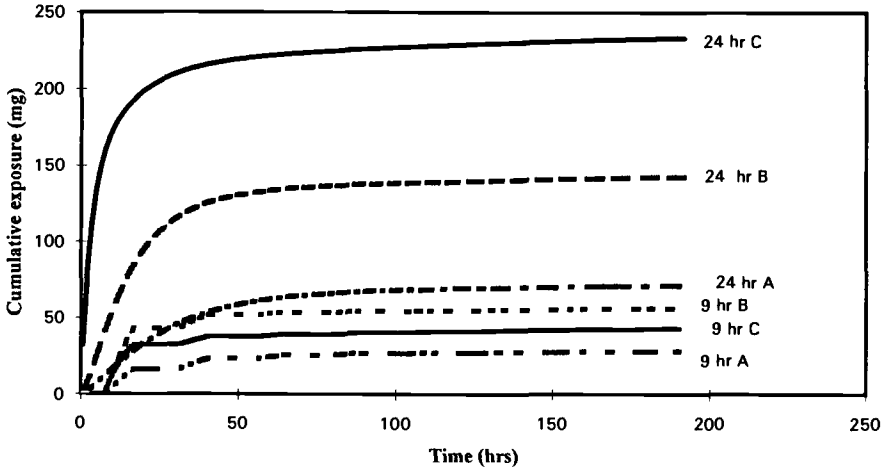

FIG. 9—*Cumulative exposure to three products with sinks.*

exposure for a person spending 24 h/day in the building. On the other hand, for a person spending 9 h/day in the building, Source C has the lowest impact. Also note that Source C has no impact on the building after about 48 h. Thus a person entering the building after 48 h would see no impact of Source C.

The second scenario is for a ventilation rate of 1 ACH and typical sinks. The concentration time profiles for the three sources are given in Fig. 8, and the cumulative exposures as a function of time are given in Fig. 9. Note that the sinks have greatly extended the time that the sources impact on the IAQ in the building. This scenario has a major effect on the impact of Source C. The impact of Source C is extended from less than 48 h to over 200 h. Again, Source C is the most important source for a person spending 24 h in the building. Note that Source C also has significant

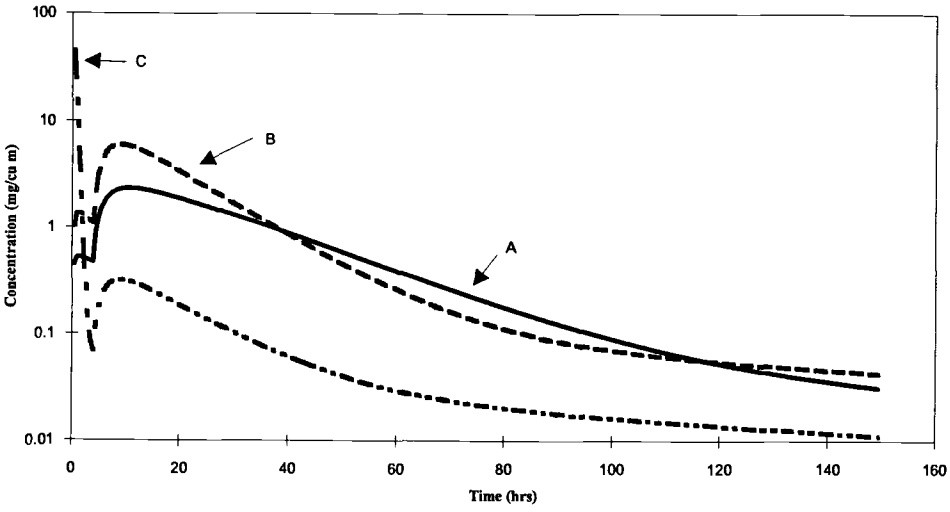

FIG. 10—*In-building concentrations of three products with 4 h of high ventilation followed by normal ventilation, with sinks.*

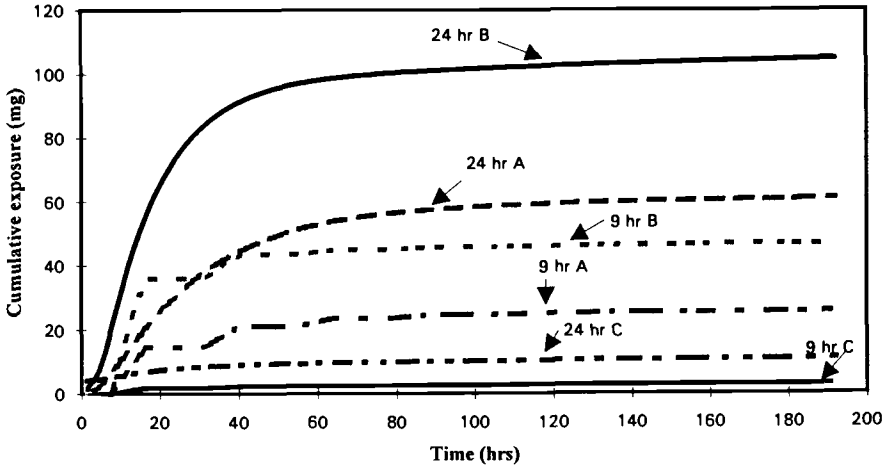

FIG. 11—*Cumulative exposure to three products with 4 h of high ventilation followed by normal ventilation, with sinks.*

impact on the person spending 9 h/day in the building. Contrast this with Scenario A where Source C had the lowest impact on the person spending 9 h/day in the building.

A final scenario is for a 4-h period of ventilation at 6 ACH followed by ventilation at 1 ACH and typical sinks. This scenario represents using the sources in a well ventilated space. The results are shown in Figs. 10 and 11. Note that under this scenario Source C again has minimal impact on the exposure of the individual spending 9 h in the building. Also note that the impact of Source C on the person spending 24 h/day in the building has been significantly reduced. The impact of the other sources has been slightly reduced but no where near as much as the impact of Source C. This scenario demonstrates an important point "fast sources are easier to control than slow sources." (Fast sources are sources with $k > 1$.)

Conclusions

The model results shown in this paper show that the impact of indoor pollutant sources on pollutant concentrations and individual exposure is determined by the interactions of sources, sinks, building operation, and individual activity patterns. Failure to consider all of these factors can lead to wrong conclusions. The calculations for various scenarios show that the impact of a particular source on exposure depends on the scenario selected. It is possible to show the impacts of a particular source ranging from major to negligible simply by selecting the scenario used to evaluate the source. If sources are to be evaluated based on their impact on exposure, a set of standard and realistic scenarios should be developed to allow comparison of the sources under equal conditions.

References

[1] Sparks, L. E., *Indoor Air Quality Model Version 1.0*, EPA-600/8-88-097a (NTIS PB89-133607), U. S. Environmental Protection Agency, Research Triangle Park, NC, 1988.

[2] Maldonado, E. A., "A Method to Characterize Air Exchange in Residences for Evaluation of Indoor Air Quality," Ph.D. dissertation in Mechanical Engineering, Iowa State University, Ames, IA, 1982.

[3] Yamamato, T., Ensor, D. S., Lawless, P. A., et al., "Fast Direct Solution Method for Multizone Indoor Air Model," *Building Systems: Room Air and Air Contaminant Distribution*, L. L. Christianson, Ed.,

American Society of Heating, Refrigerating and Air-Conditioning Engineers, Inc., Atlanta, GA, 1989, pp. 147–148.

[4] Tichenor, B. A., *Indoor Air Sources: Using Small Environmental Test Chambers to Characterize Organic Emissions from Indoor Materials and Products*, EPA-600/8-89-074 (NTIS PB90-110131), U. S. Environmental Protection Agency, Research Triangle Park, NC, 1989.

[5] Tichenor, B. A., Sparks, L. E., White, J. B., and Jackson, M. D., "Evaluating Sources of Indoor Air Pollution," *Journal of Air & Waste Management Association*, Vol. 40, No. 4, 1990, pp. 487–492.

[6] Tichenor, B. A., Guo, Z., Dunn, J. E., et al., "The Interaction of Vapour Phase Organic Compounds with Indoor Sinks," *Indoor Air*, Vol. 1, 1991, pp. 23–35.

[7] Axley, J. W., "Adsorption Modeling for Building Contaminant Dispersal Analysis," *Indoor Air*, Vol. 1, 1991, pp. 147–171.

[8] Sparks, L. E., Tichenor, B. A., White, J. B., and Jackson, M. D., "Comparison of Data from an IAQ Test House with Predictions of an IAQ Computer Model," *Indoor Air*, 1991, in press.

[9] Sparks, L. E., *EXPOSURE Version 2 A Computer Model for Analyzing the Effects of Indoor Air Pollutant Sources on Individual Exposure*, EPA-600/8-91-013 (NTIS PB91-20195), U. S. Environmental Protection Agency, Research Triangle Park, NC, 1991.

Arlene S. Rosenbaum[1] *and Gerald E. Anderson*[1]

Modeling of Indoor and Outdoor Exposures and Risk from Outdoor Benzene Emissions in Los Angeles

REFERENCE: Rosenbaum, A. S. and Anderson, G. E., **"Modeling of Indoor and Outdoor Exposures and Risk from Outdoor Benzene Emissions in Los Angeles,"** *Modeling of Indoor Air Quality and Exposure, ASTM STP 1205*, Niren L. Nagada, Ed., American Society for Testing and Materials, Philadelphia, 1993, pp. 257–270.

ABSTRACT: This paper reports on a demonstration study of the use of dispersion and exposure modeling to estimate carcinogenic risk to residents of the South Coast Air Quality Management District from benzene emitted into the atmosphere from outdoor sources. Exposures in indoor and outdoor environments are estimated throughout the basin. The distribution of individual risks across the population and among various population subgroups is assessed. The resulting expected excess lifetime cancer incidence is also evaluated. The fractions of overall risk attributable to various emission source types are compared. The results show that the contribution to overall carcinogenic risk from outdoor benzene emissions is split approximately equally between mobile sources (such as vehicles) and small, dispersed sources (for example, gasoline stations). The contribution of industrial sources (such as, large stationary sources) is negligible in comparison.

KEY WORDS: exposure, indoor, outdoor, toxics, benzene, modeling, Los Angeles, cancer risk

This paper reports on a demonstration study of the use of dispersion and exposure modeling to estimate carcinogenic risk to residents of the South Coast Air Quality Management District (SCAQMD, that is, Los Angeles) from benzene emitted into the atmosphere from outdoor sources. Concentrations resulting from outdoor emissions are estimated for indoor and outdoor microenvironments. Total risk (that is, from all outdoor sources, contributing to indoor and outdoor exposures) is estimated, along with the incremental risk produced by various categories of emission sources and the incremental risk to various segments of the population, and these incremental risks are compared. Patterns of modeled ambient benzene concentration in the SCAQMD are also compared with measured concentrations as reported by the EPA's TEAM study [*1*].

This study uses a computer model, the South Coast Risk and Exposure Assessment Model—version II (SCREAM-II) [*2*], developed by Systems Applications International under contract to the Planning Department of the SCAQMD. SCREAM-II model development was planned to address the entire District-wide problem of toxics planning anticipated under California's "Toxic Hot Spots" program, authorized under California Assembly Bill 2588. In this program, estimates of incremental risk impact from individual toxic species emitted from individual industrial sources are aggregated along with estimates for other species and sources. "Hot Spots," and the associated need for remedial action are identified from the net risk patterns. SCREAM-II can be used to

[1]Senior scientists, Systems Applications International, 101 Lucas Valley Rd., San Rafael, CA 94903.

address risk[2] associated with multi-media exposure[3] from each of an inventory of sources or from source groups in aggregate; it can address area-wide community sources such as motor vehicles, etc.; it can be used to address risk to each of 12 age-occupation groups and/or to each geographic subregion or to populations or regions in aggregate. The model structure provides for aggregating the exposure of each population group at the concentrations of each of the indoor or outdoor micro-environments they find themselves in during the course of their characteristic daily activity; risk computations address respiration rates specific to each cohort in each activity in their daily pattern. The climatologic distribution of dispersion conditions (characterized by wind speed, direction, and intensity of turbulence) is defined and used for each hour-of-the-day to match the resolution of population activity.

Emission estimates were taken from the district's inventory of toxic emissions; source categories in that inventory include industrial sources, motor vehicle sources, and commercial or residence-related sources.

Approach

Use of the SCREAM-II model for district-wide benzene emission control planning can provide the planner with data quantifying various aspects of exposure to and risk from airborne toxics. These aspects include the following:

- The spatial distribution of ambient benzene concentrations and of carcinogenic hazard from benzene on a climatologic basis. This information helps the planner in setting priorities for risk education. It may also indicate where intergovernmental cooperation is necessary, if the ambient concentration at a given location is the result of emissions from a different political jurisdiction.
- The fraction of community or individual benzene risk attributable to individual sources or to source types (for example, vehicles or industry). This measure is an indicator of the potential of available emission control measures to mitigate current risk levels.
- The distribution of exposure and risk among people of different ages or occupations. This information may show the impact of different activity patterns on exposure (for example, extended time outdoors) or may highlight the exposure of groups that might be more sensitive to a given level of exposure (for example, children or retired people).
- The frequency distribution of risk. This information addresses the issue of whether a few people assume most of the risk or whether many people share a lesser risk.

Although the algorithms of the SCREAM-II model are general and much of the data needed to apply it to any region of the U.S. are publicly available from the U.S. Census Bureau, other needed data have been collected specifically for the SCAQMD. Thus, this demonstration application was carried out for the Los Angeles metropolitan region. The region's area and population (~12.5 MM, or about 5% of the national population) are large enough to represent a microcosm of the nation. Some aspects of the climate, housing, and habits of the area are certainly not typical of all other urban areas. They do, however, represent fairly well the major, urban, warm climate, high growth areas of the country.

[2]The model can also be used to address multi-media exposures, but exposures by other than inhalation were judged not to be important for benzene-related risk.

[3]Exposures by other than inhalation depend on aerosol or gas deposition onto water or soil surfaces. No such deposition was estimated for benzene.

Benzene was chosen as the toxicant to study because of its significance to urban community risk. Benzene is used in large quantities and has a significant risk factor (carcinogenic potency). Further, the emissions inventory could be expected to be better for this species because it is handled in bulk, is a fraction of commonly used organic mixtures at known fractional concentrations and has been subject to considerable attention, along with other VOCs because of the significance of VOCs for the formation of ozone (especially in the chosen study area).

With these perspectives in mind, the required data were assembled, and the SCREAM-II model was exercised. Summary results of the model runs were evaluated, and compared with exposure concentrations measured and reported on in the EPA's TEAM study in Los Angeles.

Model Description

The model used in this study, SCREAM-II, consists of an air dispersion and deposition module (adapted from SCREAM-I, developed earlier for the SCAQMD), an inhalation exposure and risk module that also includes an indoor air model, the Indoor Air Quality Model (IAQM) [*3,4*] and a multipathway exposure and risk module. The model includes a deposition algorithm for solid or liquid aerosols or reactive gases. This capability allows analysis of exposure through ingestion of contaminated soil, water, crops, livestock, or breast milk. The multipathway exposure and risk module was not used in this application. Benzene is gaseous and gas-phase deposition to biotic, soil or water surfaces was judged to be not important; consequently, these portions of the model were not exercised. Component modules that were used are described as follows.

Air Dispersion Modeling

The SCREAM-II model incorporates modules to address exposure problems from outdoor emission sources, through transport and dispersion (including multi-media, when appropriate), and on to exposure and risk calculation. Through its modular structure, SCREAM-II can be exercised for this entire process, or it may be exercised for exposure calculations only, with concentration pattern inputs generated by any other dispersion model.

Point Sources—Two modes of air dispersion modeling are included in SCREAM-II. In the first mode SCREAM-II includes a standard gaussian dispersion plume model for point sources. Building wake effects and fugitive or other area sources are treated with the same gaussian plume algorithm with "virtual source" adjustment of the source locations. The virtual source approach is similar to, but less detailed than, the approach in the EPA's Industrial Source Complex—Long Term (ISCLT) model [*5*].

For each of the point sources included in the simulation, SCREAM-II produces an estimated air concentration at the centroid of each U.S. Census Tract (CT)[4] in the modeling region. Diurnal variations in dispersion are addressed because correlations between the atmosphere's dispersive effectiveness and the exposure of people through their daily activity are expected. For example, people are more likely to be indoors and inactive (asleep) at night, when the atmosphere in the Los Angeles basin is the most stable (low turbulence) and most often exhibits easterly winds. In the daytime, when people are more likely to be outdoors, active, and away from their homes, winds and turbulence tend to be stronger, and winds tend to be from a westerly direction.

[4]SCREAM-II can operate on various levels of spatial resolution including individual city block, U.S. Census Block Group, U.S. Census Tract, place (that is, town), or county. It was operated at the Census Tract level for this study to demonstrate spatial resolution without undue computational effort.

To compute diurnally varying exposures, the inhalation exposure module requires that hourly spatial concentration patterns be supplied as input. Computation of exposures for all 8760 h in just one simulation year, for many chemicals, and for many different sources would be very computer intensive. Moreover, for long-term chronic effects (for example, cancer) the goal is to represent the average diurnal patterns of dispersion during a period much longer than a year in order to estimate long-term average exposure concentrations.

To reduce computing requirements of calculating diurnally varying exposures, a climatologic modeling approach is used. As with other climatologic models (for example, the EPA's ISCLT) the dispersion module is supplied with a STability ARray (STAR) joint probability matrix. A STAR matrix describes the joint frequency distribution of hourly meteorological measurements sorted into classes, or "bins," by wind speed, wind direction, and atmospheric stability. The long-term concentration is calculated by simulating the average concentration for each meteorological bin and summing the averages across bins, weighting each by its frequency of occurrence.

By normal convention, a single STAR matrix is prepared for the entire simulation period, usually one or more years. In SCREAM-II a separate STAR matrix is used for each of the 24 hours in the day. For example, there is a STAR matrix for the time period from 8 a.m. to 9 a.m., reflecting the relative long-term frequency of each meteorological condition for that time of day. This was done by processing meteorological data, separated by hour of the day, for each of 30 SCAQMD stations with the same EPA processor used to create STAR matrices for ISCLT and other climatological dispersion models. The hourly STAR files are incorporated in SCREAM-II; data from the nearest site are accessed for the processing of each source.

Using the hourly STAR matrices, the SCREAM-II dispersion module is run for each hour separately, estimating long-term average air toxic concentrations.[5] These concentrations may be thought of as expected long-term averages for each hour of the day. For this study, 24 hourly expected concentrations were calculated at the centroid of each CT in the SCAQMD.

Community (Area) Sources—The second mode of dispersion modeling is used for addressing community-wide area sources. These would include motor vehicle traffic emissions or other activities that lead to a large number of small, widely distributed sources that cannot, practically, be individually defined. Examples include the home use of organic solvents, cleaners, or coatings; pesticide applications, and commercial operations such as dry cleaning plants or gasoline stations.

Dispersion from community sources involves modeling the source distribution and modeling the dispersive dilution itself. These processes are carried out on a user-specific modeling grid. Several options are available for modeling the source distribution so as to cover the most important types of community sources. Gridded motor vehicle emissions are available in many districts for use in modeling pollutants subject to national ambient air quality standards, such as ozone. These may be entered directly rather than modeled. In the SCAQMD toxics inventory, benzene emissions from community home and commercial operations are entered in the form of population-based emission factors (number/person/year). These benzene factors were applied to gridded populations to produce gridded emissions for SCREAM-II. Other source types are treated differently.

For widely distributed community sources, emission density gradients are assumed to be small; thus, dispersion is assumed to be dominated by vertical processes and by the mean transport wind past the ground level source areas. Concentrations at any point are thus proportional to the local grid emission density ($g/m^2/s$) and inversely proportional to the subregional wind speed and mixing depth. This treatment is, effectively, "box model" dispersion adjusted for the local emission den-

[5]SCREAM-II, like other gaussian climatological models such as EPA's ISCLT, computes ambient 1-h average concentrations independently for each climatological condition. Thus, these models implicitly assume that the average concentration for the current hour at any receptor is a function only of current conditions, emissions, and source characteristics.

sity. The vertical dispersion constant used was based on that in the Gifford-Hanna urban regional box model [6]. Subregional wind data were from the 30 station data set supplied by SCAQMD and incorporated in a resident SCREAM-II file.

Inhalation Exposure and Risk Modeling

The 24 hourly concentrations for each CT centroid are supplied as input to the inhalation exposure module. This module, based on algorithms from a version of the EPA's NAAQS Exposure Model (NEM) coded by Systems Applications (NEM/SAI) [7], is used to calculate basinwide and subregional population inhalation exposures. In order to address exposures that occur indoors, where most people spend more than 80% of their time and where levels of outdoor-generated air pollution may be less than outdoors, SCREAM-II estimates indoor air concentrations resulting from outdoor sources with the Indoor Air Quality Model (IAQM).

The overall approach to exposure assessment involves assigning members of population subgroups to a geographic location (that is, residential or work exposure district) and microenvironment (for example, indoors in a weatherized office, outdoors near a roadway) for each hour/day/season combination on the basis of a prototypical activity pattern. The benzene concentration in that location/microenvironment combination becomes the exposure concentration for that hour/day/season combination. All such exposures are aggregated for each population subgroup to estimate a long-term average exposure concentration. The following section presents the details of the approach.

Inhalation Exposure Module—Air toxics inhalation exposure is calculated by a module adapted from NEM/SAI urban-scale population exposure model. NEM/SAI takes into account mobility patterns, indoor-outdoor differences, and physical exercise levels. The inhalation exposure/risk module calculates exposures in each CT, aggregating reported exposure throughout the basin for 36 subregions, or exposure districts. Exposures are estimated for up to 56 different population subgroups. The following basic age-occupation groups are considered. (The 56 subgroups are defined by dividing these groups according to variations of prototypical commute and indoor-outdoor work patterns.)

Students 18 and over
Managers and professionals
Sales workers
Clerical and kindred workers
Craftsmen and kindred workers
Farmers
Operatives and laborers
Service, military, and private household workers
Housepersons
Unemployed and retired persons
Children under 5
Children 5 to 17.

At each hour, a prototypical activity pattern assigns a population subgroup to a geographical location (residential or work exposure district) and to one of six basic indoor or outdoor microenvironments (see Table 1) at one of three physical exercise levels: low, moderate, or heavy. Different population activity patterns are defined for weekdays, Saturdays, and Sundays. The population activity database [8] is the same as that used by the EPA in previous ambient standards exposure analyses.

TABLE 1—*Correspondence between basic microenvironments and site- and time-specific microenvironments used in the SCREAM-II inhalation exposure module.*

Basic Microenvironment	Corresponding Site- and Time-Specific Microenvironments
Indoors at work	Office with typical heating, ventilation, and air conditioning (HVAC) system (built before 1976, that is, not weatherized)
	Office with typical energy-efficient HVAC system (built after 1976, i.e., weatherized)
Indoors at school	School (not weatherized)
	School (weatherized)
Other indoors	Home (not weatherized), with closed windows
	Home (weatherized), with closed windows
	Home with windows open
	Home with central air conditioning operating
Inside a transportation vehicle	Same (not subdivided)
Outdoors, near a roadway	Same (not subdivided)
Outdoors, other	Same (not subdivided)

In order to address the variations in geographic location, the 56 subgroups are further divided into cohorts. A cohort is an age-occupation subgroup that has the same combination of work and residential exposure districts. For example, outdoor construction workers who lived in exposure District 4 and worked in exposure District 9 would form one cohort, while outdoor construction workers who lived in District 9 and worked in District 4 would constitute another cohort. Population subgroup and transportation data projections were obtained from the South Coast Association of Governments (SCAG) [*9*].

The six basic microenvironments map into eleven site- and time-specific categories as shown in Table 1.

Weatherization is an important determinant of the rate at which outdoor air leaks into the indoor environment, and therefore, the resulting indoor concentration of outdoor-generated pollutants. Recent changes in building codes have increased the degree of weatherization in newer buildings. In addition, utility-sponsored retrofit programs have led to higher levels of weatherization in some older buildings. The number of homes, offices, and schools of each type is estimated for each exposure district based on statistics and year-specific projections from the California Energy Commission. In addition, the configuration of the home microenvironments (for example, central air conditioner operating or windows open) is varied, as appropriate, according to time of day and season of the year.

The indoor microenvironments represent building configurations that are present in different fractions in the building stock in different study areas (for example, there are regional differences in the percentage of buildings that are air conditioned), season (for example, windows closed in the winter, air conditioners operating in the summer, etc.), and time of day (for example, windows

TABLE 2—*Estimates of benzene emissions in the South Coast Air Quality Management District. Source: Planning Department, SCAQMD* [10].

Source Type	Proportionality Factor	Total Emissions (metric tons/year)
Point	—	109
Area	0.611 kg/person/year	7182
Mobile	0.034 kg/kg ROG	6273

TABLE 3—*Summary of SCREAM results for benzene risks in the SCAQMD.*

	Excess 70 yr. Cancer Incidence (exp. val.)					Max. Individual Lifetime Risk (/MM)			
	Total	Industry	Vehicles	Community		Total	Industry	Vehicles	Community
Children <5 yrs	864	0.8	412	451		1840	8	957	878
Children 5 to 17	2262	2.0	1080	1180		1800	9	941	863
Students > = 18	910	0.8	439	470		1830	9	952	874
Housepersons	1166	1.0	560	605		1860	8	971	891
Unemployed	1161	1.0	550	610		1800	8	940	863
Professionals	352	0.3	171	181		1750	8	912	837
Clerks	244	0.2	118	126		1770	8	921	845
Laborers	221	0.2	106	115		1880	9	981	901
Farmers	15	0.0	7	8		1910	9	994	912
Service	164	0.1	79	85		1860	9	970	891
Craftsmen	160	0.2	77	83		2000	9	1040	957
Sales	130	0.1	63	67		1760	8	918	843
Total	7650	7	3662	3981	Mean	1838	9	958	880
	Exposure @ Bz > 1e − 7 $\mu g/m^3$ (people)					Mean exposure concentration ($\mu g/m^3$)			
	Total	Industry	Vehicles	Community		Total	Industry	Vehicles	Community
Children <5 yrs	1 403 000	500 000	1 383 000	1 403 000		11.62	0.03	5.62	6.07
Children 5 to 17	3 855 000	1 331 000	3 792 000	3 854 000		11.07	0.03	5.37	5.78
Students > = 18	1 439 000	538 000	1 419 000	1 438 000		11.93	0.03	5.84	6.17
Housepersons	1 969 000	662 000	1 934 000	1 968 000		11.17	0.03	5.46	5.80
Unemployed	1 698 000	708 000	1 659 000	1 696 000		12.90	0.03	6.26	6.79
Professionals	592 000	218 000	580 000	592 000		11.23	0.03	5.56	5.77
Clerks	389 000	156 000	384 000	389 000		11.84	0.02	5.80	6.11
Laborers	327 000	132 000	322 000	326 000		12.76	0.03	6.21	6.66
Farmers	26 000	8 000	25 000	26 000		10.89	0.00	5.28	5.81
Service	242 000	95 000	238 000	242 000		12.79	0.02	6.26	6.63
Craftsmen	253 000	94 000	248 000	253 000		11.95	0.04	5.86	6.19
Sales	221 000	78 000	216 000	221 000		11.11	0.02	5.50	5.72
Total	12 414 000	4 520 000	12 200 000	12 408 000	Mean	11.77	0.03	5.75	6.12

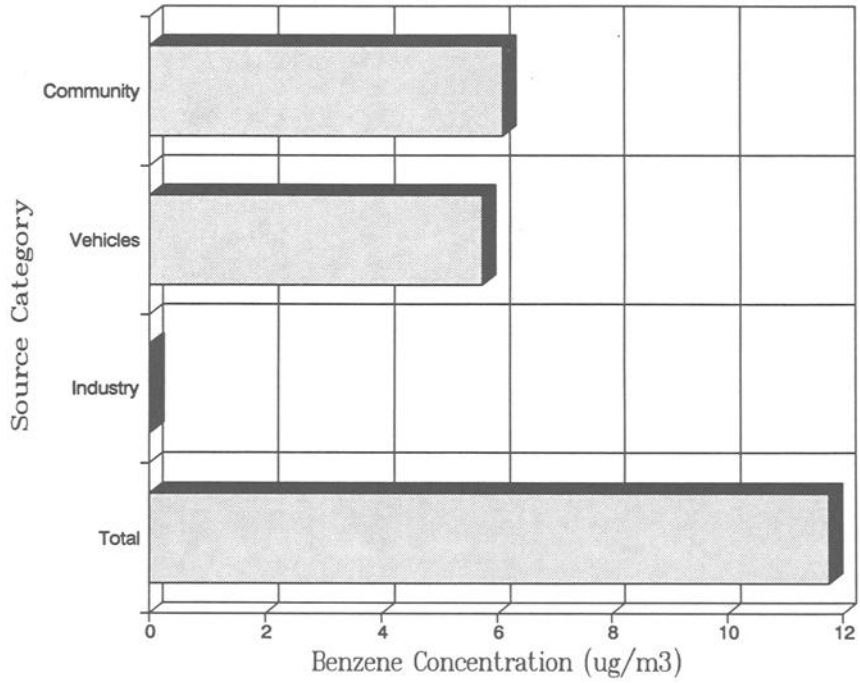

FIG. 1—*Mean exposure concentrations from benzene emissions in the SCAQMD.*

open during the day, windows closed at night, etc.). Such differences are accounted for in the inhalation exposure module by simulating air quality levels in each microenvironment and combining them with appropriate weighting factors to reflect daily and seasonal changes in building configuration.

Indoor Air Quality Submodule—Indoor pollutant concentrations are calculated in the inhalation exposure module by the IAQM submodule, an explicit indoor air quality model. IAQM simulates indoor air quality by means of a dynamic mass balance equation, with a building represented as a single compartment, a standard and satisfactory assumption for most applications, including SCREAM-II. Outdoor air is permitted to leak into and out of the building, with indoor recirculation and makeup air supplied as appropriate through a heating, ventilation, and air conditioning (HVAC) system, if present, whose design parameters are chosen as representative of the desired building stock. Filtration systems are permitted on both the makeup and recirculation portions of the HVAC system. Indoor sources are not addressed in this application.

Pollutant loss indoors is simulated in terms of adsorption onto surfaces or deposition due to settling, with reactivity or deposition rates dependent on the pollutant. Such reactivities or deposition rates are taken from published experimental data. Because benzene has a relatively low surface reactivity it was considered inert for this application.

Carcinogenic Risk Estimates—In addition to exposure concentrations, SCREAM-II estimates the individual excess[6] cancer risks resulting from exposure on the basis of unit risk factors (URF). A URF is defined as the probability of an individual developing cancer as a result of continuous

[6]The term "excess" is used to denote the risk, or probability, of an individual contracting cancer, over and above background cancer risk.

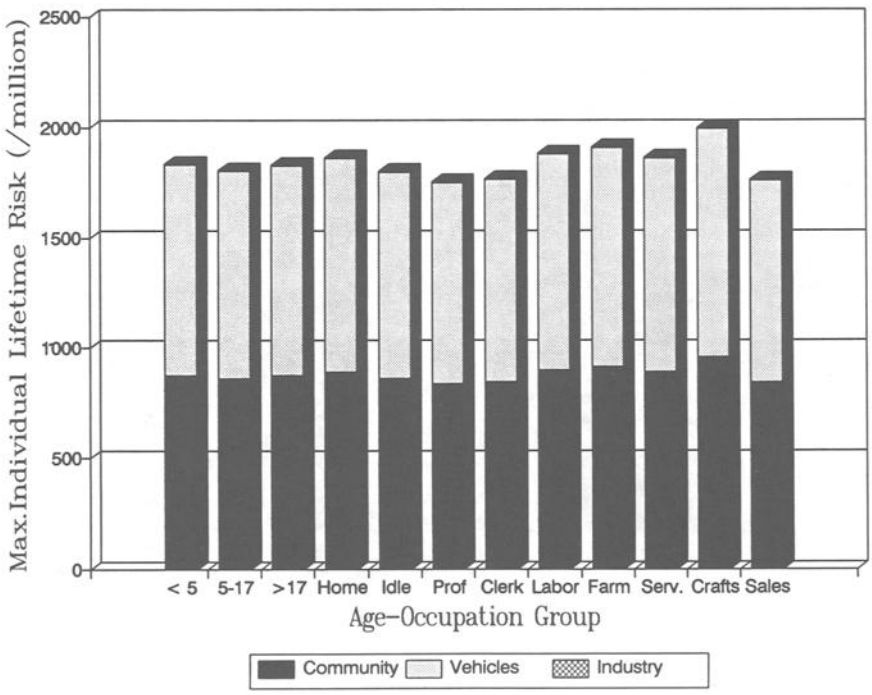

FIG. 2—*Expected cancer incidence in the SCAQMD from benzene emissions, by source type and age-occupation group.*

exposure to an airborne pollutant at a concentration of 1 $\mu g/m^3$ over a 70-year lifetime. The risk from exposure at any other concentration level is assumed to be proportional to that concentration. Thus, the individual risk, or probability, of developing cancer as a result of pollutant exposure over a 70-year period is calculated as the product of the average exposure concentration ($\mu g/m^3$) and the unit risk factor for the pollutant of interest ($[\mu g/m^3]^{-1}$). The unit risk factors assumed for benzene in this study is 5.3×10^{-5} per $\mu g/m^3$ per 70-year life.

SCREAM-II also reports the number of people exposed to individual risks exceeding a series of threshold levels along with the associated excess cancer incidence (cases), assuming a 70-year exposure. The excess cancer incidence is the number of excess cancer cases expected to occur as a result of 70 years of exposure, with emission rates, population levels, and population distribution held at current values. The excess cancer incidence is a function of both the individual excess risks and the size of the exposed population. Thus an area with a low average individual excess risk and a large population may have the same predicted number of excess cancer cases as an area with a higher average individual excess risk but a smaller population.

The excess lifetime cancer incidence is the expected number of cancer cases resulting from the exposure conditions delineated. The expected value of a random variable, a well known concept from probability theory, is the average value anticipated over a large number of realizations of the variable. It is calculated as the weighted sum of all possible values of the variable where a weight is the probability of a specific value being realized.

In this case, for each individual the possible values for cancer cases are assumed to be 0 and 1 (that is multiple cases in the same individual from exposure to a single pollutant are not considered). The probability of a cancer case is estimated as the individual risk (IR), discussed above. Therefore, the expected number of cancer cases for an individual from exposure to a particular

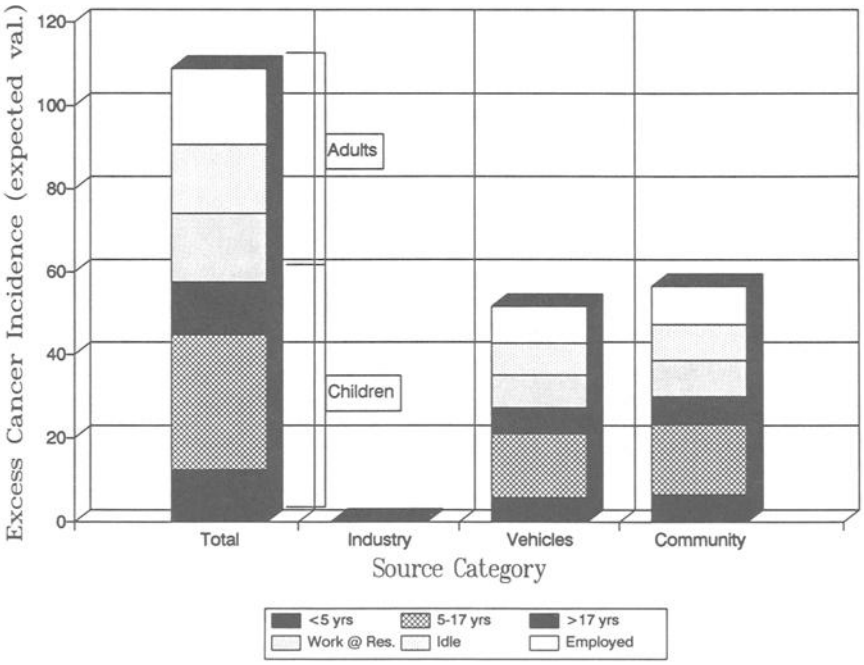

FIG. 3—*Expected cancer incidence in the SCAQMD from benzene emissions, by age-occupation group and source type.*

pollutant is calculated as:

$$E = (0 \text{ cancer cases} * [1. - IR]) + (1 \text{ cancer case} * IR)$$

or $$E = IR.$$

Assuming that the probabilities of contracting cancer due to exposure to pollutants are independent among individuals, the total expected number of cancer cases for all individuals may be calculated as:

$$T = \sum_{\text{individuals}} E_{\text{indiv}}$$

or $$T = \sum_{\text{individuals}} IR_{\text{indiv}}.$$

Model Input Data

Benzene emissions data were supplied by the South Coast Air Quality Management District. All estimates are based on pre-1978 data [*10*]. Three types of sources were included:

- relatively large stationary or "point" sources,
- relatively small, widely dispersed stationary or "area" sources, such as gasoline service stations; and
- mobile sources.

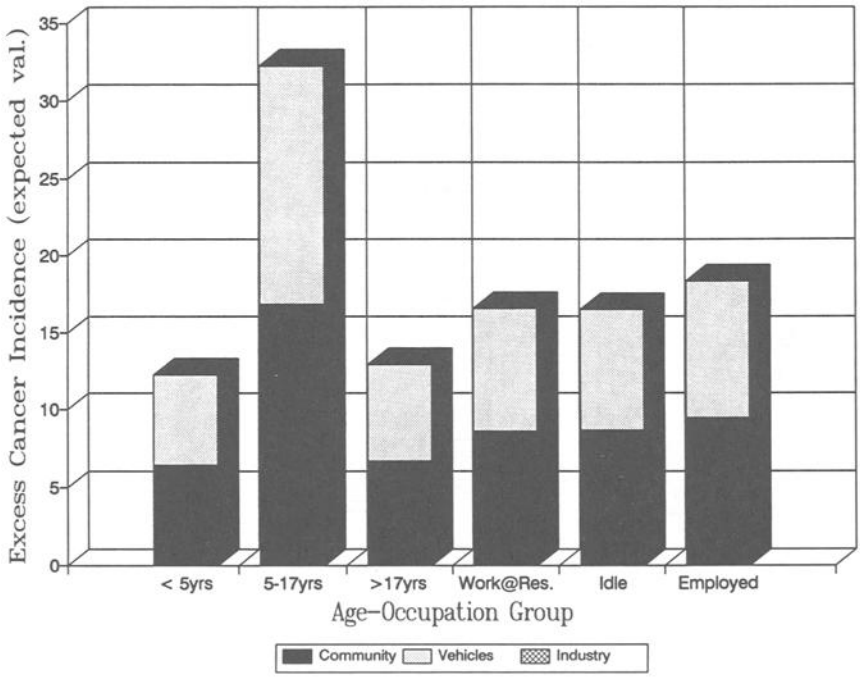

FIG. 4—*Maximum lifetime risk to individual in the SCAQMD from benzene emissions.*

Emissions from stationary sources were self-reported estimates. Benzene emissions from area sources were assumed to be proportional to population density with an identical geographic distribution. Mobile source emissions of benzene were assumed to be proportional to total reactive organic gas (ROG) emissions from mobil sources. Table 2 shows the proportionality factors and total benzene emissions from each source type.

Data on population composition by age-occupation group and their geographical distribution were obtained from the South Coast Association of Governments. They are projections for 1990 made prior to that year.

Other data inputs to the inhalation exposure model, such as the prototypical population activity patterns, population mobility data, and building stock (for example, fraction with enhanced weatherization) are discussed above.

Results

Table 3 and Figs. 2 to 5 summarize the modeling results. The lower right-hand section of Table 3 shows that the overall Mean Exposure Concentration for all population groups from all three types of outdoor sources is approximately 12 $\mu g/m^3$, with a range of approximately 20%, from 11 to 13 $\mu g/m^3$ among population groups. The differences among population groups reflect differences in the make-up of the population at different geographic sites and differences in the prototypical activity patterns between groups, particularly with respect to time spent indoors. The contribution from each source type is shown also in Fig. 1. This shows that the contribution from industrial sources is essentially negligible, while the contributions from vehicles and community sources (for example, gasoline stations) are roughly equal. All concentrations are approximately proportional to the overall emissions (Table 2) from each source type.

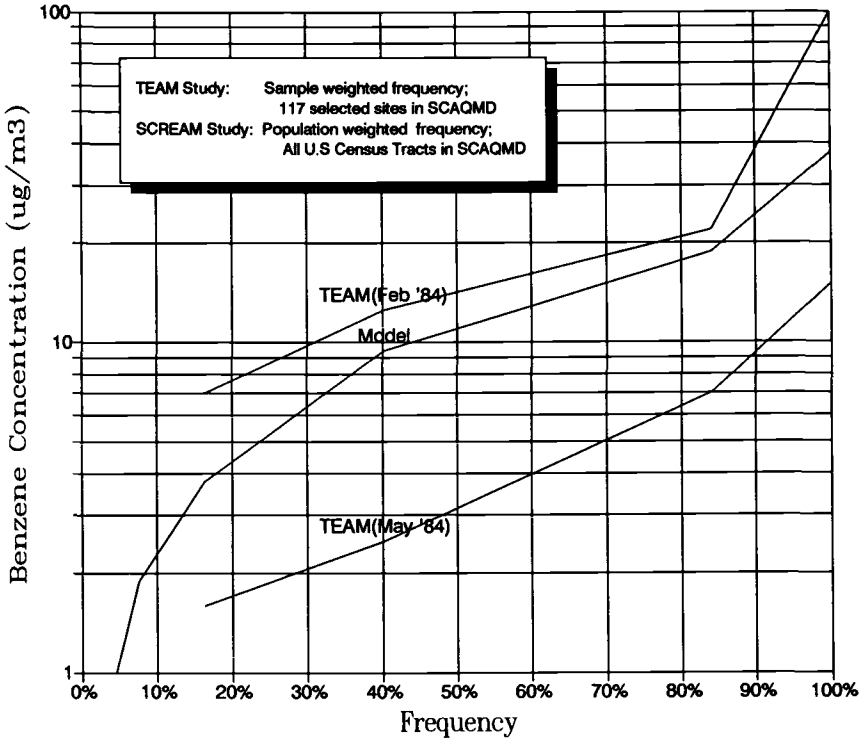

FIG. 5—*Cumulative frequency distribution of modeling results compared with measurements.*

Table 3 (upper right) and Fig. 2 summarize the Maximum Individual Lifetime Risk. They show a range from approximately 1750 to 1900 per million for the various population groups. The values of Maximum Individual Lifetime Risk for the various source types indicate that mobile sources generate the highest maximum risks, even though the overall emissions (Table 2) and Mean Exposure Concentrations from these sources are smaller than from area sources. This suggests that the geographical distribution of these emissions are less uniform than for area sources.

The lower left-hand section of Table 3 shows the number of people subject to exposure concentrations exceeding 0.1×10^{-6} $\mu g/m^3$ of benzene from the three source types. The total, 12 400 000, includes the entire population of the SoCAB. Nearly all these people are exposed above that threshold from either vehicles or community sources alone. However, only 4 500 000, or less than 40% of the population is subject to that risk level as a result of point source emissions alone.

Table 3 (upper left-hand section) shows the estimate of Excess 70 Year Cancer Incidence that would result from benzene emissions at the rates estimated by SCAQMD for each source type. These results are also presented in Figs. 3 and 4 (same results, but the variables are interchanged). The overall expected Excess 70 Year Cancer Incidence is approximately 7800 cases or about 110 cases per year of emissions. As in the case of the Mean Exposure Concentration, the contributions from the community and mobile sources appear to be approximately proportional to their overall emissions. The variation of incidence among population groups reflects both differences in the Mean Exposure Concentrations for the groups, shown in Table 3, and the different sizes of the population groups.

Comparison with TEAM Measurements—The EPA's TEAM study involved monitoring 19 organic compounds, including benzene, during two test periods in 1984 in several Los Angeles area neighborhoods. Measurements were taken with devices strapped to many dozen participating subjects (117 in February of which 52 repeated in May). Readings were taken to quantify 12 h, night and day, integrated exposures of each subject through their daily activity. Measurements were also taken at fixed outdoor sites outside the subject's residences. Subjects were chosen in the South Bay area of the Los Angeles metropolitan region, inland of Santa Monica Bay, roughly from El Segundo to Redondo Beach and inland to Carson and portions of the City of Los Angeles. They were judged to represent the expected exposures to Census Tracts with about one-third of a million residents in the studied neighborhoods (360 000 in February 1984 and 330 000 in May 1984).

Because of the climatologic setting of Los Angeles, no set of neighborhoods is fully representative of the entire region; nevertheless, the sampled population and region are impressively large. Also, any limited period of record cannot fully define a long-term (lifetime) risk, and the TEAM report suggests that dispersion conditions were not typical through the study periods. In fact, it is suggested that the dispersion conditions may bound the range of expectations. In particular, the February study period was thought to have been characterized by particularly strong night time inversions, producing uncharacteristically high concentrations.

Although this study addresses exposures in indoor and outdoor microenvironments, only outside sources are in the SCAQMD inventory. Therefore, the best comparison of present study with TEAM study results is for outdoor TEAM measurements. A comparison is made in Fig. 5 in terms of cumulative frequency distributions from the present study and from the TEAM study. The distribution from the present study consists of the concentrations computed for each of the CT's in the SCAQMD. The distribution from the TEAM study consists of all of the outdoor (fixed site) measurements in the more limited South Bay study area. Figure 5 shows that model results fall between the TEAM results for the two study periods. SCREAM-II results average about 50% lower than the maximum (winter) TEAM observations, thus giving some confidence that SCREAM-II dispersion algorithms and the SCAQMD benzene inventory are within reasonable bounds.

Future Directions

In order to estimate the relative contribution of indoor sources to benzene exposure and risk in the South Coast Air Basin with SCREAM-II, the contribution to indoor concentrations from indoor sources may be included in the input to the IAQM submodule of the inhalation exposure module. Indoor source concentration contributions may be varied by indoor microenvironment type in the model (for example, home with air conditioner running, home with windows open). Current studies at EPA and other laboratories are developing emission estimates for many indoor materials and operations. These data will provide needed input for future modeled estimates of exposures and risk.

In this study we have demonstrated a tool for estimating and comparing benzene population exposure and carcinogenic risk from various types of outdoor sources and among various population groups, including exposures that occur in the indoor environment. Additional information on exposure and risk from indoor sources would be valuable in the air quality planning process in setting priorities for emission control measures.

References

[1] USEPA, "The Total Exposure Assessment Methodology (TEAM) Study: Summary and Analysis: Vol. I," US EPA, Office of Research and Development, 1987, Washington DC, EPA/600/6-87/002A.

[2] Rosenbaum, A. S., Anderson, G. E., and Lundberg, G. W., "User's Guide to the South Coast Risk and Exposure Assessment Model—Version 2 (SCREAM-II) for the Personal Computer," Systems Applications International, 1992, San Rafael, California.

[3] Hayes, S. R. and Lundberg, G. W., "Further Improvement and Sensitivity Analysis of an Ozone Population Exposure Model," Systems Applications, Inc., San Rafael, California, for the American Petroleum Institute, 1985, Washington, DC (SYSAPP-85/061).

[4] Hayes, S. R., "Estimating the Effect of Being Indoors on Total Personal Exposure to Outdoor Air Pollution," *Journal of the Air Pollution Control Association*, Vol. 39, No. 11, 1989, pp. 1453–1461.

[5] USEPA, "User's Guide for the Industrial Source Complex (ISC2) Dispersion Models," EPA-450/4-92-008A, 1992.

[6] Hanna, S. R. and Gifford, F. A., "Modeling Urban Air Pollution," *Atmospheric Environment*, Vol. 7, pp. 131–136.

[7] Austin, B. S., Rosenbaum, A. S., and Hayes, S. R., "User's Guide to the NEM–SAI Exposure Model," Systems Applications, Inc., 1988, San Rafael, California, for the U.S. Environmental Protection Agency, Research Triangle Park, North Carolina (SYSAPP-88/051).

[8] Roddin, M. F., Ellis, H. T., and Siddiqee, M. W., "Background Data for Human Activity Patterns, Volumes 1 and 2," SRI International, 1979, Menlo Park, California, for the U.S. Environmental Protection Agency, Research Triangle Park, North Carolina.

[9] Douglas, T., "Computer Tape Data File Defining Population Mobility Parameters for Each Regional Statistical Areas in the SCAB," South Coast Association of Governments, 1987, Los Angeles, California.

[10] SCAQMD, "The Magnitude of Ambient Air Toxics Impacts from Existing Sources in the South Coast Air Basin, 1987 Air Quality Management Plan Revision Working Paper No. 3," South Coast Air Quality Management District, El Monte, California (June 1987).

Michael D. Koontz,[1] *William C. Evans,*[1] *Niren L. Nagda,*[1] *and Peggy L. Jenkins*[2]

Development of a Model for Indoor Air Pollutant Exposure Distributions

REFERENCE: Koontz, M. D., Evans, W. C., Nagda, N. L., and Jenkins, P. L., **"Development of a Model for Indoor Air Pollutant Exposure Distributions,"** *Modeling of Indoor Air Quality and Exposure, ASTM STP 1205*, Niren L. Nagda, Ed., American Society for Testing and Materials, Philadelphia, 1993, pp. 271–279.

ABSTRACT: A user-friendly computer model is being developed to estimate the distribution of Californians' indoor exposures to various pollutants. The model will be capable of operating at three levels. Level 1 will sum estimated inhalation exposures across multiple indoor locations to ultimately yield a population distribution of "total indoor air" exposures, that is, the portion of total (24-h) exposure associated with time spent indoors. Level 2 will link randomly selected location/activity profiles, collected in several California surveys, with measured or modeled concentration distributions, resulting in estimated exposure distributions for specific indoor locations such as residential environments. For each sampled location/activity profile, both time-integrated inhalation exposure and potential inhaled dose will be estimated. Level 3 will estimate concentration distributions for pollutants in locations for which measured concentrations are not available, based on the principle of conservation of mass. All information required for a model run will be supplied through a user interface. Options will be provided to save files relating to choices and inputs for a given run, so that all or selected parts of a run can be replicated. Providing this capability within Level 3 of the model will allow the user to make a series of related runs aimed at assessing the impact of one or more potential mitigation strategies.

KEY WORDS: indoor air quality, inhalation exposure, population activity patterns, mass balance, Monte Carlo simulation, computer modeling

Assessment of human exposure to toxic air pollutants in indoor environments is of interest to a number of regulator agencies, particularly because: (1) many individuals spend a significant majority of their time indoors, and (2) indoor concentrations are generally higher than those outdoors for many pollutants. To fully consider indoor exposures in assessing associated health risks, estimates are needed of both average and high-range indoor exposures for the entire population who may be exposed, as well as subgroups of that population such as sensitive individuals.

Assessment of indoor exposures can be complicated because of the considerable variety in: (1) building types and construction characteristics, (2) indoor emission sources such as interior construction materials, furnishings, appliances, and consumer products, and (3) occupant activities including: movement patterns, uses of various types of sources, operation of space-conditioning equipment, and opening or closing of doors and windows. The most direct means of quantifying population exposures to indoor air pollutants is through field monitoring surveys, but this method of generating an exposure distribution is expensive given the lengthy list of pollutants to be as-

[1]Manager, Indoor Air and Exposure Program, senior research scientist, and director, Indoor Environment Division, respectively, GEOMET Technologies, Inc., 20251 Century Boulevard, Germantown, MD 20874.

[2]Manager, Indoor Exposure Assessment Section, California Air Resources Board, Research Division, PO Box 2815, Sacramento, CA 95812.

sessed. An alternative to collecting large amounts of new field monitoring data is to use the limited indoor concentration data, together with information such as location/activity profiles, indoor-source emissions, and housing characteristics as a basis for modeling the population's exposure distribution.

A number of models have been developed to estimate indoor concentrations or exposure distributions for specific pollutants or under a limited set of conditions. Certain "physical-stochastic" models can generate population exposure distributions by utilizing Monte Carlo techniques to simulate human behavior and time-varying pollutant concentrations in specific types of locations (for example, residence, workplace, in transit, and outdoors). For example, the NAAQS Exposure Model (NEM) [*1*] was developed to estimate and analyze population exposures under current or proposed ambient air quality standards. Consequently, this model is driven primarily by ambient concentration data and relies on relatively simple empirical adjustment factors to treat indoor and in-transit environments. Models that have been developed to explicitly treat indoor environments (for example, CONTAM [*2*], INDOOR [*3*], IAQPC [*4*], and MCCEM [*5*]) generally rely on the principle of conservation of mass [*6*] to address factors such as indoor emissions, indoor volumes, airflows between indoors and outdoors and among different zones within a building, and chemical/physical decay or other removal processes. Because these models were intended to predict time-varying indoor concentrations for specific situations, using them to develop indoor concentration or exposure distributions for a variety of situations for the general population would be quite tedious. A macromodel [*7*] has been developed to estimate indoor concentration distributions across a variety of residences, but this model is currently restricted to combustion pollutants and steady-state assumptions in predicting average indoor concentrations over a one-week time interval.

None of the existing models are able to estimate indoor exposure distributions for a variety of pollutants for California residents. Consequently, a new model is being developed that can be flexible in utilizing various types of inputs (for example, location/activity patterns, indoor concentrations, and source emissions) to construct indoor exposure distributions from the best available data for each contaminant to be assessed. The model is currently in the developmental stage. This paper provides an overview of the model structure and describes its key components and features.

Model Overview

For a given model run, the user will be able to apply the model at one of three levels:

- **Level 1**—Aggregating indoor exposure distributions across environments, or
- **Level 2**—Combining indoor-air concentration distributions with location/activity profiles to produce exposure distributions for different types of indoor environments, or
- **Level 3**—Estimating indoor-air concentration distributions for different environments based on the principle of conservation of mass.

The relationships among these three levels are shown in Fig. 1. Level 1 of the model uses environment-specific exposure estimates from Level 2 as the primary inputs. Level 2 uses measured indoor concentration distributions or modeled distributions output from Level 3, together with location/activity patterns, to calculate exposure distributions for various types of environments or locations. Level 3 uses available data on indoor source emissions, air exchange rates, outdoor concentrations, removal factors, and so forth to estimate indoor concentrations when measured concentration data are not available.

The model is structured to provide estimates across major indoor environments including: homes, offices, schools, enclosed transit, public-access buildings, and restaurants or lounges. Initial emphasis in model development is being placed on the residential environment, due to greater availability of supporting data on measured concentrations and mass-balance parameters and the fact

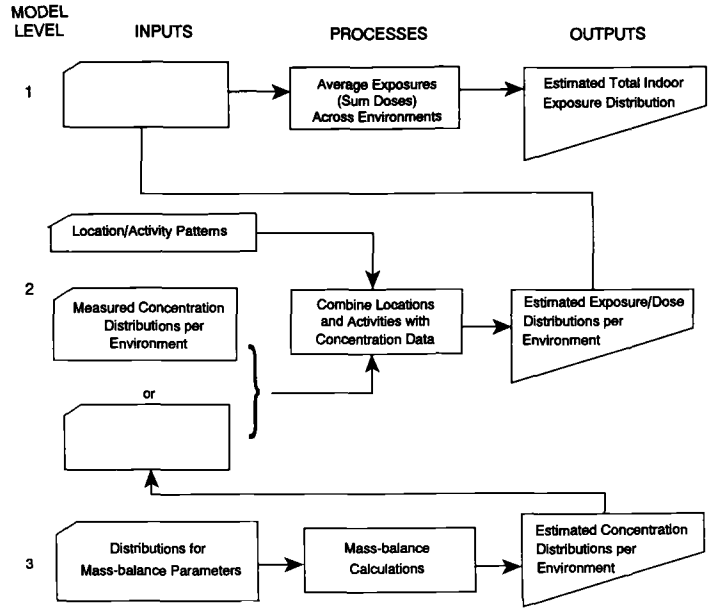

FIG. 1—*Overview of model levels and their relationships.*

TABLE 1—*Candidate contaminants for model development and associated indoor sources.*

Category/Contaminants	Examples of Indoor Sources
Volatile Organic Compounds	
Formaldehyde	pressed-wood products containing ureaformaldehyde (UF) resins, upholstered furniture/draperies with UF resin permanent-press finishes, new apparel, UF foam insulation, smoke from tobacco products, unvented combustion appliances
Benzene	unvented gas appliances, fireplaces or wood stoves, gasoline fumes, cleaning solvents, paints, smoke from tobacco products, kerosene heaters
Chlorinated hydrocarbons (trichloroethylene, perchloroethylene, chloroform)	dry-cleaned clothing, chlorinated water supply, various types of consumer products (for example, water repellents, fabric finishes, spot removers, liquid/aerosol cleaners)
Polynuclear Aromatic Compounds	
Benzo[a]pyrene	fireplaces or wood stoves, smoke from tobacco products, cooking
Inorganic Gases	
Carbon monoxide	unvented gas appliances, leakage from vented combustion appliances, smoke from tobacco products, vehicle emissions from attached/underground garages, kerosene heaters
Nitrogen dioxide	
Particulate Matter	
PM_{10}	smoke from tobacco products, fireplaces, or wood stoves, hobbies/crafts, animals, resuspension due to vacuuming, dusting, or sweeping

that this is the single indoor environment where most people spend the greatest fraction of their time. Future efforts most likely will address office environments, enclosed in-transit environments, and public-access buildings as data become available for those environments.

The initial set of contaminants to be considered in developing the model is listed in Table 1, together with examples of major indoor sources for each. Although limited in number, these contaminants cover the major classes of indoor pollutants, including volatile organic compounds (formaldehyde, benzene, and chlorinated hydrocarbons), polynuclear aromatic compounds (benzo[a]pyrene), inorganic gases (carbon monoxide and nitrogen dioxide), and particulate matter (inhalable particles, or PM_{10}).

Level 1: Aggregation Across Locations

The role of Level 1 of the model is relatively straightforward: to sum exposures across locations to ultimately yield a population distribution of "total indoor air" exposures, that is, the portion of total (24-h) exposure associated with time spent indoors. The outputs from this level of the model will have increasing completeness and validity as sufficient data become available for different types of environments. The model will allow users to save and repeatedly access the same random-number seed when selecting activity profiles to be combined with environment-specific concentration data within Level 2 of the model. In this way, environment-specific exposures can be aggregated within Level 1 across a common set of activity profiles.

Outputs from Level 1 of the model will include graphs of the histogram and cumulative frequency distribution for total indoor-air exposure as well as summary statistics such as arithmetic mean, standard deviation and percentiles for the cumulative frequency distribution. At the user's option, the exposure calculations associated with each location/activity profile can be saved in a data file for analysis in greater detail outside the model. Random-number seeds also will be shown in the outputs so that the user has the ability to replicate a given model run if desired. By running Level 1 repeatedly with different random-number seeds, the user also will be able to empirically examine the statistical stability of estimates such as the 95th percentile of the exposure distribution.

Level 2: Combining Concentration Distributions and Location/Activity Profiles

The role of Level 2 of the model is to combine randomly selected location/activity profiles with measured or modeled concentration distributions, resulting in estimated population exposure distributions for specific types of indoor locations such as residential environments. For each sampled location/activity profile, the model will estimate both inhalation exposure (that is, the time-integrated concentration encountered while in an environment) and potential inhaled dose (that is, the product of average concentration, time spent in the environment, and amount of air inhaled per unit time while in the environment). The average breathing rate while in the environment will be assigned based on activity codes in each location/activity profile; the assignment will be conditional on the individual's age and sex (adult males, adult females, and children).

Through a Monte Carlo simulation whereby a number of location/activity profiles are sampled and combined with location-specific concentration data and activity-specific breathing rates, the model will estimate a distribution of population exposures and potential inhaled doses. Location-specific concentration data, derived from prior monitoring surveys or estimated through Level 3 of the model, may be available for averaging times such as 1, 8, 12, or 24 h; the location/activity profiles available through the model will be summarized for compatibility with these averaging times. The user will be allowed to model a number of environments simultaneously at this level of model operation.

Location/activity profiles to be combined with concentration distributions will be derived from California surveys of (1) adults and adolescents and (2) children under the age of 12 years. A total

of 1762 profiles are available from the adult/adolescent survey and 1200 profiles are available from the survey of children. The survey methods, that involved three geographic strata (the southern coastal area, the San Francisco Bay area, and the remainder of the state) and a 24-h recall diary administered to randomly selected households and household members, have been described in greater detail elsewhere [*8,9*]. It will be possible to add additional profiles for sensitive subgroups of the population such as asthmatics, provided that the data are summarized in a format compatible with those from the previous California surveys.

For the currently available location/activity profiles, the user will have the ability to select population subgroups based on criteria such as geographic region, urban/suburban/rural residence, county of residence, season or weekday/weekend when the profile was recorded, and age, gender, income level, education status, or employment status of the respondent. At this point in the user interface, the model will determine the number of available location/activity profiles, display this number, and issue a warning message if the requested number of simulation trials exceeds the number of available profiles.

For the California location/activity surveys, weighting factors have been developed to compensate for uneven sampling of days of the week, seasons of the year, and regions of the state in addition to adjustments related to the number of telephones and eligible respondents in the household. It is currently envisioned that the location/activity profiles will be sampled with equal selection probabilities and that the weights will be reflected in the graphical and statistical outputs. The detailed output files containing indoor-exposure or inhaled-dose information for each sampled profile will also contain the weights for use in any further analysis outside the model. Users will have the ability to control the random-number seed for sampling from location/activity profiles and concentration distributions, so that the simulation can be repeated with identical or revised inputs.

Level 3: Estimation of Concentrations from Mass-Balance Equations

The role of Level 3 of the model is to estimate concentration distributions for pollutants in environments for which measured concentrations are not available. Based on the principle of conservation of mass within an indoor environment, the indoor concentration is increased by emissions from indoor sources and by infiltration of outdoor air, and is decreased by exfiltration of indoor air or by processes such as decay, deposition, chemical transformation, or filtration. The basic equation, or series of compound-specific equations, from which Level 3 of the model will operate can be generally expressed as follows [*6,7*]

$$\frac{dC_i}{dt} = (P \cdot a \cdot C_o) + \frac{S}{V} - (a \cdot C_i) - (k \cdot C_i) \tag{1}$$

where

P = penetration factor, or fraction of the outdoor contaminant concentration that moves through the building shell to the indoors without interception;
a = indoor-outdoor air exchange rate (1/h, or air changes per h);
C = outdoor concentration ($\mu g/m^3$),
S = indoor-source emission rate ($\mu g/h$), that may result from more than one indoor source;
V = indoor volume (m^3),
C_i = indoor concentration ($\mu g/m^3$), and
k = rate (1/h) associated with removal processes other than air exchange.

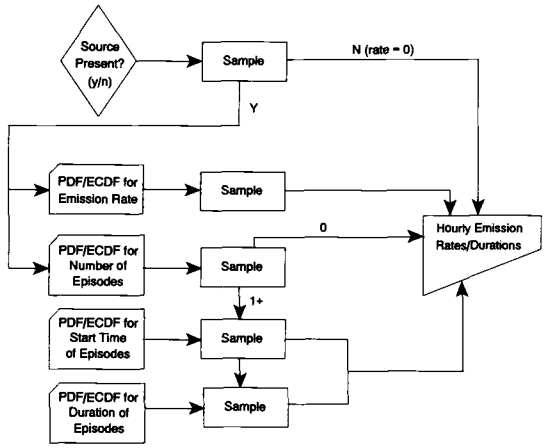

FIG. 2—*Emissions flowchart for frequent source with constant emission rate (for example, gas range, cigarette).*

It is desirable that the model provide reasonably accurate results without being overly complex, so that sufficient input data can be located to implement the model. Consequently, a single-chamber dynamic model is initially planned, even though such a model will have some limitations, such as inability to reproduce spatial concentration gradients that may exist within a building. General approaches for dealing with various terms of Level 3 of the model are discussed below.

Most of the data on air exchange rates that could be used for the model are averages over a period of several days or longer for residential environments. The air-exchange measurements were performed with perfluorocarbon tracers [*10*] as part of the design for field monitoring studies in California intended to characterize pollutant concentrations or exposure distributions [*11,12*] or residential energy consumption [*13,14*]. The majority of these data are for the southern-coastal area of the state, but several ongoing studies sponsored by the California Air Resources Board (ARB) will provide information for other areas in the near future. Information related to residential volumes has been collected by agencies such as the U.S. Department of Energy and the California Energy Commission, in addition to field studies with air-exchange measurements. Outdoor concentration data are available through networks of ambient monitoring sites established by the ARB for criteria pollutants or air toxics.

The source term in the above equation is more properly expressed as a summation of various types of sources. For combustion pollutants, for example, the sources would include gas range/oven pilot lights, use of a gas range for cooking or misuse for heating, unvented space heaters, and smoking of tobacco products. For most air toxics, the emissions result from indoor materials or furnishings, occupant use of consumer products, and public water supplies. These types of sources emit pollutants either continuously or intermittently, and associated emission rates can be nearly constant over time or can decline exponentially when the source is active.

Depending on the specific type of source, parameters such as frequency, duration, time of use, age and load factor of the source, and initial emission rate and time-related decline in the emission rate may enter into the source-related calculations. Illustrative flowcharts for sampling these parameters to determine emission rates and durations are given in Figs. 2 through 4 for sources defined according to (1) frequency of use and (2) constant versus declining rate of emitting pollutants. For example, for a frequent source such as a gas range that has a (nearly) constant emission rate when in use, the model will sample whether or not the source is present and, if so, the emission rate, the number of usage episodes on a given day, and the start time and duration for each episode

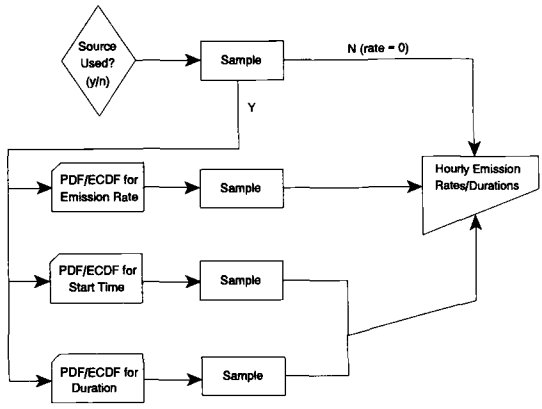

FIG. 3—*Emissions flowchart for episodic source with declining emission rate (for example, latex paint, dry-cleaned clothes).*

(Fig. 2). The inputs for these factors will be in the form of parameters describing a probability density function (PDF), such as mean and standard deviation for a normal distribution, or an empirical cumulative distribution function (ECDF), in the form of values associated with selected percentiles of the cumulative frequency distribution.

Some of the candidate compounds for the model are inert, whereas others, such as nitrogen dioxide and many of the VOCs, can be chemically reactive. For reactive species, a commonly used modeling approach is to specify a first order rate constant that represents the product of deposition velocity times surface area of contact. Reactivity rates for some compounds have been summarized by Nazaroff and Cass [*15*]. General terms for particle losses due to deposition can be specified in a similar manner [*16*]. Additional terms (that is, airflow rates and removal efficiencies) can be added for particles to account for removal through air-cleaning devices or through filters in heating, ventilating, and air-conditioning (HVAC) systems. Considerations for future enhancements to the model include (1) resuspension of deposited particles due to cleaning activities or movement of

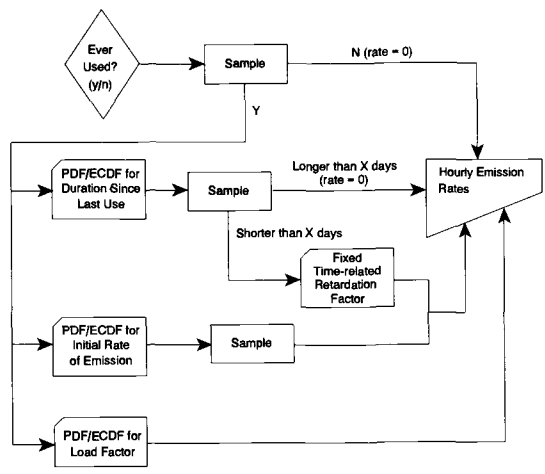

FIG. 4—*Emissions flowchart for constant source with declining emission rate (for example, construction material).*

people and (2) re-emission of reactive gases from material sinks. Models for reversible sinks have been postulated [*17*], but the information needed to support such models is currently lacking in most instances.

Current Status and Future Plans

An overall conceptual framework for the model has been developed, together with some of the supporting computer code (Microsoft QuickBASIC). Specifications for model outputs are being finalized and several methodological issues remain to be resolved. All information (for example, choice of compound, environment(s) and population subgroup, data files, and parameters describing distributions of input parameters) required for a model run will be supplied through a user interface. Options will be provided to save files related to substantive subsets of information (for example, population subgroup selections, breathing rates, concentration distributions, or mass-balance parameters). Through these files, it will be possible to call upon prior choices or previously developed information as defaults for subsequent model runs, so that all or selected parts of a run can be repeated. Providing this capability within Level 3 of the model will allow the user to make a series of related runs aimed at assessing the impact of one or more potential mitigation strategies.

An initial prototype of the model (Levels 1 and 2) was delivered in late 1992. The completed model, that will include the module for Level 3, is expected in spring 1993. Model verification/validation steps will include: independent checks on model calculations and on proper retention and use of information from user inputs, as well as some comparisons of model predictions from Level 1 or Level 3, or both, with measured data sets (for example, time-weighted-average personal exposures for Level 1, environment-specific concentrations for Level 3).

Acknowledgment/Disclaimer

The work reported in this paper is supported by the California Air Resources Board (ARB) under Contract A933-157 with GEOMET Technologies, Inc. The model is being developed as a tool for the ARB Research Division in assessing exposure to toxic air pollutants in indoor environments and identifying the relative contribution of indoor exposure to total human exposure, as mandated under Section 39660.5 of the California Health and Safety Code. The opinions and conclusions expressed in this paper are those of the authors and do not necessarily reflect the views of the California ARB.

References

[*1*] Johnson, T. and Paul, R. A., *The NAAQS Exposure Model (NEM) Applied to Carbon Monoxide*, Report EPA-450/4-83-003, U.S. Environmental Protection Agency, Research Triangle Park, NC, 1983.

[*2*] Axley, J., "Progress Toward a General Analytical Model for Predicting Indoor Air Pollution in Buildings: Phase III Report," Report NBSIR 88-3814, National Institute of Standards and Technology (NIST), Gaithersburg, MD, 1988.

[*3*] Sparks, L. E., "Indoor Air Model Version 1.0," Report EPA 600/8-88-097a, U.S. Environmental Protection Agency, Research Triangle Park, NC, 1988.

[*4*] Ensor, D. S., Yakamoto, T., Lawless, D. A., "Indoor Air Quality Simulator for Personal Computers," Paper 89–82.1, *Proceedings*, 82nd Annual Meeting of the Air and Waste Management Association, 1989.

[*5*] Koontz, M. D. and Nagda, N. L., "A Multichamber Model for Assessing Consumer Inhalation Exposure," *Indoor Air*, Vol. 4, 1991, pp. 593–605.

[*6*] Nagda, N. L., Rector, H. E., and Koontz, M. D., *Guidelines for Monitoring Indoor Air Quality*, Hemisphere Publishing Corporation, New York, 1987.

[*7*] Traynor, G. T., Aceti, J. C., and Apte, M. G., "Macromodel for Assessing Residential Concentrations of Combustion-Generated Pollutants: Model Development and Preliminary Predictions for CO, NO_2, and

Respirable Suspended Particles," Report LBL-25211, Lawrence Berkeley Laboratory, Berkeley, CA, 1989.

[8] Jenkins, P. L., Phillips, T. J., Mulberg, E. J., and Hui, S. P., "Activity Patterns of Californians: Use of and Proximity to Indoor Pollutant Sources," *Atmospheric Environment*, Vol. 26A, No. 12, 1992, pp. 2141–2148.

[9] Phillips, T. J., Jenkins, P. L., and Mulberg, E. J., "Children in California: Activity Patterns and Presence of Pollutant Sources," Paper 91-172.5, *Proceedings*, 84th Annual Meeting of the Air and Waste Management Association, 1991.

[10] Dietz, R. N. and Cote, E. A., "An Inexpensive Perfluorcarbon Tracer Technique for Wide-Scale Infiltration Measurements in Homes," *Environment International*, Vol. 8, 1982, pp. 419–433.

[11] Wallace, L. A., "The Total Exposure Assessment Methodology (TEAM) Study: Summary and Analysis: Volume I," Report EPA-600/6-87-002a, Washington, DC, 1987.

[12] Wilson, A. L., Colome, S. D., Baker, P. E., and Becker, G. W., *Residential Indoor Air Quality Study of Nitrogen Dioxide: Phase I Final Report*, prepared for Southern California Gas Company, Los Angeles, CA, 1986.

[13] Berkeley Solar Group and Xenergy, *Occupancy Patterns & Energy Consumption in California Houses (1984–1988)*, Report P400-90-009, prepared for California Energy Commission under Contract 400-87-015, 1990.

[14] Mahone, E. E., Mort, D. W., Alereza, T., *Pilot Residential Air Exchange Survey—Task 2: Pilot Infiltration Study*, prepared for California Energy Commission under Contract 400-88-020, 1990.

[15] Nazaroff, W. W. and Cass, G. R., "Mathematical Modeling of Chemically Reactive Pollutants in Indoor Air," *Environmental Science and Technology*, Vol. 20, No. 9, 1986, pp. 924–934.

[16] Nazaroff, W. W. and Cass, G. R., "Mathematical Modeling of Indoor Aerosol Dynamics," *Environmental Science and Technology*, Vol. 23, No. 2, 1989, pp. 157–166.

[17] Guo, Z., Dunn, J. E., Tichenor, B. A., "On Representing Reversible Sinks in Indoor Air Quality Models," *Indoor Air '90*, Proceedings of the 5th International Conference on Indoor Air Quality and Climate, Vol. 4, 1990, pp. 177–182.

Joseph V. Behar,[1] *Jerry N. Blancato,*[1] *Muhilan D. Pandian,*[2] *and Jacob Thomas*[3]

Modeling of Human Exposure/Dose to Benzene

REFERENCE: Behar, J. V., Blancato, J. N., Pandian, M. D., and Thomas, J., "**Modeling of Human Exposure/Dose to Benzene,**" *Modeling of Indoor Air Quality and Exposure, ASTM STP 1205*, Niren L. Nagda, Ed., American Society for Testing and Materials, Philadelphia, 1993, pp. 280–290.

ABSTRACT: This paper presents the latest developments in the modeling of population exposures to airborne pollutants in indoor environments. Population exposure estimates are composed of three basic components: (1) human activity patterns, (2) microenvironmental (primarily indoor) concentration distributions, and (3) ambient (primarily background or outdoor) concentration distributions. Human activity pattern data and concentration distribution data may be derived from experiments or by simulation. This paper reports the progress made in combining the above three components of exposure in a simulation model. Exposure estimation is a precursor to dose determination. The latest results in our attempts to incorporate pharmacokinetic modules into human exposure models are presented.

KEY WORDS: exposure, simulation, pharmacokinetics, microenvironment

Benzene has been listed by the U.S. Environmental Protection Agency (EPA) under Section 112 of the Clean Air Act as a hazardous air pollutant. As a result of its high volatility, the most likely exposure to benzene will be via inhalation. Chronic exposure to benzene may result in severe anemia. Benzene is a known leukemogen and is regarded as a human carcinogen. There are two primary exposure scenarios for benzene exposure: (1) occupational exposure and (2) general exposure. For general exposure, two conditions must be considered, transient and long term (or steady state). Occupational exposures, potentially high level exposures, usually involve only a small fraction of the total population. Transient exposures, while probably lower-level than occupational, are expected to occur for a much larger population from the use of benzene-containing consumer products, including gasoline. Steady-state exposures, expected to be chronic, low-level exposures (for example, ambient), involve the entire population.

Background

The Total Exposure Assessment Methodology (TEAM) studies executed between 1979 and 1988 by the U.S. EPA [*1–6*] have provided data that corroborates the hypothesis that exposure to certain classes of volatile organic compounds (VOCs), including benzene, occurs primarily within the confines of highly restricted environments. Such environments are located primarily indoors, although some outdoor environments exist in which human receptors are situated close to sources and

[1]Environmental scientist and research biologist, respectively, Environmental Monitoring Systems Laboratory (EMSL), Exposure Assessment Research Division, Las Vegas, NV.
[2]Environmental engineer, Harry Reid Center for Environmental Studies, UNLV, Las Vegas, NV.
[3]Statistician, Information Systems and Services, Inc., Las Vegas, NV.

the dispersion of pollutants is relatively restricted (over short distances and time scales). Such locations, when appropriately combined with human activities, are referred to as "microenvironments."

Human exposure to any pollutant can be estimated by matching the times spent by subjects in the microenvironments through which they pass with the concentrations of the pollutant in those microenvironments. Subject movements are obtained from human time-activity patterns. The latter, in the context of exposure assessment, are quantifiable descriptions of the duration and frequency with which individuals of a population occupy particular locations (microenvironments) in space and time. They are, ostensibly, a record of the things people do, where they do them, for how long and when, during the conduct of their daily lives. Information obtained from human exposure studies (TEAM) conducted by the EPA indicate that indoor microenvironments constitute a significant fraction of the locations critical to correct estimation of human exposure.

Estimation of the dose to target tissues is the next step in the risk assessment process. As in the exposure assessment process, this may be accomplished either by measurements (for example, of parent compounds, biomarkers, or metabolites taken from sampled tissues, body fluids, or various excreta), or by estimation using pharmacokinetic models. Pharmacokinetics is the study of the disposition of foreign substances and their metabolites within the body. Pharmacokinetic models are mathematical descriptions of these pharmacokinetics. They were first used to predict the dose and dosage regimen necessary for optimum therapeutic drug concentrations. In recent years, their utility in risk and exposure assessment has become more apparent [*7–11*]. Most of the models used to describe and predict internal body doses of toxins are physiologically-based pharmacokinetic (PBPK) models. When properly formulated and validated, these models give the risk assessor an estimate of dose to internal tissues, organs, or cells. With these models and some knowledge about mechanism of action, the dose portion of dose-response functions is based on a more rational estimate of the effective dose. Previous assessments have been based on some concentration or measure of exposure outside the body boundaries. This has led to considerable uncertainties in the extrapolation process between species and even between different exposure scenarios. For example, two identical time exposure products (for example, ppm-h) may result in considerably different metabolite concentrations because of inherent pharmacokinetic nonlinearities. PBPK models can be formulated to quantitatively account for many of the nonlinear biochemical and physiologic processes occurring in the living organism.

One very helpful use of such models is to examine and better describe the impact that different exposure profiles can have on internal or effective dose. The identification of the importance of different exposure scenarios can be easily accomplished with the use of these models. With such identification, better exposure and risk assessments can be performed. Equally important is the advantage that these models offer the assessor who needs to plan monitoring studies. By predetermining required resolution that will be needed in the dose-response assessment, monitoring studies can be carefully planned. As a result, costly but unnecessary data gathering is avoided while crucial and important data are appropriately collected and not overlooked as they might otherwise be.

In this paper, one such PBPK model is used to illustrate how models can be used to shed light on the impact of definitive changes in exposure concentrations that often occur in the course of daily living. Here the Benzene Exposure Assessment Model (BEAM) [*12–14*] was used to give high resolution exposure concentration profiles over time. Those profiles were then used as the input into the PBPK model. The resulting tissue concentrations were then examined.

Approach

BEAM simulates exposures of a sample of residents in an urban area during the conduct of their daily lives. To do this, the model needs three inputs: (1) activity patterns, (2) outdoor benzene concentration distributions of the urban area for the time of the year for the ambient component

of exposure, and (3) microenvironmental concentration distributions due to sources, the majority of which are indoor sources for the transient source component.

BEAM uses 16 standardized microenvironments (activity/locations) that are listed below [*15*].

1. Autoplaces
2. Restaurant or Bar
3. In-Vehicle, Internal Combustion
4. In-Vehicle, Other
5. Physical Activity, Outdoor
6. Physical Activity, Indoor
7. Work or Study at Residence
8. Work or Study, Not in Residence
9. Cooking
10. Other Activity in Kitchen
11. Chores or Child Care
12. Shop or Errands
13. Other Outdoor Activity
14. Social or Cultural Activity
15. Leisure, Indoor
16. Sleep, Indoor

In the second validation study of BEAM for the Los Angeles participants of the California TEAM studies of 1984 and 1987 [*13*], the above mentioned inputs were provided by: (1) the adult activity pattern study of the California Air Resources Board, (2) the TEAM outdoor benzene concentration distributions taken during two seasons in 1984 and two seasons in 1987 when the four VOC exposure studies were conducted in Los Angeles, and (3) indoor concentration distributions measured during the TEAM 1987 California study and the studies conducted by California's South Coast Air Quality Management District [*16*]. BEAM, using the actual activity pattern profile of selected individuals, simulates exposure using the Monte Carlo technique of sampling from distributions. For each microenvironment, the participant passes through, the ambient and the appropriate microenvironmental distributions are sampled and the concentrations added to provide the total exposure the individual experiences for the duration in minutes he or she spends in the microenvironment. Thus, BEAM provides exposure profiles over 24 h for the individuals.

For this study, four residents of the Los Angeles July 1987 TEAM study (two smokers and two nonsmokers) were chosen. Using BEAM with the three sets of inputs mentioned above, their exposure profiles were simulated. BEAM uses a smoking algorithm to superimpose the passive benzene concentrations due to smoking. It should be noted that the smoking algorithm does not currently provide benzene exposure due to the active smoke drawn in by the smoker. Hence, the present analysis underestimates the exposure profile of active smokers by the amount of direct smoke inhaled. Correction of this shortcoming is currently underway. Each person's exposure profile was simulated twice, once using both the ambient component and the microenvironmental source component (mainly indoor), and the second time using only the ambient component. The difference in concentrations between the two simulated exposure profiles in each microenvironment is mainly the indoor component of exposure. The results of the simulation of exposures to benzene for the four selected cases are given (Table 1).

The physiologically based pharmacokinetic model for benzene [*1*] was used as a basis for this illustrative work. While the exact mathematical description of the model can be found elsewhere [*17*], this particular model tracks the concentration of benzene in several of the body's tissues and in exhaled air. Included in the organs being described are the liver, fat, blood, and bone. The liver is typically included because of its metabolic capacity. Metabolism is a major elimination pathway

TABLE 1—*BEAM simulation of benzene exposures over 1440 min.*

Duration, min	Microenvironment	Benzene Exposure Concentrations		
		Indoor	Outdoor	Both
	CASE 1—MALE, AGE 30, NONSMOKER			
420	16	2.2	0.5	2.7
20	11	0.8	5.0	5.8
10	15	0.7	9.2	9.9
30	3	23.8	0.3	24.1
120	8	0.9	1.7	2.6
20	14	0.8	2.4	3.2
160	8	0.1	0.1	0.2
60	2	1.8	4.1	5.9
210	8	0.1	2.6	2.7
30	3	34.8	5.0	39.8
180	14	10.3	3.5	13.8
15	3	12.5	2.1	14.6
135	15	0.0	3.5	3.5
30	16	0.4	2.3	2.7
1440				
	CASE 2—FEMALE, AGE 35, NONSMOKER			
90	16	4.3	0.4	4.7
300	15	17.1	5.7	22.8
180	16	0.1	3.2	3.3
75	15	0.1	1.9	2.0
35	11	8.8	3.4	12.2
25	11	0.4	0.2	0.6
15	1	96.2	0.6	96.8
30	13	0.0	3.3	3.3
45	9	0.1	2.0	2.1
30	15	8.9	4.6	13.5
20	3	21.5	2.3	23.8
205	12	0.6	0.6	1.2
20	3	15.0	2.3	17.3
70	15	1.5	7.4	8.9
90	11	0.8	8.5	9.3
120	13	0.0	1.7	1.7
20	3	15.2	5.2	20.4
15	16	0.9	4.8	5.7
	CASE 3—MALE, AGE 62, SMOKER			
360	16	0.4	1.5	1.9
80	11	9.7	5.5	15.2
25	11	10.0	1.6	11.6
15	3	14.0	1.7	15.7
180	8	13.5	2.4	15.9
15	12	1.6	2.5	4.1
435	8	0.1	8.0	8.1
15	3	139.4	5.2	144.6
30	15	18.4	2.4	20.8
225	15	20.4	11.5	31.9
15	11	24.3	0.5	24.8
45	16	2.3	2.8	5.1

TABLE 1—*Continued*

Duration, min	Microenvironment	Benzene Exposure Concentrations		
		Indoor	Outdoor	Both
	CASE 4—MALE, AGE 28, SMOKER			
420	16	0.6	2.0	2.6
30	9	7.6	4.4	12.0
15	15	6.8	5.6	12.4
195	14	13.8	3.9	17.7
75	9	6.7	4.1	10.8
15	15	10.8	0.6	11.4
15	10	9.6	5.5	15.1
225	16	0.5	5.6	6.1
120	9	7.8	1.8	9.6
60	15	9.1	6.8	15.9
150	15	32.2	5.9	38.1
20	11	6.9	3.3	10.2
100	16	1.7	2.2	3.9

for benzene itself. In addition, some of the metabolites formed are believed to be responsible for some of the observed toxicity. Bone is included because it is in this tissue that many of the well known toxic effects of this compound, including bone marrow suppression and leukemia, have been observed to occur.

The model used here was altered in some of its parameter values. In the published model [*17*], blood and respiratory flows were set somewhat high to accommodate vigorous activity and smoking behavior. In this study, the values were adjusted more in accordance with resting conditions. The values chosen were based on those used by Corely, et al. [*10*], and on physiologic values reported in medical physiology textbooks [*18*]. The parameter values used in this study and those reported in Travis, et al. [*17*] are given (Table 2). In addition, while in Travis's paper there is mention of extrahepatic metabolism, no metabolism terms are explicitly introduced into any of the extrahepatic equations. Instead, the authors implied that the liver metabolism equation accounts for all metabolism. However, in Table A1 of Travis's paper, values are listed for metabolic rate constants for conversion of benzene in the bone marrow. It was decided that for this study the rate constant (V_{max}) for the bone should be added to that listed for the liver. The value for the bone rate constant is very small compared to that for liver. As a result, it's impact on total metabolism, and hence, on actual benzene concentrations, the interest of this exercise, is expected to be minimal. However, it could be very important in quantifying the amount of possible toxic metabolite reaching the bone marrow. Thus, for quantifying actual hazard at the site of toxicity, the model would be expanded to include bone marrow metabolism and for tracking concentrations of metabolite in this very important and vital tissue.

For each case, an exposure profile was simulated by the BEAM model. That profile was then used as the input for the pharmacokinetic model to calculate internal tissue concentrations. Prior to that, the actual monitored concentration in exhaled breath of each individual (*vide supra*) was used to establish the initial conditions for organ concentrations in the pharmacokinetic model. Thus, aspects of the actual exposure occurring prior to the start of the BEAM simulated input were taken into account. This was done as follows. The monitored exhaled breath concentration was used as the target for the pharmacokinetic model. Various inhalation concentrations were tried until a match between model output and monitored exhaled air was reached. The tissue concentrations that resulted with this matched pharmacokinetic model run were taken as the initial conditions for the subsequent pharmacokinetic model runs using the BEAM simulated exposure profiles. The

TABLE 2—*Pharmacokinetic parameter values.*

Parameter[a]	Travis et al. [17][b]	This Study
Alveolar ventilation	15.0	5.8
Cardiac output	12.4	5.8
Liver blood flow	3.10	1.57
Fat blood flow	0.62	0.49
Bone marrow blood flow	1.10	0.35
Internal organ blood flow	5.45	2.70
Muscle blood flow	2.72	0.87
Liver volume	1.86	1.86
Fat volume	13.3	13.3
Bone marrow volume	2.8	2.8
Internal organ volume	3.5	3.5
Muscle volume	40.6	40.6
Blood/air partition	7.4	7.4
Liver/blood partition	1.49	1.49
Fat/blood partition	54.86	54.86
Bone marrow/blood partition	13.78	13.78
Internal organ/blood partition	1.49	1.49
Muscle/blood partition	2.03	2.03
V_{MAX} for metabolism, liver	0.484	0.503
V_{MAX} for metabolism, bone	0.0008	n/a[c]
KM for metabolism, liver	0.35	0.35
KM for metabolism, bone	0.35	n/a[c]

[a]Units—Flow, L/min; Volume, L; V_{MAX}, mg/min; *KM*, mg/L.

[b]Parameters from Travis were converted as follows: Blood flows from QT[a] fractional flow to organ; volumes—total volume[a] fractional volume of organ.

[c]In the Travis et al. (1991) paper [*17*], there was no discussion of the metabolism in the bone marrow compartment, although these values were listed in the Tables. Here, *f* completeness, the values of the two reported V_{MAX} were added together.

conditions for initializing the pharmacokinetic model runs were an assumed continuous exposure for two h, using the parameters listed (Table 2). Obviously, modifying the assumptions for this "prerun" simulation results in different initial conditions. For future application, greater understanding of actual exposure conditions would reduce the uncertainties associated with this process. Pharmacokinetic model runs were then done for the BEAM simulated cases outlined above and the resulting tissue concentrations were plotted.

Results and Discussion

Figures 1 through 4 show the outputs from the BEAM, that are also the inputs to the PBPK model and the outputs from the PBPK model. The upper left panel of each figure shows the concentration in the inhaled air as simulated by the BEAM. The pharmacokinetic model simulates the entire lung as one homogeneous compartment without consideration for the flows and effects of the upper airways. In the alveolar spaces the inhaled air mixes with air in the lung. Consequently, the concentration in the inhaled breath is not the same as the concentration in the alveolar space.

The actual concentrations of benzene in the internal tissues may vary from what is visualized in Figs. 1 through 4, depending upon the exact assumptions with respect to the initializing pre-BEAM exposure run. However, of interest here are the concentration versus time profiles. Several things can be noted. First, the exhaled breath and arterial blood concentrations mirror one another and the inhaled breath concentration very closely. The times for peaks are almost identical in each. This is not surprising given that the inhaled air accounts, according to this and other models, for

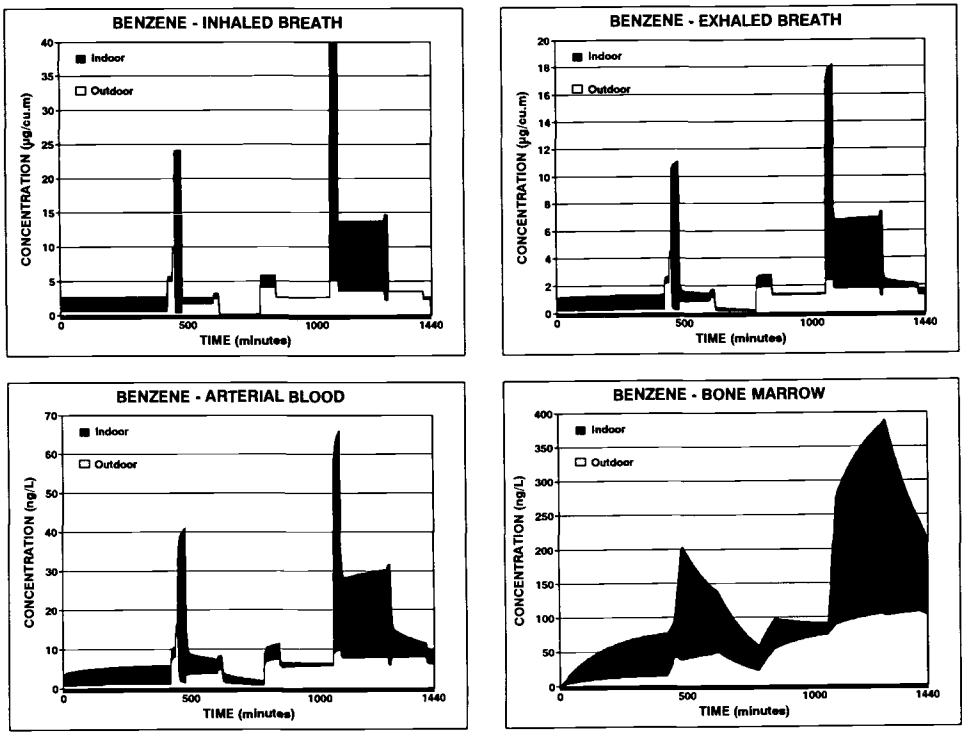

FIG. 1—*Case 1-nonsmoker, benzene exposure/dose patterns, indoor/outdoor contributions.*

30% of the alveolar air and that the blood to air partitioning for benzene favors the blood by 7.4 times. With this partition value and the low concentrations simulated here, it would be expected that benzene rapidly passes into the blood across the pulmonary membrane. The bone marrow profiles lag behind the blood and air profiles slightly. This delay is due to the several physiological and thermodynamic properties of the organ, including the lag caused by the circulation time. The initial benzene concentrations in bone marrow were set to zero.

This high correspondence between inhaled air concentrations with both exhaled air and blood concentration has implications for biomonitoring considerations. From the results of this pharmacokinetic model, it appears that concentrations of benzene in both the exhaled breath and blood are reflective of only the most recent inhalation concentration. Thus, a breath measurement taken after a 12 or 24 h study does not reveal very much information regarding the exposure concentrations before the most recent exposure. For example, observing Case 1, if exhaled breath were measured at 1000 min, one would not be able to discern anything about the peak that had occurred in the inhalation concentration at 500 min. Thus individual breath samples taken over wide time ranges are not expected to be reflective of cumulative exposure. However, if cumulative monitoring could be accomplished, then cumulative exposure could be estimated. There are practical limitations to this. However, if urinary metabolites were found to have some correspondence, and because of their relative ease of collection, they might lend themselves for estimating total exposures. It might also be useful and very powerful to biomonitor more than one matrix. For example, breath measurements could be taken periodically to reflect changes in the profile, while urine measurements could be used to reflect cumulative exposure.

The contribution of indoor air to internal concentrations can also be determined from these plots. In each plot the upper line represents concentrations when the BEAM simulation included both

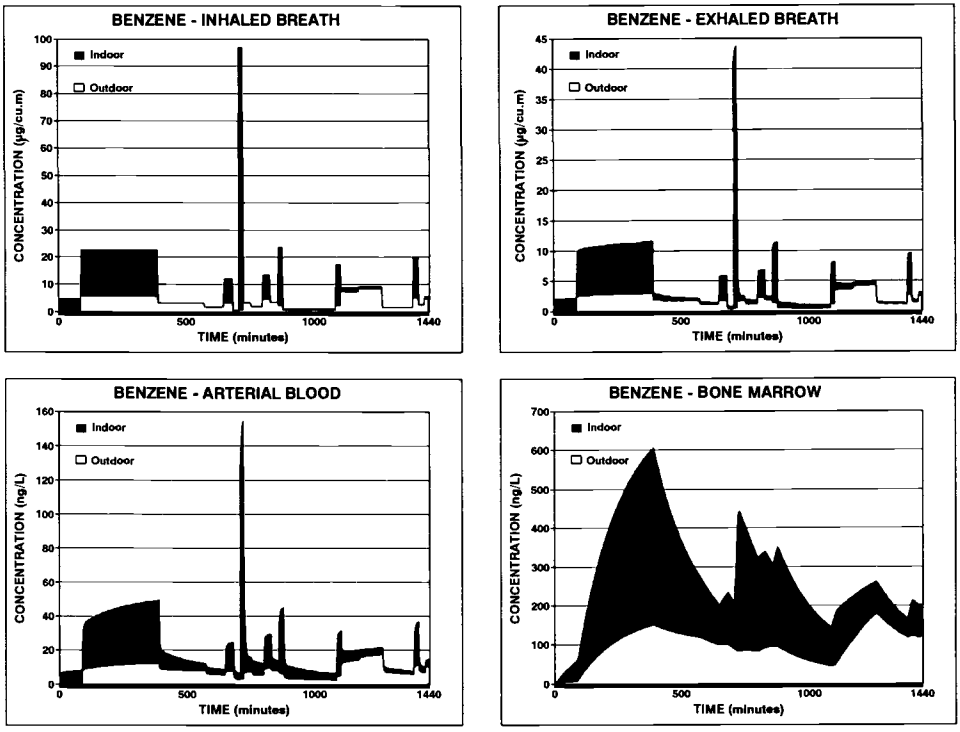

FIG. 2—*Case 2-nonsmoker, benzene exposure/dose patterns, indoor/outdoor contributions.*

ambient and indoor air components of benzene concentrations. The lower line represents concentrations when the BEAM simulation included only the ambient contribution. Thus, the difference between the two lines represents the contribution of indoor air. Hence, the large contribution from transient exposure (from indoor air) compared with the contribution from steady state exposure (from outdoor air), to exhaled air and arterial blood concentrations can be observed.

Although not shown here, total metabolite was also calculated and the difference for Case 3 is approximately 1.2-fold less when the indoor air component is omitted. Under different exposure conditions, the impact upon metabolism might be greater. With the exposure conditions used here, the difference in metabolite formation increased with time. These findings are presented here to illustrate the usefulness of interfacing exposure models such as BEAM with pharmacokinetic models. At this time no conclusions should be drawn from these observations. Further investigations will be necessary to better understand the impact of indoor concentrations on metabolite formation. This is especially important considering that metabolites are suspected to significantly contribute to the toxicity of benzene.

Summary

This paper is illustrative of the coupling of exposure models such as BEAM with physiologically-based pharmacokinetic models. The importance and impact of exposure scenarios based on actual exposure conditions on target doses can be easily determined with this approach. With appropriate analysis and well planned, limited monitoring studies, a great deal of insight can be gained. In this case, with this particular pharmacokinetic model, the following can be said.

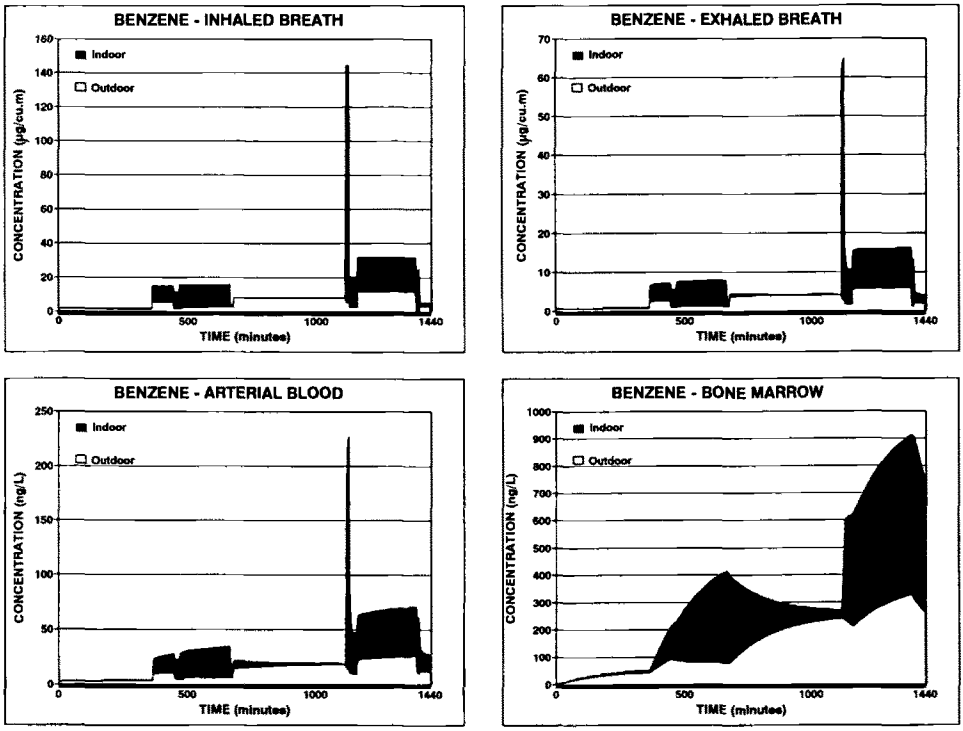

FIG. 3—*Case 3-smoker, benzene exposure/dose patterns, indoor/outdoor contributions.*

(1) It appears that slight alterations in exposure concentrations can be expected to immediately result in similar changes in blood and exhaled breath concentrations.
(2) As a result of number 1 above, it appears that exhaled breath concentrations are reflective of immediate exposure conditions rather than conditions before the last change in the microenviromental exposure concentration.
(3) Some biomarker other than exhaled air (or alternately cumulative exhaled air) will be necessary to estimate cumulative exposure.
(4) An appropriately validated pharmacokinetic model, when used with proper sampling protocols and methods, may be useful for estimating concentrations in bone marrow and amount metabolized.

Future work calls for expanding this effort to reduce the considerable uncertainties that still remain. Presently, this laboratory is engaging with others in efforts to monitor exposed individuals over time. Monitoring is expected to include exposure concentration, exhaled air, blood, and urine. The blood and urine will be analyzed for benzene metabolites. The pharmacokinetic model will be expanded to include urinary metabolite excretion. It is also likely that other pharmacokinetic models for benzene such as that published by Medinsky et al. [*19*] for rodents will be examined to see how they can be modified and adapted for our purposes. Some of these other models also include bone marrow metabolism and the transport of metabolite formed in the liver to the bone marrow. The present work does not clearly elucidate the importance of quickly changing exposure profiles upon such microscopic levels within the body. Including these components into the phar-

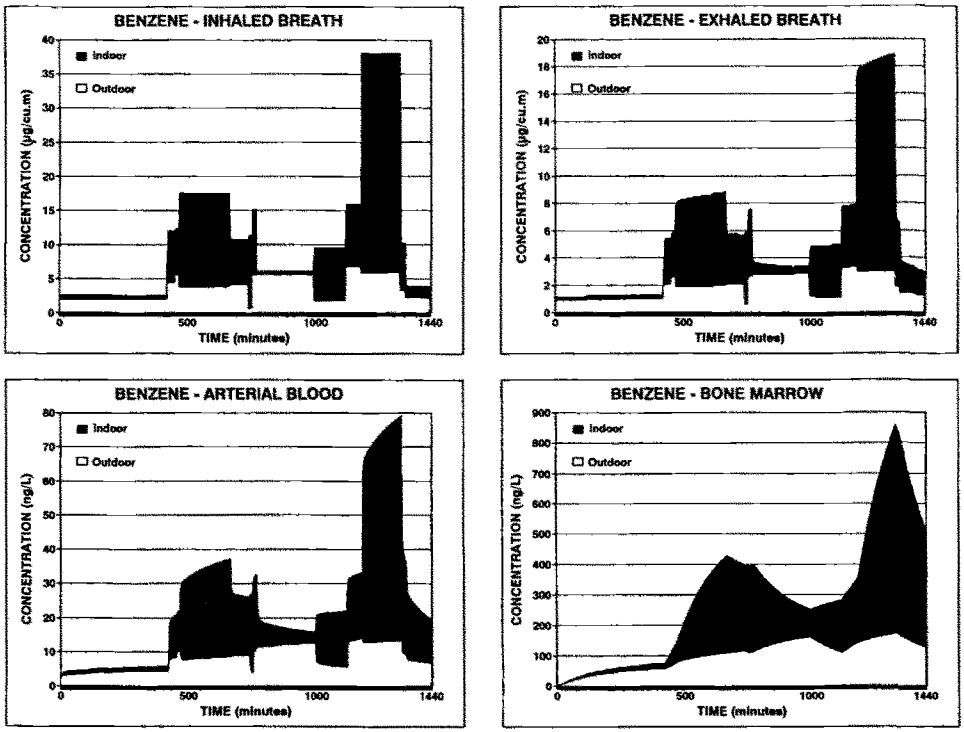

FIG. 4—*Case 4-smoker, benzene exposure/dose patterns, indoor/outdoor contributions.*

macokinetic model is extremely important as the toxic role of both bone marrow produced and liver produced metabolites is becoming clearer.

References

[1] Hartwell, T. D., *Study of Carbon Monoxide Exposure to Residents of Washington, DC and Denver, CO, Part I*, U.S. Environmental Protection Agency (EPA), National Technical Information Service (NTIS), PB84-183516, Environmental Monitoring Systems Laboratory-Research Triangle Park (EMSL-RTP), 1984.

[2] Hartwell, T. D., Clayton, C. A., Michie, R. M., Jr., Whitmore, R., Zelon, H. S., and Whitehurst, D. A., "Study of Carbon Monoxide Exposures of Residents of Washington, DC," Paper 84-121.4, *Proceedings*, 77th Annual Meeting of the Air Pollution Control Association, 1984.

[3] Pellizarri, E. D., Perritt, K., Hartwell, T. D., Michael, L. C., Whitmore, R., Handy, R. W., Smith, D., and Zelon, H., *Total Exposure Assessment Methodology (TEAM) Study: Elizabeth and Bayonne, NJ, Devils Lake, ND, and Greensboro, NC, Vol. II*, U.S. EPA, Washington, DC, 1987.

[4] Pellizarri, E. D., Perritt, K., Hartwell, T. D., Michael, L. C., Whitmore, R., Handy, R. W., Smith, D., and Zelon, H., *Total Exposure Assessment Methodology (TEAM) Study: Selected Communities in Northern and Southern California, Vol. III*, U.S. EPA, Washington, DC, 1987.

[5] Wallace, L. A., "Personal Exposures, Indoor and Outdoor Air Concentrations, and Exhaled Breath Concentrations of Selected Volatile Organic Compounds Measured for 600 Residents of New Jersey, North Dakota, North Carolina, and California," *Toxicological and Environmental Chemistry*, U.S. Environmental Protection Agency, Office of Research and Development, Benzene Bibliographic Library Information Service (EPA-ORD BBLIS), Citation 017, Washington, 1986.

[6] Wallace, L. A., *The Total Exposure Assessment Methodology (TEAM) Study: Summary and Analysis: Volume I*, U.S. EPA, Washington, DC, 1987.

[7] Chen, C. W. and Blancato, J. N., "Incorporation of Biological Mechanisms in Cancer Risk Assessment: Example—Vinyl Chloride," *Cell Biology and Toxicology*, Vol. 5, No. 4, 1989, pp. 417–444.

[8] Chen, C. W. and Blancato, J. N., "Role of Pharmacokinetic Modeling in Risk Assessment: Perchlorethylene as an Example," *Pharmacokinetics in Risk Assessment*, National Academy Press, 1987.

[9] Blancato, J. N. and Rhomberg, L., "The Impact of Pharmacokinetics on the Risk Assessment of Dichloromethane," *Biological Data for Pharmacokinetic Modeling and Risk Assessment*, U.S. EPA 600/3-90/019, U.S. EPA, Washington, DC, 1989.

[10] Corley, R. A., Mendrala, A. L., Smith, F. A., Stoats, D. A., Cargos, M. L., Connolly, R. B., Andersen, M. E., and Reitz, R. H., "Development of a Physiologically Based Pharmacokinetic Model for Chloroform," *Toxicology and Applied Pharmacology*, Vol. 103, 1990, pp. 512–527.

[11] Reitz, R. H., Mendrala, A. L., Gorier, R. A., Quast, J. F., Gargas, M. L., Andersen, M. E., Stoats, D. A., and Connolly, R. B., "Estimating the Risk of Liver Cancer Associated with Human Exposures to Chloroform Using Physiologically Based Pharmacokinetic Modeling," *Toxicology and Applied Pharmacology*, Vol. 105, 1990, pp. 443–459.

[12] Behar, J. V., Thomas, J., and Pandian, M. D., "Benzene Exposure Assessment Model (BEAM) (2nd Interim Report)," U.S. EPA 600/X-90/027, U.S. EPA, 1991.

[13] Behar, J. V., Thomas, J., and Pandian, M. D., "Benzene Exposure Assessment Model (BEAM) (3rd Report)," U.S. EPA 600/X-91/091, U.S. EPA, Washington, DC, 1991.

[14] Thomas, J., Pandian, M. D., Behar, J. V., Rheingrover, S., Hunt, H., and Ziegenfus, R. C., "Interim Report on Benzene Exposure Assessment Model (BEAM)," U.S. EPA 600/X-89/015, U.S. EPA, Washington, DC, 1989.

[15] Robinson, J. P. and Thomas, J., "Time Spent in Activities, Locations, and Microenvironments: A California-National Comparison," U.S. EPA 600/4-91/006, Environmental Monitoring Systems Laboratory-Las Vegas (EMSL-LV), U.S. EPA, Las Vegas, NV, 1991.

[16] Shikiya, D. C., Liu, C. S., Kahn, M. I., Juarros, J., and Barcikowski, W., *In-Vehicle Air Toxics Characterization Study in the South Coast Air Quality Management District, El Monte, California*, South Coast Air Quality Management District, El Monte, CA, 1989.

[17] Travis, C. C., Craig, P. H., and Bowers, J. C., "Characterization of Human Exposure to Ambient Levels of Benzene Using Pulmonary 'Wash-Out Data'," *Atmospheric Environment*, Vol. 25A, No. 8, 1991, pp. 1643–1647.

[18] *Best and Taylor's Physiological Basis of Medical Practice*, John B. West, Ed., Williams and Wilkins, Baltimore, Hong Kong, London, Sydney, 1991.

[19] Medinsky, M. A., Sobourin, P. J., Lacier, G., Birnbaum, L. S., and Henderson, R. F., "A Physiological Model for Simulation of Benzene Metabolism by Rats and Mice," *Toxicology and Applied Pharmacology*, Vol. 99, 1989, pp. 193–206.

Author Index

Subject Index

T–U

V–W

ISBN 0-8031-1875-9